



**Mercator  
Ocean**  
Ocean Forecasters



**cmcc**  
Centro Euro-Mediterraneo  
sui Cambiamenti Climatici



**NATURAL  
ENVIRONMENT  
RESEARCH COUNCIL**



---

## NEMO ocean engine

---

Gurvan Madec, and the NEMO team

`gurvan.madec@locean-ipsl.umpc.fr`

`nemo.st@locean-ipsl.umpc.fr`

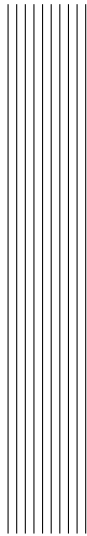
January 2017

– version 4.0 alpha –

*Note du Pôle de modélisation de l'Institut Pierre-Simon Laplace No 27*

ISSN No 1288-1619.





# Contents

<b>1</b>	<b>Introduction</b>	<b>5</b>
<b>2</b>	<b>Model basics</b>	<b>13</b>
2.1	Primitive Equations . . . . .	14
2.1.1	Vector Invariant Formulation . . . . .	14
2.1.2	Boundary Conditions . . . . .	15
2.2	The Horizontal Pressure Gradient . . . . .	17
2.2.1	Pressure Formulation . . . . .	17
2.2.2	Free Surface Formulation . . . . .	17
2.3	Curvilinear $z$ -coordinate System . . . . .	18
2.3.1	Tensorial Formalism . . . . .	18
2.3.2	Continuous Model Equations . . . . .	20
2.4	Curvilinear generalised vertical coordinate System . . . . .	24
2.4.1	The $s$ -coordinate Formulation . . . . .	25
2.4.2	Curvilinear $z^*$ -coordinate System . . . . .	27
2.4.3	Curvilinear Terrain-following $s$ -coordinate . . . . .	30
2.4.4	Curvilinear $\tilde{z}$ -coordinate . . . . .	32
2.5	Subgrid Scale Physics . . . . .	33
2.5.1	Vertical Subgrid Scale Physics . . . . .	33
2.5.2	Formulation of the Lateral Diffusive and Viscous Operators . . . . .	34
<b>3</b>	<b>Time Domain (STP)</b>	<b>39</b>
3.1	Time stepping environment . . . . .	40
3.2	Non-Diffusive Part — Leapfrog Scheme . . . . .	40

3.3	Diffusive Part — Forward or Backward Scheme . . . . .	41
3.4	Surface Pressure Gradient . . . . .	43
3.5	The Modified Leapfrog – Asselin Filter scheme . . . . .	44
3.6	Start/Restart strategy . . . . .	44
<b>4</b>	<b>Space Domain (DOM)</b> . . . . .	<b>47</b>
4.1	Fundamentals of the Discretisation . . . . .	48
4.1.1	Arrangement of Variables . . . . .	48
4.1.2	Discrete Operators . . . . .	49
4.1.3	Numerical Indexing . . . . .	51
4.2	Domain: Needed fields . . . . .	54
4.3	Domain: Horizontal Grid (mesh) ( <i>domhgr</i> ) . . . . .	54
4.3.1	Coordinates and scale factors . . . . .	54
4.3.2	Choice of horizontal grid . . . . .	55
4.3.3	Output Grid files . . . . .	57
4.4	Domain: Vertical Grid ( <i>domzgr</i> ) . . . . .	57
4.4.1	Meter Bathymetry . . . . .	59
4.4.2	<i>z</i> -coordinate ( <i>ln_zco</i> ) . . . . .	60
4.4.3	<i>z</i> -coordinate with partial step ( <i>ln_zps</i> ) . . . . .	62
4.4.4	<i>s</i> -coordinate ( <i>ln_sco</i> ) . . . . .	64
4.4.5	<i>z</i> *- or <i>s</i> *-coordinate ( <i>ln_linssh=false</i> ) . . . . .	66
4.4.6	level bathymetry and mask . . . . .	67
4.5	Domain: Initial State ( <i>istate and dtatsd</i> ) . . . . .	68
<b>5</b>	<b>Ocean Tracers (TRA)</b> . . . . .	<b>69</b>
5.1	Tracer Advection ( <i>traadv</i> ) . . . . .	71
5.1.1	Centred schemes (CEN) ( <i>ln_traadv_cen</i> ) . . . . .	73
5.1.2	Flux Corrected Transport schemes (FCT) ( <i>ln_traadv_fct</i> ) . . . . .	74
5.1.3	MUSCL scheme ( <i>ln_traadv_mus</i> ) . . . . .	75
5.1.4	Upstream-Biased Scheme (UBS) ( <i>ln_traadv_ubs</i> ) . . . . .	76
5.1.5	QUICKEST scheme (QCK) ( <i>ln_traadv_qck</i> ) . . . . .	77
5.2	Tracer Lateral Diffusion ( <i>traldf</i> ) . . . . .	77
5.2.1	Type of operator ( <i>ln_traldf_NONE, ln_traldf_lap, ln_traldf_blp</i> ) . . . . .	78
5.2.2	Direction of action ( <i>ln_traldf_lev, ln_traldf_hor, ln_traldf_iso, ln_traldf_triad</i> ) . . . . .	79
5.2.3	Iso-level (bi-)laplacian operator ( <i>ln_traldf_iso</i> ) . . . . .	79
5.2.4	Standard and triad rotated (bi-)laplacian operator ( <i>traldf_iso.F90, traldf_triad.F90</i> ) . . . . .	80
5.3	Tracer Vertical Diffusion ( <i>trazdf</i> ) . . . . .	81
5.4	External Forcing . . . . .	82
5.4.1	Surface boundary condition ( <i>trasbc</i> ) . . . . .	82
5.4.2	Solar Radiation Penetration ( <i>traqsr</i> ) . . . . .	83
5.4.3	Bottom Boundary Condition ( <i>trabbc</i> ) . . . . .	85
5.5	Bottom Boundary Layer ( <i>trabbl.F90 - key_trabbl</i> ) . . . . .	87

5.5.1	Diffusive Bottom Boundary layer ( <i>nn_bbl_ldf=1</i> ) . . . . .	88
5.5.2	Advective Bottom Boundary Layer ( <i>nn_bbl_adv= 1 or 2</i> ) . . . . .	88
5.6	Tracer damping ( <i>tradmp</i> ) . . . . .	90
5.6.1	DMP_TOOLS . . . . .	91
5.7	Tracer time evolution ( <i>tranxt</i> ) . . . . .	92
5.8	Equation of State ( <i>eosbn2</i> ) . . . . .	93
5.8.1	Equation Of Seawater ( <i>nn_eos = -1, 0, or 1</i> ) . . . . .	93
5.8.2	Brunt-Väisälä Frequency ( <i>nn_eos = 0, 1 or 2</i> ) . . . . .	95
5.8.3	Freezing Point of Seawater . . . . .	96
5.9	Horizontal Derivative in <i>zps</i> -coordinate ( <i>zpsjde</i> ) . . . . .	96
<b>6</b>	<b>Ocean Dynamics (DYN)</b> . . . . .	<b>99</b>
6.1	Sea surface height and diagnostic variables ( $\eta, \zeta, \chi, w$ ) . . . . .	101
6.1.1	Horizontal divergence and relative vorticity ( <i>divcur</i> ) . . . . .	101
6.1.2	Sea surface height evolution and vertical velocity ( <i>sshwzv</i> ) . . . . .	101
6.2	Coriolis and Advection: vector invariant form . . . . .	102
6.2.1	Vorticity term ( <i>dynvor</i> ) . . . . .	102
6.2.2	Kinetic Energy Gradient term ( <i>dynkeg</i> ) . . . . .	106
6.2.3	Vertical advection term ( <i>dynzad</i> ) . . . . .	106
6.3	Coriolis and Advection: flux form . . . . .	107
6.3.1	Coriolis plus curvature metric terms ( <i>dynvor</i> ) . . . . .	107
6.3.2	Flux form Advection term ( <i>dynadv</i> ) . . . . .	107
6.4	Hydrostatic pressure gradient ( <i>dynhpg</i> ) . . . . .	109
6.4.1	<i>z</i> -coordinate with full step ( <i>ln_dynhpg_zco</i> ) . . . . .	109
6.4.2	<i>z</i> -coordinate with partial step ( <i>ln_dynhpg_zps</i> ) . . . . .	110
6.4.3	<i>s</i> - and <i>z-s</i> -coordinates . . . . .	110
6.4.4	Ice shelf cavity . . . . .	111
6.4.5	Time-scheme ( <i>ln_dynhpg_imp</i> ) . . . . .	111
6.5	Surface pressure gradient ( <i>dynspg</i> ) . . . . .	112
6.5.1	Explicit free surface ( <b>key_dynspg_exp</b> ) . . . . .	113
6.5.2	Split-Explicit free surface ( <b>key_dynspg_ts</b> ) . . . . .	113
6.5.3	Filtered free surface ( <b>key_dynspgflt</b> ) . . . . .	116
6.6	Lateral diffusion term ( <i>dynldf</i> ) . . . . .	116
6.6.1	Iso-level laplacian operator ( <i>ln_dynldf_lap</i> ) . . . . .	117
6.6.2	Rotated laplacian operator ( <i>ln_dynldf_iso</i> ) . . . . .	117
6.6.3	Iso-level bilaplacian operator ( <i>ln_dynldf_bilap</i> ) . . . . .	118
6.7	Vertical diffusion term ( <i>dynzdf.F90</i> ) . . . . .	118
6.8	External Forcings . . . . .	120
6.9	Time evolution term ( <i>dynnxt</i> ) . . . . .	120
<b>7</b>	<b>Surface Boundary Condition (SBC, ISF, ICB)</b> . . . . .	<b>123</b>
7.1	Surface boundary condition for the ocean . . . . .	127
7.2	Input Data generic interface . . . . .	127
7.2.1	Input Data specification ( <i>fldread.F90</i> ) . . . . .	128

7.2.2	Interpolation on-the-Fly	130
7.2.3	Standalone Surface Boundary Condition Scheme	133
7.3	Analytical formulation ( <i>sbcana</i> )	134
7.4	Flux formulation ( <i>sbcflx</i> )	135
7.5	Bulk formulation ( <i>sbcblk_core</i> , <i>sbcblk_clio</i> or <i>sbcblk_mfs</i> )	135
7.5.1	CORE Bulk formulae ( <i>ln_core=true</i> )	135
7.5.2	CLIO Bulk formulae ( <i>ln_clio=true</i> )	136
7.5.3	MFS Bulk formulae ( <i>ln_mfs=true</i> )	137
7.6	Coupled formulation ( <i>sbccpl</i> )	138
7.7	Atmospheric pressure ( <i>sbcapr</i> )	139
7.8	Tidal Potential ( <i>sbctide</i> )	140
7.9	River runoffs ( <i>sbcnmf</i> )	141
7.10	Ice shelf melting ( <i>sbcisf</i> )	142
7.11	Ice sheet coupling	144
7.12	Handling of icebergs (ICB)	146
7.13	Miscellaneous options	147
7.13.1	Diurnal cycle ( <i>sbcncy</i> )	147
7.13.2	Rotation of vector pairs onto the model grid directions	149
7.13.3	Surface restoring to observed SST and/or SSS ( <i>sbcssr</i> )	150
7.13.4	Handling of ice-covered area ( <i>sbcice_...</i> )	150
7.13.5	Interface to CICE ( <i>sbcice_cice</i> )	151
7.13.6	Freshwater budget control ( <i>sbcfwb</i> )	152
7.13.7	Neutral drag coefficient from external wave model ( <i>sbcwave</i> )	152
<b>8</b>	<b>Lateral Boundary Condition (LBC)</b>	<b>153</b>
8.1	Boundary Condition at the Coast ( <i>rn_shlat</i> )	154
8.2	Model Domain Boundary Condition ( <i>jperio</i> )	157
8.2.1	Closed, cyclic, south symmetric ( <i>jperio</i> = 0, 1 or 2)	157
8.2.2	North-fold ( <i>jperio</i> = 3 to 6)	158
8.3	Exchange with neighbouring processors ( <i>lbclnk</i> , <i>lib_mpp</i> )	158
8.4	Unstructured Open Boundary Conditions (BDY)	161
8.4.1	The namelists	163
8.4.2	The Flow Relaxation Scheme	164
8.4.3	The Flather radiation scheme	165
8.4.4	Boundary geometry	165
8.4.5	Input boundary data files	167
8.4.6	Volume correction	167
8.4.7	Tidal harmonic forcing	168
<b>9</b>	<b>Lateral Ocean Physics (LDF)</b>	<b>171</b>
9.1	Direction of Lateral Mixing ( <i>ldfslp</i> )	173
9.1.1	slopes for tracer geopotential mixing in the <i>s</i> -coordinate	173
9.1.2	Slopes for tracer iso-neutral mixing	173
9.1.3	slopes for momentum iso-neutral mixing	176

9.2	Lateral Mixing Operators ( <i>ldftra, lfdyn</i> ) . . . . .	178
9.3	Lateral Mixing Coefficient ( <i>ldftra, lfdyn</i> ) . . . . .	178
9.4	Eddy Induced Velocity ( <i>traadv_eiv, ldfeiv</i> ) . . . . .	180
<b>10</b>	<b>Vertical Ocean Physics (ZDF)</b>	<b>183</b>
10.1	Vertical Mixing . . . . .	184
10.1.1	Constant ( <b>key_zdfcst</b> ) . . . . .	184
10.1.2	Richardson Number Dependent ( <b>key_zdfric</b> ) . . . . .	185
10.1.3	TKE Turbulent Closure Scheme ( <b>key_zdftke</b> ) . . . . .	186
10.1.4	TKE discretization considerations ( <b>key_zdftke</b> ) . . . . .	191
10.1.5	GLS Generic Length Scale ( <b>key_zdfgls</b> ) . . . . .	194
10.2	Convection . . . . .	196
10.2.1	Non-Penetrative Convective Adjustment ( <i>ln_tranpc</i> ) . . . . .	197
10.2.2	Enhanced Vertical Diffusion ( <i>ln_zdfevd</i> ) . . . . .	198
10.2.3	Turbulent Closure Scheme ( <b>key_zdftke</b> or <b>key_zdfgls</b> ) . . . . .	199
10.3	Double Diffusion Mixing ( <b>key_zdfddm</b> ) . . . . .	200
10.4	Bottom and Top Friction ( <i>zdfbfr</i> ) . . . . .	201
10.4.1	Linear Bottom Friction ( <i>nn_botfr = 0</i> or <i>1</i> ) . . . . .	202
10.4.2	Non-Linear Bottom Friction ( <i>nn_botfr = 2</i> ) . . . . .	203
10.4.3	Log-layer Bottom Friction enhancement ( <i>nn_botfr = 2, ln_loglayer = .true.</i> ) . . . . .	204
10.4.4	Bottom Friction stability considerations . . . . .	204
10.4.5	Implicit Bottom Friction ( <i>ln_bfrimp=T</i> ) . . . . .	205
10.4.6	Bottom Friction with split-explicit time splitting ( <i>ln_bfrimp=F</i> ) . . . . .	206
10.5	Tidal Mixing ( <b>key_zdftmx</b> ) . . . . .	207
10.5.1	Bottom intensified tidal mixing . . . . .	207
10.5.2	Indonesian area specific treatment ( <i>ln_zdftmx_itf</i> ) . . . . .	208
10.6	Internal wave-driven mixing ( <b>key_zdftmx_new</b> ) . . . . .	210
<b>11</b>	<b>Output and Diagnostics (IOM, DIA, TRD, FLO)</b>	<b>213</b>
11.1	Old Model Output (default) . . . . .	214
11.2	Standard model Output (IOM) . . . . .	214
11.2.1	XIOS: the IO_SERVER . . . . .	216
11.2.2	Practical issues . . . . .	217
11.2.3	XML fundamentals . . . . .	218
11.2.4	Detailed functionalities . . . . .	222
11.2.5	XML reference tables . . . . .	224
11.2.6	CF metadata standard compliance . . . . .	231
11.3	NetCDF4 Support ( <b>key_netcdf4</b> ) . . . . .	231
11.4	Tracer/Dynamics Trends (TRD) . . . . .	234
11.5	On-line Floats trajectories (FLO) ( <b>key_floats</b> ) . . . . .	235
11.6	Harmonic analysis of tidal constituents ( <b>key_diaharm</b> ) . . . . .	236
11.7	Transports across sections ( <b>key_diadct</b> ) . . . . .	237
11.8	Diagnosing the Steric effect in sea surface height . . . . .	239

---

11.9	Other Diagnostics ( <b>key_diahth</b> , <b>key_diaar5</b> ) . . . . .	242
11.9.1	Depth of various quantities ( <i>diahth.F90</i> ) . . . . .	242
11.9.2	Poleward heat and salt transports ( <i>diaptr.F90</i> ) . . . . .	243
11.9.3	CMIP specific diagnostics ( <i>diaar5.F90</i> ) . . . . .	243
11.9.4	25 hour mean output for tidal models . . . . .	243
11.9.5	Top Middle and Bed hourly output . . . . .	244
11.9.6	Courant numbers . . . . .	244
<b>12</b>	<b>Observation and model comparison (OBS)</b>	<b>245</b>
12.1	Running the observation operator code example . . . . .	246
12.2	Technical details . . . . .	247
12.2.1	Profile feedback type observation file header . . . . .	248
12.2.2	Sea level anomaly feedback type observation file header . . . . .	250
12.2.3	Sea surface temperature feedback type observation file header . . . . .	252
12.3	Theoretical details . . . . .	253
12.3.1	Horizontal interpolation methods . . . . .	253
12.3.2	Grid search . . . . .	255
12.3.3	Parallel aspects of horizontal interpolation . . . . .	255
12.3.4	Vertical interpolation operator . . . . .	258
12.4	Offline observation operator . . . . .	259
12.4.1	Concept . . . . .	259
12.4.2	Using the offline observation operator . . . . .	259
12.4.3	Configuring the offline observation operator . . . . .	260
12.4.4	Advanced usage . . . . .	264
12.5	Observation Utilities . . . . .	265
12.5.1	Obstools . . . . .	265
12.5.2	building the obstools . . . . .	268
12.5.3	Dataplot . . . . .	268
<b>13</b>	<b>Apply assimilation increments (ASM)</b>	<b>271</b>
13.1	Direct initialization . . . . .	272
13.2	Incremental Analysis Updates . . . . .	272
13.3	Divergence damping initialisation . . . . .	273
13.4	Implementation details . . . . .	273
<b>14</b>	<b>Stochastic parametrization of EOS (STO)</b>	<b>275</b>
14.1	Stochastic processes . . . . .	276
14.2	Implementation details . . . . .	277
<b>15</b>	<b>Miscellaneous Topics</b>	<b>279</b>
15.1	Representation of Unresolved Straits . . . . .	280
15.1.1	Hand made geometry changes . . . . .	280
15.2	Closed seas ( <i>closea.F90</i> ) . . . . .	282
15.3	Sub-Domain Functionality . . . . .	282



---

15.3.1	Simple subsetting of input files via netCDF attributes . . . .	282
15.4	Accuracy and Reproducibility ( <i>lib_fortran.F90</i> ) . . . . .	283
15.4.1	Issues with intrinsic SIGN function ( <b>key_nosignedzero</b> ) . . . . .	283
15.4.2	MPP reproducibility . . . . .	284
15.4.3	MPP scalability . . . . .	284
15.5	Model Optimisation, Control Print and Benchmark . . . . .	285
<b>16</b>	<b>Configurations</b> . . . . .	<b>287</b>
16.1	Introduction . . . . .	288
16.2	Water column model: 1D model (C1D) ( <b>key_c1d</b> ) . . . . .	288
16.3	ORCA family: global ocean with tripolar grid . . . . .	289
16.3.1	ORCA tripolar grid . . . . .	289
16.3.2	ORCA pre-defined resolution . . . . .	292
16.4	GYRE family: double gyre basin . . . . .	293
16.5	AMM: atlantic margin configuration . . . . .	294
<b>A</b>	<b>Curvilinear <math>s</math>-Coordinate Equations</b> . . . . .	<b>295</b>
A.1	The chain rule for $s$ -coordinates . . . . .	296
A.2	Continuity Equation in $s$ -coordinates . . . . .	296
A.3	Momentum Equation in $s$ -coordinate . . . . .	298
A.4	Tracer Equation . . . . .	302
<b>B</b>	<b>Appendix B : Diffusive Operators</b> . . . . .	<b>303</b>
B.1	Horizontal/Vertical 2nd Order Tracer Diffusive Operators . . . . .	304
B.2	Iso/diapycnal 2nd Order Tracer Diffusive Operators . . . . .	306
B.3	Lateral/Vertical Momentum Diffusive Operators . . . . .	308
<b>C</b>	<b>Discrete Invariants of the Equations</b> . . . . .	<b>311</b>
C.1	Introduction / Notations . . . . .	312
C.2	Continuous conservation . . . . .	313
C.3	Discrete total energy conservation : vector invariant form . . . . .	316
C.3.1	Total energy conservation . . . . .	316
C.3.2	Vorticity term (coriolis + vorticity part of the advection) . . . . .	316
C.3.3	Pressure Gradient Term . . . . .	320
C.4	Discrete total energy conservation : flux form . . . . .	322
C.4.1	Total energy conservation . . . . .	322
C.4.2	Coriolis and advection terms: flux form . . . . .	323
C.5	Discrete enstrophy conservation . . . . .	324
C.6	Conservation Properties on Tracers . . . . .	326
C.6.1	Advection Term . . . . .	326
C.7	Conservation Properties on Lateral Momentum Physics . . . . .	327
C.7.1	Conservation of Potential Vorticity . . . . .	327
C.7.2	Dissipation of Horizontal Kinetic Energy . . . . .	328
C.7.3	Dissipation of Enstrophy . . . . .	329

---

C.7.4	Conservation of Horizontal Divergence . . . . .	329
C.7.5	Dissipation of Horizontal Divergence Variance . . . . .	329
C.8	Conservation Properties on Vertical Momentum Physics . . . . .	330
C.9	Conservation Properties on Tracer Physics . . . . .	333
C.9.1	Conservation of Tracers . . . . .	333
C.9.2	Dissipation of Tracer Variance . . . . .	334
<b>D</b>	<b>Iso-neutral diffusion and eddy advection using triads</b>	<b>335</b>
D.1	Choice of <i>namtra_ldf</i> namelist parameters . . . . .	336
D.2	Triad formulation of iso-neutral diffusion . . . . .	337
D.2.1	The iso-neutral diffusion operator . . . . .	337
D.2.2	The standard discretization . . . . .	338
D.2.3	Expression of the skew-flux in terms of triad slopes . . . . .	339
D.2.4	The full triad fluxes . . . . .	341
D.2.5	Ensuring the scheme does not increase tracer variance . . . . .	342
D.2.6	Triad volumes in Griffes's scheme and in <i>NEMO</i> . . . . .	343
D.2.7	Summary of the scheme . . . . .	344
D.2.8	Treatment of the triads at the boundaries . . . . .	345
D.2.9	Limiting of the slopes within the interior . . . . .	347
D.2.10	Tapering within the surface mixed layer . . . . .	347
D.3	Eddy induced advection formulated as a skew flux . . . . .	350
D.3.1	The continuous skew flux formulation . . . . .	350
D.3.2	The discrete skew flux formulation . . . . .	352
D.3.3	Treatment of the triads at the boundaries . . . . .	353
D.3.4	Limiting of the slopes within the interior . . . . .	354
D.3.5	Tapering within the surface mixed layer . . . . .	354
D.3.6	Streamfunction diagnostics . . . . .	354
<b>E</b>	<b>Coding Rules</b>	<b>357</b>
E.1	The program structure . . . . .	358
E.2	Coding conventions . . . . .	358
E.3	Naming Conventions . . . . .	360
E.4	The program structure . . . . .	361
	<b>Index</b>	<b>361</b>
	<b>Index</b>	<b>362</b>
	<b>Bibliography</b>	<b>371</b>



## Abstract / Résumé

The ocean engine of NEMO (Nucleus for European Modelling of the Ocean) is a primitive equation model adapted to regional and global ocean circulation problems. It is intended to be a flexible tool for studying the ocean and its interactions with the others components of the earth climate system over a wide range of space and time scales. Prognostic variables are the three-dimensional velocity field, a non-linear sea surface height, the *Conservative* Temperature and the *Absolute* Salinity. In the horizontal direction, the model uses a curvilinear orthogonal grid and in the vertical direction, a full or partial step  $z$ -coordinate, or  $s$ -coordinate, or a mixture of the two. The distribution of variables is a three-dimensional Arakawa C-type grid. Various physical choices are available to describe ocean physics, including TKE, and GLS vertical physics. Within NEMO, the ocean is interfaced with a sea-ice model (LIM or CICE), passive tracer and biogeochemical models (TOP) and, via the OASIS coupler, with several atmospheric general circulation models. It also support two-way grid embedding via the AGRIF software.





## Disclaimer

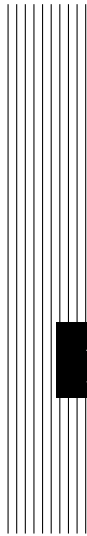
Like all components of NEMO, the ocean component is developed under the CE-CILL license, which is a French adaptation of the GNU GPL (General Public License). Anyone may use it freely for research purposes, and is encouraged to communicate back to the NEMO team its own developments and improvements. The model and the present document have been made available as a service to the community. We cannot certify that the code and its manual are free of errors. Bugs are inevitable and some have undoubtedly survived the testing phase. Users are encouraged to bring them to our attention. The author assumes no responsibility for problems, errors, or incorrect usage of NEMO.

NEMO reference in papers and other publications is as follows:

Madec, G., and the NEMO team, 2008: NEMO ocean engine. *Note du Pôle de modélisation*, Institut Pierre-Simon Laplace (IPSL), France, No 27, ISSN No 1288-1619.

Additional information can be found on [nemo-ocean.eu](http://nemo-ocean.eu) website.





# 1 Introduction

The Nucleus for European Modelling of the Ocean (*NEMO*) is a framework of ocean related engines, namely OPA<sup>1</sup> for the ocean dynamics and thermodynamics, LIM<sup>2</sup> for the sea-ice dynamics and thermodynamics, TOP<sup>3</sup> for the biogeochemistry (both transport (TRP) and sources minus sinks (LOBSTER, PISCES)<sup>4</sup>. It is intended to be a flexible tool for studying the ocean and its interactions with the other components of the earth climate system (atmosphere, sea-ice, biogeochemical tracers, ...) over a wide range of space and time scales. This documentation provides information about the physics represented by the ocean component of *NEMO* and the rationale for the choice of numerical schemes and the model design. More specific information about running the model on different computers, or how to set up a configuration, are found on the *NEMO* web site ([www.nemo-ocean.eu](http://www.nemo-ocean.eu)).

The ocean component of *NEMO* has been developed from the OPA model, release 8.2, described in Madec et al. [1998]. This model has been used for a wide range of applications, both regional or global, as a forced ocean model and as a model coupled with the sea-ice and/or the atmosphere.

This manual is organised in as follows. Chapter 2 presents the model basics, *i.e.* the equations and their assumptions, the vertical coordinates used, and the subgrid scale physics. This part deals with the continuous equations of the model (primitive equations, with temperature, salinity and an equation of seawater). The equations are written in a curvilinear coordinate system, with a choice of vertical coordinates ( $z$ ,  $s$ ,  $z^*$ ,  $s^*$ ,  $\tilde{z}$ ,  $\tilde{s}$ , and a mixture of them). Momentum equations are formulated in vector invariant or flux form. Dimensional units in the meter, kilogram, second (MKS) international system are used throughout.

---

<sup>1</sup>OPA = Océan PARallélisté

<sup>2</sup>LIM= Louvain)la-neuve Ice Model

<sup>3</sup>TOP = Tracer in the Ocean Paradigm

<sup>4</sup>Both LOBSTER and PISCES are not acronyms just name

The following chapters deal with the discrete equations. Chapter 3 presents the time domain. The model time stepping environment is a three level scheme in which the tendency terms of the equations are evaluated either centered in time, or forward, or backward depending of the nature of the term. Chapter 4 presents the space domain. The model is discretised on a staggered grid (Arakawa C grid) with masking of land areas. Vertical discretisation used depends on both how the bottom topography is represented and whether the free surface is linear or not. Full step or partial step  $z$ -coordinate or  $s$ - (terrain-following) coordinate is used with linear free surface (level position are then fixed in time). In non-linear free surface, the corresponding rescaled height coordinate formulation ( $z^*$  or  $s^*$ ) is used (the level position then vary in time as a function of the sea surface heigh). The following two chapters (5 and 6) describe the discretisation of the prognostic equations for the active tracers and the momentum. Explicit, split-explicit and filtered free surface formulations are implemented. A number of numerical schemes are available for momentum advection, for the computation of the pressure gradients, as well as for the advection of tracers (second or higher order advection schemes, including positive ones).

Surface boundary conditions (chapter 7) can be implemented as prescribed fluxes, or bulk formulations for the surface fluxes (wind stress, heat, freshwater). The model allows penetration of solar radiation There is an optional geothermal heating at the ocean bottom. Within the *NEMO* system the ocean model is interactively coupled with a sea ice model (LIM) and with biogeochemistry models (PISCES, LOBSTER). Interactive coupling to Atmospheric models is possible via the OASIS coupler [Valcke 2006]. Two-way nesting is also available through an interface to the AGRIF package (Adaptative Grid Refinement in FORTRAN) [Debreu et al. 2008]. The interface code for coupling to an alternative sea ice model (CICE, Hunke and Lipscomb [2008]) has now been upgraded so that it works for both global and regional domains, although AGRIF is still not available.

Other model characteristics are the lateral boundary conditions (chapter 8). Global configurations of the model make use of the ORCA tripolar grid, with special north fold boundary condition. Free-slip or no-slip boundary conditions are allowed at land boundaries. Closed basin geometries as well as periodic domains and open boundary conditions are possible.

Physical parameterisations are described in chapters 9 and 10. The model includes an implicit treatment of vertical viscosity and diffusivity. The lateral Laplacian and biharmonic viscosity and diffusion can be rotated following a geopotential or neutral direction. There is an optional eddy induced velocity [Gent and McWilliams 1990] with a space and time variable coefficient Tréguier et al. [1997]. The model has vertical harmonic viscosity and diffusion with a space and time variable coefficient, with options to compute the coefficients with Blanke and Delecluse [1993], Pacanowski and Philander [1981], or Umlauf and Burchard [2003] mixing schemes.



CPP keys and namelists are used for inputs to the code.

### CPP keys

Some CPP keys are implemented in the FORTRAN code to allow code selection at compiling step. This selection of code at compilation time reduces the reliability of the whole platform since it changes the code from one set of CPP keys to the other. It is used only when the addition/suppression of the part of code highly changes the amount of memory at run time. Usual coding looks like :

```
#if defined key_option1
    This part of the FORTRAN code will be active
    only if key_option1 is activated at compiling step
#endif
```

### Namelists

The namelist allows to input variables (character, logical, real and integer) into the code. There is one namelist file for each component of NEMO (dynamics, sea-ice, biogeochemistry...) containing all the FORTRAN namelists needed. The implementation in NEMO uses a two step process. For each FORTRAN namelist, two files are read:

1. A reference namelist ( in *CONFIG/SHARED/namelist\_ref* ) is read first. This file contains all the namelist variables which are initialised to default values
2. A configuration namelist ( in *CONFIG/CFG\_NAME/EXP00/namelist\_cfg* ) is read afterwards. This file contains only the namelist variables which are changed from default values, and overwrites those.

A template can be found in *NEMO/OPA\_SRC/module.example* The effective namelist, taken in account during the run, is stored at execution time in an *output\_namelist\_dyn* (or *\_ice* or *\_top*) file.

Model outputs management and specific online diagnostics are described in chapters 11. The diagnostics includes the output of all the tendencies of the momentum and tracers equations, the output of tracers tendencies averaged over the time evolving mixed layer, the output of the tendencies of the barotropic vorticity equation, the computation of on-line floats trajectories... Chapter 12 describes a tool which reads in observation files (profile temperature and salinity, sea surface temperature, sea level anomaly and sea ice concentration) and calculates an interpolated model equivalent value at the observation location and nearest model timestep. Originally developed of data assimilation, it is a fantastic tool for model and data comparison. Chapter 13 describes how increments produced by data assimilation may be applied to the model equations. Finally, Chapter 16 provides a brief introduction to the pre-defined model configurations (water column model, ORCA and GYRE families of configurations).

**Table 1.1:** Organization of Chapters mimicking the one of the model directories.

Chapter 3	-	model time STePping environment
Chapter 4	DOM	model DOMain
Chapter 5	TRA	TRAcEr equations (potential temperature and salinity)
Chapter 6	DYN	DYNamic equations (momentum)
Chapter 7	SBC	Surface Boundary Conditions
Chapter 8	LBC	Lateral Boundary Conditions (also OBC and BDY)
Chapter 9	LDF	Lateral DiFfusion (parameterisations)
Chapter 10	ZDF	vertical (Z) DiFfusion (parameterisations)
Chapter 11	DIA	I/O and DIAGnostics (also IOM, FLO and TRD)
Chapter 12	OBS	OBServation and model comparison
Chapter 13	ASM	ASsiMilation increment
Chapter 15	SOL	Miscellaneous topics (including solvers)
Chapter 16	-	predefined configurations (including C1D)

The model is implemented in FORTRAN 90, with preprocessing (C-pre-processor). It runs under UNIX. It is optimized for vector computers and parallelised by domain decomposition with MPI. All input and output is done in NetCDF (Network Common Data Format) with a optional direct access format for output. To ensure the clarity and readability of the code it is necessary to follow coding rules. The coding rules for OPA include conventions for naming variables, with different starting letters for different types of variables (real, integer, parameter. . .). Those rules are briefly presented in Appendix E and a more complete document is available on the *NEMO* web site.

The model is organized with a high internal modularity based on physics. For example, each trend (*i.e.*, a term in the RHS of the prognostic equation) for momentum and tracers is computed in a dedicated module. To make it easier for the user to find his way around the code, the module names follow a three-letter rule. For example, *traldf.F90* is a module related to the TRAcers equation, computing the Lateral DiFfusion. Furthermore, modules are organized in a few directories that correspond to their category, as indicated by the first three letters of their name (Tab. 1.1).

The manual mirrors the organization of the model. After the presentation of the continuous equations (Chapter 2), the following chapters refer to specific terms of the equations each associated with a group of modules (Tab. 1.1).

### Changes between releases

NEMO/OPA, like all research tools, is in perpetual evolution. The present document describes the OPA version include in the release 3.4 of NEMO. This release differs significantly from version 8, documented in Madec et al. [1998].

- The main modifications from OPA v8 and NEMO/OPA v3.2 are :

1. transition to full native FORTRAN 90, deep code restructuring and drastic reduction of CPP keys;
2. introduction of partial step representation of bottom topography [Barnier et al. 2006, Le Sommer et al. 2009, Penduff et al. 2007];
3. partial reactivation of a terrain-following vertical coordinate ( $s$ - and hybrid  $s$ - $z$ ) with the addition of several options for pressure gradient computation<sup>5</sup>;
4. more choices for the treatment of the free surface: full explicit, split-explicit or filtered schemes, and suppression of the rigid-lid option;
5. non linear free surface associated with the rescaled height coordinate  $z^*$  or  $s$ ;
6. additional schemes for vector and flux forms of the momentum advection;
7. additional advection schemes for tracers;
8. implementation of the AGRIF package (Adaptative Grid Refinement in FORTRAN) [Debreu et al. 2008];
9. online diagnostics : tracers trend in the mixed layer and vorticity balance;
10. rewriting of the I/O management with the use of an I/O server;
11. generalized ocean-ice-atmosphere-CO2 coupling interface, interfaced with OASIS 3 coupler ;
12. surface module (SBC) that simplify the way the ocean is forced and include two bulk formulae (CLIO and CORE) and which includes an on-the-fly interpolation of input forcing fields ;
13. RGB light penetration and optional use of ocean color
14. major changes in the TKE schemes: it now includes a Langmuir cell parameterization [Axell 2002], the Mellor and Blumberg [2004] surface wave breaking parameterization, and has a time discretization which is energetically consistent with the ocean model equations [Burchard 2002, Marsaleix et al. 2008];

---

<sup>5</sup>Partial support of  $s$ -coordinate: there is presently no support for neutral physics in  $s$ - coordinate and for the new options for horizontal pressure gradient computation with a non-linear equation of state.

15. tidal mixing parametrisation (bottom intensification) + Indonesian specific tidal mixing [[Koch-Larrouy et al. 2007](#)];
16. introduction of LIM-3, the new Louvain-la-Neuve sea-ice model (C-grid rheology and new thermodynamics including bulk ice salinity) [[Vancoppenolle et al. 2009b;a](#)]

• The main modifications from NEMO/OPA v3.2 and v3.3 are :

1. introduction of a modified leapfrog-Asselin filter time stepping scheme [[Leclair and Madec 2009](#)];
2. additional scheme for iso-neutral mixing [[Griffies et al. 1998](#)], although it is still a "work in progress";
3. a rewriting of the bottom boundary layer scheme, following [Campin and Goosse \[1999\]](#);
4. addition of a Generic Length Scale vertical mixing scheme, following [Umlauf and Burchard \[2003\]](#);
5. addition of the atmospheric pressure as an external forcing on both ocean and sea-ice dynamics;
6. addition of a diurnal cycle on solar radiation [[Bernie et al. 2007](#)];
7. river runoffs added through a non-zero depth, and having its own temperature and salinity;
8. CORE II normal year forcing set as the default forcing of ORCA2-LIM configuration ;
9. generalisation of the use of *fldread.F90* for all input fields (ocean climatology, sea-ice damping...) ;
10. addition of an on-line observation and model comparison (thanks to NEMOVAR project);
11. optional application of an assimilation increment (thanks to NEMOVAR project);
12. coupling interface adjusted for WRF atmospheric model;
13. C-grid ice rheology now available for both LIM-2 and LIM-3 [[Bouillon et al. 2009](#)];
14. LIM-3 ice-ocean momentum coupling applied to LIM-2 ;

15. a deep re-writing and simplification of the off-line tracer component (OFF\_SRC) ;
16. the merge of passive and active advection and diffusion modules ;
17. Use of the Flexible Configuration Manager (FCM) to build configurations, generate the Makefile and produce the executable ;
18. Linear-tangent and Adjoint component (TAM) added, phased with v3.0

In addition, several minor modifications in the coding have been introduced with the constant concern of improving the model performance.

- The main modifications from NEMO/OPA v3.3 and v3.4 are :

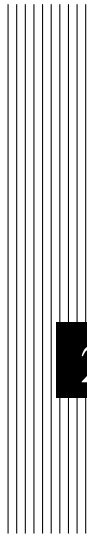
1. finalisation of above iso-neutral mixing [[Griffies et al. 1998](#)];
2. "Neptune effect" parametrisation;
3. horizontal pressure gradient suitable for s-coordinate;
4. semi-implicit bottom friction;
5. finalisation of the merge of passive and active tracers advection-diffusion modules;
6. a new bulk formulae (so-called MFS);
7. use fldread for the off-line tracer component (OFF\_SRC) ;
8. use MPI point to point communications for north fold;
9. diagnostic of transport ;

- The main modifications from NEMO/OPA v3.4 and v3.6 are :

1. ... ;

- The main modifications from NEMO/OPA v3.6 and v4.0 are :

1. new definition of configurations ;
2. bulk formulation ;
3. ... ;



## 2 Model basics

### Contents

---

<b>2.1</b>	<b>Primitive Equations</b> . . . . .	<b>14</b>
2.1.1	Vector Invariant Formulation . . . . .	14
2.1.2	Boundary Conditions . . . . .	15
<b>2.2</b>	<b>The Horizontal Pressure Gradient</b> . . . . .	<b>17</b>
2.2.1	Pressure Formulation . . . . .	17
2.2.2	Free Surface Formulation . . . . .	17
<b>2.3</b>	<b>Curvilinear <math>z</math>-coordinate System</b> . . . . .	<b>18</b>
2.3.1	Tensorial Formalism . . . . .	18
2.3.2	Continuous Model Equations . . . . .	20
<b>2.4</b>	<b>Curvilinear generalised vertical coordinate System</b> . . . . .	<b>24</b>
2.4.1	The $s$ -coordinate Formulation . . . . .	25
2.4.2	Curvilinear $z^*$ -coordinate System . . . . .	27
2.4.3	Curvilinear Terrain-following $s$ -coordinate . . . . .	30
2.4.4	Curvilinear $\tilde{z}$ -coordinate . . . . .	32
<b>2.5</b>	<b>Subgrid Scale Physics</b> . . . . .	<b>33</b>
2.5.1	Vertical Subgrid Scale Physics . . . . .	33
2.5.2	Formulation of the Lateral Diffusive and Viscous Operators . . . . .	34

---

## 2.1 Primitive Equations

### 2.1.1 Vector Invariant Formulation

The ocean is a fluid that can be described to a good approximation by the primitive equations, *i.e.* the Navier-Stokes equations along with a nonlinear equation of state which couples the two active tracers (temperature and salinity) to the fluid velocity, plus the following additional assumptions made from scale considerations:

(1) *spherical earth approximation*: the geopotential surfaces are assumed to be spheres so that gravity (local vertical) is parallel to the earth's radius

(2) *thin-shell approximation*: the ocean depth is neglected compared to the earth's radius

(3) *turbulent closure hypothesis*: the turbulent fluxes (which represent the effect of small scale processes on the large-scale) are expressed in terms of large-scale features

(4) *Boussinesq hypothesis*: density variations are neglected except in their contribution to the buoyancy force

(5) *Hydrostatic hypothesis*: the vertical momentum equation is reduced to a balance between the vertical pressure gradient and the buoyancy force (this removes convective processes from the initial Navier-Stokes equations and so convective processes must be parameterized instead)

(6) *Incompressibility hypothesis*: the three dimensional divergence of the velocity vector is assumed to be zero.

Because the gravitational force is so dominant in the equations of large-scale motions, it is useful to choose an orthogonal set of unit vectors ( $\mathbf{i}, \mathbf{j}, \mathbf{k}$ ) linked to the earth such that  $\mathbf{k}$  is the local upward vector and ( $\mathbf{i}, \mathbf{j}$ ) are two vectors orthogonal to  $\mathbf{k}$ , *i.e.* tangent to the geopotential surfaces. Let us define the following variables:  $\mathbf{U}$  the vector velocity,  $\mathbf{U} = \mathbf{U}_h + w \mathbf{k}$  (the subscript  $h$  denotes the local horizontal vector, *i.e.* over the ( $\mathbf{i}, \mathbf{j}$ ) plane),  $T$  the potential temperature,  $S$  the salinity,  $\rho$  the *in situ* density. The vector invariant form of the primitive equations in the ( $\mathbf{i}, \mathbf{j}, \mathbf{k}$ ) vector system provides the following six equations (namely the momentum balance, the hydrostatic equilibrium, the incompressibility equation, the heat and salt conservation equations and an equation of state):

$$\frac{\partial \mathbf{U}_h}{\partial t} = - \left[ (\nabla \times \mathbf{U}) \times \mathbf{U} + \frac{1}{2} \nabla (\mathbf{U}^2) \right]_h - f \mathbf{k} \times \mathbf{U}_h - \frac{1}{\rho_o} \nabla_h p + \mathbf{D}^{\mathbf{U}} + \mathbf{F}^{\mathbf{U}} \quad (2.1a)$$

$$\frac{\partial p}{\partial z} = -\rho g \quad (2.1b)$$

$$\nabla \cdot \mathbf{U} = 0 \quad (2.1c)$$



$$\frac{\partial T}{\partial t} = -\nabla \cdot (T \mathbf{U}) + D^T + F^T \quad (2.1d)$$

$$\frac{\partial S}{\partial t} = -\nabla \cdot (S \mathbf{U}) + D^S + F^S \quad (2.1e)$$

$$\rho = \rho(T, S, p) \quad (2.1f)$$

where  $\nabla$  is the generalised derivative vector operator in  $(\mathbf{i}, \mathbf{j}, \mathbf{k})$  directions,  $t$  is the time,  $z$  is the vertical coordinate,  $\rho$  is the *in situ* density given by the equation of state (2.1f),  $\rho_o$  is a reference density,  $p$  the pressure,  $f = 2\Omega \cdot \mathbf{k}$  is the Coriolis acceleration (where  $\Omega$  is the Earth's angular velocity vector), and  $g$  is the gravitational acceleration.  $\mathbf{D}^U$ ,  $D^T$  and  $D^S$  are the parameterisations of small-scale physics for momentum, temperature and salinity, and  $\mathbf{F}^U$ ,  $F^T$  and  $F^S$  surface forcing terms. Their nature and formulation are discussed in §2.5 and page §2.1.2.

### 2.1.2 Boundary Conditions

An ocean is bounded by complex coastlines, bottom topography at its base and an air-sea or ice-sea interface at its top. These boundaries can be defined by two surfaces,  $z = -H(i, j)$  and  $z = \eta(i, j, k, t)$ , where  $H$  is the depth of the ocean bottom and  $\eta$  is the height of the sea surface. Both  $H$  and  $\eta$  are usually referenced to a given surface,  $z = 0$ , chosen as a mean sea surface (Fig. 2.1). Through these two boundaries, the ocean can exchange fluxes of heat, fresh water, salt, and momentum with the solid earth, the continental margins, the sea ice and the atmosphere. However, some of these fluxes are so weak that even on climatic time scales of thousands of years they can be neglected. In the following, we briefly review the fluxes exchanged at the interfaces between the ocean and the other components of the earth system.

**Land - ocean interface:** the major flux between continental margins and the ocean is a mass exchange of fresh water through river runoff. Such an exchange modifies the sea surface salinity especially in the vicinity of major river mouths. It can be neglected for short range integrations but has to be taken into account for long term integrations as it influences the characteristics of water masses formed (especially at high latitudes). It is required in order to close the water cycle of the climate system. It is usually specified as a fresh water flux at the air-sea interface in the vicinity of river mouths.

**Solid earth - ocean interface:** heat and salt fluxes through the sea floor are small, except in special areas of little extent. They are usually neglected in the model<sup>1</sup>. The boundary condition is thus set to no flux of heat and salt across

<sup>1</sup>In fact, it has been shown that the heat flux associated with the solid Earth cooling (*i.e.* the geothermal heating) is not negligible for the thermohaline circulation of the world ocean (see 5.4.3).

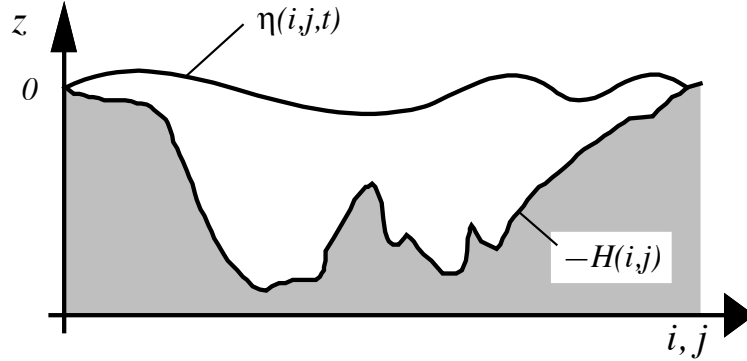


**Figure 2.1:** The ocean is bounded by two surfaces,  $z = -H(i, j)$  and  $z = \eta(i, j, t)$ , where  $H$  is the depth of the sea floor and  $\eta$  the height of the sea surface. Both  $H$  and  $\eta$  are referenced to  $z = 0$ .

solid boundaries. For momentum, the situation is different. There is no flow across solid boundaries, *i.e.* the velocity normal to the ocean bottom and coastlines is zero (in other words, the bottom velocity is parallel to solid boundaries). This kinematic boundary condition can be expressed as:

$$w = -\mathbf{U}_h \cdot \nabla_h (H) \quad (2.2)$$

In addition, the ocean exchanges momentum with the earth through frictional processes. Such momentum transfer occurs at small scales in a boundary layer. It must be parameterized in terms of turbulent fluxes using bottom and/or lateral boundary conditions. Its specification depends on the nature of the physical parameterisation used for  $\mathbf{D}^U$  in (2.1a). It is discussed in §2.5.1, page 33.

**Atmosphere - ocean interface:** the kinematic surface condition plus the mass flux of fresh water PE (the precipitation minus evaporation budget) leads to:

$$w = \frac{\partial \eta}{\partial t} + \mathbf{U}_h|_{z=\eta} \cdot \nabla_h (\eta) + P - E \quad (2.3)$$

The dynamic boundary condition, neglecting the surface tension (which removes capillary waves from the system) leads to the continuity of pressure across the interface  $z = \eta$ . The atmosphere and ocean also exchange horizontal momentum (wind stress), and heat.

**Sea ice - ocean interface:** the ocean and sea ice exchange heat, salt, fresh water and momentum. The sea surface temperature is constrained to be at the freezing point at the interface. Sea ice salinity is very low ( $\sim 4 - 6 \text{ psu}$ ) compared to those of the ocean ( $\sim 34 \text{ psu}$ ). The cycle of freezing/melting is associated with fresh water and salt fluxes that cannot be neglected.

## 2.2 The Horizontal Pressure Gradient

### 2.2.1 Pressure Formulation

The total pressure at a given depth  $z$  is composed of a surface pressure  $p_s$  at a reference geopotential surface ( $z = 0$ ) and a hydrostatic pressure  $p_h$  such that:  $p(i, j, k, t) = p_s(i, j, t) + p_h(i, j, k, t)$ . The latter is computed by integrating (2.1b), assuming that pressure in decibars can be approximated by depth in meters in (2.1f). The hydrostatic pressure is then given by:

$$p_h(i, j, z, t) = \int_{\varsigma=z}^{\varsigma=0} g \rho(T, S, \varsigma) d\varsigma \quad (2.4)$$

Two strategies can be considered for the surface pressure term: (a) introduce of a new variable  $\eta$ , the free-surface elevation, for which a prognostic equation can be established and solved; (b) assume that the ocean surface is a rigid lid, on which the pressure (or its horizontal gradient) can be diagnosed. When the former strategy is used, one solution of the free-surface elevation consists of the excitation of external gravity waves. The flow is barotropic and the surface moves up and down with gravity as the restoring force. The phase speed of such waves is high (some hundreds of metres per second) so that the time step would have to be very short if they were present in the model. The latter strategy filters out these waves since the rigid lid approximation implies  $\eta = 0$ , *i.e.* the sea surface is the surface  $z = 0$ . This well known approximation increases the surface wave speed to infinity and modifies certain other longwave dynamics (*e.g.* barotropic Rossby or planetary waves). The rigid-lid hypothesis is an obsolescent feature in modern OGCMs. It has been available until the release 3.1 of *NEMO*, and it has been removed in release 3.2 and followings. Only the free surface formulation is now described in the this document (see the next sub-section).

### 2.2.2 Free Surface Formulation

In the free surface formulation, a variable  $\eta$ , the sea-surface height, is introduced which describes the shape of the air-sea interface. This variable is solution of a prognostic equation which is established by forming the vertical average of the kinematic surface condition (2.2):

$$\frac{\partial \eta}{\partial t} = -D + P - E \quad \text{where } D = \nabla \cdot [(H + \eta) \bar{\mathbf{U}}_h] \quad (2.5)$$

and using (2.1b) the surface pressure is given by:  $p_s = \rho g \eta$ .

Allowing the air-sea interface to move introduces the external gravity waves (EGWs) as a class of solution of the primitive equations. These waves are barotropic because of hydrostatic assumption, and their phase speed is quite high. Their time scale is short with respect to the other processes described by the primitive equations.

Two choices can be made regarding the implementation of the free surface in the model, depending on the physical processes of interest.

- If one is interested in EGWs, in particular the tides and their interaction with the baroclinic structure of the ocean (internal waves) possibly in shallow seas, then a non linear free surface is the most appropriate. This means that no approximation is made in (2.5) and that the variation of the ocean volume is fully taken into account. Note that in order to study the fast time scales associated with EGWs it is necessary to minimize time filtering effects (use an explicit time scheme with very small time step, or a split-explicit scheme with reasonably small time step, see §6.5.1 or §6.5.2.

- If one is not interested in EGW but rather sees them as high frequency noise, it is possible to apply an explicit filter to slow down the fastest waves while not altering the slow barotropic Rossby waves. If further, an approximative conservation of heat and salt contents is sufficient for the problem solved, then it is sufficient to solve a linearized version of (2.5), which still allows to take into account freshwater fluxes applied at the ocean surface [Roullet and Madec 2000]. Nevertheless, with the linearization, an exact conservation of heat and salt contents is lost.

The filtering of EGWs in models with a free surface is usually a matter of discretisation of the temporal derivatives, using a split-explicit method [Killworth et al. 1991, Zhang and Endoh 1992] or the implicit scheme [Dukowicz and Smith 1994] or the addition of a filtering force in the momentum equation [Roullet and Madec 2000]. With the present release, *NEMO* offers the choice between an explicit free surface (see §6.5.1) or a split-explicit scheme strongly inspired the one proposed by Shchepetkin and McWilliams [2005] (see §6.5.2).

## 2.3 Curvilinear $z$ -coordinate System

### 2.3.1 Tensorial Formalism

In many ocean circulation problems, the flow field has regions of enhanced dynamics (*i.e.* surface layers, western boundary currents, equatorial currents, or ocean fronts). The representation of such dynamical processes can be improved by specifically increasing the model resolution in these regions. As well, it may be convenient to use a lateral boundary-following coordinate system to better represent coastal dynamics. Moreover, the common geographical coordinate system has a singular point at the North Pole that cannot be easily treated in a global model without filtering. A solution consists of introducing an appropriate coordinate transformation that shifts the singular point onto land [Madec and Imbard 1996, Murray 1996]. As a consequence, it is important to solve the primitive equations in various curvilinear coordinate systems. An efficient way of introducing an appropriate coordinate transform can be found when using a tensorial formalism. This formalism is suited to any multidimensional curvilinear coordinate system. Ocean modellers mainly use three-dimensional orthogonal grids on the sphere (spherical earth approximation), with preservation of the local vertical. Here we give the simplified

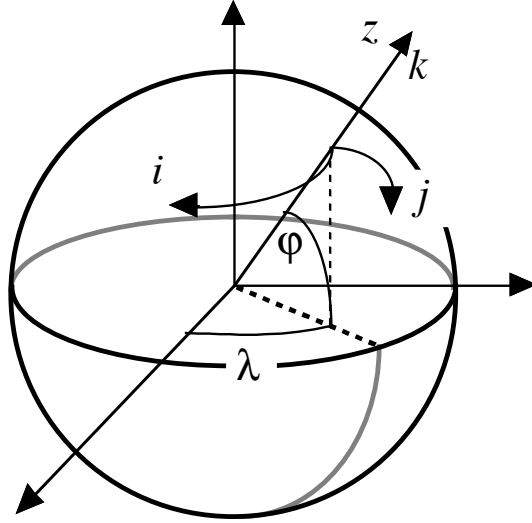


**Figure 2.2:** the geographical coordinate system  $(\lambda, \varphi, z)$  and the curvilinear coordinate system  $(\mathbf{i}, \mathbf{j}, \mathbf{k})$ .

equations for this particular case. The general case is detailed by [Eiseman and Stone \[1980\]](#) in their survey of the conservation laws of fluid dynamics.

Let  $(i, j, k)$  be a set of orthogonal curvilinear coordinates on the sphere associated with the positively oriented orthogonal set of unit vectors  $(\mathbf{i}, \mathbf{j}, \mathbf{k})$  linked to the earth such that  $\mathbf{k}$  is the local upward vector and  $(\mathbf{i}, \mathbf{j})$  are two vectors orthogonal to  $\mathbf{k}$ , *i.e.* along geopotential surfaces (Fig.2.2). Let  $(\lambda, \varphi, z)$  be the geographical coordinate system in which a position is defined by the latitude  $\varphi(i, j)$ , the longitude  $\lambda(i, j)$  and the distance from the centre of the earth  $a + z(k)$  where  $a$  is the earth's radius and  $z$  the altitude above a reference sea level (Fig.2.2). The local deformation of the curvilinear coordinate system is given by  $e_1, e_2$  and  $e_3$ , the three scale factors:

$$\begin{aligned}
 e_1 &= (a + z) \left[ \left( \frac{\partial \lambda}{\partial i} \cos \varphi \right)^2 + \left( \frac{\partial \varphi}{\partial i} \right)^2 \right]^{1/2} \\
 e_2 &= (a + z) \left[ \left( \frac{\partial \lambda}{\partial j} \cos \varphi \right)^2 + \left( \frac{\partial \varphi}{\partial j} \right)^2 \right]^{1/2} \\
 e_3 &= \left( \frac{\partial z}{\partial k} \right)
 \end{aligned} \tag{2.6}$$

Since the ocean depth is far smaller than the earth's radius,  $a + z$ , can be replaced by  $a$  in (2.6) (thin-shell approximation). The resulting horizontal scale factors  $e_1, e_2$  are independent of  $k$  while the vertical scale factor is a single function of  $k$  as  $\mathbf{k}$  is parallel to  $\mathbf{z}$ . The scalar and vector operators that appear in the primitive

equations (Eqs. (2.1a) to (2.1f)) can be written in the tensorial form, invariant in any orthogonal horizontal curvilinear coordinate system transformation:

$$\nabla q = \frac{1}{e_1} \frac{\partial q}{\partial i} \mathbf{i} + \frac{1}{e_2} \frac{\partial q}{\partial j} \mathbf{j} + \frac{1}{e_3} \frac{\partial q}{\partial k} \mathbf{k} \quad (2.7a)$$

$$\nabla \cdot \mathbf{A} = \frac{1}{e_1 e_2} \left[ \frac{\partial (e_2 a_1)}{\partial i} + \frac{\partial (e_1 a_2)}{\partial j} \right] + \frac{1}{e_3} \left[ \frac{\partial a_3}{\partial k} \right] \quad (2.7b)$$

$$\begin{aligned} \nabla \times \mathbf{A} = & \left[ \frac{1}{e_2} \frac{\partial a_3}{\partial j} - \frac{1}{e_3} \frac{\partial a_2}{\partial k} \right] \mathbf{i} + \left[ \frac{1}{e_3} \frac{\partial a_1}{\partial k} - \frac{1}{e_1} \frac{\partial a_3}{\partial i} \right] \mathbf{j} \\ & + \frac{1}{e_1 e_2} \left[ \frac{\partial (e_2 a_2)}{\partial i} - \frac{\partial (e_1 a_1)}{\partial j} \right] \mathbf{k} \end{aligned} \quad (2.7c)$$

$$\Delta q = \nabla \cdot (\nabla q) \quad (2.7d)$$

$$\Delta \mathbf{A} = \nabla (\nabla \cdot \mathbf{A}) - \nabla \times (\nabla \times \mathbf{A}) \quad (2.7e)$$

where  $q$  is a scalar quantity and  $\mathbf{A} = (a_1, a_2, a_3)$  a vector in the  $(i, j, k)$  coordinate system.

### 2.3.2 Continuous Model Equations

In order to express the Primitive Equations in tensorial formalism, it is necessary to compute the horizontal component of the non-linear and viscous terms of the equation using (2.7a) to (2.7e). Let us set  $\mathbf{U} = (u, v, w) = \mathbf{U}_h + w \mathbf{k}$ , the velocity in the  $(i, j, k)$  coordinate system and define the relative vorticity  $\zeta$  and the divergence of the horizontal velocity field  $\chi$ , by:

$$\zeta = \frac{1}{e_1 e_2} \left[ \frac{\partial (e_2 v)}{\partial i} - \frac{\partial (e_1 u)}{\partial j} \right] \quad (2.8)$$

$$\chi = \frac{1}{e_1 e_2} \left[ \frac{\partial (e_2 u)}{\partial i} + \frac{\partial (e_1 v)}{\partial j} \right] \quad (2.9)$$

Using the fact that the horizontal scale factors  $e_1$  and  $e_2$  are independent of  $k$  and that  $e_3$  is a function of the single variable  $k$ , the nonlinear term of (2.1a) can be transformed as follows:

$$\begin{aligned} & \left[ (\nabla \times \mathbf{U}) \times \mathbf{U} + \frac{1}{2} \nabla (\mathbf{U}^2) \right]_h \\ & = \left( \begin{array}{c} \left[ \frac{1}{e_3} \frac{\partial u}{\partial k} - \frac{1}{e_1} \frac{\partial w}{\partial i} \right] w - \zeta v \\ \zeta u - \left[ \frac{1}{e_2} \frac{\partial w}{\partial j} - \frac{1}{e_3} \frac{\partial v}{\partial k} \right] w \end{array} \right) + \frac{1}{2} \left( \begin{array}{c} \frac{1}{e_1} \frac{\partial (u^2 + v^2 + w^2)}{\partial i} \\ \frac{1}{e_2} \frac{\partial (u^2 + v^2 + w^2)}{\partial j} \end{array} \right) \end{aligned}$$

$$= \begin{pmatrix} -\zeta v \\ \zeta u \end{pmatrix} + \frac{1}{2} \begin{pmatrix} \frac{1}{e_1} \frac{\partial(u^2+v^2)}{\partial i} \\ \frac{1}{e_2} \frac{\partial(u^2+v^2)}{\partial j} \end{pmatrix} + \frac{1}{e_3} \begin{pmatrix} w \frac{\partial u}{\partial k} \\ w \frac{\partial v}{\partial k} \end{pmatrix} - \begin{pmatrix} \frac{w}{e_1} \frac{\partial w}{\partial i} - \frac{1}{2e_1} \frac{\partial w^2}{\partial i} \\ \frac{w}{e_2} \frac{\partial w}{\partial j} - \frac{1}{2e_2} \frac{\partial w^2}{\partial j} \end{pmatrix}$$

The last term of the right hand side is obviously zero, and thus the nonlinear term of (2.1a) is written in the  $(i, j, k)$  coordinate system:

$$\left[ (\nabla \times \mathbf{U}) \times \mathbf{U} + \frac{1}{2} \nabla (\mathbf{U}^2) \right]_h = \zeta \mathbf{k} \times \mathbf{U}_h + \frac{1}{2} \nabla_h (\mathbf{U}_h^2) + \frac{1}{e_3} w \frac{\partial \mathbf{U}_h}{\partial k} \quad (2.10)$$

This is the so-called *vector invariant form* of the momentum advection term. For some purposes, it can be advantageous to write this term in the so-called flux form, *i.e.* to write it as the divergence of fluxes. For example, the first component of (2.10) (the  $i$ -component) is transformed as follows:

$$\begin{aligned} [(\nabla \times \mathbf{U}) \times \mathbf{U} + \frac{1}{2} \nabla (\mathbf{U}^2)]_i &= -\zeta v + \frac{1}{2e_1} \frac{\partial(u^2+v^2)}{\partial i} + \frac{1}{e_3} w \frac{\partial u}{\partial k} \\ &= \frac{1}{e_1 e_2} \left( -v \frac{\partial(e_2 v)}{\partial i} + v \frac{\partial(e_1 u)}{\partial j} \right) + \frac{1}{e_1 e_2} \left( +e_2 u \frac{\partial u}{\partial i} + e_2 v \frac{\partial v}{\partial i} \right) + \frac{1}{e_3} \left( w \frac{\partial u}{\partial k} \right) \\ &= \frac{1}{e_1 e_2} \left\{ - \left( v^2 \frac{\partial e_2}{\partial i} + e_2 v \frac{\partial v}{\partial i} \right) + \left( \frac{\partial(e_1 u v)}{\partial j} - e_1 u \frac{\partial v}{\partial j} \right) \right. \\ &\quad \left. + \left( \frac{\partial(e_2 u u)}{\partial i} - u \frac{\partial(e_2 u)}{\partial i} \right) + e_2 v \frac{\partial v}{\partial i} \right\} + \frac{1}{e_3} \left( \frac{\partial(w u)}{\partial k} - u \frac{\partial w}{\partial k} \right) \\ &= \frac{1}{e_1 e_2} \left( \frac{\partial(e_2 u u)}{\partial i} + \frac{\partial(e_1 u v)}{\partial j} \right) + \frac{1}{e_3} \frac{\partial(w u)}{\partial k} \\ &\quad + \frac{1}{e_1 e_2} \left( -u \left( \frac{\partial(e_1 v)}{\partial j} - v \frac{\partial e_1}{\partial j} \right) - u \frac{\partial(e_2 u)}{\partial i} \right) - \frac{1}{e_3} \frac{\partial w}{\partial k} u + \frac{1}{e_1 e_2} \left( -v^2 \frac{\partial e_2}{\partial i} \right) \\ &= \nabla \cdot (\mathbf{U} u) - (\nabla \cdot \mathbf{U}) u + \frac{1}{e_1 e_2} \left( -v^2 \frac{\partial e_2}{\partial i} + u v \frac{\partial e_1}{\partial j} \right) \end{aligned}$$

as  $\nabla \cdot \mathbf{U} = 0$  (incompressibility) it comes:

$$= \nabla \cdot (\mathbf{U} u) + \frac{1}{e_1 e_2} \left( v \frac{\partial e_2}{\partial i} - u \frac{\partial e_1}{\partial j} \right) (-v)$$

The flux form of the momentum advection term is therefore given by:

$$\begin{aligned} \left[ (\nabla \times \mathbf{U}) \times \mathbf{U} + \frac{1}{2} \nabla (\mathbf{U}^2) \right]_h \\ = \nabla \cdot \begin{pmatrix} \mathbf{U} u \\ \mathbf{U} v \end{pmatrix} + \frac{1}{e_1 e_2} \left( v \frac{\partial e_2}{\partial i} - u \frac{\partial e_1}{\partial j} \right) \mathbf{k} \times \mathbf{U}_h \quad (2.11) \end{aligned}$$

The flux form has two terms, the first one is expressed as the divergence of momentum fluxes (hence the flux form name given to this formulation) and the second one is due to the curvilinear nature of the coordinate system used. The

latter is called the *metric* term and can be viewed as a modification of the Coriolis parameter:

$$f \rightarrow f + \frac{1}{e_1 e_2} \left( v \frac{\partial e_2}{\partial i} - u \frac{\partial e_1}{\partial j} \right) \quad (2.12)$$

Note that in the case of geographical coordinate, *i.e.* when  $(i, j) \rightarrow (\lambda, \varphi)$  and  $(e_1, e_2) \rightarrow (a \cos \varphi, a)$ , we recover the commonly used modification of the Coriolis parameter  $f \rightarrow f + (u/a) \tan \varphi$ .

To sum up, the curvilinear  $z$ -coordinate equations solved by the ocean model can be written in the following tensorial formalism:

• **Vector invariant form of the momentum equations :**

$$\begin{aligned} \frac{\partial u}{\partial t} = & + (\zeta + f) v - \frac{1}{2 e_1} \frac{\partial}{\partial i} (u^2 + v^2) - \frac{1}{e_3} w \frac{\partial u}{\partial k} \\ & - \frac{1}{e_1} \frac{\partial}{\partial i} \left( \frac{p_s + p_h}{\rho_o} \right) + D_u^{\mathbf{U}} + F_u^{\mathbf{U}} \end{aligned} \quad (2.13a)$$

$$\begin{aligned} \frac{\partial v}{\partial t} = & - (\zeta + f) u - \frac{1}{2 e_2} \frac{\partial}{\partial j} (u^2 + v^2) - \frac{1}{e_3} w \frac{\partial v}{\partial k} \\ & - \frac{1}{e_2} \frac{\partial}{\partial j} \left( \frac{p_s + p_h}{\rho_o} \right) + D_v^{\mathbf{U}} + F_v^{\mathbf{U}} \end{aligned}$$

• **flux form of the momentum equations :**

$$\begin{aligned} \frac{\partial u}{\partial t} = & + \left( f + \frac{1}{e_1 e_2} \left( v \frac{\partial e_2}{\partial i} - u \frac{\partial e_1}{\partial j} \right) \right) v \\ & - \frac{1}{e_1 e_2} \left( \frac{\partial (e_2 u u)}{\partial i} + \frac{\partial (e_1 v u)}{\partial j} \right) - \frac{1}{e_3} \frac{\partial (w u)}{\partial k} \\ & - \frac{1}{e_1} \frac{\partial}{\partial i} \left( \frac{p_s + p_h}{\rho_o} \right) + D_u^{\mathbf{U}} + F_u^{\mathbf{U}} \end{aligned} \quad (2.14a)$$

$$\begin{aligned} \frac{\partial v}{\partial t} = & - \left( f + \frac{1}{e_1 e_2} \left( v \frac{\partial e_2}{\partial i} - u \frac{\partial e_1}{\partial j} \right) \right) u \\ & + \frac{1}{e_1 e_2} \left( \frac{\partial (e_2 u v)}{\partial i} + \frac{\partial (e_1 v v)}{\partial j} \right) - \frac{1}{e_3} \frac{\partial (w v)}{\partial k} \\ & - \frac{1}{e_2} \frac{\partial}{\partial j} \left( \frac{p_s + p_h}{\rho_o} \right) + D_v^{\mathbf{U}} + F_v^{\mathbf{U}} \end{aligned} \quad (2.14b)$$



where  $\zeta$ , the relative vorticity, is given by (2.8) and  $p_s$ , the surface pressure, is given by:

$$p_s = \rho g \eta \quad (2.15)$$

with  $\eta$  is solution of (2.5)

The vertical velocity and the hydrostatic pressure are diagnosed from the following equations:

$$\frac{\partial w}{\partial k} = -\chi e_3 \quad (2.16)$$

$$\frac{\partial p_h}{\partial k} = -\rho g e_3 \quad (2.17)$$

where the divergence of the horizontal velocity,  $\chi$  is given by (2.9).

• *tracer equations* :

$$\frac{\partial T}{\partial t} = -\frac{1}{e_1 e_2} \left[ \frac{\partial (e_2 T u)}{\partial i} + \frac{\partial (e_1 T v)}{\partial j} \right] - \frac{1}{e_3} \frac{\partial (T w)}{\partial k} + D^T + F^T \quad (2.18)$$

$$\frac{\partial S}{\partial t} = -\frac{1}{e_1 e_2} \left[ \frac{\partial (e_2 S u)}{\partial i} + \frac{\partial (e_1 S v)}{\partial j} \right] - \frac{1}{e_3} \frac{\partial (S w)}{\partial k} + D^S + F^S \quad (2.19)$$

$$\rho = \rho(T, S, z(k)) \quad (2.20)$$

The expression of  $\mathbf{D}^U$ ,  $D^S$  and  $D^T$  depends on the subgrid scale parameterisation used. It will be defined in §2.5.1. The nature and formulation of  $\mathbf{F}^U$ ,  $F^T$  and  $F^S$ , the surface forcing terms, are discussed in Chapter 7.

## 2.4 Curvilinear generalised vertical coordinate System

The ocean domain presents a huge diversity of situation in the vertical. First the ocean surface is a time dependent surface (moving surface). Second the ocean floor depends on the geographical position, varying from more than 6,000 meters in abyssal trenches to zero at the coast. Last but not least, the ocean stratification exerts a strong barrier to vertical motions and mixing. Therefore, in order to represent the ocean with respect to the first point a space and time dependent vertical coordinate that follows the variation of the sea surface height *e.g.* an  $z^*$ -coordinate; for the second point, a space variation to fit the change of bottom topography *e.g.* a terrain-following or  $\sigma$ -coordinate; and for the third point, one will be tempted to use a space and time dependent coordinate that follows the isopycnal surfaces, *e.g.* an isopycnic coordinate.

In order to satisfy two or more constrains one can even be tempted to mixed these coordinate systems, as in HYCOM (mixture of  $z$ -coordinate at the surface, isopycnic coordinate in the ocean interior and  $\sigma$  at the ocean bottom) [Chassignet et al. 2003] or OPA (mixture of  $z$ -coordinate in vicinity the surface and steep topography areas and  $\sigma$ -coordinate elsewhere) [Madec et al. 1996] among others.

In fact one is totally free to choose any space and time vertical coordinate by introducing an arbitrary vertical coordinate :

$$s = s(i, j, k, t) \quad (2.21)$$

with the restriction that the above equation gives a single-valued monotonic relationship between  $s$  and  $k$ , when  $i$ ,  $j$  and  $t$  are held fixed. (2.21) is a transformation from the  $(i, j, k, t)$  coordinate system with independent variables into the  $(i, j, s, t)$  generalised coordinate system with  $s$  depending on the other three variables through (2.21). This so-called *generalised vertical coordinate* [Kasahara 1974] is in fact an Arbitrary Lagrangian–Eulerian (ALE) coordinate. Indeed, choosing an expression for  $s$  is an arbitrary choice that determines which part of the vertical velocity (defined from a fixed referential) will cross the levels (Eulerian part) and which part will be used to move them (Lagrangian part). The coordinate is also sometime referenced as an adaptive coordinate [Hofmeister et al. 2009], since the coordinate system is adapted in the course of the simulation. Its most often used implementation is via an ALE algorithm, in which a pure lagrangian step is followed by regridding and remapping steps, the later step implicitly embedding the vertical advection [Hirt et al. 1974, Chassignet et al. 2003, White et al. 2009]. Here we follow the [Kasahara 1974] strategy : a regridding step (an update of the vertical coordinate) followed by an eulerian step with an explicit computation of vertical advection relative to the moving  $s$ -surfaces.

the generalized vertical coordinates used in ocean modelling are not orthogonal, which contrasts with many other applications in mathematical physics. Hence, it is useful to keep in mind the following properties that may seem odd on initial encounter.

The horizontal velocity in ocean models measures motions in the horizontal plane, perpendicular to the local gravitational field. That is, horizontal velocity is mathematically the same regardless the vertical coordinate, be it geopotential, isopycnal, pressure, or terrain following. The key motivation for maintaining the same horizontal velocity component is that the hydrostatic and geostrophic balances are dominant in the large-scale ocean. Use of an alternative quasi-horizontal velocity, for example one oriented parallel to the generalized surface, would lead to unacceptable numerical errors. Correspondingly, the vertical direction is anti-parallel to the gravitational force in all of the coordinate systems. We do not choose the alternative of a quasi-vertical direction oriented normal to the surface of a constant generalized vertical coordinate.

It is the method used to measure transport across the generalized vertical coordinate surfaces which differs between the vertical coordinate choices. That is, computation of the dia-surface velocity component represents the fundamental distinction between the various coordinates. In some models, such as geopotential, pressure, and terrain following, this transport is typically diagnosed from volume or mass conservation. In other models, such as isopycnal layered models, this transport is prescribed based on assumptions about the physical processes producing a flux across the layer interfaces.

In this section we first establish the PE in the generalised vertical  $s$ -coordinate, then we discuss the particular cases available in *NEMO*, namely  $z$ ,  $z^*$ ,  $s$ , and  $\tilde{z}$ .

### 2.4.1 The $s$ -coordinate Formulation

Starting from the set of equations established in §2.3 for the special case  $k = z$  and thus  $e_3 = 1$ , we introduce an arbitrary vertical coordinate  $s = s(i, j, k, t)$ , which includes  $z$ -,  $z^*$ - and  $\sigma$ -coordinates as special cases ( $s = z$ ,  $s = z^*$ , and  $s = \sigma = z/H$  or  $= z/(H + \eta)$ , resp.). A formal derivation of the transformed equations is given in Appendix A. Let us define the vertical scale factor by  $e_3 = \partial_s z$  ( $e_3$  is now a function of  $(i, j, k, t)$ ), and the slopes in the  $(\mathbf{i}, \mathbf{j})$  directions between  $s$ - and  $z$ -surfaces by :

$$\sigma_1 = \frac{1}{e_1} \left. \frac{\partial z}{\partial i} \right|_s, \quad \text{and} \quad \sigma_2 = \frac{1}{e_2} \left. \frac{\partial z}{\partial j} \right|_s \quad (2.22)$$

We also introduce  $\omega$ , a dia-surface velocity component, defined as the velocity relative to the moving  $s$ -surfaces and normal to them:

$$\omega = w - e_3 \frac{\partial s}{\partial t} - \sigma_1 u - \sigma_2 v \quad (2.23)$$

The equations solved by the ocean model (2.1) in  $s$ -coordinate can be written as follows (see Appendix A.3):

- Vector invariant form of the momentum equation :

$$\begin{aligned} \frac{\partial u}{\partial t} = & + (\zeta + f) v - \frac{1}{2e_1} \frac{\partial}{\partial i} (u^2 + v^2) - \frac{1}{e_3} \omega \frac{\partial u}{\partial k} \\ & - \frac{1}{e_1} \frac{\partial}{\partial i} \left( \frac{p_s + p_h}{\rho_o} \right) + g \frac{\rho}{\rho_o} \sigma_1 + D_u^{\mathbf{U}} + F_u^{\mathbf{U}} \end{aligned} \quad (2.24)$$

$$\begin{aligned} \frac{\partial v}{\partial t} = & - (\zeta + f) u - \frac{1}{2e_2} \frac{\partial}{\partial j} (u^2 + v^2) - \frac{1}{e_3} \omega \frac{\partial v}{\partial k} \\ & - \frac{1}{e_2} \frac{\partial}{\partial j} \left( \frac{p_s + p_h}{\rho_o} \right) + g \frac{\rho}{\rho_o} \sigma_2 + D_v^{\mathbf{U}} + F_v^{\mathbf{U}} \end{aligned} \quad (2.25)$$

- Vector invariant form of the momentum equation :

$$\begin{aligned} \frac{1}{e_3} \frac{\partial (e_3 u)}{\partial t} = & + \left( f + \frac{1}{e_1 e_2} \left( v \frac{\partial e_2}{\partial i} - u \frac{\partial e_1}{\partial j} \right) \right) v \\ & - \frac{1}{e_1 e_2 e_3} \left( \frac{\partial (e_2 e_3 u u)}{\partial i} + \frac{\partial (e_1 e_3 v u)}{\partial j} \right) - \frac{1}{e_3} \frac{\partial (\omega u)}{\partial k} \\ & - \frac{1}{e_1} \frac{\partial}{\partial i} \left( \frac{p_s + p_h}{\rho_o} \right) + g \frac{\rho}{\rho_o} \sigma_1 + D_u^{\mathbf{U}} + F_u^{\mathbf{U}} \end{aligned} \quad (2.26)$$

$$\begin{aligned} \frac{1}{e_3} \frac{\partial (e_3 v)}{\partial t} = & - \left( f + \frac{1}{e_1 e_2} \left( v \frac{\partial e_2}{\partial i} - u \frac{\partial e_1}{\partial j} \right) \right) u \\ & - \frac{1}{e_1 e_2 e_3} \left( \frac{\partial (e_2 e_3 u v)}{\partial i} + \frac{\partial (e_1 e_3 v v)}{\partial j} \right) - \frac{1}{e_3} \frac{\partial (\omega v)}{\partial k} \\ & - \frac{1}{e_2} \frac{\partial}{\partial j} \left( \frac{p_s + p_h}{\rho_o} \right) + g \frac{\rho}{\rho_o} \sigma_2 + D_v^{\mathbf{U}} + F_v^{\mathbf{U}} \end{aligned} \quad (2.27)$$

where the relative vorticity,  $\zeta$ , the surface pressure gradient, and the hydrostatic pressure have the same expressions as in  $z$ -coordinates although they do not represent exactly the same quantities.  $\omega$  is provided by the continuity equation (see Appendix A):

$$\frac{\partial e_3}{\partial t} + e_3 \chi + \frac{\partial \omega}{\partial s} = 0 \quad \text{with} \quad \chi = \frac{1}{e_1 e_2 e_3} \left[ \frac{\partial (e_2 e_3 u)}{\partial i} + \frac{\partial (e_1 e_3 v)}{\partial j} \right] \quad (2.28)$$

- tracer equations:

$$\begin{aligned} \frac{1}{e_3} \frac{\partial (e_3 T)}{\partial t} = & - \frac{1}{e_1 e_2 e_3} \left[ \frac{\partial (e_2 e_3 u T)}{\partial i} + \frac{\partial (e_1 e_3 v T)}{\partial j} \right] \\ & - \frac{1}{e_3} \frac{\partial (T \omega)}{\partial k} + D^T + F^S \end{aligned} \quad (2.29)$$

$$\frac{1}{e_3} \frac{\partial (e_3 S)}{\partial t} = -\frac{1}{e_1 e_2 e_3} \left[ \frac{\partial (e_2 e_3 u S)}{\partial i} + \frac{\partial (e_1 e_3 v S)}{\partial j} \right] - \frac{1}{e_3} \frac{\partial (S \omega)}{\partial k} + D^S + F^S \quad (2.30)$$

The equation of state has the same expression as in  $z$ -coordinate, and similar expressions are used for mixing and forcing terms.

### 2.4.2 Curvilinear $z^*$ -coordinate System

In that case, the free surface equation is nonlinear, and the variations of volume are fully taken into account. These coordinates systems is presented in a report [Levier et al. 2007] available on the *NEMO* web site.

The  $z^*$  coordinate approach is an unapproximated, non-linear free surface implementation which allows one to deal with large amplitude free-surface variations relative to the vertical resolution [Adcroft and Campin 2004]. In the  $z^*$  formulation, the variation of the column thickness due to sea-surface undulations is not concentrated in the surface level, as in the  $z$ -coordinate formulation, but is equally

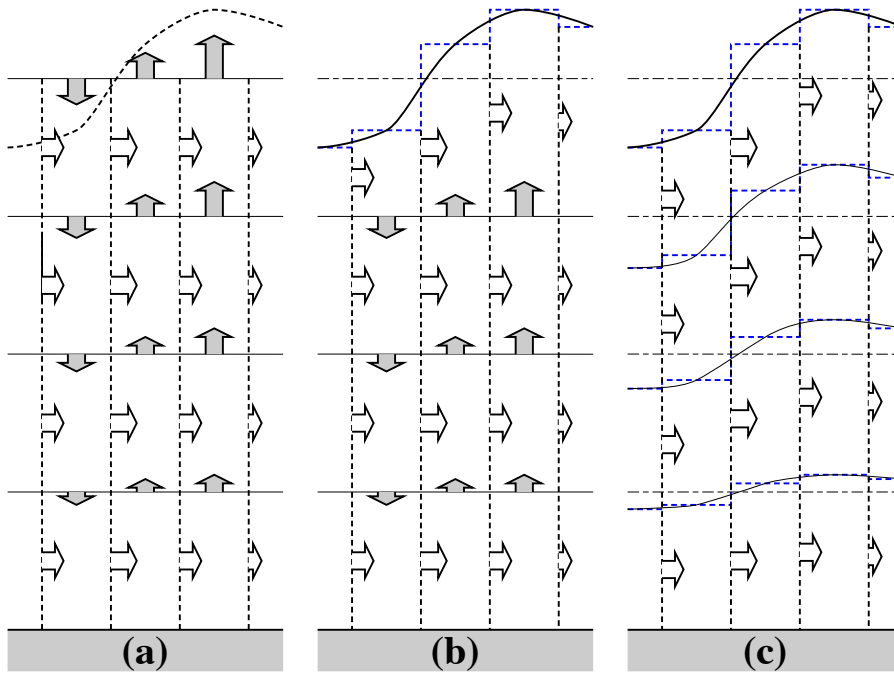


**Figure 2.3:** (a)  $z$ -coordinate in linear free-surface case ; (b)  $z$ -coordinate in non-linear free surface case ; (c) re-scaled height coordinate (become popular as the  $z^*$ -coordinate [Adcroft and Campin 2004] ).

distributed over the full water column. Thus vertical levels naturally follow sea-surface variations, with a linear attenuation with depth, as illustrated by figure fig.1c . Note that with a flat bottom, such as in fig.1c, the bottom-following  $z$  coordinate and  $z^*$  are equivalent. The definition and modified oceanic equations for the rescaled vertical coordinate  $z^*$ , including the treatment of fresh-water flux at the surface, are detailed in Adcroft and Campin (2004). The major points are summarized here. The position ( $z^*$ ) and vertical discretization ( $\delta z^*$ ) are expressed as:

$$H + z^* = (H + z)/r \quad \text{and} \quad \delta z^* = \delta z/r \quad \text{with} \quad r = \frac{H + \eta}{H} \quad (2.31)$$

Since the vertical displacement of the free surface is incorporated in the vertical coordinate  $z^*$ , the upper and lower boundaries are at fixed  $z^*$  position,  $z^* = 0$  and  $z^* = -H$  respectively. Also the divergence of the flow field is no longer zero as shown by the continuity equation:

$$\frac{\partial r}{\partial t} = \nabla_{z^*} \cdot (r \mathbf{U}_h) (r w^*) = 0$$

To overcome problems with vanishing surface and/or bottom cells, we consider the  $z^*$  coordinate

$$z^* = H \left( \frac{z - \eta}{H + \eta} \right) \quad (2.32)$$

This coordinate is closely related to the "eta" coordinate used in many atmospheric models (see Black (1994) for a review of eta coordinate atmospheric models). It was originally used in ocean models by Stacey et al. (1995) for studies of tides next to shelves, and it has been recently promoted by Adcroft and Campin (2004) for global climate modelling.

The surfaces of constant  $z^*$  are quasi-horizontal. Indeed, the  $z^*$  coordinate reduces to  $z$  when  $\eta$  is zero. In general, when noting the large differences between undulations of the bottom topography versus undulations in the surface height, it is clear that surfaces constant  $z^*$  are very similar to the depth surfaces. These properties greatly reduce difficulties of computing the horizontal pressure gradient relative to terrain following sigma models discussed in §2.4.3. Additionally, since  $z^*$  when  $\eta = 0$ , no flow is spontaneously generated in an unforced ocean starting from rest, regardless the bottom topography. This behaviour is in contrast to the case with "s"-models, where pressure gradient errors in the presence of nontrivial topographic variations can generate nontrivial spontaneous flow from a resting state, depending on the sophistication of the pressure gradient solver. The quasi-horizontal nature of the coordinate surfaces also facilitates the implementation of neutral physics parameterizations in  $z^*$  models using the same techniques as in  $z$ -models (see Chapters 13-16 of Griffies [2004]) for a discussion of neutral physics in  $z$ -models, as well as Section §9.1 in this document for treatment in *NEMO*).

The range over which  $z^*$  varies is time independent  $-H \leq z^* \leq 0$ . Hence, all cells remain nonvanishing, so long as the surface height maintains  $\eta > -H$ . This

is a minor constraint relative to that encountered on the surface height when using  $s = z$  or  $s = z - \eta$ .

Because  $z^*$  has a time independent range, all grid cells have static increments  $ds$ , and the sum of the vertical increments yields the time independent ocean depth. The  $z^*$  coordinate is therefore invisible to undulations of the free surface, since it moves along with the free surface. This property means that no spurious vertical transport is induced across surfaces of constant  $z^*$  by the motion of external gravity waves. Such spurious transport can be a problem in  $z$ -models, especially those with tidal forcing. Quite generally, the time independent range for the  $z^*$  coordinate is a very convenient property that allows for a nearly arbitrary vertical resolution even in the presence of large amplitude fluctuations of the surface height, again so long as  $\eta > -H$ .

### 2.4.3 Curvilinear Terrain-following $s$ -coordinate

#### Introduction

Several important aspects of the ocean circulation are influenced by bottom topography. Of course, the most important is that bottom topography determines deep ocean sub-basins, barriers, sills and channels that strongly constrain the path of water masses, but more subtle effects exist. For example, the topographic  $\beta$ -effect is usually larger than the planetary one along continental slopes. Topographic Rossby waves can be excited and can interact with the mean current. In the  $z$ -coordinate system presented in the previous section (§2.3),  $z$ -surfaces are geopotential surfaces. The bottom topography is discretised by steps. This often leads to a misrepresentation of a gradually sloping bottom and to large localized depth gradients associated with large localized vertical velocities. The response to such a velocity field often leads to numerical dispersion effects. One solution to strongly reduce this error is to use a partial step representation of bottom topography instead of a full step one [Pacanowski and Gnanadesikan \[1998\]](#). Another solution is to introduce a terrain-following coordinate system (hereafter  $s$ -coordinate)

The  $s$ -coordinate avoids the discretisation error in the depth field since the layers of computation are gradually adjusted with depth to the ocean bottom. Relatively small topographic features as well as gentle, large-scale slopes of the sea floor in the deep ocean, which would be ignored in typical  $z$ -model applications with the largest grid spacing at greatest depths, can easily be represented (with relatively low vertical resolution). A terrain-following model (hereafter  $s$ -model) also facilitates the modelling of the boundary layer flows over a large depth range, which in the framework of the  $z$ -model would require high vertical resolution over the whole depth range. Moreover, with a  $s$ -coordinate it is possible, at least in principle, to have the bottom and the sea surface as the only boundaries of the domain (no more lateral boundary condition to specify). Nevertheless, a  $s$ -coordinate also has its drawbacks. Perfectly adapted to a homogeneous ocean, it has strong limitations as soon as stratification is introduced. The main two problems come from the truncation error in the horizontal pressure gradient and a possibly increased diapycnal diffusion. The horizontal pressure force in  $s$ -coordinate consists of two terms (see [Appendix A](#)),

$$\nabla p|_z = \nabla p|_s - \frac{\partial p}{\partial s} \nabla z|_s \quad (2.33)$$

The second term in (2.33) depends on the tilt of the coordinate surface and introduces a truncation error that is not present in a  $z$ -model. In the special case of a  $\sigma$ -coordinate (i.e. a depth-normalised coordinate system  $\sigma = z/H$ ), [Haney \[1991\]](#) and [Beckmann and Haidvogel \[1993\]](#) have given estimates of the magnitude of this truncation error. It depends on topographic slope, stratification, horizontal and vertical resolution, the equation of state, and the finite difference scheme. This error limits the possible topographic slopes that a model can handle at a given horizontal and vertical resolution. This is a severe restriction for large-scale appli-



cations using realistic bottom topography. The large-scale slopes require high horizontal resolution, and the computational cost becomes prohibitive. This problem can be at least partially overcome by mixing  $s$ -coordinate and step-like representation of bottom topography [Gerdes 1993a;b, Madec et al. 1996]. However, the definition of the model domain vertical coordinate becomes then a non-trivial thing for a realistic bottom topography: an envelope topography is defined in  $s$ -coordinate on which a full or partial step bottom topography is then applied in order to adjust the model depth to the observed one (see §4.4).

For numerical reasons a minimum of diffusion is required along the coordinate surfaces of any finite difference model. It causes spurious diapycnal mixing when coordinate surfaces do not coincide with isoneutral surfaces. This is the case for a  $z$ -model as well as for a  $s$ -model. However, density varies more strongly on  $s$ -surfaces than on horizontal surfaces in regions of large topographic slopes, implying larger diapycnal diffusion in a  $s$ -model than in a  $z$ -model. Whereas such a diapycnal diffusion in a  $z$ -model tends to weaken horizontal density (pressure) gradients and thus the horizontal circulation, it usually reinforces these gradients in a  $s$ -model, creating spurious circulation. For example, imagine an isolated bump of topography in an ocean at rest with a horizontally uniform stratification. Spurious diffusion along  $s$ -surfaces will induce a bump of isoneutral surfaces over the topography, and thus will generate there a baroclinic eddy. In contrast, the ocean will stay at rest in a  $z$ -model. As for the truncation error, the problem can be reduced by introducing the terrain-following coordinate below the strongly stratified portion of the water column (*i.e.* the main thermocline) [Madec et al. 1996]. An alternate solution consists of rotating the lateral diffusive tensor to geopotential or to isoneutral surfaces (see §2.5.2. Unfortunately, the slope of isoneutral surfaces relative to the  $s$ -surfaces can very large, strongly exceeding the stability limit of such an operator when it is discretized (see Chapter 9).

The  $s$ -coordinates introduced here [Lott et al. 1990, Madec et al. 1996] differ mainly in two aspects from similar models: it allows a representation of bottom topography with mixed full or partial step-like/terrain following topography ; It also offers a completely general transformation,  $s = s(i, j, z)$  for the vertical coordinate.

#### 2.4.4 Curvilinear $\tilde{z}$ -coordinate

The  $\tilde{z}$ -coordinate has been developed by [Leclair and Madec \[2011\]](#). It is available in *NEMO* since the version 3.4. Nevertheless, it is currently not robust enough to be used in all possible configurations. Its use is therefore not recommended.

## 2.5 Subgrid Scale Physics

The primitive equations describe the behaviour of a geophysical fluid at space and time scales larger than a few kilometres in the horizontal, a few meters in the vertical and a few minutes. They are usually solved at larger scales: the specified grid spacing and time step of the numerical model. The effects of smaller scale motions (coming from the advective terms in the Navier-Stokes equations) must be represented entirely in terms of large-scale patterns to close the equations. These effects appear in the equations as the divergence of turbulent fluxes (*i.e.* fluxes associated with the mean correlation of small scale perturbations). Assuming a turbulent closure hypothesis is equivalent to choose a formulation for these fluxes. It is usually called the subgrid scale physics. It must be emphasized that this is the weakest part of the primitive equations, but also one of the most important for long-term simulations as small scale processes *in fine* balance the surface input of kinetic energy and heat.

The control exerted by gravity on the flow induces a strong anisotropy between the lateral and vertical motions. Therefore subgrid-scale physics  $\mathbf{D}^U$ ,  $D^S$  and  $D^T$  in (2.1a), (2.1d) and (2.1e) are divided into a lateral part  $\mathbf{D}^{lU}$ ,  $D^{lS}$  and  $D^{lT}$  and a vertical part  $\mathbf{D}^{vU}$ ,  $D^{vS}$  and  $D^{vT}$ . The formulation of these terms and their underlying physics are briefly discussed in the next two subsections.

### 2.5.1 Vertical Subgrid Scale Physics

The model resolution is always larger than the scale at which the major sources of vertical turbulence occur (shear instability, internal wave breaking...). Turbulent motions are thus never explicitly solved, even partially, but always parameterized. The vertical turbulent fluxes are assumed to depend linearly on the gradients of large-scale quantities (for example, the turbulent heat flux is given by  $\overline{T'w'} = -A^{vT} \partial_z \overline{T}$ , where  $A^{vT}$  is an eddy coefficient). This formulation is analogous to that of molecular diffusion and dissipation. This is quite clearly a necessary compromise: considering only the molecular viscosity acting on large scale severely underestimates the role of turbulent diffusion and dissipation, while an accurate consideration of the details of turbulent motions is simply impractical. The resulting vertical momentum and tracer diffusive operators are of second order:

$$\begin{aligned} \mathbf{D}^{vU} &= \frac{\partial}{\partial z} \left( A^{vm} \frac{\partial \mathbf{U}_h}{\partial z} \right), \\ D^{vT} &= \frac{\partial}{\partial z} \left( A^{vT} \frac{\partial T}{\partial z} \right), \quad D^{vS} = \frac{\partial}{\partial z} \left( A^{vT} \frac{\partial S}{\partial z} \right) \end{aligned} \quad (2.34)$$

where  $A^{vm}$  and  $A^{vT}$  are the vertical eddy viscosity and diffusivity coefficients, respectively. At the sea surface and at the bottom, turbulent fluxes of momentum, heat and salt must be specified (see Chap. 7 and 10 and §5.5). All the vertical physics is embedded in the specification of the eddy coefficients. They can be assumed to be either constant, or function of the local fluid properties (*e.g.*

Richardson number, Brunt-Vaisälä frequency...), or computed from a turbulent closure model. The choices available in *NEMO* are discussed in §10).

## 2.5.2 Formulation of the Lateral Diffusive and Viscous Operators

Lateral turbulence can be roughly divided into a mesoscale turbulence associated with eddies (which can be solved explicitly if the resolution is sufficient since their underlying physics are included in the primitive equations), and a sub mesoscale turbulence which is never explicitly solved even partially, but always parameterized. The formulation of lateral eddy fluxes depends on whether the mesoscale is below or above the grid-spacing (*i.e.* the model is eddy-resolving or not).

In non-eddy-resolving configurations, the closure is similar to that used for the vertical physics. The lateral turbulent fluxes are assumed to depend linearly on the lateral gradients of large-scale quantities. The resulting lateral diffusive and dissipative operators are of second order. Observations show that lateral mixing induced by mesoscale turbulence tends to be along isopycnal surfaces (or more precisely neutral surfaces [McDougall \[1987\]](#)) rather than across them. As the slope of neutral surfaces is small in the ocean, a common approximation is to assume that the ‘lateral’ direction is the horizontal, *i.e.* the lateral mixing is performed along geopotential surfaces. This leads to a geopotential second order operator for lateral subgrid scale physics. This assumption can be relaxed: the eddy-induced turbulent fluxes can be better approached by assuming that they depend linearly on the gradients of large-scale quantities computed along neutral surfaces. In such a case, the diffusive operator is an isoneutral second order operator and it has components in the three space directions. However, both horizontal and isoneutral operators have no effect on mean (*i.e.* large scale) potential energy whereas potential energy is a main source of turbulence (through baroclinic instabilities). [Gent and McWilliams \[1990\]](#) have proposed a parameterisation of mesoscale eddy-induced turbulence which associates an eddy-induced velocity to the isoneutral diffusion. Its mean effect is to reduce the mean potential energy of the ocean. This leads to a formulation of lateral subgrid-scale physics made up of an isoneutral second order operator and an eddy induced advective part. In all these lateral diffusive formulations, the specification of the lateral eddy coefficients remains the problematic point as there is no really satisfactory formulation of these coefficients as a function of large-scale features.

In eddy-resolving configurations, a second order operator can be used, but usually the more scale selective biharmonic operator is preferred as the grid-spacing is usually not small enough compared to the scale of the eddies. The role devoted to the subgrid-scale physics is to dissipate the energy that cascades toward the grid scale and thus to ensure the stability of the model while not interfering with the resolved mesoscale activity. Another approach is becoming more and more popular: instead of specifying explicitly a sub-grid scale term in the momentum and tracer time evolution equations, one uses a advective scheme which is diffusive enough to maintain the model stability. It must be emphasised that then, all the sub-grid

scale physics is included in the formulation of the advection scheme.

All these parameterisations of subgrid scale physics have advantages and drawbacks. There are not all available in *NEMO*. For active tracers (temperature and salinity) the main ones are: Laplacian and bilaplacian operators acting along geopotential or iso-neutral surfaces, [Gent and McWilliams \[1990\]](#) parameterisation, and various slightly diffusive advection schemes. For momentum, the main ones are: Laplacian and bilaplacian operators acting along geopotential surfaces, and UBS advection schemes when flux form is chosen for the momentum advection.

### Lateral Laplacian tracer diffusive operator

The lateral Laplacian tracer diffusive operator is defined by (see [Appendix B](#)):

$$D^{lT} = \nabla \cdot \left( A^{lT} \mathfrak{R} \nabla T \right) \quad \text{with} \quad \mathfrak{R} = \begin{pmatrix} 1 & 0 & -r_1 \\ 0 & 1 & -r_2 \\ -r_1 & -r_2 & r_1^2 + r_2^2 \end{pmatrix} \quad (2.35)$$

where  $r_1$  and  $r_2$  are the slopes between the surface along which the diffusive operator acts and the model level (*e.g.*  $z$ - or  $s$ -surfaces). Note that the formulation [\(2.35\)](#) is exact for the rotation between geopotential and  $s$ -surfaces, while it is only an approximation for the rotation between isoneutral and  $z$ - or  $s$ -surfaces. Indeed, in the latter case, two assumptions are made to simplify [\(2.35\)](#) [[Cox 1987](#)]. First, the horizontal contribution of the dianeutral mixing is neglected since the ratio between iso and dia-neutral diffusive coefficients is known to be several orders of magnitude smaller than unity. Second, the two isoneutral directions of diffusion are assumed to be independent since the slopes are generally less than  $10^{-2}$  in the ocean (see [Appendix B](#)).

For *iso-level* diffusion,  $r_1$  and  $r_2$  are zero.  $\mathfrak{R}$  reduces to the identity in the horizontal direction, no rotation is applied.

For *geopotential* diffusion,  $r_1$  and  $r_2$  are the slopes between the geopotential and computational surfaces: they are equal to  $\sigma_1$  and  $\sigma_2$ , respectively (see [\(2.22\)](#)).

For *isoneutral* diffusion  $r_1$  and  $r_2$  are the slopes between the isoneutral and computational surfaces. Therefore, they are different quantities, but have similar expressions in  $z$ - and  $s$ -coordinates. In  $z$ -coordinates:

$$r_1 = \frac{e_3}{e_1} \left( \frac{\partial \rho}{\partial i} \right) \left( \frac{\partial \rho}{\partial k} \right)^{-1} \quad r_2 = \frac{e_3}{e_2} \left( \frac{\partial \rho}{\partial j} \right) \left( \frac{\partial \rho}{\partial k} \right)^{-1} \quad (2.36)$$

while in  $s$ -coordinates  $\frac{\partial}{\partial k}$  is replaced by  $\frac{\partial}{\partial s}$ .

### Eddy induced velocity

When the *eddy induced velocity* parametrisation (eiv) [[Gent and McWilliams 1990](#)] is used, an additional tracer advection is introduced in combination with the isoneutral diffusion of tracers:

$$D^{lT} = \nabla \cdot \left( A^{lT} \mathfrak{R} \nabla T \right) + \nabla \cdot (\mathbf{U}^* T) \quad (2.37)$$

where  $\mathbf{U}^* = (u^*, v^*, w^*)$  is a non-divergent, eddy-induced transport velocity. This velocity field is defined by:

$$\begin{aligned} u^* &= +\frac{1}{e_3} \frac{\partial}{\partial k} [A^{ev} \tilde{r}_1] \\ v^* &= +\frac{1}{e_3} \frac{\partial}{\partial k} [A^{ev} \tilde{r}_2] \\ w^* &= -\frac{1}{e_1 e_2} \left[ \frac{\partial}{\partial i} (A^{ev} e_2 \tilde{r}_1) + \frac{\partial}{\partial j} (A^{ev} e_1 \tilde{r}_2) \right] \end{aligned} \quad (2.38)$$

where  $A^{ev}$  is the eddy induced velocity coefficient (or equivalently the isoneutral thickness diffusivity coefficient), and  $\tilde{r}_1$  and  $\tilde{r}_2$  are the slopes between isoneutral and *geopotential* surfaces. Their values are thus independent of the vertical coordinate, but their expression depends on the coordinate:

$$\tilde{r}_n = \begin{cases} r_n & \text{in } z\text{-coordinate} \\ r_n + \sigma_n & \text{in } z^* \text{ and } s\text{-coordinates} \end{cases} \quad \text{where } n = 1, 2 \quad (2.39)$$

The normal component of the eddy induced velocity is zero at all the boundaries. This can be achieved in a model by tapering either the eddy coefficient or the slopes to zero in the vicinity of the boundaries. The latter strategy is used in *NEMO* (cf. Chap. 9).

### Lateral bilaplacian tracer diffusive operator

The lateral bilaplacian tracer diffusive operator is defined by:

$$D^{lT} = -\Delta (\Delta T) \quad \text{where } \Delta \bullet = \nabla \left( \sqrt{B^{lT}} \Re \nabla \bullet \right) \quad (2.40)$$

It is the Laplacian operator given by (2.35) applied twice with the harmonic eddy diffusion coefficient set to the square root of the biharmonic one.

### Lateral Laplacian momentum diffusive operator

The Laplacian momentum diffusive operator along  $z$ - or  $s$ -surfaces is found by applying (2.7e) to the horizontal velocity vector (see Appendix B):

$$\begin{aligned} \mathbf{D}^{lU} &= \nabla_h (A^{lm} \chi) - \nabla_h \times (A^{lm} \zeta \mathbf{k}) \\ &= \begin{pmatrix} \frac{1}{e_1} \frac{\partial}{\partial i} (A^{lm} \chi) - \frac{1}{e_2 e_3} \frac{\partial}{\partial j} (A^{lm} e_3 \zeta) \\ \frac{1}{e_2} \frac{\partial}{\partial j} (A^{lm} \chi) + \frac{1}{e_1 e_3} \frac{\partial}{\partial i} (A^{lm} e_3 \zeta) \end{pmatrix} \end{aligned} \quad (2.41)$$

Such a formulation ensures a complete separation between the vorticity and horizontal divergence fields (see Appendix C). Unfortunately, it is only available

in *iso-level* direction. When a rotation is required (*i.e.* geopotential diffusion in  $s$ -coordinates or isoneutral diffusion in both  $z$ - and  $s$ -coordinates), the  $u$  and  $v$ -fields are considered as independent scalar fields, so that the diffusive operator is given by:

$$\begin{aligned} D_u^{lU} &= \nabla \cdot (A^{lm} \mathfrak{R} \nabla u) \\ D_v^{lU} &= \nabla \cdot (A^{lm} \mathfrak{R} \nabla v) \end{aligned} \tag{2.42}$$

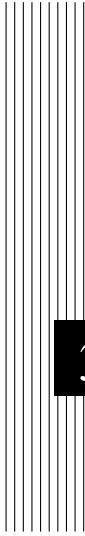
where  $\mathfrak{R}$  is given by (2.35). It is the same expression as those used for diffusive operator on tracers. It must be emphasised that such a formulation is only exact in a Cartesian coordinate system, *i.e.* on a  $f$ - or  $\beta$ -plane, not on the sphere. It is also a very good approximation in vicinity of the Equator in a geographical coordinate system [Lengaigne et al. 2003].

#### **lateral bilaplacian momentum diffusive operator**

As for tracers, the bilaplacian order momentum diffusive operator is a re-entering Laplacian operator with the harmonic eddy diffusion coefficient set to the square root of the biharmonic one. Nevertheless it is currently not available in the isoneutral case.







## **3** Time Domain (STP)

### **Contents**

---

<b>3.1</b>	<b>Time stepping environment</b>	<b>40</b>
<b>3.2</b>	<b>Non-Diffusive Part — Leapfrog Scheme</b>	<b>40</b>
<b>3.3</b>	<b>Diffusive Part — Forward or Backward Scheme</b>	<b>41</b>
<b>3.4</b>	<b>Surface Pressure Gradient</b>	<b>43</b>
<b>3.5</b>	<b>The Modified Leapfrog – Asselin Filter scheme</b>	<b>44</b>
<b>3.6</b>	<b>Start/Restart strategy</b>	<b>44</b>

---

Having defined the continuous equations in Chap. 2, we need now to choose a time discretization, a key feature of an ocean model as it exerts a strong influence on the structure of the computer code (*i.e.* on its flowchart). In the present chapter, we provide a general description of the *NEMO* time stepping strategy and the consequences for the order in which the equations are solved.

### 3.1 Time stepping environment

The time stepping used in *NEMO* is a three level scheme that can be represented as follows:

$$x^{t+\Delta t} = x^{t-\Delta t} + 2 \Delta t \text{RHS}_x^{t-\Delta t, t, t+\Delta t} \quad (3.1)$$

where  $x$  stands for  $u$ ,  $v$ ,  $T$  or  $S$ ; RHS is the Right-Hand-Side of the corresponding time evolution equation;  $\Delta t$  is the time step; and the superscripts indicate the time at which a quantity is evaluated. Each term of the RHS is evaluated at a specific time step depending on the physics with which it is associated.

The choice of the time step used for this evaluation is discussed below as well as the implications for starting or restarting a model simulation. Note that the time stepping calculation is generally performed in a single operation. With such a complex and nonlinear system of equations it would be dangerous to let a prognostic variable evolve in time for each term separately.

The three level scheme requires three arrays for each prognostic variable. For each variable  $x$  there is  $x_b$  (before),  $x_n$  (now) and  $x_a$ . The third array, although referred to as  $x_a$  (after) in the code, is usually not the variable at the after time step; but rather it is used to store the time derivative (RHS in (3.1)) prior to time-stepping the equation. Generally, the time stepping is performed once at each time step in the *tranxt.F90* and *dynnxt.F90* modules, except when using implicit vertical diffusion or calculating sea surface height in which case time-splitting options are used.

### 3.2 Non-Diffusive Part — Leapfrog Scheme

The time stepping used for processes other than diffusion is the well-known leapfrog scheme [Mesinger and Arakawa 1976]. This scheme is widely used for advection processes in low-viscosity fluids. It is a time centred scheme, *i.e.* the RHS in (3.1) is evaluated at time step  $t$ , the now time step. It may be used for momentum and tracer advection, pressure gradient, and Coriolis terms, but not for diffusion terms. It is an efficient method that achieves second-order accuracy with just one right hand side evaluation per time step. Moreover, it does not artificially damp

linear oscillatory motion nor does it produce instability by amplifying the oscillations. These advantages are somewhat diminished by the large phase-speed error of the leapfrog scheme, and the unsuitability of leapfrog differencing for the representation of diffusion and Rayleigh damping processes. However, the scheme allows the coexistence of a numerical and a physical mode due to its leading third order dispersive error. In other words a divergence of odd and even time steps may occur. To prevent it, the leapfrog scheme is often used in association with a Robert-Asselin time filter (hereafter the LF-RA scheme). This filter, first designed by Robert [1966] and more comprehensively studied by Asselin [1972], is a kind of laplacian diffusion in time that mixes odd and even time steps:

$$x_F^t = x^t + \gamma \left[ x_F^{t-\Delta t} - 2x^t + x^{t+\Delta t} \right] \quad (3.2)$$

where the subscript  $F$  denotes filtered values and  $\gamma$  is the Asselin coefficient.  $\gamma$  is initialized as *rn\_atfp* (namelist parameter). Its default value is *rn\_atfp*= $10^{-3}$  (see § 3.5), causing only a weak dissipation of high frequency motions ([Farge 1987]). The addition of a time filter degrades the accuracy of the calculation from second to first order. However, the second order truncation error is proportional to  $\gamma$ , which is small compared to 1. Therefore, the LF-RA is a quasi second order accurate scheme. The LF-RA scheme is preferred to other time differencing schemes such as predictor corrector or trapezoidal schemes, because the user has an explicit and simple control of the magnitude of the time diffusion of the scheme. When used with the 2nd order space centred discretisation of the advection terms in the momentum and tracer equations, LF-RA avoids implicit numerical diffusion: diffusion is set explicitly by the user through the Robert-Asselin filter parameter and the viscosity and diffusion coefficients.

### 3.3 Diffusive Part — Forward or Backward Scheme

The leapfrog differencing scheme is unsuitable for the representation of diffusion and damping processes. For a tendency  $D_x$ , representing a diffusion term or a restoring term to a tracer climatology (when present, see § 5.6), a forward time differencing scheme is used :

$$x^{t+\Delta t} = x^{t-\Delta t} + 2 \Delta t D_x^{t-\Delta t} \quad (3.3)$$

This is diffusive in time and conditionally stable. The conditions for stability of second and fourth order horizontal diffusion schemes are [Griffies 2004]:

$$A^h < \begin{cases} \frac{e^2}{8 \Delta t} & \text{laplacian diffusion} \\ \frac{e^4}{64 \Delta t} & \text{bilaplacian diffusion} \end{cases} \quad (3.4)$$

where  $e$  is the smallest grid size in the two horizontal directions and  $A^h$  is the mixing coefficient. The linear constraint (3.4) is a necessary condition, but not

sufficient. If it is not satisfied, even mildly, then the model soon becomes wildly unstable. The instability can be removed by either reducing the length of the time steps or reducing the mixing coefficient.

For the vertical diffusion terms, a forward time differencing scheme can be used, but usually the numerical stability condition imposes a strong constraint on the time step. Two solutions are available in *NEMO* to overcome the stability constraint: (a) a forward time differencing scheme using a time splitting technique (*ln\_zdfexp* = true) or (b) a backward (or implicit) time differencing scheme (*ln\_zdfexp* = false). In (a), the master time step  $\Delta t$  is cut into  $N$  fractional time steps so that the stability criterion is reduced by a factor of  $N$ . The computation is performed as follows:

$$\begin{aligned} x_*^{t-\Delta t} &= x^{t-\Delta t} \\ x_*^{t-\Delta t+L\frac{2\Delta t}{N}} &= x_*^{t-\Delta t+(L-1)\frac{2\Delta t}{N}} + \frac{2\Delta t}{N} \text{DF}^{t-\Delta t+(L-1)\frac{2\Delta t}{N}} \quad \text{for } L = 1 \text{ to } N \\ x_*^{t+\Delta t} &= x_*^{t+\Delta t} \end{aligned} \quad (3.5)$$

with DF a vertical diffusion term. The number of fractional time steps,  $N$ , is given by setting *nn\_zdfexp*, (namelist parameter). The scheme (b) is unconditionally stable but diffusive. It can be written as follows:

$$x^{t+\Delta t} = x^{t-\Delta t} + 2 \Delta t \text{RHS}_x^{t+\Delta t} \quad (3.6)$$

This scheme is rather time consuming since it requires a matrix inversion, but it becomes attractive since a value of 3 or more is needed for  $N$  in the forward time differencing scheme. For example, the finite difference approximation of the temperature equation is:

$$\frac{T(k)^{t+1} - T(k)^{t-1}}{2 \Delta t} \equiv \text{RHS} + \frac{1}{e_{3t}} \delta_k \left[ \frac{A_w^{vT}}{e_{3w}} \delta_{k+1/2} [T^{t+1}] \right] \quad (3.7)$$

where RHS is the right hand side of the equation except for the vertical diffusion term. We rewrite (3.6) as:

$$-c(k+1) T^{t+1}(k+1) + d(k) T^{t+1}(k) - c(k) T^{t+1}(k-1) \equiv b(k) \quad (3.8)$$

where

$$\begin{aligned} c(k) &= A_w^{vT}(k) / e_{3w}(k) \\ d(k) &= e_{3t}(k) / (2\Delta t) + c_k + c_{k+1} \\ b(k) &= e_{3t}(k) (T^{t-1}(k) / (2\Delta t) + \text{RHS}) \end{aligned}$$

(3.8) is a linear system of equations with an associated matrix which is tridiagonal. Moreover,  $c(k)$  and  $d(k)$  are positive and the diagonal term is greater than the sum of the two extra-diagonal terms, therefore a special adaptation of the Gauss elimination procedure is used to find the solution (see for example [Richtmyer and Morton \[1967\]](#)).

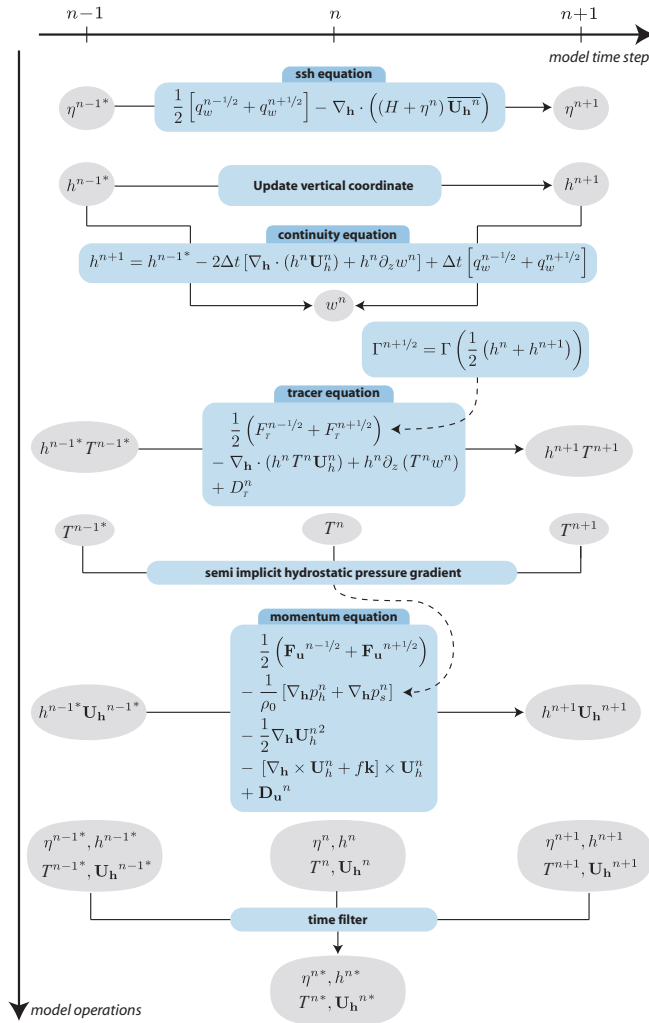


**Figure 3.1:** Sketch of the leapfrog time stepping sequence in *NEMO* from [Leclair and Madec \[2009\]](#). The use of a semi-implicit computation of the hydrostatic pressure gradient requires the tracer equation to be stepped forward prior to the momentum equation. The need for knowledge of the vertical scale factor (here denoted as  $h$ ) requires the sea surface height and the continuity equation to be stepped forward prior to the computation of the tracer equation. Note that the method for the evaluation of the surface pressure gradient  $\nabla p_s$  is not presented here (see § 6.5).

### 3.4 Surface Pressure Gradient

====*llll* TO BE written.... :-)

### 3.5 The Modified Leapfrog – Asselin Filter scheme

Significant changes have been introduced by [Leclair and Madec \[2009\]](#) in the LF-RA scheme in order to ensure tracer conservation and to allow the use of a much smaller value of the Asselin filter parameter. The modifications affect both the forcing and filtering treatments in the LF-RA scheme.

In a classical LF-RA environment, the forcing term is centred in time, *i.e.* it is time-stepped over a  $2\Delta t$  period:  $x^t = x^{t-2\Delta t} + 2\Delta t Q^t$  where  $Q$  is the forcing applied to  $x$ , and the time filter is given by (3.2) so that  $Q$  is redistributed over several time step. In the modified LF-RA environment, these two formulations have been replaced by:

$$x^{t+\Delta t} = x^{t-\Delta t} + \Delta t \left( Q^{t-\Delta t/2} + Q^{t+\Delta t/2} \right) \quad (3.9)$$

$$x_F^t = x^t + \gamma \left[ x_F^{t-\Delta t} - 2x^t + x^{t+\Delta t} \right] - \gamma \Delta t \left[ Q^{t+\Delta t/2} - Q^{t-\Delta t/2} \right] \quad (3.10)$$

The change in the forcing formulation given by (3.9) (see Fig.3.2) has a significant effect: the forcing term no longer excites the divergence of odd and even time steps [[Leclair and Madec 2009](#)]. This property improves the LF-RA scheme in two respects. First, the LF-RA can now ensure the local and global conservation of tracers. Indeed, time filtering is no longer required on the forcing part. The influence of the Asselin filter on the forcing is removed by adding a new term in the filter (last term in (3.10) compared to (3.2)). Since the filtering of the forcing was the source of non-conservation in the classical LF-RA scheme, the modified formulation becomes conservative [[Leclair and Madec 2009](#)]. Second, the LF-RA becomes a truly quasi-second order scheme. Indeed, (3.9) used in combination with a careful treatment of static instability (§10.2.2) and of the TKE physics (§10.1.4), the two other main sources of time step divergence, allows a reduction by two orders of magnitude of the Asselin filter parameter.

Note that the forcing is now provided at the middle of a time step:  $Q^{t+\Delta t/2}$  is the forcing applied over the  $[t, t + \Delta t]$  time interval. This and the change in the time filter, (3.10), allows an exact evaluation of the contribution due to the forcing term between any two time steps, even if separated by only  $\Delta t$  since the time filter is no longer applied to the forcing term.

### 3.6 Start/Restart strategy

```

!-----
$namrun      !  parameters of the run
!-----
nn_no        =      0      !  job number (no more used...)
cn_exp       = "ORCA2"    !  experience name
nn_it000     =      1      !  first time step
nn_itend     =    5475     !  last time step (std 5475)
nn_date0     = 010101     !  date at nit_0000 (format yyyymmdd) used if ln_rstart=F or (ln_rstart=T and nn_rstctl=0 or 1)
nn_time0     =      0      !  initial time of day in hhmm
nn_leapy     =      0      !  Leap year calendar (1) or not (0)
ln_rstart    = .false.    !  start from rest (F) or from a restart file (T)
  nn_euler    =      1      !  = 0 : start with forward time step if ln_rstart=T
  nn_rstctl   =      0      !  restart control ==> activated only if ln_rstart=T
  !           !  = 0 nn_date0 read in namelist ; nn_it000 : read in namelist

```

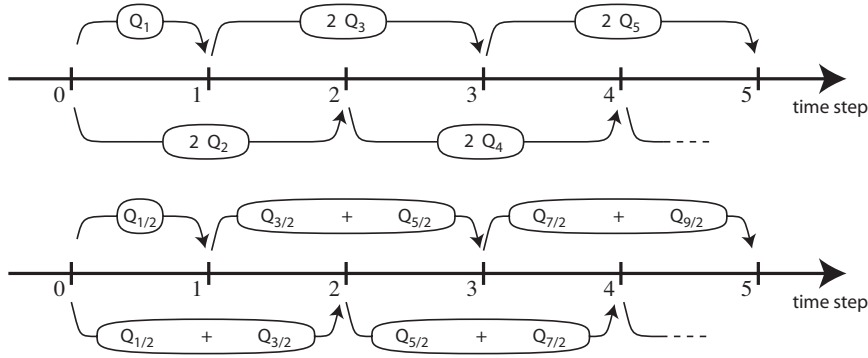


**Figure 3.2:** Illustration of forcing integration methods. (top) "Traditional" formulation : the forcing is defined at the same time as the variable to which it is applied (integer value of the time step index) and it is applied over a  $2\Delta t$  period. (bottom) modified formulation : the forcing is defined in the middle of the time (integer and a half value of the time step index) and the mean of two successive forcing values ( $n - 1/2, n + 1/2$ ). is applied over a  $2\Delta t$  period.

```

!                                     ! = 1 nn_date0 read in namelist ; nn_it000 : check consistency between namelist and restart
!                                     ! = 2 nn_date0 read in restart ; nn_it000 : check consistency between namelist and restart
cn_oceerst_in   = "restart"           ! suffix of ocean restart name (input)
cn_oceerst_indir = "."                ! directory from which to read input ocean restarts
cn_oceerst_out  = "restart"           ! suffix of ocean restart name (output)
cn_oceerst_outdir = "."               ! directory in which to write output ocean restarts
ln_iscpl       = .false.             ! cavity evolution forcing or coupling to ice sheet model
nn_istate      = 0                   ! output the initial state (1) or not (0)
ln_rst_list    = .false.             ! output restarts at list of times using nn_stocklist (T) or at set frequency with nn_stock (F)
nn_stock       = 5475                ! frequency of creation of a restart file (modulo referenced to 1)
nn_stocklist  = 0,0,0,0,0,0,0,0,0,0 ! List of timesteps when a restart file is to be written
nn_write       = 5475                ! frequency of write in the output file (modulo referenced to nn_it000)
ln_mskland    = .false.             ! mask land points in NetCDF outputs (costly: + ~15%)
ln_cfmeta     = .false.             ! output additional data to netCDF files required for compliance with the CF metadata standard
ln_clobber    = .true.              ! clobber (overwrite) an existing file
nn_chunksz    = 0                    ! chunksize (bytes) for NetCDF file (works only with iom_nf90 routines)
/

```

The first time step of this three level scheme when starting from initial conditions is a forward step (Euler time integration):

$$x^1 = x^0 + \Delta t \text{ RHS}^0 \quad (3.11)$$

This is done simply by keeping the leapfrog environment (*i.e.* the (3.1) three level time stepping) but setting all  $x^0$  (*before*) and  $x^1$  (*now*) fields equal at the first time step and using half the value of  $\Delta t$ .

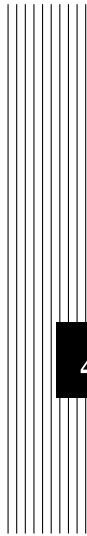
It is also possible to restart from a previous computation, by using a restart file. The restart strategy is designed to ensure perfect restartability of the code: the user should obtain the same results to machine precision either by running the model for  $2N$  time steps in one go, or by performing two consecutive experiments of  $N$  steps with a restart. This requires saving two time levels and many auxiliary data in the restart files in machine precision.

Note that when a semi-implicit scheme is used to evaluate the hydrostatic pressure gradient (see §6.4.5), an extra three-dimensional field has to be added to the restart file to ensure an exact restartability. This is done optionally via the

*nn\_dynhpg\_rst* namelist parameter, so that the size of the restart file can be reduced when restartability is not a key issue (operational oceanography or in ensemble simulations for seasonal forecasting).

Note the size of the time step used,  $\Delta t$ , is also saved in the restart file. When restarting, if the the time step has been changed, a restart using an Euler time stepping scheme is imposed. Options are defined through the *namrun* namelist variables.





## 4 Space Domain (DOM)

### Contents

---

<b>4.1</b>	<b>Fundamentals of the Discretisation</b>	<b>48</b>
4.1.1	Arrangement of Variables	48
4.1.2	Discrete Operators	49
4.1.3	Numerical Indexing	51
<b>4.2</b>	<b>Domain: Needed fields</b>	<b>54</b>
<b>4.3</b>	<b>Domain: Horizontal Grid (mesh) (<i>domhgr</i>)</b>	<b>54</b>
4.3.1	Coordinates and scale factors	54
4.3.2	Choice of horizontal grid	55
4.3.3	Output Grid files	57
<b>4.4</b>	<b>Domain: Vertical Grid (<i>domzgr</i>)</b>	<b>57</b>
4.4.1	Meter Bathymetry	59
4.4.2	$z$ -coordinate ( <i>ln_zco</i> )	60
4.4.3	$z$ -coordinate with partial step ( <i>ln_zps</i> )	62
4.4.4	$s$ -coordinate ( <i>ln_sco</i> )	64
4.4.5	$z^*$ - or $s^*$ -coordinate ( <i>ln_linssh=false</i> )	66
4.4.6	level bathymetry and mask	67
<b>4.5</b>	<b>Domain: Initial State (<i>istate and dtatsd</i>)</b>	<b>68</b>

---

Having defined the continuous equations in Chap. 2 and chosen a time discretization Chap. 3, we need to choose a discretization on a grid, and numerical algorithms. In the present chapter, we provide a general description of the staggered grid used in *NEMO*, and other information relevant to the main directory routines as well as the DOM (DOMain) directory.

## 4.1 Fundamentals of the Discretisation

### 4.1.1 Arrangement of Variables

The numerical techniques used to solve the Primitive Equations in this model are based on the traditional, centred second-order finite difference approximation. Special attention has been given to the homogeneity of the solution in the three space directions. The arrangement of variables is the same in all directions. It consists of cells centred on scalar points  $(t, S, p, \rho)$  with vector points  $(u, v, w)$  defined in the centre of each face of the cells (Fig. 4.1). This is the generalisation to three dimensions of the well-known ‘‘C’’ grid in Arakawa’s classification [Mesinger and Arakawa 1976]. The relative and planetary vorticity,  $\zeta$  and  $f$ , are defined in the centre of each vertical edge and the barotropic stream function  $\psi$  is defined at horizontal points overlying the  $\zeta$  and  $f$ -points.

The ocean mesh (*i.e.* the position of all the scalar and vector points) is defined by the transformation that gives  $(\lambda, \varphi, z)$  as a function of  $(i, j, k)$ . The grid-points are located at integer or integer and a half value of  $(i, j, k)$  as indicated on Table 4.1. In all the following, subscripts  $u, v, w, f, uw, vw$  or  $fw$  indicate the position of the grid-point where the scale factors are defined. Each scale factor is defined as the local analytical value provided by (2.6). As a result, the mesh on which partial derivatives  $\frac{\partial}{\partial \lambda}$ ,  $\frac{\partial}{\partial \varphi}$ , and  $\frac{\partial}{\partial z}$  are evaluated is a uniform mesh with a grid size of unity. Discrete partial derivatives are formulated by the traditional, centred second order finite difference approximation while the scale factors are chosen equal to their local analytical value. An important point here is that the partial derivative of the scale factors must be evaluated by centred finite difference approximation, not from their analytical expression. This preserves the symmetry of the discrete set of equations and therefore satisfies many of the continuous properties (see Appendix C). A similar, related remark can be made about the domain size: when needed, an area, volume, or the total ocean depth must be evaluated as the sum of the relevant scale factors (see (4.8)) in the next section).

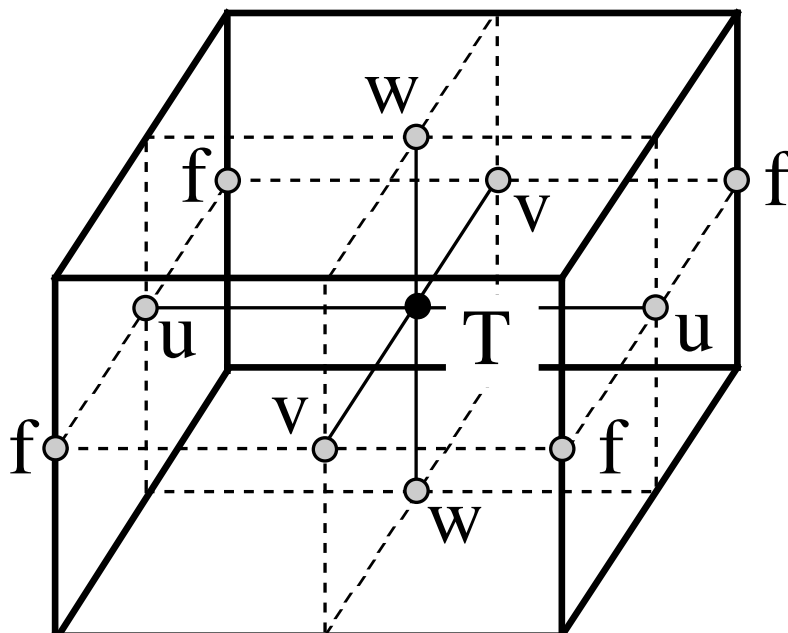


**Figure 4.1:** Arrangement of variables.  $t$  indicates scalar points where temperature, salinity, density, pressure and horizontal divergence are defined.  $(u, v, w)$  indicates vector points, and  $f$  indicates vorticity points where both relative and planetary vorticities are defined

### 4.1.2 Discrete Operators

Given the values of a variable  $q$  at adjacent points, the differencing and averaging operators at the midpoint between them are:

$$\delta_i[q] = q(i + 1/2) - q(i - 1/2) \quad (4.1a)$$

$$\bar{q}^i = \{q(i + 1/2) + q(i - 1/2)\} / 2 \quad (4.1b)$$

Similar operators are defined with respect to  $i + 1/2$ ,  $j$ ,  $j + 1/2$ ,  $k$ , and  $k + 1/2$ . Following (2.7a) and (2.7d), the gradient of a variable  $q$  defined at a  $t$ -point has its three components defined at  $u$ -,  $v$ - and  $w$ -points while its Laplacian is defined at  $t$ -point. These operators have the following discrete forms in the curvilinear  $s$ -coordinate system:

$$\nabla q \equiv \frac{1}{e_{1u}} \delta_{i+1/2}[q] \mathbf{i} + \frac{1}{e_{2v}} \delta_{j+1/2}[q] \mathbf{j} + \frac{1}{e_{3w}} \delta_{k+1/2}[q] \mathbf{k} \quad (4.2)$$

**Table 4.1:** Location of grid-points as a function of integer or integer and a half value of the column, line or level. This indexing is only used for the writing of the semi-discrete equation. In the code, the indexing uses integer values only and has a reverse direction in the vertical (see §4.1.3)

T	$i$	$j$	$k$
u	$i + 1/2$	$j$	$k$
v	$i$	$j + 1/2$	$k$
w	$i$	$j$	$k + 1/2$
f	$i + 1/2$	$j + 1/2$	$k$
uw	$i + 1/2$	$j$	$k + 1/2$
vw	$i$	$j + 1/2$	$k + 1/2$
fw	$i + 1/2$	$j + 1/2$	$k + 1/2$

$$\Delta q \equiv \frac{1}{e_{1t} e_{2t} e_{3t}} \left( \delta_i \left[ \frac{e_{2u} e_{3u}}{e_{1u}} \delta_{i+1/2}[q] \right] + \delta_j \left[ \frac{e_{1v} e_{3v}}{e_{2v}} \delta_{j+1/2}[q] \right] \right) + \frac{1}{e_{3t}} \delta_k \left[ \frac{1}{e_{3w}} \delta_{k+1/2}[q] \right] \quad (4.3)$$

Following (2.7c) and (2.7b), a vector  $\mathbf{A} = (a_1, a_2, a_3)$  defined at vector points  $(u, v, w)$  has its three curl components defined at  $vw$ -,  $uw$ -, and  $f$ -points, and its divergence defined at  $t$ -points:

$$\nabla \times \mathbf{A} \equiv \frac{1}{e_{2v} e_{3vw}} (\delta_{j+1/2} [e_{3w} a_3] - \delta_{k+1/2} [e_{2v} a_2]) \quad \mathbf{i} \quad (4.4)$$

$$+ \frac{1}{e_{2u} e_{3uw}} (\delta_{k+1/2} [e_{1u} a_1] - \delta_{i+1/2} [e_{3w} a_3]) \quad \mathbf{j} \quad (4.5)$$

$$+ \frac{1}{e_{1f} e_{2f}} (\delta_{i+1/2} [e_{2v} a_2] - \delta_{j+1/2} [e_{1u} a_1]) \quad \mathbf{k} \quad (4.6)$$

$$\nabla \cdot \mathbf{A} \equiv \frac{1}{e_{1t} e_{2t} e_{3t}} (\delta_i [e_{2u} e_{3u} a_1] + \delta_j [e_{1v} e_{3v} a_2]) + \frac{1}{e_{3t}} \delta_k [a_3] \quad (4.7)$$

The vertical average over the whole water column denoted by an overbar becomes for a quantity  $q$  which is a masked field (i.e. equal to zero inside solid area):

$$\bar{q} = \frac{1}{H} \int_{k^b}^{k^o} q e_{3q} dk \equiv \frac{1}{H_q} \sum_k q e_{3q} \quad (4.8)$$

where  $H_q$  is the ocean depth, which is the masked sum of the vertical scale factors at  $q$  points,  $k^b$  and  $k^o$  are the bottom and surface  $k$ -indices, and the symbol  $k^o$  refers to a summation over all grid points of the same type in the direction indicated by the subscript (here  $k$ ).

In continuous form, the following properties are satisfied:

$$\nabla \times \nabla q = \mathbf{0} \quad (4.9)$$

$$\nabla \cdot (\nabla \times \mathbf{A}) = 0 \quad (4.10)$$

It is straightforward to demonstrate that these properties are verified locally in discrete form as soon as the scalar  $q$  is taken at  $t$ -points and the vector  $\mathbf{A}$  has its components defined at vector points  $(u, v, w)$ .

Let  $a$  and  $b$  be two fields defined on the mesh, with value zero inside continental area. Using integration by parts it can be shown that the differencing operators ( $\delta_i, \delta_j$  and  $\delta_k$ ) are skew-symmetric linear operators, and further that the averaging operators  $\bar{\cdot}^i, \bar{\cdot}^k$  and  $\bar{\cdot}^k$ ) are symmetric linear operators, *i.e.*

$$\sum_i a_i \delta_i [b] \equiv - \sum_i \delta_{i+1/2} [a] b_{i+1/2} \quad (4.11)$$

$$\sum_i a_i \bar{b}^i \equiv \sum_i \bar{a}^{i+1/2} b_{i+1/2} \quad (4.12)$$

In other words, the adjoint of the differencing and averaging operators are  $\delta_i^* = \delta_{i+1/2}$  and  $(\bar{\cdot}^i)^* = \bar{\cdot}^{i+1/2}$ , respectively. These two properties will be used extensively in the Appendix C to demonstrate integral conservative properties of the discrete formulation chosen.

### 4.1.3 Numerical Indexing

The array representation used in the FORTRAN code requires an integer indexing while the analytical definition of the mesh (see §4.1.1) is associated with the use of integer values for  $t$ -points and both integer and integer and a half values for all the other points. Therefore a specific integer indexing must be defined for points other than  $t$ -points (*i.e.* velocity and vorticity grid-points). Furthermore, the direction of the vertical indexing has been changed so that the surface level is at  $k = 1$ .

#### Horizontal Indexing

The indexing in the horizontal plane has been chosen as shown in Fig.4.2. For an increasing  $i$  index ( $j$  index), the  $t$ -point and the eastward  $u$ -point (northward  $v$ -point) have the same index (see the dashed area in Fig.4.2). A  $t$ -point and its nearest northeast  $f$ -point have the same  $i$ - and  $j$ -indices.

#### Vertical Indexing

In the vertical, the chosen indexing requires special attention since the  $k$ -axis is re-orientated downward in the FORTRAN code compared to the indexing used in the semi-discrete equations and given in §4.1.1. The sea surface corresponds to the  $w$ -level  $k = 1$  which is the same index as  $t$ -level just below (Fig.4.3). The last  $w$ -level ( $k = jpk$ ) either corresponds to the ocean floor or is inside the bathymetry while the last  $t$ -level is always inside the bathymetry (Fig.4.3). Note that for an increasing  $k$  index, a  $w$ -point and the  $t$ -point just below have the same  $k$  index, in

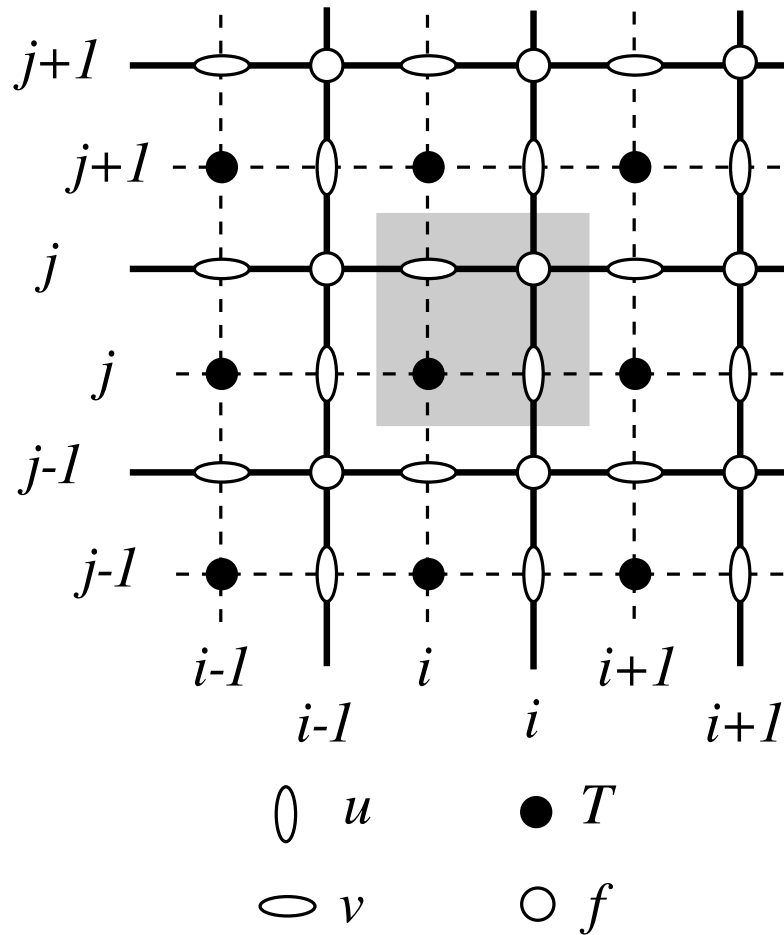


**Figure 4.2:** Horizontal integer indexing used in the FORTRAN code. The dashed area indicates the cell in which variables contained in arrays have the same  $i$ - and  $j$ -indices

opposition to what is done in the horizontal plane where it is the  $t$ -point and the nearest velocity points in the direction of the horizontal axis that have the same  $i$  or  $j$  index (compare the dashed area in Fig.4.2 and 4.3). Since the scale factors are chosen to be strictly positive, a *minus sign* appears in the FORTRAN code *before all the vertical derivatives* of the discrete equations given in this documentation.

### Domain Size

The total size of the computational domain is set by the parameters  $jpiglo$ ,  $jjjglo$  and  $jjkglo$  in the  $i$ ,  $j$  and  $k$  directions respectively. They are given as namelist variables in the *namecfg* namelist. Parameters  $jpj$  and  $jjj$  refer to the size of each processor subdomain when the code is run in parallel using domain decomposition

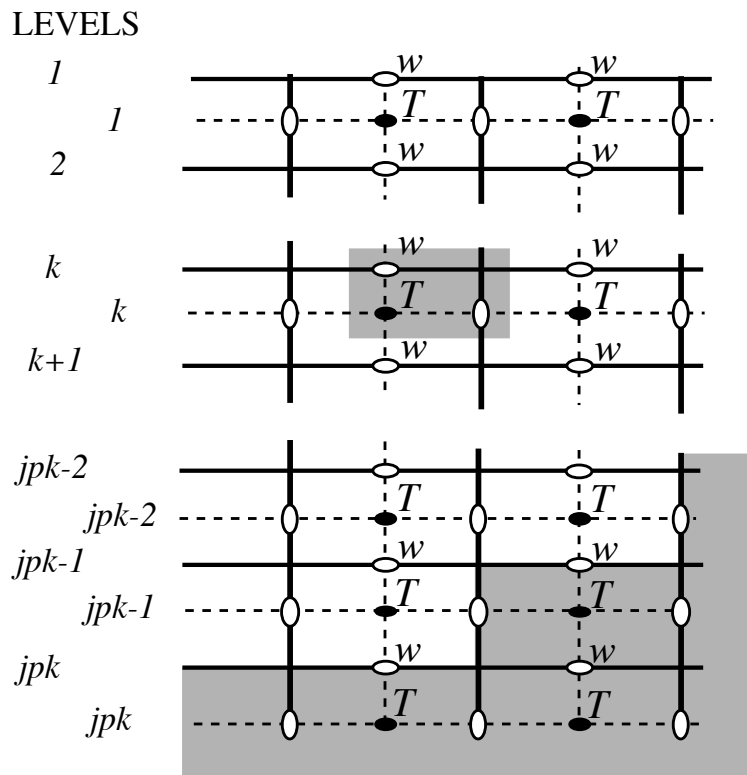


**Figure 4.3:** Vertical integer indexing used in the FORTRAN code. Note that the  $k$ -axis is orientated downward. The dashed area indicates the cell in which variables contained in arrays have the same  $k$ -index.

(`key_mpp_mpi` defined, see §8.3).

## 4.2 Domain: Needed fields

The ocean mesh (*i.e.* the position of all the scalar and vector points) is defined by the transformation that gives  $(\lambda, \varphi, z)$  as a function of  $(i, j, k)$ . The grid-points are located at integer or integer and a half values of as indicated in Table 4.1. The associated scale factors are defined using the analytical first derivative of the transformation (2.6). These definitions are done in two modules given by example, `userdef_hgr.F90` and `userdef_zgr.F90`, which provide the horizontal and vertical meshes, respectively. Otherwise all needed fields can be read in file `cn_domcfg` specified in `namcfg`.

The needed fields for domain are:

geographic position :

longitude : `glamt` , `glamu` , `glamv` and `glamf` (at T, U, V and F point)

latitude : `gphit` , `gphiu` , `gphiv` and `gphif` (at T, U, V and F point)

Coriolis parameter (if domain not on the sphere): `ff.f` and `ff.t` (at T and F point)

Scale factors : `e1t`, `e1u`, `e1v` and `e1f` (on i direction),

`e2t`, `e2u`, `e2v` and `e2f` (on j direction)

and `ie1e2u_v`, `e1e2u` , `e1e2v`

## 4.3 Domain: Horizontal Grid (mesh) (`domhgr.F90` module)

### 4.3.1 Coordinates and scale factors

The ocean mesh (*i.e.* the position of all the scalar and vector points) is defined by the transformation that gives  $(\lambda, \varphi, z)$  as a function of  $(i, j, k)$ . The grid-points are located at integer or integer and a half values of as indicated in Table 4.1. The associated scale factors are defined using the analytical first derivative of the transformation (2.6). These definitions are done in two modules, `domhgr.F90` and `domzgr.F90`, which provide the horizontal and vertical meshes, respectively. This section deals with the horizontal mesh parameters.

In a horizontal plane, the location of all the model grid points is defined from the analytical expressions of the longitude  $\lambda$  and latitude  $\varphi$  as a function of  $(i, j)$ . The horizontal scale factors are calculated using (2.6). For example, when the longitude and latitude are function of a single value ( $i$  and  $j$ , respectively) (geographical configuration of the mesh), the horizontal mesh definition reduces to define the wanted  $\lambda(i)$ ,  $\varphi(j)$ , and their derivatives  $\lambda'(i)$   $\varphi'(j)$  in the `domhgr.F90` module. The model computes the grid-point positions and scale factors in the horizontal



plane as follows:

$$\begin{array}{ll}
 \lambda_t \equiv \text{glamt} = \lambda(i) & \varphi_t \equiv \text{gphit} = \varphi(j) \\
 \lambda_u \equiv \text{glamu} = \lambda(i + 1/2) & \varphi_u \equiv \text{gphiu} = \varphi(j) \\
 \lambda_v \equiv \text{glamv} = \lambda(i) & \varphi_v \equiv \text{gphiv} = \varphi(j + 1/2) \\
 \lambda_f \equiv \text{glamf} = \lambda(i + 1/2) & \varphi_f \equiv \text{gphif} = \varphi(j + 1/2)
 \end{array}$$

$$\begin{array}{ll}
 e_{1t} \equiv \mathbf{e1t} = r_a |\lambda'(i) \cos \varphi(j)| & e_{2t} \equiv \mathbf{e2t} = r_a |\varphi'(j)| \\
 e_{1u} \equiv \mathbf{e1t} = r_a |\lambda'(i + 1/2) \cos \varphi(j)| & e_{2u} \equiv \mathbf{e2t} = r_a |\varphi'(j)| \\
 e_{1v} \equiv \mathbf{e1t} = r_a |\lambda'(i) \cos \varphi(j + 1/2)| & e_{2v} \equiv \mathbf{e2t} = r_a |\varphi'(j + 1/2)| \\
 e_{1f} \equiv \mathbf{e1t} = r_a |\lambda'(i + 1/2) \cos \varphi(j + 1/2)| & e_{2f} \equiv \mathbf{e2t} = r_a |\varphi'(j + 1/2)|
 \end{array}$$

where the last letter of each computational name indicates the grid point considered and  $r_a$  is the earth radius (defined in *phycst.F90* along with all universal constants). Note that the horizontal position of and scale factors at  $w$ -points are exactly equal to those of  $t$ -points, thus no specific arrays are defined at  $w$ -points.

Note that the definition of the scale factors (*i.e.* as the analytical first derivative of the transformation that gives  $(\lambda, \varphi, z)$  as a function of  $(i, j, k)$ ) is specific to the *NEMO* model [Martí et al. 1992]. As an example,  $e_{1t}$  is defined locally at a  $t$ -point, whereas many other models on a C grid choose to define such a scale factor as the distance between the  $U$ -points on each side of the  $t$ -point. Relying on an analytical transformation has two advantages: firstly, there is no ambiguity in the scale factors appearing in the discrete equations, since they are first introduced in the continuous equations; secondly, analytical transformations encourage good practice by the definition of smoothly varying grids (rather than allowing the user to set arbitrary jumps in thickness between adjacent layers) [Tréguier et al. 1996]. An example of the effect of such a choice is shown in Fig. 4.4.

### 4.3.2 Choice of horizontal grid

The user has three options available in defining a horizontal grid, which involve the namelist variable *jphgr\_mesh* of the *namcfg* namelist.

***jphgr\_mesh=0*** The most general curvilinear orthogonal grids. The coordinates and their first derivatives with respect to  $i$  and  $j$  are provided in a input file (*coordinates.nc*), read in *hgr\_read* subroutine of the *domhgr* module.

***jphgr\_mesh=1 to 5*** A few simple analytical grids are provided (see below). For other analytical grids, the *domhgr.F90* module must be modified by the user.

There are two simple cases of geographical grids on the sphere. With *jphgr\_mesh=1*, the grid (expressed in degrees) is regular in space, with grid sizes specified by parameters *ppe1\_deg* and *ppe2\_deg*, respectively. Such a geographical grid can be very anisotropic at high latitudes because of the convergence of meridians (the

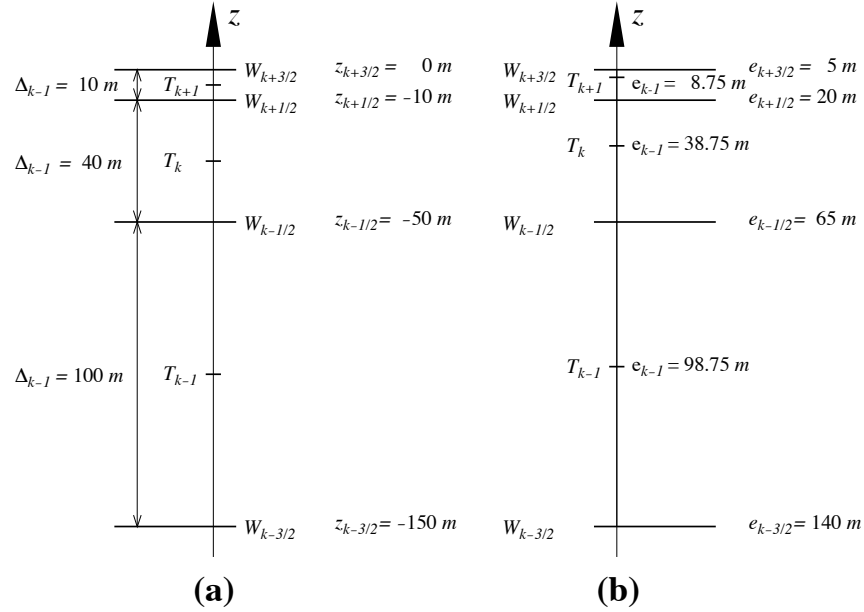


**Figure 4.4:** Comparison of (a) traditional definitions of grid-point position and grid-size in the vertical, and (b) analytically derived grid-point position and scale factors. For both grids here, the same  $w$ -point depth has been chosen but in (a) the  $t$ -points are set half way between  $w$ -points while in (b) they are defined from an analytical function:  $z(k) = 5(k - 1/2)^3 - 45(k - 1/2)^2 + 140(k - 1/2) - 150$ . Note the resulting difference between the value of the grid-size  $\Delta_k$  and those of the scale factor  $e_k$ .

zonal scale factors  $e_1$  become much smaller than the meridional scale factors  $e_2$ ). The Mercator grid ( $jphgr\_mesh=4$ ) avoids this anisotropy by refining the meridional scale factors in the same way as the zonal ones. In this case, meridional scale factors and latitudes are calculated analytically using the formulae appropriate for a Mercator projection, based on  $ppe1\_deg$  which is a reference grid spacing at the equator (this applies even when the geographical equator is situated outside the model domain). In these two cases ( $jphgr\_mesh=1$  or  $4$ ), the grid position is defined by the longitude and latitude of the south-westernmost point ( $ppglamt0$  and  $ppgphi0$ ). Note that for the Mercator grid the user need only provide an approximate starting latitude: the real latitude will be recalculated analytically, in order to ensure that the equator corresponds to line passing through  $t$ - and  $u$ -points.

Rectangular grids ignoring the spherical geometry are defined with  $jphgr\_mesh = 2, 3, 5$ . The domain is either an  $f$ -plane ( $jphgr\_mesh = 2$ , Coriolis factor is constant) or a beta-plane ( $jphgr\_mesh = 3$ , the Coriolis factor is linear in the  $j$ -direction). The grid size is uniform in meter in each direction, and given by the parameters  $ppe1\_m$  and  $ppe2\_m$  respectively. The zonal grid coordinate ( $glam$  arrays)

is in kilometers, starting at zero with the first  $t$ -point. The meridional coordinate ( $gphi$ . arrays) is in kilometers, and the second  $t$ -point corresponds to coordinate  $gphit = 0$ . The input variable  $ppglam0$  is ignored.  $ppgphi0$  is used to set the reference latitude for computation of the Coriolis parameter. In the case of the beta plane,  $ppgphi0$  corresponds to the center of the domain. Finally, the special case  $jphgr\_mesh=5$  corresponds to a beta plane in a rotated domain for the GYRE configuration, representing a classical mid-latitude double gyre system. The rotation allows us to maximize the jet length relative to the gyre areas (and the number of grid points).

The choice of the grid must be consistent with the boundary conditions specified by  $jperio$ , a parameter found in *namcfg* namelist (see §8).

### 4.3.3 Output Grid files

All the arrays relating to a particular ocean model configuration (grid-point position, scale factors, masks) can be saved in files if  $nn\_msh \neq 0$  (namelist variable in *namdom*). This can be particularly useful for plots and off-line diagnostics. In some cases, the user may choose to make a local modification of a scale factor in the code. This is the case in global configurations when restricting the width of a specific strait (usually a one-grid-point strait that happens to be too wide due to insufficient model resolution). An example is Gibraltar Strait in the ORCA2 configuration. When such modifications are done, the output grid written when  $nn\_msh \neq 0$  is no more equal to the input grid.

## 4.4 Domain: Vertical Grid (*domzgr.F90* module)

```
!-----
&namdom      !   time and space domain
!-----
  ln_linssh   = .false.  ! =T linear free surface ==>> model level are fixed in time
  nn_closea   =    0     ! remove (=0) or keep (=1) closed seas and lakes (ORCA)
  !
  nn_msh      =    0     ! create (>0) a mesh file or not (=0)
  rn_isfmin   =   1.00   ! threshold (m) to discriminate grounding ice to floating ice
  !
  rn_rdt      =  5760.   ! time step for the dynamics and tracer
  rn_atfp     =    0.1   ! asselin time filter parameter
  !
  ln_crs      = .false.  ! Logical switch for coarsening module      (T => fill namcrs)
/
```

Variables are defined through the *namzgr* and *namdom* namelists. In the vertical, the model mesh is determined by four things: (1) the bathymetry given in meters ; (2) the number of levels of the model ( $jpk$ ) ; (3) the analytical transformation  $z(i, j, k)$  and the vertical scale factors (derivatives of the transformation) ; and (4) the masking system, *i.e.* the number of wet model levels at each  $(i, j)$  column of points.

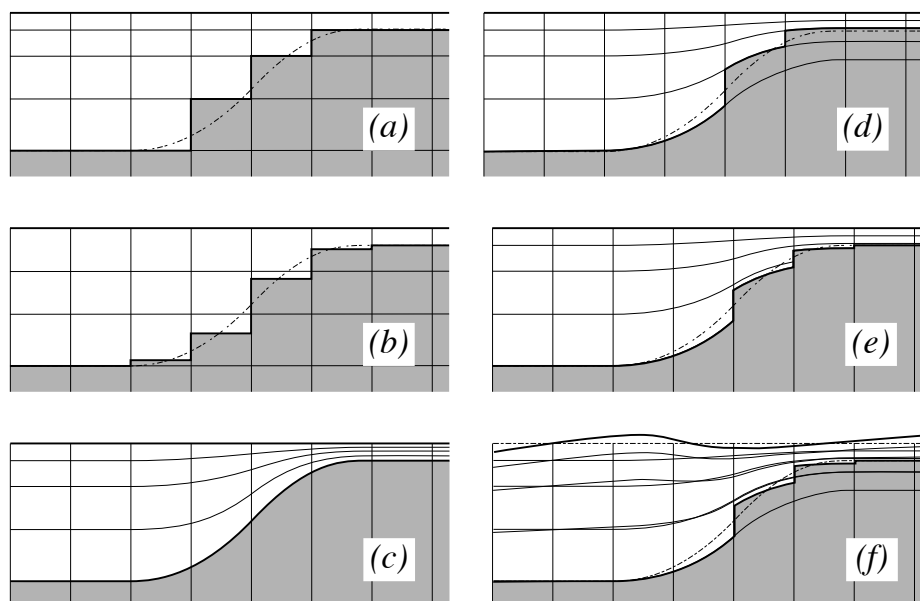


**Figure 4.5:** The ocean bottom as seen by the model: (a)  $z$ -coordinate with full step, (b)  $z$ -coordinate with partial step, (c)  $s$ -coordinate: terrain following representation, (d) hybrid  $s - z$  coordinate, (e) hybrid  $s - z$  coordinate with partial step, and (f) same as (e) but in the non-linear free surface ( $ln\_linssh=false$ ). Note that the non-linear free surface can be used with any of the 5 coordinates (a) to (e).

The choice of a vertical coordinate, even if it is made through *namzgr* namelist parameters, must be done once of all at the beginning of an experiment. It is not intended as an option which can be enabled or disabled in the middle of an experiment. Three main choices are offered (Fig. 4.5a to c):  $z$ -coordinate with full step bathymetry ( $ln\_zco = true$ ),  $z$ -coordinate with partial step bathymetry ( $ln\_zps = true$ ), or generalized,  $s$ -coordinate ( $ln\_sco = true$ ). Hybridation of the three main coordinates are available:  $s - z$  or  $s - zps$  coordinate (Fig. 4.5d and 4.5e). By default a non-linear free surface is used: the coordinate follow the time-variation of the free surface so that the transformation is time dependent:  $z(i, j, k, t)$  (Fig. 4.5f). When a linear free surface is assumed ( $ln\_linssh=true$ ), the vertical coordinate are fixed in time, but the seawater can move up and down across the  $z=0$  surface (in other words, the top of the ocean in not a rigid-lid). The last choice in terms of vertical coordinate concerns the presence (or not) in the model domain of ocean cavities beneath ice shelves. Setting  $ln\_isfcav$  to true allows to manage ocean cavities, otherwise they are filled in. This option is currently only available in  $z$ - or  $zps$ -coordinate, and partial step are also applied at the ocean/ice shelf interface.

Contrary to the horizontal grid, the vertical grid is computed in the code and no provision is made for reading it from a file. The only input file is the bathymetry (in

meters) (*bathy\_meter.nc*). <sup>1</sup>. If *ln\_isfcav* = true, an extra file input file describing the ice shelf draft (in meters) (*isf\_draft\_meter.nc*) is needed.

After reading the bathymetry, the algorithm for vertical grid definition differs between the different options:

**zco** set a reference coordinate transformation  $z_0(k)$ , and set  $z(i, j, k, t) = z_0(k)$ .

**zps** set a reference coordinate transformation  $z_0(k)$ , and calculate the thickness of the deepest level at each  $(i, j)$  point using the bathymetry, to obtain the final three-dimensional depth and scale factor arrays.

**sco** smooth the bathymetry to fulfil the hydrostatic consistency criteria and set the three-dimensional transformation.

**s-z and s-zps** smooth the bathymetry to fulfil the hydrostatic consistency criteria and set the three-dimensional transformation  $z(i, j, k)$ , and possibly introduce masking of extra land points to better fit the original bathymetry file

Unless a linear free surface is used (*ln\_linssh*=false), the arrays describing the grid point depths and vertical scale factors are three set of three dimensional arrays  $(i, j, k)$  defined at *before*, *now* and *after* time step. The time at which they are defined is indicated by a suffix: *\_b*, *\_n*, or *\_a*, respectively. They are updated at each model time step using a fixed reference coordinate system which computer names have a *\_0* suffix. When the linear free surface option is used (*ln\_linssh*=true), *before*, *now* and *after* arrays are simply set one for all to their reference counterpart.

#### 4.4.1 Meter Bathymetry

Three options are possible for defining the bathymetry, according to the namelist variable *nn\_bathy* (found in *namdom* namelist):

**nn\_bathy = 0** a flat-bottom domain is defined. The total depth  $z_w(jpk)$  is given by the coordinate transformation. The domain can either be a closed basin or a periodic channel depending on the parameter *jperio*.

**nn\_bathy = -1** a domain with a bump of topography one third of the domain width at the central latitude. This is meant for the "EEL-R5" configuration, a periodic or open boundary channel with a seamount.

**nn\_bathy = 1** read a bathymetry and ice shelf draft (if needed). The *bathy\_meter.nc* file (Netcdf format) provides the ocean depth (positive, in meters) at each grid point of the model grid. The bathymetry is usually built by interpolating a standard bathymetry product (*e.g.* ETOPO2) onto the horizontal ocean mesh. Defining the bathymetry also defines the coastline: where the bathymetry is zero, no model levels are defined (all levels are masked).

<sup>1</sup>N.B. in full step *z*-coordinate, a *bathy\_level.nc* file can replace the *bathy\_meter.nc* file, so that the computation of the number of wet ocean point in each water column is by-passed

The *isfdraft\_meter.nc* file (Netcdf format) provides the ice shelf draft (positive, in meters) at each grid point of the model grid. This file is only needed if *ln\_isfcav* = true. Defining the ice shelf draft will also define the ice shelf edge and the grounding line position.

When a global ocean is coupled to an atmospheric model it is better to represent all large water bodies (e.g. great lakes, Caspian sea...) even if the model resolution does not allow their communication with the rest of the ocean. This is unnecessary when the ocean is forced by fixed atmospheric conditions, so these seas can be removed from the ocean domain. The user has the option to set the bathymetry in closed seas to zero (see §15.2), but the code has to be adapted to the user's configuration.

#### 4.4.2 $z$ -coordinate (*ln\_zco=true*) and reference coordinate

The reference coordinate transformation  $z_0(k)$  defines the arrays  $gdept_0$  and  $gdepw_0$  for  $t$ - and  $w$ -points, respectively. As indicated on Fig.4.3  $jpgk$  is the number of  $w$ -levels.  $gdepw_0(1)$  is the ocean surface. There are at most  $jpgk-1$   $t$ -points inside the ocean, the additional  $t$ -point at  $jk = jpgk$  is below the sea floor and is not used. The vertical location of  $w$ - and  $t$ -levels is defined from the analytic expression of the depth  $z_0(k)$  whose analytical derivative with respect to  $k$  provides the vertical scale factors. The user must provide the analytical expression of both  $z_0$  and its first derivative with respect to  $k$ . This is done in routine *domzgr.F90* through statement functions, using parameters provided in the *namcfg* namelist.

It is possible to define a simple regular vertical grid by giving zero stretching (*ppacr=0*). In that case, the parameters  $jpgk$  (number of  $w$ -levels) and *pphmax* (total ocean depth in meters) fully define the grid.

For climate-related studies it is often desirable to concentrate the vertical resolution near the ocean surface. The following function is proposed as a standard for a  $z$ -coordinate (with either full or partial steps):

$$\begin{aligned} z_0(k) &= h_{sur} - h_0 k - h_1 \log [\cosh((k - h_{th})/h_{cr})] \\ e_3^0(k) &= |-h_0 - h_1 \tanh((k - h_{th})/h_{cr})| \end{aligned} \quad (4.13)$$

where  $k = 1$  to  $jpgk$  for  $w$ -levels and  $k = 1$  to  $k = 1$  for  $T$ -levels. Such an expression allows us to define a nearly uniform vertical location of levels at the ocean top and bottom with a smooth hyperbolic tangent transition in between (Fig. 4.6).

If the ice shelf cavities are opened (*ln\_isfcav=true*), the definition of  $z_0$  is the same. However, definition of  $e_3^0$  at  $t$ - and  $w$ -points is respectively changed to:

$$\begin{aligned} e_3^T(k) &= z_W(k+1) - z_W(k) \\ e_3^W(k) &= z_T(k) - z_T(k-1) \end{aligned} \quad (4.14)$$

This formulation decrease the self-generated circulation into the ice shelf cavity (which can, in extreme case, leads to blow up).

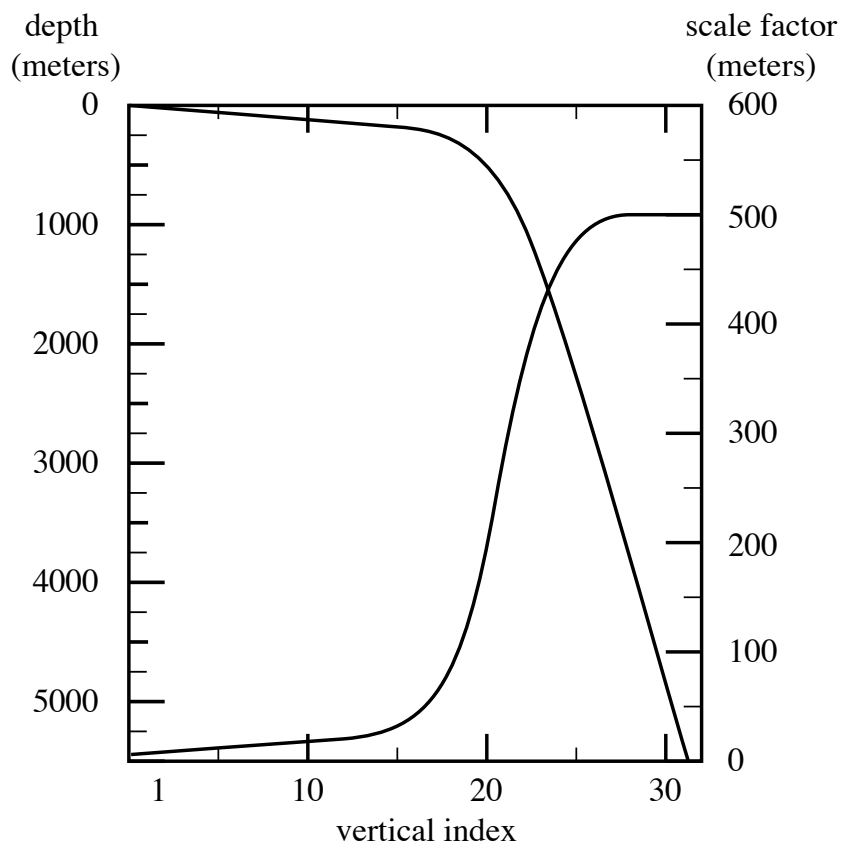


**Figure 4.6:** Default vertical mesh for ORCA2: 30 ocean levels (L30). Vertical level functions for (a) T-point depth and (b) the associated scale factor as computed from (4.14) using (4.15) in  $z$ -coordinate.

The most used vertical grid for ORCA2 has 10  $m$  (500  $m$ ) resolution in the surface (bottom) layers and a depth which varies from 0 at the sea surface to a minimum of  $-5000 m$ . This leads to the following conditions:

$$\begin{aligned}
 e_3(1 + 1/2) &= 10. \\
 e_3(jpk - 1/2) &= 500. \\
 z(1) &= 0. \\
 z(jpk) &= -5000.
 \end{aligned}
 \tag{4.15}$$

With the choice of the stretching  $h_{cr} = 3$  and the number of levels  $jpk=31$ , the four coefficients  $h_{sur}$ ,  $h_0$ ,  $h_1$ , and  $h_{th}$  in (4.14) have been determined such that (4.15) is satisfied, through an optimisation procedure using a bisection method. For the first standard ORCA2 vertical grid this led to the following values:  $h_{sur} =$

4762.96,  $h_0 = 255.58$ ,  $h_1 = 245.5813$ , and  $h_{th} = 21.43336$ . The resulting depths and scale factors as a function of the model levels are shown in Fig. 4.6 and given in Table 4.2. Those values correspond to the parameters  $pps_{sur}$ ,  $ppa_0$ ,  $ppa_1$ ,  $ppk_{th}$  in *namcfg* namelist.

Rather than entering parameters  $h_{sur}$ ,  $h_0$ , and  $h_1$  directly, it is possible to recalculate them. In that case the user sets  $pps_{sur}=ppa_0=ppa_1=999999.$ , in *namcfg* namelist, and specifies instead the four following parameters:

- $ppacr=h_{cr}$ : stretching factor (nondimensional). The larger  $ppacr$ , the smaller the stretching. Values from 3 to 10 are usual.
- $ppk_{th}=h_{th}$ : is approximately the model level at which maximum stretching occurs (nondimensional, usually of order 1/2 or 2/3 of  $jp_k$ )
- $ppdz_{min}$ : minimum thickness for the top layer (in meters)
- $pph_{max}$ : total depth of the ocean (meters).

As an example, for the 45 layers used in the DRAKKAR configuration those parameters are:  $jp_k=46$ ,  $ppacr=9$ ,  $ppk_{th}=23.563$ ,  $ppdz_{min}=6m$ ,  $pph_{max}=5750m$ .

#### 4.4.3 $z$ -coordinate with partial step (*ln\_zps=.true.*)

```

!-----
&namdom      !   time and space domain
!-----
  ln_linssh   = .false.  ! -T linear free surface ==> model level are fixed in time
  nn_closea   =    0     ! remove (=0) or keep (=1) closed seas and lakes (ORCA)
  !
  nn_msh      =    0     ! create (>0) a mesh file or not (=0)
  rn_isfhmin  =    1.00  ! threshold (m) to discriminate grounding ice to floating ice
  !
  rn_rdt      =  5760.   ! time step for the dynamics and tracer
  rn_atfp     =    0.1   ! asselin time filter parameter
  !
  ln_crs      = .false.  ! Logical switch for coarsening module      (T => fill namcrs)
/

```

In  $z$ -coordinate partial step, the depths of the model levels are defined by the reference analytical function  $z_0(k)$  as described in the previous section, *except* in the bottom layer. The thickness of the bottom layer is allowed to vary as a function of geographical location  $(\lambda, \varphi)$  to allow a better representation of the bathymetry, especially in the case of small slopes (where the bathymetry varies by less than one level thickness from one grid point to the next). The reference layer thicknesses  $e_{3t}^0$  have been defined in the absence of bathymetry. With partial steps, layers from 1 to  $jp_k-2$  can have a thickness smaller than  $e_{3t}(jp_k)$ . The model deepest layer ( $jp_k-1$ ) is allowed to have either a smaller or larger thickness than  $e_{3t}(jp_k)$ : the maximum thickness allowed is  $2 * e_{3t}(jp_k - 1)$ . This has to be kept in mind when specifying values in *namdom* namelist, as the maximum depth  $pph_{max}$  in partial steps: for example, with  $pph_{max}= 5750 m$  for the DRAKKAR 45 layer grid, the maximum ocean depth allowed is actually  $6000 m$  (the default thickness  $e_{3t}(jp_k - 1)$  being  $250 m$ ). Two variables in the *namdom* namelist are used to define the partial step vertical grid. The minimum water thickness (in meters) allowed for a cell partially filled with bathymetry at level  $jk$  is the minimum of  $rn.e3zps_{min}$  (thickness in



**Table 4.2:** Default vertical mesh in  $z$ -coordinate for 30 layers ORCA2 configuration as computed from (4.14) using the coefficients given in (4.15)

LEVEL	<b>gdept_1d</b>	<b>gdepw_1d</b>	<b>e3t_1d</b>	<b>e3w_1d</b>
1	<b>5.00</b>	0.00	<b>10.00</b>	10.00
2	<b>15.00</b>	10.00	<b>10.00</b>	10.00
3	<b>25.00</b>	20.00	<b>10.00</b>	10.00
4	<b>35.01</b>	30.00	<b>10.01</b>	10.00
5	<b>45.01</b>	40.01	<b>10.01</b>	10.01
6	<b>55.03</b>	50.02	<b>10.02</b>	10.02
7	<b>65.06</b>	60.04	<b>10.04</b>	10.03
8	<b>75.13</b>	70.09	<b>10.09</b>	10.06
9	<b>85.25</b>	80.18	<b>10.17</b>	10.12
10	<b>95.49</b>	90.35	<b>10.33</b>	10.24
11	<b>105.97</b>	100.69	<b>10.65</b>	10.47
12	<b>116.90</b>	111.36	<b>11.27</b>	10.91
13	<b>128.70</b>	122.65	<b>12.47</b>	11.77
14	<b>142.20</b>	135.16	<b>14.78</b>	13.43
15	<b>158.96</b>	150.03	<b>19.23</b>	16.65
16	<b>181.96</b>	169.42	<b>27.66</b>	22.78
17	<b>216.65</b>	197.37	<b>43.26</b>	34.30
18	<b>272.48</b>	241.13	<b>70.88</b>	55.21
19	<b>364.30</b>	312.74	<b>116.11</b>	90.99
20	<b>511.53</b>	429.72	<b>181.55</b>	146.43
21	<b>732.20</b>	611.89	<b>261.03</b>	220.35
22	<b>1033.22</b>	872.87	<b>339.39</b>	301.42
23	<b>1405.70</b>	1211.59	<b>402.26</b>	373.31
24	<b>1830.89</b>	1612.98	<b>444.87</b>	426.00
25	<b>2289.77</b>	2057.13	<b>470.55</b>	459.47
26	<b>2768.24</b>	2527.22	<b>484.95</b>	478.83
27	<b>3257.48</b>	3011.90	<b>492.70</b>	489.44
28	<b>3752.44</b>	3504.46	<b>496.78</b>	495.07
29	<b>4250.40</b>	4001.16	<b>498.90</b>	498.02
30	<b>4749.91</b>	4500.02	<b>500.00</b>	499.54
31	<b>5250.23</b>	5000.00	<b>500.56</b>	500.33

meters, usually 20 *m*) or  $e_{3t}(jk) * rn\_e3zps\_rat$  (a fraction, usually 10%, of the default thickness  $e_{3t}(jk)$ ).

#### 4.4.4 *s*-coordinate (*ln\_sco=true*)

Options are defined in *namzgr\_sco*. In *s*-coordinate (*ln\_sco = true*), the depth and thickness of the model levels are defined from the product of a depth field and either a stretching function or its derivative, respectively:

$$\begin{aligned} z(k) &= h(i, j) z_0(k) \\ e_3(k) &= h(i, j) z'_0(k) \end{aligned} \quad (4.16)$$

where  $h$  is the depth of the last  $w$ -level ( $z_0(k)$ ) defined at the  $t$ -point location in the horizontal and  $z_0(k)$  is a function which varies from 0 at the sea surface to 1 at the ocean bottom. The depth field  $h$  is not necessary the ocean depth, since a mixed step-like and bottom-following representation of the topography can be used (Fig. 4.5d-e) or an envelop bathymetry can be defined (Fig. 4.5f). The namelist parameter *rn\_rmax* determines the slope at which the terrain-following coordinate intersects the sea bed and becomes a pseudo  $z$ -coordinate. The coordinate can also be hybridised by specifying *rn\_sbot\_min* and *rn\_sbot\_max* as the minimum and maximum depths at which the terrain-following vertical coordinate is calculated.

Options for stretching the coordinate are provided as examples, but care must be taken to ensure that the vertical stretch used is appropriate for the application.

The original default NEMO *s*-coordinate stretching is available if neither of the other options are specified as true (*ln\_s\_SH94 = false* and *ln\_s\_SF12 = false*). This uses a depth independent tanh function for the stretching [Madec et al. 1996]:

$$z = s_{min} + C(s)(H - s_{min}) \quad (4.17)$$

where  $s_{min}$  is the depth at which the *s*-coordinate stretching starts and allows a  $z$ -coordinate to be placed on top of the stretched coordinate, and  $z$  is the depth (negative down from the sea surface).

$$s = -\frac{k}{n-1} \quad \text{and} \quad 0 \leq k \leq n-1 \quad (4.18)$$

$$C(s) = \frac{[\tanh(\theta(s+b)) - \tanh(\theta b)]}{2 \sinh(\theta)} \quad (4.19)$$

A stretching function, modified from the commonly used Song and Haidvogel [1994] stretching (*ln\_s\_SH94 = true*), is also available and is more commonly used for shelf seas modelling:

$$C(s) = (1-b) \frac{\sinh(\theta s)}{\sinh(\theta)} + b \frac{\tanh[\theta(s + \frac{1}{2})] - \tanh(\frac{\theta}{2})}{2 \tanh(\frac{\theta}{2})} \quad (4.20)$$

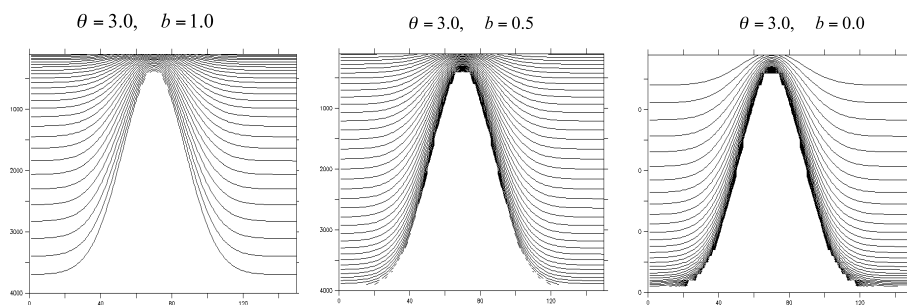


**Figure 4.7:** Examples of the stretching function applied to a seamount; from left to right: surface, surface and bottom, and bottom intensified resolutions

where  $H_c$  is the critical depth (*rn\_hc*) at which the coordinate transitions from pure  $\sigma$  to the stretched coordinate, and  $\theta$  (*rn\_theta*) and  $b$  (*rn\_bb*) are the surface and bottom control parameters such that  $0 \leq \theta \leq 20$ , and  $0 \leq b \leq 1$ .  $b$  has been designed to allow surface and/or bottom increase of the vertical resolution (Fig. 4.7).

Another example has been provided at version 3.5 (*ln\_s\_SF12*) that allows a fixed surface resolution in an analytical terrain-following stretching Siddorn and Furner [2012]. In this case the a stretching function  $\gamma$  is defined such that:

$$z = -\gamma h \quad \text{with} \quad 0 \leq \gamma \leq 1 \quad (4.21)$$

The function is defined with respect to  $\sigma$ , the unstretched terrain-following coordinate:

$$\gamma = A \left( \sigma - \frac{1}{2} (\sigma^2 + f(\sigma)) \right) + B (\sigma^3 - f(\sigma)) + f(\sigma) \quad (4.22)$$

Where:

$$f(\sigma) = (\alpha + 2) \sigma^{\alpha+1} - (\alpha + 1) \sigma^{\alpha+2} \quad \text{and} \quad \sigma = \frac{k}{n-1} \quad (4.23)$$

This gives an analytical stretching of  $\sigma$  that is solvable in  $A$  and  $B$  as a function of the user prescribed stretching parameter  $\alpha$  (*rn\_alpha*) that stretches towards the surface ( $\alpha > 1.0$ ) or the bottom ( $\alpha < 1.0$ ) and user prescribed surface (*rn\_zs*) and bottom depths. The bottom cell depth in this example is given as a function of water depth:

$$Z_b = ha + b \quad (4.24)$$

where the namelist parameters *rn\_zb\_a* and *rn\_zb\_b* are  $a$  and  $b$  respectively.

This gives a smooth analytical stretching in computational space that is constrained to given specified surface and bottom grid cell thicknesses in real space.

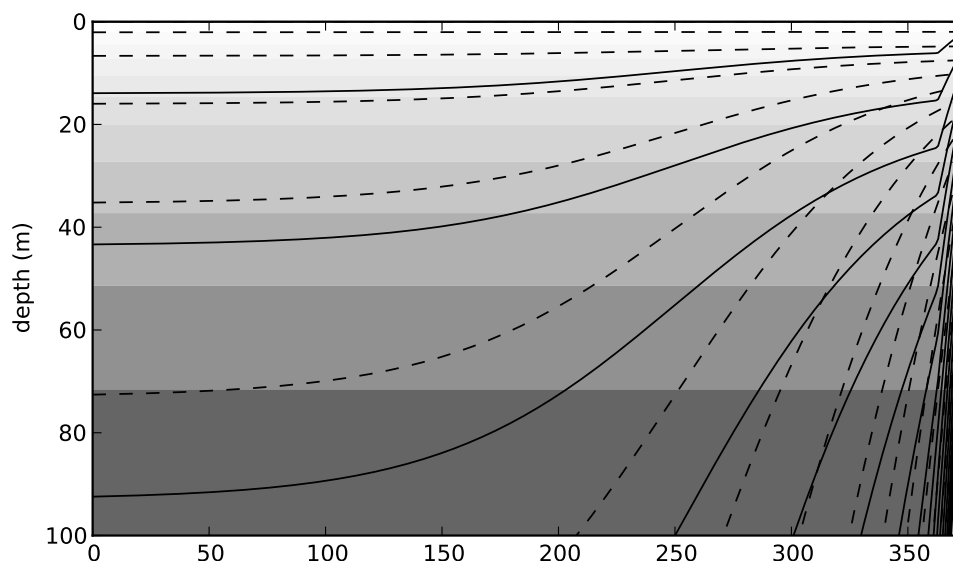


**Figure 4.8:** A comparison of the [Song and Haidvogel \[1994\]](#)  $S$ -coordinate (solid lines), a 50 level  $Z$ -coordinate (contoured surfaces) and the [Siddorn and Furner \[2012\]](#)  $S$ -coordinate (dashed lines) in the surface 100m for a idealised bathymetry that goes from 50m to 5500m depth. For clarity every third coordinate surface is shown.

This is not to be confused with the hybrid schemes that superimpose geopotential coordinates on terrain following coordinates thus creating a non-analytical vertical coordinate that therefore may suffer from large gradients in the vertical resolutions. This stretching is less straightforward to implement than the [Song and Haidvogel \[1994\]](#) stretching, but has the advantage of resolving diurnal processes in deep water and has generally flatter slopes.

As with the [Song and Haidvogel \[1994\]](#) stretching the stretch is only applied at depths greater than the critical depth  $h_c$ . In this example two options are available in depths shallower than  $h_c$ , with pure sigma being applied if the `ln_sigcrit` is true and pure  $z$ -coordinates if it is false (the  $z$ -coordinate being equal to the depths of the stretched coordinate at  $h_c$ ).

Minimising the horizontal slope of the vertical coordinate is important in terrain-following systems as large slopes lead to hydrostatic consistency. A hydrostatic consistency parameter diagnostic following [Haney \[1991\]](#) has been implemented, and is output as part of the model mesh file at the start of the run.

#### 4.4.5 $z^*$ - or $s^*$ -coordinate (`ln_linssh=false`)

This option is described in the Report by [Levier \*et al.\* \(2007\)](#), available on the *NEMO* web site.

#### 4.4.6 level bathymetry and mask

Whatever the vertical coordinate used, the model offers the possibility of representing the bottom topography with steps that follow the face of the model cells (step like topography) [Madec et al. 1996]. The distribution of the steps in the horizontal is defined in a 2D integer array, *mbathy*, which gives the number of ocean levels (*i.e.* those that are not masked) at each *t*-point. *mbathy* is computed from the meter bathymetry using the definition of *gdept* as the number of *t*-points which  $gdept \leq bathy$ .

Modifications of the model bathymetry are performed in the *bat\_ctl* routine (see *domzgr.F90* module) after *mbathy* is computed. Isolated grid points that do not communicate with another ocean point at the same level are eliminated.

As for the representation of bathymetry, a 2D integer array, *misfdep*, is created. *misfdep* defines the level of the first wet *t*-point. All the cells between  $k = 1$  and  $misfdep(i, j) - 1$  are masked. By default,  $misfdep(:, :) = 1$  and no cells are masked.

In case of ice shelf cavities, modifications of the model bathymetry and ice shelf draft into the cavities are performed in the *zgr\_isf* routine. The compatibility between ice shelf draft and bathymetry is checked. All the locations where the ice shelf is thinnest than *rn\_isfmin* meters are grounded (*i.e.* masked). If only one cell on the water column is opened at *t*-, *u*- or *v*-points, the bathymetry or the ice shelf draft is dug to fit this constrain. If the incompatibility is too strong (need to dig more than 1 cell), the cell is masked.

From the *mbathy* and *misfdep* array, the mask fields are defined as follows:

$$tmask(i, j, k) = \begin{cases} 0 & \text{if } k < misfdep(i, j) \\ 1 & \text{if } misfdep(i, j) \leq k \leq mbathy(i, j) \\ 0 & \text{if } k > mbathy(i, j) \end{cases}$$

$$umask(i, j, k) = tmask(i, j, k) * tmask(i + 1, j, k)$$

$$vmask(i, j, k) = tmask(i, j, k) * tmask(i, j + 1, k)$$

$$fmask(i, j, k) = tmask(i, j, k) * tmask(i + 1, j, k) \\ * tmask(i, j, k) * tmask(i + 1, j, k)$$

$$wmask(i, j, k) = tmask(i, j, k) * tmask(i, j, k - 1) \text{ with } wmask(i, j, 1) = tmask(i, j, 1)$$

Note that, without ice shelves cavities, masks at *t*- and *w*-points are identical with the numerical indexing used (§ 4.1.3). Nevertheless, *wmask* are required with ocean cavities to deal with the top boundary (ice shelf/ocean interface) exactly in the same way as for the bottom boundary.

The specification of closed lateral boundaries requires that at least the first and last rows and columns of the *mbathy* array are set to zero. In the particular case of an east-west cyclical boundary condition, *mbathy* has its last column equal to the second one and its first column equal to the last but one (and so too the mask arrays) (see § 8.2).

## 4.5 Domain: Initial State (*istate.F90* and *dtatsd.F90* modules)

```

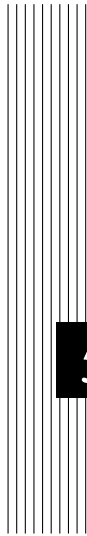
!-----
&namtsd      ! data : Temperature & Salinity
!-----
!           ! file name           ! frequency (hours) ! variable ! time interp.! clim ! 'yearly' / ! weights ! rot
!           ! (if <0 months) ! name ! (logical) ! (T/F) ! 'monthly' ! filename ! pair
sn_tem = 'data_lm_potential_temperature_nomask', -1 , 'votemper', .true. , .true. , 'yearly' , ' ' , ' '
sn_sal = 'data_lm_salinity_nomask' , -1 , 'vosaline', .true. , .true. , 'yearly' , ' ' , ' '
!
cn_dir      = './'           ! root directory for the location of the runoff files
ln_tsd_init = .true.        ! Initialisation of ocean T & S with T & S input data (T) or not (F)
ln_tsd_tradmp = .true.     ! damping of ocean T & S toward T & S input data (T) or not (F)
/

```

Options are defined in *namtsd*. By default, the ocean start from rest (the velocity field is set to zero) and the initialization of temperature and salinity fields is controlled through the *ln\_tsd.ini* namelist parameter.

**ln\_tsd\_init = .true.** use a T and S input files that can be given on the model grid itself or on their native input data grid. In the latter case, the data will be interpolated on-the-fly both in the horizontal and the vertical to the model grid (see § 7.2.2). The information relative to the input files are given in the *sn\_tem* and *sn\_sal* structures. The computation is done in the *dtatsd.F90* module.

**ln\_tsd\_init = .false.** use constant salinity value of 35.5 psu and an analytical profile of temperature (typical of the tropical ocean), see *istate.t.s* subroutine called from *istate.F90* module.



## 5 Ocean Tracers (TRA)

### Contents

---

<b>5.1</b>	<b>Tracer Advection (<i>traadv</i>)</b> . . . . .	<b>71</b>
5.1.1	Centred schemes (CEN) ( <i>ln_traadv_cen</i> ) . . . . .	73
5.1.2	Flux Corrected Transport schemes (FCT) ( <i>ln_traadv_fct</i> )	74
5.1.3	MUSCL scheme ( <i>ln_traadv_mus</i> ) . . . . .	75
5.1.4	Upstream-Biased Scheme (UBS) ( <i>ln_traadv_ubs</i> ) . . . . .	76
5.1.5	QUICKEST scheme (QCK) ( <i>ln_traadv_qck</i> ) . . . . .	77
<b>5.2</b>	<b>Tracer Lateral Diffusion (<i>traldf</i>)</b> . . . . .	<b>77</b>
5.2.1	Type of operator ( <i>ln_traldf_NONE</i> , <i>ln_traldf_lap</i> , <i>ln_traldf_blp</i> )	78
5.2.2	Direction of action ( <i>ln_traldf_lev</i> , <i>ln_traldf_hor</i> , <i>ln_traldf_iso</i> , <i>ln_traldf_triad</i> ) . . . . .	79
5.2.3	Iso-level (bi-)laplacian operator ( <i>ln_traldf_iso</i> ) . . . . .	79
5.2.4	Standard and triad rotated (bi-)laplacian operator ( <i>traldf_iso.F90</i> , <i>traldf_triad.F90</i> ) . . . . .	80
<b>5.3</b>	<b>Tracer Vertical Diffusion (<i>trazdf</i>)</b> . . . . .	<b>81</b>
<b>5.4</b>	<b>External Forcing</b> . . . . .	<b>82</b>
5.4.1	Surface boundary condition ( <i>trasbc</i> ) . . . . .	82
5.4.2	Solar Radiation Penetration ( <i>traqsr</i> ) . . . . .	83
5.4.3	Bottom Boundary Condition ( <i>trabbc</i> ) . . . . .	85
<b>5.5</b>	<b>Bottom Boundary Layer (<i>trabbl.F90</i> - <i>key_trabbl</i>)</b> . . . . .	<b>87</b>
5.5.1	Diffusive Bottom Boundary layer ( <i>nn_bbl_ldf=1</i> ) . . . . .	88
5.5.2	Advective Bottom Boundary Layer ( <i>nn_bbl_adv= 1 or 2</i> )	88
<b>5.6</b>	<b>Tracer damping (<i>tradmp</i>)</b> . . . . .	<b>90</b>
5.6.1	DMP_TOOLS . . . . .	91

---

<b>5.7</b>	<b>Tracer time evolution (<i>tranxt</i>)</b> . . . . .	<b>92</b>
<b>5.8</b>	<b>Equation of State (<i>eosbn2</i>)</b> . . . . .	<b>93</b>
5.8.1	Equation Of Seawater ( <i>nn_eos</i> = -1, 0, or 1) . . . . .	93
5.8.2	Brunt-Väisälä Frequency ( <i>nn_eos</i> = 0, 1 or 2) . . . . .	95
5.8.3	Freezing Point of Seawater . . . . .	96
<b>5.9</b>	<b>Horizontal Derivative in <i>zps</i>-coordinate (<i>zpsjde</i>)</b> . . . . .	<b>96</b>

---

Using the representation described in Chap. 4, several semi-discrete space forms of the tracer equations are available depending on the vertical coordinate used and on the physics used. In all the equations presented here, the masking has been omitted for simplicity. One must be aware that all the quantities are masked fields and that each time a mean or difference operator is used, the resulting field is multiplied by a mask.

The two active tracers are potential temperature and salinity. Their prognostic equations can be summarized as follows:

$$\text{NXT} = \text{ADV} + \text{LDF} + \text{ZDF} + \text{SBC} (+\text{QSR}) (+\text{BBC}) (+\text{BBL}) (+\text{DMP})$$

NXT stands for next, referring to the time-stepping. From left to right, the terms on the rhs of the tracer equations are the advection (ADV), the lateral diffusion (LDF), the vertical diffusion (ZDF), the contributions from the external forcings (SBC: Surface Boundary Condition, QSR: penetrative Solar Radiation, and BBC: Bottom Boundary Condition), the contribution from the bottom boundary Layer (BBL) parametrisation, and an internal damping (DMP) term. The terms QSR, BBC, BBL and DMP are optional. The external forcings and parameterisations require complex inputs and complex calculations (*e.g.* bulk formulae, estimation of mixing coefficients) that are carried out in the SBC, LDF and ZDF modules and described in chapters §7, §9 and §10, respectively. Note that *tranpc.F90*, the non-penetrative convection module, although located in the NEMO/OPA/TRA directory as it directly modifies the tracer fields, is described with the model vertical physics (ZDF) together with other available parameterization of convection.

In the present chapter we also describe the diagnostic equations used to compute the sea-water properties (density, Brunt-Väisälä frequency, specific heat and freezing point with associated modules *eosbn2.F90* and *phycst.F90*).

The different options available to the user are managed by namelist logicals or CPP keys. For each equation term *TTT*, the namelist logicals are *ln\_traTTT\_xxx*, where *xxx* is a 3 or 4 letter acronym corresponding to each optional scheme. The CPP key (when it exists) is **key\_traTTT**. The equivalent code can be found in the *traTTT* or *traTTT\_xxx* module, in the NEMO/OPA/TRA directory.



The user has the option of extracting each tendency term on the RHS of the tracer equation for output (*ln\_tra\_trd* or *ln\_tra\_mxl* = true), as described in Chap. 11.

## 5.1 Tracer Advection (*traadv.F90*)

```

!-----
&namtra_adv  !  advection scheme for tracer                               (default: NO selection)
!-----
ln_traadv_NONE= .false. ! No tracer advection
ln_traadv_cen = .false. ! 2nd order centered scheme
  nn_cen_h   = 4          ! =2/4, horizontal 2nd order CEN / 4th order CEN
  nn_cen_v   = 4          ! =2/4, vertical 2nd order CEN / 4th order COMPACT
ln_traadv_fct = .false. ! FCT scheme
  nn_fct_h   = 2          ! =2/4, horizontal 2nd / 4th order
  nn_fct_v   = 2          ! =2/4, vertical 2nd / COMPACT 4th order
ln_traadv_mus = .false. ! MUSCL scheme
  ln_mus_ups = .false.   ! use upstream scheme near river mouths
ln_traadv_ubs = .false. ! UBS scheme
  nn_ubs_v   = 2          ! =2, vertical 2nd order FCT / COMPACT 4th order
ln_traadv_qck = .false. ! QUICKEST scheme
/

```

When considered (*i.e.* when *ln\_traadv\_NONE* is not set to *true*), the advection tendency of a tracer is expressed in flux form, *i.e.* as the divergence of the advective fluxes. Its discrete expression is given by :

$$ADV_{\tau} = -\frac{1}{b_t} ( \delta_i [e_{2u} e_{3u} u \tau_u] + \delta_j [e_{1v} e_{3v} v \tau_v] ) - \frac{1}{e_{3t}} \delta_k [w \tau_w] \quad (5.1)$$

where  $\tau$  is either T or S, and  $b_t = e_{1t} e_{2t} e_{3t}$  is the volume of  $T$ -cells. The flux form in (5.1) implicitly requires the use of the continuity equation. Indeed, it is obtained by using the following equality :  $\nabla \cdot (\mathbf{U} T) = \mathbf{U} \cdot \nabla T$  which results from the use of the continuity equation,  $\partial_t e_3 + e_3 \nabla \cdot \mathbf{U} = 0$  (which reduces to  $\nabla \cdot \mathbf{U} = 0$  in linear free surface, *i.e.* *ln\_linssh*=true). Therefore it is of paramount importance to design the discrete analogue of the advection tendency so that it is consistent with the continuity equation in order to enforce the conservation properties of the continuous equations. In other words, by setting  $\tau = 1$  in (5.1) we recover the discrete form of the continuity equation which is used to calculate the vertical velocity.

The key difference between the advection schemes available in *NEMO* is the choice made in space and time interpolation to define the value of the tracer at the velocity points (Fig. 5.1).

Along solid lateral and bottom boundaries a zero tracer flux is automatically specified, since the normal velocity is zero there. At the sea surface the boundary condition depends on the type of sea surface chosen:

**linear free surface:** (*ln\_linssh*=true) the first level thickness is constant in time: the vertical boundary condition is applied at the fixed surface  $z = 0$  rather than on the moving surface  $z = \eta$ . There is a non-zero advective flux which is set for all advection schemes as  $\tau_w|_{k=1/2} = T_{k=1}$ , *i.e.* the product of surface velocity (at  $z = 0$ ) by the first level tracer value.

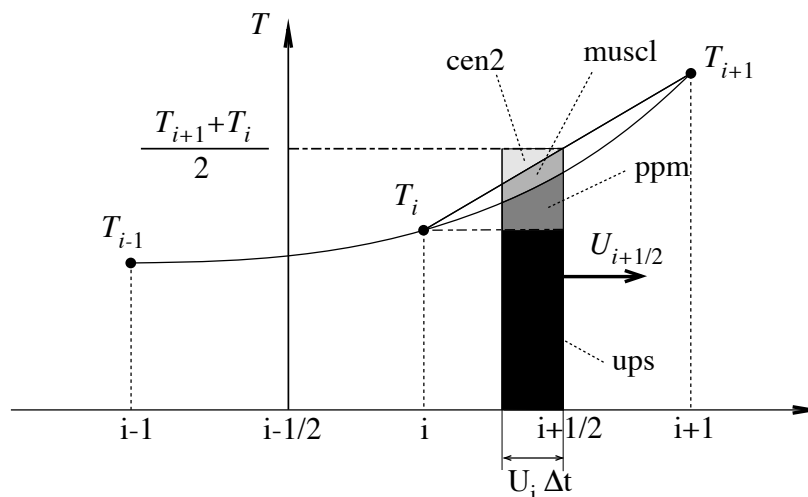


**Figure 5.1:** Schematic representation of some ways used to evaluate the tracer value at  $u$ -point and the amount of tracer exchanged between two neighbouring grid points. Upstream biased scheme (ups): the upstream value is used and the black area is exchanged. Piecewise parabolic method (ppm): a parabolic interpolation is used and the black and dark grey areas are exchanged. Monotonic upstream scheme for conservative laws (muscl): a parabolic interpolation is used and black, dark grey and grey areas are exchanged. Second order scheme (cen2): the mean value is used and black, dark grey, grey and light grey areas are exchanged. Note that this illustration does not include the flux limiter used in ppm and muscl schemes.

**non-linear free surface:** ( $ln\_linssh=false$ ) convergence/divergence in the first ocean level moves the free surface up/down. There is no tracer advection through it so that the advective fluxes through the surface are also zero

In all cases, this boundary condition retains local conservation of tracer. Global conservation is obtained in non-linear free surface case, but *not* in the linear free surface case. Nevertheless, in the latter case, it is achieved to a good approximation since the non-conservative term is the product of the time derivative of the tracer and the free surface height, two quantities that are not correlated [Roullet and Madec 2000, Griffies et al. 2001, Campin et al. 2004].

The velocity field that appears in (5.1) and (??) is the centred (*now*) *effective* ocean velocity, *i.e.* the *eulerian* velocity (see Chap. 6) plus the eddy induced velocity (*eiv*) and/or the mixed layer eddy induced velocity (*eiv*) when those parameterisations are used (see Chap. 9).

Several tracer advection scheme are proposed, namely a  $2^{nd}$  or  $4^{th}$  order centred schemes (CEN), a  $2^{nd}$  or  $4^{th}$  order Flux Corrected Transport scheme (FCT),

a Monotone Upstream Scheme for Conservative Laws scheme (MUSCL), a 3<sup>rd</sup> Upstream Biased Scheme (UBS, also often called UP3), and a Quadratic Upstream Interpolation for Convective Kinematics with Estimated Streaming Terms scheme (QUICKEST). The choice is made in the *namtra\_adv* namelist, by setting to *true* one of the logicals *ln\_traadv\_xxx*. The corresponding code can be found in the *traadv\_xxx.F90* module, where *xxx* is a 3 or 4 letter acronym corresponding to each scheme. By default (*i.e.* in the reference namelist, *namelist\_ref*), all the logicals are set to *false*. If the user does not select an advection scheme in the configuration namelist (*namelist\_cfg*), the tracers will *not* be advected !

Details of the advection schemes are given below. The choosing an advection scheme is a complex matter which depends on the model physics, model resolution, type of tracer, as well as the issue of numerical cost. In particular, we note that (1) CEN and FCT schemes require an explicit diffusion operator while the other schemes are diffusive enough so that they do not necessarily need additional diffusion ; (2) CEN and UBS are not *positive* schemes <sup>1</sup>, implying that false extrema are permitted. Their use is not recommended on passive tracers ; (3) It is recommended that the same advection-diffusion scheme is used on both active and passive tracers. Indeed, if a source or sink of a passive tracer depends on an active one, the difference of treatment of active and passive tracers can create very nice-looking frontal structures that are pure numerical artefacts. Nevertheless, most of our users set a different treatment on passive and active tracers, that's the reason why this possibility is offered. We strongly suggest them to perform a sensitivity experiment using a same treatment to assess the robustness of their results.

### 5.1.1 Centred schemes (CEN) (*ln\_traadv\_cen=true*)

The centred advection scheme (CEN) is used when *ln\_traadv\_cen = true*. Its order (2<sup>nd</sup> or 4<sup>th</sup>) can be chosen independently on horizontal (iso-level) and vertical direction by setting *nn\_cen\_h* and *nn\_cen\_v* to 2 or 4. CEN implementation can be found in the *traadv\_cen.F90* module.

In the 2<sup>nd</sup> order centred formulation (CEN2), the tracer at velocity points is evaluated as the mean of the two neighbouring *T*-point values. For example, in the *i*-direction :

$$\tau_u^{cen2} = \bar{T}^{i+1/2} \quad (5.2)$$

CEN2 is non diffusive (*i.e.* it conserves the tracer variance,  $\tau^2$ ) but dispersive (*i.e.* it may create false extrema). It is therefore notoriously noisy and must be used in conjunction with an explicit diffusion operator to produce a sensible solution. The associated time-stepping is performed using a leapfrog scheme in conjunction with an Asselin time-filter, so *T* in (5.2) is the *now* tracer value.

Note that using the CEN2, the overall tracer advection is of second order accuracy since both (5.1) and (5.2) have this order of accuracy.

<sup>1</sup>negative values can appear in an initially strictly positive tracer field which is advected

In the 4<sup>th</sup> order formulation (CEN4), tracer values are evaluated at u- and v-points as a 4<sup>th</sup> order interpolation, and thus depend on the four neighbouring  $T$ -points. For example, in the  $i$ -direction:

$$\tau_u^{cen4} = T - \frac{1}{6} \delta_i [\delta_{i+1/2}[T]]^{i+1/2} \quad (5.3)$$

In the vertical direction ( $nn\_cen\_v=4$ ), a 4<sup>th</sup> COMPACT interpolation has been preferred [Demange 2014]. In the COMPACT scheme, both the field and its derivative are interpolated, which leads, after a matrix inversion, spectral characteristics similar to schemes of higher order [Lele 1992].

Strictly speaking, the CEN4 scheme is not a 4<sup>th</sup> order advection scheme but a 4<sup>th</sup> order evaluation of advective fluxes, since the divergence of advective fluxes (5.1) is kept at 2<sup>nd</sup> order. The expression 4<sup>th</sup> order scheme used in oceanographic literature is usually associated with the scheme presented here. Introducing a true 4<sup>th</sup> order advection scheme is feasible but, for consistency reasons, it requires changes in the discretisation of the tracer advection together with changes in the continuity equation, and the momentum advection and pressure terms.

A direct consequence of the pseudo-fourth order nature of the scheme is that it is not non-diffusive, *i.e.* the global variance of a tracer is not preserved using CEN4. Furthermore, it must be used in conjunction with an explicit diffusion operator to produce a sensible solution. As in CEN2 case, the time-stepping is performed using a leapfrog scheme in conjunction with an Asselin time-filter, so  $T$  in (5.3) is the *now* tracer.

At a  $T$ -grid cell adjacent to a boundary (coastline, bottom and surface), an additional hypothesis must be made to evaluate  $\tau_u^{cen4}$ . This hypothesis usually reduces the order of the scheme. Here we choose to set the gradient of  $T$  across the boundary to zero. Alternative conditions can be specified, such as a reduction to a second order scheme for these near boundary grid points.

### 5.1.2 Flux Corrected Transport schemes (FCT) (*ln\_traadv\_fct=true*)

The Flux Corrected Transport schemes (FCT) is used when *ln\_traadv\_fct = true*. Its order (2<sup>nd</sup> or 4<sup>th</sup>) can be chosen independently on horizontal (iso-level) and vertical direction by setting *nn\_fct\_h* and *nn\_fct\_v* to 2 or 4. FCT implementation can be found in the *traadv\_fct.F90* module.

In FCT formulation, the tracer at velocity points is evaluated using a combination of an upstream and a centred scheme. For example, in the  $i$ -direction :

$$\tau_u^{ups} = \begin{cases} T_{i+1} & \text{if } u_{i+1/2} < 0 \\ T_i & \text{if } u_{i+1/2} \geq 0 \end{cases} \quad (5.4)$$

$$\tau_u^{fct} = \tau_u^{ups} + c_u (\tau_u^{cen} - \tau_u^{ups})$$

where  $c_u$  is a flux limiter function taking values between 0 and 1. The FCT order is the one of the centred scheme used (*i.e.* it depends on the setting of *nn\_fct\_h* and *nn\_fct\_v*). There exist many ways to define  $c_u$ , each corresponding to a different FCT scheme. The one chosen in *NEMO* is described in Zalesak [1979].  $c_u$  only departs from 1 when the advective term produces a local extremum in the tracer field. The resulting scheme is quite expensive but *positive*. It can be used on both active and passive tracers. A comparison of FCT-2 with MUSCL and a MPDATA scheme can be found in Lévy et al. [2001].

An additional option has been added controlled by *nn\_fct\_zts*. By setting this integer to a value larger than zero, a  $2^{nd}$  order FCT scheme is used on both horizontal and vertical direction, but on the latter, a split-explicit time stepping is used, with a number of sub-timestep equals to *nn\_fct\_zts*. This option can be useful when the size of the timestep is limited by vertical advection [Lemarié et al. 2015]. Note that in this case, a similar split-explicit time stepping should be used on vertical advection of momentum to insure a better stability (see §6.2.3).

For stability reasons (see §3),  $\tau_u^{cen}$  is evaluated in (5.4) using the *now* tracer while  $\tau_u^{ups}$  is evaluated using the *before* tracer. In other words, the advective part of the scheme is time stepped with a leap-frog scheme while a forward scheme is used for the diffusive part.

### 5.1.3 Monotone Upstream Scheme for Conservative Laws (MUSCL) (*ln\_traadv\_mus=T*)

The Monotone Upstream Scheme for Conservative Laws (MUSCL) is used when *ln\_traadv\_mus = true*. MUSCL implementation can be found in the *traadv\_mus.F90* module.

MUSCL has been first implemented in *NEMO* by Lévy et al. [2001]. In its formulation, the tracer at velocity points is evaluated assuming a linear tracer variation between two *T*-points (Fig.5.1). For example, in the *i*-direction :

$$\tau_u^{mus} = \begin{cases} \tau_i & + \frac{1}{2} \left( 1 - \frac{u_{i+1/2} \Delta t}{e_{1u}} \right) \widetilde{\partial}_i \tau & \text{if } u_{i+1/2} \geq 0 \\ \tau_{i+1/2} & + \frac{1}{2} \left( 1 + \frac{u_{i+1/2} \Delta t}{e_{1u}} \right) \widetilde{\partial}_{i+1/2} \tau & \text{if } u_{i+1/2} < 0 \end{cases} \quad (5.5)$$

where  $\widetilde{\partial}_i \tau$  is the slope of the tracer on which a limitation is imposed to ensure the *positive* character of the scheme.

The time stepping is performed using a forward scheme, that is the *before* tracer field is used to evaluate  $\tau_u^{mus}$ .

For an ocean grid point adjacent to land and where the ocean velocity is directed toward land, an upstream flux is used. This choice ensure the *positive* character of the scheme. In addition, fluxes round a grid-point where a runoff is applied can optionally be computed using upstream fluxes (*ln\_mus\_ups = true*).

### 5.1.4 Upstream-Biased Scheme (UBS) (*ln\_traadv\_ubs=true*)

The Upstream-Biased Scheme (UBS) is used when *ln\_traadv\_ubs = true*. UBS implementation can be found in the *traadv\_mus.F90* module.

The UBS scheme, often called UP3, is also known as the Cell Averaged QUICK scheme (Quadratic Upstream Interpolation for Convective Kinematics). It is an upstream-biased third order scheme based on an upstream-biased parabolic interpolation. For example, in the *i*-direction :

$$\tau_u^{ubs} = \bar{T}^{i+1/2} - \frac{1}{6} \begin{cases} \tau''_i & \text{if } u_{i+1/2} \geq 0 \\ \tau''_{i+1} & \text{if } u_{i+1/2} < 0 \end{cases} \quad (5.6)$$

where  $\tau''_i = \delta_i [\delta_{i+1/2} [\tau]]$ .

This results in a dissipatively dominant (i.e. hyper-diffusive) truncation error [Shchepetkin and McWilliams 2005]. The overall performance of the advection scheme is similar to that reported in Farrow and Stevens [1995]. It is a relatively good compromise between accuracy and smoothness. Nevertheless the scheme is not *positive*, meaning that false extrema are permitted, but the amplitude of such are significantly reduced over the centred second or fourth order method. therefore it is not recommended that it should be applied to a passive tracer that requires positivity.

The intrinsic diffusion of UBS makes its use risky in the vertical direction where the control of artificial diapycnal fluxes is of paramount importance [Shchepetkin and McWilliams 2005, Demange 2014]. Therefore the vertical flux is evaluated using either a  $2^{\text{nd}}$  order FCT scheme or a  $4^{\text{th}}$  order COMPACT scheme (*nn\_cen\_v=2* or *4*).

For stability reasons (see §3), the first term in (5.6) (which corresponds to a second order centred scheme) is evaluated using the *now* tracer (centred in time) while the second term (which is the diffusive part of the scheme), is evaluated using the *before* tracer (forward in time). This choice is discussed by Webb et al. [1998] in the context of the QUICK advection scheme. UBS and QUICK schemes only differ by one coefficient. Replacing 1/6 with 1/8 in (5.6) leads to the QUICK advection scheme [Webb et al. 1998]. This option is not available through a namelist parameter, since the 1/6 coefficient is hard coded. Nevertheless it is quite easy to make the substitution in the *traadv\_ubs.F90* module and obtain a QUICK scheme.

Note that it is straightforward to rewrite (5.6) as follows:

$$\tau_u^{ubs} = \tau_u^{cen4} + \frac{1}{12} \begin{cases} + \tau''_i & \text{if } u_{i+1/2} \geq 0 \\ - \tau''_{i+1} & \text{if } u_{i+1/2} < 0 \end{cases} \quad (5.7)$$

or equivalently

$$u_{i+1/2} \tau_u^{ubs} = u_{i+1/2} T - \frac{1}{6} \delta_i [\delta_{i+1/2} [T]]^{i+1/2} - \frac{1}{2} |u|_{i+1/2} \frac{1}{6} \delta_{i+1/2} [\tau''_i] \quad (5.8)$$

(5.7) has several advantages. Firstly, it clearly reveals that the UBS scheme is based on the fourth order scheme to which an upstream-biased diffusion term is added. Secondly, this emphasises that the 4<sup>th</sup> order part (as well as the 2<sup>nd</sup> order part as stated above) has to be evaluated at the *now* time step using (5.6). Thirdly, the diffusion term is in fact a biharmonic operator with an eddy coefficient which is simply proportional to the velocity:  $A_u^{lm} = \frac{1}{12} e_{1u}^3 |u|$ . Note the current version of NEMO uses the computationally more efficient formulation (5.6).

### 5.1.5 QUICKEST scheme (QCK) (*ln\_traadv\_qck=true*)

The Quadratic Upstream Interpolation for Convective Kinematics with Estimated Streaming Terms (QUICKEST) scheme proposed by Leonard [1979] is used when *ln\_traadv\_qck = true*. QUICKEST implementation can be found in the *traadv\_qck.F90* module.

QUICKEST is the third order Godunov scheme which is associated with the ULTIMATE QUICKEST limiter [Leonard 1991]. It has been implemented in NEMO by G. Reffray (MERCATOR-ocean) and can be found in the *traadv\_qck.F90* module. The resulting scheme is quite expensive but *positive*. It can be used on both active and passive tracers. However, the intrinsic diffusion of QCK makes its use risky in the vertical direction where the control of artificial diapycnal fluxes is of paramount importance. Therefore the vertical flux is evaluated using the CEN2 scheme. This no longer guarantees the positivity of the scheme. The use of FCT in the vertical direction (as for the UBS case) should be implemented to restore this property.

## 5.2 Tracer Lateral Diffusion (*traldf.F90*)

```

!-----
! namtra_ldf      ! lateral diffusion scheme for tracers                (default: NO selection)
!-----
!
! Operator type:
ln_traldf_NONE = .false. ! No explicit diffusion
ln_traldf_lap  = .false. ! laplacian operator
ln_traldf_blp  = .false. ! bilaplacian operator
!
! Direction of action:
ln_traldf_lev  = .false. ! iso-level
ln_traldf_hor  = .false. ! horizontal (geopotential)
ln_traldf_iso  = .false. ! iso-neutral (standard operator)
ln_traldf_triad = .false. ! iso-neutral (triad operator)
!
! iso-neutral options:
ln_traldf_msc  = .false. ! Method of Stabilizing Correction (both operators)
rn_slpmax     = 0.01    ! slope limit                                (both operators)
ln_triad_iso   = .false. ! pure horizontal mixing in ML                (triad only)
rn_sw_triad    = 1      ! =1 switching triad ; =0 all 4 triads used (triad only)
ln_botmix_triad = .false. ! lateral mixing on bottom                (triad only)
!
! Coefficients:
nn_aht_ijk_t   = 0      ! space/time variation of eddy coef
!
! = -20 (= -30) read in eddy_diffusivity_2D.nc (...3D.nc) file
! = 0 constant
! = 10 F(k) =ldf_c1d
! = 20 F(i,j) =ldf_c2d
! = 21 F(i,j,t) =Treguier et al. JPO 1997 formulation
! = 30 F(i,j,k) =ldf_c2d * ldf_c1d
! = 31 F(i,j,k,t)=F(local velocity and grid-spacing)
rn_aht_0       = 2000.  ! lateral eddy diffusivity (lap. operator) [m2/s]
rn_bht_0       = 1.e+12 ! lateral eddy diffusivity (bilap. operator) [m4/s]

```

Options are defined through the *namtra\_ldf* namelist variables. They are re-grouped in four items, allowing to specify (i) the type of operator used (none, laplacian, bilaplacian), (ii) the direction along which the operator acts (iso-level, horizontal, iso-neutral), (iii) some specific options related to the rotated operators (*i.e.* non-iso-level operator), and (iv) the specification of eddy diffusivity coefficient (either constant or variable in space and time). Item (iv) will be described in Chap.9 . The direction along which the operators act is defined through the slope between this direction and the iso-level surfaces. The slope is computed in the *ldfslp.F90* module and will also be described in Chap. 9.

The lateral diffusion of tracers is evaluated using a forward scheme, *i.e.* the tracers appearing in its expression are the *before* tracers in time, except for the pure vertical component that appears when a rotation tensor is used. This latter component is solved implicitly together with the vertical diffusion term (see §3). When *ln\_traldf\_msc = true*, a Method of Stabilizing Correction is used in which the pure vertical component is split into an explicit and an implicit part [Lemarié et al. 2012].

### 5.2.1 Type of operator (*ln\_traldf\_NONE*, *ln\_traldf\_lap*, or *ln\_traldf\_blp = true*)

Three operator options are proposed and, one and only one of them must be selected:

*ln\_traldf\_NONE* = true : no operator selected, the lateral diffusive tendency will not be applied to the tracer equation. This option can be used when the selected advection scheme is diffusive enough (MUSCL scheme for example).

*ln\_traldf\_lap* = true : a laplacian operator is selected. This harmonic operator takes the following expression:  $\mathcal{L}(T) = \nabla \cdot A_{ht} \nabla T$ , where the gradient operates along the selected direction (see §5.2.2), and  $A_{ht}$  is the eddy diffusivity coefficient expressed in  $m^2/s$  (see Chap. 9).

*ln\_traldf\_blp* = true : a bilaplacian operator is selected. This biharmonic operator takes the following expression:  $\mathcal{B} = -\mathcal{L}(\mathcal{L}(T)) = -\nabla \cdot b \nabla (\nabla \cdot b \nabla T)$  where the gradient operates along the selected direction, and  $b^2 = B_{ht}$  is the eddy diffusivity coefficient expressed in  $m^4/s$  (see Chap. 9). In the code, the bilaplacian operator is obtained by calling the laplacian twice.

Both laplacian and bilaplacian operators ensure the total tracer variance decrease. Their primary role is to provide strong dissipation at the smallest scale supported by the grid while minimizing the impact on the larger scale features. The main difference between the two operators is the scale selectiveness. The bilaplacian damping time (*i.e.* its spin down time) scales like  $\lambda^{-4}$  for disturbances of wavelength  $\lambda$  (so that short waves damped more rapidly than long ones), whereas the laplacian damping time scales only like  $\lambda^{-2}$ .



### 5.2.2 Direction of action (*ln\_traldf\_lev*, ... *hor*, ... *iso*, or ... *triad* = true)

The choice of a direction of action determines the form of operator used. The operator is a simple (re-entrant) laplacian acting in the (*i,j*) plane when iso-level option is used (*ln\_traldf\_lev* = true) or when a horizontal (*i.e.* geopotential) operator is demanded in *z*-coordinate (*ln\_traldf\_hor* and *ln\_zco* equal true). The associated code can be found in the *traldf\_lap\_blp.F90* module. The operator is a rotated (re-entrant) laplacian when the direction along which it acts does not coincide with the iso-level surfaces, that is when standard or triad iso-neutral option is used (*ln\_traldf\_iso* or *ln\_traldf\_triad* equals true, see *traldf\_iso.F90* or *traldf\_triad.F90* module, resp.), or when a horizontal (*i.e.* geopotential) operator is demanded in *s*-coordinate (*ln\_traldf\_hor* and *ln\_sco* equal true)<sup>2</sup>. In that case, a rotation is applied to the gradient(s) that appears in the operator so that diffusive fluxes acts on the three spatial direction.

The resulting discret form of the three operators (one iso-level and two rotated one) is given in the next two sub-sections.

### 5.2.3 Iso-level (bi-)laplacian operator (*ln\_traldf\_iso*)

The laplacian diffusion operator acting along the model (*i,j*)-surfaces is given by:

$$D_i^{IT} = \frac{1}{b_t} \left( \delta_i \left[ A_u^{IT} \frac{e_{2u} e_{3u}}{e_{1u}} \delta_{i+1/2}[T] \right] + \delta_j \left[ A_v^{IT} \frac{e_{1v} e_{3v}}{e_{2v}} \delta_{j+1/2}[T] \right] \right) \quad (5.9)$$

where  $b_t = e_{1t} e_{2t} e_{3t}$  is the volume of *T*-cells and where zero diffusive fluxes is assumed across solid boundaries, first (and third in bilaplacian case) horizontal tracer derivative are masked. It is implemented in the *traldf\_lap* subroutine found in the *traldf\_lap.F90* module. The module also contains *traldf\_blp*, the subroutine calling twice *traldf\_lap* in order to compute the iso-level bilaplacian operator.

It is a *horizontal* operator (*i.e.* acting along geopotential surfaces) in the *z*-coordinate with or without partial steps, but is simply an iso-level operator in the *s*-coordinate. It is thus used when, in addition to *ln\_traldf\_lap* or *ln\_traldf\_blp* = true, we have *ln\_traldf\_lev* = true or *ln\_traldf\_hor* = *ln\_zco* = true. In both cases, it significantly contributes to diapycnal mixing. It is therefore never recommended, even when using it in the bilaplacian case.

Note that in the partial step *z*-coordinate (*ln\_zps*=true), tracers in horizontally adjacent cells are located at different depths in the vicinity of the bottom. In this case, horizontal derivatives in (5.9) at the bottom level require a specific treatment. They are calculated in the *zpsjde.F90* module, described in §5.9.

<sup>2</sup>In this case, the standard iso-neutral operator will be automatically selected

## 5.2.4 Standard and triad (bi-)laplacian operator (*traldf\_iso.F90*, *traldf\_triad.F90*)

### Standard rotated (bi-)laplacian operator (*traldf\_iso.F90*)

The general form of the second order lateral tracer subgrid scale physics (2.34) takes the following semi-discrete space form in  $z$ - and  $s$ -coordinates:

$$\begin{aligned}
 D_T^{lT} = \frac{1}{b_t} \left\{ \delta_i \left[ A_u^{lT} \left( \frac{e_{2u} e_{3u}}{e_{1u}} \delta_{i+1/2}[T] - e_{2u} r_{1u} \overline{\overline{\delta_{k+1/2}[T]}}^{i+1/2,k} \right) \right] \right. \\
 + \delta_j \left[ A_v^{lT} \left( \frac{e_{1v} e_{3v}}{e_{2v}} \delta_{j+1/2}[T] - e_{1v} r_{2v} \overline{\overline{\delta_{k+1/2}[T]}}^{j+1/2,k} \right) \right] \\
 + \delta_k \left[ A_w^{lT} \left( - e_{2w} r_{1w} \overline{\overline{\delta_{i+1/2}[T]}}^{i,k+1/2} \right. \right. \\
 \left. \left. - e_{1w} r_{2w} \overline{\overline{\delta_{j+1/2}[T]}}^{j,k+1/2} \right. \right. \\
 \left. \left. + \frac{e_{1w} e_{2w}}{e_{3w}} (r_{1w}^2 + r_{2w}^2) \delta_{k+1/2}[T] \right) \right] \left. \right\} \quad (5.10)
 \end{aligned}$$

where  $b_t = e_{1t} e_{2t} e_{3t}$  is the volume of  $T$ -cells,  $r_1$  and  $r_2$  are the slopes between the surface of computation ( $z$ - or  $s$ -surfaces) and the surface along which the diffusion operator acts (*i.e.* horizontal or iso-neutral surfaces). It is thus used when, in addition to  $ln\_traldf\_lap = true$ , we have  $ln\_traldf\_iso = true$ , or both  $ln\_traldf\_hor = true$  and  $ln\_zco = true$ . The way these slopes are evaluated is given in §9.1. At the surface, bottom and lateral boundaries, the turbulent fluxes of heat and salt are set to zero using the mask technique (see §8.1).

The operator in (5.10) involves both lateral and vertical derivatives. For numerical stability, the vertical second derivative must be solved using the same implicit time scheme as that used in the vertical physics (see §5.3). For computer efficiency reasons, this term is not computed in the *traldf\_iso.F90* module, but in the *trazdf.F90* module where, if iso-neutral mixing is used, the vertical mixing coefficient is simply increased by  $\frac{e_{1w} e_{2w}}{e_{3w}} (r_{1w}^2 + r_{2w}^2)$ .

This formulation conserves the tracer but does not ensure the decrease of the tracer variance. Nevertheless the treatment performed on the slopes (see §9) allows the model to run safely without any additional background horizontal diffusion [Guilyardi et al. 2001].

Note that in the partial step  $z$ -coordinate ( $ln\_zps = true$ ), the horizontal derivatives at the bottom level in (5.10) require a specific treatment. They are calculated in module *zpsbde*, described in §5.9.

### Triad rotated (bi-)laplacian operator (*ln\_traldf\_triad*)

If the Griffies triad scheme is employed ( $ln\_traldf\_triad = true$ ; see App.D)

An alternative scheme developed by Griffies et al. [1998] which ensures tracer variance decreases is also available in *NEMO* ( $ln\_traldf\_grif = true$ ). A complete description of the algorithm is given in App.D.

The lateral fourth order bilaplacian operator on tracers is obtained by applying (5.9) twice. The operator requires an additional assumption on boundary conditions: both first and third derivative terms normal to the coast are set to zero.

The lateral fourth order operator formulation on tracers is obtained by applying (5.10) twice. It requires an additional assumption on boundary conditions: first and third derivative terms normal to the coast, normal to the bottom and normal to the surface are set to zero.

### Option for the rotated operators

*ln\_traldf\_msc* = Method of Stabilizing Correction (both operators)

*rn\_slpmax* = slope limit (both operators)

*ln\_triad\_iso* = pure horizontal mixing in ML (triad only)

*rn\_sw\_triad* = 1 switching triad ; =0 all 4 triads used (triad only)

*ln\_botmix\_triad* = lateral mixing on bottom (triad only)

## 5.3 Tracer Vertical Diffusion (*trazdf.F90*)

```

!-----
&namzdf      ! vertical physics                                (default: NO selection)
!-----
!
! type of vertical closure (required)
ln_zdfcst   = .false.   ! constant mixing
ln_zdftric = .false.   ! local Richardson dependent formulation (T => fill namzdf_ric)
ln_zdfcke   = .false.   ! Turbulent Kinetic Energy closure (T => fill namzdf_tke)
ln_zdfgls   = .false.   ! Generic Length Scale closure (T => fill namzdf_gls)
!
! convection
ln_zdfevd   = .false.   ! enhanced vertical diffusion
nn_evdm     = 0         ! apply on tracer (=0) or on tracer and momentum (=1)
rn_evd      = 100.      ! mixing coefficient [m2/s]
ln_zdfnpc   = .false.   ! Non-Penetrative Convective algorithm
nn_npc      = 1         ! frequency of application of npc
nn_npcp     = 365       ! npc control print frequency
!
ln_zdfddm   = .false.   ! double diffusive mixing
rn_avts     = 1.e-4     ! maximum avs (vertical mixing on salinity)
rn_hsbfr    = 1.6       ! heat/salt buoyancy flux ratio
!
! gravity wave-driven vertical mixing
ln_zdfiwm   = .false.   ! internal wave-induced mixing (T => fill namzdf_iwm)
ln_zdfswm   = .false.   ! surface wave-induced mixing (T => ln_wave=ln_sdw=T)
!
! coefficients
rn_avm0     = 1.2e-4    ! vertical eddy viscosity [m2/s] (background Kz if ln_zdfcst=F)
rn_avt0     = 1.2e-5    ! vertical eddy diffusivity [m2/s] (background Kz if ln_zdfcst=F)
nn_avb      = 0         ! profile for background avt & avm (=1) or not (=0)
nn_havtb    = 0         ! horizontal shape for avtb (=1) or not (=0)
/

```

Options are defined through the *namzdf* namelist variables. The formulation of the vertical subgrid scale tracer physics is the same for all the vertical coordinates, and is based on a laplacian operator. The vertical diffusion operator given by (2.34) takes the following semi-discrete space form:

$$\begin{aligned}
 D_T^{vT} &= \frac{1}{e_{3t}} \delta_k \left[ \frac{A_w^{vT}}{e_{3w}} \delta_{k+1/2}[T] \right] \\
 D_T^{vS} &= \frac{1}{e_{3t}} \delta_k \left[ \frac{A_w^{vS}}{e_{3w}} \delta_{k+1/2}[S] \right]
 \end{aligned}
 \tag{5.11}$$

where  $A_w^{vT}$  and  $A_w^{vS}$  are the vertical eddy diffusivity coefficients on temperature and salinity, respectively. Generally,  $A_w^{vT} = A_w^{vS}$  except when double diffusive mixing is parameterised (*i.e.* `key_zdfddm` is defined). The way these coefficients are evaluated is given in §10 (ZDF). Furthermore, when iso-neutral mixing is used, both mixing coefficients are increased by  $\frac{e_{1w} e_{2w}}{e_{3w}} (r_{1w}^2 + r_{2w}^2)$  to account for the vertical second derivative of (5.10).

At the surface and bottom boundaries, the turbulent fluxes of heat and salt must be specified. At the surface they are prescribed from the surface forcing and added in a dedicated routine (see §5.4.1), whilst at the bottom they are set to zero for heat and salt unless a geothermal flux forcing is prescribed as a bottom boundary condition (see §5.4.3).

The large eddy coefficient found in the mixed layer together with high vertical resolution implies that in the case of explicit time stepping (`ln_zdfexp=true`) there would be too restrictive a constraint on the time step. Therefore, the default implicit time stepping is preferred for the vertical diffusion since it overcomes the stability constraint. A forward time differencing scheme (`ln_zdfexp=true`) using a time splitting technique (`nn_zdfexp > 1`) is provided as an alternative. Namelist variables `ln_zdfexp` and `nn_zdfexp` apply to both tracers and dynamics.

## 5.4 External Forcing

### 5.4.1 Surface boundary condition (`trasbc.F90`)

The surface boundary condition for tracers is implemented in a separate module (`trasbc.F90`) instead of entering as a boundary condition on the vertical diffusion operator (as in the case of momentum). This has been found to enhance readability of the code. The two formulations are completely equivalent; the forcing terms in `trasbc` are the surface fluxes divided by the thickness of the top model layer.

Due to interactions and mass exchange of water ( $F_{mass}$ ) with other Earth system components (*i.e.* atmosphere, sea-ice, land), the change in the heat and salt content of the surface layer of the ocean is due both to the heat and salt fluxes crossing the sea surface (not linked with  $F_{mass}$ ) and to the heat and salt content of the mass exchange. They are both included directly in  $Q_{ns}$ , the surface heat flux, and  $F_{salt}$ , the surface salt flux (see §7 for further details). By doing this, the forcing formulation is the same for any tracer (including temperature and salinity).

The surface module (`sbcmod.F90`, see §7) provides the following forcing fields (used on tracers):

- $Q_{ns}$ , the non-solar part of the net surface heat flux that crosses the sea surface (*i.e.* the difference between the total surface heat flux and the fraction of the short wave flux that penetrates into the water column, see §5.4.2) plus the heat content associated with of the mass exchange with the atmosphere and lands.
- $sfx$ , the salt flux resulting from ice-ocean mass exchange (freezing, melting, ridging...)

- *emp*, the mass flux exchanged with the atmosphere (evaporation minus precipitation) and possibly with the sea-ice and ice-shelves.
- *rnf*, the mass flux associated with runoff (see §7.9 for further detail of how it acts on temperature and salinity tendencies)
- *fwfssf*, the mass flux associated with ice shelf melt, (see §7.10 for further details on how the ice shelf melt is computed and applied).

The surface boundary condition on temperature and salinity is applied as follows:

$$\begin{aligned} F^T &= \frac{1}{\rho_o C_p e_{3t}|_{k=1}} \overline{Q_{ns}}^t \\ F^S &= \frac{1}{\rho_o e_{3t}|_{k=1}} \overline{sfx}^t \end{aligned} \quad (5.12)$$

where  $\overline{x}^t$  means that  $x$  is averaged over two consecutive time steps ( $t - \Delta t/2$  and  $t + \Delta t/2$ ). Such time averaging prevents the divergence of odd and even time step (see §3).

In the linear free surface case (*ln\_linssh = true*), an additional term has to be added on both temperature and salinity. On temperature, this term remove the heat content associated with mass exchange that has been added to  $Q_{ns}$ . On salinity, this term mimics the concentration/dilution effect that would have resulted from a change in the volume of the first level. The resulting surface boundary condition is applied as follows:

$$\begin{aligned} F^T &= \frac{1}{\rho_o C_p e_{3t}|_{k=1}} \overline{(Q_{ns} - emp C_p T|_{k=1})}^t \\ F^S &= \frac{1}{\rho_o e_{3t}|_{k=1}} \overline{(sfx - emp S|_{k=1})}^t \end{aligned} \quad (5.13)$$

Note that an exact conservation of heat and salt content is only achieved with non-linear free surface. In the linear free surface case, there is a small imbalance. The imbalance is larger than the imbalance associated with the Asselin time filter [Leclair and Madec 2009]. This is the reason why the modified filter is not applied in the linear free surface case (see §3).

#### 5.4.2 Solar Radiation Penetration (*traqsr.F90*)

```

!-----
&namtra_qsr      ! penetrative solar radiation              (ln_traqsr =T)
!-----
!
!   ! file name ! frequency (hours) ! variable ! time interp. ! clim ! 'yearly' / ! weights ! rotation ! land/sea mask !
!   !           ! (if <0 months) ! name      ! (logical) ! (T/F) ! 'monthly' ! filename ! pairing ! filename      !
!   sn_chl      = 'chlorophyll',      -1      , 'CHLA'      , .true.      , .true.      , 'yearly' , ' '      , ' '      , ' '
!
!   cn_dir      = './'                ! root directory for the location of the runoff files
!   ln_qsr_rgb  = .true.                ! RGB (Red-Green-Blue) light penetration
!   ln_qsr_2bd  = .false.               ! 2 bands light penetration
!   ln_qsr_bio  = .false.               ! bio-model light penetration
!   nn_chldta   = 1                    ! RGB : Chl data (=1) or cst value (=0)
!   rn_abs      = 0.58                 ! RGB & 2 bands: fraction of light (rn_sil)
!   rn_si0      = 0.35                 ! RGB & 2 bands: shortness depth of extinction
!   rn_sil      = 23.0                 ! 2 bands: longest depth of extinction
/

```

Options are defined through the *namtra\_qsr* namelist variables. When the penetrative solar radiation option is used (*ln\_fluxqsr=true*), the solar radiation penetrates the top few tens of meters of the ocean. If it is not used (*ln\_fluxqsr=false*) all the heat flux is absorbed in the first ocean level. Thus, in the former case a term is added to the time evolution equation of temperature (2.1d) and the surface boundary condition is modified to take into account only the non-penetrative part of the surface heat flux:

$$\frac{\partial T}{\partial t} = \dots + \frac{1}{\rho_o C_p e_3} \frac{\partial I}{\partial k} \quad (5.14)$$

$$Q_{ns} = Q_{\text{Total}} - Q_{sr}$$

where  $Q_{sr}$  is the penetrative part of the surface heat flux (*i.e.* the shortwave radiation) and  $I$  is the downward irradiance ( $I|_{z=\eta} = Q_{sr}$ ). The additional term in (5.14) is discretized as follows:

$$\frac{1}{\rho_o C_p e_3} \frac{\partial I}{\partial k} \equiv \frac{1}{\rho_o C_p e_{3t}} \delta_k [I_w] \quad (5.15)$$

The shortwave radiation,  $Q_{sr}$ , consists of energy distributed across a wide spectral range. The ocean is strongly absorbing for wavelengths longer than 700 nm and these wavelengths contribute to heating the upper few tens of centimetres. The fraction of  $Q_{sr}$  that resides in these almost non-penetrative wavebands,  $R$ , is  $\sim 58\%$  (specified through namelist parameter *rn\_abs*). It is assumed to penetrate the ocean with a decreasing exponential profile, with an e-folding depth scale,  $\xi_0$ , of a few tens of centimetres (typically  $\xi_0 = 0.35$  m set as *rn\_si0* in the *namtra\_qsr* namelist). For shorter wavelengths (400-700 nm), the ocean is more transparent, and solar energy propagates to larger depths where it contributes to local heating. The way this second part of the solar energy penetrates into the ocean depends on which formulation is chosen. In the simple 2-waveband light penetration scheme (*ln\_qsr\_2bd=true*) a chlorophyll-independent monochromatic formulation is chosen for the shorter wavelengths, leading to the following expression [Paulson and Simpson 1977]:

$$I(z) = Q_{sr} \left[ R e^{-z/\xi_0} + (1 - R) e^{-z/\xi_1} \right] \quad (5.16)$$

where  $\xi_1$  is the second extinction length scale associated with the shorter wavelengths. It is usually chosen to be 23 m by setting the *rn\_si0* namelist parameter. The set of default values ( $\xi_0$ ,  $\xi_1$ ,  $R$ ) corresponds to a Type I water in Jerlov's (1968) classification (oligotrophic waters).

Such assumptions have been shown to provide a very crude and simplistic representation of observed light penetration profiles (Morel [1988], see also Fig.5.2). Light absorption in the ocean depends on particle concentration and is spectrally selective. Morel [1988] has shown that an accurate representation of light penetration can be provided by a 61 waveband formulation. Unfortunately, such a

model is very computationally expensive. Thus, [Lengaigne et al. \[2007\]](#) have constructed a simplified version of this formulation in which visible light is split into three wavebands: blue (400-500 nm), green (500-600 nm) and red (600-700nm). For each wave-band, the chlorophyll-dependent attenuation coefficient is fitted to the coefficients computed from the full spectral model of [Morel \[1988\]](#) (as modified by [Morel and Maritorena \[2001\]](#)), assuming the same power-law relationship. As shown in Fig.5.2, this formulation, called RGB (Red-Green-Blue), reproduces quite closely the light penetration profiles predicted by the full spectral model, but with much greater computational efficiency. The 2-bands formulation does not reproduce the full model very well.

The RGB formulation is used when `ln_qsr_rgb=true`. The RGB attenuation coefficients (*i.e.* the inverses of the extinction length scales) are tabulated over 61 nonuniform chlorophyll classes ranging from 0.01 to 10 g.Chl/L (see the routine `trc_oce_rgb` in `trc_oce.F90` module). Four types of chlorophyll can be chosen in the RGB formulation:

**`nn_chdta=0`** a constant 0.05 g.Chl/L value everywhere ;

**`nn_chdta=1`** an observed time varying chlorophyll deduced from satellite surface ocean color measurement spread uniformly in the vertical direction ;

**`nn_chdta=2`** same as previous case except that a vertical profile of chlorophyll is used. Following [Morel and Berthon \[1989\]](#), the profile is computed from the local surface chlorophyll value ;

**`ln_qsr_bio=true`** simulated time varying chlorophyll by TOP biogeochemical model. In this case, the RGB formulation is used to calculate both the phytoplankton light limitation in PISCES or LOBSTER and the oceanic heating rate.

The trend in (5.15) associated with the penetration of the solar radiation is added to the temperature trend, and the surface heat flux is modified in routine `traqsr.F90`.

When the  $z$ -coordinate is preferred to the  $s$ -coordinate, the depth of  $w$ -levels does not significantly vary with location. The level at which the light has been totally absorbed (*i.e.* it is less than the computer precision) is computed once, and the trend associated with the penetration of the solar radiation is only added down to that level. Finally, note that when the ocean is shallow ( $< 200$  m), part of the solar radiation can reach the ocean floor. In this case, we have chosen that all remaining radiation is absorbed in the last ocean level (*i.e.*  $I$  is masked).

### 5.4.3 Bottom Boundary Condition (`trabbc.F90`)

```

!-----
&nambbc      !   bottom temperature boundary condition           (default: NO)
!-----
!           !   file name           ! frequency (hours) ! variable ! time interp.! clim  ! 'yearly'// ! weights ! rotation ! land/sea mask !
!           !           ! (if <0 months) ! name      ! (logical) ! (T/F) ! 'monthly' ! filename ! pairing ! filename !
sn_qgh      ='geothermal_heating.nc', -12.      , 'heatflow', .false. , .true. , 'yearly' , ' ' , ' ' , ' '
!
ln_trabbc   = .false.   ! Apply a geothermal heating at the ocean bottom
nn_geoflx   = 2         ! geothermal heat flux: = 0 no flux
              !         = 1 constant flux

```

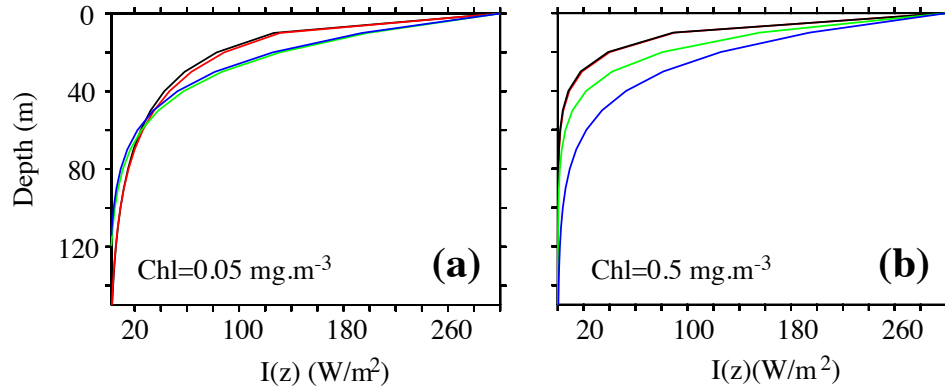


**Figure 5.2:** Penetration profile of the downward solar irradiance calculated by four models. Two waveband chlorophyll-independent formulation (blue), a chlorophyll-dependent monochromatic formulation (green), 4 waveband RGB formulation (red), 61 waveband Morel (1988) formulation (black) for a chlorophyll concentration of (a)  $\text{Chl}=0.05 \text{ mg/m}^3$  and (b)  $\text{Chl}=0.5 \text{ mg/m}^3$ . From [Lengaigne et al. \[2007\]](#).

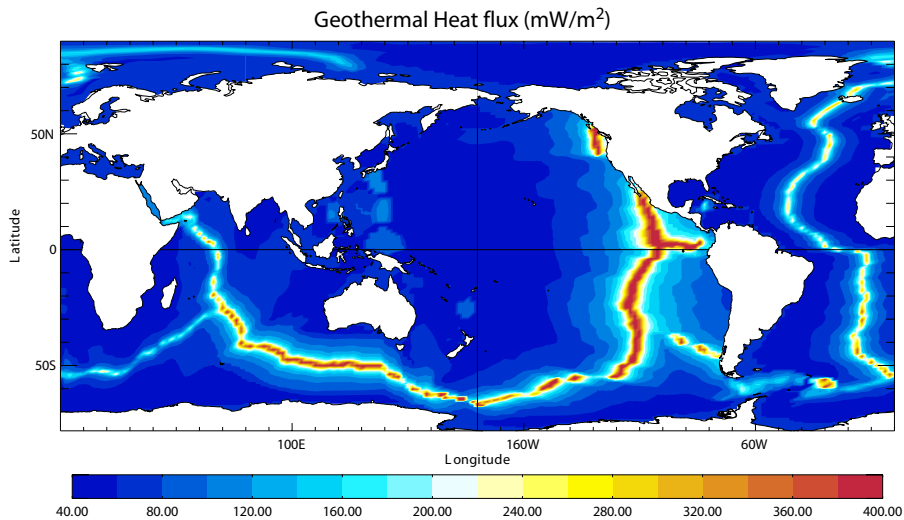


**Figure 5.3:** Geothermal Heat flux (in  $\text{mW}\cdot\text{m}^{-2}$ ) used by [Emile-Geay and Madec \[2009\]](#). It is inferred from the age of the sea floor and the formulae of [Stein and Stein \[1992\]](#).

```

/
!           = 2 variable flux (read in geothermal_heating.nc in mW/m2)
rn_geoflx_cst = 86.4e-3 ! Constant value of geothermal heat flux [W/m2]
cn_dir       = './'    ! root directory for the location of the runoff files

```

Usually it is assumed that there is no exchange of heat or salt through the



ocean bottom, *i.e.* a no flux boundary condition is applied on active tracers at the bottom. This is the default option in *NEMO*, and it is implemented using the masking technique. However, there is a non-zero heat flux across the seafloor that is associated with solid earth cooling. This flux is weak compared to surface fluxes (a mean global value of  $\sim 0.1 \text{ W/m}^2$  [Stein and Stein 1992]), but it warms systematically the ocean and acts on the densest water masses. Taking this flux into account in a global ocean model increases the deepest overturning cell (*i.e.* the one associated with the Antarctic Bottom Water) by a few Sverdrups [Emile-Geay and Madec 2009].

Options are defined through the *namtra\_bbc* namelist variables. The presence of geothermal heating is controlled by setting the namelist parameter *ln\_trabbc* to true. Then, when *nn\_geoflx* is set to 1, a constant geothermal heating is introduced whose value is given by the *nn\_geoflx\_cst*, which is also a namelist parameter. When *nn\_geoflx* is set to 2, a spatially varying geothermal heat flux is introduced which is provided in the *geothermal\_heating.nc* NetCDF file (Fig.5.3) [Emile-Geay and Madec 2009].

## 5.5 Bottom Boundary Layer (*trabbl.F90* - key\_trabbl)

```

!-----
&namtbl      !   bottom boundary layer scheme                      (default: NO)
!-----
  ln_trabbl   = .false.    ! Bottom Boundary Layer parameterisation flag
  nn_bbl_ldf  = 1          ! diffusive bbl (=1) or not (=0)
  nn_bbl_adv  = 0          ! advective bbl (=1/2) or not (=0)
  rn_ahtbl   = 1000.      ! lateral mixing coefficient in the bbl [m2/s]
  rn_gamtbl  = 10.        ! advective bbl coefficient [s]
/

```

Options are defined through the *namtbl* namelist variables. In a *z*-coordinate configuration, the bottom topography is represented by a series of discrete steps. This is not adequate to represent gravity driven downslope flows. Such flows arise either downstream of sills such as the Strait of Gibraltar or Denmark Strait, where dense water formed in marginal seas flows into a basin filled with less dense water, or along the continental slope when dense water masses are formed on a continental shelf. The amount of entrainment that occurs in these gravity plumes is critical in determining the density and volume flux of the densest waters of the ocean, such as Antarctic Bottom Water, or North Atlantic Deep Water. *z*-coordinate models tend to overestimate the entrainment, because the gravity flow is mixed vertically by convection as it goes "downstairs" following the step topography, sometimes over a thickness much larger than the thickness of the observed gravity plume. A similar problem occurs in the *s*-coordinate when the thickness of the bottom level varies rapidly downstream of a sill [Willebrand et al. 2001], and the thickness of the plume is not resolved.

The idea of the bottom boundary layer (BBL) parameterisation, first introduced by Beckmann and Döscher [1997], is to allow a direct communication between two adjacent bottom cells at different levels, whenever the densest water is located above the less dense water. The communication can be by a diffusive flux (diffusive BBL), an advective flux (advective BBL), or both. In the current implementation

of the BBL, only the tracers are modified, not the velocities. Furthermore, it only connects ocean bottom cells, and therefore does not include all the improvements introduced by [Campin and Goosse \[1999\]](#).

### 5.5.1 Diffusive Bottom Boundary layer (*nn\_bbl\_ldf=1*)

When applying sigma-diffusion (**key\_trabbl** defined and *nn\_bbl\_ldf* set to 1), the diffusive flux between two adjacent cells at the ocean floor is given by

$$\mathbf{F}_\sigma = A_l^\sigma \nabla_\sigma T \quad (5.17)$$

with  $\nabla_\sigma$  the lateral gradient operator taken between bottom cells, and  $A_l^\sigma$  the lateral diffusivity in the BBL. Following [Beckmann and Döscher \[1997\]](#), the latter is prescribed with a spatial dependence, *i.e.* in the conditional form

$$A_l^\sigma(i, j, t) = \begin{cases} A_{bbl} & \text{if } \nabla_\sigma \rho \cdot \nabla H < 0 \\ 0 & \text{otherwise} \end{cases} \quad (5.18)$$

where  $A_{bbl}$  is the BBL diffusivity coefficient, given by the namelist parameter *rn\_ahbbl* and usually set to a value much larger than the one used for lateral mixing in the open ocean. The constraint in (5.18) implies that sigma-like diffusion only occurs when the density above the sea floor, at the top of the slope, is larger than in the deeper ocean (see green arrow in Fig.5.4). In practice, this constraint is applied separately in the two horizontal directions, and the density gradient in (5.18) is evaluated with the log gradient formulation:

$$\nabla_\sigma \rho / \rho = \alpha \nabla_\sigma T + \beta \nabla_\sigma S \quad (5.19)$$

where  $\rho$ ,  $\alpha$  and  $\beta$  are functions of  $\bar{T}^\sigma$ ,  $\bar{S}^\sigma$  and  $\bar{H}^\sigma$ , the along bottom mean temperature, salinity and depth, respectively.

### 5.5.2 Advective Bottom Boundary Layer (*nn\_bbl\_adv= 1 or 2*)

When applying an advective BBL (*nn\_bbl\_adv* = 1 or 2), an overturning circulation is added which connects two adjacent bottom grid-points only if dense water overlies less dense water on the slope. The density difference causes dense water to move down the slope.

*nn\_bbl\_adv* = 1 : the downslope velocity is chosen to be the Eulerian ocean velocity just above the topographic step (see black arrow in Fig.5.4) [[Beckmann and Döscher 1997](#)]. It is a *conditional advection*, that is, advection is allowed only if dense water overlies less dense water on the slope (*i.e.*  $\nabla_\sigma \rho \cdot \nabla H < 0$ ) and if the velocity is directed towards greater depth (*i.e.*  $\mathbf{U} \cdot \nabla H > 0$ ).

*nn\_bbl\_adv* = 2 : the downslope velocity is chosen to be proportional to  $\Delta\rho$ , the density difference between the higher cell and lower cell densities [[Campin and Goosse 1999](#)]. The advection is allowed only if dense water overlies less dense

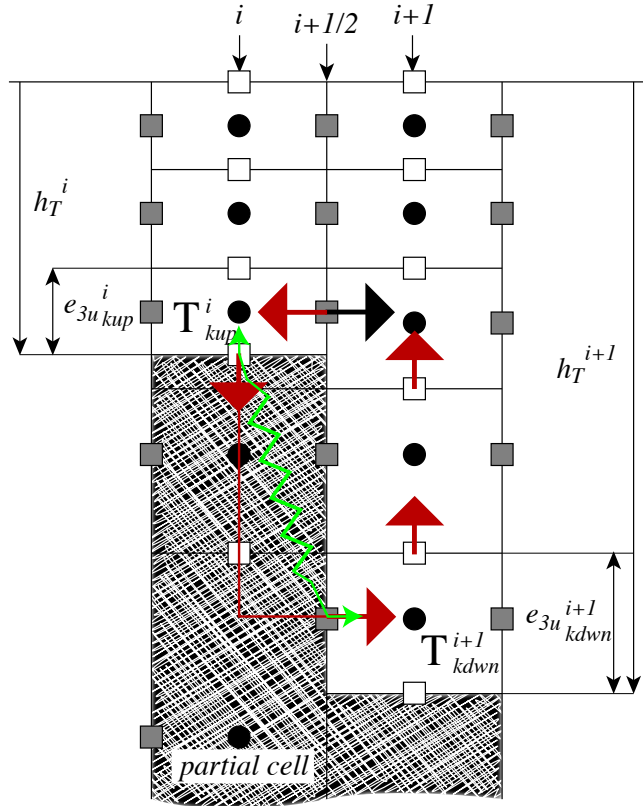


**Figure 5.4:** Advective/diffusive Bottom Boundary Layer. The BBL parameterisation is activated when  $\rho_{kup}^i$  is larger than  $\rho_{kdwn}^{i+1}$ . Red arrows indicate the additional overturning circulation due to the advective BBL. The transport of the downslope flow is defined either as the transport of the bottom ocean cell (black arrow), or as a function of the along slope density gradient. The green arrow indicates the diffusive BBL flux directly connecting *kup* and *kdwn* ocean bottom cells. connection

water on the slope (*i.e.*  $\nabla_{\sigma\rho} \cdot \nabla H < 0$ ). For example, the resulting transport of the downslope flow, here in the *i*-direction (Fig.5.4), is simply given by the following expression:

$$u_{bbl}^{tr} = \gamma g \frac{\Delta\rho}{\rho_o} e_{1u} \min(e_{3ukup}, e_{3ukdwn}) \quad (5.20)$$

where  $\gamma$ , expressed in seconds, is the coefficient of proportionality provided as *rn\_gambbl*, a namelist parameter, and *kup* and *kdwn* are the vertical index of the higher and lower cells, respectively. The parameter  $\gamma$  should take a different value for each bathymetric step, but for simplicity, and because no direct estimation of this parameter is available, a uniform value has been assumed. The possible values for  $\gamma$  range between 1 and 10 s [Campin and Goosse 1999].

Scalar properties are advected by this additional transport ( $u_{bbl}^{tr}, v_{bbl}^{tr}$ ) using the

upwind scheme. Such a diffusive advective scheme has been chosen to mimic the entrainment between the downslope plume and the surrounding water at intermediate depths. The entrainment is replaced by the vertical mixing implicit in the advection scheme. Let us consider as an example the case displayed in Fig.5.4 where the density at level  $(i, kup)$  is larger than the one at level  $(i, kdw)$ . The advective BBL scheme modifies the tracer time tendency of the ocean cells near the topographic step by the downslope flow (5.21), the horizontal (5.22) and the upward (5.23) return flows as follows:

$$\partial_t T_{kdw}^{do} \equiv \partial_t T_{kdw}^{do} + \frac{u_{bbl}^{tr}}{b_{t_{kdw}}^{do}} \left( T_{kup}^{sh} - T_{kdw}^{do} \right) \quad (5.21)$$

$$\partial_t T_{kup}^{sh} \equiv \partial_t T_{kup}^{sh} + \frac{u_{bbl}^{tr}}{b_{t_{kup}}^{sh}} \left( T_{kdw}^{do} - T_{kup}^{sh} \right) \quad (5.22)$$

and for  $k = kdw - 1, \dots, kup$ :

$$\partial_t T_k^{do} \equiv \partial_t T_k^{do} + \frac{u_{bbl}^{tr}}{b_{t_k}^{do}} \left( T_{k+1}^{do} - T_k^{do} \right) \quad (5.23)$$

where  $b_t$  is the  $T$ -cell volume.

Note that the BBL transport,  $(u_{bbl}^{tr}, v_{bbl}^{tr})$ , is available in the model outputs. It has to be used to compute the effective velocity as well as the effective overturning circulation.

## 5.6 Tracer damping (*tradmp.F90*)

```

!-----
&namtra_dmp ! tracer: T & S newtonian damping (default: NO)
!-----
ln_tradmp = .true. ! add a damping term
nn_zdmp = 0 ! vertical shape =0 damping throughout the water column
! ! ! =1 no damping in the mixing layer (kz criteria)
! ! ! =2 no damping in the mixed layer (rho criteria)
cn_resto = 'resto.nc' ! Name of file containing restoration coeff. field (use dmp_tools to create this)
/

```

In some applications it can be useful to add a Newtonian damping term into the temperature and salinity equations:

$$\begin{aligned} \frac{\partial T}{\partial t} &= \dots - \gamma (T - T_o) \\ \frac{\partial S}{\partial t} &= \dots - \gamma (S - S_o) \end{aligned} \quad (5.24)$$

where  $\gamma$  is the inverse of a time scale, and  $T_o$  and  $S_o$  are given temperature and salinity fields (usually a climatology). Options are defined through the *namtra\_dmp* namelist variables. The restoring term is added when the namelist parameter *ln\_tradmp* is set to true. It also requires that both *ln\_tsd\_init* and *ln\_tsd\_tradmp* are set to true in *namtsd* namelist as well as *sn\_tem* and *sn\_sal* structures are correctly set (*i.e.* that  $T_o$  and  $S_o$  are provided in input files and read using *fldread.F90*, see

§7.2.1). The restoring coefficient  $\gamma$  is a three-dimensional array read in during the *tra\_dmp\_init* routine. The file name is specified by the namelist variable *cn\_resto*. The DMP\_TOOLS tool is provided to allow users to generate the netcdf file.

The two main cases in which (5.24) is used are (a) the specification of the boundary conditions along artificial walls of a limited domain basin and (b) the computation of the velocity field associated with a given  $T$ - $S$  field (for example to build the initial state of a prognostic simulation, or to use the resulting velocity field for a passive tracer study). The first case applies to regional models that have artificial walls instead of open boundaries. In the vicinity of these walls,  $\gamma$  takes large values (equivalent to a time scale of a few days) whereas it is zero in the interior of the model domain. The second case corresponds to the use of the robust diagnostic method [Sarmiento and Bryan 1982]. It allows us to find the velocity field consistent with the model dynamics whilst having a  $T$ ,  $S$  field close to a given climatological field ( $T_o$ ,  $S_o$ ).

The robust diagnostic method is very efficient in preventing temperature drift in intermediate waters but it produces artificial sources of heat and salt within the ocean. It also has undesirable effects on the ocean convection. It tends to prevent deep convection and subsequent deep-water formation, by stabilising the water column too much.

The namelist parameter *nn\_zdmp* sets whether the damping should be applied in the whole water column or only below the mixed layer (defined either on a density or  $S_o$  criterion). It is common to set the damping to zero in the mixed layer as the adjustment time scale is short here [Madec et al. 1996].

### 5.6.1 Generating *resto.nc* using DMP\_TOOLS

DMP\_TOOLS can be used to generate a netcdf file containing the restoration coefficient  $\gamma$ . Note that in order to maintain bit comparison with previous NEMO versions DMP\_TOOLS must be compiled and run on the same machine as the NEMO model. A *mesh\_mask.nc* file for the model configuration is required as an input. This can be generated by carrying out a short model run with the namelist parameter *nn\_msh* set to 1. The namelist parameter *ln\_tradmp* will also need to be set to *.false.* for this to work. The *nam\_dmp\_create* namelist in the DMP\_TOOLS directory is used to specify options for the restoration coefficient.

*cp\_cfg*, *cp\_cpz*, *jp\_cfg* and *jperio* specify the model configuration being used and should be the same as specified in *namcfg*. The variable *lzoom* is used to specify that the damping is being used as in case *a* above to provide boundary conditions to a zoom configuration. In the case of the arctic or antarctic zoom configurations this includes some specific treatment. Otherwise damping is applied to the 6 grid points along the ocean boundaries. The open boundaries are specified by the variables *lzoom\_n*, *lzoom\_e*, *lzoom\_s*, *lzoom\_w* in the *nam\_zoom\_dmp* name list.

The remaining switch namelist variables determine the spatial variation of the restoration coefficient in non-zoom configurations. *ln\_full\_field* specifies that newtonian damping should be applied to the whole model domain. *ln\_med\_red\_seas* specifies grid specific restoration coefficients in the Mediterranean Sea for the ORCA4, ORCA2 and ORCA05 configurations. If *ln\_old\_31\_lev\_code* is set then the depth variation of the coefficients will be specified as a function of the model number. This option is included to allow backwards compatibility of the ORCA2 reference configurations with previous model versions. *ln\_coast* specifies that the restoration coefficient should be reduced near to coastlines. This option only has an effect if *ln\_full\_field* is true. *ln\_zero\_top\_layer* specifies that the restoration coefficient should be zero in the surface layer. Finally *ln\_custom* specifies that the custom module will be called. This module is contained in the file custom.F90 and can be edited by users. For example damping could be applied in a specific region.

The restoration coefficient can be set to zero in equatorial regions by specifying a positive value of *nn\_hdmp*. Equatorward of this latitude the restoration coefficient will be zero with a smooth transition to the full values of a 10° latitude band. This is often used because of the short adjustment time scale in the equatorial region [Reverdin et al. 1991, Fujio and Imasato 1991, Marti 1992]. The time scale associated with the damping depends on the depth as a hyperbolic tangent, with *rn\_surf* as surface value, *rn\_bot* as bottom value and a transition depth of *rn\_dep*.

## 5.7 Tracer time evolution (*tranxt.F90*)

```
!-----
&namdom      !   time and space domain
!-----
ln_linssh    = .false. ! =T linear free surface ==> model level are fixed in time
nn_closea    = 0       ! remove (=0) or keep (=1) closed seas and lakes (ORCA)
!
nn_msh       = 0       ! create (>0) a mesh file or not (=0)
rn_isfhmin   = 1.00    ! threshold (m) to discriminate grounding ice to floating ice
!
rn_rdt       = 5760.   ! time step for the dynamics and tracer
rn_atfp      = 0.1     ! asselin time filter parameter
!
ln_crs       = .false. ! Logical switch for coarsening module      (T => fill namcrs)
/
```

Options are defined through the *namdom* namelist variables. The general framework for tracer time stepping is a modified leap-frog scheme [Leclair and Madec 2009], *i.e.* a three level centred time scheme associated with a Asselin time filter (cf. §3.5):

$$(e_{3t}T)^{t+\Delta t} = (e_{3t}T)_f^{t-\Delta t} + 2 \Delta t e_{3t}^t \text{RHS}^t$$

$$(e_{3t}T)_f^t = (e_{3t}T)^t + \gamma \left[ (e_{3t}T)_f^{t-\Delta t} - 2(e_{3t}T)^t + (e_{3t}T)^{t+\Delta t} \right] - \gamma \Delta t \left[ Q^{t+\Delta t/2} - Q^{t-\Delta t/2} \right] \quad (5.25)$$

where RHS is the right hand side of the temperature equation, the subscript *f* denotes filtered values,  $\gamma$  is the Asselin coefficient, and *S* is the total forcing applied on *T* (*i.e.* fluxes plus content in mass exchanges).  $\gamma$  is initialized as *rn\_atfp*

(**namelist** parameter). Its default value is  $rn\_atfp=10^{-3}$ . Note that the forcing correction term in the filter is not applied in linear free surface ( $lk\_vvl=false$ ) (see §5.4.1). Not also that in constant volume case, the time stepping is performed on  $T$ , not on its content,  $e_{3t}T$ .

When the vertical mixing is solved implicitly, the update of the *next* tracer fields is done in module *trazdf.F90*. In this case only the swapping of arrays and the Asselin filtering is done in the *tranxt.F90* module.

In order to prepare for the computation of the *next* time step, a swap of tracer arrays is performed:  $T^{t-\Delta t} = T^t$  and  $T^t = T_f$ .

## 5.8 Equation of State (*eosbn2.F90*)

```

!-----
&nameos      !   ocean Equation Of Seawater                               (default: NO)
!-----
ln_teos10   = .false.           ! = Use TEOS-10
ln_eos80    = .false.           ! = Use EOS80
ln_seos     = .false.           ! = Use S-EOS (simplified Eq.)
!
! S-EOS coefficients (ln_seos=T):
! rd(T,S,Z)*rau0 = -a0*(1+.5*lambda*dT+mu*Z+nu*dS)*dT+b0*dS
rn_a0       = 1.6550e-1         ! thermal expansion coefficient
rn_b0       = 7.6554e-1         ! saline expansion coefficient
rn_lambda1  = 5.9520e-2         ! cabbeling coeff in T^2  (=0 for linear eos)
rn_lambda2  = 7.4914e-4         ! cabbeling coeff in S^2  (=0 for linear eos)
rn_mu1      = 1.4970e-4         ! thermobaric coeff. in T (=0 for linear eos)
rn_mu2      = 1.1090e-5         ! thermobaric coeff. in S (=0 for linear eos)
rn_nu       = 2.4341e-3         ! cabbeling coeff in T*S  (=0 for linear eos)
/

```

### 5.8.1 Equation Of Seawater (*nn\_eos = -1, 0, or 1*)

The Equation Of Seawater (EOS) is an empirical nonlinear thermodynamic relationship linking seawater density,  $\rho$ , to a number of state variables, most typically temperature, salinity and pressure. Because density gradients control the pressure gradient force through the hydrostatic balance, the equation of state provides a fundamental bridge between the distribution of active tracers and the fluid dynamics. Nonlinearities of the EOS are of major importance, in particular influencing the circulation through determination of the static stability below the mixed layer, thus controlling rates of exchange between the atmosphere and the ocean interior [Roquet et al. 2015a]. Therefore an accurate EOS based on either the 1980 equation of state (EOS-80, UNESCO [1983]) or TEOS-10 [IOC et al. 2010] standards should be used anytime a simulation of the real ocean circulation is attempted [Roquet et al. 2015a]. The use of TEOS-10 is highly recommended because (i) it is the new official EOS, (ii) it is more accurate, being based on an updated database of laboratory measurements, and (iii) it uses Conservative Temperature and Absolute Salinity (instead of potential temperature and practical salinity for EOS-980, both variables being more suitable for use as model variables [IOC et al. 2010, Graham and McDougall 2013]). EOS-80 is an obsolescent feature of the NEMO system, kept only for backward compatibility. For process studies, it is often convenient to use an approximation of the EOS. To that purposed, a simplified EOS (S-EOS) inspired by Vallis [2006] is also available.

In the computer code, a density anomaly,  $d_a = \rho/\rho_o - 1$ , is computed, with  $\rho_o$  a reference density. Called *rau0* in the code,  $\rho_o$  is set in *phycst.F90* to a value of  $1,026 \text{ Kg/m}^3$ . This is a sensible choice for the reference density used in a Boussinesq ocean climate model, as, with the exception of only a small percentage of the ocean, density in the World Ocean varies by no more than 2% from that value [Gill 1982].

Options are defined through the *nameos* namelist variables, and in particular *nn\_eos* which controls the EOS used (= -1 for TEOS10 ; = 0 for EOS-80 ; = 1 for S-EOS).

***nn\_eos* = -1** the polyTEOS10-bsq equation of seawater [Roquet et al. 2015b] is used. The accuracy of this approximation is comparable to the TEOS-10 rational function approximation, but it is optimized for a boussinesq fluid and the polynomial expressions have simpler and more computationally efficient expressions for their derived quantities which make them more adapted for use in ocean models. Note that a slightly higher precision polynomial form is now used replacement of the TEOS-10 rational function approximation for hydrographic data analysis [IOC et al. 2010]. A key point is that conservative state variables are used: Absolute Salinity (unit: g/kg, notation:  $S_A$ ) and Conservative Temperature (unit:  $^{\circ}\text{C}$ , notation:  $\Theta$ ). The pressure in decibars is approximated by the depth in meters. With TEOS10, the specific heat capacity of sea water,  $C_p$ , is a constant. It is set to  $C_p = 3991.86795711963 \text{ J Kg}^{-1} \text{ }^{\circ}\text{K}^{-1}$ , according to IOC et al. [2010].

Choosing polyTEOS10-bsq implies that the state variables used by the model are  $\Theta$  and  $S_A$ . In particular, the initial state defined by the user have to be given as *Conservative Temperature* and *Absolute Salinity*. In addition, setting *ln\_useCT* to *true* convert the Conservative SST to potential SST prior to either computing the air-sea and ice-sea fluxes (forced mode) or sending the SST field to the atmosphere (coupled mode).

***nn\_eos* = 0** the polyEOS80-bsq equation of seawater is used. It takes the same polynomial form as the polyTEOS10, but the coefficients have been optimized to accurately fit EOS80 (Roquet, personal comm.). The state variables used in both the EOS80 and the ocean model are: the Practical Salinity ((unit: psu, notation:  $S_p$ )) and Potential Temperature (unit:  $^{\circ}\text{C}$ , notation:  $\theta$ ). The pressure in decibars is approximated by the depth in meters. With this EOS, the specific heat capacity of sea water,  $C_p$ , is a function of temperature, salinity and pressure [UNESCO 1983]. Nevertheless, a severe assumption is made in order to have a heat content ( $C_p T_p$ ) which is conserved by the model:  $C_p$  is set to a constant value, the TEOS10 value.

***nn\_eos* = 1** a simplified EOS (S-EOS) inspired by Vallis [2006] is chosen, the coefficients of which has been optimized to fit the behavior of TEOS10 (Roquet, personal comm.) (see also Roquet et al. [2015a]). It provides a simplistic linear representation of both cabbeling and thermobaricity effects which is



**Table 5.1:** Standard value of S-EOS coefficients.

coeff.	computer name	S-EOS	description
$a_0$	<i>rn_a0</i>	$1.6550 \cdot 10^{-1}$	linear thermal expansion coeff.
$b_0$	<i>rn_b0</i>	$7.6554 \cdot 10^{-1}$	linear haline expansion coeff.
$\lambda_1$	<i>rn_lambda1</i>	$5.9520 \cdot 10^{-2}$	cabbeling coeff. in $T^2$
$\lambda_2$	<i>rn_lambda2</i>	$5.4914 \cdot 10^{-4}$	cabbeling coeff. in $S^2$
$\nu$	<i>rn_nu</i>	$2.4341 \cdot 10^{-3}$	cabbeling coeff. in $T S$
$\mu_1$	<i>rn_mu1</i>	$1.4970 \cdot 10^{-4}$	thermobaric coeff. in T
$\mu_2$	<i>rn_mu2</i>	$1.1090 \cdot 10^{-5}$	thermobaric coeff. in S

enough for a proper treatment of the EOS in theoretical studies [Roquet et al. 2015a]. With such an equation of state there is no longer a distinction between *conservative* and *potential* temperature, as well as between *absolute* and *practical* salinity. S-EOS takes the following expression:

$$d_a(T, S, z) = (-a_0 (1 + 0.5 \lambda_1 T_a + \mu_1 z) * T_a + b_0 (1 - 0.5 \lambda_2 S_a - \mu_2 z) * S_a - \nu T_a S_a) / \rho_o \quad (5.26)$$

$$\text{with } T_a = T - 10 ; S_a = S - 35 ; \rho_o = 1026 \text{ Kg/m}^3$$

where the computer name of the coefficients as well as their standard value are given in 5.1. In fact, when choosing S-EOS, various approximation of EOS can be specified simply by changing the associated coefficients. Setting to zero the two thermobaric coefficients ( $\mu_1, \mu_2$ ) remove thermobaric effect from S-EOS. setting to zero the three cabbeling coefficients ( $\lambda_1, \lambda_2, \nu$ ) remove cabbeling effect from S-EOS. Keeping non-zero value to  $a_0$  and  $b_0$  provide a linear EOS function of T and S.

### 5.8.2 Brunt-Väisälä Frequency (*nn\_eos* = 0, 1 or 2)

An accurate computation of the ocean stability (i.e. of  $N$ , the brunt-Väisälä frequency) is of paramount importance as determine the ocean stratification and is used in several ocean parameterisations (namely TKE, GLS, Richardson number dependent vertical diffusion, enhanced vertical diffusion, non-penetrative convection, tidal mixing parameterisation, iso-neutral diffusion). In particular,  $N^2$  has to be computed at the local pressure (pressure in decibar being approximated by the depth in meters). The expression for  $N^2$  is given by:

$$N^2 = \frac{g}{e_{3w}} (\beta \delta_{k+1/2}[S] - \alpha \delta_{k+1/2}[T]) \quad (5.27)$$

where  $(T, S) = (\Theta, S_A)$  for TEOS10,  $= (\theta, S_p)$  for TEOS-80, or  $= (T, S)$  for S-EOS, and,  $\alpha$  and  $\beta$  are the thermal and haline expansion coefficients. The coef-

ficients are a polynomial function of temperature, salinity and depth which expression depends on the chosen EOS. They are computed through *eos\_rab*, a FORTRAN function that can be found in *eosbn2.F90*.

### 5.8.3 Freezing Point of Seawater

The freezing point of seawater is a function of salinity and pressure [UNESCO 1983]:

$$T_f(S, p) = \left( -0.0575 + 1.710523 \cdot 10^{-3} \sqrt{S} - 2.154996 \cdot 10^{-4} S \right) S - 7.53 \cdot 10^{-3} p \quad (5.28)$$

(5.28) is only used to compute the potential freezing point of sea water (*i.e.* referenced to the surface  $p = 0$ ), thus the pressure dependent terms in (5.28) (last term) have been dropped. The freezing point is computed through *eos\_fzp*, a FORTRAN function that can be found in *eosbn2.F90*.

## 5.9 Horizontal Derivative in *zps*-coordinate (*zpsjde.F90*)

With partial cells (*ln\_zps=true*) at bottom and top (*ln\_isfcav=true*), in general, tracers in horizontally adjacent cells live at different depths. Horizontal gradients of tracers are needed for horizontal diffusion (*traldf.F90* module) and the hydrostatic pressure gradient calculations (*dynhpg.F90* module). The partial cell properties at the top (*ln\_isfcav=true*) are computed in the same way as for the bottom. So, only the bottom interpolation is explained below.

Before taking horizontal gradients between the tracers next to the bottom, a linear interpolation in the vertical is used to approximate the deeper tracer as if it actually lived at the depth of the shallower tracer point (Fig. 5.5). For example, for temperature in the  $i$ -direction the needed interpolated temperature,  $\tilde{T}$ , is:

$$\tilde{T} = \begin{cases} T^{i+1} - \frac{(e_{3w}^{i+1} - e_{3w}^i)}{e_{3w}^{i+1}} \delta_k T^{i+1} & \text{if } e_{3w}^{i+1} \geq e_{3w}^i \\ T^i + \frac{(e_{3w}^{i+1} - e_{3w}^i)}{e_{3w}^i} \delta_k T^{i+1} & \text{if } e_{3w}^{i+1} < e_{3w}^i \end{cases}$$

and the resulting forms for the horizontal difference and the horizontal average

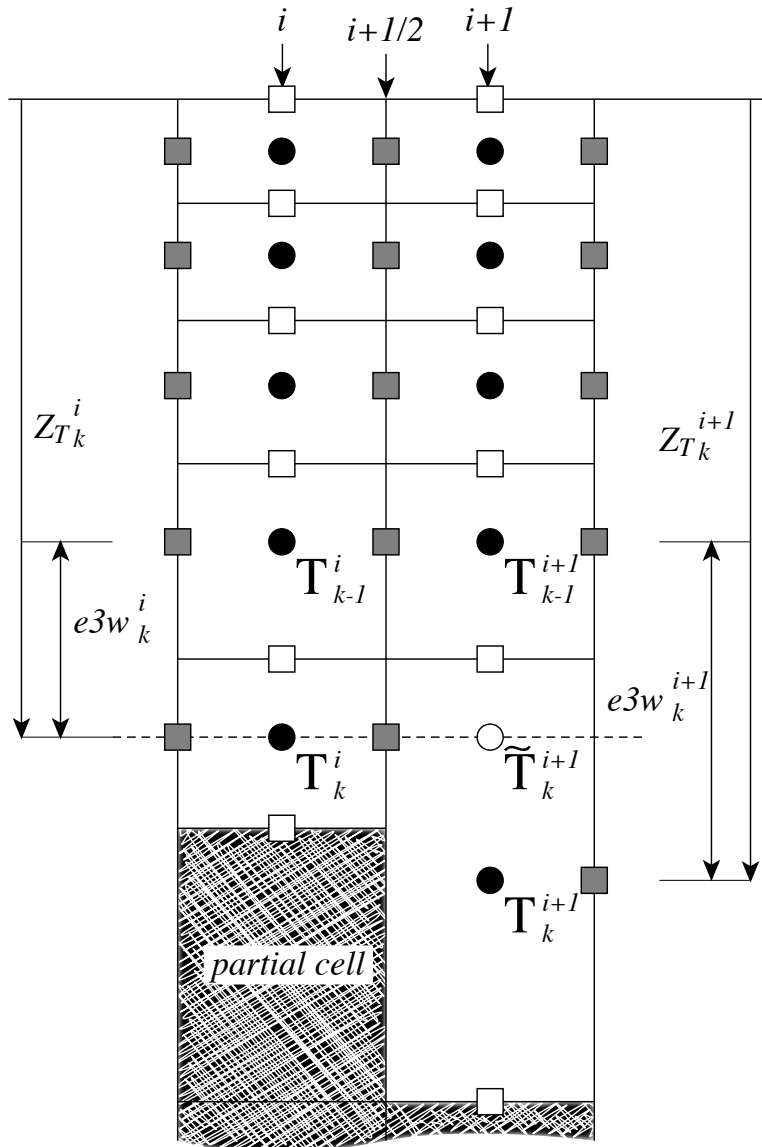


**Figure 5.5:** Discretisation of the horizontal difference and average of tracers in the  $z$ -partial step coordinate ( $ln\_zps=true$ ) in the case  $(e3w_k^{i+1} - e3w_k^i) > 0$ . A linear interpolation is used to estimate  $\tilde{T}_k^{i+1}$ , the tracer value at the depth of the shallower tracer point of the two adjacent bottom  $T$ -points. The horizontal difference is then given by:  $\delta_{i+1/2}T_k = \tilde{T}_k^{i+1} - T_k^i$  and the average by:  $\bar{T}_k^{i+1/2} = (\tilde{T}_k^{i+1/2} - T_k^i)/2$ .

value of  $T$  at a  $U$ -point are:

$$\delta_{i+1/2}T = \begin{cases} \tilde{T} - T^i & \text{if } e_{3w}^{i+1} \geq e_{3w}^i \\ T^{i+1} - \tilde{T} & \text{if } e_{3w}^{i+1} < e_{3w}^i \end{cases} \quad (5.29)$$

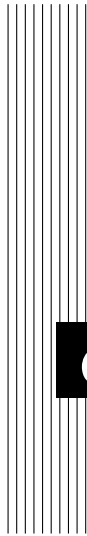
$$\bar{T}^{i+1/2} = \begin{cases} (\tilde{T} - T^i)/2 & \text{if } e_{3w}^{i+1} \geq e_{3w}^i \\ (T^{i+1} - \tilde{T})/2 & \text{if } e_{3w}^{i+1} < e_{3w}^i \end{cases}$$

The computation of horizontal derivative of tracers as well as of density is performed once for all at each time step in *zpsjde.F90* module and stored in shared arrays to be used when needed. It has to be emphasized that the procedure used to compute the interpolated density,  $\tilde{\rho}$ , is not the same as that used for  $T$  and  $S$ . Instead of forming a linear approximation of density, we compute  $\tilde{\rho}$  from the interpolated values of  $T$  and  $S$ , and the pressure at a  $u$ -point (in the equation of state pressure is approximated by depth, see §5.8.1) :

$$\tilde{\rho} = \rho(\tilde{T}, \tilde{S}, z_u) \quad \text{where } z_u = \min(z_T^{i+1}, z_T^i) \quad (5.30)$$

This is a much better approximation as the variation of  $\rho$  with depth (and thus pressure) is highly non-linear with a true equation of state and thus is badly approximated with a linear interpolation. This approximation is used to compute both the horizontal pressure gradient (§6.4) and the slopes of neutral surfaces (§9.1)

Note that in almost all the advection schemes presented in this Chapter, both averaging and differencing operators appear. Yet (5.29) has not been used in these schemes: in contrast to diffusion and pressure gradient computations, no correction for partial steps is applied for advection. The main motivation is to preserve the domain averaged mean variance of the advected field when using the  $2^{nd}$  order centred scheme. Sensitivity of the advection schemes to the way horizontal averages are performed in the vicinity of partial cells should be further investigated in the near future.



## 6 Ocean Dynamics (DYN)

### Contents

---

<b>6.1</b>	<b>Sea surface height and diagnostic variables (<math>\eta, \zeta, \chi, w</math>) . . .</b>	<b>101</b>
6.1.1	Horizontal divergence and relative vorticity ( <i>divcur</i> ) . . .	101
6.1.2	Sea surface height evolution and vertical velocity ( <i>ssh-wzv</i> ) . . . . .	101
<b>6.2</b>	<b>Coriolis and Advection: vector invariant form . . . . .</b>	<b>102</b>
6.2.1	Vorticity term ( <i>dynvor</i> ) . . . . .	102
6.2.2	Kinetic Energy Gradient term ( <i>dynkeg</i> ) . . . . .	106
6.2.3	Vertical advection term ( <i>dynzad</i> ) . . . . .	106
<b>6.3</b>	<b>Coriolis and Advection: flux form . . . . .</b>	<b>107</b>
6.3.1	Coriolis plus curvature metric terms ( <i>dynvor</i> ) . . . . .	107
6.3.2	Flux form Advection term ( <i>dynadv</i> ) . . . . .	107
<b>6.4</b>	<b>Hydrostatic pressure gradient (<i>dynhpg</i>) . . . . .</b>	<b>109</b>
6.4.1	<i>z</i> -coordinate with full step ( <i>ln_dynhpg_zco</i> ) . . . . .	109
6.4.2	<i>z</i> -coordinate with partial step ( <i>ln_dynhpg_zps</i> ) . . . . .	110
6.4.3	<i>s</i> - and <i>z-s</i> -coordinates . . . . .	110
6.4.4	Ice shelf cavity . . . . .	111
6.4.5	Time-scheme ( <i>ln_dynhpg_imp</i> ) . . . . .	111
<b>6.5</b>	<b>Surface pressure gradient (<i>dynspg</i>) . . . . .</b>	<b>112</b>
6.5.1	Explicit free surface ( <b>key_dynspg_exp</b> ) . . . . .	113
6.5.2	Split-Explicit free surface ( <b>key_dynspg_ts</b> ) . . . . .	113
6.5.3	Filtered free surface ( <b>key_dynspg_fft</b> ) . . . . .	116
<b>6.6</b>	<b>Lateral diffusion term (<i>dynldf</i>) . . . . .</b>	<b>116</b>
6.6.1	Iso-level laplacian operator ( <i>ln_dynldf_lap</i> ) . . . . .	117

---

6.6.2	Rotated laplacian operator ( <i>ln_dynldf_iso</i> ) . . . . .	117
6.6.3	Iso-level bilaplacian operator ( <i>ln_dynldf_bilap</i> ) . . . . .	118
<b>6.7</b>	<b>Vertical diffusion term (<i>dynzdf.F90</i>) . . . . .</b>	<b>118</b>
<b>6.8</b>	<b>External Forcings . . . . .</b>	<b>120</b>
<b>6.9</b>	<b>Time evolution term (<i>dynnxt</i>) . . . . .</b>	<b>120</b>

---

Using the representation described in Chapter 4, several semi-discrete space forms of the dynamical equations are available depending on the vertical coordinate used and on the conservation properties of the vorticity term. In all the equations presented here, the masking has been omitted for simplicity. One must be aware that all the quantities are masked fields and that each time an average or difference operator is used, the resulting field is multiplied by a mask.

The prognostic ocean dynamics equation can be summarized as follows:

$$\text{NXT} = \begin{pmatrix} \text{VOR} + \text{KEG} + \text{ZAD} \\ \text{COR} + \text{ADV} \end{pmatrix} + \text{HPG} + \text{SPG} + \text{LDF} + \text{ZDF}$$

NXT stands for next, referring to the time-stepping. The first group of terms on the rhs of this equation corresponds to the Coriolis and advection terms that are decomposed into either a vorticity part (VOR), a kinetic energy part (KEG) and a vertical advection part (ZAD) in the vector invariant formulation, or a Coriolis and advection part (COR+ADV) in the flux formulation. The terms following these are the pressure gradient contributions (HPG, Hydrostatic Pressure Gradient, and SPG, Surface Pressure Gradient); and contributions from lateral diffusion (LDF) and vertical diffusion (ZDF), which are added to the rhs in the *dynldf.F90* and *dynzdf.F90* modules. The vertical diffusion term includes the surface and bottom stresses. The external forcings and parameterisations require complex inputs (surface wind stress calculation using bulk formulae, estimation of mixing coefficients) that are carried out in modules SBC, LDF and ZDF and are described in Chapters 7, 9 and 10, respectively.

In the present chapter we also describe the diagnostic equations used to compute the horizontal divergence, curl of the velocities (*divcur* module) and the vertical velocity (*wzvm* module).

The different options available to the user are managed by namelist variables. For term *ttt* in the momentum equations, the logical namelist variables are *ln\_dynntt\_XXX*, where *XXX* is a 3 or 4 letter acronym corresponding to each optional scheme. If a CPP key is used for this term its name is **key\_ttt**. The corresponding code can be found in the *dynntt\_XXX* module in the DYN directory, and it is usually computed in the *dyn\_ttt\_XXX* subroutine.

The user has the option of extracting and outputting each tendency term from the 3D momentum equations (**key\_trddyn** defined), as described in Chap.15. Furthermore, the tendency terms associated with the 2D barotropic vorticity balance (when **key\_trdvor** is defined) can be derived from the 3D terms.

## 6.1 Sea surface height and diagnostic variables ( $\eta, \zeta, \chi, w$ )

### 6.1.1 Horizontal divergence and relative vorticity (*divcur.F90*)

The vorticity is defined at an  $f$ -point (*i.e.* corner point) as follows:

$$\zeta = \frac{1}{e_{1f} e_{2f}} \left( \delta_{i+1/2} [e_{2v} v] - \delta_{j+1/2} [e_{1u} u] \right) \quad (6.1)$$

The horizontal divergence is defined at a  $T$ -point. It is given by:

$$\chi = \frac{1}{e_{1t} e_{2t} e_{3t}} \left( \delta_i [e_{2u} e_{3u} u] + \delta_j [e_{1v} e_{3v} v] \right) \quad (6.2)$$

Note that although the vorticity has the same discrete expression in  $z$ - and  $s$ -coordinates, its physical meaning is not identical.  $\zeta$  is a pseudo vorticity along  $s$ -surfaces (only pseudo because  $(u, v)$  are still defined along geopotential surfaces, but are not necessarily defined at the same depth).

The vorticity and divergence at the *before* step are used in the computation of the horizontal diffusion of momentum. Note that because they have been calculated prior to the Asselin filtering of the *before* velocities, the *before* vorticity and divergence arrays must be included in the restart file to ensure perfect restartability. The vorticity and divergence at the *now* time step are used for the computation of the nonlinear advection and of the vertical velocity respectively.

### 6.1.2 Horizontal divergence and relative vorticity (*sshwzv.F90*)

The sea surface height is given by :

$$\begin{aligned} \frac{\partial \eta}{\partial t} &\equiv \frac{1}{e_{1t} e_{2t}} \sum_k \{ \delta_i [e_{2u} e_{3u} u] + \delta_j [e_{1v} e_{3v} v] \} - \frac{emp}{\rho_w} \\ &\equiv \sum_k \chi e_{3t} - \frac{emp}{\rho_w} \end{aligned} \quad (6.3)$$

where  $emp$  is the surface freshwater budget (evaporation minus precipitation), expressed in  $\text{Kg/m}^2/\text{s}$  (which is equal to  $\text{mm/s}$ ), and  $\rho_w = 1,035 \text{ Kg/m}^3$  is the reference density of sea water (Boussinesq approximation). If river runoff is expressed as a surface freshwater flux (see §7) then  $emp$  can be written as the evaporation minus precipitation, minus the river runoff. The sea-surface height is evaluated using exactly the same time stepping scheme as the tracer equation (5.25): a leapfrog scheme in combination with an Asselin time filter, *i.e.* the velocity appearing in (6.3) is centred in time (*now* velocity). This is of paramount importance. Replacing  $T$  by the number 1 in the tracer equation and summing over the water column

must lead to the sea surface height equation otherwise tracer content will not be conserved [Griffies et al. 2001, Leclair and Madec 2009].

The vertical velocity is computed by an upward integration of the horizontal divergence starting at the bottom, taking into account the change of the thickness of the levels :

$$\begin{cases} w|_{k_b-1/2} = 0 & \text{where } k_b \text{ is the level just above the sea floor} \\ w|_{k+1/2} = w|_{k-1/2} + e_{3t}|_k \chi|_k - \frac{1}{2\Delta t} (e_{3t}^{t+1}|_k - e_{3t}^{t-1}|_k) \end{cases} \quad (6.4)$$

In the case of a non-linear free surface (**key\_vv1**), the top vertical velocity is  $-emp/\rho_w$ , as changes in the divergence of the barotropic transport are absorbed into the change of the level thicknesses, re-orientated downward. In the case of a linear free surface, the time derivative in (6.4) disappears. The upper boundary condition applies at a fixed level  $z = 0$ . The top vertical velocity is thus equal to the divergence of the barotropic transport (*i.e.* the first term in the right-hand-side of (6.3)).

Note also that whereas the vertical velocity has the same discrete expression in  $z$ - and  $s$ -coordinates, its physical meaning is not the same: in the second case,  $w$  is the velocity normal to the  $s$ -surfaces. Note also that the  $k$ -axis is re-orientated downwards in the FORTRAN code compared to the indexing used in the semi-discrete equations such as (6.4) (see §4.1.3).

## 6.2 Coriolis and Advection: vector invariant form

```
!-----
&namdyn_adv ! formulation of the momentum advection (default: NO selection)
!-----
ln_dynadv_NONE= .false. ! linear dynamics (no momentum advection)
ln_dynadv_vec = .false. ! vector form - 2nd centered scheme
nn_dynkeg = 0 ! grad(KE) scheme: =0 C2 ; =1 Hollingsworth correction
ln_dynadv_cen2= .false. ! flux form - 2nd order centered scheme
ln_dynadv_ubs = .false. ! flux form - 3rd order UBS scheme
/
```

The vector invariant form of the momentum equations is the one most often used in applications of the *NEMO* ocean model. The flux form option (see next section) has been present since version 2. Options are defined through the *namdyn\_adv* namelist variables Coriolis and momentum advection terms are evaluated using a leapfrog scheme, *i.e.* the velocity appearing in these expressions is centred in time (*now* velocity). At the lateral boundaries either free slip, no slip or partial slip boundary conditions are applied following Chap.8.

### 6.2.1 Vorticity term (*dynvor.F90*)

```
!-----
&namdyn_vor ! Vorticity / Coriolis scheme (default: NO)
!-----
ln_dynvor_ene = .false. ! enstrophy conserving scheme
ln_dynvor_ens = .false. ! energy conserving scheme
ln_dynvor_mix = .false. ! mixed scheme
ln_dynvor_eeen = .false. ! energy & enstrophy scheme
nn_eeen_e3f = 1 ! e3f = masked averaging of e3t divided by 4 (=0) or by the sum of mask (=1)
ln_dynvor_msk = .false. ! vorticity multiplied by fmask (=T) or not (=F) (all vorticity schemes) ! PLEASE DO NOT ACTIVATE
/
```



Options are defined through the *namdyn\_vor* namelist variables. Four discretisations of the vorticity term (*ln\_dynvor\_xxx=true*) are available: conserving potential enstrophy of horizontally non-divergent flow (ENS scheme) ; conserving horizontal kinetic energy (ENE scheme) ; conserving potential enstrophy for the relative vorticity term and horizontal kinetic energy for the planetary vorticity term (MIX scheme) ; or conserving both the potential enstrophy of horizontally non-divergent flow and horizontal kinetic energy (EEN scheme) (see Appendix C.5). In the case of ENS, ENE or MIX schemes the land sea mask may be slightly modified to ensure the consistency of vorticity term with analytical equations (*ln\_dynvor\_con=true*). The vorticity terms are all computed in dedicated routines that can be found in the *dynvor.F90* module.

### Enstrophy conserving scheme (*ln\_dynvor\_ens=true*)

In the enstrophy conserving case (ENS scheme), the discrete formulation of the vorticity term provides a global conservation of the enstrophy ( $[(\zeta + f)/e_{3f}]^2$  in *s*-coordinates) for a horizontally non-divergent flow (*i.e.*  $\chi=0$ ), but does not conserve the total kinetic energy. It is given by:

$$\begin{cases} + \frac{1}{e_{1u}} \overline{\left(\frac{\zeta + f}{e_{3f}}\right)^i} \overline{(e_{1v} e_{3v} v)}^{i,j+1/2} \\ - \frac{1}{e_{2v}} \overline{\left(\frac{\zeta + f}{e_{3f}}\right)^j} \overline{(e_{2u} e_{3u} u)}^{i+1/2,j} \end{cases} \quad (6.5)$$

### Energy conserving scheme (*ln\_dynvor\_ene=true*)

The kinetic energy conserving scheme (ENE scheme) conserves the global kinetic energy but not the global enstrophy. It is given by:

$$\begin{cases} + \frac{1}{e_{1u}} \overline{\left(\frac{\zeta + f}{e_{3f}}\right)} \overline{(e_{1v} e_{3v} v)}^{i+1/2,j} \\ - \frac{1}{e_{2v}} \overline{\left(\frac{\zeta + f}{e_{3f}}\right)} \overline{(e_{2u} e_{3u} u)}^{j+1/2,i} \end{cases} \quad (6.6)$$

### Mixed energy/enstrophy conserving scheme (*ln\_dynvor\_mix=true*)

For the mixed energy/enstrophy conserving scheme (MIX scheme), a mixture of the two previous schemes is used. It consists of the ENS scheme (C.13) for the relative vorticity term, and of the ENE scheme (6.6) applied to the planetary vorticity

term.

$$\left\{ \begin{array}{l} +\frac{1}{e_{1u}} \left( \frac{\zeta}{e_{3f}} \right)^i \overline{\overline{(e_{1v} e_{3v} v)}}^{i,j+1/2} - \frac{1}{e_{1u}} \left( \frac{f}{e_{3f}} \right) \overline{\overline{(e_{1v} e_{3v} v)}}^{i+1/2,j} \\ -\frac{1}{e_{2v}} \left( \frac{\zeta}{e_{3f}} \right)^j \overline{\overline{(e_{2u} e_{3u} u)}}^{i+1/2,j} + \frac{1}{e_{2v}} \left( \frac{f}{e_{3f}} \right) \overline{\overline{(e_{2u} e_{3u} u)}}^{j+1/2,i} \end{array} \right. \quad (6.7)$$

### Energy and enstrophy conserving scheme (*ln\_dynvor\_een=true*)

In both the ENS and ENE schemes, it is apparent that the combination of  $i$  and  $j$  averages of the velocity allows for the presence of grid point oscillation structures that will be invisible to the operator. These structures are *computational modes* that will be at least partly damped by the momentum diffusion operator (*i.e.* the subgrid-scale advection), but not by the resolved advection term. The ENS and ENE schemes therefore do not contribute to dump any grid point noise in the horizontal velocity field. Such noise would result in more noise in the vertical velocity field, an undesirable feature. This is a well-known characteristic of  $C$ -grid discretization where  $u$  and  $v$  are located at different grid points, a price worth paying to avoid a double averaging in the pressure gradient term as in the  $B$ -grid.

A very nice solution to the problem of double averaging was proposed by Arakawa and Hsu [1990]. The idea is to get rid of the double averaging by considering triad combinations of vorticity. It is noteworthy that this solution is conceptually quite similar to the one proposed by [Griffies et al. 1998] for the discretization of the iso-neutral diffusion operator (see App.C).

The Arakawa and Hsu [1990] vorticity advection scheme for a single layer is modified for spherical coordinates as described by Arakawa and Lamb [1981] to obtain the EEN scheme. First consider the discrete expression of the potential vorticity,  $q$ , defined at an  $f$ -point:

$$q = \frac{\zeta + f}{e_{3f}} \quad (6.8)$$

where the relative vorticity is defined by (6.1), the Coriolis parameter is given by  $f = 2\Omega \sin \varphi_f$  and the layer thickness at  $f$ -points is:

$$e_{3f} = \overline{\overline{e_{3t}}}^{i+1/2,j+1/2} \quad (6.9)$$

A key point in (6.9) is how the averaging in the  $\mathbf{i}$ - and  $\mathbf{j}$ - directions is made. It uses the sum of masked  $t$ -point vertical scale factor divided either by the sum of the four  $t$ -point masks ( $nn\_een\_e3f = 1$ ), or just by 4 ( $nn\_een\_e3f = \text{true}$ ). The latter case preserves the continuity of  $e_{3f}$  when one or more of the neighbouring  $e_{3t}$  tends to zero and extends by continuity the value of  $e_{3f}$  into the land areas. This case introduces a sub-grid-scale topography at  $f$ -points (with a systematic reduction of  $e_{3f}$  when a model level intercept the bathymetry) that tends to reinforce

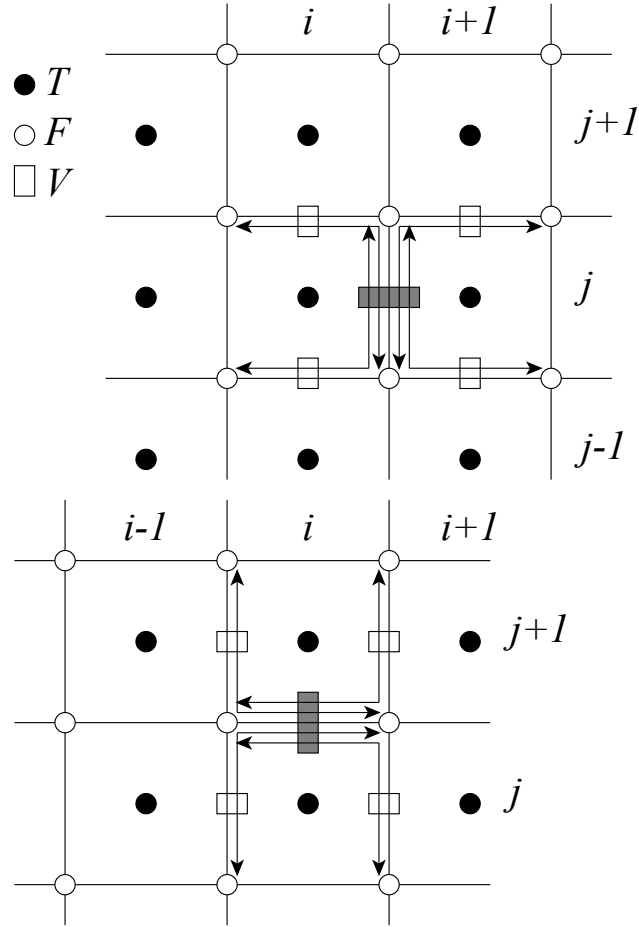


**Figure 6.1:** Triads used in the energy and enstrophy conserving scheme (een) for  $u$ -component (upper panel) and  $v$ -component (lower panel).

the topostrophy of the flow (*i.e.* the tendency of the flow to follow the isobaths) [Penduff et al. 2007].

Next, the vorticity triads,  ${}^i_j Q_{j_p}^{i_p}$  can be defined at a  $T$ -point as the following triad combinations of the neighbouring potential vorticities defined at  $f$ -points (Fig. 6.1):

$${}^j_i Q_{j_p}^{i_p} = \frac{1}{12} \left( q_{j+j_p}^{i-i_p} + q_{j+i_p}^{i+j_p} + q_{j-j_p}^{i+i_p} \right) \quad (6.10)$$

where the indices  $i_p$  and  $k_p$  take the values:  $i_p = -1/2$  or  $1/2$  and  $j_p = -1/2$  or  $1/2$ .

Finally, the vorticity terms are represented as:

$$\begin{cases} +q e_3 v \equiv +\frac{1}{e_{1u}} \sum_{i_p, k_p}^{i+1/2-i_p} \mathbb{Q}_{j_p}^{i_p} (e_{1v} e_{3v} v)_{j+j_p}^{i+1/2-i_p} \\ -q e_3 u \equiv -\frac{1}{e_{2v}} \sum_{i_p, k_p}^i \mathbb{Q}_{j_p}^{i_p} (e_{2u} e_{3u} u)_{j+1/2-j_p}^{i+i_p} \end{cases} \quad (6.11)$$

This EEN scheme in fact combines the conservation properties of the ENS and ENE schemes. It conserves both total energy and potential enstrophy in the limit of horizontally nondivergent flow (*i.e.*  $\chi=0$ ) (see Appendix C.5). Applied to a realistic ocean configuration, it has been shown that it leads to a significant reduction of the noise in the vertical velocity field [Le Sommer et al. 2009]. Furthermore, used in combination with a partial steps representation of bottom topography, it improves the interaction between current and topography, leading to a larger topography of the flow [Barnier et al. 2006, Penduff et al. 2007].

### 6.2.2 Kinetic Energy Gradient term (*dynkeg.F90*)

As demonstrated in Appendix C, there is a single discrete formulation of the kinetic energy gradient term that, together with the formulation chosen for the vertical advection (see below), conserves the total kinetic energy:

$$\begin{cases} -\frac{1}{2 e_{1u}} \delta_{i+1/2} [\overline{u^2}^i + \overline{v^2}^j] \\ -\frac{1}{2 e_{2v}} \delta_{j+1/2} [\overline{u^2}^i + \overline{v^2}^j] \end{cases} \quad (6.12)$$

### 6.2.3 Vertical advection term (*dynzad.F90*)

The discrete formulation of the vertical advection, together with the formulation chosen for the gradient of kinetic energy (KE) term, conserves the total kinetic energy. Indeed, the change of KE due to the vertical advection is exactly balanced by the change of KE due to the gradient of KE (see Appendix C).

$$\begin{cases} -\frac{1}{e_{1u} e_{2u} e_{3u}} \frac{\overline{e_{1t} e_{2t} w^{i+1/2} \delta_{k+1/2} [u]}^k}{e_{1t} e_{2t} w^{i+1/2} \delta_{k+1/2} [u]} \\ -\frac{1}{e_{1v} e_{2v} e_{3v}} \frac{\overline{e_{1t} e_{2t} w^{j+1/2} \delta_{k+1/2} [u]}^k}{e_{1t} e_{2t} w^{j+1/2} \delta_{k+1/2} [u]} \end{cases} \quad (6.13)$$

When `ln_dynzad_zts = true`, a split-explicit time stepping with 5 sub-timesteps is used on the vertical advection term. This option can be useful when the value of the timestep is limited by vertical advection [Lemarié et al. 2015]. Note that in this case, a similar split-explicit time stepping should be used on vertical advection of tracer to ensure a better stability, an option which is only available with a TVD scheme (see `ln_traadv_tvd_zts` in §5.1.2).

### 6.3 Coriolis and Advection: flux form

```

!-----
&namdyn_adv    !    formulation of the momentum advection                (default: NO selection)
!-----
ln_dynadv_NONE= .false. ! linear dynamics (no momentum advection)
ln_dynadv_vec = .false. ! vector form - 2nd centered scheme
nn_dynkeg     = 0      ! grad(KE) scheme: =0  C2 ; =1 Hollingsworth correction
ln_dynadv_cen2= .false. ! flux form - 2nd order centered scheme
ln_dynadv_ubs = .false. ! flux form - 3rd order UBS      scheme
/

```

Options are defined through the *namdyn\_adv* namelist variables. In the flux form (as in the vector invariant form), the Coriolis and momentum advection terms are evaluated using a leapfrog scheme, *i.e.* the velocity appearing in their expressions is centred in time (*now* velocity). At the lateral boundaries either free slip, no slip or partial slip boundary conditions are applied following Chap.8.

#### 6.3.1 Coriolis plus curvature metric terms (*dynvor.F90*)

In flux form, the vorticity term reduces to a Coriolis term in which the Coriolis parameter has been modified to account for the "metric" term. This altered Coriolis parameter is thus discretised at *f*-points. It is given by:

$$f + \frac{1}{e_1 e_2} \left( v \frac{\partial e_2}{\partial i} - u \frac{\partial e_1}{\partial j} \right) \equiv f + \frac{1}{e_{1f} e_{2f}} \left( \bar{v}^{i+1/2} \delta_{i+1/2} [e_{2u}] - \bar{u}^{j+1/2} \delta_{j+1/2} [e_{1u}] \right) \quad (6.14)$$

Any of the (C.13), (6.6) and (C.15) schemes can be used to compute the product of the Coriolis parameter and the vorticity. However, the energy-conserving scheme (C.15) has exclusively been used to date. This term is evaluated using a leapfrog scheme, *i.e.* the velocity is centred in time (*now* velocity).

#### 6.3.2 Flux form Advection term (*dynadv.F90*)

The discrete expression of the advection term is given by :

$$\left\{ \begin{array}{l} \frac{1}{e_{1u} e_{2u} e_{3u}} \left( \delta_{i+1/2} [e_{2u} e_{3u} \bar{u}^i u_t] + \delta_j [e_{1u} e_{3u} \bar{v}^{i+1/2} u_f] \right. \\ \quad \left. + \delta_k [e_{1w} e_{2w} \bar{w}^{i+1/2} u_{uw}] \right) \\ \\ \frac{1}{e_{1v} e_{2v} e_{3v}} \left( \delta_i [e_{2u} e_{3u} \bar{u}^{j+1/2} v_f] + \delta_{j+1/2} [e_{1u} e_{3u} \bar{v}^i v_t] \right. \\ \quad \left. + \delta_k [e_{1w} e_{2w} \bar{w}^{j+1/2} v_{vw}] \right) \end{array} \right\} \quad (6.15)$$

Two advection schemes are available: a  $2^{nd}$  order centered finite difference scheme, CEN2, or a  $3^{rd}$  order upstream biased scheme, UBS. The latter is described in Shepetkin and McWilliams [2005]. The schemes are selected using

the namelist logicals `ln_dynadv_cen2` and `ln_dynadv_ubs`. In flux form, the schemes differ by the choice of a space and time interpolation to define the value of  $u$  and  $v$  at the centre of each face of  $u$ - and  $v$ -cells, *i.e.* at the  $T$ -,  $f$ -, and  $uw$ -points for  $u$  and at the  $f$ -,  $T$ - and  $vw$ -points for  $v$ .

### $2^{nd}$ order centred scheme (cen2) (`ln_dynadv_cen2=true`)

In the centred  $2^{nd}$  order formulation, the velocity is evaluated as the mean of the two neighbouring points :

$$\begin{cases} u_T^{cen2} = \bar{u}^i & u_F^{cen2} = \bar{u}^{j+1/2} & u_{uw}^{cen2} = \bar{u}^{k+1/2} \\ v_F^{cen2} = \bar{v}^{i+1/2} & v_T^{cen2} = \bar{v}^j & v_{vw}^{cen2} = \bar{v}^{k+1/2} \end{cases} \quad (6.16)$$

The scheme is non diffusive (*i.e.* conserves the kinetic energy) but dispersive (*i.e.* it may create false extrema). It is therefore notoriously noisy and must be used in conjunction with an explicit diffusion operator to produce a sensible solution. The associated time-stepping is performed using a leapfrog scheme in conjunction with an Asselin time-filter, so  $u$  and  $v$  are the *now* velocities.

### Upstream Biased Scheme (UBS) (`ln_dynadv_ubs=true`)

The UBS advection scheme is an upstream biased third order scheme based on an upstream-biased parabolic interpolation. For example, the evaluation of  $u_T^{ubs}$  is done as follows:

$$u_T^{ubs} = \bar{u}^i - \frac{1}{6} \begin{cases} u''_{i-1/2} & \text{if } \overline{e_{2u} e_{3u} u^i} \geq 0 \\ u''_{i+1/2} & \text{if } \overline{e_{2u} e_{3u} u^i} < 0 \end{cases} \quad (6.17)$$

where  $u''_{i+1/2} = \delta_{i+1/2} [\delta_i [u]]$ . This results in a dissipatively dominant (*i.e.* hyper-diffusive) truncation error [Shchepetkin and McWilliams 2005]. The overall performance of the advection scheme is similar to that reported in Farrow and Stevens [1995]. It is a relatively good compromise between accuracy and smoothness. It is not a *positive* scheme, meaning that false extrema are permitted. But the amplitudes of the false extrema are significantly reduced over those in the centred second order method. As the scheme already includes a diffusion component, it can be used without explicit lateral diffusion on momentum (*i.e.* `ln_dynldf_lap=ln_dynldf_bilap=false`), and it is recommended to do so.

The UBS scheme is not used in all directions. In the vertical, the centred  $2^{nd}$  order evaluation of the advection is preferred, *i.e.*  $u_{uw}^{ubs}$  and  $u_{vw}^{ubs}$  in (6.16) are used. UBS is diffusive and is associated with vertical mixing of momentum.

For stability reasons, the first term in (6.17), which corresponds to a second order centred scheme, is evaluated using the *now* velocity (centred in time), while the second term, which is the diffusion part of the scheme, is evaluated using the *before* velocity (forward in time). This is discussed by Webb et al. [1998] in the context of the Quick advection scheme.

Note that the UBS and QUICK (Quadratic Upstream Interpolation for Convective Kinematics) schemes only differ by one coefficient. Replacing 1/6 by 1/8 in (6.17) leads to the QUICK advection scheme [Webb et al. 1998]. This option is not available through a namelist parameter, since the 1/6 coefficient is hard coded. Nevertheless it is quite easy to make the substitution in the *dynadv\_ubs.F90* module and obtain a QUICK scheme.

Note also that in the current version of *dynadv\_ubs.F90*, there is also the possibility of using a 4<sup>th</sup> order evaluation of the advective velocity as in ROMS. This is an error and should be suppressed soon.

## 6.4 Hydrostatic pressure gradient (*dynhpg.F90*)

```
!-----
&namdyn_hpg      ! Hydrostatic pressure gradient option           (default: NO selection)
!-----
ln_hpg_zco = .false. ! z-coordinate - full steps
ln_hpg_zps = .false. ! z-coordinate - partial steps (interpolation)
ln_hpg_sco = .false. ! s-coordinate (standard jacobian formulation)
ln_hpg_isf = .false. ! s-coordinate (sco ) adapted to isf
ln_hpg_djc = .false. ! s-coordinate (Density Jacobian with Cubic polynomial)
ln_hpg_prj = .false. ! s-coordinate (Pressure Jacobian scheme)
/
```

Options are defined through the *namdyn\_hpg* namelist variables. The key distinction between the different algorithms used for the hydrostatic pressure gradient is the vertical coordinate used, since HPG is a *horizontal* pressure gradient, *i.e.* computed along geopotential surfaces. As a result, any tilt of the surface of the computational levels will require a specific treatment to compute the hydrostatic pressure gradient.

The hydrostatic pressure gradient term is evaluated either using a leapfrog scheme, *i.e.* the density appearing in its expression is centred in time (*now*  $\rho$ ), or a semi-implicit scheme. At the lateral boundaries either free slip, no slip or partial slip boundary conditions are applied.

### 6.4.1 *z*-coordinate with full step (*ln\_dynhpg\_zco=true*)

The hydrostatic pressure can be obtained by integrating the hydrostatic equation vertically from the surface. However, the pressure is large at great depth while its horizontal gradient is several orders of magnitude smaller. This may lead to large truncation errors in the pressure gradient terms. Thus, the two horizontal components of the hydrostatic pressure gradient are computed directly as follows:

for  $k = km$  (surface layer,  $jk = 1$  in the code)

$$\begin{cases} \delta_{i+1/2} [p^h] \Big|_{k=km} = \frac{1}{2} g \delta_{i+1/2} [e_{3w} \rho] \Big|_{k=km} \\ \delta_{j+1/2} [p^h] \Big|_{k=km} = \frac{1}{2} g \delta_{j+1/2} [e_{3w} \rho] \Big|_{k=km} \end{cases} \quad (6.18)$$

for  $1 < k < km$  (interior layer)

$$\begin{cases} \delta_{i+1/2} [p^h] \Big|_k = \delta_{i+1/2} [p^h] \Big|_{k-1} + \frac{1}{2} g \delta_{i+1/2} \left[ e_{3w} \bar{\rho}^{k+1/2} \right] \Big|_k \\ \delta_{j+1/2} [p^h] \Big|_k = \delta_{j+1/2} [p^h] \Big|_{k-1} + \frac{1}{2} g \delta_{j+1/2} \left[ e_{3w} \bar{\rho}^{k+1/2} \right] \Big|_k \end{cases} \quad (6.19)$$

Note that the  $1/2$  factor in (6.18) is adequate because of the definition of  $e_{3w}$  as the vertical derivative of the scale factor at the surface level ( $z = 0$ ). Note also that in case of variable volume level (`key_vvl` defined), the surface pressure gradient is included in (6.18) and (6.19) through the space and time variations of the vertical scale factor  $e_{3w}$ .

#### 6.4.2 $z$ -coordinate with partial step (`ln_dynhpg_zps=true`)

With partial bottom cells, tracers in horizontally adjacent cells generally live at different depths. Before taking horizontal gradients between these tracer points, a linear interpolation is used to approximate the deeper tracer as if it actually lived at the depth of the shallower tracer point.

Apart from this modification, the horizontal hydrostatic pressure gradient evaluated in the  $z$ -coordinate with partial step is exactly as in the pure  $z$ -coordinate case. As explained in detail in section §5.9, the nonlinearity of pressure effects in the equation of state is such that it is better to interpolate temperature and salinity vertically before computing the density. Horizontal gradients of temperature and salinity are needed for the TRA modules, which is the reason why the horizontal gradients of density at the deepest model level are computed in module `zpsdhe.F90` located in the TRA directory and described in §5.9.

#### 6.4.3 $s$ - and $z$ - $s$ -coordinates

Pressure gradient formulations in an  $s$ -coordinate have been the subject of a vast number of papers (*e.g.*, Song [1998], Shchepetkin and McWilliams [2005]). A number of different pressure gradient options are coded but the ROMS-like, density Jacobian with cubic polynomial method is currently disabled whilst known bugs are under investigation.

- Traditional coding (see for example Madec et al. [1996]): (`ln_dynhpg_sco=true`)

$$\begin{cases} -\frac{1}{\rho_o e_{1u}} \delta_{i+1/2} [p^h] + \frac{g \bar{\rho}^{i+1/2}}{\rho_o e_{1u}} \delta_{i+1/2} [z_t] \\ -\frac{1}{\rho_o e_{2v}} \delta_{j+1/2} [p^h] + \frac{g \bar{\rho}^{j+1/2}}{\rho_o e_{2v}} \delta_{j+1/2} [z_t] \end{cases} \quad (6.20)$$

Where the first term is the pressure gradient along coordinates, computed as in (6.18) - (6.19), and  $z_T$  is the depth of the  $T$ -point evaluated from the sum of the vertical scale factors at the  $w$ -point ( $e_{3w}$ ).



- Traditional coding with adaptation for ice shelf cavities (*ln\_dynhpg\_isf=true*). This scheme need the activation of ice shelf cavities (*ln\_isfcav=true*).
- Pressure Jacobian scheme (*prj*) (a research paper in preparation) (*ln\_dynhpg\_prj=true*)
- Density Jacobian with cubic polynomial scheme (DJC) [Shchepetkin and McWilliams 2005] (*ln\_dynhpg\_djc=true*) (currently disabled; under development)

Note that expression (6.20) is commonly used when the variable volume formulation is activated (**key\_vvl**) because in that case, even with a flat bottom, the coordinate surfaces are not horizontal but follow the free surface [Levier et al. 2007]. The pressure jacobian scheme (*ln\_dynhpg\_prj=true*) is available as an improved option to *ln\_dynhpg\_sco=true* when **key\_vvl** is active. The pressure Jacobian scheme uses a constrained cubic spline to reconstruct the density profile across the water column. This method maintains the monotonicity between the density nodes. The pressure can be calculated by analytical integration of the density profile and a pressure Jacobian method is used to solve the horizontal pressure gradient. This method can provide a more accurate calculation of the horizontal pressure gradient than the standard scheme.

#### 6.4.4 Ice shelf cavity

Beneath an ice shelf, the total pressure gradient is the sum of the pressure gradient due to the ice shelf load and the pressure gradient due to the ocean load. If cavity opened (*ln\_isfcav = true*) these 2 terms can be calculated by setting *ln\_dynhpg\_isf = true*. No other scheme are working with the ice shelf.

- The main hypothesis to compute the ice shelf load is that the ice shelf is in an isostatic equilibrium. The top pressure is computed integrating from surface to the base of the ice shelf a reference density profile (prescribed as density of a water at 34.4 PSU and  $-1.9^{\circ}C$ ) and corresponds to the water replaced by the ice shelf. This top pressure is constant over time. A detailed description of this method is described in Losch [2008].

- The ocean load is computed using the expression (6.20) described in 6.4.3.

#### 6.4.5 Time-scheme (*ln\_dynhpg\_imp= true/false*)

The default time differencing scheme used for the horizontal pressure gradient is a leapfrog scheme and therefore the density used in all discrete expressions given above is the *now* density, computed from the *now* temperature and salinity. In some specific cases (usually high resolution simulations over an ocean domain which includes weakly stratified regions) the physical phenomenon that controls the time-step is internal gravity waves (IGWs). A semi-implicit scheme for doubling the stability limit associated with IGWs can be used [Brown and Campana 1978, Maltrod et al. 1998]. It involves the evaluation of the hydrostatic pressure gradient as an average over the three time levels  $t - \Delta t$ ,  $t$ , and  $t + \Delta t$  (*i.e. before, now and after*

time-steps), rather than at the central time level  $t$  only, as in the standard leapfrog scheme.

- leapfrog scheme ( $ln\_dynhpg\_imp=true$ ):

$$\frac{u^{t+\Delta t} - u^{t-\Delta t}}{2\Delta t} = \dots - \frac{1}{\rho_o e_{1u}} \delta_{i+1/2} [p_h^t] \quad (6.21)$$

- semi-implicit scheme ( $ln\_dynhpg\_imp=true$ ):

$$\frac{u^{t+\Delta t} - u^{t-\Delta t}}{2\Delta t} = \dots - \frac{1}{4\rho_o e_{1u}} \delta_{i+1/2} [p_h^{t+\Delta t} + 2p_h^t + p_h^{t-\Delta t}] \quad (6.22)$$

The semi-implicit time scheme (6.22) is made possible without significant additional computation since the density can be updated to time level  $t + \Delta t$  before computing the horizontal hydrostatic pressure gradient. It can be easily shown that the stability limit associated with the hydrostatic pressure gradient doubles using (6.22) compared to that using the standard leapfrog scheme (6.21). Note that (6.22) is equivalent to applying a time filter to the pressure gradient to eliminate high frequency IGWs. Obviously, when using (6.22), the doubling of the time-step is achievable only if no other factors control the time-step, such as the stability limits associated with advection or diffusion.

In practice, the semi-implicit scheme is used when  $ln\_dynhpg\_imp=true$ . In this case, we choose to apply the time filter to temperature and salinity used in the equation of state, instead of applying it to the hydrostatic pressure or to the density, so that no additional storage array has to be defined. The density used to compute the hydrostatic pressure gradient (whatever the formulation) is evaluated as follows:

$$\rho^t = \rho(\tilde{T}, \tilde{S}, z_t) \quad \text{with} \quad \tilde{X} = 1/4 (X^{t+\Delta t} + 2X^t + X^{t-\Delta t}) \quad (6.23)$$

Note that in the semi-implicit case, it is necessary to save the filtered density, an extra three-dimensional field, in the restart file to restart the model with exact reproducibility. This option is controlled by  $nn\_dynhpg\_rst$ , a namelist parameter.

## 6.5 Surface pressure gradient (*dynspg.F90*)

```
!-----
&namdyn_spg      !   surface pressure gradient                               (default: NO)
!-----
ln_dynspg_exp = .false.   ! explicit free surface
ln_dynspg_ts  = .false.   ! split-explicit free surface
ln_bt_fw      = .true.    ! Forward integration of barotropic Eqs.
ln_bt_av      = .true.    ! Time filtering of barotropic variables
nn_btflt      = 1         ! Time filter choice = 0 None
!                                     !                                     = 1 Boxcar over nn_baro sub-steps
!                                     !                                     = 2 Boxcar over 2*nn_baro " "
ln_bt_auto    = .true.    ! Number of sub-step defined from:
rn_bt_cmax    = 0.8       ! =T : the Maximum Courant Number allowed
nn_baro       = 30        ! =F : the number of sub-step in rn_rdt seconds
/
```

Options are defined through the *namdyn\_spg* namelist variables. The surface pressure gradient term is related to the representation of the free surface (§2.2). The main distinction is between the fixed volume case (linear free surface) and the variable volume case (nonlinear free surface, **key\_vvl** is defined). In the linear free surface case (§2.2.2) the vertical scale factors  $e_3$  are fixed in time, while they are time-dependent in the nonlinear case (§2.2.2). With both linear and nonlinear free surface, external gravity waves are allowed in the equations, which imposes a very small time step when an explicit time stepping is used. Two methods are proposed to allow a longer time step for the three-dimensional equations: the filtered free surface, which is a modification of the continuous equations (see (??)), and the split-explicit free surface described below. The extra term introduced in the filtered method is calculated implicitly, so that the update of the next velocities is done in module *dynspg\_ft.F90* and not in *dynnxt.F90*.

The form of the surface pressure gradient term depends on how the user wants to handle the fast external gravity waves that are a solution of the analytical equation (§2.2). Three formulations are available, all controlled by a CPP key (`ln_dynspg_XXX`): an explicit formulation which requires a small time step ; a filtered free surface formulation which allows a larger time step by adding a filtering term into the momentum equation ; and a split-explicit free surface formulation, described below, which also allows a larger time step.

The extra term introduced in the filtered method is calculated implicitly, so that a solver is used to compute it. As a consequence the update of the *next* velocities is done in module *dynspg\_ft.F90* and not in *dynnxt.F90*.

### 6.5.1 Explicit free surface (**key\_dynspg\_exp**)

In the explicit free surface formulation (**key\_dynspg\_exp** defined), the model time step is chosen to be small enough to resolve the external gravity waves (typically a few tens of seconds). The surface pressure gradient, evaluated using a leap-frog scheme (*i.e.* centered in time), is thus simply given by :

$$\begin{cases} -\frac{1}{e_{1u} \rho_o} \delta_{i+1/2} [\rho \eta] \\ -\frac{1}{e_{2v} \rho_o} \delta_{j+1/2} [\rho \eta] \end{cases} \quad (6.24)$$

Note that in the non-linear free surface case (*i.e.* **key\_vvl** defined), the surface pressure gradient is already included in the momentum tendency through the level thickness variation allowed in the computation of the hydrostatic pressure gradient. Thus, nothing is done in the *dynspg\_exp.F90* module.

### 6.5.2 Split-Explicit free surface (**key\_dynspg\_ts**)

The split-explicit free surface formulation used in *NEMO* (**key\_dynspg\_ts** defined), also called the time-splitting formulation, follows the one proposed by Shchepetkin and McWilliams [2005]. The general idea is to solve the free surface equation and the associated barotropic velocity equations with a smaller time step than  $\Delta t$ , the time step used for the three dimensional prognostic variables (Fig. 6.2). The size of the small time step,  $\Delta t_e$  (the external mode or barotropic time step) is provided through the *nn\_baro* namelist parameter as:  $\Delta t_e = \Delta t / nn\_baro$ . This parameter can be optionally defined automatically (*ln\_bt\_nn\_auto=true*) considering that the stability of the barotropic system is essentially controlled by external waves propagation. Maximum Courant number is in that case time independent, and easily computed online from the input bathymetry. Therefore,  $\Delta t_e$  is adjusted so that the Maximum allowed Courant number is smaller than *rn\_bt\_cmax*.

The barotropic mode solves the following equations:

$$\frac{\partial \bar{\mathbf{U}}_h}{\partial t} = -f \mathbf{k} \times \bar{\mathbf{U}}_h - g \nabla_h \eta - \frac{c_b^U}{H + \eta} \bar{\mathbf{U}}_h + \bar{\mathbf{G}} \quad (6.25a)$$

$$\frac{\partial \eta}{\partial t} = -\nabla \cdot [(H + \eta) \bar{\mathbf{U}}_h] + P - E \quad (6.25b)$$

where  $\bar{\mathbf{G}}$  is a forcing term held constant, containing coupling term between modes, surface atmospheric forcing as well as slowly varying barotropic terms not explicitly computed to gain efficiency. The third term on the right hand side of (6.25a) represents the bottom stress (see section §10.4), explicitly accounted for at each barotropic iteration. Temporal discretization of the system above follows a three-time step Generalized Forward Backward algorithm detailed in Shchepetkin and McWilliams [2005]. AB3-AM4 coefficients used in *NEMO* follow the second-order accurate, "multi-purpose" stability compromise as defined in Shchepetkin and McWilliams [2008] (see their figure 12, lower left).

In the default case (*ln\_bt\_fw=true*), the external mode is integrated between *now* and *after* baroclinic time-steps (Fig. 6.2a). To avoid aliasing of fast barotropic motions into three dimensional equations, time filtering is eventually applied on barotropic quantities (*ln\_bt\_av=true*). In that case, the integration is extended slightly beyond *after* time step to provide time filtered quantities. These are used for the subsequent initialization of the barotropic mode in the following baroclinic step. Since external mode equations written at baroclinic time steps finally follow a forward time stepping scheme, asselin filtering is not applied to barotropic quantities. Alternatively, one can choose to integrate barotropic equations starting from *before* time step (*ln\_bt\_fw=false*). Although more computationally expensive (*nn\_baro* additional iterations are indeed necessary), the baroclinic to barotropic forcing term given at *now* time step become centred in the middle of the integration window. It can easily be shown that this property removes part of splitting errors between modes, which increases the overall numerical robustness.

As far as tracer conservation is concerned, barotropic velocities used to advect tracers must also be updated at *now* time step. This implies to change the

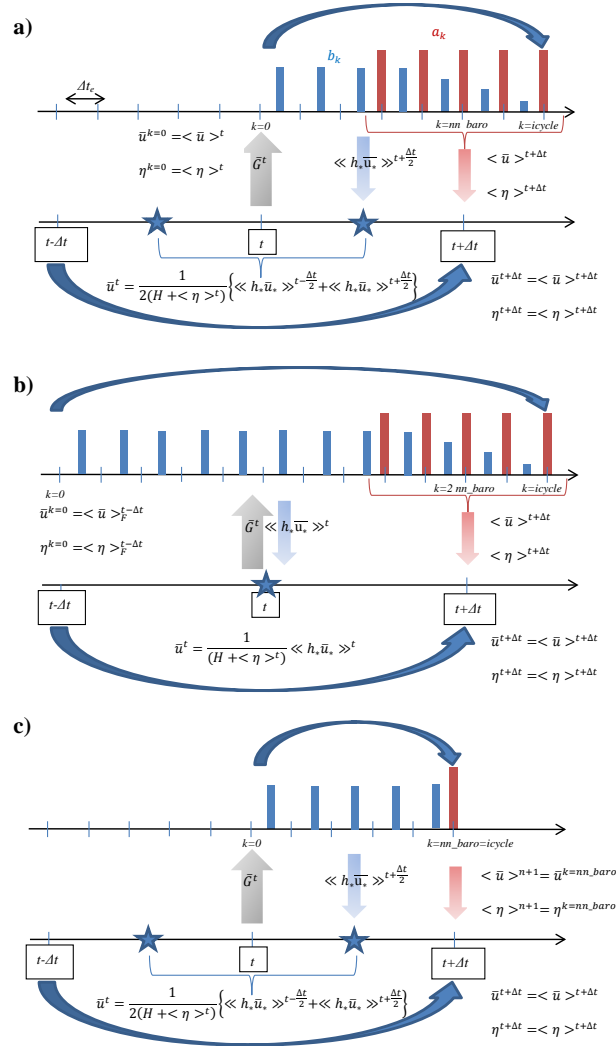


**Figure 6.2:** Schematic of the split-explicit time stepping scheme for the external and internal modes. Time increases to the right. In this particular example, a box-car averaging window over  $nn\_baro$  barotropic time steps is used ( $nn\_bt\_flt = 1$ ) and  $nn\_baro = 5$ . Internal mode time steps (which are also the model time steps) are denoted by  $t - \Delta t$ ,  $t$  and  $t + \Delta t$ . Variables with  $k$  superscript refer to instantaneous barotropic variables,  $\langle \rangle$  and  $\langle \langle \rangle \rangle$  operator refer to time filtered variables using respectively primary (red vertical bars) and secondary weights (blue vertical bars). The former are used to obtain time filtered quantities at  $t + \Delta t$  while the latter are used to obtain time averaged transports to advect tracers. a) Forward time integration:  $ln\_bt\_fw=true$ ,  $ln\_bt\_av=true$ . b) Centred time integration:  $ln\_bt\_fw=false$ ,  $ln\_bt\_av=true$ . c) Forward time integration with no time filtering (POM-like scheme):  $ln\_bt\_fw=true$ ,  $ln\_bt\_av=false$ .

traditional order of computations in *NEMO*: most of momentum trends (including the barotropic mode calculation) updated first, tracers' after. This *de facto* makes semi-implicit hydrostatic pressure gradient (see section §6.4.5) and time splitting not compatible. Advective barotropic velocities are obtained by using a secondary set of filtering weights, uniquely defined from the filter coefficients used for the time averaging (Shchepetkin and McWilliams [2005]). Consistency between the time averaged continuity equation and the time stepping of tracers is here the key to obtain exact conservation.

One can eventually choose to feedback instantaneous values by not using any time filter (*ln\_bt\_av=false*). In that case, external mode equations are continuous in time, ie they are not re-initialized when starting a new sub-stepping sequence. This is the method used so far in the POM model, the stability being maintained by refreshing at (almost) each barotropic time step advection and horizontal diffusion terms. Since the latter terms have not been added in *NEMO* for computational efficiency, removing time filtering is not recommended except for debugging purposes. This may be used for instance to appreciate the damping effect of the standard formulation on external gravity waves in idealized or weakly non-linear cases. Although the damping is lower than for the filtered free surface, it is still significant as shown by Levier et al. [2007] in the case of an analytical barotropic Kelvin wave.

### 6.5.3 Filtered free surface (key\_dynspgflt)

The filtered formulation follows the Roulet and Madec [2000] implementation. The extra term introduced in the equations (see §2.2.2) is solved implicitly. The elliptic solvers available in the code are documented in §15.

Note that in the linear free surface formulation (**key\_vvl** not defined), the ocean depth is time-independent and so is the matrix to be inverted. It is computed once and for all and applies to all ocean time steps.

## 6.6 Lateral diffusion term (*dynldf.F90*)

```

!-----
&namdyn_ldf      ! lateral diffusion on momentum                (default: NO selection)
!-----
!
!      ! Type of the operator :
ln_dynldf_NONE= .false.  ! No operator (i.e. no explicit diffusion)
ln_dynldf_lap = .false.  ! laplacian operator
ln_dynldf_blp = .false.  ! bilaplacian operator
!
!      ! Direction of action :
ln_dynldf_lev = .false.  ! iso-level
ln_dynldf_hor = .false.  ! horizontal (geopotential)
ln_dynldf_iso = .false.  ! iso-neutral
!
!      ! Coefficient
nn_ahm_ijk_t = 0        ! space/time variation of eddy coef
!      ! ==30 read in eddy_viscosity_3D.nc file
!      ! ==20 read in eddy_viscosity_2D.nc file
!      ! = 0 constant
!      ! = 10 F(k)=c1d
!      ! = 20 F(i,j)=F(grid spacing)=c2d
!      ! = 30 F(i,j,k)=c2d*c1d
!      ! = 31 F(i,j,k)=F(grid spacing and local velocity)
!      ! = 32 F(i,j,k)=F(local gridscale and deformation rate)
! Caution in 20 and 30 cases the coefficient have to be given for a 1 degree grid (~111km)
rn_ahm_0        = 40000. ! horizontal laplacian eddy viscosity [m2/s]

```

```

rn_ahm_b      = 0.      ! background eddy viscosity for ldf_iso [m2/s]
rn_bhm_0     = 1.e+12  ! horizontal bilaplacian eddy viscosity [m4/s]
!           ! Smagorinsky settings (nn_ahm_ijk_t = 32) :
rn_csmc      = 3.5    ! Smagorinsky constant of proportionality
rn_minfac    = 1.0    ! multiplier of theoretical lower limit
rn_maxfac    = 1.0    ! multiplier of theoretical upper limit
/

```

Options are defined through the *namdyn\_ldf* namelist variables. The options available for lateral diffusion are to use either laplacian (rotated or not) or biharmonic operators. The coefficients may be constant or spatially variable; the description of the coefficients is found in the chapter on lateral physics (Chap.9). The lateral diffusion of momentum is evaluated using a forward scheme, *i.e.* the velocity appearing in its expression is the *before* velocity in time, except for the pure vertical component that appears when a tensor of rotation is used. This latter term is solved implicitly together with the vertical diffusion term (see §3)

At the lateral boundaries either free slip, no slip or partial slip boundary conditions are applied according to the user's choice (see Chap.8).

### 6.6.1 Iso-level laplacian operator (*ln\_dynldf\_lap=true*)

For lateral iso-level diffusion, the discrete operator is:

$$\begin{cases} D_u^{lU} = \frac{1}{e_{1u}} \delta_{i+1/2} [A_T^{lm} \chi] - \frac{1}{e_{2u} e_{3u}} \delta_j [A_f^{lm} e_{3f} \zeta] \\ D_v^{lU} = \frac{1}{e_{2v}} \delta_{j+1/2} [A_T^{lm} \chi] + \frac{1}{e_{1v} e_{3v}} \delta_i [A_f^{lm} e_{3f} \zeta] \end{cases} \quad (6.26)$$

As explained in §2.5.2, this formulation (as the gradient of a divergence and curl of the vorticity) preserves symmetry and ensures a complete separation between the vorticity and divergence parts of the momentum diffusion.

### 6.6.2 Rotated laplacian operator (*ln\_dynldf\_iso=true*)

A rotation of the lateral momentum diffusion operator is needed in several cases: for iso-neutral diffusion in the *z*-coordinate (*ln\_dynldf\_iso=true*) and for either iso-neutral (*ln\_dynldf\_iso=true*) or geopotential (*ln\_dynldf\_hor=true*) diffusion in the *s*-coordinate. In the partial step case, coordinates are horizontal except at the deepest level and no rotation is performed when *ln\_dynldf\_hor=true*. The diffusion operator is defined simply as the divergence of down gradient momentum fluxes on each momentum component. It must be emphasized that this formulation ignores constraints on the stress tensor such as symmetry. The resulting discrete representation

is:

$$D_u^U = \frac{1}{e_{1u} e_{2u} e_{3u}} \left\{ \begin{aligned} & \delta_{i+1/2} \left[ A_T^{lm} \left( \frac{e_{2t} e_{3t}}{e_{1t}} \delta_i[u] - e_{2t} r_{1t} \overline{\overline{\delta_{k+1/2}[u]}}^{i,k} \right) \right] \\ & + \delta_j \left[ A_f^{lm} \left( \frac{e_{1f} e_{3f}}{e_{2f}} \delta_{j+1/2}[u] - e_{1f} r_{2f} \overline{\overline{\delta_{k+1/2}[u]}}^{j+1/2,k} \right) \right] \\ & + \delta_k \left[ A_{uw}^{lm} \left( -e_{2u} r_{1uw} \overline{\overline{\delta_{i+1/2}[u]}}^{i+1/2,k+1/2} \right. \right. \\ & \quad \left. \left. - e_{1u} r_{2uw} \overline{\overline{\delta_{j+1/2}[u]}}^{j,k+1/2} \right. \right. \\ & \quad \left. \left. + \frac{e_{1u} e_{2u}}{e_{3uw}} (r_{1uw}^2 + r_{2uw}^2) \delta_{k+1/2}[u] \right) \right] \end{aligned} \right\} \quad (6.27)$$

$$D_v^V = \frac{1}{e_{1v} e_{2v} e_{3v}} \left\{ \begin{aligned} & \delta_{i+1/2} \left[ A_f^{lm} \left( \frac{e_{2f} e_{3f}}{e_{1f}} \delta_{i+1/2}[v] - e_{2f} r_{1f} \overline{\overline{\delta_{k+1/2}[v]}}^{i+1/2,k} \right) \right] \\ & + \delta_j \left[ A_T^{lm} \left( \frac{e_{1t} e_{3t}}{e_{2t}} \delta_j[v] - e_{1t} r_{2t} \overline{\overline{\delta_{k+1/2}[v]}}^{j,k} \right) \right] \\ & + \delta_k \left[ A_{vw}^{lm} \left( -e_{2v} r_{1vw} \overline{\overline{\delta_{i+1/2}[v]}}^{i+1/2,k+1/2} \right. \right. \\ & \quad \left. \left. - e_{1v} r_{2vw} \overline{\overline{\delta_{j+1/2}[v]}}^{j+1/2,k+1/2} \right. \right. \\ & \quad \left. \left. + \frac{e_{1v} e_{2v}}{e_{3vw}} (r_{1vw}^2 + r_{2vw}^2) \delta_{k+1/2}[v] \right) \right] \end{aligned} \right\}$$

where  $r_1$  and  $r_2$  are the slopes between the surface along which the diffusion operator acts and the surface of computation ( $z$ - or  $s$ -surfaces). The way these slopes are evaluated is given in the lateral physics chapter (Chap.9).

### 6.6.3 Iso-level bilaplacian operator (*ln\_dynldf\_bilap=true*)

The lateral fourth order operator formulation on momentum is obtained by applying (6.26) twice. It requires an additional assumption on boundary conditions: the first derivative term normal to the coast depends on the free or no-slip lateral boundary conditions chosen, while the third derivative terms normal to the coast are set to zero (see Chap.8).

## 6.7 Vertical diffusion term (*dynzdf.F90*)

```
!-----
!&namzdf          ! vertical physics          (default: NO selection)
```



```

!-----
!
! type of vertical closure (required)
ln_zdfcst = .false. ! constant mixing
ln_zdfcric = .false. ! local Richardson dependent formulation (T => fill namzdf_ric)
ln_zdfktke = .false. ! Turbulent Kinetic Energy closure (T => fill namzdf_tke)
ln_zdfgls = .false. ! Generic Length Scale closure (T => fill namzdf_gls)
!
! convection
ln_zdfevd = .false. ! enhanced vertical diffusion
nn_evdm = 0 ! apply on tracer (=0) or on tracer and momentum (=1)
rn_evd = 100. ! mixing coefficient [m2/s]
ln_zdfnpc = .false. ! Non-Penetrative Convective algorithm
nn_npc = 1 ! frequency of application of npc
nn_npcp = 365 ! npc control print frequency
!
ln_zdfddm = .false. ! double diffusive mixing
rn_avts = 1.e-4 ! maximum avs (vertical mixing on salinity)
rn_hsbfr = 1.6 ! heat/salt buoyancy flux ratio
!
! gravity wave-driven vertical mixing
ln_zdfiwm = .false. ! internal wave-induced mixing (T => fill namzdf_iwm)
ln_zdfswm = .false. ! surface wave-induced mixing (T => ln_wave=ln_sdw=T)
!
! coefficients
rn_avm0 = 1.2e-4 ! vertical eddy viscosity [m2/s] (background Kz if ln_zdfcst=F)
rn_avt0 = 1.2e-5 ! vertical eddy diffusivity [m2/s] (background Kz if ln_zdfcst=F)
nn_avb = 0 ! profile for background avt & avm (=1) or not (=0)
nn_havtb = 0 ! horizontal shape for avtb (=1) or not (=0)
/

```

Options are defined through the *namzdf* namelist variables. The large vertical diffusion coefficient found in the surface mixed layer together with high vertical resolution implies that in the case of explicit time stepping there would be too restrictive a constraint on the time step. Two time stepping schemes can be used for the vertical diffusion term : (a) a forward time differencing scheme (*ln\_zdfexp=true*) using a time splitting technique (*nn\_zdfexp > 1*) or (b) a backward (or implicit) time differencing scheme (*ln\_zdfexp=false*) (see §3). Note that namelist variables *ln\_zdfexp* and *nn\_zdfexp* apply to both tracers and dynamics.

The formulation of the vertical subgrid scale physics is the same whatever the vertical coordinate is. The vertical diffusion operators given by (2.34) take the following semi-discrete space form:

$$\left\{ \begin{array}{l} D_u^{vm} \equiv \frac{1}{e_{3u}} \delta_k \left[ \frac{A_{uw}^{vm}}{e_{3uw}} \delta_{k+1/2} [u] \right] \\ D_v^{vm} \equiv \frac{1}{e_{3v}} \delta_k \left[ \frac{A_{vw}^{vm}}{e_{3vw}} \delta_{k+1/2} [v] \right] \end{array} \right. \quad (6.28)$$

where  $A_{uw}^{vm}$  and  $A_{vw}^{vm}$  are the vertical eddy viscosity and diffusivity coefficients. The way these coefficients are evaluated depends on the vertical physics used (see §10).

The surface boundary condition on momentum is the stress exerted by the wind. At the surface, the momentum fluxes are prescribed as the boundary condition on the vertical turbulent momentum fluxes,

$$\left( \frac{A^{vm}}{e_3} \frac{\partial \mathbf{U}_h}{\partial k} \right) \Big|_{z=1} = \frac{1}{\rho_o} \begin{pmatrix} \tau_u \\ \tau_v \end{pmatrix} \quad (6.29)$$

where  $(\tau_u, \tau_v)$  are the two components of the wind stress vector in the  $(\mathbf{i}, \mathbf{j})$  coordinate system. The high mixing coefficients in the surface mixed layer ensure that

the surface wind stress is distributed in the vertical over the mixed layer depth. If the vertical mixing coefficient is small (when no mixed layer scheme is used) the surface stress enters only the top model level, as a body force. The surface wind stress is calculated in the surface module routines (SBC, see Chap.7)

The turbulent flux of momentum at the bottom of the ocean is specified through a bottom friction parameterisation (see §10.4)

## 6.8 External Forcings

Besides the surface and bottom stresses (see the above section) which are introduced as boundary conditions on the vertical mixing, three other forcings may enter the dynamical equations by affecting the surface pressure gradient.

(1) When `ln_apr_dyn = true` (see §7.7), the atmospheric pressure is taken into account when computing the surface pressure gradient.

(2) When `ln_tide_pot = true` and `ln_tide = true` (see §7.8), the tidal potential is taken into account when computing the surface pressure gradient.

(3) When `nn_ice_embd = 2` and LIM or CICE is used (*i.e.* when the sea-ice is embedded in the ocean), the snow-ice mass is taken into account when computing the surface pressure gradient.

## 6.9 Time evolution term (*dynnxt.F90*)

```
!-----
&namdom      !   time and space domain
!-----
ln_linssh   = .false. ! =T linear free surface ==> model level are fixed in time
nn_closea   = 0       ! remove (=0) or keep (=1) closed seas and lakes (ORCA)
!
nn_msh      = 0       ! create (>0) a mesh file or not (=0)
rn_isfhmin  = 1.00    ! threshold (m) to discriminate grounding ice to floating ice
!
rn_rdt      = 5760.   ! time step for the dynamics and tracer
rn_atfp     = 0.1     ! asselin time filter parameter
!
ln_crs      = .false. ! Logical switch for coarsening module      (T => fill namcrs)
/
```

Options are defined through the *namdom* namelist variables. The general framework for dynamics time stepping is a leap-frog scheme, *i.e.* a three level centred time scheme associated with an Asselin time filter (cf. Chap.3). The scheme is applied to the velocity, except when using the flux form of momentum advection (cf. §6.3) in the variable volume case (**key\_vvl** defined), where it has to be applied to the thickness weighted velocity (see §A.3)

• vector invariant form or linear free surface (`ln_dynhpg_vec=true` ; **key\_vvl** not defined):

$$\begin{cases} u^{t+\Delta t} = u_f^{t-\Delta t} + 2\Delta t \text{ RHS}_u^t \\ u_f^t = u^t + \gamma \left[ u_f^{t-\Delta t} - 2u^t + u^{t+\Delta t} \right] \end{cases} \quad (6.30)$$

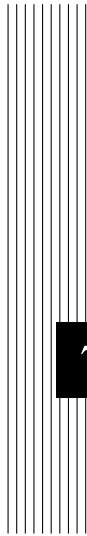
• flux form and nonlinear free surface (`ln_dynhpg_vec=false` ; **key\_vvl** defined):

$$\begin{cases} (e_{3u} u)^{t+\Delta t} = (e_{3u} u)_f^{t-\Delta t} + 2\Delta t e_{3u} \text{RHS}_u^t \\ (e_{3u} u)_f^t = (e_{3u} u)^t + \gamma \left[ (e_{3u} u)_f^{t-\Delta t} - 2(e_{3u} u)^t + (e_{3u} u)^{t+\Delta t} \right] \end{cases} \quad (6.31)$$

where RHS is the right hand side of the momentum equation, the subscript *f* denotes filtered values and  $\gamma$  is the Asselin coefficient.  $\gamma$  is initialized as *nn\_atfp* (namelist parameter). Its default value is *nn\_atfp* =  $10^{-3}$ . In both cases, the modified Asselin filter is not applied since perfect conservation is not an issue for the momentum equations.

Note that with the filtered free surface, the update of the *after* velocities is done in the *dynsp\_ft.F90* module, and only array swapping and Asselin filtering is done in *dynnxt.F90*.





# 7 Surface Boundary Condition (SBC, ISF, ICB)

## Contents

---

<b>7.1</b>	<b>Surface boundary condition for the ocean</b>	<b>127</b>
<b>7.2</b>	<b>Input Data generic interface</b>	<b>127</b>
7.2.1	Input Data specification ( <i>fdread.F90</i> )	128
7.2.2	Interpolation on-the-Fly	130
7.2.3	Standalone Surface Boundary Condition Scheme	133
<b>7.3</b>	<b>Analytical formulation (<i>sbcana</i>)</b>	<b>134</b>
<b>7.4</b>	<b>Flux formulation (<i>sbcflx</i>)</b>	<b>135</b>
<b>7.5</b>	<b>Bulk formulation (<i>sbcblk_core</i>, <i>sbcblk_clio</i> or <i>sbcblk_mfs</i>)</b>	<b>135</b>
7.5.1	CORE Bulk formulae ( <i>ln_core=true</i> )	135
7.5.2	CLIO Bulk formulae ( <i>ln_clio=true</i> )	136
7.5.3	MFS Bulk formulae ( <i>ln_mfs=true</i> )	137
<b>7.6</b>	<b>Coupled formulation (<i>sbcopl</i>)</b>	<b>138</b>
<b>7.7</b>	<b>Atmospheric pressure (<i>sbcapr</i>)</b>	<b>139</b>
<b>7.8</b>	<b>Tidal Potential (<i>sbc tide</i>)</b>	<b>140</b>
<b>7.9</b>	<b>River runoffs (<i>sbc rnf</i>)</b>	<b>141</b>
<b>7.10</b>	<b>Ice shelf melting (<i>sbc isf</i>)</b>	<b>142</b>
<b>7.11</b>	<b>Ice sheet coupling</b>	<b>144</b>
<b>7.12</b>	<b>Handling of icebergs (ICB)</b>	<b>146</b>
<b>7.13</b>	<b>Miscellaneous options</b>	<b>147</b>
7.13.1	Diurnal cycle ( <i>sbc dcy</i> )	147
7.13.2	Rotation of vector pairs onto the model grid directions	149
7.13.3	Surface restoring to observed SST and/or SSS ( <i>sbc sst</i> )	150
7.13.4	Handling of ice-covered area ( <i>sbc ice...</i> )	150

7.13.5	Interface to CICE ( <i>sbice_cice</i> ) . . . . .	151
7.13.6	Freshwater budget control ( <i>sbcfwb</i> ) . . . . .	152
7.13.7	Neutral drag coefficient from external wave model ( <i>sbwave</i> )	152

---

```

!-----
&namsbc      !   Surface Boundary Condition (surface module)
!-----
nn_fsbc      = 5          !   frequency of surface boundary condition computation
                    !   (also = the frequency of sea-ice & iceberg model call)
                    !   Type of air-sea fluxes
ln_usr       = .false.   !   user defined formulation              (T => check usrdef_sbc)
ln_flx       = .false.   !   flux formulation                  (T => fill namsbc_flux)
ln_blk       = .false.   !   Bulk formulation                      (T => fill namsbc_blk)
                    !   Type of coupling (Ocean/Ice/Atmosphere) :
ln_cpl       = .false.   !   atmosphere coupled formulation          ( requires key_oasis3 )
ln_mixcpl    = .false.   !   forced-coupled mixed formulation        ( requires key_oasis3 )
nn_components = 0        !   configuration of the opa-sas OASIS coupling
                    !   =0 no opa-sas OASIS coupling: default single executable config.
                    !   =1 opa-sas OASIS coupling: multi executable config., OPA component
                    !   =2 opa-sas OASIS coupling: multi executable config., SAS component
                    !   Sea-ice :
nn_ice       = 0        !   =0 no ice boundary condition      ,
                    !   =1 use observed ice-cover      ,
                    !   =2 or 3 automatically for LIM3 or CICE ("key_lim3" or "key_cice")
                    !   except in AGRIF zoom where it has to be specified
ln_ice_embd  = .false.  !   =T embedded sea-ice (pressure + mass and salt exchanges)
                    !   =F levitating ice (no pressure, mass and salt exchanges)
                    !   Misc. options of sbc :
ln_traqsr   = .true.   !   Light penetration in the ocean          (T => fill namtra_qsr)
ln_dm2dc    = .false.  !   daily mean to diurnal cycle on short wave
ln_rnf      = .true.   !   runoffs                                (T => fill namsbc_rnf)
ln_ssr      = .true.   !   Sea Surface Restoring on T and/or S      (T => fill namsbc_ssr)
nn_fwb      = 2        !   FreshWater Budget: =0 unchecked
                    !   =1 global mean of e-p-r set to zero at each time step
                    !   =2 annual global mean of e-p-r set to zero
ln_apr_dyn  = .false.  !   Patm gradient added in ocean & ice Eqs. (T => fill namsbc_apr)
ln_isf      = .false.  !   ice shelf                              (T => fill namsbc_isf)
ln_wave     = .false.  !   Activate coupling with wave            (T => fill namsbc_wave)
ln_cdgw     = .false.  !   Neutral drag coefficient read from wave model (T => ln_wave=.true. & fill namsbc_wave)
ln_sdw      = .false.  !   Read 2D Surf Stokes Drift & Computation of 3D stokes drift (T => ln_wave=.true. & fill namsbc_wave)
ln_tauoc    = .false.  !   Activate ocean stress modified by external wave induced stress (T => ln_wave=.true. & fill namsbc_wave)
ln_stcor    = .false.  !   Activate Stokes Coriolis term (T => ln_wave=.true. & ln_sdw=.true. & fill namsbc_wave)
nn_lsm      = 0        !   =0 land/sea mask for input fields is not applied (keep empty land/sea mask filename field) ,
                    !   =1:n number of iterations of land/sea mask application for input fields (fill land/sea mask filename field)
/

```

The ocean needs six fields as surface boundary condition:

- the two components of the surface ocean stress ( $\tau_u$ ,  $\tau_v$ )
- the incoming solar and non solar heat fluxes ( $Q_{ns}$ ,  $Q_{sr}$ )
- the surface freshwater budget ( $emp$ )
- the surface salt flux associated with freezing/melting of seawater ( $sfx$ )

plus an optional field:

- the atmospheric pressure at the ocean surface ( $p_a$ )

Five different ways to provide the first six fields to the ocean are available which are controlled by namelist *namsbc* variables: an analytical formulation (*ln\_ana* = true), a flux formulation (*ln\_flux* = true), a bulk formulae formulation (CORE (*ln\_blk\_core* = true), CLIO (*ln\_blk\_clio* = true) or MFS<sup>1</sup> (*ln\_blk\_mfs* = true) bulk formulae) and a coupled or mixed forced/coupled formulation (exchanges with a atmospheric model

<sup>1</sup> Note that MFS bulk formulae compute fluxes only for the ocean component

via the OASIS coupler) (*ln\_cpl* or *ln\_mixcpl* = true). When used (*i.e.* *ln\_apr\_dyn* = true), the atmospheric pressure forces both ocean and ice dynamics.

The frequency at which the forcing fields have to be updated is given by the *nn\_fsbc* namelist parameter. When the fields are supplied from data files (flux and bulk formulations), the input fields need not be supplied on the model grid. Instead a file of coordinates and weights can be supplied which maps the data from the supplied grid to the model points (so called "Interpolation on the Fly", see §7.2.2). If the Interpolation on the Fly option is used, input data belonging to land points (in the native grid), can be masked to avoid spurious results in proximity of the coasts as large sea-land gradients characterize most of the atmospheric variables.

In addition, the resulting fields can be further modified using several namelist options. These options control

- the rotation of vector components supplied relative to an east-north coordinate system onto the local grid directions in the model ;
- the addition of a surface restoring term to observed SST and/or SSS (*ln\_ssr* = true) ;
- the modification of fluxes below ice-covered areas (using observed ice-cover or a sea-ice model) (*nn\_ice* = 0, 1, 2 or 3) ;
- the addition of river runoffs as surface freshwater fluxes or lateral inflow (*ln\_rnf* = true) ;
- the addition of isf melting as lateral inflow (parameterisation) or as fluxes applied at the land-ice ocean interface (*ln\_isf*) ;
- the addition of a freshwater flux adjustment in order to avoid a mean sea-level drift (*nn\_fwb* = 0, 1 or 2) ;
- the transformation of the solar radiation (if provided as daily mean) into a diurnal cycle (*ln\_dm2dc* = true) ; and a neutral drag coefficient can be read from an external wave model (*ln\_cdgw* = true).

The latter option is possible only in case core or mfs bulk formulas are selected.

In this chapter, we first discuss where the surface boundary condition appears in the model equations. Then we present the five ways of providing the surface boundary condition, followed by the description of the atmospheric pressure and the river runoff. Next the scheme for interpolation on the fly is described. Finally, the different options that further modify the fluxes applied to the ocean are discussed. One of these is modification by icebergs (see §7.12), which act as drifting sources of fresh water. Another example of modification is that due to the ice shelf melting/freezing (see §7.10), which provides additional sources of fresh water.



**Table 7.1:** Ocean variables provided by the ocean to the surface module (SBC). The variable are averaged over *nn\_fsbc* time step, *i.e.* the frequency of computation of surface fluxes.

Variable description	Model variable	Units	point
i-component of the surface current	ssu_m	$m.s^{-1}$	U
j-component of the surface current	ssv_m	$m.s^{-1}$	V
Sea surface temperature	sst_m	$^{\circ}K$	T
Sea surface salinty	sss_m	<i>psu</i>	T

## 7.1 Surface boundary condition for the ocean

The surface ocean stress is the stress exerted by the wind and the sea-ice on the ocean. It is applied in *dynzdf.F90* module as a surface boundary condition of the computation of the momentum vertical mixing trend (see (6.29) in §6.7). As such, it has to be provided as a 2D vector interpolated onto the horizontal velocity ocean mesh, *i.e.* resolved onto the model (**i,j**) direction at *u*- and *v*-points.

The surface heat flux is decomposed into two parts, a non solar and a solar heat flux,  $Q_{ns}$  and  $Q_{sr}$ , respectively. The former is the non penetrative part of the heat flux (*i.e.* the sum of sensible, latent and long wave heat fluxes plus the heat content of the mass exchange with the atmosphere and sea-ice). It is applied in *trasbc.F90* module as a surface boundary condition trend of the first level temperature time evolution equation (see (5.12) and (5.13) in §5.4.1). The latter is the penetrative part of the heat flux. It is applied as a 3D trends of the temperature equation (*traqsr.F90* module) when *ln\_traqsr=true*. The way the light penetrates inside the water column is generally a sum of decreasing exponentials (see §5.4.2).

The surface freshwater budget is provided by the *emp* field. It represents the mass flux exchanged with the atmosphere (evaporation minus precipitation) and possibly with the sea-ice and ice shelves (freezing minus melting of ice). It affects both the ocean in two different ways: (*i*) it changes the volume of the ocean and therefore appears in the sea surface height equation as a volume flux, and (*ii*) it changes the surface temperature and salinity through the heat and salt contents of the mass exchanged with the atmosphere, the sea-ice and the ice shelves.

The ocean model provides, at each time step, to the surface module (*sbc-mod.F90*) the surface currents, temperature and salinity. These variables are averaged over *nn\_fsbc* time-step (7.1), and it is these averaged fields which are used to computes the surface fluxes at a frequency of *nn\_fsbc* time-step.

## 7.2 Input Data generic interface

A generic interface has been introduced to manage the way input data (2D or 3D fields, like surface forcing or ocean T and S) are specify in *NEMO*. This task is

archieved by *fldread.F90*. The module was design with four main objectives in mind:

1. optionally provide a time interpolation of the input data at model time-step, whatever their input frequency is, and according to the different calendars available in the model.
2. optionally provide an on-the-fly space interpolation from the native input data grid to the model grid.
3. make the run duration independent from the period cover by the input files.
4. provide a simple user interface and a rather simple developer interface by limiting the number of prerequisite information.

As a results the user have only to fill in for each variable a structure in the namelist file to defined the input data file and variable names, the frequency of the data (in hours or months), whether its is climatological data or not, the period covered by the input file (one year, month, week or day), and three additional parameters for on-the-fly interpolation. When adding a new input variable, the developer has to add the associated structure in the namelist, read this information by mirroring the namelist read in *sbc\_blk\_init* for example, and simply call *fld\_read* to obtain the desired input field at the model time-step and grid points.

The only constraints are that the input file is a NetCDF file, the file name follows a nomenclature (see §7.2.1), the period it cover is one year, month, week or day, and, if on-the-fly interpolation is used, a file of weights must be supplied (see §7.2.2).

Note that when an input data is archived on a disc which is accessible directly from the workspace where the code is executed, then the use can set the *cn\_dir* to the pathway leading to the data. By default, the data are assumed to have been copied so that *cn\_dir*='./'.

### 7.2.1 Input Data specification (*fldread.F90*)

The structure associated with an input variable contains the following information:

```
! file name ! frequency (hours) ! variable ! time interp. ! clim ! 'yearly' / ! weights ! rotation ! land/sea mask !
!           ! (if <0 months) ! name      ! (logical) ! (T/F) ! 'monthly' ! filename ! pairing ! filename      !
```

where

**File name** : the stem name of the NetCDF file to be open. This stem will be completed automatically by the model, with the addition of a '.nc' at its end and by date information and possibly a prefix (when using AGRIF). Tab.7.2 provides the resulting file name in all possible cases according to whether it is a climatological file or not, and to the open/close frequency (see below for definition).

**Table 7.2:** naming nomenclature for climatological or interannual input file, as a function of the Open/close frequency. The stem name is assumed to be 'fn'. For weekly files, the 'LLL' corresponds to the first three letters of the first day of the week (*i.e.* 'sun', 'sat', 'fri', 'thu', 'wed', 'tue', 'mon'). The 'YYYY', 'MM' and 'DD' should be replaced by the actual year/month/day, always coded with 4 or 2 digits. Note that (1) in mpp, if the file is split over each subdomain, the suffix '.nc' is replaced by '\_PPPP.nc', where 'PPPP' is the process number coded with 4 digits; (2) when using AGRIF, the prefix '\_N' is added to files, where 'N' is the child grid number.

	daily or weekLLL	monthly	yearly
clim = false	fn_yYYYYmMMdDD	fn_yYYYYmMM	fn_yYYYY
clim = true	not possible	fn_m??.nc	fn

**Record frequency** : the frequency of the records contained in the input file. Its unit is in hours if it is positive (for example 24 for daily forcing) or in months if negative (for example -1 for monthly forcing or -12 for annual forcing). Note that this frequency must really be an integer and not a real. On some computers, setting it to '24.' can be interpreted as 240!

**Variable name** : the name of the variable to be read in the input NetCDF file.

**Time interpolation** : a logical to activate, or not, the time interpolation. If set to 'false', the forcing will have a steplike shape remaining constant during each forcing period. For example, when using a daily forcing without time interpolation, the forcing remaining constant from 00h00'00" to 23h59'59". If set to 'true', the forcing will have a broken line shape. Records are assumed to be dated the middle of the forcing period. For example, when using a daily forcing with time interpolation, linear interpolation will be performed between mid-day of two consecutive days.

**Climatological forcing** : a logical to specify if a input file contains climatological forcing which can be cycle in time, or an interannual forcing which will requires additional files if the period covered by the simulation exceed the one of the file. See the above the file naming strategy which impacts the expected name of the file to be opened.

**Open/close frequency** : the frequency at which forcing files must be opened/closed. Four cases are coded: 'daily', 'weekLLL' (with 'LLL' the first 3 letters of the first day of the week), 'monthly' and 'yearly' which means the forcing files will contain data for one day, one week, one month or one year. Files are assumed to contain data from the beginning of the open/close period. For example, the first record of a yearly file containing daily data is Jan 1st even if the experiment is not starting at the beginning of the year.

**Others** : 'weights filename', 'pairing rotation' and 'land/sea mask' are associated with on-the-fly interpolation which is described in §7.2.2.

Additional remarks:

(1) The time interpolation is a simple linear interpolation between two consecutive records of the input data. The only tricky point is therefore to specify the date at which we need to do the interpolation and the date of the records read in the input files. Following [Leclair and Madec \[2009\]](#), the date of a time step is set at the middle of the time step. For example, for an experiment starting at 0h00'00" with a one hour time-step, a time interpolation will be performed at the following time: 0h30'00", 1h30'00", 2h30'00", etc. However, for forcing data related to the surface module, values are not needed at every time-step but at every *nn.fsbc* time-step. For example with *nn.fsbc* = 3, the surface module will be called at time-steps 1, 4, 7, etc. The date used for the time interpolation is thus redefined to be at the middle of *nn.fsbc* time-step period. In the previous example, this leads to: 1h30'00", 4h30'00", 7h30'00", etc.

(2) For code readability and maintenance issues, we don't take into account the NetCDF input file calendar. The calendar associated with the forcing field is build according to the information provided by user in the record frequency, the open/close frequency and the type of temporal interpolation. For example, the first record of a yearly file containing daily data that will be interpolated in time is assumed to be start Jan 1st at 12h00'00" and end Dec 31st at 12h00'00".

(3) If a time interpolation is requested, the code will pick up the needed data in the previous (next) file when interpolating data with the first (last) record of the open/close period. For example, if the input file specifications are "yearly, containing daily data to be interpolated in time", the values given by the code between 00h00'00" and 11h59'59" on Jan 1st will be interpolated values between Dec 31st 12h00'00" and Jan 1st 12h00'00". If the forcing is climatological, Dec and Jan will be keep-up from the same year. However, if the forcing is not climatological, at the end of the open/close period the code will automatically close the current file and open the next one. Note that, if the experiment is starting (ending) at the beginning (end) of an open/close period we do accept that the previous (next) file is not existing. In this case, the time interpolation will be performed between two identical values. For example, when starting an experiment on Jan 1st of year Y with yearly files and daily data to be interpolated, we do accept that the file related to year Y-1 is not existing. The value of Jan 1st will be used as the missing one for Dec 31st of year Y-1. If the file of year Y-1 exists, the code will read its last record. Therefore, this file can contain only one record corresponding to Dec 31st, a useful feature for user considering that it is too heavy to manipulate the complete file for year Y-1.

### 7.2.2 Interpolation on-the-Fly

Interpolation on the Fly allows the user to supply input files required for the surface forcing on grids other than the model grid. To do this he or she must supply, in addition to the source data file, a file of weights to be used to interpolate from the data grid to the model grid. The original development of this code used the

SCRIP package (freely available [here](#) under a copyright agreement). In principle, any package can be used to generate the weights, but the variables in the input weights file must have the same names and meanings as assumed by the model. Two methods are currently available: bilinear and bicubic interpolation. Prior to the interpolation, providing a land/sea mask file, the user can decide to remove land points from the input file and substitute the corresponding values with the average of the 8 neighbouring points in the native external grid. Only "sea points" are considered for the averaging. The land/sea mask file must be provided in the structure associated with the input variable. The netcdf land/sea mask variable name must be 'LSM' it must have the same horizontal and vertical dimensions of the associated variable and should be equal to 1 over land and 0 elsewhere. The procedure can be recursively applied setting `nn_lsm = 1` in `namsbc` namelist. Note that `nn_lsm=0` forces the code to not apply the procedure even if a file for land/sea mask is supplied.

### Bilinear Interpolation

The input weights file in this case has two sets of variables: `src01`, `src02`, `src03`, `src04` and `wgt01`, `wgt02`, `wgt03`, `wgt04`. The "src" variables correspond to the point in the input grid to which the weight "wgt" is to be applied. Each src value is an integer corresponding to the index of a point in the input grid when written as a one dimensional array. For example, for an input grid of size 5x10, point (3,2) is referenced as point 8, since  $(2-1)*5+3=8$ . There are four of each variable because bilinear interpolation uses the four points defining the grid box containing the point to be interpolated. All of these arrays are on the model grid, so that values `src01(i,j)` and `wgt01(i,j)` are used to generate a value for point (i,j) in the model.

Symbolically, the algorithm used is:

$$f_m(i, j) = f_m(i, j) + \sum_{k=1}^4 wgt(k) f(idx(src(k))) \quad (7.1)$$

where function `idx()` transforms a one dimensional index `src(k)` into a two dimensional index, and `wgt(1)` corresponds to variable "wgt01" for example.

### Bicubic Interpolation

Again there are two sets of variables: "src" and "wgt". But in this case there are 16 of each. The symbolic algorithm used to calculate values on the model grid is now:

$$\begin{aligned}
f_m(i, j) = f_m(i, j) &+ \sum_{k=1}^4 wgt(k) f(idx(src(k))) + \sum_{k=5}^8 wgt(k) \left. \frac{\partial f}{\partial i} \right|_{idx(src(k))} \\
&+ \sum_{k=9}^{12} wgt(k) \left. \frac{\partial f}{\partial j} \right|_{idx(src(k))} + \sum_{k=13}^{16} wgt(k) \left. \frac{\partial^2 f}{\partial i \partial j} \right|_{idx(src(k))}
\end{aligned}$$

The gradients here are taken with respect to the horizontal indices and not distances since the spatial dependency has been absorbed into the weights.

### Implementation

To activate this option, a non-empty string should be supplied in the weights file-name column of the relevant namelist; if this is left as an empty string no action is taken. In the model, weights files are read in and stored in a structured type (WGT) in the fldread module, as and when they are first required. This initialisation procedure determines whether the input data grid should be treated as cyclical or not by inspecting a global attribute stored in the weights input file. This attribute must be called "ew\_wrap" and be of integer type. If it is negative, the input non-model grid is assumed not to be cyclic. If zero or greater, then the value represents the number of columns that overlap. *E.g.* if the input grid has columns at longitudes 0, 1, 2, ..., 359, then ew\_wrap should be set to 0; if longitudes are 0.5, 2.5, ..., 358.5, 360.5, 362.5, ew\_wrap should be 2. If the model does not find attribute ew\_wrap, then a value of -999 is assumed. In this case the *fld\_read* routine defaults ew\_wrap to value 0 and therefore the grid is assumed to be cyclic with no overlapping columns. (In fact this only matters when bicubic interpolation is required.) Note that no testing is done to check the validity in the model, since there is no way of knowing the name used for the longitude variable, so it is up to the user to make sure his or her data is correctly represented.

Next the routine reads in the weights. Bicubic interpolation is assumed if it finds a variable with name "src05", otherwise bilinear interpolation is used. The WGT structure includes dynamic arrays both for the storage of the weights (on the model grid), and when required, for reading in the variable to be interpolated (on the input data grid). The size of the input data array is determined by examining the values in the "src" arrays to find the minimum and maximum i and j values required. Since bicubic interpolation requires the calculation of gradients at each point on the grid, the corresponding arrays are dimensioned with a halo of width one grid point all the way around. When the array of points from the data file is adjacent to an edge of the data grid, the halo is either a copy of the row/column next to it (non-cyclical case), or is a copy of one from the first few columns on the opposite side of the grid (cyclical case).

### Limitations

1. The case where input data grids are not logically rectangular has not been tested.
2. This code is not guaranteed to produce positive definite answers from positive definite inputs when a bicubic interpolation method is used.
3. The cyclic condition is only applied on left and right columns, and not to top and bottom rows.
4. The gradients across the ends of a cyclical grid assume that the grid spacing between the two columns involved are consistent with the weights used.
5. Neither interpolation scheme is conservative. (There is a conservative scheme available in SCRIP, but this has not been implemented.)

### Utilities

A set of utilities to create a weights file for a rectilinear input grid is available (see the directory NEMOGCM/TOOLS/WEIGHTS).

#### 7.2.3 Standalone Surface Boundary Condition Scheme

```

!-----
&namcbc_sas      ! Stand-Alone Surface boundary condition
!-----
!
!   ! file name ! frequency (hours) ! variable ! time interp.! clim ! 'yearly'// ! weights ! rotation ! land/sea mask !
!   !           ! (if <0 months) ! name      ! (logical) ! (T/F) ! 'monthly' ! filename ! pairing ! filename !
sn_ustp      = 'sas_grid_U',    120      , 'uos'      , .true.    , .true.    , 'yearly' , ''      , ''      , ''      , ''
sn_vstp      = 'sas_grid_V',    120      , 'vos'      , .true.    , .true.    , 'yearly' , ''      , ''      , ''      , ''
sn_tem       = 'sas_grid_T',    120      , 'sosstst'  , .true.    , .true.    , 'yearly' , ''      , ''      , ''      , ''
sn_sal       = 'sas_grid_T',    120      , 'sosaline' , .true.    , .true.    , 'yearly' , ''      , ''      , ''      , ''
sn_ssh       = 'sas_grid_T',    120      , 'sosshg'   , .true.    , .true.    , 'yearly' , ''      , ''      , ''      , ''
sn_e3t       = 'sas_grid_T',    120      , 'e3t_m'    , .true.    , .true.    , 'yearly' , ''      , ''      , ''      , ''
sn_frq       = 'sas_grid_T',    120      , 'frq_m'    , .true.    , .true.    , 'yearly' , ''      , ''      , ''      , ''

l_sasread    = .true.    ! =T Read the above fields in a file, =F initialize to 0. in sbcssm.F90
ln_3d_uve    = .false.   ! specify whether we are supplying a 3D u,v and e3 field
ln_read_frq  = .false.   ! specify whether we must read frq or not
cn_dir       = './'      ! root directory for the location of the bulk files are
/

```

In some circumstances it may be useful to avoid calculating the 3D temperature, salinity and velocity fields and simply read them in from a previous run or receive them from OASIS. For example:

- Multiple runs of the model are required in code development to see the effect of different algorithms in the bulk formulae.
- The effect of different parameter sets in the ice model is to be examined.
- Development of sea-ice algorithms or parameterizations.
- spinup of the iceberg floats
- ocean/sea-ice simulation with both media running in parallel (*ln\_mixcpl = true*)

The StandAlone Surface scheme provides this utility. Its options are defined through the *namsbc\_sas* namelist variables. A new copy of the model has to be compiled with a configuration based on ORCA2\_SAS\_LIM. However no namelist parameters need be changed from the settings of the previous run (except perhaps *nn\_date0*) In this configuration, a few routines in the standard model are overridden by new versions. Routines replaced are:

- *nemogcm.F90* : This routine initialises the rest of the model and repeatedly calls the *stp* time stepping routine (*step.F90*) Since the ocean state is not calculated all associated initialisations have been removed.
- *step.F90* : The main time stepping routine now only needs to call the *sbc* routine (and a few utility functions).
- *sbcmod.F90* : This has been cut down and now only calculates surface forcing and the ice model required. New surface modules that can function when only the surface level of the ocean state is defined can also be added (e.g. icebergs).
- *daymod.F90* : No ocean restarts are read or written (though the ice model restarts are retained), so calls to restart functions have been removed. This also means that the calendar cannot be controlled by time in a restart file, so the user must make sure that *nn\_date0* in the model namelist is correct for his or her purposes.
- *stpctl.F90* : Since there is no free surface solver, references to it have been removed from *stp\_ctl* module.
- *diawri.F90* : All 3D data have been removed from the output. The surface temperature, salinity and velocity components (which have been read in) are written along with relevant forcing and ice data.

One new routine has been added:

- *sbc\_sas.F90* : This module initialises the input files needed for reading temperature, salinity and velocity arrays at the surface. These filenames are supplied in namelist *namsbc\_sas*. Unfortunately because of limitations with the *iom.F90* module, the full 3D fields from the mean files have to be read in and interpolated in time, before using just the top level. Since *fldread* is used to read in the data, Interpolation on the Fly may be used to change input data resolution.

### 7.3 Analytical formulation (*sbcana.F90* module)



The analytical formulation of the surface boundary condition is the default scheme. In this case, all the six fluxes needed by the ocean are assumed to be uniform in space. They take constant values given in the namelist *namcbc\_ana* by the variables *rn\_utau0*, *rn\_vtau0*, *rn\_qns0*, *rn\_qsr0*, and *rn\_emp0* (*emp* = *emp<sub>S</sub>*). The runoff is set to zero. In addition, the wind is allowed to reach its nominal value within a given number of time steps (*nn\_tau000*).

If a user wants to apply a different analytical forcing, the *sbcana.F90* module can be modified to use another scheme. As an example, the *sbc\_ana\_gyre.F90* routine provides the analytical forcing for the GYRE configuration (see GYRE configuration manual, in preparation).

## 7.4 Flux formulation (*sbcflx.F90* module)

```

!-----
&namcbc_flux ! surface boundary condition : flux formulation
!-----
!
! ! file name ! frequency (hours) ! variable ! time interp. ! clim ! 'yearly'/' ! weights ! rotation ! land/sea mask !
! ! ! (if <0 months) ! name ! (logical) ! (T/F) ! 'monthly' ! filename ! pairing ! filename !
!
sn_utau = 'utau' , 24 , 'utau' , .false. , .false. , 'yearly' , '' , '' , ''
sn_vtau = 'vtau' , 24 , 'vtau' , .false. , .false. , 'yearly' , '' , '' , ''
sn_qtot = 'qtot' , 24 , 'qtot' , .false. , .false. , 'yearly' , '' , '' , ''
sn_qsr = 'qsr' , 24 , 'qsr' , .false. , .false. , 'yearly' , '' , '' , ''
sn_emp = 'emp' , 24 , 'emp' , .false. , .false. , 'yearly' , '' , '' , ''
!
!
cn_dir = './' ! root directory for the location of the flux files
/

```

In the flux formulation (*ln\_flux=true*), the surface boundary condition fields are directly read from input files. The user has to define in the namelist *namcbc\_flux* the name of the file, the name of the variable read in the file, the time frequency at which it is given (in hours), and a logical setting whether a time interpolation to the model time step is required for this field. See §7.2.1 for a more detailed description of the parameters.

Note that in general, a flux formulation is used in associated with a restoring term to observed SST and/or SSS. See §7.13.3 for its specification.

## 7.5 Bulk formulation (*sbcblk\_core.F90 sbcblk\_clio.F90 sbcblk\_mfs.F90* modules)

In the bulk formulation, the surface boundary condition fields are computed using bulk formulae and atmospheric fields and ocean (and ice) variables.

The atmospheric fields used depend on the bulk formulae used. Three bulk formulations are available : the CORE, the CLIO and the MFS bulk formulae. The choice is made by setting to true one of the following namelist variable : *ln\_core* ; *ln\_clio* or *ln\_mfs*.

Note : in forced mode, when a sea-ice model is used, a bulk formulation (CLIO or CORE) have to be used. Therefore the two bulk (CLIO and CORE) formulae include the computation of the fluxes over both an ocean and an ice surface.

### 7.5.1 CORE Bulk formulae (*ln\_core=true, sbcblk\_core.F90*)

The CORE bulk formulae have been developed by [Large and Yeager \[2004\]](#). They have been designed to handle the CORE forcing, a mixture of NCEP re-analysis and satellite data. They use an inertial dissipative method to compute the turbulent transfer coefficients (momentum, sensible heat and evaporation) from the 10 metre wind speed, air temperature and specific humidity. This [Large and Yeager \[2004\]](#) dataset is available through the [GFDL web site](#).

Note that substituting ERA40 to NCEP reanalysis fields does not require changes in the bulk formulae themselves. This is the so-called DRAKKAR Forcing Set (DFS) [[Brodeau et al. 2009](#)].

Options are defined through the *namsbc\_core* namelist variables. The required 8 input fields are:

Variable description	Model variable	Units	point
i-component of the 10m air velocity	utau	$m.s^{-1}$	T
j-component of the 10m air velocity	vtau	$m.s^{-1}$	T
10m air temperature	tair	$^{\circ}K$	T
Specific humidity	humi	%	T
Incoming long wave radiation	qlw	$W.m^{-2}$	T
Incoming short wave radiation	qsr	$W.m^{-2}$	T
Total precipitation (liquid + solid)	precip	$Kg.m^{-2}.s^{-1}$	T
Solid precipitation	snow	$Kg.m^{-2}.s^{-1}$	T

Note that the air velocity is provided at a tracer ocean point, not at a velocity ocean point (*u*- and *v*-points). It is simpler and faster (less fields to be read), but it is not the recommended method when the ocean grid size is the same or larger than the one of the input atmospheric fields.

The *sn\_wndi*, *sn\_wndj*, *sn\_qsr*, *sn\_qlw*, *sn\_tair*, *sn\_humi*, *sn\_prec*, *sn\_snow*, *sn\_tdif* parameters describe the fields and the way they have to be used (spatial and temporal interpolations).

*cn\_dir* is the directory of location of bulk files *ln\_taudif* is the flag to specify if we use High Frequency (HF) tau information (.true.) or not (.false.) *rn\_zqt*: is the height of humidity and temperature measurements (m) *rn\_zu*: is the height of wind measurements (m)

Three multiplicative factors are available: *rn\_pfac* and *rn\_efac* allows to adjust (if necessary) the global freshwater budget by increasing/reducing the precipitations (total and snow) and or evaporation, respectively. The third one, *rn\_vfac*, control to which extent the ice/ocean velocities are taken into account in the calculation of surface wind stress. Its range should be between zero and one, and it is recommended to set it to 0.

### 7.5.2 CLIO Bulk formulae (*ln\_clio=true, sbcblk\_clio.F90*)

The CLIO bulk formulae were developed several years ago for the Louvain-la-neuve coupled ice-ocean model (CLIO, [Goosse et al. \[1999\]](#)). They are simpler bulk formulae. They assume the stress to be known and compute the radiative fluxes from a climatological cloud cover.

Options are defined through the *namsbc\_clio* namelist variables. The required 7 input fields are:

Variable description	Model variable	Units	point
i-component of the ocean stress	utau	$N.m^{-2}$	U
j-component of the ocean stress	vtau	$N.m^{-2}$	V
Wind speed module	vatm	$m.s^{-1}$	T
10m air temperature	tair	$^{\circ}K$	T
Specific humidity	humi	%	T
Cloud cover		%	T
Total precipitation (liquid + solid)	precip	$Kg.m^{-2}.s^{-1}$	T
Solid precipitation	snow	$Kg.m^{-2}.s^{-1}$	T

As for the flux formulation, information about the input data required by the model is provided in the *namsbc\_blk\_core* or *namsbc\_blk\_clio* namelist (see §7.2.1).

### 7.5.3 MFS Bulk formulae (*ln\_mfs=true*, *sbcblk\_mfs.F90*)

The MFS (Mediterranean Forecasting System) bulk formulae have been developed by [Castellari et al. \[1998\]](#). They have been designed to handle the ECMWF operational data and are currently in use in the MFS operational system [[Tonani et al. 2008](#)], [[Oddo et al. 2009](#)]. The wind stress computation uses a drag coefficient computed according to [Hellerman and Rosenstein \[1983\]](#). The surface boundary condition for temperature involves the balance between surface solar radiation, net long-wave radiation, the latent and sensible heat fluxes. Solar radiation is dependent on cloud cover and is computed by means of an astronomical formula [[Reed 1977](#)]. Albedo monthly values are from [Payne \[1972\]](#) as means of the values at  $40^{\circ}N$  and  $30^{\circ}N$  for the Atlantic Ocean (hence the same latitudinal band of the Mediterranean Sea). The net long-wave radiation flux [[Bignami et al. 1995](#)] is a function of air temperature, sea-surface temperature, cloud cover and relative humidity. Sensible heat and latent heat fluxes are computed by classical bulk formulae parameterised according to [Kondo \[1975\]](#). Details on the bulk formulae used can be found in [Maggiore et al. \[1998\]](#) and [Castellari et al. \[1998\]](#).

Options are defined through the *namsbc\_mfs* namelist variables. The required 7 input fields must be provided on the model Grid-T and are:

- Zonal Component of the 10m wind ( $m.s^{-1}$ ) (*sn\_windi*)
- Meridional Component of the 10m wind ( $m.s^{-1}$ ) (*sn\_windj*)

- Total Cloud Cover (%) (*sn\_clc*)
- 2m Air Temperature (*K*) (*sn\_tair*)
- 2m Dew Point Temperature (*K*) (*sn\_rhm*)
- Total Precipitation  $Kgm^{-2}s^{-1}$  (*sn\_prec*)
- Mean Sea Level Pressure (*Pa*) (*sn\_msl*)

## 7.6 Coupled formulation (*sbccpl.F90* module)

```

!-----
!$namsbc_cpl ! coupled ocean/atmosphere model ("key_oasis3")
!-----
!
! description ! multiple ! vector ! vector ! vector !
! ! categories ! reference ! orientation ! grids !
! send
sn_snd_temp = 'weighted oce and ice' , 'no' , '' , '' , '' , ''
sn_snd_alb = 'weighted ice' , 'no' , '' , '' , '' , ''
sn_snd_thick = 'none' , 'no' , '' , '' , '' , ''
sn_snd_crt = 'none' , 'no' , 'spherical' , 'eastward-northward' , 'T' , ''
sn_snd_co2 = 'coupled' , 'no' , '' , '' , '' , ''
sn_snd_crtw = 'none' , 'no' , '' , '' , '' , 'U,V'
sn_snd_ifrac = 'none' , 'no' , '' , '' , '' , ''
sn_snd_wlev = 'coupled' , 'no' , '' , '' , '' , ''
! receive
sn_rcv_w10m = 'none' , 'no' , '' , '' , '' , ''
sn_rcv_tauomod = 'coupled' , 'no' , '' , '' , '' , ''
sn_rcv_tau = 'oce only' , 'no' , 'cartesian' , 'eastward-northward' , 'U,V' , ''
sn_rcv_dqnsdt = 'coupled' , 'no' , '' , '' , '' , ''
sn_rcv_qsr = 'oce and ice' , 'no' , '' , '' , '' , ''
sn_rcv_qns = 'oce and ice' , 'no' , '' , '' , '' , ''
sn_rcv_emp = 'conservative' , 'no' , '' , '' , '' , ''
sn_rcv_rnf = 'coupled' , 'no' , '' , '' , '' , ''
sn_rcv_cal = 'coupled' , 'no' , '' , '' , '' , ''
sn_rcv_co2 = 'coupled' , 'no' , '' , '' , '' , ''
sn_rcv_hsig = 'none' , 'no' , '' , '' , '' , ''
sn_rcv_iceflx = 'none' , 'no' , '' , '' , '' , ''
sn_rcv_mslp = 'none' , 'no' , '' , '' , '' , ''
sn_rcv_phioc = 'none' , 'no' , '' , '' , '' , ''
sn_rcv_sdrfx = 'none' , 'no' , '' , '' , '' , ''
sn_rcv_sdrfy = 'none' , 'no' , '' , '' , '' , ''
sn_rcv_wper = 'none' , 'no' , '' , '' , '' , ''
sn_rcv_wnum = 'none' , 'no' , '' , '' , '' , ''
sn_rcv_wstrf = 'none' , 'no' , '' , '' , '' , ''
sn_rcv_wdrag = 'none' , 'no' , '' , '' , '' , ''
!
nn_cplmodel = 1 ! Maximum number of models to/from which NEMO is potentially sending/receiving data
ln_usecpmask = .false. ! use a coupling mask file to merge data received from several models
! ! -> file cplmask.nc with the float variable called cplmask (jpi,jpj,nn_cplmodel)
/

```

In the coupled formulation of the surface boundary condition, the fluxes are provided by the OASIS coupler at a frequency which is defined in the OASIS coupler, while sea and ice surface temperature, ocean and ice albedo, and ocean currents are sent to the atmospheric component.

A generalised coupled interface has been developed. It is currently interfaced with OASIS-3-MCT (**key\_oasis3**). It has been successfully used to interface *NEMO* to most of the European atmospheric GCM (ARPEGE, ECHAM, ECMWF, HadAM, HadGAM, LMDz), as well as to **WRF** (Weather Research and Forecasting Model).

Note that in addition to the setting of *ln\_cpl* to true, the **key\_coupled** have to be defined. The CPP key is mainly used in sea-ice to ensure that the atmospheric

fluxes are actually recieved by the ice-ocean system (no calculation of ice sublimation in coupled mode). When PISCES biogeochemical model (**key\_top** and **key\_pisces**) is also used in the coupled system, the whole carbon cycle is computed by defining **key\_cpl\_carbon\_cycle**. In this case, CO<sub>2</sub> fluxes will be exchanged between the atmosphere and the ice-ocean system (and need to be activated in *namsbc\_cpl*).

The namelist above allows control of various aspects of the coupling fields (particularly for vectors) and now allows for any coupling fields to have multiple sea ice categories (as required by LIM3 and CICE). When indicating a multi-category coupling field in *namsbc\_cpl* the number of categories will be determined by the number used in the sea ice model. In some limited cases it may be possible to specify single category coupling fields even when the sea ice model is running with multiple categories - in this case the user should examine the code to be sure the assumptions made are satisfactory. In cases where this is definitely not possible the model should abort with an error message. The new code has been tested using ECHAM with LIM2, and HadGAM3 with CICE but although it will compile with **key\_lim3** additional minor code changes may be required to run using LIM3.

## 7.7 Atmospheric pressure (*sbcapr.F90*)

```

!-----
&namsbc_apr      ! Atmospheric pressure used as ocean forcing          (ln_apr_dyn =T)
!-----
!               ! file name ! frequency (hours) ! variable ! time interp.! clim ! 'yearly'/ ! weights ! rotation ! land/sea mask !
!               ! (if <0 months) ! name ! (logical) ! (T/F) ! 'monthly' ! filename ! pairing ! filename !
!   sn_apr      = 'patm'   ,      -1      , 'somspre' , .true.   , .true. , 'yearly' , ' ' , ' ' , ' '
!
!   cn_dir      = './'     ! root directory for the location of the bulk files
!   rn_pref     = 101000.  ! reference atmospheric pressure [N/m2]/
!   ln_ref_apr  = .false.  ! ref. pressure: global mean Patm (T) or a constant (F)
!   ln_apr_abc  = .false.  ! inverse barometer added to OBC ssh data
/

```

The optional atmospheric pressure can be used to force ocean and ice dynamics (*ln\_apr\_dyn* = true, *namsbc* namelist). The input atmospheric forcing defined via *sn\_apr* structure (*namsbc\_apr* namelist) can be interpolated in time to the model time step, and even in space when the interpolation on-the-fly is used. When used to force the dynamics, the atmospheric pressure is further transformed into an equivalent inverse barometer sea surface height,  $\eta_{ib}$ , using:

$$\eta_{ib} = -\frac{1}{g \rho_o} (P_{atm} - P_o) \quad (7.2)$$

where  $P_{atm}$  is the atmospheric pressure and  $P_o$  a reference atmospheric pressure. A value of 101,000 N/m<sup>2</sup> is used unless *ln\_ref\_apr* is set to true. In this case  $P_o$  is set to the value of  $P_{atm}$  averaged over the ocean domain, *i.e.* the mean value of  $\eta_{ib}$  is kept to zero at all time step.

The gradient of  $\eta_{ib}$  is added to the RHS of the ocean momentum equation (see *dynspg.F90* for the ocean). For sea-ice, the sea surface height,  $\eta_m$ , which is provided to the sea ice model is set to  $\eta - \eta_{ib}$  (see *sbcssr.F90* module).  $\eta_{ib}$  can be set in the output. This can simplify altimetry data and model comparison as

inverse barometer sea surface height is usually removed from these data prior to their distribution.

When using time-splitting and BDY package for open boundaries conditions, the equivalent inverse barometer sea surface height  $\eta_{ib}$  can be added to BDY ssh data: *ln\_apr\_obc* might be set to true.

## 7.8 Tidal Potential (*sbctide.F90*)

```
!-----
&nam_tide      !   tide parameters
!-----
  ln_tide      = .false.
  ln_tide_pot  = .true.  ! use tidal potential forcing
  ln_tide_ramp = .false. !
  rdtideramp  =  0.     !
  clname(1)   = 'DUMMY' ! name of constituent - all tidal components must be set in namelist_cfg
/
```

A module is available to compute the tidal potential and use it in the momentum equation. This option is activated when *ln\_tide* is set to true in *nam\_tide*.

Some parameters are available in namelist *nam\_tide*:

- *ln\_tide\_pot* activate the tidal potential forcing
- *nb\_harmo* is the number of constituent used
- *clname* is the name of constituent

The tide is generated by the forces of gravity of the Earth-Moon and Earth-Sun system; they are expressed as the gradient of the astronomical potential ( $\vec{\nabla}\Pi_a$ ).

The potential astronomical expressed, for the three types of tidal frequencies following, by :

Tide long period :

$$\Pi_a = gA_k \left( \frac{1}{2} - \frac{3}{2} \sin^2 \phi \right) \cos(\omega_k t + V_{0k}) \quad (7.3)$$

diurnal Tide :

$$\Pi_a = gA_k (\sin 2\phi) \cos(\omega_k t + \lambda + V_{0k}) \quad (7.4)$$

Semi-diurnal tide:

$$\Pi_a = gA_k (\cos^2 \phi) \cos(\omega_k t + 2\lambda + V_{0k}) \quad (7.5)$$

$A_k$  is the amplitude of the wave  $k$ ,  $\omega_k$  the pulsation of the wave  $k$ ,  $V_{0k}$  the astronomical phase of the wave  $k$  to Greenwich.

We make corrections to the astronomical potential. We obtain :

$$\Pi - g\delta = (1 + k - h)\Pi_A(\lambda, \phi) \quad (7.6)$$

with  $k$  a number of Love estimated to 0.6 which parameterised the astronomical tidal land, and  $h$  a number of Love to 0.3 which parameterised the parameterisation due to the astronomical tidal land.

## 7.9 River runoffs (*sbc\_rnf.F90*)

```

!-----
&nam_sbc_rnf ! runoffs namelist surface boundary condition (ln_rnf =T)
!-----
! ! file name ! frequency (hours) ! variable ! time interp. ! clim ! 'yearly' ! weights ! rotation ! land/sea
! ! ! (if <0 months) ! name ! (logical) ! (T/F) ! 'monthly' ! filename ! pairing ! filename
sn_rnf = 'runoff_core_monthly', -1 , 'sorunoff', .true. , .true. , 'yearly' , '' , '' , ''
sn_cnf = 'runoff_core_monthly', 0 , 'socoefr0', .false. , .true. , 'yearly' , '' , '' , ''
sn_s_rnf = 'runoffs' , 24 , 'rosaline', .true. , .true. , 'yearly' , '' , '' , ''
sn_t_rnf = 'runoffs' , 24 , 'rotemper', .true. , .true. , 'yearly' , '' , '' , ''
sn_dep_rnf = 'runoffs' , 0 , 'rodepth', .false. , .true. , 'yearly' , '' , '' , ''

cn_dir = './' ! root directory for the location of the runoff files
ln_rnf_mouth= .true. ! specific treatment at rivers mouths
rn_hrnf = 15.e0 ! depth over which enhanced vertical mixing is used (ln_rnf_mouth=T)
rn_avt_rnf = 1.e-3 ! value of the additional vertical mixing coef. [m2/s] (ln_rnf_mouth=T)
rn_rfact = 1.e0 ! multiplicative factor for runoff
ln_rnf_depth= .false. ! read in depth information for runoff
ln_rnf_tem = .false. ! read in temperature information for runoff
ln_rnf_sal = .false. ! read in salinity information for runoff
ln_rnf_depth_ini = .false. ! compute depth at initialisation from runoff file
rn_rnf_max = 5.735e-4 ! max value of the runoff climatologie over global domain ( ln_rnf_depth_ini = .true )
rn_dep_max = 150. ! depth over which runoffs is spread ( ln_rnf_depth_ini = .true )
nn_rnf_depth_file = 0 ! create (=1) a runoff depth file or not (=0)
/

```

River runoff generally enters the ocean at a nonzero depth rather than through the surface. Many models, however, have traditionally inserted river runoff to the top model cell. This was the case in *NEMO* prior to the version 3.3, and was combined with an option to increase vertical mixing near the river mouth.

However, with this method numerical and physical problems arise when the top grid cells are of the order of one meter. This situation is common in coastal modelling and is becoming more common in open ocean and climate modelling <sup>2</sup>.

As such from V 3.3 onwards it is possible to add river runoff through a non-zero depth, and for the temperature and salinity of the river to effect the surrounding ocean. The user is able to specify, in a NetCDF input file, the temperature and salinity of the river, along with the depth (in metres) which the river should be added to.

Namelist variables in *nam\_sbc\_rnf*, *ln\_rnf\_depth*, *ln\_rnf\_sal* and *ln\_rnf\_tem* control whether the river attributes (depth, salinity and temperature) are read in and used. If these are set as false the river is added to the surface box only, assumed to be fresh (0 psu), and/or taken as surface temperature respectively.

The runoff value and attributes are read in in *sbc\_rnf*. For temperature -999 is taken as missing data and the river temperature is taken to be the surface temperature at the river point. For the depth parameter a value of -1 means the river is added to the surface box only, and a value of -999 means the river is added through the entire water column. After being read in the temperature and salinity variables are multiplied by the amount of runoff (converted into m/s) to give the heat and salt content of the river runoff. After the user specified depth is read in, the number of grid boxes this corresponds to is calculated and stored in the variable *nz\_rnf*. The variable *h\_dep* is then calculated to be the depth (in metres) of the bottom of the lowest box the river water is being added to (i.e. the total depth that river water is being added to in the model).

<sup>2</sup>At least a top cells thickness of 1 meter and a 3 hours forcing frequency are required to properly represent the diurnal cycle [Bernie et al. 2005]. see also §7.13.1.

The mass/volume addition due to the river runoff is, at each relevant depth level, added to the horizontal divergence (*hdivn*) in the subroutine *sbc\_rnf\_div* (called from *divcur.F90*). This increases the diffusion term in the vicinity of the river, thereby simulating a momentum flux. The sea surface height is calculated using the sum of the horizontal divergence terms, and so the river runoff indirectly forces an increase in sea surface height.

The *hdivn* terms are used in the tracer advection modules to force vertical velocities. This causes a mass of water, equal to the amount of runoff, to be moved into the box above. The heat and salt content of the river runoff is not included in this step, and so the tracer concentrations are diluted as water of ocean temperature and salinity is moved upward out of the box and replaced by the same volume of river water with no corresponding heat and salt addition.

For the linear free surface case, at the surface box the tracer advection causes a flux of water (of equal volume to the runoff) through the sea surface out of the domain, which causes a salt and heat flux out of the model. As such the volume of water does not change, but the water is diluted.

For the non-linear free surface case (**key\_vvl**), no flux is allowed through the surface. Instead in the surface box (as well as water moving up from the boxes below) a volume of runoff water is added with no corresponding heat and salt addition and so as happens in the lower boxes there is a dilution effect. (The runoff addition to the top box along with the water being moved up through boxes below means the surface box has a large increase in volume, whilst all other boxes remain the same size)

In *trasbc* the addition of heat and salt due to the river runoff is added. This is done in the same way for both *vvl* and *non-vvl*. The temperature and salinity are increased through the specified depth according to the heat and salt content of the river.

In the non-linear free surface case (*vvl*), near the end of the time step the change in sea surface height is redistributed through the grid boxes, so that the original ratios of grid box heights are restored. In doing this water is moved into boxes below, throughout the water column, so the large volume addition to the surface box is spread between all the grid boxes.

It is also possible for runoff to be specified as a negative value for modelling flow through straits, i.e. modelling the Baltic flow in and out of the North Sea. When the flow is out of the domain there is no change in temperature and salinity, regardless of the namelist options used, as the ocean water leaving the domain removes heat and salt (at the same concentration) with it.

## 7.10 Ice shelf melting (*sbcisf.F90*)

```
!-----
!namsbc_isf      ! Top boundary layer (ISF)                                (nn_isf >0)
!-----
!               ! file name ! frequency (hours) ! variable ! time interp.! clim ! 'yearly'/ ! weights ! rotation ! land/sea
!               !           ! (if <0 months) ! name      ! (logical) ! (T/F) ! 'monthly' ! filename ! pairing ! filename
! nn_isf == 4
!   sn_fwfisf = 'rnfisf' ,          -12          , 'sowflisf' , .false. , .true. , 'yearly' , '' , '' , ''
```



```

! nn_isf == 3
  sn_rnfisf = 'rnfisf' ,          -12      , 'sofwfisf' , .false. , .true. , 'yearly' , '' , '' , ''
! nn_isf == 2 and 3
  sn_depmax_isf='rnfisf' ,          -12      , 'sozisfmax' , .false. , .true. , 'yearly' , '' , '' , ''
  sn_depmin_isf='rnfisf' ,          -12      , 'sozisfmin' , .false. , .true. , 'yearly' , '' , '' , ''
! nn_isf == 2
  sn_Leff_isf = 'rnfisf' ,          -12      , 'Leff' , .false. , .true. , 'yearly' , '' , '' , ''
!
! for all case
  nn_isf = 1      ! ice shelf melting/freezing
                  ! 1 = presence of ISF   2 = bg03 parametrisation
                  ! 3 = rnf file for isf   4 = ISF fwf specified
                  ! option 1 and 4 need ln_isfcav = .true. (domzgr)
! only for nn_isf = 1 or 2
  rn_gammat0 = 1.e-4 ! gammat coefficient used in blk formula
  rn_gammas0 = 1.e-4 ! gammas coefficient used in blk formula
! only for nn_isf = 1 or 4
  rn_hisf_tbl = 30. ! thickness of the top boundary layer (Losh et al. 2008)
  !              ! 0 => thickness of the tbl = thickness of the first wet cell
! only for nn_isf = 1
  nn_isfblk = 1    ! 1 ISOMIP like: 2 equations formulation (Hunter et al., 2006)
  !              ! 2 ISOMIP+ like: 3 equations formulation (Asay-Davis et al., 2015)
  nn_gammabl = 1  ! 0 = cst Gammat (= gammat/s)
  !              ! 1 = velocity dependent Gamma (u* * gammat/s) (Jenkins et al. 2010)
  !              ! 2 = velocity and stability dependent Gamma (Holland et al. 1999)
/

```

Namelist variable in *namsbc*, *nn\_isf*, controls the ice shelf representation used.

***nn\_isf* = 1** The ice shelf cavity is represented (*ln\_isfcav* = true needed). The fwf and heat flux are computed. Two different bulk formula are available:

***nn\_isfblk* = 1** The bulk formula used to compute the melt is based the one described in [Hunter \[2006\]](#). This formulation is based on a balance between the upward ocean heat flux and the latent heat flux at the ice shelf base.

***nn\_isfblk* = 2** The bulk formula used to compute the melt is based the one described in [Jenkins \[1991\]](#). This formulation is based on a 3 equations formulation (a heat flux budget, a salt flux budget and a linearised freezing point temperature equation).

For this 2 bulk formulations, there are 3 different ways to compute the exchange coefficient:

***nn\_gammabl* = 0** The salt and heat exchange coefficients are constant and defined by *rn\_gammas0* and *rn\_gammat0*

***nn\_gammabl* = 1** The salt and heat exchange coefficients are velocity dependent and defined as  $rn\_gammas0 \times u_*$  and  $rn\_gammat0 \times u_*$  where  $u_*$  is the friction velocity in the top boundary layer (ie first *rn\_hisf\_tbl* meters). See [Jenkins \[2010\]](#) for all the details on this formulation.

***nn\_gammabl* = 2** The salt and heat exchange coefficients are velocity and stability dependent and defined as  $\gamma_{T,S} = \frac{u_*}{\Gamma_{Turb} + \Gamma_{Mole}^{T,S}}$  where  $u_*$  is the friction velocity in the top boundary layer (ie first *rn\_hisf\_tbl* meters),  $\Gamma_{Turb}$  the contribution of the ocean stability and  $\Gamma_{Mole}^{T,S}$  the contribution of the molecular diffusion. See [Holland and Jenkins \[1999\]](#) for all the details on this formulation.

***nn\_isf = 2*** A parameterisation of *isf* is used. The ice shelf cavity is not represented. The *fwf* is distributed along the ice shelf edge between the depth of the average grounding line (GL) (*sn\_depmax\_isf*) and the base of the ice shelf along the calving front (*sn\_depmin\_isf*) as in (*nn\_isf = 3*). Furthermore the *fwf* and heat flux are computed using the Beckmann and Goosse [2003] parameterisation of *isf* melting. The effective melting length (*sn\_Leff\_isf*) is read from a file.

***nn\_isf = 3*** A simple parameterisation of *isf* is used. The ice shelf cavity is not represented. The *fwf* (*sn\_rnfisf*) is prescribed and distributed along the ice shelf edge between the depth of the average grounding line (GL) (*sn\_depmax\_isf*) and the base of the ice shelf along the calving front (*sn\_depmin\_isf*). The heat flux ( $Q_h$ ) is computed as  $Q_h = fwf \times L_f$ .

***nn\_isf = 4*** The ice shelf cavity is opened (*ln\_isfcav = true* needed). However, the *fwf* is not computed but specified from file *sn\_fwfisf*). The heat flux ( $Q_h$ ) is computed as  $Q_h = fwf \times L_f$ .

- *nn\_isf = 1* and *nn\_isf = 2* compute a melt rate based on the water mass properties, ocean velocities and depth. This flux is thus highly dependent of the model resolution (horizontal and vertical), realism of the water masses onto the shelf ...

- *nn\_isf = 3* and *nn\_isf = 4* read the melt rate from a file. You have total control of the *fwf* forcing. This can be useful if the water masses on the shelf are not realistic or the resolution (horizontal/vertical) are too coarse to have realistic melting or for studies where you need to control your heat and fw input.

A namelist parameters control over how many meters the heat and fw fluxes are spread. *rn\_hisf\_tbl*] is the top boundary layer thickness as defined in Losch [2008]. This parameter is only used if *nn\_isf = 1* or *nn\_isf = 4*

If *rn\_hisf\_tbl = 0.*, the fluxes are put in the top level whatever is its tickness.

If *rn\_hisf\_tbl > 0.*, the fluxes are spread over the first *rn\_hisf\_tbl* m (ie over one or several cells).

The ice shelf melt is implemented as a volume flux with in the same way as for the runoff. The fw addition due to the ice shelf melting is, at each relevant depth level, added to the horizontal divergence (*hdivn*) in the subroutine *sbc\_isf\_div*, called from *divcur.F90*. See the runoff section 7.9 for all the details about the divergence correction.

## 7.11 Ice sheet coupling

```
!-----
&namcbc_iscpl ! land ice / ocean coupling option
!-----
```

```

nn_drown   = 10      ! number of iteration of the extrapolation loop (fill the new wet cells)
ln_hsb     = .false. ! activate conservation module (conservation exact after a time of rn_fiscpl)
nn_fiscpl  = 43800   ! (number of time step) conservation period (maybe should be fix to the coupling frequency of restart frequency)
/

```

Ice sheet/ocean coupling is done through file exchange at the restart step. NEMO, at each restart step, read the bathymetry and ice shelf draft variable in a netcdf file. If *ln\_iscpl* = *true*, the isf draft is assume to be different at each restart step with potentially some new wet/dry cells due to the ice sheet dynamics/thermodynamics. The wetting and drying scheme applied on the restart is very simple and described below for the 6 different cases:

**Thin a cell down:** T/S/ssh are unchanged and U/V in the top cell are corrected to keep the barotropic transport (bt) constant ( $bt_b = bt_n$ ).

**Enlarge a cell:** See case "Thin a cell down"

**Dry a cell:** mask, T/S, U/V and ssh are set to 0. Furthermore, U/V into the water column are modified to satisfy ( $bt_b = bt_n$ ).

**Wet a cell:** mask is set to 1, T/S is extrapolated from neighbours,  $ssh_n = ssh_b$  and U/V set to 0. If no neighbours along i,j and k, T/S/U/V and mask are set to 0.

**Dry a column:** mask, T/S, U/V are set to 0 everywhere in the column and ssh set to 0.

**Wet a column:** set mask to 1, T/S is extrapolated from neighbours, ssh is extrapolated from neighbours and U/V set to 0. If no neighbour, T/S/U/V and mask set to 0.

The extrapolation is call *nn\_drown* times. It means that if the grounding line retreat by more than *nn\_drown* cells between 2 coupling steps, the code will be unable to fill all the new wet cells properly. The default number is set up for the MISOMIP idealised experiments.

This coupling procedure is able to take into account grounding line and calving front migration. However, it is a non-conservative processe. This could lead to a trend in heat/salt content and volume. In order to remove the trend and keep the conservation level as close to 0 as possible, a simple conservation scheme is available with *ln\_hsb* = *true*. The heat/salt/vol. gain/loss is diagnose, as well as the location. Based on what is done on sbrcnf to prescribed a source of heat/salt/vol., the heat/salt/vol. gain/loss is removed/added, over a period of *rn\_fiscpl* time step, into the system. So after *rn\_fiscpl* time step, all the heat/salt/vol. gain/loss due to extrapolation process is canceled.

As the before and now fields are not compatible (modification of the geometry), the restart time step is prescribed to be an euler time step instead of a leap frog and  $fields_b = fields_n$ .

## 7.12 Handling of icebergs (ICB)

```

!-----
&namberg      !   iceberg parameters                                (default: No iceberg)
!-----
ln_icebergs   = .false.                ! iceberg floats or not
ln_bergdia   = .true.                  ! Calculate budgets
nn_verbose_level = 1                    ! Turn on more verbose output if level > 0
nn_verbose_write = 15                  ! Timesteps between verbose messages
nn_sample_rate = 1                      ! Timesteps between sampling for trajectory storage
rn_initial_mass = 8.8e7, 4.1e8, 3.3e9, 1.8e10, 3.8e10, 7.5e10, 1.2e11, 2.2e11, 3.9e11, 7.4e11
! Initial mass required for an iceberg of each class
rn_distribution = 0.24, 0.12, 0.15, 0.18, 0.12, 0.07, 0.03, 0.03, 0.03, 0.02
! Proportion of calving mass to apportion to each class
! Ratio between effective and real iceberg mass (non-dim)
! i.e. number of icebergs represented at a point
rn_mass_scaling = 2000, 200, 50, 20, 10, 5, 2, 1, 1, 1
! thickness of newly calved bergs (m)
rn_initial_thickness = 40., 67., 133., 175., 250., 250., 250., 250., 250., 250.
rn_rho_bergs = 850.                    ! Density of icebergs
rn_LoW_ratio = 1.5                      ! Initial ratio L/W for newly calved icebergs
ln_operator_splitting = .true.          ! Use first order operator splitting for thermodynamics
rn_bits_erosion_fraction = 0.           ! Fraction of erosion melt flux to divert to bergy bits
rn_sicn_shift = 0.                      ! Shift of sea-ice concn in erosion flux (0<sicn_shift<1)
ln_passive_mode = .false.               ! Iceberg - ocean decoupling
nn_test_icebergs = 10                   ! Create test icebergs of this class (-1 = no)
! Put a test iceberg at each gridpoint in box (lon1,lon2,lat1,lat2)
rn_test_box = 108.0, 116.0, -66.0, -58.0
rn_speed_limit = 0.                     ! CFL speed limit for a berg

!          ! file name ! frequency (hours) ! variable ! time interp. ! clim ! 'yearly' / ! weights ! rotation ! land/sea
!          !          ! (if <0 months) ! name ! (logical) ! (T/F) ! 'monthly' ! filename ! pairing ! filename
sn_icb = 'calving', -1, , 'calvingmask', .true. , .true. , 'yearly' , '' , '' , ''

cn_dir = './'
/

```

Icebergs are modelled as lagrangian particles in NEMO [Marsh et al. 2015]. Their physical behaviour is controlled by equations as described in Martin and Adcroft [2010]). (Note that the authors kindly provided a copy of their code to act as a basis for implementation in NEMO). Icebergs are initially spawned into one of ten classes which have specific mass and thickness as described in the *namberg* namelist: *rn\_initial\_mass* and *rn\_initial\_thickness*. Each class has an associated scaling (*rn\_mass\_scaling*), which is an integer representing how many icebergs of this class are being described as one lagrangian point (this reduces the numerical problem of tracking every single iceberg). They are enabled by setting *ln\_icebergs* = true.

Two initialisation schemes are possible.

***nn\_test\_icebergs* > 0** In this scheme, the value of *nn\_test\_icebergs* represents the class of iceberg to generate (so between 1 and 10), and *nn\_test\_icebergs* provides a lon/lat box in the domain at each grid point of which an iceberg is generated at the beginning of the run. (Note that this happens each time the timestep equals *nn\_nit000*.) *nn\_test\_icebergs* is defined by four numbers in *nn\_test\_box* representing the corners of the geographical box: lonmin,lonmax,latmin,latmax

***nn\_test\_icebergs* = -1** In this scheme the model reads a calving file supplied in the *sn\_icb* parameter. This should be a file with a field on the configuration grid (typically ORCA) representing ice accumulation rate at each model point. These should be ocean points adjacent to land where icebergs are known to calve. Most points in this input grid are going to have value zero. When

the model runs, ice is accumulated at each grid point which has a non-zero source term. At each time step, a test is performed to see if there is enough ice mass to calve an iceberg of each class in order (1 to 10). Note that this is the initial mass multiplied by the number each particle represents (*i.e.* the scaling). If there is enough ice, a new iceberg is spawned and the total available ice reduced accordingly.

Icebergs are influenced by wind, waves and currents, bottom melt and erosion. The latter act to disintegrate the iceberg. This is either all melted freshwater, or (if *rn\_bits\_erosion\_fraction* > 0) into melt and additionally small ice bits which are assumed to propagate with their larger parent and thus delay fluxing into the ocean. Melt water (and other variables on the configuration grid) are written into the main NEMO model output files.

Extensive diagnostics can be produced. Separate output files are maintained for human-readable iceberg information. A separate file is produced for each processor (independent of *ln\_ctl*). The amount of information is controlled by two integer parameters:

*nn\_verbose\_level* takes a value between one and four and represents an increasing number of points in the code at which variables are written, and an increasing level of obscurity.

*nn\_verbose\_write* is the number of timesteps between writes

Iceberg trajectories can also be written out and this is enabled by setting *nn\_sample\_rate* > 0. A non-zero value represents how many timesteps between writes of information into the output file. These output files are in NETCDF format. When **key\_mpp\_mpi** is defined, each output file contains only those icebergs in the corresponding processor. Trajectory points are written out in the order of their parent iceberg in the model's "linked list" of icebergs. So care is needed to recreate data for individual icebergs, since its trajectory data may be spread across multiple files.

## 7.13 Miscellaneous options

### 7.13.1 Diurnal cycle (*sbcncy.F90*)

Bernie et al. [2005] have shown that to capture 90% of the diurnal variability of SST requires a vertical resolution in upper ocean of 1 m or better and a temporal resolution of the surface fluxes of 3 h or less. Unfortunately high frequency forcing fields are rare, not to say inexistent. Nevertheless, it is possible to obtain a reasonable diurnal cycle of the SST knowing only short wave flux (SWF) at high frequency [Bernie et al. 2007]. Furthermore, only the knowledge of daily mean value of SWF is needed, as higher frequency variations can be reconstructed from them, assuming that the diurnal cycle of SWF is a scaling of the top of the atmosphere diurnal cycle of incident SWF. The Bernie et al. [2007] reconstruction

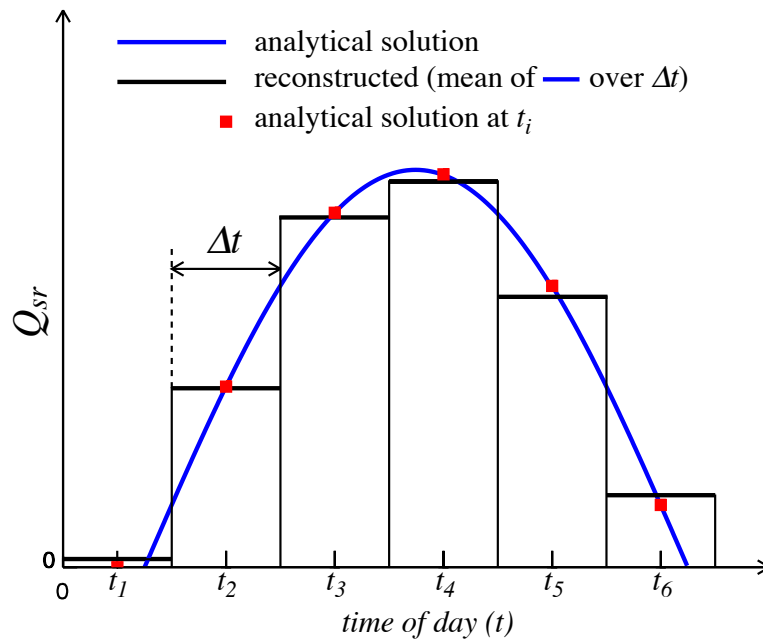


**Figure 7.1:** Example of reconstruction of the diurnal cycle variation of short wave flux from daily mean values. The reconstructed diurnal cycle (black line) is chosen as the mean value of the analytical cycle (blue line) over a time step, not as the mid time step value of the analytically cycle (red square). From [Bernie et al. \[2007\]](#).

algorithm is available in *NEMO* by setting `ln_dm2dc = true` (a `namsbc` namelist variable) when using CORE bulk formulae (`ln_blk_core = true`) or the flux formulation (`ln_flux = true`). The reconstruction is performed in the `sbcscy.F90` module. The detail of the algorithm used can be found in the appendix A of [Bernie et al. \[2007\]](#). The algorithm preserve the daily mean incoming SWF as the reconstructed SWF at a given time step is the mean value of the analytical cycle over this time step (Fig.7.1). The use of diurnal cycle reconstruction requires the input SWF to be daily (*i.e.* a frequency of 24 and a time interpolation set to true in `sn_qsr` namelist parameter). Furthermore, it is recommended to have a least 8 surface module time step per day, that is  $\Delta t \text{ nn.fsbc} < 10,800 \text{ s} = 3 \text{ h}$ . An example of reconstructed SWF is given in Fig.7.2 for a 12 reconstructed diurnal cycle, one every 2 hours (from 1am to 11pm).

Note also that the setting a diurnal cycle in SWF is highly recommended when the top layer thickness approach 1 m or less, otherwise large error in SST can appear due to an inconsistency between the scale of the vertical resolution and the forcing acting on that scale.

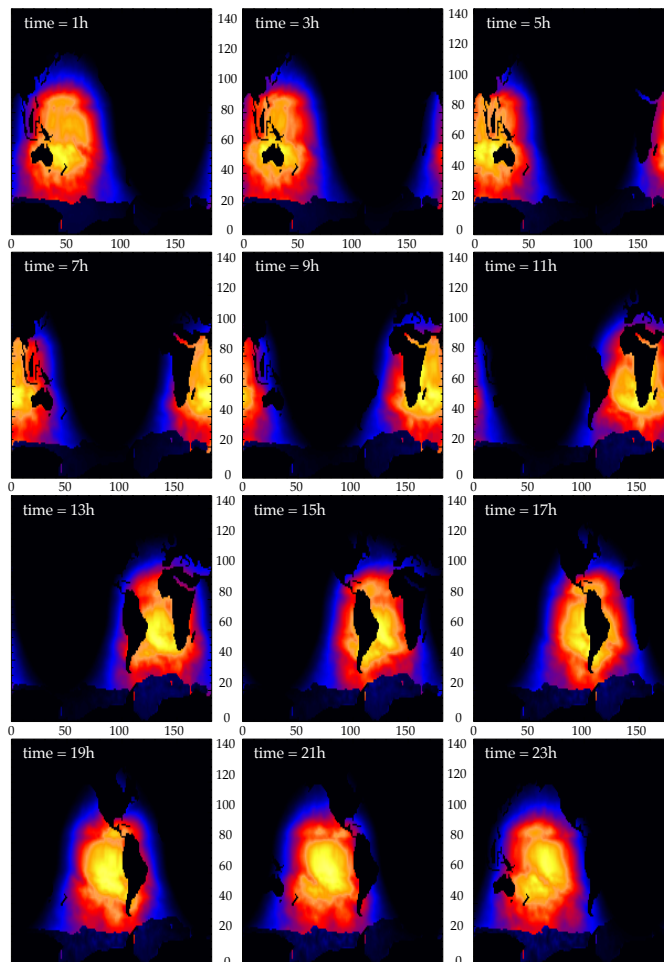


**Figure 7.2:** Example of reconstruction of the diurnal cycle variation of short wave flux from daily mean values on an ORCA2 grid with a time sampling of 2 hours (from 1am to 11pm). The display is on (i,j) plane.

### 7.13.2 Rotation of vector pairs onto the model grid directions

When using a flux (*ln\_flux=true*) or bulk (*ln\_clio=true* or *ln\_core=true*) formulation, pairs of vector components can be rotated from east-north directions onto the local grid directions. This is particularly useful when interpolation on the fly is used since here any vectors are likely to be defined relative to a rectilinear grid. To activate this option a non-empty string is supplied in the rotation pair column of the relevant namelist. The eastward component must start with "U" and the northward component with "V". The remaining characters in the strings are used to identify which pair of components go together. So for example, strings "U1" and "V1" next to "utau" and "vtau" would pair the wind stress components together and

rotate them on to the model grid directions; "U2" and "V2" could be used against a second pair of components, and so on. The extra characters used in the strings are arbitrary. The `rot_rep` routine from the `geo2ocean.F90` module is used to perform the rotation.

### 7.13.3 Surface restoring to observed SST and/or SSS (*sbcssr.F90*)

```

!-----
&namcbc_ssr ! surface boundary condition : sea surface restoring (ln_ssr =T)
!-----
!
! ! file name ! frequency (hours) ! variable ! time interp. ! clim ! 'yearly' / ! weights ! rotation ! land/sea
! ! ! (if <0 months) ! name ! (logical) ! (T/F) ! 'monthly' ! filename ! pairing ! filename
sn_sst = 'sst_data', 24, 'sst', .false., .false., 'yearly', ' ', ' ', ' ', ' '
sn_sss = 'sss_data', -1, 'sss', .true., .true., 'yearly', ' ', ' ', ' ', ' '

cn_dir = './' ! root directory for the location of the runoff files
nn_sstr = 0 ! add a retroaction term in the surface heat flux (=1) or not (=0)
nn_ssr = 2 ! add a damping term in the surface freshwater flux (=2)
! ! or to SSS only (=1) or no damping term (=0)
rn_dqdt = -40. ! magnitude of the retroaction on temperature [W/m2/K]
rn_deds = -166.67 ! magnitude of the damping on salinity [mm/day]
ln_ssr_bnd = .true. ! flag to bound erp term (associated with nn_ssr=2)
rn_ssr_bnd = 4.e0 ! ABS(Max/Min) value of the damping erp term [mm/day]
/

```

IOptions are defined through the `namcbc_ssr` namelist variables. n forced mode using a flux formulation (`ln_flux = true`), a feedback term *must* be added to the surface heat flux  $Q_{ns}^o$ :

$$Q_{ns} = Q_{ns}^o + \frac{dQ}{dT} (T|_{k=1} - SST_{Obs}) \quad (7.7)$$

where SST is a sea surface temperature field (observed or climatological),  $T$  is the model surface layer temperature and  $\frac{dQ}{dT}$  is a negative feedback coefficient usually taken equal to  $-40 \text{ W/m}^2/\text{K}$ . For a 50 m mixed-layer depth, this value corresponds to a relaxation time scale of two months. This term ensures that if  $T$  perfectly matches the supplied SST, then  $Q$  is equal to  $Q_o$ .

In the fresh water budget, a feedback term can also be added. Converted into an equivalent freshwater flux, it takes the following expression :

$$emp = emp_o + \gamma_s^{-1} e_{3t} \frac{(S|_{k=1} - SSS_{Obs})}{S|_{k=1}} \quad (7.8)$$

where  $emp_o$  is a net surface fresh water flux (observed, climatological or an atmospheric model product),  $SSS_{Obs}$  is a sea surface salinity (usually a time interpolation of the monthly mean Polar Hydrographic Climatology [Steele et al. 2001]),  $S|_{k=1}$  is the model surface layer salinity and  $\gamma_s$  is a negative feedback coefficient which is provided as a namelist parameter. Unlike heat flux, there is no physical justification for the feedback term in 7.8 as the atmosphere does not care about ocean surface salinity [Madec and Delecluse 1997]. The SSS restoring term should be viewed as a flux correction on freshwater fluxes to reduce the uncertainties we have on the observed freshwater budget.

### 7.13.4 Handling of ice-covered area (*sbice...*)

The presence at the sea surface of an ice covered area modifies all the fluxes transmitted to the ocean. There are several way to handle sea-ice in the system depend-



ing on the value of the *nn\_ice* namelist parameter found in *namsbc* namelist.

**nn\_ice = 0** there will never be sea-ice in the computational domain. This is a typical namelist value used for tropical ocean domain. The surface fluxes are simply specified for an ice-free ocean. No specific things is done for sea-ice.

**nn\_ice = 1** sea-ice can exist in the computational domain, but no sea-ice model is used. An observed ice covered area is read in a file. Below this area, the SST is restored to the freezing point and the heat fluxes are set to  $-4 W/m^2$  ( $-2 W/m^2$ ) in the northern (southern) hemisphere. The associated modification of the freshwater fluxes are done in such a way that the change in buoyancy fluxes remains zero. This prevents deep convection to occur when trying to reach the freezing point (and so ice covered area condition) while the SSS is too large. This manner of managing sea-ice area, just by using *si IF* case, is usually referred as the *ice-if* model. It can be found in the *sbcice\_if.F90* module.

**nn\_ice = 2 or more** A full sea ice model is used. This model computes the ice-ocean fluxes, that are combined with the air-sea fluxes using the ice fraction of each model cell to provide the surface ocean fluxes. Note that the activation of a sea-ice model is done by defining a CPP key (**key\_lim3** or **key\_ice**). The activation automatically overwrites the read value of *nn\_ice* to its appropriate value (*i.e.* 2 for LIM-3 or 3 for CICE).

### 7.13.5 Interface to CICE (*sbcice\_ice.F90*)

It is now possible to couple a regional or global NEMO configuration (without AGRIF) to the CICE sea-ice model by using **key\_ice**. The CICE code can be obtained from [LANL](#) and the additional 'hadgem3' drivers will be required, even with the latest code release. Input grid files consistent with those used in NEMO will also be needed, and CICE CPP keys **ORCA\_GRID**, **CICE\_IN\_NEMO** and **coupled** should be used (seek advice from UKMO if necessary). Currently the code is only designed to work when using the CORE forcing option for NEMO (with *calc\_strair = true* and *calc\_Tsfc = true* in the CICE name-list), or alternatively when NEMO is coupled to the HadGAM3 atmosphere model (with *calc\_strair = false* and *calc\_Tsfc = false*). The code is intended to be used with *nn\_fsbc* set to 1 (although coupling ocean and ice less frequently should work, it is possible the calculation of some of the ocean-ice fluxes needs to be modified slightly - the user should check that results are not significantly different to the standard case).

There are two options for the technical coupling between NEMO and CICE. The standard version allows complete flexibility for the domain decompositions in the individual models, but this is at the expense of global gather and scatter operations in the coupling which become very expensive on larger numbers of processors. The alternative option (using **key\_nemocice\_decomp** for both NEMO and

CICE) ensures that the domain decomposition is identical in both models (provided domain parameters are set appropriately, and *processor\_shape* = *square-ice* and *distribution\_wght* = *block* in the CICE name-list) and allows much more efficient direct coupling on individual processors. This solution scales much better although it is at the expense of having more idle CICE processors in areas where there is no sea ice.

### 7.13.6 Freshwater budget control (*sbcfwb.F90*)

For global ocean simulation it can be useful to introduce a control of the mean sea level in order to prevent unrealistic drift of the sea surface height due to inaccuracy in the freshwater fluxes. In *NEMO*, two way of controlling the the freshwater budget.

***nn.fwb=0*** no control at all. The mean sea level is free to drift, and will certainly do so.

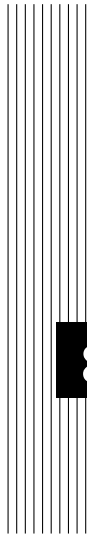
***nn.fwb=1*** global mean *emp* set to zero at each model time step.

***nn.fwb=2*** freshwater budget is adjusted from the previous year annual mean budget which is read in the *EMPave\_old.dat* file. As the model uses the Boussinesq approximation, the annual mean fresh water budget is simply evaluated from the change in the mean sea level at January the first and saved in the *EMPav.dat* file.

### 7.13.7 Neutral drag coefficient from external wave model (*sbcwave.F90*)

```
!-----
&namsbc_wave ! External fields from wave model (ln_wave=T)
!-----
!
! file name ! frequency (hours) ! variable ! time interp. ! clim ! 'yearly' / ! weights ! rotation !
! ! ! (if <0 months) ! name ! (logical) ! (T/F) ! 'monthly' ! filename ! pairing ! fi
sn_cdg = 'sdw_wave' , 1 , 'drag_coeff' , .true. , .false. , 'daily' , '' , '' , ''
sn_usd = 'sdw_wave' , 1 , 'u_sd2d' , .true. , .false. , 'daily' , '' , '' , ''
sn_vsd = 'sdw_wave' , 1 , 'v_sd2d' , .true. , .false. , 'daily' , '' , '' , ''
sn_hsw = 'sdw_wave' , 1 , 'hs' , .true. , .false. , 'daily' , '' , '' , ''
sn_wmp = 'sdw_wave' , 1 , 'wmp' , .true. , .false. , 'daily' , '' , '' , ''
sn_wnum = 'sdw_wave' , 1 , 'wave_num' , .true. , .false. , 'daily' , '' , '' , ''
sn_tauoc = 'sdw_wave' , 1 , 'wave_stress' , .true. , .false. , 'daily' , '' , '' , ''
!
cn_dir = './' ! root directory for the location of drag coefficient files
/
```

In order to read a neutral drag coeff, from an external data source (*i.e.* a wave model), the logical variable *ln\_cdgw* in *namsbc* namelist must be set to *true*. The *sbcwave.F90* module containing the routine *sbc\_wave* reads the namelist *namsbc\_wave* (for external data names, locations, frequency, interpolation and all the miscellaneous options allowed by Input Data generic Interface see §7.2) and a 2D field of neutral drag coefficient. Then using the routine *TURB\_CORE\_1Z* or *TURB\_CORE\_2Z*, and starting from the neutral drag coefficient provided, the drag coefficient is computed according to stable/unstable conditions of the air-sea interface following Large and Yeager [2004].



## 8 Lateral Boundary Condition (LBC)

### Contents

---

<b>8.1</b>	<b>Boundary Condition at the Coast (<i>rn_shlat</i>)</b>	<b>154</b>
<b>8.2</b>	<b>Model Domain Boundary Condition (<i>jperio</i>)</b>	<b>157</b>
8.2.1	Closed, cyclic, south symmetric ( <i>jperio</i> = 0, 1 or 2)	157
8.2.2	North-fold ( <i>jperio</i> = 3 to 6)	158
<b>8.3</b>	<b>Exchange with neighbouring processors (<i>lbclnk</i>, <i>lib_mpp</i>)</b>	<b>158</b>
<b>8.4</b>	<b>Unstructured Open Boundary Conditions (BDY)</b>	<b>161</b>
8.4.1	The namelists	163
8.4.2	The Flow Relaxation Scheme	164
8.4.3	The Flather radiation scheme	165
8.4.4	Boundary geometry	165
8.4.5	Input boundary data files	167
8.4.6	Volume correction	167
8.4.7	Tidal harmonic forcing	168

---

## 8.1 Boundary Condition at the Coast (*rn\_shlat*)

```

!-----
&namlbc      ! lateral momentum boundary condition
!-----
!
! free slip ! partial slip ! no slip ! strong slip
rn_shlat    = 2.      ! shlat = 0 ! 0 < shlat < 2 ! shlat = 2 ! 2 < shlat
ln_vorlat   = .false. ! consistency of vorticity boundary condition with analytical Eqs.
/

```

Options are defined through the *namlbc* namelist variables. The discrete representation of a domain with complex boundaries (coastlines and bottom topography) leads to arrays that include large portions where a computation is not required as the model variables remain at zero. Nevertheless, vectorial supercomputers are far more efficient when computing over a whole array, and the readability of a code is greatly improved when boundary conditions are applied in an automatic way rather than by a specific computation before or after each computational loop. An efficient way to work over the whole domain while specifying the boundary conditions, is to use multiplication by mask arrays in the computation. A mask array is a matrix whose elements are 1 in the ocean domain and 0 elsewhere. A simple multiplication of a variable by its own mask ensures that it will remain zero over land areas. Since most of the boundary conditions consist of a zero flux across the solid boundaries, they can be simply applied by multiplying variables by the correct mask arrays, *i.e.* the mask array of the grid point where the flux is evaluated. For example, the heat flux in the *i*-direction is evaluated at *u*-points. Evaluating this quantity as,

$$\frac{A^{iT}}{e_1} \frac{\partial T}{\partial i} \equiv \frac{A_u^{iT}}{e_{1u}} \delta_{i+1/2} [T] \text{ mask}_u \quad (8.1)$$

(where  $\text{mask}_u$  is the mask array at a *u*-point) ensures that the heat flux is zero inside land and at the boundaries, since  $\text{mask}_u$  is zero at solid boundaries which in this case are defined at *u*-points (normal velocity *u* remains zero at the coast) (Fig. 8.1).

For momentum the situation is a bit more complex as two boundary conditions must be provided along the coast (one each for the normal and tangential velocities). The boundary of the ocean in the C-grid is defined by the velocity-faces. For example, at a given *T*-level, the lateral boundary (a coastline or an intersection with the bottom topography) is made of segments joining *f*-points, and normal velocity points are located between two *f*-points (Fig. 8.1). The boundary condition on the normal velocity (no flux through solid boundaries) can thus be easily implemented using the mask system. The boundary condition on the tangential velocity requires a more specific treatment. This boundary condition influences the relative vorticity and momentum diffusive trends, and is required in order to compute the vorticity at the coast. Four different types of lateral boundary condition are available, controlled by the value of the *rn\_shlat* namelist parameter. (The value of the  $\text{mask}_f$  array along the coastline is set equal to this parameter.) These are:

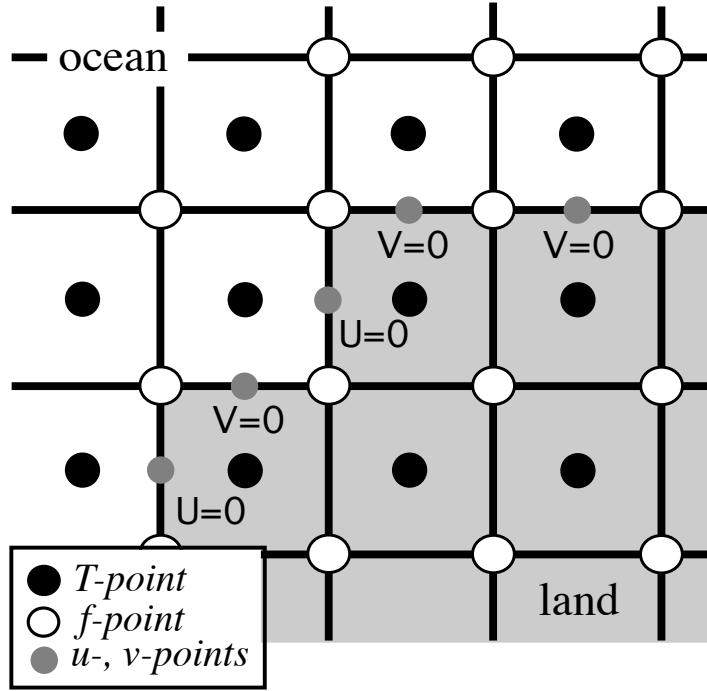


**Figure 8.1:** Lateral boundary (thick line) at T-level. The velocity normal to the boundary is set to zero.

**free-slip boundary condition (*rn\_shlat=0*):** the tangential velocity at the coastline is equal to the offshore velocity, *i.e.* the normal derivative of the tangential velocity is zero at the coast, so the vorticity:  $\text{mask}_f$  array is set to zero inside the land and just at the coast (Fig. 8.2-a).

**no-slip boundary condition (*rn\_shlat=2*):** the tangential velocity vanishes at the coastline. Assuming that the tangential velocity decreases linearly from the closest ocean velocity grid point to the coastline, the normal derivative is evaluated as if the velocities at the closest land velocity gridpoint and the closest ocean velocity gridpoint were of the same magnitude but in the opposite direction (Fig. 8.2-b). Therefore, the vorticity along the coastlines is given by:

$$\zeta \equiv 2 (\delta_{i+1/2} [e_{2v} v] - \delta_{j+1/2} [e_{1u} u]) / (e_{1f} e_{2f}) ,$$

where  $u$  and  $v$  are masked fields. Setting the  $\text{mask}_f$  array to 2 along the coastline provides a vorticity field computed with the no-slip boundary condition, simply by multiplying it by the  $\text{mask}_f$  :

$$\zeta \equiv \frac{1}{e_{1f} e_{2f}} (\delta_{i+1/2} [e_{2v} v] - \delta_{j+1/2} [e_{1u} u]) \text{mask}_f \quad (8.2)$$

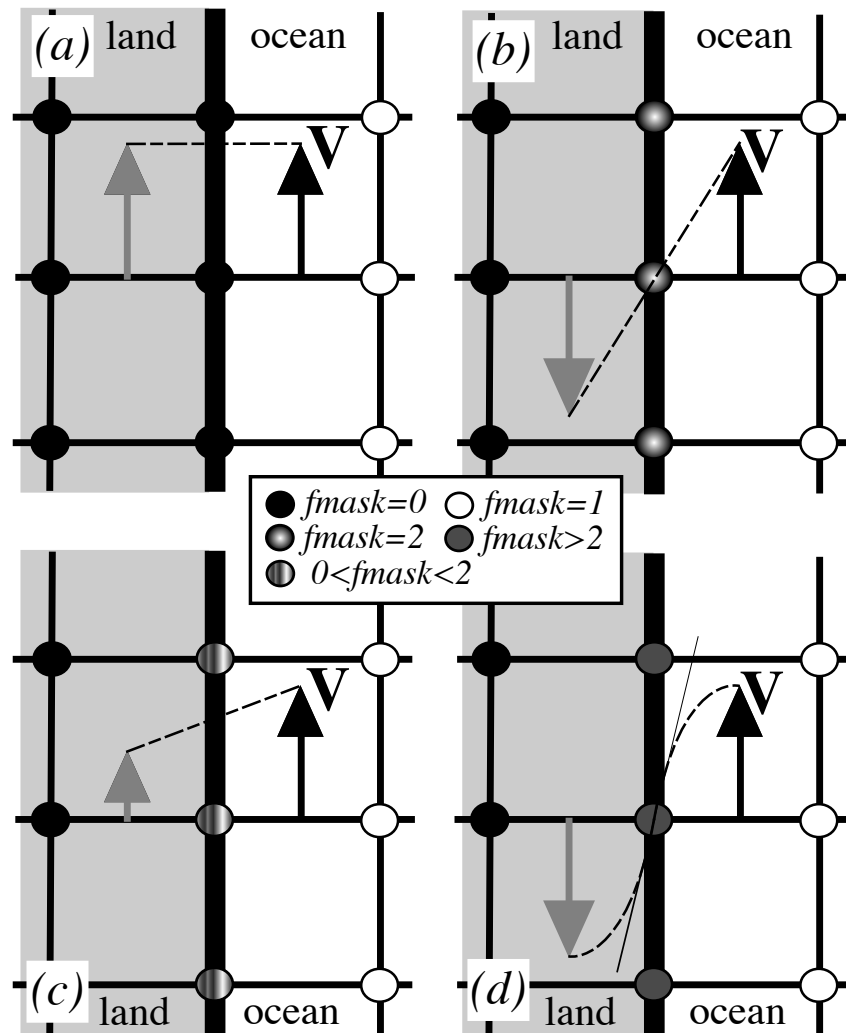


**Figure 8.2:** lateral boundary condition (a) free-slip ( $rn\_shlat = 0$ ) ; (b) no-slip ( $rn\_shlat = 2$ ) ; (c) "partial" free-slip ( $0 < rn\_shlat < 2$ ) and (d) "strong" no-slip ( $2 < rn\_shlat$ ). Implied "ghost" velocity inside land area is display in grey.

**”partial” free-slip boundary condition ( $0 < rn\_shlat < 2$ ):** the tangential velocity at the coastline is smaller than the offshore velocity, *i.e.* there is a lateral friction but not strong enough to make the tangential velocity at the coast vanish (Fig. 8.2-c). This can be selected by providing a value of  $mask_f$  strictly inbetween 0 and 2.

**”strong” no-slip boundary condition ( $2 < rn\_shlat$ ):** the viscous boundary layer is assumed to be smaller than half the grid size (Fig. 8.2-d). The friction is thus larger than in the no-slip case.

Note that when the bottom topography is entirely represented by the *s*-coordinates (pure *s*-coordinate), the lateral boundary condition on tangential velocity is of much less importance as it is only applied next to the coast where the minimum water depth can be quite shallow.

## 8.2 Model Domain Boundary Condition (*jperio*)

At the model domain boundaries several choices are offered: closed, cyclic east-west, south symmetric across the equator, a north-fold, and combination closed-north fold or cyclic-north-fold. The north-fold boundary condition is associated with the 3-pole ORCA mesh.

### 8.2.1 Closed, cyclic, south symmetric (*jperio* = 0, 1 or 2)

The choice of closed, cyclic or symmetric model domain boundary condition is made by setting *jperio* to 0, 1 or 2 in namelist *namcfg*. Each time such a boundary condition is needed, it is set by a call to routine *lbclnk.F90*. The computation of momentum and tracer trends proceeds from  $i = 2$  to  $i = jpi - 1$  and from  $j = 2$  to  $j = jpj - 1$ , *i.e.* in the model interior. To choose a lateral model boundary condition is to specify the first and last rows and columns of the model variables.

**For closed boundary (*jperio*=0)** , solid walls are imposed at all model boundaries: first and last rows and columns are set to zero.

**For cyclic east-west boundary (*jperio*=1)** , first and last rows are set to zero (closed) whilst the first column is set to the value of the last-but-one column and the last column to the value of the second one (Fig. 8.3-a). Whatever flows out of the eastern (western) end of the basin enters the western (eastern) end. Note that there is no option for north-south cyclic or for doubly cyclic cases.

**For symmetric boundary condition across the equator (*jperio*=2)** , last rows, and first and last columns are set to zero (closed). The row of symmetry is chosen to be the *u*- and *T*-points equator line ( $j = 2$ , *i.e.* at the southern end of the domain). For arrays defined at *u*- or *T*-points, the first row is set to the value of the third row while for most of *v*- and *f*-point arrays (*v*,  $\zeta$ , *jψ*, but

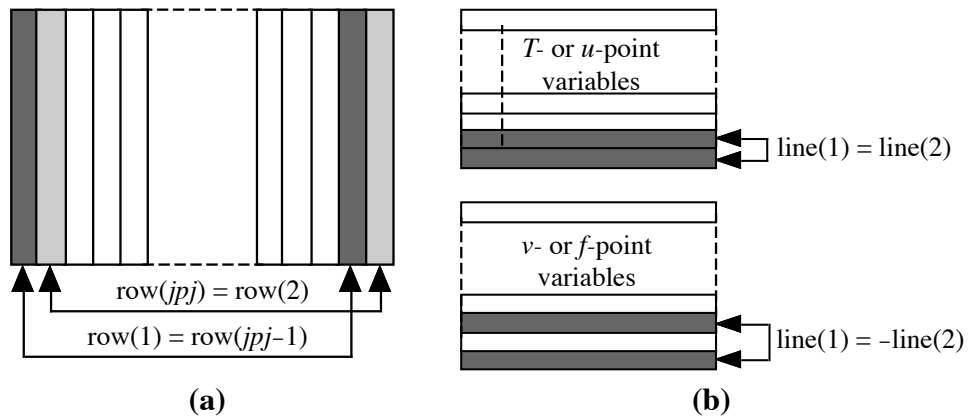


**Figure 8.3:** setting of (a) east-west cyclic (b) symmetric across the equator boundary conditions.

scalar arrays such as eddy coefficients) the first row is set to minus the value of the second row (Fig. 8.3-b). Note that this boundary condition is not yet available for the case of a massively parallel computer (**key\_mpp** defined).

### 8.2.2 North-fold ( $j_{perio} = 3$ to 6)

The north fold boundary condition has been introduced in order to handle the north boundary of a three-polar ORCA grid. Such a grid has two poles in the northern hemisphere (Fig. 16.1, and thus requires a specific treatment illustrated in Fig. 8.4. Further information can be found in *lbcnfd.F90* module which applies the north fold boundary condition.

## 8.3 Exchange with neighbouring processors (*lbclnk.F90*, *lib\_mpp.F90*)

For massively parallel processing (mpp), a domain decomposition method is used. The basic idea of the method is to split the large computation domain of a numerical experiment into several smaller domains and solve the set of equations by addressing independent local problems. Each processor has its own local memory and computes the model equation over a subdomain of the whole model domain. The subdomain boundary conditions are specified through communications between processors which are organized by explicit statements (message passing method).

A big advantage is that the method does not need many modifications of the initial FORTRAN code. From the modeller's point of view, each sub domain running on a processor is identical to the "mono-domain" code. In addition, the programmer manages the communications between subdomains, and the code is faster when the number of processors is increased. The porting of OPA code on an



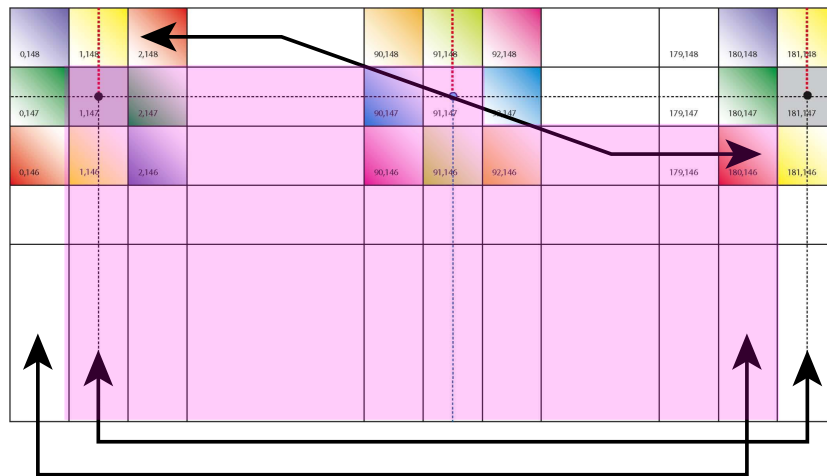


**Figure 8.4:** North fold boundary with a  $T$ -point pivot and cyclic east-west boundary condition ( $j_{perio} = 4$ ), as used in ORCA 2, 1/4, and 1/12. Pink shaded area corresponds to the inner domain mask (see text).

iPSC860 was achieved during Guyon's PhD [Guyon et al. 1994, 1995] in collaboration with CETIIS and ONERA. The implementation in the operational context and the studies of performance on a T3D and T3E Cray computers have been made in collaboration with IDRIS and CNRS. The present implementation is largely inspired by Guyon's work [Guyon 1995].

The parallelization strategy is defined by the physical characteristics of the ocean model. Second order finite difference schemes lead to local discrete operators that depend at the very most on one neighbouring point. The only non-local computations concern the vertical physics (implicit diffusion, turbulent closure scheme, ...) (delocalization over the whole water column), and the solving of the elliptic equation associated with the surface pressure gradient computation (delocalization over the whole horizontal domain). Therefore, a pencil strategy is used for the data sub-structuring: the 3D initial domain is laid out on local processor memories following a 2D horizontal topological splitting. Each sub-domain computes its own surface and bottom boundary conditions and has a side wall overlapping interface which defines the lateral boundary conditions for computations in the inner sub-domain. The overlapping area consists of the two rows at each edge of the sub-domain. After a computation, a communication phase starts: each processor sends to its neighbouring processors the update values of the points corresponding to the interior overlapping area to its neighbouring sub-domain (*i.e.* the innermost of the two overlapping rows). The communication is done through the Message Passing Interface (MPI). The data exchanges between processors are required at the very place where lateral domain boundary conditions are set in the mono-domain computation: the *lbc\_lnk* routine (found in *lbclnk.F90* module)

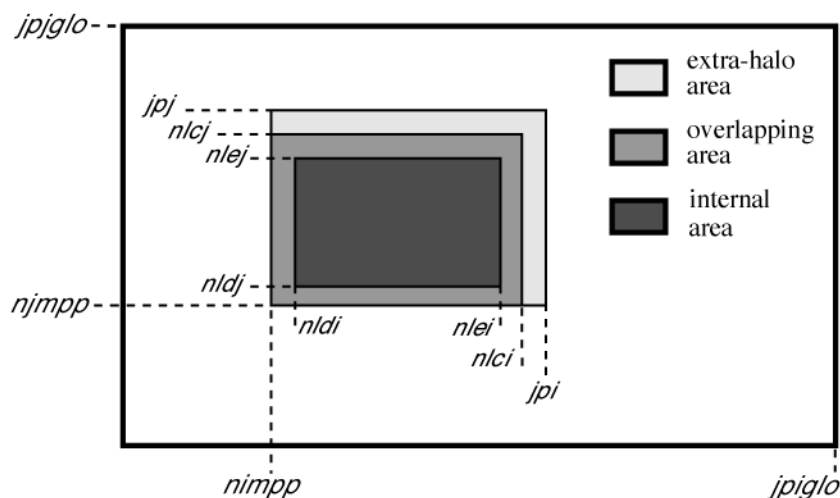


**Figure 8.5:** Positioning of a sub-domain when massively parallel processing is used.

which manages such conditions is interfaced with routines found in *lib.mpp.F90* module when running on an MPP computer (*i.e.* when **key\_mpp\_mpi** defined). It has to be pointed out that when using the MPP version of the model, the east-west cyclic boundary condition is done implicitly, whilst the south-symmetric boundary condition option is not available.

In the standard version of *NEMO*, the splitting is regular and arithmetic. The *i*-axis is divided by *jpni* and the *j*-axis by *jpnj* for a number of processors *jpni* most often equal to  $jpni \times jpni$  (parameters set in *nammpp* namelist). Each processor is independent and without message passing or synchronous process, programs run alone and access just its own local memory. For this reason, the main model dimensions are now the local dimensions of the subdomain (pencil) that are named *jpi*, *npj*, *jpj*. These dimensions include the internal domain and the overlapping rows. The number of rows to exchange (known as the halo) is usually set to one (*jpnci*=1, in *par\_oce.F90*). The whole domain dimensions are named *jpiglo*, *jpjglo* and *jpj*. The relationship between the whole domain and a sub-domain is:

$$\begin{aligned} jpi &= (jpiglo - 2 * jpnci + (jpni - 1)) / jpni + 2 * jpnci \\ npj &= (jpjglo - 2 * jpncj + (jpni - 1)) / jpni + 2 * jpncj \end{aligned} \quad (8.3)$$

where *jpni*, *jpni* are the number of processors following the *i*- and *j*-axis.

One also defines variables *nldi* and *nlei* which correspond to the internal domain bounds, and the variables *nimpp* and *njmpp* which are the position of the (1,1) grid-point in the global domain. An element of  $T_l$ , a local array (subdomain) corresponds to an element of  $T_g$ , a global array (whole domain) by the relationship:

$$T_g(i + nimpp - 1, j + njmpp - 1, k) = T_l(i, j, k), \quad (8.4)$$

with  $1 \leq i \leq jpi$ ,  $1 \leq j \leq jpj$ , and  $1 \leq k \leq jpk$ .

Processors are numbered from 0 to  $jpnij - 1$ , the number is saved in the variable `nproc`. In the standard version, a processor has no more than four neighbouring processors named `nono` (for north), `noea` (east), `noso` (south) and `nowe` (west) and two variables, `nbondi` and `nbondj`, indicate the relative position of the processor :

- `nbondi = -1` an east neighbour, no west processor,
- `nbondi = 0` an east neighbour, a west neighbour,
- `nbondi = 1` no east processor, a west neighbour,
- `nbondi = 2` no splitting following the i-axis.

During the simulation, processors exchange data with their neighbours. If there is effectively a neighbour, the processor receives variables from this processor on its overlapping row, and sends the data issued from internal domain corresponding to the overlapping row of the other processor.

The *NEMO* model computes equation terms with the help of mask arrays (0 on land points and 1 on sea points). It is easily readable and very efficient in the context of a computer with vectorial architecture. However, in the case of a scalar processor, computations over the land regions become more expensive in terms of CPU time. It is worse when we use a complex configuration with a realistic bathymetry like the global ocean where more than 50 % of points are land points. For this reason, a pre-processing tool can be used to choose the mpp domain decomposition with a maximum number of only land points processors, which can then be eliminated (Fig. 8.6) (For example, the `mpp_optimiz` tools, available from the DRAKKAR web site). This optimisation is dependent on the specific bathymetry employed. The user then chooses optimal parameters `jpni`, `jpnj` and `jpnij` with  $jpnij < jpni \times jpnj$ , leading to the elimination of  $jpni \times jpnj - jpnij$  land processors. When those parameters are specified in `nammpp` namelist, the algorithm in the `inimpp2` routine sets each processor's parameters (`nbound`, `nono`, `noea`,...) so that the land-only processors are not taken into account.

When land processors are eliminated, the value corresponding to these locations in the model output files is undefined. Note that this is a problem for the `meshmask` file which requires to be defined over the whole domain. Therefore, user should not eliminate land processors when creating a `meshmask` file (*i.e.* when setting a non-zero value to `nn_msh`).

## 8.4 Unstructured Open Boundary Conditions (BDY)

```
!-----
&nambdy      ! unstructured open boundaries
!-----
```

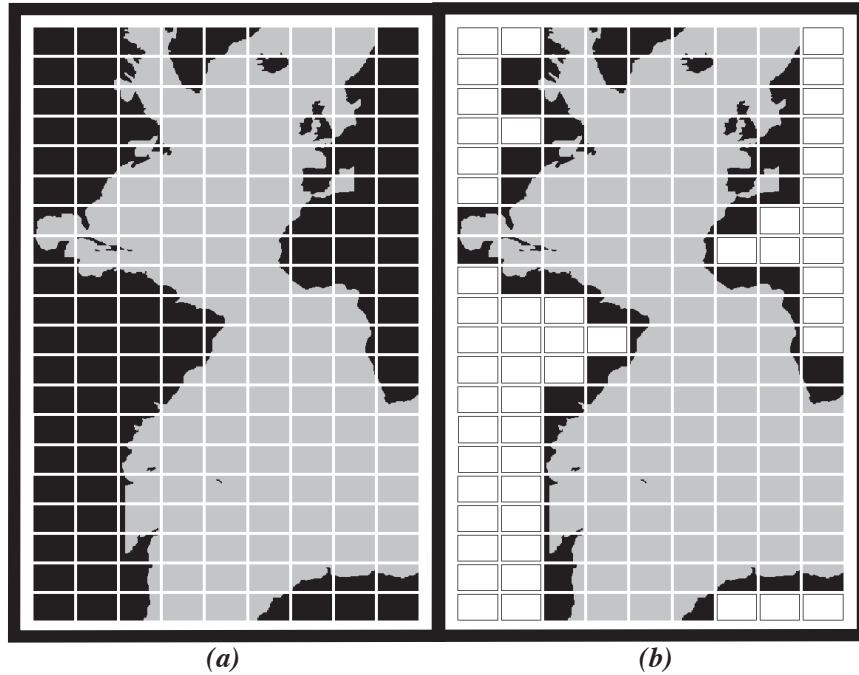


**Figure 8.6:** Example of Atlantic domain defined for the CLIPPER projet. Initial grid is composed of 773 x 1236 horizontal points. (a) the domain is split onto 9 subdomains ( $jpmi=9$ ,  $jpmj=20$ ). 52 subdomains are land areas. (b) 52 subdomains are eliminated (white rectangles) and the resulting number of processors really used during the computation is  $jpmij=128$ .

```

ln_bdy          = .false.          ! Use unstructured open boundaries
nb_bdy         = 0                 ! number of open boundary sets
ln_coords_file = .true.           ! =T : read bdy coordinates from file
cn_coords_file = 'coordinates.bdy.nc' ! bdy coordinates files
ln_mask_file   = .false.         ! =T : read mask from file
cn_mask_file   = ''              ! name of mask file (if ln_mask_file=.TRUE.)
cn_dyn2d       = 'none'          !
nn_dyn2d_dta   = 0               ! = 0, bdy data are equal to the initial state
                                     ! = 1, bdy data are read in 'bdydata .nc' files
                                     ! = 2, use tidal harmonic forcing data from files
                                     ! = 3, use external data AND tidal harmonic forcing

cn_dyn3d       = 'none'          !
nn_dyn3d_dta   = 0               ! = 0, bdy data are equal to the initial state
                                     ! = 1, bdy data are read in 'bdydata .nc' files

cn_tra         = 'none'          !
nn_tra_dta     = 0               ! = 0, bdy data are equal to the initial state
                                     ! = 1, bdy data are read in 'bdydata .nc' files

cn_ice_lim     = 'none'          !
nn_ice_lim_dta = 0               ! = 0, bdy data are equal to the initial state
                                     ! = 1, bdy data are read in 'bdydata .nc' files

rn_ice_tem     = 270.            ! lim3 only: arbitrary temperature of incoming sea ice
rn_ice_sal     = 10.            ! lim3 only:  -- salinity  --
rn_ice_age     = 30.            ! lim3 only:  -- age      --

ln_tra_dmp     = .false.         ! open boundaries conditions for tracers
ln_dyn3d_dmp   = .false.         ! open boundary condition for baroclinic velocities
rn_time_dmp    = 1.             ! Damping time scale in days
rn_time_dmp_out = 1.           ! Outflow damping time scale
nn_rimwidth    = 10             ! width of the relaxation zone
ln_vol         = .false.         ! total volume correction (see nn_volctl parameter)
nn_volctl     = 1               ! = 0, the total water flux across open boundaries is zero
nb_jpk_bdy    = -1              ! number of levels in the bdy data (set < 0 if consistent with planned run)

```

```

!-----
&nambdy_dta ! open boundaries - external data
!-----
!
! file name ! frequency (hours) ! variable ! time interp.! clim ! 'yearly'/ ! weights ! rotation ! land/sea mask !
! ! ! (if <0 months) ! name ! (logical) ! (T/F) ! 'monthly' ! filename ! pairing ! filename !
bn_ssh = 'amm12_bdyT_u2d', 24 , 'sossheig', .true. , .false. , 'daily' , '' , '' , '' , ''
bn_u2d = 'amm12_bdyU_u2d', 24 , 'vobtcrtx', .true. , .false. , 'daily' , '' , '' , '' , ''
bn_v2d = 'amm12_bdyV_u2d', 24 , 'vobtcrtx', .true. , .false. , 'daily' , '' , '' , '' , ''
bn_u3d = 'amm12_bdyU_u3d', 24 , 'vozocrtx', .true. , .false. , 'daily' , '' , '' , '' , ''
bn_v3d = 'amm12_bdyV_u3d', 24 , 'vomecrty', .true. , .false. , 'daily' , '' , '' , '' , ''
bn_tem = 'amm12_bdyT_tra', 24 , 'votemper', .true. , .false. , 'daily' , '' , '' , '' , ''
bn_sal = 'amm12_bdyT_tra', 24 , 'vosaline', .true. , .false. , 'daily' , '' , '' , '' , ''
! for lim3
! bn_a_i = 'amm12_bdyT_ice', 24 , 'ileadfra', .true. , .false. , 'daily' , '' , '' , '' , ''
! bn_h_i = 'amm12_bdyT_ice', 24 , 'iicethic', .true. , .false. , 'daily' , '' , '' , '' , ''
! bn_h_s = 'amm12_bdyT_ice', 24 , 'isnowth1', .true. , .false. , 'daily' , '' , '' , '' , ''

cn_dir = 'bdydata/' ! root directory for the location of the bulk files
ln_full_vel = .false. !
/

```

Options are defined through the *nambdy nambdy\_index nambdy\_dta nambdy\_dta2* namelist variables. The BDY module is the core implementation of open boundary conditions for regional configurations. It implements the Flow Relaxation Scheme algorithm for temperature, salinity, velocities and ice fields, and the Flather radiation condition for the depth-mean transports. The specification of the location of the open boundary is completely flexible and allows for example the open boundary to follow an isobath or other irregular contour.

The BDY module was modelled on the OBC module (see NEMO 3.4) and shares many features and a similar coding structure [Chanut 2005].

Boundary data files used with earlier versions of NEMO may need to be re-ordered to work with this version. See the section on the Input Boundary Data Files for details.

### 8.4.1 The namelists

The BDY module is activated by setting *ln\_bdy* to true. It is possible to define more than one boundary “set” and apply different boundary conditions to each set. The number of boundary sets is defined by *nb\_bdy*. Each boundary set may be defined as a set of straight line segments in a namelist (*ln\_coords\_file=.false.*) or read in from a file (*ln\_coords\_file=.true.*). If the set is defined in a namelist, then the namelists *nambdy\_index* must be included separately, one for each set. If the set is defined by a file, then a “coordinates.bdy.nc” file must be provided. The coordinates.bdy file is analogous to the usual NEMO “coordinates.nc” file. In the example above, there are two boundary sets, the first of which is defined via a file and the second is defined in a namelist. For more details of the definition of the boundary geometry see section 8.4.4.

For each boundary set a boundary condition has to be chosen for the barotropic solution (“u2d”: sea-surface height and barotropic velocities), for the baroclinic velocities (“u3d”), and for the active tracers<sup>1</sup> (“tra”). For each set of variables

<sup>1</sup>The BDY module does not deal with passive tracers at this version

there is a choice of algorithm and a choice for the data, eg. for the active tracers the algorithm is set by *nn\_tra* and the choice of data is set by *nn\_tra\_dta*.

The choice of algorithm is currently as follows:

0. No boundary condition applied. So the solution will “see” the land points around the edge of the edge of the domain.
1. Flow Relaxation Scheme (FRS) available for all variables.
2. Flather radiation scheme for the barotropic variables. The Flather scheme is not compatible with the filtered free surface (*dynspg\_ts*).

The main choice for the boundary data is to use initial conditions as boundary data (*nn\_tra\_dta=0*) or to use external data from a file (*nn\_tra\_dta=1*). For the barotropic solution there is also the option to use tidal harmonic forcing either by itself or in addition to other external data.

If external boundary data is required then the *nambdy\_dta* namelist must be defined. One *nambdy\_dta* namelist is required for each boundary set in the order in which the boundary sets are defined in *nambdy*. In the example given, two boundary sets have been defined and so there are two *nambdy\_dta* namelists. The boundary data is read in using the *fldread* module, so the *nambdy\_dta* namelist is in the format required for *fldread*. For each variable required, the filename, the frequency of the files and the frequency of the data in the files is given. Also whether or not time-interpolation is required and whether the data is climatological (time-cyclic) data. Note that on-the-fly spatial interpolation of boundary data is not available at this version.

In the example namelists given, two boundary sets are defined. The first set is defined via a file and applies FRS conditions to temperature and salinity and Flather conditions to the barotropic variables. External data is provided in daily files (from a large-scale model). Tidal harmonic forcing is also used. The second set is defined in a namelist. FRS conditions are applied on temperature and salinity and climatological data is read from external files.

#### 8.4.2 The Flow Relaxation Scheme

The Flow Relaxation Scheme (FRS) [Davies 1976, Engerdahl 1995], applies a simple relaxation of the model fields to externally-specified values over a zone next to the edge of the model domain. Given a model prognostic variable  $\Phi$

$$\Phi(d) = \alpha(d)\Phi_e(d) + (1 - \alpha(d))\Phi_m(d) \quad d = 1, N \quad (8.5)$$

where  $\Phi_m$  is the model solution and  $\Phi_e$  is the specified external field,  $d$  gives the discrete distance from the model boundary and  $\alpha$  is a parameter that varies from 1

at  $d = 1$  to a small value at  $d = N$ . It can be shown that this scheme is equivalent to adding a relaxation term to the prognostic equation for  $\Phi$  of the form:

$$-\frac{1}{\tau} (\Phi - \Phi_e) \quad (8.6)$$

where the relaxation time scale  $\tau$  is given by a function of  $\alpha$  and the model time step  $\Delta t$ :

$$\tau = \frac{1 - \alpha}{\alpha} \Delta t \quad (8.7)$$

Thus the model solution is completely prescribed by the external conditions at the edge of the model domain and is relaxed towards the external conditions over the rest of the FRS zone. The application of a relaxation zone helps to prevent spurious reflection of outgoing signals from the model boundary.

The function  $\alpha$  is specified as a *tanh* function:

$$\alpha(d) = 1 - \tanh\left(\frac{d-1}{2}\right), \quad d = 1, N \quad (8.8)$$

The width of the FRS zone is specified in the namelist as *nn\_rimwidth*. This is typically set to a value between 8 and 10.

### 8.4.3 The Flather radiation scheme

The [Flather \[1994\]](#) scheme is a radiation condition on the normal, depth-mean transport across the open boundary. It takes the form

$$U = U_e + \frac{c}{h} (\eta - \eta_e), \quad (8.9)$$

where  $U$  is the depth-mean velocity normal to the boundary and  $\eta$  is the sea surface height, both from the model. The subscript  $e$  indicates the same fields from external sources. The speed of external gravity waves is given by  $c = \sqrt{gh}$ , and  $h$  is the depth of the water column. The depth-mean normal velocity along the edge of the model domain is set equal to the external depth-mean normal velocity, plus a correction term that allows gravity waves generated internally to exit the model boundary. Note that the sea-surface height gradient in (8.9) is a spatial gradient across the model boundary, so that  $\eta_e$  is defined on the  $T$  points with  $nbr = 1$  and  $\eta$  is defined on the  $T$  points with  $nbr = 2$ .  $U$  and  $U_e$  are defined on the  $U$  or  $V$  points with  $nbr = 1$ , *i.e.* between the two  $T$  grid points.

### 8.4.4 Boundary geometry

Each open boundary set is defined as a list of points. The information is stored in the arrays *nbi*, *nbj*, and *nbr* in the *idx\_bdy* structure. The *nbi* and *nbj* arrays define the local  $(i, j)$  indices of each point in the boundary zone and the *nbr* array defines the discrete distance from the boundary with  $nbr = 1$  meaning that the

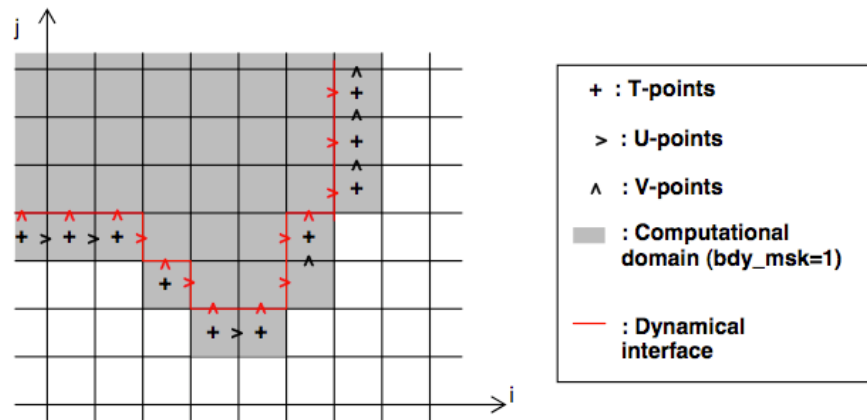


**Figure 8.7:** Example of geometry of unstructured open boundary

point is next to the edge of the model domain and  $nbr > 1$  showing that the point is increasingly further away from the edge of the model domain. A set of  $nbi$ ,  $nbj$ , and  $nbr$  arrays is defined for each of the  $T$ ,  $U$  and  $V$  grids. Figure 8.7 shows an example of an irregular boundary.

The boundary geometry for each set may be defined in a namelist `nambdy_index` or by reading in a “`coordinates.bdy.nc`” file. The `nambdy_index` namelist defines a series of straight-line segments for north, east, south and west boundaries. For the northern boundary, `nbdysegn` gives the number of segments, `jpjnob` gives the  $j$  index for each segment and `jpindt` and `jpifnt` give the start and end  $i$  indices for each segment with similar for the other boundaries. These segments define a list of  $T$  grid points along the outermost row of the boundary ( $nbr = 1$ ). The code deduces the  $U$  and  $V$  points and also the points for  $nbr > 1$  if `nn_rimwidth > 1`.

The boundary geometry may also be defined from a “`coordinates.bdy.nc`” file. Figure 8.8 gives an example of the header information from such a file. The file should contain the index arrays for each of the  $T$ ,  $U$  and  $V$  grids. The arrays must be in order of increasing  $nbr$ . Note that the  $nbi$ ,  $nbj$  values in the file are global values and are converted to local values in the code. Typically this file will be used to generate external boundary data via interpolation and so will also contain the latitudes and longitudes of each point as shown. However, this is not necessary to run the model.

For some choices of irregular boundary the model domain may contain areas of ocean which are not part of the computational domain. For example if an open boundary is defined along an isobath, say at the shelf break, then the areas of ocean outside of this boundary will need to be masked out. This can be done by reading a mask file defined as `cn_mask_file` in the `nam_bdy` namelist. Only one mask file is used even if multiple boundary sets are defined.



### 8.4.5 Input boundary data files

The data files contain the data arrays in the order in which the points are defined in the *nbi* and *nbi* arrays. The data arrays are dimensioned on: a time dimension; *xb* which is the index of the boundary data point in the horizontal; and *yb* which is a degenerate dimension of 1 to enable the file to be read by the standard NEMO I/O routines. The 3D fields also have a depth dimension.

At Version 3.4 there are new restrictions on the order in which the boundary points are defined (and therefore restrictions on the order of the data in the file). In particular:

1. The data points must be in order of increasing *nbr*, ie. all the  $nbr = 1$  points, then all the  $nbr = 2$  points etc.
2. All the data for a particular boundary set must be in the same order. (Prior to 3.4 it was possible to define barotropic data in a different order to the data for tracers and baroclinic velocities).

These restrictions mean that data files used with previous versions of the model may not work with version 3.4. A fortran utility *bdy\_reorder* exists in the TOOLS directory which will re-order the data in old BDY data files.

### 8.4.6 Volume correction

There is an option to force the total volume in the regional model to be constant, similar to the option in the OBC module. This is controlled by the *nn\_volctl* parameter in the namelist. A value of *nn\_volctl* = 0 indicates that this option is not used. If *nn\_volctl* = 1 then a correction is applied to the normal velocities around the boundary at each timestep to ensure that the integrated volume flow through the boundary is zero. If *nn\_volctl* = 2 then the calculation of the volume change on the timestep includes the change due to the freshwater flux across the surface and the correction velocity corrects for this as well.

If more than one boundary set is used then volume correction is applied to all boundaries at once.

```

netcdf med12.obc.coordinates {
dimensions:
  yb = 1 ;
  xbT = 3218 ;
  xbU = 3200 ;
  xbV = 3201 ;
variables:
  int nbit(yb, xbT) ;
  int nbu(yb, xbU) ;
  int nbiv(yb, xbV) ;
  int nbjt(yb, xbT) ;
  int nbju(yb, xbU) ;
  int nbjv(yb, xbV) ;
  int nbrt(yb, xbT) ;
  int nbru(yb, xbU) ;
  int nbrv(yb, xbV) ;
  float elt(yb, xbT) ;
    elt:units = "metres" ;
  float elu(yb, xbU) ;
    elu:units = "metres" ;
  float elv(yb, xbV) ;
    elv:units = "metres" ;
  float e2t(yb, xbT) ;
    e2t:units = "metres" ;
  float e2u(yb, xbU) ;
    e2u:units = "metres" ;
  float e2v(yb, xbV) ;
    e2v:units = "metres" ;
  float glamt(yb, xbT) ;
    glamt:units = "degrees_east" ;
  float glamu(yb, xbU) ;
    glamu:units = "degrees_east" ;
  float glamv(yb, xbV) ;
    glamv:units = "degrees_east" ;
  float gphit(yb, xbT) ;
    gphit:units = "degrees_north" ;
  float gphiu(yb, xbU) ;
    gphiu:units = "degrees_north" ;
  float gphiv(yb, xbV) ;
    gphiv:units = "degrees_north" ;

// global attributes:
  :file_name = "med12.obc.coordinates.reorder.nc" ;
  :rimwidth = 9 ;
  :NCO = "3.9.9" ;
}

```

**Figure 8.8:** Example of the header for a coordinates.bdy.nc file

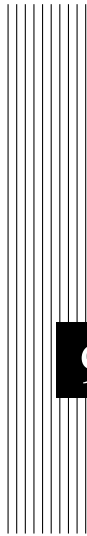
## 8.4.7 Tidal harmonic forcing

!-----

```
&nambdy_tide ! tidal forcing at open boundaries
!-----
  filtide      = 'bdydtb/amm12_bdytide_' ! file name root of tidal forcing files
  ln_bdytide_2ddta = .false.             !
  ln_bdytide_conj = .false.             !
/
```

Options are defined through the *nambdy\_tide* namelist variables. To be written....





## 9 Lateral Ocean Physics (LDF)

### Contents

---

<b>9.1</b>	<b>Direction of Lateral Mixing (<i>ldfslp</i>)</b>	<b>173</b>
9.1.1	slopes for tracer geopotential mixing in the <i>s</i> -coordinate	173
9.1.2	Slopes for tracer iso-neutral mixing	173
9.1.3	slopes for momentum iso-neutral mixing	176
<b>9.2</b>	<b>Lateral Mixing Operators (<i>ldftra, lfdyn</i>)</b>	<b>178</b>
<b>9.3</b>	<b>Lateral Mixing Coefficient (<i>ldftra, lfdyn</i>)</b>	<b>178</b>
<b>9.4</b>	<b>Eddy Induced Velocity (<i>traadv_eiv, ldfeiv</i>)</b>	<b>180</b>

---

The lateral physics terms in the momentum and tracer equations have been described in §2.5.1 and their discrete formulation in §5.2 and §6.6). In this section we further discuss each lateral physics option. Choosing one lateral physics scheme means for the user defining, (1) the type of operator used (laplacian or bilaplacian operators, or no lateral mixing term) ; (2) the direction along which the lateral diffusive fluxes are evaluated (model level, geopotential or isopycnal surfaces) ; and (3) the space and time variations of the eddy coefficients. These three aspects of the lateral diffusion are set through namelist parameters (see the *nam\_traldf* and *nam\_dynldf* below). Note that this chapter describes the standard implementation of iso-neutral tracer mixing, and Griffies's implementation, which is used if *traldf\_grif=true*, is described in AppdxD

```

!-----
&namtra_ldf      ! lateral diffusion scheme for tracers                (default: NO selection)
!-----
!
! Operator type:
ln_traldf_NONE = .false. ! No explicit diffusion
ln_traldf_lap  = .false. ! laplacian operator
ln_traldf_blp  = .false. ! bilaplacian operator
!
! Direction of action:
ln_traldf_lev = .false. ! iso-level
ln_traldf_hor = .false. ! horizontal (geopotential)
ln_traldf_iso = .false. ! iso-neutral (standard operator)
ln_traldf_triad = .false. ! iso-neutral (triad operator)
!
! iso-neutral options:
ln_traldf_msc = .false. ! Method of Stabilizing Correction (both operators)
rn_slpmax     = 0.01    ! slope limit (both operators)
ln_triad_iso  = .false. ! pure horizontal mixing in ML (triad only)
rn_sw_triad   = 1       ! =1 switching triad ; =0 all 4 triads used (triad only)
ln_botmix_triad = .false. ! lateral mixing on bottom (triad only)
!
! Coefficients:
nn_ahm_ijk_t = 0       ! space/time variation of eddy coef
!
!   = -20 (= -30) read in eddy_diffusivity_2D.nc (..._3D.nc) file
!   = 0 constant
!   = 10 F(k) =ldf_c1d
!   = 20 F(i,j) =ldf_c2d
!   = 21 F(i,j,t) =Treguier et al. JPO 1997 formulation
!   = 30 F(i,j,k) =ldf_c2d * ldf_c1d
!   = 31 F(i,j,k,t)=F(local velocity and grid-spacing)
rn_ahm_0      = 2000.   ! lateral eddy diffusivity (lap. operator) [m2/s]
rn_bht_0      = 1.e+12 ! lateral eddy diffusivity (bilap. operator) [m4/s]
/

!-----
&namdyn_ldf     ! lateral diffusion on momentum                    (default: NO selection)
!-----
!
! Type of the operator :
ln_dynldf_NONE= .false. ! No operator (i.e. no explicit diffusion)
ln_dynldf_lap  = .false. ! laplacian operator
ln_dynldf_blp  = .false. ! bilaplacian operator
!
! Direction of action :
ln_dynldf_lev = .false. ! iso-level
ln_dynldf_hor = .false. ! horizontal (geopotential)
ln_dynldf_iso = .false. ! iso-neutral
!
! Coefficient
nn_ahm_ijk_t = 0       ! space/time variation of eddy coef
!
!   = -30 read in eddy_viscosity_3D.nc file
!   = -20 read in eddy_viscosity_2D.nc file
!   = 0 constant
!   = 10 F(k)=c1d
!   = 20 F(i,j)=F(grid spacing)=c2d
!   = 30 F(i,j,k)=c2d*c1d
!   = 31 F(i,j,k)=F(grid spacing and local velocity)
!   = 32 F(i,j,k)=F(local gridscale and deformation rate)
! Caution in 20 and 30 cases the coefficient have to be given for a 1 degree grid (~111km)
rn_ahm_0      = 40000. ! horizontal laplacian eddy viscosity [m2/s]
rn_ahm_b      = 0.     ! background eddy viscosity for ldf_iso [m2/s]

```

```

rn_bhm_0      = 1.e+12      ! horizontal bilaplacian eddy viscosity [m4/s]
!             ! Smagorinsky settings (nn_ahm_ijk_t = 32) :
rn_csmc       = 3.5        ! Smagorinsky constant of proportionality
rn_minfac     = 1.0        ! multiplier of theoretical lower limit
rn_maxfac     = 1.0        ! multiplier of theoretical upper limit
/

```

## 9.1 Direction of Lateral Mixing (*ldfslp.F90*)

A direction for lateral mixing has to be defined when the desired operator does not act along the model levels. This occurs when (a) horizontal mixing is required on tracer or momentum (*ln\_traldf\_hor* or *ln\_dynldf\_hor*) in *s*- or mixed *s-z*- coordinates, and (b) isoneutral mixing is required whatever the vertical coordinate is. This direction of mixing is defined by its slopes in the *i*- and *j*-directions at the face of the cell of the quantity to be diffused. For a tracer, this leads to the following four slopes :  $r_{1u}$ ,  $r_{1w}$ ,  $r_{2v}$ ,  $r_{2w}$  (see (5.10)), while for momentum the slopes are  $r_{1t}$ ,  $r_{1uw}$ ,  $r_{2f}$ ,  $r_{2uw}$  for *u* and  $r_{1f}$ ,  $r_{1vw}$ ,  $r_{2t}$ ,  $r_{2vw}$  for *v*.

### 9.1.1 slopes for tracer geopotential mixing in the *s*-coordinate

In *s*-coordinates, geopotential mixing (*i.e.* horizontal mixing)  $r_1$  and  $r_2$  are the slopes between the geopotential and computational surfaces. Their discrete formulation is found by locally solving (5.10) when the diffusive fluxes in the three directions are set to zero and  $T$  is assumed to be horizontally uniform, *i.e.* a linear function of  $z_T$ , the depth of a  $T$ -point.

$$\begin{aligned}
r_{1u} &= \frac{e_{3u}}{\left(e_{1u} \overline{\overline{i+1/2, k}}\right)} \delta_{i+1/2}[z_t] \approx \frac{1}{e_{1u}} \delta_{i+1/2}[z_t] \\
r_{2v} &= \frac{e_{3v}}{\left(e_{2v} \overline{\overline{j+1/2, k}}\right)} \delta_{j+1/2}[z_t] \approx \frac{1}{e_{2v}} \delta_{j+1/2}[z_t] \\
r_{1w} &= \frac{1}{e_{1w}} \overline{\overline{\delta_{i+1/2}[z_t]}}^{i, k+1/2} \approx \frac{1}{e_{1w}} \delta_{i+1/2}[z_{uw}] \\
r_{2w} &= \frac{1}{e_{2w}} \overline{\overline{\delta_{j+1/2}[z_t]}}^{j, k+1/2} \approx \frac{1}{e_{2w}} \delta_{j+1/2}[z_{vw}]
\end{aligned} \tag{9.1}$$

These slopes are computed once in *ldfslp\_init* when *ln\_sco*=True, and either *ln\_traldf\_hor*=True or *ln\_dynldf\_hor*=True.

### 9.1.2 Slopes for tracer iso-neutral mixing

In iso-neutral mixing  $r_1$  and  $r_2$  are the slopes between the iso-neutral and computational surfaces. Their formulation does not depend on the vertical coordinate used. Their discrete formulation is found using the fact that the diffusive fluxes of locally referenced potential density (*i.e.* *insitu* density) vanish. So, substituting  $T$

by  $\rho$  in (5.10) and setting the diffusive fluxes in the three directions to zero leads to the following definition for the neutral slopes:

$$\begin{aligned}
 r_{1u} &= \frac{e_{3u}}{e_{1u}} \frac{\delta_{i+1/2}[\rho]}{\overline{\overline{\delta_{k+1/2}[\rho]}}^{i+1/2,k}} \\
 r_{2v} &= \frac{e_{3v}}{e_{2v}} \frac{\delta_{j+1/2}[\rho]}{\overline{\overline{\delta_{k+1/2}[\rho]}}^{j+1/2,k}} \\
 r_{1w} &= \frac{e_{3w}}{e_{1w}} \frac{\overline{\overline{\delta_{i+1/2}[\rho]}}^{i,k+1/2}}{\delta_{k+1/2}[\rho]} \\
 r_{2w} &= \frac{e_{3w}}{e_{2w}} \frac{\overline{\overline{\delta_{j+1/2}[\rho]}}^{j,k+1/2}}{\delta_{k+1/2}[\rho]}
 \end{aligned} \tag{9.2}$$

As the mixing is performed along neutral surfaces, the gradient of  $\rho$  in (9.2) has to be evaluated at the same local pressure (which, in decibars, is approximated by the depth in meters in the model). Therefore (9.2) cannot be used as such, but further transformation is needed depending on the vertical coordinate used:

***z*-coordinate with full step :** in (9.2) the densities appearing in the *i* and *j* derivatives are taken at the same depth, thus the *insitu* density can be used. This is not the case for the vertical derivatives:  $\delta_{k+1/2}[\rho]$  is replaced by  $-\rho N^2/g$ , where  $N^2$  is the local Brunt-Vaisälä frequency evaluated following McDougall [1987] (see §5.8.2).

***z*-coordinate with partial step :** this case is identical to the full step case except that at partial step level, the *horizontal* density gradient is evaluated as described in §5.9.

***s*- or hybrid *s*-*z*- coordinate :** in the current release of *NEMO*, iso-neutral mixing is only employed for *s*-coordinates if the Griffies scheme is used (*traldf\_grif=true*; see Appdx D). In other words, iso-neutral mixing will only be accurately represented with a linear equation of state (*mn\_eos=1* or *2*). In the case of a "true" equation of state, the evaluation of *i* and *j* derivatives in (9.2) will include a pressure dependent part, leading to the wrong evaluation of the neutral slopes.

Note: The solution for *s*-coordinate passes through the use of different (and better) expression for the constraint on iso-neutral fluxes. Following Griffies [2004], instead of specifying directly that there is a zero neutral diffusive flux of locally referenced potential density, we stay in the *T-S* plane and consider the balance between the neutral direction diffusive fluxes of potential temperature and salinity:

$$\alpha \mathbf{F}(T) = \beta \mathbf{F}(S) \tag{9.3}$$



This constraint leads to the following definition for the slopes:

$$\begin{aligned}
r_{1u} &= \frac{e_{3u}}{e_{1u}} \frac{\alpha_u \overline{\delta_{i+1/2}[T]}^{i+1/2,k} - \beta_u \overline{\delta_{i+1/2}[S]}^{i+1/2,k}}{\alpha_u \overline{\delta_{k+1/2}[T]}^{i+1/2,k} - \beta_u \overline{\delta_{k+1/2}[S]}^{i+1/2,k}} \\
r_{2v} &= \frac{e_{3v}}{e_{2v}} \frac{\alpha_v \overline{\delta_{j+1/2}[T]}^{j+1/2,k} - \beta_v \overline{\delta_{j+1/2}[S]}^{j+1/2,k}}{\alpha_v \overline{\delta_{k+1/2}[T]}^{j+1/2,k} - \beta_v \overline{\delta_{k+1/2}[S]}^{j+1/2,k}} \\
r_{1w} &= \frac{e_{3w}}{e_{1w}} \frac{\alpha_w \overline{\delta_{i+1/2}[T]}^{i,k+1/2} - \beta_w \overline{\delta_{i+1/2}[S]}^{i,k+1/2}}{\alpha_w \overline{\delta_{k+1/2}[T]}^{i,k+1/2} - \beta_w \overline{\delta_{k+1/2}[S]}^{i,k+1/2}} \\
r_{2w} &= \frac{e_{3w}}{e_{2w}} \frac{\alpha_w \overline{\delta_{j+1/2}[T]}^{j,k+1/2} - \beta_w \overline{\delta_{j+1/2}[S]}^{j,k+1/2}}{\alpha_w \overline{\delta_{k+1/2}[T]}^{j,k+1/2} - \beta_w \overline{\delta_{k+1/2}[S]}^{j,k+1/2}}
\end{aligned} \tag{9.4}$$

where  $\alpha$  and  $\beta$ , the thermal expansion and saline contraction coefficients introduced in §5.8.2, have to be evaluated at the three velocity points. In order to save computation time, they should be approximated by the mean of their values at  $T$ -points (for example in the case of  $\alpha$ :  $\alpha_u = \overline{\alpha_T}^{i+1/2}$ ,  $\alpha_v = \overline{\alpha_T}^{j+1/2}$  and  $\alpha_w = \overline{\alpha_T}^{k+1/2}$ ).

Note that such a formulation could be also used in the  $z$ -coordinate and  $z$ -coordinate with partial steps cases.

This implementation is a rather old one. It is similar to the one proposed by Cox [1987], except for the background horizontal diffusion. Indeed, the Cox implementation of isopycnal diffusion in GFDL-type models requires a minimum background horizontal diffusion for numerical stability reasons. To overcome this problem, several techniques have been proposed in which the numerical schemes of the ocean model are modified [Weaver and Eby 1997, Griffies et al. 1998]. Griffies's scheme is now available in *NEMO* if *traldf\_grif\_iso* is set true; see Appdx D. Here, another strategy is presented [Lazar 1997]: a local filtering of the iso-neutral slopes (made on 9 grid-points) prevents the development of grid point noise generated by the iso-neutral diffusion operator (Fig. 9.1). This allows an iso-neutral diffusion scheme without additional background horizontal mixing. This technique can be viewed as a diffusion operator that acts along large-scale ( $2 \Delta x$ ) iso-neutral surfaces. The diapycnal diffusion required for numerical stability is thus minimized and its net effect on the flow is quite small when compared to the effect of an horizontal background mixing.

Nevertheless, this iso-neutral operator does not ensure that variance cannot increase, contrary to the Griffies et al. [1998] operator which has that property.

For numerical stability reasons [Cox 1987, Griffies 2004], the slopes must also be bounded by 1/100 everywhere. This constraint is applied in a piecewise linear fashion, increasing from zero at the surface to 1/100 at 70 metres and thereafter

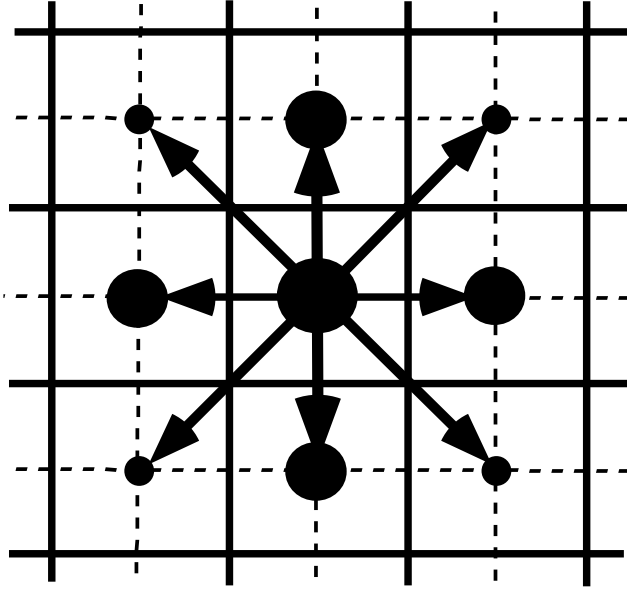


**Figure 9.1:** averaging procedure for isopycnal slope computation.

decreasing to zero at the bottom of the ocean. (the fact that the eddies "feel" the surface motivates this flattening of isopycnals near the surface).

add here a discussion about the flattening of the slopes, vs tapering the coefficient.

### 9.1.3 slopes for momentum iso-neutral mixing

The iso-neutral diffusion operator on momentum is the same as the one used on tracers but applied to each component of the velocity separately (see (6.27) in section 6.6.2). The slopes between the surface along which the diffusion operator acts and the surface of computation ( $z$ - or  $s$ -surfaces) are defined at  $T$ -,  $f$ -, and  $uw$ -points for the  $u$ -component, and  $T$ -,  $f$ - and  $vw$ - points for the  $v$ -component. They are computed from the slopes used for tracer diffusion, *i.e.* (9.1) and (9.2) :

$$\begin{aligned}
 r_{1t} &= \overline{r_{1u}}^i & r_{1f} &= \overline{r_{1u}}^{i+1/2} \\
 r_{2f} &= \overline{r_{2v}}^{j+1/2} & r_{2t} &= \overline{r_{2v}}^j \\
 r_{1uw} &= \overline{r_{1w}}^{i+1/2} & \text{and} & r_{1vw} &= \overline{r_{1w}}^{j+1/2} \\
 r_{2uw} &= \overline{r_{2w}}^{j+1/2} & & r_{2vw} &= \overline{r_{2w}}^{j+1/2}
 \end{aligned} \tag{9.5}$$

The major issue remaining is in the specification of the boundary conditions. The same boundary conditions are chosen as those used for lateral diffusion along model level surfaces, *i.e.* using the shear computed along the model levels and with no additional friction at the ocean bottom (see §8.1).

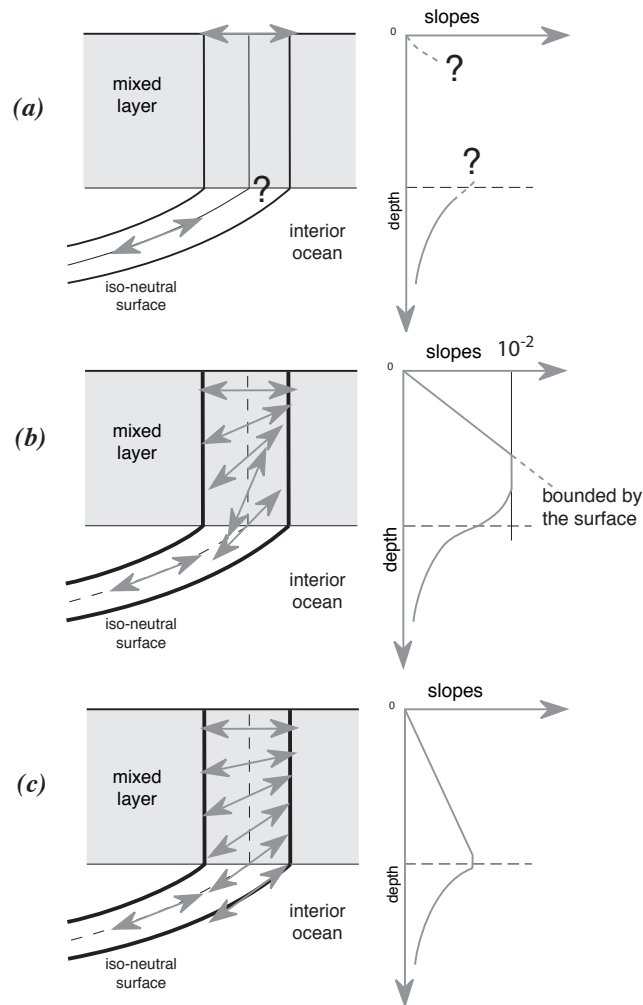


**Figure 9.2:** Vertical profile of the slope used for lateral mixing in the mixed layer : (a) in the real ocean the slope is the iso-neutral slope in the ocean interior, which has to be adjusted at the surface boundary (i.e. it must tend to zero at the surface since there is no mixing across the air-sea interface: wall boundary condition). Nevertheless, the profile between the surface zero value and the interior iso-neutral one is unknown, and especially the value at the base of the mixed layer ; (b) profile of slope using a linear tapering of the slope near the surface and imposing a maximum slope of  $1/100$  ; (c) profile of slope actually used in *NEMO*: a linear decrease of the slope from zero at the surface to its ocean interior value computed just below the mixed layer. Note the huge change in the slope at the base of the mixed layer between (b) and (c).

## 9.2 Lateral Mixing Operators (*traldf.F90*, *traldf.F90*)

## 9.3 Lateral Mixing Coefficient (*ldfra.F90*, *ldfdyn.F90*)

Introducing a space variation in the lateral eddy mixing coefficients changes the model core memory requirement, adding up to four extra three-dimensional arrays for the geopotential or isopycnal second order operator applied to momentum. Six CPP keys control the space variation of eddy coefficients: three for momentum and three for tracer. The three choices allow: a space variation in the three space directions (**key\_traldf\_c3d**, **key\_dynldf\_c3d**), in the horizontal plane (**key\_traldf\_c2d**, **key\_dynldf\_c2d**), or in the vertical only (**key\_traldf\_c1d**, **key\_dynldf\_c1d**). The default option is a constant value over the whole ocean on both momentum and tracers.

The number of additional arrays that have to be defined and the gridpoint position at which they are defined depend on both the space variation chosen and the type of operator used. The resulting eddy viscosity and diffusivity coefficients can be a function of more than one variable. Changes in the computer code when switching from one option to another have been minimized by introducing the eddy coefficients as statement functions (include file *ldfra\_substitute.h90* and *ldfdyn\_substitute.h90*). The functions are replaced by their actual meaning during the preprocessing step (CPP). The specification of the space variation of the coefficient is made in *ldfra.F90* and *ldfdyn.F90*, or more precisely in include files *traldf\_cNd.h90* and *dynldf\_cNd.h90*, with N=1, 2 or 3. The user can modify these include files as he/she wishes. The way the mixing coefficient are set in the reference version can be briefly described as follows:

### Constant Mixing Coefficients (default option)

When none of the **key\_dynldf...** and **key\_traldf...** keys are defined, a constant value is used over the whole ocean for momentum and tracers, which is specified through the *rn\_ahm0* and *rn\_aht0* namelist parameters.

### Vertically varying Mixing Coefficients (**key\_traldf\_c1d** and **key\_dynldf\_c1d**)

The 1D option is only available when using the *z*-coordinate with full step. Indeed in all the other types of vertical coordinate, the depth is a 3D function of (**i,j,k**) and therefore, introducing depth-dependent mixing coefficients will require 3D arrays. In the 1D option, a hyperbolic variation of the lateral mixing coefficient is introduced in which the surface value is *rn\_aht0* (*rn\_ahm0*), the bottom value is 1/4 of the surface value, and the transition takes place around *z*=300 m with a width of 300 m (*i.e.* both the depth and the width of the inflection point are set to 300 m). This profile is hard coded in file *traldf\_c1d.h90*, but can be easily modified by users.

**Horizontally Varying Mixing Coefficients (key\_traldf\_c2d and key\_dynldf\_c2d)**

By default the horizontal variation of the eddy coefficient depends on the local mesh size and the type of operator used:

$$A_l = \begin{cases} \frac{\max(e_1, e_2)}{e_{max}} A_o^l & \text{for laplacian operator} \\ \frac{\max(e_1, e_2)^3}{e_{max}^3} A_o^l & \text{for bilaplacian operator} \end{cases} \quad (9.6)$$

where  $e_{max}$  is the maximum of  $e_1$  and  $e_2$  taken over the whole masked ocean domain, and  $A_o^l$  is the *rn\_ahm0* (momentum) or *rn\_aht0* (tracer) namelist parameter. This variation is intended to reflect the lesser need for subgrid scale eddy mixing where the grid size is smaller in the domain. It was introduced in the context of the DYNAMO modelling project [Willebrand et al. 2001]. Note that such a grid scale dependance of mixing coefficients significantly increase the range of stability of model configurations presenting large changes in grid pacing such as global ocean models. Indeed, in such a case, a constant mixing coefficient can lead to a blow up of the model due to large coefficient compare to the smallest grid size (see §3.3), especially when using a bilaplacian operator.

Other formulations can be introduced by the user for a given configuration. For example, in the ORCA2 global ocean model (see Configurations), the laplacian viscosity operator uses  $rn_ahm0 = 4.10^4 \text{ m}^2/\text{s}$  poleward of  $20^\circ$  north and south and decreases linearly to  $rn_aht0 = 2.10^3 \text{ m}^2/\text{s}$  at the equator [Madec et al. 1996, Delecluse and Madec 2000]. This modification can be found in routine *ldf\_dyn\_c2d\_orca* defined in *ldfdyn\_c2d.F90*. Similar modified horizontal variations can be found with the Antarctic or Arctic sub-domain options of ORCA2 and ORCA05 (see &namcfg namelist).

**Space Varying Mixing Coefficients (key\_traldf\_c3d and key\_dynldf\_c3d)**

The 3D space variation of the mixing coefficient is simply the combination of the 1D and 2D cases, *i.e.* a hyperbolic tangent variation with depth associated with a grid size dependence of the magnitude of the coefficient.

**Space and Time Varying Mixing Coefficients**

There is no default specification of space and time varying mixing coefficient. The only case available is specific to the ORCA2 and ORCA05 global ocean configurations. It provides only a tracer mixing coefficient for eddy induced velocity (ORCA2) or both iso-neutral and eddy induced velocity (ORCA05) that depends on the local growth rate of baroclinic instability. This specification is actually used when an ORCA key and both **key\_traldf\_eiv** and **key\_traldf\_c2d** are defined.

The following points are relevant when the eddy coefficient varies spatially:

(1) the momentum diffusion operator acting along model level surfaces is written in terms of curl and divergent components of the horizontal current (see §2.5.2). Although the eddy coefficient could be set to different values in these two terms, this option is not currently available.

(2) with an horizontally varying viscosity, the quadratic integral constraints on enstrophy and on the square of the horizontal divergence for operators acting along model-surfaces are no longer satisfied (Appendix C.7).

(3) for isopycnal diffusion on momentum or tracers, an additional purely horizontal background diffusion with uniform coefficient can be added by setting a non zero value of `rn_ahmb0` or `rn_ahb0`, a background horizontal eddy viscosity or diffusivity coefficient (namelist parameters whose default values are 0). However, the technique used to compute the isopycnal slopes is intended to get rid of such a background diffusion, since it introduces spurious diapycnal diffusion (see §9.1).

(4) when an eddy induced advection term is used (`key_traldf_eiv`),  $A^{eiv}$ , the eddy induced coefficient has to be defined. Its space variations are controlled by the same CPP variable as for the eddy diffusivity coefficient (*i.e.* `key_traldf_cNd`).

(5) the eddy coefficient associated with a biharmonic operator must be set to a *negative* value.

(6) it is possible to use both the laplacian and biharmonic operators concurrently.

(7) it is possible to run without explicit lateral diffusion on momentum (`ln_dynldf_lap = ln_dynldf_bilap = false`). This is recommended when using the UBS advection scheme on momentum (`ln_dynadv_ubs = true`, see 6.3.2) and can be useful for testing purposes.

## 9.4 Eddy Induced Velocity (`traadv_eiv.F90`, `ldfeiv.F90`)

When Gent and McWilliams [1990] diffusion is used (`key_traldf_eiv` defined), an eddy induced tracer advection term is added, the formulation of which depends on the slopes of iso-neutral surfaces. Contrary to the case of iso-neutral mixing, the slopes used here are referenced to the geopotential surfaces, *i.e.* (9.1) is used in  $z$ -coordinates, and the sum (9.1) + (9.2) in  $s$ -coordinates. The eddy induced velocity is given by:

$$\begin{aligned} u^* &= \frac{1}{e_{2u}e_{3u}} \delta_k \left[ e_{2u} A_{uw}^{eiv} \overline{r_{1w}}^{i+1/2} \right] \\ v^* &= \frac{1}{e_{1u}e_{3v}} \delta_k \left[ e_{1v} A_{vw}^{eiv} \overline{r_{2w}}^{j+1/2} \right] \\ w^* &= \frac{1}{e_{1w}e_{2w}} \left\{ \delta_i \left[ e_{2u} A_{uw}^{eiv} \overline{r_{1w}}^{i+1/2} \right] + \delta_j \left[ e_{1v} A_{vw}^{eiv} \overline{r_{2w}}^{j+1/2} \right] \right\} \end{aligned} \quad (9.7)$$

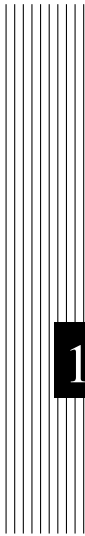
where  $A^{eiv}$  is the eddy induced velocity coefficient whose value is set through `rn_aeiv`, a `nam_traldf` namelist parameter. The three components of the eddy in-

duced velocity are computed and add to the eulerian velocity in *traadv\_eiv.F90*. This has been preferred to a separate computation of the advective trends associated with the *eiv* velocity, since it allows us to take advantage of all the advection schemes offered for the tracers (see §5.1) and not just the 2<sup>nd</sup> order advection scheme as in previous releases of OPA [Madec et al. 1998]. This is particularly useful for passive tracers where *positivity* of the advection scheme is of paramount importance.

At the surface, lateral and bottom boundaries, the eddy induced velocity, and thus the advective eddy fluxes of heat and salt, are set to zero.







# 10 Vertical Ocean Physics (ZDF)

## Contents

---

<b>10.1 Vertical Mixing</b> . . . . .	<b>184</b>
10.1.1 Constant ( <b>key_zdfest</b> ) . . . . .	184
10.1.2 Richardson Number Dependent ( <b>key_zdfric</b> ) . . . . .	185
10.1.3 TKE Turbulent Closure Scheme ( <b>key_zdftke</b> ) . . . . .	186
10.1.4 TKE discretization considerations ( <b>key_zdftke</b> ) . . . . .	191
10.1.5 GLS Generic Length Scale ( <b>key_zdfgls</b> ) . . . . .	194
<b>10.2 Convection</b> . . . . .	<b>196</b>
10.2.1 Non-Penetrative Convective Adjustment ( <i>ln_tranpc</i> ) . . . . .	197
10.2.2 Enhanced Vertical Diffusion ( <i>ln_zdfevd</i> ) . . . . .	198
10.2.3 Turbulent Closure Scheme ( <b>key_zdftke</b> or <b>key_zdfgls</b> ) . . . . .	199
<b>10.3 Double Diffusion Mixing (<b>key_zdfddm</b>)</b> . . . . .	<b>200</b>
<b>10.4 Bottom and Top Friction (<i>zdfbfr</i>)</b> . . . . .	<b>201</b>
10.4.1 Linear Bottom Friction ( <i>nn_botfr</i> = 0 or 1) . . . . .	202
10.4.2 Non-Linear Bottom Friction ( <i>nn_botfr</i> = 2) . . . . .	203
10.4.3 Log-layer Bottom Friction enhancement ( <i>nn_botfr</i> = 2, <i>ln_loglayer</i> = .true.) . . . . .	204
10.4.4 Bottom Friction stability considerations . . . . .	204
10.4.5 Implicit Bottom Friction ( <i>ln_bfrimp</i> =T) . . . . .	205
10.4.6 Bottom Friction with split-explicit time splitting ( <i>ln_bfrimp</i> =F)206	
<b>10.5 Tidal Mixing (<b>key_zdftmx</b>)</b> . . . . .	<b>207</b>
10.5.1 Bottom intensified tidal mixing . . . . .	207
10.5.2 Indonesian area specific treatment ( <i>ln_zdftmx_itf</i> ) . . . . .	208
<b>10.6 Internal wave-driven mixing (<b>key_zdftmx_new</b>)</b> . . . . .	<b>210</b>

---

## 10.1 Vertical Mixing

The discrete form of the ocean subgrid scale physics has been presented in §5.3 and §6.7. At the surface and bottom boundaries, the turbulent fluxes of momentum, heat and salt have to be defined. At the surface they are prescribed from the surface forcing (see Chap. 7), while at the bottom they are set to zero for heat and salt, unless a geothermal flux forcing is prescribed as a bottom boundary condition (*i.e.* **key\_trabbl** defined, see §5.4.3), and specified through a bottom friction parameterisation for momentum (see §10.4).

In this section we briefly discuss the various choices offered to compute the vertical eddy viscosity and diffusivity coefficients,  $A_u^{vm}$ ,  $A_v^{vm}$  and  $A^{vT}$  ( $A^{vS}$ ), defined at  $ww$ -,  $vw$ - and  $w$ - points, respectively (see §5.3 and §6.7). These coefficients can be assumed to be either constant, or a function of the local Richardson number, or computed from a turbulent closure model (either TKE or GLS formulation). The computation of these coefficients is initialized in the *zdfini.F90* module and performed in the *zdftric.F90*, *zdfтке.F90* or *zdfgls.F90* modules. The trends due to the vertical momentum and tracer diffusion, including the surface forcing, are computed and added to the general trend in the *dynzdf.F90* and *trazdf.F90* modules, respectively. These trends can be computed using either a forward time stepping scheme (namelist parameter *ln\_zdfexp=true*) or a backward time stepping scheme (*ln\_zdfexp=false*) depending on the magnitude of the mixing coefficients, and thus of the formulation used (see §3).

### 10.1.1 Constant (key\_zdfcst)

```

!-----
&namzdf      !   vertical physics                                (default: NO selection)
!-----
!
!   ! type of vertical closure (required)
ln_zdfcst   = .false.    ! constant mixing
ln_zdftric  = .false.    ! local Richardson dependent formulation (T => fill namzdf_ric)
ln_zdfтке   = .false.    ! Turbulent Kinetic Energy closure      (T => fill namzdf_tke)
ln_zdfgls   = .false.    ! Generic Length Scale closure        (T => fill namzdf_gls)
!
!   ! convection
ln_zdfevd   = .false.    ! enhanced vertical diffusion
nn_evdm     = 0          ! apply on tracer (=0) or on tracer and momentum (=1)
rn_evd      = 100.       ! mixing coefficient [m2/s]
ln_zdfnpc   = .false.    ! Non-Penetrative Convective algorithm
nn_npc      = 1          ! frequency of application of npc
nn_npcp     = 365        ! npc control print frequency
!
ln_zdfddm   = .false.    ! double diffusive mixing
rn_avts     = 1.e-4      ! maximum avts (vertical mixing on salinity)
rn_hsbfr    = 1.6        ! heat/salt buoyancy flux ratio
!
!   ! gravity wave-driven vertical mixing
ln_zdfiwm   = .false.    ! internal wave-induced mixing      (T => fill namzdf_iwm)
ln_zdfswm   = .false.    ! surface wave-induced mixing      (T => ln_wave=ln_sdw=T )
!
!   ! coefficients
rn_avm0     = 1.2e-4     ! vertical eddy viscosity [m2/s]    (background Kz if ln_zdfcst=F)
rn_avt0     = 1.2e-5     ! vertical eddy diffusivity [m2/s]  (background Kz if ln_zdfcst=F)
nn_avb      = 0          ! profile for background avt & avm (=1) or not (=0)
nn_havtb    = 0          ! horizontal shape for avtb (=1) or not (=0)

```

/

Options are defined through the *namzdf* namelist variables. When **key\_zdfcst** is defined, the momentum and tracer vertical eddy coefficients are set to constant values over the whole ocean. This is the crudest way to define the vertical ocean physics. It is recommended that this option is only used in process studies, not in basin scale simulations. Typical values used in this case are:

$$\begin{aligned} A_u^{vm} &= A_v^{vm} = 1.2 \cdot 10^{-4} \text{ m}^2 \cdot \text{s}^{-1} \\ A^{vT} &= A^{vS} = 1.2 \cdot 10^{-5} \text{ m}^2 \cdot \text{s}^{-1} \end{aligned}$$

These values are set through the *rn\_avm0* and *rn\_avt0* namelist parameters. In all cases, do not use values smaller than those associated with the molecular viscosity and diffusivity, that is  $\sim 10^{-6} \text{ m}^2 \cdot \text{s}^{-1}$  for momentum,  $\sim 10^{-7} \text{ m}^2 \cdot \text{s}^{-1}$  for temperature and  $\sim 10^{-9} \text{ m}^2 \cdot \text{s}^{-1}$  for salinity.

### 10.1.2 Richardson Number Dependent (key\_zdfcric)

```

!-----
&namzdf_ric ! richardson number dependent vertical diffusion (ln_zdfcric =T)
!-----
rn_avmri = 100.e-4 ! maximum value of the vertical viscosity
rn_alp = 5. ! coefficient of the parameterization
nn_ric = 2 ! coefficient of the parameterization
ln_mldw = .false. ! enhanced mixing in the Ekman layer
rn_ekmfc = 0.7 ! Factor in the Ekman depth Equation
rn_mldmin = 1.0 ! minimum allowable mixed-layer depth estimate (m)
rn_mldmax = 1000.0 ! maximum allowable mixed-layer depth estimate (m)
rn_wtmix = 10.0 ! vertical eddy viscosity coeff [m2/s] in the mixed-layer
rn_wvmix = 10.0 ! vertical eddy diffusion coeff [m2/s] in the mixed-layer

```

When **key\_zdfcric** is defined, a local Richardson number dependent formulation for the vertical momentum and tracer eddy coefficients is set through the *namzdf\_ric* namelist variables. The vertical mixing coefficients are diagnosed from the large scale variables computed by the model. *In situ* measurements have been used to link vertical turbulent activity to large scale ocean structures. The hypothesis of a mixing mainly maintained by the growth of Kelvin-Helmholtz like instabilities leads to a dependency between the vertical eddy coefficients and the local Richardson number (*i.e.* the ratio of stratification to vertical shear). Following Pacanowski and Philander [1981], the following formulation has been implemented:

$$\begin{cases} A^{vT} = \frac{A_{ric}^{vT}}{(1 + a Ri)^n} + A_b^{vT} \\ A^{vm} = \frac{A^{vT}}{(1 + a Ri)} + A_b^{vm} \end{cases} \quad (10.1)$$

where  $Ri = N^2 / (\partial_z \mathbf{U}_h)^2$  is the local Richardson number,  $N$  is the local Brunt-Vaisälä frequency (see §5.8.2),  $A_b^{vT}$  and  $A_b^{vm}$  are the constant background values set as in the constant case (see §10.1.1), and  $A_{ric}^{vT} = 10^{-4} \text{ m}^2 \cdot \text{s}^{-1}$  is the maximum value that can be reached by the coefficient when  $Ri \leq 0$ ,  $a = 5$  and  $n = 2$ . The last three values can be modified by setting the *rn\_avmri*, *rn\_alp* and *nn\_ric* namelist parameters, respectively.

A simple mixing-layer model to transfer and dissipate the atmospheric forcings (wind-stress and buoyancy fluxes) can be activated setting the `ln_mldw = .true.` in the namelist.

In this case, the local depth of turbulent wind-mixing or "Ekman depth"  $h_e(x, y, t)$  is evaluated and the vertical eddy coefficients prescribed within this layer.

This depth is assumed proportional to the "depth of frictional influence" that is limited by rotation:

$$h_e = Ek \frac{u^*}{f_0} \quad (10.2)$$

where,  $Ek$  is an empirical parameter,  $u^*$  is the friction velocity and  $f_0$  is the Coriolis parameter.

In this similarity height relationship, the turbulent friction velocity:

$$u^* = \sqrt{\frac{|\tau|}{\rho_o}} \quad (10.3)$$

is computed from the wind stress vector  $|\tau|$  and the reference density  $\rho_o$ . The final  $h_e$  is further constrained by the adjustable bounds `rn_mldmin` and `rn_mldmax`. Once  $h_e$  is computed, the vertical eddy coefficients within  $h_e$  are set to the empirical values `rn_wtmix` and `rn_wvmix` [Lermusiaux 2001].

### 10.1.3 TKE Turbulent Closure Scheme (key\_zdftke)

```

!-----
&namzdf_tke      !   turbulent eddy kinetic dependent vertical diffusion   (ln_zdftke =T)
!-----
rn_ediff        = 0.1      !   coef. for vertical eddy coef. (avt=rn_ediff*mx1*sqrt(e) )
rn_ediss        = 0.7      !   coef. of the Kolmogoroff dissipation
rn_ebb          = 67.83    !   coef. of the surface input of tke (=67.83 suggested when ln_mx10=T)
rn_emin         = 1.e-6    !   minimum value of tke [m2/s2]
rn_emin0        = 1.e-4    !   surface minimum value of tke [m2/s2]
rn_bshear       = 1.e-20   !   background shear (>0) currently a numerical threshold (do not change it)
nn_pdl          = 1       !   Prandtl number function of richarson number (=1, avt=pd1(Ri)*avm) or not (=0, avt=avm)
nn_mx1          = 2       !   mixing length: = 0 bounded by the distance to surface and bottom
!               !               = 1 bounded by the local vertical scale factor
!               !               = 2 first vertical derivative of mixing length bounded by 1
!               !               = 3 as =2 with distinct dissipation an mixing length scale
ln_mx10         = .true.   !   surface mixing length scale = F(wind stress) (T) or not (F)
rn_mx10         = 0.04     !   surface buoyancy length scale minimum value
ln_drq          = .false.  !   top/bottom friction added as boundary condition of TKE
ln_lc           = .true.   !   Langmuir cell parameterisation (Axell 2002)
  rn_lc          = 0.15    !   coef. associated to Langmuir cells
nn_etau         = 1       !   penetration of tke below the mixed layer (ML) due to NIWs
!               !               = 0 none ; = 1 add a tke source below the ML
!               !               = 2 add a tke source just at the base of the ML
!               !               = 3 as = 1 applied on HF part of the stress           (ln_cpl=T)
rn_efr          = 0.05    !   fraction of surface tke value which penetrates below the ML (nn_etau=1 or 2)
nn_htau         = 1       !   type of exponential decrease of tke penetration below the ML
!               !               = 0 constant 10 m length scale
!               !               = 1 0.5m at the equator to 30m poleward of 40 degrees
/

```

The vertical eddy viscosity and diffusivity coefficients are computed from a TKE turbulent closure model based on a prognostic equation for  $\bar{e}$ , the turbulent kinetic energy, and a closure assumption for the turbulent length scales. This turbulent closure model has been developed by Bougeault and Lacarrere [1989] in the atmospheric case, adapted by Gaspar et al. [1990] for the oceanic case, and embedded in OPA, the ancestor of NEMO, by Blanke and Delecluse [1993] for

equatorial Atlantic simulations. Since then, significant modifications have been introduced by [Madec et al. \[1998\]](#) in both the implementation and the formulation of the mixing length scale. The time evolution of  $\bar{e}$  is the result of the production of  $\bar{e}$  through vertical shear, its destruction through stratification, its vertical diffusion, and its dissipation of [Kolmogorov \[1942\]](#) type:

$$\frac{\partial \bar{e}}{\partial t} = \frac{K_m}{e_3^2} \left[ \left( \frac{\partial u}{\partial k} \right)^2 + \left( \frac{\partial v}{\partial k} \right)^2 \right] - K_\rho N^2 + \frac{1}{e_3} \frac{\partial}{\partial k} \left[ \frac{A^{vm}}{e_3} \frac{\partial \bar{e}}{\partial k} \right] - c_\epsilon \frac{\bar{e}^{3/2}}{l_\epsilon} \quad (10.4)$$

$$\begin{aligned} K_m &= C_k l_k \sqrt{\bar{e}} \\ K_\rho &= A^{vm} / P_{rt} \end{aligned} \quad (10.5)$$

where  $N$  is the local Brunt-Vaisälä frequency (see §5.8.2),  $l_\epsilon$  and  $l_\kappa$  are the dissipation and mixing length scales,  $P_{rt}$  is the Prandtl number,  $K_m$  and  $K_\rho$  are the vertical eddy viscosity and diffusivity coefficients. The constants  $C_k = 0.1$  and  $C_\epsilon = \sqrt{2}/2 \approx 0.7$  are designed to deal with vertical mixing at any depth [[Gaspar et al. 1990](#)]. They are set through namelist parameters *nn\_ediff* and *nn\_ediss*.  $P_{rt}$  can be set to unity or, following [Blanke and Delecluse \[1993\]](#), be a function of the local Richardson number,  $R_i$ :

$$P_{rt} = \begin{cases} 1 & \text{if } R_i \leq 0.2 \\ 5 R_i & \text{if } 0.2 \leq R_i \leq 2 \\ 10 & \text{if } 2 \leq R_i \end{cases}$$

Options are defined through the *namzdfy\_tke* namelist variables. The choice of  $P_{rt}$  is controlled by the *nn\_pdl* namelist variable.

At the sea surface, the value of  $\bar{e}$  is prescribed from the wind stress field as  $\bar{e}_o = e_{bb} |\tau| / \rho_o$ , with  $e_{bb}$  the *rn\_ebb* namelist parameter. The default value of  $e_{bb}$  is 3.75. [[Gaspar et al. 1990](#)]), however a much larger value can be used when taking into account the surface wave breaking (see below Eq. (10.10)). The bottom value of TKE is assumed to be equal to the value of the level just above. The time integration of the  $\bar{e}$  equation may formally lead to negative values because the numerical scheme does not ensure its positivity. To overcome this problem, a cut-off in the minimum value of  $\bar{e}$  is used (*rn\_emin* namelist parameter). Following [Gaspar et al. \[1990\]](#), the cut-off value is set to  $\sqrt{2}/2 \cdot 10^{-6} \text{ m}^2 \cdot \text{s}^{-2}$ . This allows the subsequent formulations to match that of [Gargett \[1984\]](#) for the diffusion in the thermocline and deep ocean:  $K_\rho = 10^{-3}/N$ . In addition, a cut-off is applied on  $K_m$  and  $K_\rho$  to avoid numerical instabilities associated with too weak vertical diffusion. They must be specified at least larger than the molecular values, and are set through *rn\_avm0* and *rn\_avt0* (*namzdf* namelist, see §10.1.1).

### Turbulent length scale

For computational efficiency, the original formulation of the turbulent length scales proposed by Gaspar et al. [1990] has been simplified. Four formulations are proposed, the choice of which is controlled by the *nn\_mxl* namelist parameter. The first two are based on the following first order approximation [Blanke and Delecluse 1993]:

$$l_k = l_\epsilon = \sqrt{2\bar{e}}/N \quad (10.6)$$

which is valid in a stable stratified region with constant values of the Brunt- Vaisälä frequency. The resulting length scale is bounded by the distance to the surface or to the bottom (*nn\_mxl* = 0) or by the local vertical scale factor (*nn\_mxl* = 1). Blanke and Delecluse [1993] notice that this simplification has two major drawbacks: it makes no sense for locally unstable stratification and the computation no longer uses all the information contained in the vertical density profile. To overcome these drawbacks, Madec et al. [1998] introduces the *nn\_mxl* = 2 or 3 cases, which add an extra assumption concerning the vertical gradient of the computed length scale. So, the length scales are first evaluated as in (10.6) and then bounded such that:

$$\frac{1}{e_3} \left| \frac{\partial l}{\partial k} \right| \leq 1 \quad \text{with } l = l_k = l_\epsilon \quad (10.7)$$

(10.7) means that the vertical variations of the length scale cannot be larger than the variations of depth. It provides a better approximation of the Gaspar et al. [1990] formulation while being much less time consuming. In particular, it allows the length scale to be limited not only by the distance to the surface or to the ocean bottom but also by the distance to a strongly stratified portion of the water column such as the thermocline (Fig. 10.1). In order to impose the (10.7) constraint, we introduce two additional length scales:  $l_{up}$  and  $l_{down}$ , the upward and downward length scales, and evaluate the dissipation and mixing length scales as (and note that here we use numerical indexing):

$$\begin{aligned} l_{up}^{(k)} &= \min \left( l^{(k)}, l_{up}^{(k+1)} + e_{3t}^{(k)} \right) & \text{from } k = 1 \text{ to } jpk \\ l_{down}^{(k)} &= \min \left( l^{(k)}, l_{down}^{(k-1)} + e_{3t}^{(k-1)} \right) & \text{from } k = jpk \text{ to } 1 \end{aligned} \quad (10.8)$$

where  $l^{(k)}$  is computed using (10.6), *i.e.*  $l^{(k)} = \sqrt{2\bar{e}^{(k)}/N^2^{(k)}}$ .

In the *nn\_mxl* = 2 case, the dissipation and mixing length scales take the same value:  $l_k = l_\epsilon = \min(l_{up}, l_{down})$ , while in the *nn\_mxl* = 3 case, the dissipation and mixing turbulent length scales are give as in Gaspar et al. [1990]:

$$\begin{aligned} l_k &= \sqrt{l_{up} l_{down}} \\ l_\epsilon &= \min(l_{up}, l_{down}) \end{aligned} \quad (10.9)$$

At the ocean surface, a non zero length scale is set through the *rn\_mxl0* namelist parameter. Usually the surface scale is given by  $l_o = \kappa z_o$  where  $\kappa = 0.4$  is von

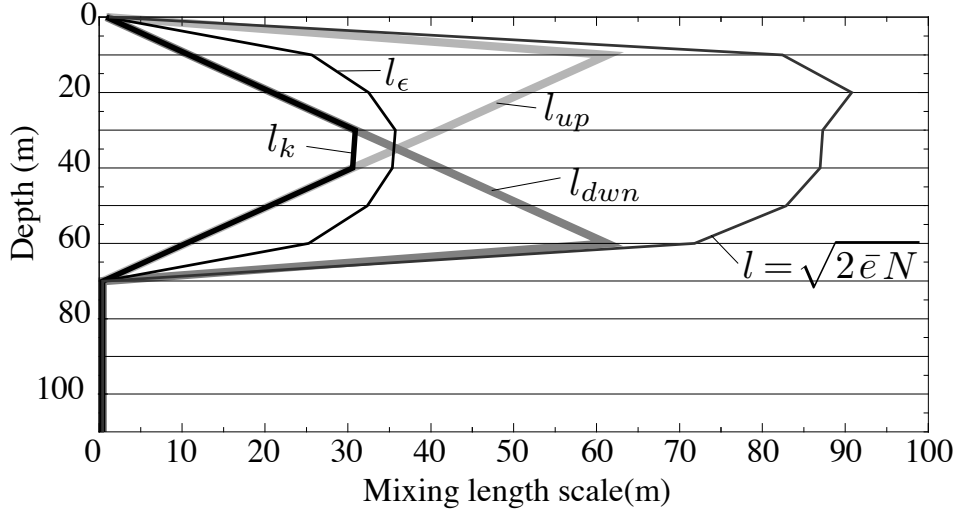


**Figure 10.1:** Illustration of the mixing length computation.

Karman's constant and  $z_o$  the roughness parameter of the surface. Assuming  $z_o = 0.1$  m [Craig and Banner 1994] leads to a 0.04 m, the default value of  $rn\_mxl0$ . In the ocean interior a minimum length scale is set to recover the molecular viscosity when  $\bar{\epsilon}$  reach its minimum value ( $1 \cdot 10^{-6} = C_k l_{min} \sqrt{\bar{\epsilon}_{min}}$ ).

### Surface wave breaking parameterization

Following Mellor and Blumberg [2004], the TKE turbulence closure model has been modified to include the effect of surface wave breaking energetics. This results in a reduction of summertime surface temperature when the mixed layer is relatively shallow. The Mellor and Blumberg [2004] modifications acts on surface length scale and TKE values and air-sea drag coefficient. The latter concerns the bulk formulae and is not discussed here.

Following Craig and Banner [1994], the boundary condition on surface TKE value is :

$$\bar{\epsilon}_o = \frac{1}{2} (15.8 \alpha_{CB})^{2/3} \frac{|\tau|}{\rho_o} \quad (10.10)$$

where  $\alpha_{CB}$  is the Craig and Banner [1994] constant of proportionality which depends on the "wave age", ranging from 57 for mature waves to 146 for younger waves [Mellor and Blumberg 2004]. The boundary condition on the turbulent length scale follows the Charnock's relation:

$$l_o = \kappa \beta \frac{|\tau|}{g \rho_o} \quad (10.11)$$

where  $\kappa = 0.40$  is the von Karman constant, and  $\beta$  is the Charnock's constant. Mellor and Blumberg [2004] suggest  $\beta = 2.10^5$  the value chosen by Stacey [1999] citing observation evidence, and  $\alpha_{CB} = 100$  the Craig and Banner's value. As the surface boundary condition on TKE is prescribed through  $\bar{e}_o = e_{bb}|\tau|/\rho_o$ , with  $e_{bb}$  the *rn\_ebb* namelist parameter, setting *rn\_ebb* = 67.83 corresponds to  $\alpha_{CB} = 100$ . Further setting *ln\_mx10* to true applies (10.11) as surface boundary condition on length scale, with  $\beta$  hard coded to the Stacey's value. Note that a minimal threshold of *rn\_emin0* =  $10^{-4} \text{ m}^2 \cdot \text{s}^{-2}$  (namelist parameters) is applied on surface  $\bar{e}$  value.

### Langmuir cells

Langmuir circulations (LC) can be described as ordered large-scale vertical motions in the surface layer of the oceans. Although LC have nothing to do with convection, the circulation pattern is rather similar to so-called convective rolls in the atmospheric boundary layer. The detailed physics behind LC is described in, for example, Craik and Leibovich [1976]. The prevailing explanation is that LC arise from a nonlinear interaction between the Stokes drift and wind drift currents.

Here we introduced in the TKE turbulent closure the simple parameterization of Langmuir circulations proposed by [Axell 2002] for a  $k - \epsilon$  turbulent closure. The parameterization, tuned against large-eddy simulation, includes the whole effect of LC in an extra source terms of TKE,  $P_{LC}$ . The presence of  $P_{LC}$  in (10.4), the TKE equation, is controlled by setting *ln\_lc* to *true* in the *namtke* namelist.

By making an analogy with the characteristic convective velocity scale (*e.g.*, D'Alessio et al. [1998]),  $P_{LC}$  is assumed to be :

$$P_{LC}(z) = \frac{w_{LC}^3(z)}{H_{LC}} \quad (10.12)$$

where  $w_{LC}(z)$  is the vertical velocity profile of LC, and  $H_{LC}$  is the LC depth. With no information about the wave field,  $w_{LC}$  is assumed to be proportional to the Stokes drift  $u_s = 0.377 |\tau|^{1/2}$ , where  $|\tau|$  is the surface wind stress module <sup>1</sup>. For the vertical variation,  $w_{LC}$  is assumed to be zero at the surface as well as at a finite depth  $H_{LC}$  (which is often close to the mixed layer depth), and simply varies as a sine function in between (a first-order profile for the Langmuir cell structures). The resulting expression for  $w_{LC}$  is :

$$w_{LC} = \begin{cases} c_{LC} u_s \sin(-\pi z/H_{LC}) & \text{if } -z \leq H_{LC} \\ 0 & \text{otherwise} \end{cases} \quad (10.13)$$

where  $c_{LC} = 0.15$  has been chosen by [Axell 2002] as a good compromise to fit LES data. The chosen value yields maximum vertical velocities  $w_{LC}$  of the order

<sup>1</sup>Following Li and Garrett [1993], the surface Stoke drift velocity may be expressed as  $u_s = 0.016 |U_{10m}|$ . Assuming an air density of  $\rho_a = 1.22 \text{ Kg/m}^3$  and a drag coefficient of  $1.5 \cdot 10^{-3}$  give the expression used of  $u_s$  as a function of the module of surface stress



of a few centimeters per second. The value of  $c_{LC}$  is set through the *mlc* namelist parameter, having in mind that it should stay between 0.15 and 0.54 [Axell 2002].

The  $H_{LC}$  is estimated in a similar way as the turbulent length scale of TKE equations:  $H_{LC}$  is depth to which a water parcel with kinetic energy due to Stoke drift can reach on its own by converting its kinetic energy to potential energy, according to

$$-\int_{-H_{LC}}^0 N^2 z dz = \frac{1}{2} u_s^2 \quad (10.14)$$

### Mixing just below the mixed layer

Vertical mixing parameterizations commonly used in ocean general circulation models tend to produce mixed-layer depths that are too shallow during summer months and windy conditions. This bias is particularly acute over the Southern Ocean. To overcome this systematic bias, an ad hoc parameterization is introduced into the TKE scheme Rodgers et al. [2014]. The parameterization is an empirical one, *i.e.* not derived from theoretical considerations, but rather is meant to account for observed processes that affect the density structure of the oceans planetary boundary layer that are not explicitly captured by default in the TKE scheme (*i.e.* near-inertial oscillations and ocean swells and waves).

When using this parameterization (*i.e.* when *nn\_etau* = 1), the TKE input to the ocean ( $S$ ) imposed by the winds in the form of near-inertial oscillations, swell and waves is parameterized by (10.10) the standard TKE surface boundary condition, plus a depth depend one given by:

$$S = (1 - f_i) f_r e_s e^{-z/h_\tau} \quad (10.15)$$

where  $z$  is the depth,  $e_s$  is TKE surface boundary condition,  $f_r$  is the fraction of the surface TKE that penetrate in the ocean,  $h_\tau$  is a vertical mixing length scale that controls exponential shape of the penetration, and  $f_i$  is the ice concentration (no penetration if  $f_i = 1$ , that is if the ocean is entirely covered by sea-ice). The value of  $f_r$ , usually a few percents, is specified through *m\_efr* namelist parameter. The vertical mixing length scale,  $h_\tau$ , can be set as a 10 m uniform value (*nn\_etau* = 0) or a latitude dependent value (varying from 0.5 m at the Equator to a maximum value of 30 m at high latitudes (*nn\_etau* = 1)).

Note that two other option existe, *nn\_etau* = 2, or 3. They correspond to applying (10.15) only at the base of the mixed layer, or to using the high frequency part of the stress to evaluate the fraction of TKE that penetrate the ocean. Those two options are obsolescent features introduced for test purposes. They will be removed in the next release.

#### 10.1.4 TKE discretization considerations (key\_zdfake)

The production of turbulence by vertical shear (the first term of the right hand side of (10.4)) should balance the loss of kinetic energy associated with the vertical

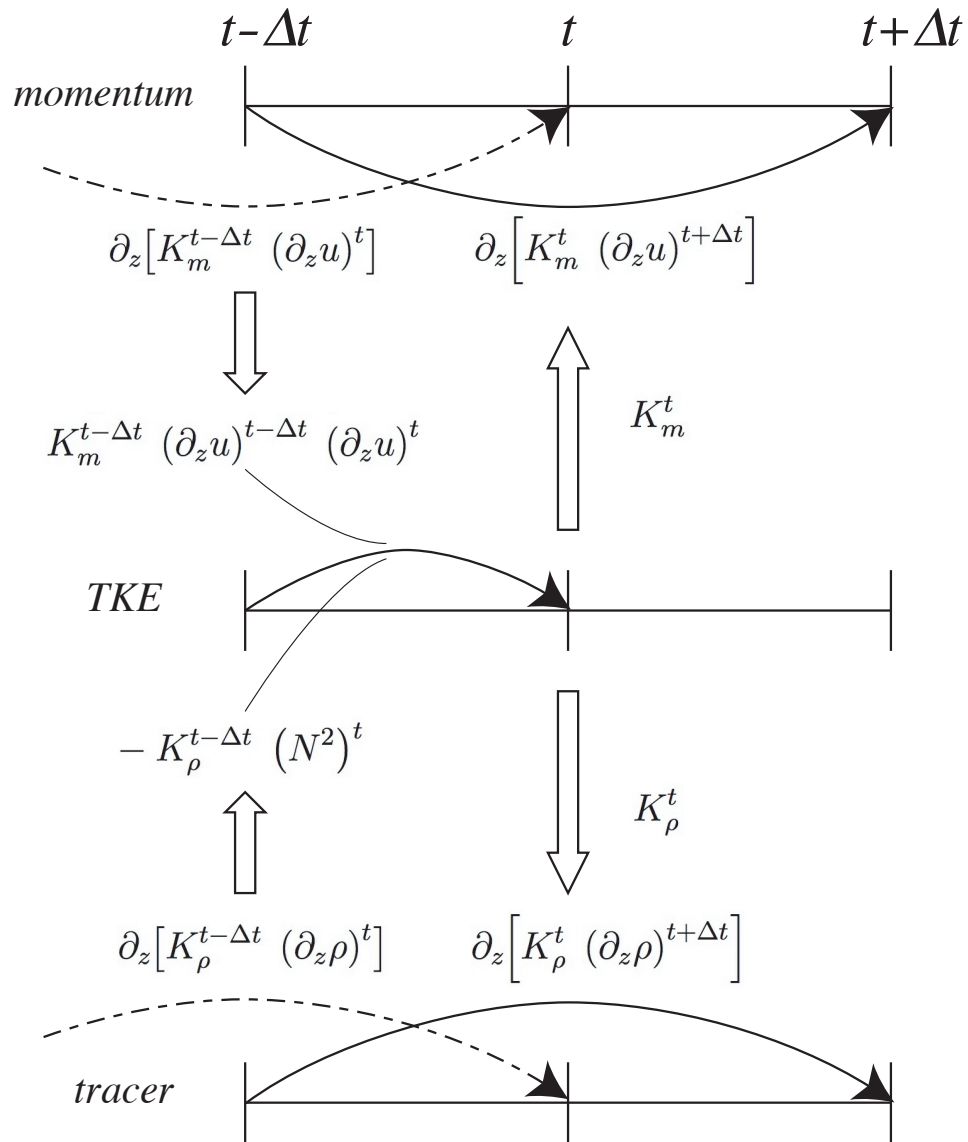


**Figure 10.2:** Illustration of the TKE time integration and its links to the momentum and tracer time integration.

momentum diffusion (first line in (2.34)). To do so a special care have to be taken for both the time and space discretization of the TKE equation [Burchard 2002, Marsaleix et al. 2008].

Let us first address the time stepping issue. Fig. 10.2 shows how the two-level Leap-Frog time stepping of the momentum and tracer equations interplays with the one-level forward time stepping of TKE equation. With this framework, the total loss of kinetic energy (in 1D for the demonstration) due to the vertical momentum

diffusion is obtained by multiplying this quantity by  $u^t$  and summing the result vertically:

$$\begin{aligned} & \int_{-H}^{\eta} u^t \partial_z (K_m^t (\partial_z u)^{t+\Delta t}) dz \\ &= \left[ u^t K_m^t (\partial_z u)^{t+\Delta t} \right]_{-H}^{\eta} - \int_{-H}^{\eta} K_m^t \partial_z u^t \partial_z u^{t+\Delta t} dz \end{aligned} \quad (10.16)$$

Here, the vertical diffusion of momentum is discretized backward in time with a coefficient,  $K_m$ , known at time  $t$  (Fig. 10.2), as it is required when using the TKE scheme (see §3.3). The first term of the right hand side of (10.16) represents the kinetic energy transfer at the surface (atmospheric forcing) and at the bottom (friction effect). The second term is always negative. It is the dissipation rate of kinetic energy, and thus minus the shear production rate of  $\bar{e}$ . (10.16) implies that, to be energetically consistent, the production rate of  $\bar{e}$  used to compute  $(\bar{e})^t$  (and thus  $K_m^t$ ) should be expressed as  $K_m^{t-\Delta t} (\partial_z u)^{t-\Delta t} (\partial_z u)^t$  (and not by the more straightforward  $K_m (\partial_z u)^2$  expression taken at time  $t$  or  $t - \Delta t$ ).

A similar consideration applies on the destruction rate of  $\bar{e}$  due to stratification (second term of the right hand side of (10.4)). This term must balance the input of potential energy resulting from vertical mixing. The rate of change of potential energy (in 1D for the demonstration) due vertical mixing is obtained by multiplying vertical density diffusion tendency by  $g z$  and and summing the result vertically:

$$\begin{aligned} & \int_{-H}^{\eta} g z \partial_z (K_\rho^t (\partial_k \rho)^{t+\Delta t}) dz \\ &= \left[ g z K_\rho^t (\partial_k \rho)^{t+\Delta t} \right]_{-H}^{\eta} - \int_{-H}^{\eta} g K_\rho^t (\partial_k \rho)^{t+\Delta t} dz \\ &= - \left[ z K_\rho^t (N^2)^{t+\Delta t} \right]_{-H}^{\eta} + \int_{-H}^{\eta} \rho^{t+\Delta t} K_\rho^t (N^2)^{t+\Delta t} dz \end{aligned} \quad (10.17)$$

where we use  $N^2 = -g \partial_k \rho / (e_3 \rho)$ . The first term of the right hand side of (10.17) is always zero because there is no diffusive flux through the ocean surface and bottom). The second term is minus the destruction rate of  $\bar{e}$  due to stratification. Therefore (10.16) implies that, to be energetically consistent, the product  $K_\rho^{t-\Delta t} (N^2)^t$  should be used in (10.4), the TKE equation.

Let us now address the space discretization issue. The vertical eddy coefficients are defined at  $w$ -point whereas the horizontal velocity components are in the centre of the side faces of a  $t$ -box in staggered C-grid (Fig.4.1). A space averaging is thus required to obtain the shear TKE production term. By redoing the (10.16) in the 3D case, it can be shown that the product of eddy coefficient by the shear at  $t$  and  $t - \Delta t$  must be performed prior to the averaging. Furthermore, the possible time variation of  $e_3$  (**key\_vvl** case) have to be taken into account.

The above energetic considerations leads to the following final discrete form

for the TKE equation:

$$\begin{aligned}
\frac{(\bar{e})^t - (\bar{e})^{t-\Delta t}}{\Delta t} \equiv & \left\{ \left( \overline{\left( \frac{K_m}{\sigma_e e_3} \right)^{i+1/2}} \right)^{t-\Delta t} \frac{\delta_{k+1/2}[u^{t+\Delta t}]}{e_3 u^{t+\Delta t}} \frac{\delta_{k+1/2}[u^t]}{e_3 u^t} \right\}^i \\
& + \left\{ \left( \overline{\left( \frac{K_m}{\sigma_e e_3} \right)^{j+1/2}} \right)^{t-\Delta t} \frac{\delta_{k+1/2}[v^{t+\Delta t}]}{e_3 v^{t+\Delta t}} \frac{\delta_{k+1/2}[v^t]}{e_3 v^t} \right\}^j \\
& - K_\rho^{t-\Delta t} (N^2)^t \\
& + \frac{1}{e_3 w^{t+\Delta t}} \delta_{k+1/2} \left[ K_m^{t-\Delta t} \frac{\delta_k[(\bar{e})^{t+\Delta t}]}{e_3 w^{t+\Delta t}} \right] \\
& - c_\epsilon \left( \frac{\sqrt{\bar{e}}}{l_\epsilon} \right)^{t-\Delta t} (\bar{e})^{t+\Delta t}
\end{aligned} \tag{10.18}$$

where the last two terms in (10.18) (vertical diffusion and Kolmogorov dissipation) are time stepped using a backward scheme (see§3.3). Note that the Kolmogorov term has been linearized in time in order to render the implicit computation possible. The restart of the TKE scheme requires the storage of  $\bar{e}$ ,  $K_m$ ,  $K_\rho$  and  $l_\epsilon$  as they all appear in the right hand side of (10.18). For the latter, it is in fact the ratio  $\sqrt{\bar{e}}/l_\epsilon$  which is stored.

### 10.1.5 GLS Generic Length Scale (key `zdfgls`)

```

!-----
&namzdf_gls      !   GLS vertical diffusion                                (ln_zdfgls =T)
!-----
rn_emin          = 1.e-7  ! minimum value of e   [m2/s2]
rn_epsmin        = 1.e-12 ! minimum value of eps [m2/s3]
ln_length_lim    = .true. ! limit on the dissipation rate under stable stratification (Galperin et al., 1988)
rn_clim_galp     = 0.267  ! galperin limit
ln_sigpsi        = .true. ! Activate or not Burchard 2001 mods on psi schmidt number in the wb case
rn_crban         = 100.   ! Craig and Banner 1994 constant for wb tke flux
rn_charn         = 70000. ! Charnock constant for wb induced roughness length
rn_hspro         = 0.02   ! Minimum surface roughness
rn_frac_hs       = 1.3    ! Fraction of wave height as roughness (if nn_z0_met>1)
nn_z0_met        = 2      ! Method for surface roughness computation (0/1/2/3)
!                 ! =3 requires ln_wave=T
nn_bc_surf       = 1      ! surface condition (0/1=Dir/Neum)
nn_bc_bot        = 1      ! bottom condition (0/1=Dir/Neum)
nn_stab_func     = 2      ! stability function (0=Galp, 1= KC94, 2=CanutoA, 3=CanutoB)
nn_clos          = 1      ! predefined closure type (0=MY82, 1=k-eps, 2=k-w, 3=Gen)
/

```

The Generic Length Scale (GLS) scheme is a turbulent closure scheme based on two prognostic equations: one for the turbulent kinetic energy  $\bar{e}$ , and another for the generic length scale,  $\psi$  [Umlauf and Burchard 2003; 2005]. This later variable is defined as :  $\psi = C_{0\mu}^p \bar{e}^m l^n$ , where the triplet  $(p, m, n)$  value given in Tab.10.1 allows to recover a number of well-known turbulent closures ( $k$ - $kl$  [Mellor and Yamada 1982],  $k$ - $\epsilon$  [Rodi 1987],  $k$ - $\omega$  [Wilcox 1988] among others [Umlauf and Burchard 2003, Kantha and Carniel 2005]). The GLS scheme is given by the following set of equations:

$$\frac{\partial \bar{e}}{\partial t} = \frac{K_m}{\sigma_e e_3} \left[ \left( \frac{\partial u}{\partial k} \right)^2 + \left( \frac{\partial v}{\partial k} \right)^2 \right] - K_\rho N^2 + \frac{1}{e_3} \frac{\partial}{\partial k} \left[ \frac{K_m}{e_3} \frac{\partial \bar{e}}{\partial k} \right] - \epsilon \tag{10.19}$$

$$\frac{\partial \psi}{\partial t} = \frac{\psi}{\bar{e}} \left\{ \frac{C_1 K_m}{\sigma_\psi e_3} \left[ \left( \frac{\partial u}{\partial k} \right)^2 + \left( \frac{\partial v}{\partial k} \right)^2 \right] - C_3 K_\rho N^2 - C_2 \epsilon Fw \right\} + \frac{1}{e_3} \frac{\partial}{\partial k} \left[ \frac{K_m}{e_3} \frac{\partial \psi}{\partial k} \right] \quad (10.20)$$

$$K_m = C_\mu \sqrt{\bar{e}} l \quad (10.21)$$

$$K_\rho = C_{\mu'} \sqrt{\bar{e}} l$$

$$\epsilon = C_{0\mu} \frac{\bar{e}^{3/2}}{l} \quad (10.22)$$

where  $N$  is the local Brunt-Vaisälä frequency (see §5.8.2) and  $\epsilon$  the dissipation rate. The constants  $C_1, C_2, C_3, \sigma_e, \sigma_\psi$  and the wall function ( $Fw$ ) depends of the choice of the turbulence model. Four different turbulent models are pre-defined (Tab.10.1). They are made available through the *nn\_clo* namelist parameter.

**Table 10.1:** Set of predefined GLS parameters, or equivalently predefined turbulence models available with **key\_zdfgls** and controlled by the *nn\_clos* namelist variable in *namzdf\_gls*.

	$k - kl$	$k - \epsilon$	$k - \omega$	generic
<i>nn_clo</i>	<b>0</b>	<b>1</b>	<b>2</b>	<b>3</b>
$(p, n, m)$	(0, 1, 1)	(3, 1.5, -1)	(-1, 0.5, -1)	(2, 1, -0.67)
$\sigma_k$	2.44	1.	2.	0.8
$\sigma_\psi$	2.44	1.3	2.	1.07
$C_1$	0.9	1.44	0.555	1.
$C_2$	0.5	1.92	0.833	1.22
$C_3$	1.	1.	1.	1.
$F_{wall}$	Yes	–	–	–

In the Mellor-Yamada model, the negativity of  $n$  allows to use a wall function to force the convergence of the mixing length towards  $Kz_b$  ( $K$ : Kappa and  $z_b$ : rugosity length) value near physical boundaries (logarithmic boundary layer law).  $C_\mu$  and  $C_{\mu'}$  are calculated from stability function proposed by Galperin et al. [1988], or by Kantha and Clayson [1994] or one of the two functions suggested by Canuto et al. [2001] (*nn\_stab\_func* = 0, 1, 2 or 3, resp.). The value of  $C_{0\mu}$  depends of the choice of the stability function.

The surface and bottom boundary condition on both  $\bar{e}$  and  $\psi$  can be calculated thanks to Dirichlet or Neumann condition through *nn\_tkebc\_surf* and *nn\_tkebc\_bot*, resp. As for TKE closure, the wave effect on the mixing is considered when *ln\_crban* = true [Craig and Banner 1994, Mellor and Blumberg 2004]. The *rn\_crban*

namelist parameter is  $\alpha_{CB}$  in (10.10) and  $rn\_charn$  provides the value of  $\beta$  in (10.11).

The  $\psi$  equation is known to fail in stably stratified flows, and for this reason almost all authors apply a clipping of the length scale as an *ad hoc* remedy. With this clipping, the maximum permissible length scale is determined by  $l_{max} = c_{lim}\sqrt{2\bar{\epsilon}}/N$ . A value of  $c_{lim} = 0.53$  is often used [Galperin et al. 1988]. Umlauf and Burchard [2005] show that the value of the clipping factor is of crucial importance for the entrainment depth predicted in stably stratified situations, and that its value has to be chosen in accordance with the algebraic model for the turbulent fluxes. The clipping is only activated if  $ln\_length\_lim=true$ , and the  $c_{lim}$  is set to the  $rn\_clim\_galp$  value.

The time and space discretization of the GLS equations follows the same energetic consideration as for the TKE case described in §10.1.4 [Burchard 2002]. Examples of performance of the 4 turbulent closure scheme can be found in Warner et al. [2005].

## 10.2 Convection

```

!-----
&namzdf      ! vertical physics                                     (default: NO selection)
!-----
!
! type of vertical closure (required)
ln_zdfcst   = .false.      ! constant mixing
ln_zdfcfric = .false.      ! local Richardson dependent formulation (T => fill namzdf_ric)
ln_zdfktke  = .false.      ! Turbulent Kinetic Energy closure (T => fill namzdf_tke)
ln_zdfgls   = .false.      ! Generic Length Scale closure (T => fill namzdf_gls)
!
!
! convection
ln_zdfevd   = .false.      ! enhanced vertical diffusion
nn_evdm     = 0             ! apply on tracer (=0) or on tracer and momentum (=1)
rn_evd      = 100.         ! mixing coefficient [m2/s]
ln_zdfnpc   = .false.      ! Non-Penetrative Convective algorithm
nn_npc      = 1           ! frequency of application of npc
nn_npcp     = 365         ! npc control print frequency
!
!
! double diffusive mixing
ln_zdfddm   = .false.      ! double diffusive mixing
rn_avts     = 1.e-4        ! maximum avs (vertical mixing on salinity)
rn_hsbfr    = 1.6         ! heat/salt buoyancy flux ratio
!
!
! gravity wave-driven vertical mixing
ln_zdfiwm   = .false.      ! internal wave-induced mixing (T => fill namzdf_iwm)
ln_zdfswm   = .false.      ! surface wave-induced mixing (T => ln_wave=ln_sdw=T )
!
!
! coefficients
rn_avm0     = 1.2e-4        ! vertical eddy viscosity [m2/s] (background Kz if ln_zdfcst=F)
rn_avt0     = 1.2e-5        ! vertical eddy diffusivity [m2/s] (background Kz if ln_zdfcst=F)
nn_avb      = 0             ! profile for background avt & avm (=1) or not (=0)
nn_havtb    = 0             ! horizontal shape for avtb (=1) or not (=0)
/

```

Static instabilities (i.e. light potential densities under heavy ones) may occur at particular ocean grid points. In nature, convective processes quickly re-establish the static stability of the water column. These processes have been removed from the model via the hydrostatic assumption so they must be parameterized. Three parameterisations are available to deal with convective processes: a non-penetrative convective adjustment or an enhanced vertical diffusion, or/and the use of a turbulent closure scheme.

### 10.2.1 Non-Penetrative Convective Adjustment (*ln\_tranpc=.true.*)

```

!-----
&namzdf      ! vertical physics                                (default: NO selection)
!-----
!
! ! type of vertical closure (required)
ln_zdfcst   = .false.   ! constant mixing
ln_zdfric   = .false.   ! local Richardson dependent formulation (T => fill namzdf_ric)
ln_zdf_tke  = .false.   ! Turbulent Kinetic Energy closure (T => fill namzdf_tke)
ln_zdfgls   = .false.   ! Generic Length Scale closure (T => fill namzdf_gls)
!
! ! convection
ln_zdfevd   = .false.   ! enhanced vertical diffusion
nn_evdm     = 0         ! apply on tracer (=0) or on tracer and momentum (=1)
rn_evd      = 100.     ! mixing coefficient [m2/s]
ln_zdfnpc   = .false.   ! Non-Penetrative Convective algorithm
nn_npc      = 1        ! frequency of application of npc
nn_npcp     = 365      ! npc control print frequency
!
ln_zdfddm   = .false.   ! double diffusive mixing
rn_avts     = 1.e-4    ! maximum avts (vertical mixing on salinity)
rn_hsbfr    = 1.6      ! heat/salt buoyancy flux ratio
!
! ! gravity wave-driven vertical mixing
ln_zdfiwm   = .false.   ! internal wave-induced mixing (T => fill namzdf_iwm)
ln_zdfswm   = .false.   ! surface wave-induced mixing (T => ln_wave=ln_sdw=T)
!
! ! coefficients
rn_avm0     = 1.2e-4   ! vertical eddy viscosity [m2/s] (background Kz if ln_zdfcst=F)
rn_avt0     = 1.2e-5   ! vertical eddy diffusivity [m2/s] (background Kz if ln_zdfcst=F)
nn_avb      = 0        ! profile for background avt & avm (=1) or not (=0)
nn_havtb    = 0        ! horizontal shape for avtb (=1) or not (=0)
/

```

Options are defined through the *namzdf* namelist variables. The non-penetrative convective adjustment is used when *ln\_zdfnpc = true*. It is applied at each *nn\_npc* time step and mixes downwards instantaneously the statically unstable portion of the water column, but only until the density structure becomes neutrally stable (*i.e.* until the mixed portion of the water column has *exactly* the density of the water just below) [Madec et al. 1991b]. The associated algorithm is an iterative process used in the following way (Fig. 10.3): starting from the top of the ocean, the first instability is found. Assume in the following that the instability is located between levels  $k$  and  $k + 1$ . The temperature and salinity in the two levels are vertically mixed, conserving the heat and salt contents of the water column. The new density is then computed by a linear approximation. If the new density profile is still unstable between levels  $k + 1$  and  $k + 2$ , levels  $k$ ,  $k + 1$  and  $k + 2$  are then mixed. This process is repeated until stability is established below the level  $k$  (the mixing process can go down to the ocean bottom). The algorithm is repeated to check if the density profile between level  $k - 1$  and  $k$  is unstable and/or if there is no deeper instability.

This algorithm is significantly different from mixing statically unstable levels two by two. The latter procedure cannot converge with a finite number of iterations for some vertical profiles while the algorithm used in *NEMO* converges for any profile in a number of iterations which is less than the number of vertical levels. This property is of paramount importance as pointed out by Killworth [1989]: it avoids the existence of permanent and unrealistic static instabilities at the sea surface. This non-penetrative convective algorithm has been proved successful in studies of the deep water formation in the north-western Mediterranean Sea [Madec et al. 1991b;a, Madec and Crépon 1991].

The current implementation has been modified in order to deal with any non

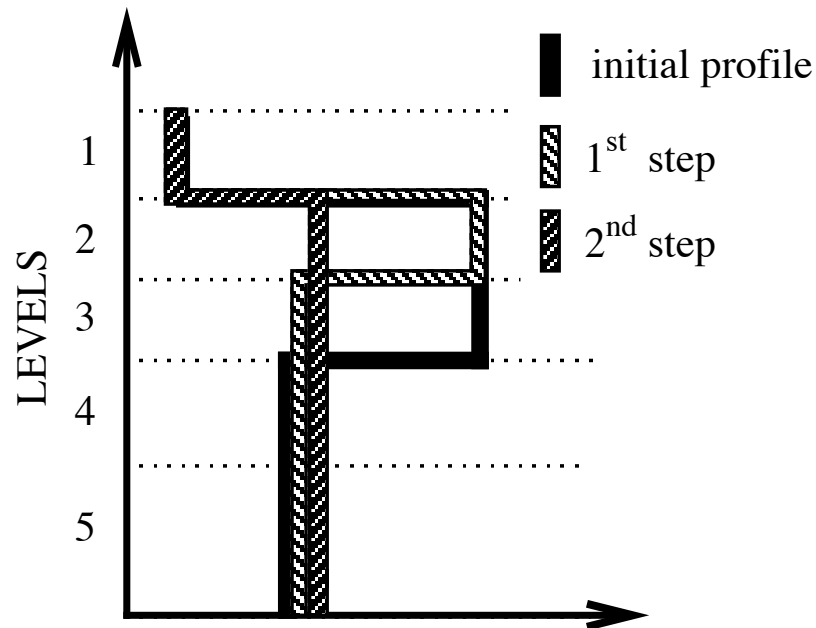


**Figure 10.3:** Example of an unstable density profile treated by the non penetrative convective adjustment algorithm. 1<sup>st</sup> step: the initial profile is checked from the surface to the bottom. It is found to be unstable between levels 3 and 4. They are mixed. The resulting  $\rho$  is still larger than  $\rho(5)$ : levels 3 to 5 are mixed. The resulting  $\rho$  is still larger than  $\rho(6)$ : levels 3 to 6 are mixed. The 1<sup>st</sup> step ends since the density profile is then stable below the level 3. 2<sup>nd</sup> step: the new  $\rho$  profile is checked following the same procedure as in 1<sup>st</sup> step: levels 2 to 5 are mixed. The new density profile is checked. It is found stable: end of algorithm.

linear equation of seawater (L. Brodeau, personal communication). Two main differences have been introduced compared to the original algorithm: (*i*) the stability is now checked using the Brunt-Väisälä frequency (not the the difference in potential density) ; (*ii*) when two levels are found unstable, their thermal and haline expansion coefficients are vertically mixed in the same way their temperature and salinity has been mixed. These two modifications allow the algorithm to perform properly and accurately with TEOS10 or EOS-80 without having to recompute the expansion coefficients at each mixing iteration.

### 10.2.2 Enhanced Vertical Diffusion (*ln\_zdfevd=true*)

```

!-----
&namzdf      !   vertical physics                                     (default: NO selection)
!-----
!
!   ! type of vertical closure (required)
ln_zdfcst   = .false.      ! constant mixing
ln_zdfric   = .false.      ! local Richardson dependent formulation (T => fill namzdf_ric)
ln_zdf_tke  = .false.      ! Turbulent Kinetic Energy closure      (T => fill namzdf_tke)
ln_zdf_gls  = .false.      ! Generic Length Scale closure      (T => fill namzdf_gls)
!
!   ! convection

```



```

ln_zdfevd = .false.      ! enhanced vertical diffusion
  nn_evdm  = 0           ! apply on tracer (=0) or on tracer and momentum (=1)
  rn_evd   = 100.       ! mixing coefficient [m2/s]
ln_zdfnpc = .false.     ! Non-Penetrative Convective algorithm
  nn_npc   = 1          ! frequency of application of npc
  nn_npcp  = 365        ! npc control print frequency
!
ln_zdfddm = .false.     ! double diffusive mixing
  rn_avts  = 1.e-4      ! maximum avts (vertical mixing on salinity)
  rn_hsbfr = 1.6        ! heat/salt buoyancy flux ratio
!
! gravity wave-driven vertical mixing
ln_zdfiwm = .false.     ! internal wave-induced mixing          (T => fill namzdf_iwm)
ln_zdfswm = .false.     ! surface wave-induced mixing          (T => ln_wave=ln_sdw=T )
!
! coefficients
rn_avm0   = 1.2e-4      ! vertical eddy viscosity [m2/s]          (background Kz if ln_zdfcst=F)
rn_avt0   = 1.2e-5     ! vertical eddy diffusivity [m2/s]       (background Kz if ln_zdfcst=F)
nn_avb    = 0           ! profile for background avt & avm (=1) or not (=0)
nn_havtb  = 0           ! horizontal shape for avtb (=1) or not (=0)
/

```

Options are defined through the *namzdf* namelist variables. The enhanced vertical diffusion parameterisation is used when *ln\_zdfevd*=true. In this case, the vertical eddy mixing coefficients are assigned very large values (a typical value is  $10 \text{ m}^2 \text{ s}^{-1}$ ) in regions where the stratification is unstable (*i.e.* when  $N^2$  the Brunt-Vaisälä frequency is negative) [Lazar 1997, Lazar et al. 1999]. This is done either on tracers only (*nn\_evdm*=0) or on both momentum and tracers (*nn\_evdm*=1).

In practice, where  $N^2 \leq 10^{-12}$ ,  $A_T^{vS}$  and  $A_T^{vS}$ , and if *nn\_evdm*=1, the four neighbouring  $A_u^{vm}$  and  $A_v^{vm}$  values also, are set equal to the namelist parameter *rn\_avevd*. A typical value for *rn\_avevd* is between 1 and  $100 \text{ m}^2 \cdot \text{s}^{-1}$ . This parameterisation of convective processes is less time consuming than the convective adjustment algorithm presented above when mixing both tracers and momentum in the case of static instabilities. It requires the use of an implicit time stepping on vertical diffusion terms (*i.e.* *ln\_zdfexp*=false).

Note that the stability test is performed on both *before* and *now* values of  $N^2$ . This removes a potential source of divergence of odd and even time step in a leapfrog environment [Leclair 2010] (see §3.5).

### 10.2.3 Turbulent Closure Scheme (key\_zdftke or key\_zdfgls)

The turbulent closure scheme presented in §10.1.3 and §10.1.5 (**key\_zdftke** or **key\_zdftke** is defined) in theory solves the problem of statically unstable density profiles. In such a case, the term corresponding to the destruction of turbulent kinetic energy through stratification in (10.4) or (10.19) becomes a source term, since  $N^2$  is negative. It results in large values of  $A_T^{vT}$  and  $A_T^{vT}$ , and also the four neighbouring  $A_u^{vm}$  and  $A_v^{vm}$  (up to  $1 \text{ m}^2 \text{ s}^{-1}$ ). These large values restore the static stability of the water column in a way similar to that of the enhanced vertical diffusion parameterisation (§10.2.2). However, in the vicinity of the sea surface (first ocean layer), the eddy coefficients computed by the turbulent closure scheme do not usually exceed  $10^{-2} \text{ m} \cdot \text{s}^{-1}$ , because the mixing length scale is bounded by the distance to the sea surface. It can thus be useful to combine the enhanced vertical diffusion with the turbulent closure scheme, *i.e.* setting the *ln\_zdfnpc* namelist parameter to true and defining the turbulent closure CPP key all together.

The KPP turbulent closure scheme already includes enhanced vertical diffusion in the case of convection, as governed by the variables *bvsqcon* and *difcon* found in *zdfkpp.F90*, therefore *ln\_zdfevd=false* should be used with the KPP scheme.

### 10.3 Double Diffusion Mixing (key\_zdfddm)

Options are defined through the *namzdf\_ddm* namelist variables. Double diffusion occurs when relatively warm, salty water overlies cooler, fresher water, or vice versa. The former condition leads to salt fingering and the latter to diffusive convection. Double-diffusive phenomena contribute to diapycnal mixing in extensive regions of the ocean. [Merryfield et al. \[1999\]](#) include a parameterisation of such phenomena in a global ocean model and show that it leads to relatively minor changes in circulation but exerts significant regional influences on temperature and salinity. This parameterisation has been introduced in *zdfddm.F90* module and is controlled by the **key\_zdfddm** CPP key.

Diapycnal mixing of S and T are described by diapycnal diffusion coefficients

$$\begin{aligned} A^{vT} &= A_o^{vT} + A_f^{vT} + A_d^{vT} \\ A^{vS} &= A_o^{vS} + A_f^{vS} + A_d^{vS} \end{aligned}$$

where subscript *f* represents mixing by salt fingering, *d* by diffusive convection, and *o* by processes other than double diffusion. The rates of double-diffusive mixing depend on the buoyancy ratio  $R_\rho = \alpha \partial_z T / \beta \partial_z S$ , where  $\alpha$  and  $\beta$  are coefficients of thermal expansion and saline contraction (see §5.8.1). To represent mixing of *S* and *T* by salt fingering, we adopt the diapycnal diffusivities suggested by Schmitt (1981):

$$A_f^{vS} = \begin{cases} \frac{A^{*v}}{1+(R_\rho/R_c)^n} & \text{if } R_\rho > 1 \text{ and } N^2 > 0 \\ 0 & \text{otherwise} \end{cases} \quad (10.23)$$

$$A_f^{vT} = 0.7 A_f^{vS} / R_\rho \quad (10.24)$$

The factor 0.7 in (10.24) reflects the measured ratio  $\alpha F_T / \beta F_S \approx 0.7$  of buoyancy flux of heat to buoyancy flux of salt (*e.g.*, [McDougall and Taylor \[1984\]](#)). Following [Merryfield et al. \[1999\]](#), we adopt  $R_c = 1.6$ ,  $n = 6$ , and  $A^{*v} = 10^{-4} \text{ m}^2 \cdot \text{s}^{-1}$ .

To represent mixing of S and T by diffusive layering, the diapycnal diffusivities

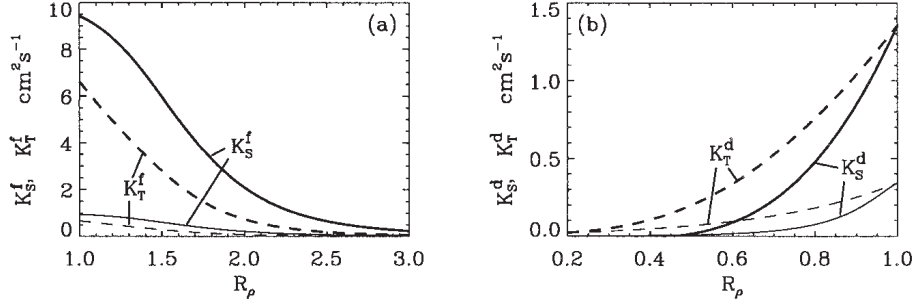


**Figure 10.4:** From Merryfield et al. [1999] : (a) Diapycnal diffusivities  $A_f^{vT}$  and  $A_f^{vS}$  for temperature and salt in regions of salt fingering. Heavy curves denote  $A^{*v} = 10^{-3} m^2.s^{-1}$  and thin curves  $A^{*v} = 10^{-4} m^2.s^{-1}$  ; (b) diapycnal diffusivities  $A_d^{vT}$  and  $A_d^{vS}$  for temperature and salt in regions of diffusive convection. Heavy curves denote the Federov parameterisation and thin curves the Kelley parameterisation. The latter is not implemented in *NEMO*.

suggested by Federov (1988) is used:

$$A_d^{vT} = \begin{cases} 1.3635 \exp(4.6 \exp[-0.54(R_\rho^{-1} - 1)]) & \text{if } 0 < R_\rho < 1 \text{ and } N^2 > 0 \\ 0 & \text{otherwise} \end{cases} \quad (10.25)$$

$$A_d^{vS} = \begin{cases} A_d^{vT} (1.85 R_\rho - 0.85) & \text{if } 0.5 \leq R_\rho < 1 \text{ and } N^2 > 0 \\ A_d^{vT} 0.15 R_\rho & \text{if } 0 < R_\rho < 0.5 \text{ and } N^2 > 0 \\ 0 & \text{otherwise} \end{cases} \quad (10.26)$$

The dependencies of (10.23) to (10.26) on  $R_\rho$  are illustrated in Fig. 10.4. Implementing this requires computing  $R_\rho$  at each grid point on every time step. This is done in *eosbn2.F90* at the same time as  $N^2$  is computed. This avoids duplication in the computation of  $\alpha$  and  $\beta$  (which is usually quite expensive).

## 10.4 Bottom and Top Friction (*zdfbfr.F90* module)

Options to define the top and bottom friction are defined through the *nambfr* namelist variables. The bottom friction represents the friction generated by the bathymetry. The top friction represents the friction generated by the ice shelf/ocean interface. As the friction processes at the top and bottom are treated in similar way, only the bottom friction is described in detail below.

Both the surface momentum flux (wind stress) and the bottom momentum flux (bottom friction) enter the equations as a condition on the vertical diffusive flux. For the bottom boundary layer, one has:

$$A^{vm} (\partial \mathbf{U}_h / \partial z) = \mathcal{F}_h^{\mathbf{U}} \quad (10.27)$$

where  $\mathcal{F}_h^{\mathbf{U}}$  is represents the downward flux of horizontal momentum outside the logarithmic turbulent boundary layer (thickness of the order of 1 m in the ocean). How  $\mathcal{F}_h^{\mathbf{U}}$  influences the interior depends on the vertical resolution of the model near the bottom relative to the Ekman layer depth. For example, in order to obtain an Ekman layer depth  $d = \sqrt{2 A^{vm} / f} = 50$  m, one needs a vertical diffusion coefficient  $A^{vm} = 0.125 \text{ m}^2 \text{ s}^{-1}$  (for a Coriolis frequency  $f = 10^{-4} \text{ m}^2 \text{ s}^{-1}$ ). With a background diffusion coefficient  $A^{vm} = 10^{-4} \text{ m}^2 \text{ s}^{-1}$ , the Ekman layer depth is only 1.4 m. When the vertical mixing coefficient is this small, using a flux condition is equivalent to entering the viscous forces (either wind stress or bottom friction) as a body force over the depth of the top or bottom model layer. To illustrate this, consider the equation for  $u$  at  $k$ , the last ocean level:

$$\frac{\partial u_k}{\partial t} = \frac{1}{e_{3u}} \left[ \frac{A_{uw}^{vm}}{e_{3uw}} \delta_{k+1/2} [u] - \mathcal{F}_h^u \right] \approx -\frac{\mathcal{F}_h^u}{e_{3u}} \quad (10.28)$$

If the bottom layer thickness is 200 m, the Ekman transport will be distributed over that depth. On the other hand, if the vertical resolution is high (1 m or less) and a turbulent closure model is used, the turbulent Ekman layer will be represented explicitly by the model. However, the logarithmic layer is never represented in current primitive equation model applications: it is *necessary* to parameterize the flux  $\mathcal{F}_h^u$ . Two choices are available in *NEMO*: a linear and a quadratic bottom friction. Note that in both cases, the rotation between the interior velocity and the bottom friction is neglected in the present release of *NEMO*.

In the code, the bottom friction is imposed by adding the trend due to the bottom friction to the general momentum trend in *dynbfr.F90*. For the time-split surface pressure gradient algorithm, the momentum trend due to the barotropic component needs to be handled separately. For this purpose it is convenient to compute and store coefficients which can be simply combined with bottom velocities and geometric values to provide the momentum trend due to bottom friction. These coefficients are computed in *zdfbfr.F90* and generally take the form  $c_b^{\mathbf{U}}$  where:

$$\frac{\partial \mathbf{U}_h}{\partial t} = -\frac{\mathcal{F}_h^{\mathbf{U}}}{e_{3u}} = \frac{c_b^{\mathbf{U}}}{e_{3u}} \mathbf{U}_h^b \quad (10.29)$$

where  $\mathbf{U}_h^b = (u_b, v_b)$  is the near-bottom, horizontal, ocean velocity.

#### 10.4.1 Linear Bottom Friction (*nn\_botfr* = 0 or 1)

The linear bottom friction parameterisation (including the special case of a free-slip condition) assumes that the bottom friction is proportional to the interior velocity

(i.e. the velocity of the last model level):

$$\mathcal{F}_h^{\mathbf{U}} = \frac{A^{vm}}{e_3} \frac{\partial \mathbf{U}_h}{\partial k} = r \mathbf{U}_h^b \quad (10.30)$$

where  $r$  is a friction coefficient expressed in  $\text{ms}^{-1}$ . This coefficient is generally estimated by setting a typical decay time  $\tau$  in the deep ocean, and setting  $r = H/\tau$ , where  $H$  is the ocean depth. Commonly accepted values of  $\tau$  are of the order of 100 to 200 days [Weatherly 1984]. A value  $\tau^{-1} = 10^{-7} \text{ s}^{-1}$  equivalent to 115 days, is usually used in quasi-geostrophic models. One may consider the linear friction as an approximation of quadratic friction,  $r \approx 2 C_D U_{av}$  (Gill [1982], Eq. 9.6.6). For example, with a drag coefficient  $C_D = 0.002$ , a typical speed of tidal currents of  $U_{av} = 0.1 \text{ m s}^{-1}$ , and assuming an ocean depth  $H = 4000 \text{ m}$ , the resulting friction coefficient is  $r = 4 \cdot 10^{-4} \text{ m s}^{-1}$ . This is the default value used in *NEMO*. It corresponds to a decay time scale of 115 days. It can be changed by specifying *rn\_bfri1* (namelist parameter).

For the linear friction case the coefficients defined in the general expression (10.29) are:

$$\begin{aligned} c_b^u &= -r \\ c_b^v &= -r \end{aligned} \quad (10.31)$$

When *nn\_botfr*=1, the value of  $r$  used is *rn\_bfri1*. Setting *nn\_botfr*=0 is equivalent to setting  $r = 0$  and leads to a free-slip bottom boundary condition. These values are assigned in *zdfbfr.F90*. From v3.2 onwards there is support for local enhancement of these values via an externally defined 2D mask array (*ln\_bfr2d=true*) given in the *bfr\_coef.nc* input NetCDF file. The mask values should vary from 0 to 1. Locations with a non-zero mask value will have the friction coefficient increased by *mask\_value\*rn\_bfri1*.

#### 10.4.2 Non-Linear Bottom Friction (*nn\_botfr = 2*)

The non-linear bottom friction parameterisation assumes that the bottom friction is quadratic:

$$\mathcal{F}_h^{\mathbf{U}} = \frac{A^{vm}}{e_3} \frac{\partial \mathbf{U}_h}{\partial k} = C_D \sqrt{u_b^2 + v_b^2 + e_b} \mathbf{U}_h^b \quad (10.32)$$

where  $C_D$  is a drag coefficient, and  $e_b$  a bottom turbulent kinetic energy due to tides, internal waves breaking and other short time scale currents. A typical value of the drag coefficient is  $C_D = 10^{-3}$ . As an example, the CME experiment [Tréguier 1992] uses  $C_D = 10^{-3}$  and  $e_b = 2.5 \cdot 10^{-3} \text{ m}^2 \text{ s}^{-2}$ , while the FRAM experiment [Killworth 1992] uses  $C_D = 1.4 \cdot 10^{-3}$  and  $e_b = 2.5 \cdot 10^{-3} \text{ m}^2 \text{ s}^{-2}$ . The CME choices have been set as default values (*rn\_bfri2* and *rn\_bfeb2* namelist parameters).

As for the linear case, the bottom friction is imposed in the code by adding the trend due to the bottom friction to the general momentum trend in *dynbfr.F90*. For

the non-linear friction case the terms computed in *zdfbfr.F90* are:

$$\begin{aligned} c_b^u &= -C_D \left[ u^2 + (\bar{v}^{i+1,j})^2 + e_b \right]^{1/2} \\ c_b^v &= -C_D \left[ (\bar{u}^{i,j+1})^2 + v^2 + e_b \right]^{1/2} \end{aligned} \quad (10.33)$$

The coefficients that control the strength of the non-linear bottom friction are initialised as namelist parameters:  $C_D = rn\_bfri2$ , and  $e_b = rn\_bfeb2$ . Note for applications which treat tides explicitly a low or even zero value of *rn\_bfeb2* is recommended. From v3.2 onwards a local enhancement of  $C_D$  is possible via an externally defined 2D mask array (*ln\_bfr2d=true*). This works in the same way as for the linear bottom friction case with non-zero masked locations increased by  $mask\_value * rn\_bfrien * rn\_bfri2$ .

#### 10.4.3 Log-layer Bottom Friction enhancement (*nn\_botfr = 2*, *ln\_loglayer = .true.*)

In the non-linear bottom friction case, the drag coefficient,  $C_D$ , can be optionally enhanced using a "law of the wall" scaling. If *ln\_loglayer = .true.*,  $C_D$  is no longer constant but is related to the thickness of the last wet layer in each column by:

$$C_D = \left( \frac{\kappa}{\log(0.5e_{3t}/rn\_bfrz0)} \right)^2 \quad (10.34)$$

where  $\kappa$  is the von-Karman constant and *rn\_bfrz0* is a roughness length provided via the namelist.

For stability, the drag coefficient is bounded such that it is kept greater or equal to the base *rn\_bfri2* value and it is not allowed to exceed the value of an additional namelist parameter: *rn\_bfri2\_max*, i.e.:

$$rn\_bfri2 \leq C_D \leq rn\_bfri2\_max \quad (10.35)$$

Note also that a log-layer enhancement can also be applied to the top boundary friction if under ice-shelf cavities are in use (*ln\_isfcav=.true.*). In this case, the relevant namelist parameters are *rn\_tfrz0*, *rn\_tfri2* and *rn\_tfri2\_max*.

#### 10.4.4 Bottom Friction stability considerations

Some care needs to be exercised over the choice of parameters to ensure that the implementation of bottom friction does not induce numerical instability. For the purposes of stability analysis, an approximation to (10.28) is:

$$\begin{aligned} \Delta u &= -\frac{\mathcal{F}_h^u}{e_{3u}} 2\Delta t \\ &= -\frac{ru}{e_{3u}} 2\Delta t \end{aligned} \quad (10.36)$$

where linear bottom friction and a leapfrog timestep have been assumed. To ensure that the bottom friction cannot reverse the direction of flow it is necessary to have:

$$|\Delta u| < |u| \quad (10.37)$$

which, using (10.36), gives:

$$r \frac{2\Delta t}{e_{3u}} < 1 \quad \Rightarrow \quad r < \frac{e_{3u}}{2\Delta t} \quad (10.38)$$

This same inequality can also be derived in the non-linear bottom friction case if a velocity of  $1 \text{ m.s}^{-1}$  is assumed. Alternatively, this criterion can be rearranged to suggest a minimum bottom box thickness to ensure stability:

$$e_{3u} > 2 r \Delta t \quad (10.39)$$

which it may be necessary to impose if partial steps are being used. For example, if  $|u| = 1 \text{ m.s}^{-1}$ ,  $r dt = 1800 \text{ s}$ ,  $r = 10^{-3}$  then  $e_{3u}$  should be greater than 3.6 m. For most applications, with physically sensible parameters these restrictions should not be of concern. But caution may be necessary if attempts are made to locally enhance the bottom friction parameters. To ensure stability limits are imposed on the bottom friction coefficients both during initialisation and at each time step. Checks at initialisation are made in *zdfbfr.F90* (assuming a  $1 \text{ m.s}^{-1}$  velocity in the non-linear case). The number of breaches of the stability criterion are reported as well as the minimum and maximum values that have been set. The criterion is also checked at each time step, using the actual velocity, in *dynbfr.F90*. Values of the bottom friction coefficient are reduced as necessary to ensure stability; these changes are not reported.

Limits on the bottom friction coefficient are not imposed if the user has elected to handle the bottom friction implicitly (see §10.4.5). The number of potential breaches of the explicit stability criterion are still reported for information purposes.

#### 10.4.5 Implicit Bottom Friction (*ln\_bfrimp=T*)

An optional implicit form of bottom friction has been implemented to improve model stability. We recommend this option for shelf sea and coastal ocean applications, especially for split-explicit time splitting. This option can be invoked by setting *ln\_bfrimp* to *true* in the *nambfr* namelist. This option requires *ln\_zdfexp* to be *false* in the *namzdf* namelist.

This implementation is realised in *dynzdf\_imp.F90* and *dynspg\_ts.F90*. In *dynzdf\_imp.F90*, the bottom boundary condition is implemented implicitly.

$$\left( \frac{A^{vm}}{e_3} \frac{\partial \mathbf{U}_h}{\partial k} \right) \Big|_{mbk} = \begin{pmatrix} c_b^u u_{mbk}^{n+1} \\ c_b^v v_{mbk}^{n+1} \end{pmatrix} \quad (10.40)$$

where  $mbk$  is the layer number of the bottom wet layer. superscript  $n + 1$  means the velocity used in the friction formula is to be calculated, so, it is implicit.

If split-explicit time splitting is used, care must be taken to avoid the double counting of the bottom friction in the 2-D barotropic momentum equations. As NEMO only updates the barotropic pressure gradient and Coriolis' forcing terms in the 2-D barotropic calculation, we need to remove the bottom friction induced by these two terms which has been included in the 3-D momentum trend and update it with the latest value. On the other hand, the bottom friction contributed by the other terms (e.g. the advection term, viscosity term) has been included in the 3-D momentum equations and should not be added in the 2-D barotropic mode.

The implementation of the implicit bottom friction in *dynspg\_ts.F90* is done in two steps as the following:

$$\frac{\mathbf{U}_{med} - \mathbf{U}^{m-1}}{2\Delta t} = -g\nabla\eta - f\mathbf{k} \times \mathbf{U}^m + c_b (\mathbf{U}_{med} - \mathbf{U}^{m-1}) \quad (10.41)$$

$$\frac{\mathbf{U}^{m+1} - \mathbf{U}_{med}}{2\Delta t} = \mathbf{T} + \left( g\nabla\eta' + f\mathbf{k} \times \mathbf{U}' \right) - 2\Delta t_{bc} c_b \left( g\nabla\eta' + f\mathbf{k} \times \mathbf{u}_b \right) \quad (10.42)$$

where  $\mathbf{T}$  is the vertical integrated 3-D momentum trend. We assume the leap-frog time-stepping is used here.  $\Delta t$  is the barotropic mode time step and  $\Delta t_{bc}$  is the baroclinic mode time step.  $c_b$  is the friction coefficient.  $\eta$  is the sea surface level calculated in the barotropic loops while  $\eta'$  is the sea surface level used in the 3-D baroclinic mode.  $\mathbf{u}_b$  is the bottom layer horizontal velocity.

#### 10.4.6 Bottom Friction with split-explicit time splitting (*ln\_bfrimp=F*)

When calculating the momentum trend due to bottom friction in *dynbfr.F90*, the bottom velocity at the before time step is used. This velocity includes both the baroclinic and barotropic components which is appropriate when using either the explicit or filtered surface pressure gradient algorithms (**key\_dynspg\_exp** or **key\_dynspg\_ftt**). Extra attention is required, however, when using split-explicit time stepping (**key\_dynspg\_ts**). In this case the free surface equation is solved with a small time step *rn\_rdt/nn\_baro*, while the three dimensional prognostic variables are solved with the longer time step of *rn\_rdt* seconds. The trend in the barotropic momentum due to bottom friction appropriate to this method is that given by the selected parameterisation (*i.e.* linear or non-linear bottom friction) computed with the evolving velocities at each barotropic timestep.

In the case of non-linear bottom friction, we have elected to partially linearise the problem by keeping the coefficients fixed throughout the barotropic time-stepping to those computed in *zdfbfr.F90* using the now timestep. This decision allows an efficient use of the  $c_b^U$  coefficients to:



1. On entry to *dyn\_spg\_ts*, remove the contribution of the before barotropic velocity to the bottom friction component of the vertically integrated momentum trend. Note the same stability check that is carried out on the bottom friction coefficient in *dynbfr.F90* has to be applied here to ensure that the trend removed matches that which was added in *dynbfr.F90*.
2. At each barotropic step, compute the contribution of the current barotropic velocity to the trend due to bottom friction. Add this contribution to the vertically integrated momentum trend. This contribution is handled implicitly which eliminates the need to impose a stability criteria on the values of the bottom friction coefficient within the barotropic loop.

Note that the use of an implicit formulation within the barotropic loop for the bottom friction trend means that any limiting of the bottom friction coefficient in *dynbfr.F90* does not adversely affect the solution when using split-explicit time splitting. This is because the major contribution to bottom friction is likely to come from the barotropic component which uses the unrestricted value of the coefficient. However, if the limiting is thought to be having a major effect (a more likely prospect in coastal and shelf seas applications) then the fully implicit form of the bottom friction should be used (see §10.4.5) which can be selected by setting *ln\_bfrimp = true*.

Otherwise, the implicit formulation takes the form:

$$\bar{U}^{t+\Delta t} = [\bar{U}^{t-\Delta t} + 2\Delta t RHS] / [1 - 2\Delta t c_b^u / H_e] \quad (10.43)$$

where  $\bar{U}$  is the barotropic velocity,  $H_e$  is the full depth (including sea surface height),  $c_b^u$  is the bottom friction coefficient as calculated in *zdf\_bfr* and *RHS* represents all the components to the vertically integrated momentum trend except for that due to bottom friction.

## 10.5 Tidal Mixing (key\_zdftmx)

### 10.5.1 Bottom intensified tidal mixing

Options are defined through the *namzdf\_tmx* namelist variables. The parameterization of tidal mixing follows the general formulation for the vertical eddy diffusivity proposed by St. Laurent et al. [2002] and first introduced in an OGCM by [Simmons et al. 2004]. In this formulation an additional vertical diffusivity resulting from internal tide breaking,  $A_{tides}^{vT}$  is expressed as a function of  $E(x, y)$ , the energy transfer from barotropic tides to baroclinic tides :

$$A_{tides}^{vT} = q \Gamma \frac{E(x, y) F(z)}{\rho N^2} \quad (10.44)$$

where  $\Gamma$  is the mixing efficiency,  $N$  the Brunt-Vaisälä frequency (see §5.8.2),  $\rho$  the density,  $q$  the tidal dissipation efficiency, and  $F(z)$  the vertical structure function.

The mixing efficiency of turbulence is set by  $\Gamma$  (*rn\_me* namelist parameter) and is usually taken to be the canonical value of  $\Gamma = 0.2$  (Osborn 1980). The tidal dissipation efficiency is given by the parameter  $q$  (*rn\_tfe* namelist parameter) represents the part of the internal wave energy flux  $E(x, y)$  that is dissipated locally, with the remaining  $1 - q$  radiating away as low mode internal waves and contributing to the background internal wave field. A value of  $q = 1/3$  is typically used [St. Laurent et al. \[2002\]](#). The vertical structure function  $F(z)$  models the distribution of the turbulent mixing in the vertical. It is implemented as a simple exponential decaying upward away from the bottom, with a vertical scale of  $h_o$  (*rn\_htmx* namelist parameter, with a typical value of 500 m) [[St. Laurent and Nash 2004](#)],

$$F(i, j, k) = \frac{e^{-\frac{H+z}{h_o}}}{h_o \left(1 - e^{-\frac{H}{h_o}}\right)} \quad (10.45)$$

and is normalized so that vertical integral over the water column is unity.

The associated vertical viscosity is calculated from the vertical diffusivity assuming a Prandtl number of 1, *i.e.*  $A_{tides}^{vm} = A_{tides}^v$ . In the limit of  $N \rightarrow 0$  (or becoming negative), the vertical diffusivity is capped at  $300 \text{ cm}^2/\text{s}$  and impose a lower limit on  $N^2$  of *rn\_n2min* usually set to  $10^{-8} \text{ s}^{-2}$ . These bounds are usually rarely encountered.

The internal wave energy map,  $E(x, y)$  in (10.44), is derived from a barotropic model of the tides utilizing a parameterization of the conversion of barotropic tidal energy into internal waves. The essential goal of the parameterization is to represent the momentum exchange between the barotropic tides and the unrepresented internal waves induced by the tidal flow over rough topography in a stratified ocean. In the current version of *NEMO*, the map is built from the output of the barotropic global ocean tide model MOG2D-G [[Carrère and Lyard 2003](#)]. This model provides the dissipation associated with internal wave energy for the M2 and K1 tides component (Fig. 10.5). The S2 dissipation is simply approximated as being 1/4 of the M2 one. The internal wave energy is thus :  $E(x, y) = 1.25E_{M2} + E_{K1}$ . Its global mean value is 1.1 TW, in agreement with independent estimates [[Egbert and Ray 2000; 2001](#)].

### 10.5.2 Indonesian area specific treatment (*ln\_zdfmx\_itf*)

When the Indonesian Through Flow (ITF) area is included in the model domain, a specific treatment of tidal induced mixing in this area can be used. It is activated through the namelist logical *ln\_tmx\_itf*, and the user must provide an input NetCDF file, *mask\_itf.nc*, which contains a mask array defining the ITF area where the specific treatment is applied.

When *ln\_tmx\_itf*=true, the two key parameters  $q$  and  $F(z)$  are adjusted following the parameterisation developed by [Koch-Larrouy et al. \[2007\]](#):

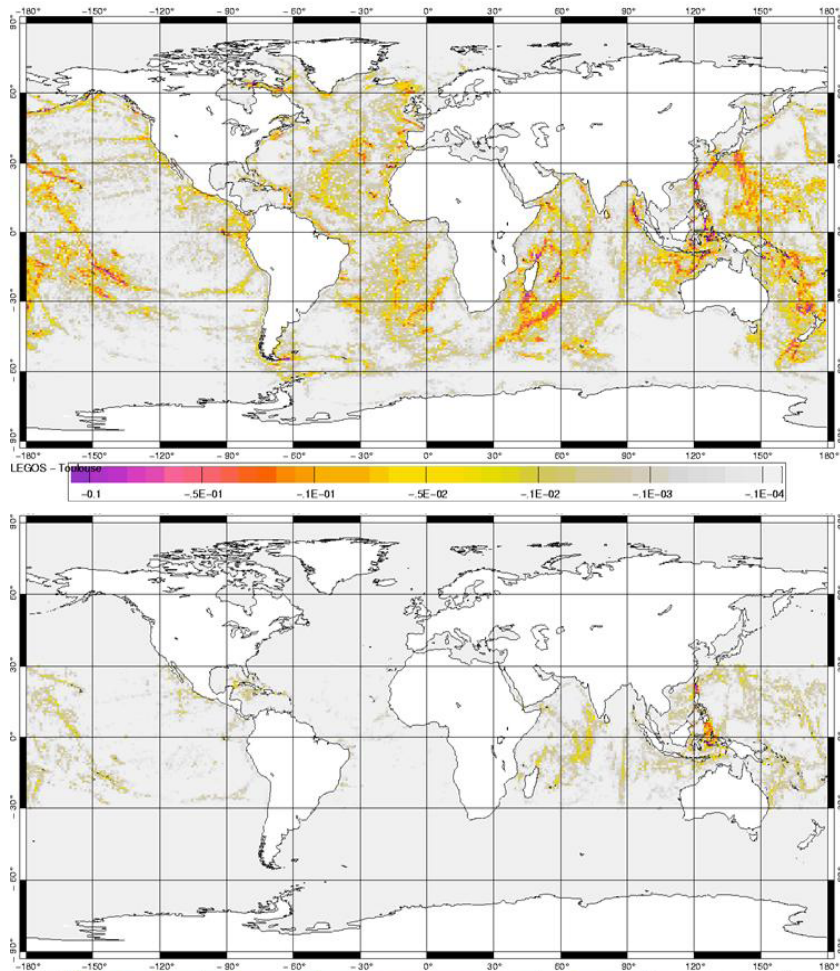


**Figure 10.5:** (a) M2 and (b) K1 internal wave drag energy from Carrère and Lyard [2003] ( $W/m^2$ ).

First, the Indonesian archipelago is a complex geographic region with a series of large, deep, semi-enclosed basins connected via numerous narrow straits. Once generated, internal tides remain confined within this semi-enclosed area and hardly radiate away. Therefore all the internal tides energy is consumed within this area. So it is assumed that  $q = 1$ , *i.e.* all the energy generated is available for mixing. Note that for test purposes, the ITF tidal dissipation efficiency is a namelist parameter (*rn\_tfe\_itf*). A value of 1 or close to is this recommended for this parameter.

Second, the vertical structure function,  $F(z)$ , is no more associated with a bottom intensification of the mixing, but with a maximum of energy available within the thermocline. Koch-Larrouy et al. [2007] have suggested that the vertical distri-

bution of the energy dissipation proportional to  $N^2$  below the core of the thermocline and to  $N$  above. The resulting  $F(z)$  is:

$$F(i, j, k) \sim \begin{cases} \frac{q \Gamma E(i, j)}{\rho N \int N dz} & \text{when } \partial_z N < 0 \\ \frac{q \Gamma E(i, j)}{\rho \int N^2 dz} & \text{when } \partial_z N > 0 \end{cases} \quad (10.46)$$

Averaged over the ITF area, the resulting tidal mixing coefficient is  $1.5 \text{ cm}^2/\text{s}$ , which agrees with the independent estimates inferred from observations. Introduced in a regional OGCM, the parameterization improves the water mass characteristics in the different Indonesian seas, suggesting that the horizontal and vertical distributions of the mixing are adequately prescribed [Koch-Larrouy et al. 2007; 2008b;a]. Note also that such a parameterisation has a significant impact on the behaviour of global coupled GCMs [Koch-Larrouy et al. 2010].

## 10.6 Internal wave-driven mixing (key `zdftmx_new`)

The parameterization of mixing induced by breaking internal waves is a generalization of the approach originally proposed by St. Laurent et al. [2002]. A three-dimensional field of internal wave energy dissipation  $\epsilon(x, y, z)$  is first constructed, and the resulting diffusivity is obtained as

$$A_{wave}^{vT} = R_f \frac{\epsilon}{\rho N^2} \quad (10.47)$$

where  $R_f$  is the mixing efficiency and  $\epsilon$  is a specified three dimensional distribution of the energy available for mixing. If the `ln_mevr` namelist parameter is set to false, the mixing efficiency is taken as constant and equal to 1/6 [Osborn 1980]. In the opposite (recommended) case,  $R_f$  is instead a function of the turbulence intensity parameter  $Re_b = \frac{\epsilon}{\nu N^2}$ , with  $\nu$  the molecular viscosity of seawater, following the model of Bouffard and Boegman [2013] and the implementation of de Lavergne et al. [2016]. Note that  $A_{wave}^{vT}$  is bounded by  $10^{-2} \text{ m}^2/\text{s}$ , a limit that is often reached when the mixing efficiency is constant.

In addition to the mixing efficiency, the ratio of salt to heat diffusivities can chosen to vary as a function of  $Re_b$  by setting the `ln_tsdiff` parameter to true, a recommended choice). This parameterization of differential mixing, due to Jackson and Rehmann [2014], is implemented as in de Lavergne et al. [2016].

The three-dimensional distribution of the energy available for mixing,  $\epsilon(i, j, k)$ , is constructed from three static maps of column-integrated internal wave energy dissipation,  $E_{cri}(i, j)$ ,  $E_{pyc}(i, j)$ , and  $E_{bot}(i, j)$ , combined to three corresponding

vertical structures (de Lavergne et al., in prep):

$$\begin{aligned} F_{cri}(i, j, k) &\propto e^{-h_{ab}/h_{cri}} \\ F_{pyc}(i, j, k) &\propto N^{n-p} \\ F_{bot}(i, j, k) &\propto N^2 e^{-h_{wkb}/h_{bot}} \end{aligned}$$

In the above formula,  $h_{ab}$  denotes the height above bottom,  $h_{wkb}$  denotes the WKB-stretched height above bottom, defined by

$$h_{wkb} = H \frac{\int_{-H}^z N dz'}{\int_{-H}^{\eta} N dz'} ,$$

The  $n_p$  parameter (given by `nm_zpyc` in `namzdf_tmx_new` namelist) controls the stratification-dependence of the pycnocline-intensified dissipation. It can take values of 1 (recommended) or 2. Finally, the vertical structures  $F_{cri}$  and  $F_{bot}$  require the specification of the decay scales  $h_{cri}(i, j)$  and  $h_{bot}(i, j)$ , which are defined by two additional input maps.  $h_{cri}$  is related to the large-scale topography of the ocean (etopo2) and  $h_{bot}$  is a function of the energy flux  $E_{bot}$ , the characteristic horizontal scale of the abyssal hill topography [Goff 2010] and the latitude.





# 11 Output and Diagnostics (IOM, DIA, TRD, FLO)

## Contents

---

<b>11.1 Old Model Output (default)</b>	<b>214</b>
<b>11.2 Standard model Output (IOM)</b>	<b>214</b>
11.2.1 XIOS: the IO_SERVER	216
11.2.2 Practical issues	217
11.2.3 XML fundamentals	218
11.2.4 Detailed functionalities	222
11.2.5 XML reference tables	224
11.2.6 CF metadata standard compliance	231
<b>11.3 NetCDF4 Support (key_netcdf4)</b>	<b>231</b>
<b>11.4 Tracer/Dynamics Trends (TRD)</b>	<b>234</b>
<b>11.5 On-line Floats trajectories (FLO) (key_floats)</b>	<b>235</b>
<b>11.6 Harmonic analysis of tidal constituents (key_diaharm)</b>	<b>236</b>
<b>11.7 Transports across sections (key_diadct)</b>	<b>237</b>
<b>11.8 Diagnosing the Steric effect in sea surface height</b>	<b>239</b>
<b>11.9 Other Diagnostics (key_diahth, key_diaar5)</b>	<b>242</b>
11.9.1 Depth of various quantities ( <i>diahth.F90</i> )	242
11.9.2 Poleward heat and salt transports ( <i>diaptr.F90</i> )	243
11.9.3 CMIP specific diagnostics ( <i>diaar5.F90</i> )	243
11.9.4 25 hour mean output for tidal models	243
11.9.5 Top Middle and Bed hourly output	244
11.9.6 Courant numbers	244

---

## 11.1 Old Model Output (default)

The model outputs are of three types: the restart file, the output listing, and the diagnostic output file(s). The restart file is used internally by the code when the user wants to start the model with initial conditions defined by a previous simulation. It contains all the information that is necessary in order for there to be no changes in the model results (even at the computer precision) between a run performed with several restarts and the same run performed in one step. It should be noted that this requires that the restart file contain two consecutive time steps for all the prognostic variables, and that it is saved in the same binary format as the one used by the computer that is to read it (in particular, 32 bits binary IEEE format must not be used for this file).

The output listing and file(s) are predefined but should be checked and eventually adapted to the user's needs. The output listing is stored in the *ocean.output* file. The information is printed from within the code on the logical unit *numout*. To locate these prints, use the UNIX command "*grep -i numout*" in the source code directory.

By default, diagnostic output files are written in NetCDF format. Since version 3.2, when defining **key\_iomput**, an I/O server has been added which provides more flexibility in the choice of the fields to be written as well as how the writing work is distributed over the processors in massively parallel computing. A complete description of the use of this I/O server is presented in the next section.

By default, **key\_iomput** is not defined, NEMO produces NetCDF with the old IOIPSL library which has been kept for compatibility and its easy installation. However, the IOIPSL library is quite inefficient on parallel machines and, since version 3.2, many diagnostic options have been added presuming the use of **key\_iomput**. The usefulness of the default IOIPSL-based option is expected to reduce with each new release. If **key\_iomput** is not defined, output files and content are defined in the *diawri.F90* module and contain mean (or instantaneous if **key\_diainstant** is defined) values over a regular period of *nn\_write* time-steps (namelist parameter).

## 11.2 Standard model Output (IOM)

Since version 3.2, *iomput* is the NEMO output interface of choice. It has been designed to be simple to use, flexible and efficient. The two main purposes of *iomput* are:

1. The complete and flexible control of the output files through external XML files adapted by the user from standard templates.



2. To achieve high performance and scalable output through the optional distribution of all diagnostic output related tasks to dedicated processes.

The first functionality allows the user to specify, without code changes or recompilation, aspects of the diagnostic output stream, such as:

- The choice of output frequencies that can be different for each file (including real months and years).
- The choice of file contents; includes complete flexibility over which data are written in which files (the same data can be written in different files).
- The possibility to split output files at a chosen frequency.
- The possibility to extract a vertical or an horizontal subdomain.
- The choice of the temporal operation to perform, e.g.: average, accumulate, instantaneous, min, max and once.
- Control over metadata via a large XML "database" of possible output fields.

In addition, `iomput` allows the user to add in the code the output of any new variable (scalar, 2D or 3D) in a very easy way. All details of `iomput` functionalities are listed in the following subsections. Examples of the XML files that control the outputs can be found in:

```
NEMOGCM/CONFIG/ORCA2_LIM/EXP00/iodef.xml
NEMOGCM/CONFIG/SHARED/field_def.xml
and
NEMOGCM/CONFIG/SHARED/domain_def.xml.
```

The second functionality targets output performance when running in parallel (**key `mpp_mpi`**). `Iomput` provides the possibility to specify `N` dedicated I/O processes (in addition to the NEMO processes) to collect and write the outputs. With an appropriate choice of `N` by the user, the bottleneck associated with the writing of the output files can be greatly reduced.

In version 3.6, the `iomput` interface depends on an external code called [XIOS-1.0](#) (use of revision 618 or higher is required). This new IO server can take advantage of the parallel I/O functionality of NetCDF4 to create a single output file and therefore to bypass the rebuilding phase. Note that writing in parallel into the same NetCDF files requires that your NetCDF4 library is linked to an HDF5 library that has been correctly compiled (*i.e.* with the configure option `--enable-parallel`). Note that the files created by `iomput` through XIOS are incompatible with NetCDF3. All post-processing and visualization tools must therefore be compatible with NetCDF4 and not only NetCDF3.

Even if not using the parallel I/O functionality of NetCDF4, using `N` dedicated I/O servers, where `N` is typically much less than the number of NEMO processors,

will reduce the number of output files created. This can greatly reduce the post-processing burden usually associated with using large numbers of NEMO processors. Note that for smaller configurations, the rebuilding phase can be avoided, even without a parallel-enabled NetCDF4 library, simply by employing only one dedicated I/O server.

### 11.2.1 XIOS: the IO\_SERVER

#### Attached or detached mode?

Iomput is based on [XIOS](#), the `io_server` developed by Yann Meurdesoif from IPSL. The behaviour of the I/O subsystem is controlled by settings in the external XML files listed above. Key settings in the `iodef.xml` file are `using_server` and the `type` tag associated with each defined file. The `using_server` setting determines whether or not the server will be used in *attached mode* (as a library) [`false`] or in *detached mode* (as an external executable on N additional, dedicated cpus) [`true`]. The *attached mode* is simpler to use but much less efficient for massively parallel applications. The type of each file can be either "multiple\_file" or "one\_file".

In *attached mode* and if the type of file is "multiple\_file", then each NEMO process will also act as an IO server and produce its own set of output files. Superficially, this emulates the standard behaviour in previous versions. However, the subdomain written out by each process does not correspond to the  $j_{pi} \times j_{pj} \times j_{pk}$  domain actually computed by the process (although it may if  $j_{pni}=1$ ). Instead each process will have collected and written out a number of complete longitudinal strips. If the "one\_file" option is chosen then all processes will collect their longitudinal strips and write (in parallel) to a single output file.

In *detached mode* and if the type of file is "multiple\_file", then each stand-alone XIOS process will collect data for a range of complete longitudinal strips and write to its own set of output files. If the "one\_file" option is chosen then all XIOS processes will collect their longitudinal strips and write (in parallel) to a single output file. Note running in detached mode requires launching a Multiple Process Multiple Data (MPMD) parallel job. The following subsection provides a typical example but the syntax will vary in different MPP environments.

#### Number of cpu used by XIOS in detached mode

The number of cores used by the XIOS is specified when launching the model. The number of cores dedicated to XIOS should be from 1/10 to 1/50 of the number of cores dedicated to NEMO. Some manufacturers suggest using  $O(\sqrt{N})$  dedicated IO processors for N processors but this is a general recommendation and not specific to NEMO. It is difficult to provide precise recommendations because the optimal choice will depend on the particular hardware properties of the target system (parallel filesystem performance, available memory, memory bandwidth etc.)

and the volume and frequency of data to be created. Here is an example of 2 cpus for the `io_server` and 62 cpu for `nemo` using `mpirun`:

```
mpirun -np 62 ./nemo.exe : -np 2 ./xios_server.exe
```

### Control of XIOS: the XIOS context in `iodef.xml`

As well as the `using_server` flag, other controls on the use of XIOS are set in the XIOS context in `iodef.xml`. See the XML basics section below for more details on XML syntax and rules.

variable name	description	example
<code>buffer_size</code>	buffer size used by XIOS to send data from NEMO to XIOS. Larger is more efficient. Note that needed/used buffer sizes are summarized at the end of the job	25000000
<code>buffer_server_factor_size</code>	ratio between NEMO and XIOS buffer size. Should be 2.	2
<code>info_level</code>	verbosity level (0 to 100)	0
<code>using_server</code>	activate attached(false) or detached(true) mode	true
<code>using_oasis</code>	XIOS is used with OASIS(true) or not (false)	false
<code>oasis_codes_id</code>	when using oasis, define the identifier of NEMO in the <code>namcouple</code> . Note that the identifier of XIOS is <code>xios.x</code>	oceanx

## 11.2.2 Practical issues

### Installation

As mentioned, XIOS is supported separately and must be downloaded and compiled before it can be used with NEMO. See the installation guide on the [XIOS](#) wiki for help and guidance. NEMO will need to link to the compiled XIOS library. The [XIOS with NEMO](#) guide provides an example illustration of how this can be achieved.

### Add your own outputs

It is very easy to add your own outputs with `iomput`. Many standard fields and diagnostics are already prepared (*i.e.*, steps 1 to 3 below have been done) and simply need to be activated by including the required output in a file definition in `iodef.xml` (step 4). To add new output variables, all 4 of the following steps must be taken.

1. in NEMO code, add a
 

```
CALL iom_put( 'identifier', array )
```

 where you want to output a 2D or 3D array.
2. If necessary, add
 

```
USE iom ! I/O manager library
```

 to the list of used modules in the upper part of your module.
3. in the field\_def.xml file, add the definition of your variable using the same identifier you used in the f90 code (see subsequent sections for a details of the XML syntax and rules). For example:

```
<field_definition>
  <!-- T grid -->

  <field_group id="grid_T" grid_ref="grid_T_3D">
    ...
    <field id="identifier" long_name="blabla" ... />
    ...
  </field_definition>
```

Note your definition must be added to the field\_group whose reference grid is consistent with the size of the array passed to iomput. The grid\_ref attribute refers to definitions set in iodef.xml which, in turn, reference grids and axes either defined in the code (iom.set\_domain\_attr and iom.set\_axis\_attr in iom.F90) or defined in the domain\_def.xml file. *e.g.*:

```
<grid id="grid_T_3D" domain_ref="grid_T" axis_ref="deptht"/>
```

Note, if your array is computed within the surface module each nn\_fsbc time\_step, add the field definition within the field\_group defined with the id "SBC": <field\_group id="SBC"...> which has been defined with the correct frequency of operations (iom.set\_field\_attr in iom.F90)

4. add your field in one of the output files defined in iodef.xml (again see subsequent sections for syntax and rules)

```
<file id="file1" .../>
  ...
  <field field_ref="identifier" />
  ...
</file>
```

### 11.2.3 XML fundamentals

#### XML basic rules

XML tags begin with the less-than character ("<") and end with the greater-than character (">"). You use tags to mark the start and end of elements, which are

the logical units of information in an XML document. In addition to marking the beginning of an element, XML start tags also provide a place to specify attributes. An attribute specifies a single property for an element, using a name/value pair, for example: `<a b="x" c="y" b="z"> ... </a>`. See [here](#) for more details.

### Structure of the xml file used in NEMO

The XML file used in XIOS is structured by 7 families of tags: context, axis, domain, grid, field, file and variable. Each tag family has hierarchy of three flavors (except for context):

flavor	description	example
root	declaration of the root element that can contain element groups or elements	<code>&lt; file_definition ... &gt;</code>
group	declaration of a group element that can contain element groups or elements	<code>&lt; file_group ... &gt;</code>
element	declaration of an element that can contain elements	<code>&lt; file ... &gt;</code>

Each element may have several attributes. Some attributes are mandatory, other are optional but have a default value and other are completely optional. Id is a special attribute used to identify an element or a group of elements. It must be unique for a kind of element. It is optional, but no reference to the corresponding element can be done if it is not defined.

The XML file is split into context tags that are used to isolate IO definition from different codes or different parts of a code. No interference is possible between 2 different contexts. Each context has its own calendar and an associated timestep. In *NEMO*, we used the following contexts (that can be defined in any order):

context	description	example
context xios	context containing information for XIOS	<code>&lt;context id="xios" ...</code>
context nemo	context containing IO information for NEMO (mother grid when using AGRIF)	<code>&lt;context id="nemo" ...</code>
context l_nemo	context containing IO information for NEMO child grid 1 (when using AGRIF)	<code>&lt;context id="l_nemo" ...</code>
context n_nemo	context containing IO information for NEMO child grid n (when using AGRIF)	<code>&lt;context id="n_nemo" ...</code>

The xios context contains only 1 tag:

context tag	description	example
variable_definition	define variables needed by XIOS. This can be seen as a kind of namelist for XIOS.	<variable_definition ...

Each context tag related to NEMO (mother or child grids) is divided into 5 parts (that can be defined in any order):

context tag	description	example
field_definition	define all variables that can potentially be outputted	<field_definition ...
file_definition	define the netcdf files to be created and the variables they will contain	<file_definition ...
axis_definition	define vertical axis	<axis_definition ...
domain_definition	define the horizontal grids	<domain_definition ...
grid_definition	define the 2D and 3D grids (association of an axis and a domain)	<grid_definition ...

### Nesting XML files

The XML file can be split in different parts to improve its readability and facilitate its use. The inclusion of XML files into the main XML file can be done through the attribute src:

```
<context src="./nemo_def.xml" />
```

In NEMO, by default, the field and domain definition is done in 2 separate files:

```
NEMOGCM/CONFIG/SHARED/field_def.xml
and
NEMOGCM/CONFIG/SHARED/domain_def.xml
```

that are included in the main iodef.xml file through the following commands:

```
<field_definition src="./field_def.xml" />
<domain_definition src="./domain_def.xml" />
```

### Use of inheritance

XML extensively uses the concept of inheritance. XML has a tree based structure with a parent-child oriented relation: all children inherit attributes from parent, but an attribute defined in a child replace the inherited attribute value. Note that the special attribute "id" is never inherited.

example 1: Direct inheritance.

```

<field_definition operation="average" >
  <field id="sst" /> <!-- averaged sst -->
  <field id="sss" operation="instant"/> <!-- instantaneous sss -->
</field_definition>

```

The field "sst" which is part (or a child) of the field\_definition will inherit the value "average" of the attribute "operation" from its parent. Note that a child can overwrite the attribute definition inherited from its parents. In the example above, the field "sss" will for example output instantaneous values instead of average values.

example 2: Inheritance by reference.

```

<field_definition>
  <field id="sst" long_name="sea surface temperature" />
  <field id="sss" long_name="sea surface salinity" />
</field_definition>

<file_definition>
  <file id="myfile" output_freq="1d" />
  <field field_ref="sst" /> <!-- default def -->
  <field field_ref="sss" long_name="my description" /> <!-- overwrite -->
</file>
</file_definition>

```

Inherit (and overwrite, if needed) the attributes of a tag you are referring to.

### Use of Groups

Groups can be used for 2 purposes. Firstly, the group can be used to define common attributes to be shared by the elements of the group through inheritance. In the following example, we define a group of field that will share a common grid "grid\_T\_2D". Note that for the field "toce", we overwrite the grid definition inherited from the group by "grid\_T\_3D".

```

<field_group id="grid_T" grid_ref="grid_T_2D">
  <field id="toce" long_name="temperature" unit="degC" grid_ref="grid_T_3D"/>
  <field id="sst" long_name="sea surface temperature" unit="degC" />
  <field id="sss" long_name="sea surface salinity" unit="psu" />
  <field id="ssh" long_name="sea surface height" unit="m" />
  ...

```

Secondly, the group can be used to replace a list of elements. Several examples of groups of fields are proposed at the end of the file CONFIG/SHARED/field\_def.xml. For example, a short list of the usual variables related to the U grid:

```

<field_group id="groupU" >
  <field field_ref="uoce" />
  <field field_ref="suoce" />
  <field field_ref="utau" />
</field_group>

```

that can be directly included in a file through the following syntax:

```

<file id="myfile_U" output_freq="1d" />
  <field_group group_ref="groupU"/>
  <field field_ref="uocetr_eff" /> <!-- add another field -->
</file>

```

### 11.2.4 Detailed functionalities

The file `NEMOGCM/CONFIG/ORCA2_LIM/iodef_demo.xml` provides several examples of the use of the new functionalities offered by the XML interface of XIOS.

#### Define horizontal subdomains

Horizontal subdomains are defined through the attributes `zoom_ibegin`, `zoom_jbegin`, `zoom_ni`, `zoom_nj` of the tag family domain. It must therefore be done in the domain part of the XML file. For example, in `CONFIG/SHARED/domain_def.xml`, we provide the following example of a definition of a 5 by 5 box with the bottom left corner at point (10,10).

```
<domain_group id="grid_T">
  <domain id="myzoom" zoom_ibegin="10" zoom_jbegin="10" zoom_ni="5" zoom_nj="5" />
```

The use of this subdomain is done through the redefinition of the attribute `domain_ref` of the tag family field. For example:

```
<file id="myfile_vzoom" output_freq="1d" >
  <field field_ref="toce" domain_ref="myzoom"/>
</file>
```

Moorings are seen as an extrem case corresponding to a 1 by 1 subdomain. The Equatorial section, the TAO, RAMA and PIRATA moorings are already registered in the code and can therefore be outputted without taking care of their (i,j) position in the grid. These predefined domains can be activated by the use of specific `domain_ref`: "EqT", "EqU" or "EqW" for the equatorial sections and the mooring position for TAO, RAMA and PIRATA followed by "T" (for example: "8s137eT", "1.5s80.5eT" ...)

```
<file id="myfile_vzoom" output_freq="1d" >
  <field field_ref="toce" domain_ref="0n180wT"/>
</file>
```

Note that if the domain decomposition used in XIOS cuts the subdomain in several parts and if you use the "multiple\_file" type for your output files, you will end up with several files you will need to rebuild using unprovided tools (like `ncpdq` and `ncrcat`, see [nco manual](#)). We are therefore advising to use the "one\_file" type in this case.

#### Define vertical zooms

Vertical zooms are defined through the attributes `zoom_begin` and `zoom_end` of the tag family axis. It must therefore be done in the axis part of the XML file. For example, in `NEMOGCM/CONFIG/ORCA2_LIM/iodef_demo.xml`, we provide the following example:



```
<axis_group id="deptht" long_name="Vertical T levels" unit="m" positive="down" >
  <axis id="deptht" />
  <axis id="deptht_myzoom" zoom_begin="1" zoom_end="10" />
```

The use of this vertical zoom is done through the redefinition of the attribute `axis_ref` of the tag family field. For example:

```
<file id="myfile_hzoom" output_freq="1d" >
  <field field_ref="toce" axis_ref="deptht_myzoom"/>
</file>
```

### Control of the output file names

The output file names are defined by the attributes "name" and "name\_suffix" of the tag family file. for example:

```
<file_group id="1d" output_freq="1d" name="myfile_1d" >
  <file id="myfileA" name_suffix="_AAA" > <!-- will create file "myfile_1d_AAA" -->
  ...
</file>
  <file id="myfileB" name_suffix="_BBB" > <!-- will create file "myfile_1d_BBB" -->
  ...
</file>
</file_group>
```

However it is often very convenient to define the file name with the name of the experiment, the output file frequency and the date of the beginning and the end of the simulation (which are informations stored either in the namelist or in the XML file). To do so, we added the following rule: if the id of the tag file is "fileN" (where N = 1 to 999 on 1 to 3 digits) or one of the predefined sections or moorings (see next subsection), the following part of the name and the name\_suffix (that can be inherited) will be automatically replaced by:

placeholder string	automatically replaced by
@expname@	the experiment name (from <code>cn_exp</code> in the namelist)
@freq@	output frequency (from attribute <code>output_freq</code> )
@startdate@	starting date of the simulation (from <code>nn_date0</code> in the restart or the namelist). <code>yyyymmdd</code> format
@startdatefull@	starting date of the simulation (from <code>nn_date0</code> in the restart or the namelist). <code>yyyymmdd_hh:mm:ss</code> format
@enddate@	ending date of the simulation (from <code>nn_date0</code> and <code>nn_itend</code> in the namelist). <code>yyyymmdd</code> format
@enddatefull@	ending date of the simulation (from <code>nn_date0</code> and <code>nn_itend</code> in the namelist). <code>yyyymmdd_hh:mm:ss</code> format

For example,

```
<file id="myfile_hzoom" name="myfile_@expname@_@startdate@_freq@freq@" output_freq="1d" >
```

with the namelist:

```
cn_exp      = "ORCA2"
nn_date0    = 19891231
ln_rstart   = .false.
```

will give the following file name radical:

```
myfile_ORCA2_19891231_freq1d
```

### Other controls of the xml attributes from NEMO

The values of some attributes are defined by subroutine calls within NEMO (calls to `iom_set_domain_attr`, `iom_set_axis_attr` and `iom_set_field_attr` in `iom.F90`). Any definition given in the xml file will be overwritten. By convention, these attributes are defined to "auto" (for string) or "0000" (for integer) in the xml file (but this is not necessary).

Here is the list of these attributes:

tag ids affected by automatic definition of some of their attributes	name attribute	attribute value
field_definition	freq_op	<i>rn_rdt</i>
SBC	freq_op	<i>rn_rdt</i> × <i>nn_fsbc</i>
ptrc_T	freq_op	<i>rn_rdt</i> × <i>nn_dttrc</i>
diad_T	freq_op	<i>rn_rdt</i> × <i>nn_dttrc</i>
EqT, EqU, EqW	jbegin, ni, name_suffix	according to the grid
TAO, RAMA and PIRATA moorings	zoom_ibegin, zoom_jbegin, name_suffix	according to the grid

### Advanced use of XIOS functionalities

#### 11.2.5 XML reference tables

(1) Simple computation: directly define the computation when referring to the variable in the file definition.

```
<field field\_ref="sst" name="tosK" unit="degK" > sst + 273.15 </field>
<field field\_ref="taum" name="taum2" unit="N2/m4" long\_name="square of wind stress module" >
<field field\_ref="qt" name="stupid\_check" > qt - qsr - qns </field>
```

(2) Simple computation: define a new variable and use it in the file definition.  
in `field_definition`:

```
<field id="sst2" long\_name="square of sea surface temperature" unit="degC2" > sst * sst </fi
```

in `file_definition`:

```
<field field\_ref="sst2" > sst2 </field>
```

Note that in this case, the following syntaxe `<field field_ref="sst2" />` is not working as `sst2` won't be evaluated.

(3) Change of variable precision:

```
<!-- force to keep real 8 -->
<field field\_ref="sst" name="tos\_r8" prec="8" />
  <!-- integer 2 with add\_offset and scale\_factor attributes -->
<field field\_ref="sss" name="sos\_i2" prec="2" add\_offset="20." scale\_factor="1.e-3" />
```

Note that, then the code is crashing, writting real4 variables forces a numerical convection from real8 to real4 which will create an internal error in NetCDF and will avoid the creation of the output files. Forcing double precision outputs with `prec="8"` (for example in the `field_definition`) will avoid this problem.

(4) add user defined attributes:

```
<file\_group id="1d" output\_freq="1d" output\_level="10" enabled=".TRUE."> <!-- 1d files -->
<file id="file1" name\_suffix="\_grid\_T" description="ocean T grid variables" >
  <field field\_ref="sst" name="tos" >
    <variable id="my\_attribute1" type="string" > blabla </variable>
    <variable id="my\_attribute2" type="integer" > 3 </variable>
    <variable id="my\_attribute3" type="float" > 5.0 </variable>
  </field>
  <variable id="my\_global\_attribute" type="string" > blabla\_global </variable>
</file>
</file\_group>
```

(5) use of the “@” function: example 1, weighted temporal average

- define a new variable in `field_definition`

```
<field id="toce\_e3t" long\_name="temperature * e3t" unit="degC*m" grid\_ref="grid\_T\_3D" > toce * e3t
```

- use it when defining your file.

```
<file\_group id="5d" output\_freq="5d" output\_level="10" enabled=".TRUE." > <!-- 5d files -->
  <file id="file1" name\_suffix="\_grid\_T" description="ocean T grid variables" >
    <field field\_ref="toce" operation="instant" freq\_op="5d" > @toce\_e3t / @e3t </field>
  </file>
</file\_group>
```

The `freq_op="5d"` attribute is used to define the operation frequency of the “@” function: here 5 day. The temporal operation done by the “@” is the one defined in the field definition: here we use the default, average. So, in the above case, `@toce_e3t` will do the 5-day mean of `toce*e3t`. `Operation="instant"` refers to the temporal operation to be performed on the field “`@toce_e3t / @e3t`”: here the temporal average is already done by the “@” function so we just use `instant` to do the ratio of the 2 mean values. `field_ref="toce"` means that attributes not explicitly defined, are inherited from `toce` field. Note that in this case, `freq_op` must be equal to the file `output_freq`.

(6) use of the “@” function: example 2, monthly SSH standard deviation

- define a new variable in `field_definition`

```
<field id="ssh2" long\_name="square of sea surface temperature" unit="degC2" > ssh * ssh </field >
```

- use it when defining your file.

```
<file\_group id="1m" output\_freq="1m" output\_level="10" enabled=".TRUE." > <!-- 1m files --
<file id="file1" name\_suffix="\_grid\_T" description="ocean T grid variables" >
  <field field\_ref="ssh" name="sshstd" long\_name="sea\_surface\_temperature\_standard\_deviat
</file>
</file\_group>
```

The freq\_op="1m" attribute is used to define the operation frequency of the "@" function: here 1 month. The temporal operation done by the "@" is the one defined in the field definition: here we use the default, average. So, in the above case, @ssh2 will do the monthly mean of ssh\*ssh. Operation="instant" refers to the temporal operation to be performed on the field "sqrt( @ssh2 - @ssh \* @ssh)": here the temporal average is already done by the "@" function so we just use instant. field\_ref="ssh" means that attributes not explicitly defined, are inherited from ssh field. Note that in this case, freq\_op must be equal to the file output\_freq.

(7) use of the "@" function: example 3, monthly average of SST diurnal cycle  
- define 2 new variables in field\_definition

```
<field id="sstmax" field\_ref="sst" long\_name="max of sea surface temperature" operation="max
<field id="sstmin" field\_ref="sst" long\_name="min of sea surface temperature" operation="min
```

- use these 2 new variables when defining your file.

```
<file\_group id="1m" output\_freq="1m" output\_level="10" enabled=".TRUE." > <!-- 1m files --
<file id="file1" name\_suffix="\_grid\_T" description="ocean T grid variables" >
  <field field\_ref="sst" name="sstdcy" long\_name="amplitude of sst diurnal cycle" operation="
</file>
</file\_group>
```

The freq\_op="1d" attribute is used to define the operation frequency of the "@" function: here 1 day. The temporal operation done by the "@" is the one defined in the field definition: here maximum for sstmax and minimum for sstmin. So, in the above case, @sstmax will do the daily max and @sstmin the daily min. Operation="average" refers to the temporal operation to be performed on the field "@sstmax - @sstmin": here monthly mean (of daily max - daily min of the sst). field\_ref="sst" means that attributes not explicitly defined, are inherited from sst field.

### Tag list

tag name	description	accepted attribute	child of	parent of
simulation	this tag is the root tag which encapsulates all the content of the xml file	none	none	context

tag name	description	accepted attribute	child of	parent of
context	encapsulates parts of the xml file dedicated to different codes or different parts of a code	id ("xios", "nemo" or "n_nemo" for the nth AGRIF zoom), src, time_origin	simulation	all root tags: ... _definition
field_definition	encapsulates the definition of all the fields that can potentially be outputted	axis_ref, default_value, domain_ref, enabled, grid_ref, level, operation, prec, src	context	field or field_group
field_group	encapsulates a group of fields	axis_ref, default_value, domain_ref, enabled, group_ref, grid_ref, id, level, operation, prec, src	field_definition, field_group, file	field or field_group
field	define a specific field	axis_ref, default_value, domain_ref, enabled, field_ref, grid_ref, id, level, long_name, name, operation, prec, standard_name, unit	field_definition, field_group, file	none
file_definition	encapsulates the definition of all the files that will be outputted	enabled, min_digits, name, name_suffix, output_level, split_freq_format, split_freq, sync_freq, type, src	context	file or file_group
file_group	encapsulates a group of files that will be outputted	enabled, description, id, min_digits, name, name_suffix, output_freq, output_level, split_freq_format, split_freq, sync_freq, type, src	file_definition, file_group	file or file_group
file	define the contents of a file to be outputted	enabled, description, id, min_digits, name, name_suffix, output_freq, output_level, split_freq_format, split_freq, sync_freq, type, src	file_definition, file_group	file

tag name	description	accepted attribute	child of	parent of
axis_definition	define all the vertical axis potentially used by the variables	src	context	axis_group, axis
axis_group	encapsulates a group of vertical axis	id, lon_name, positive, src, standard_name, unit, zoom_begin, zoom_end, zoom_size	axis_definition, axis_group	axis_group, axis
axis	define a vertical axis	id, lon_name, positive, src, standard_name, unit, zoom_begin, zoom_end, zoom_size	axis_definition, axis_group	none
domain_definition	define all the horizontal domains potentially used by the variables	src	context	domain_group, domain
domain_group	encapsulates a group of horizontal domains	id, lon_name, src, zoom_ibegin, zoom_jbegin, zoom_ni, zoom_nj	domain_definition, domain_group	domain_group, domain
domain	define an horizontal domain	id, lon_name, src, zoom_ibegin, zoom_jbegin, zoom_ni, zoom_nj	domain_definition, domain_group	none
grid_definition	define all the grid (association of a domain and/or an axis) potentially used by the variables	src	context	grid_group, grid
grid_group	encapsulates a group of grids	id, domain_ref, axis_ref	grid_definition, grid_group	grid_group, grid
grid	define a grid	id, domain_ref, axis_ref	grid_definition, grid_group	none

**Attributes list**

attribute name	description	example	accepted by
axis_ref	refers to the id of a vertical axis	axis_ref="deptht"	field, grid families

attribute name	description	example	accepted by
enabled	switch on/off the output of a field or a file	enabled=".TRUE."	field, file families
default_value	missing_value definition	default_value="1.e20"	field family
description	just for information, not used	description="ocean T grid variables"	all tags
domain_ref	refers to the id of a domain	domain_ref="grid_T"	field or grid families
field_ref	id of the field we want to add in a file	field_ref="toce"	field
grid_ref	refers to the id of a grid	grid_ref="grid_T_2D"	field family
group_ref	refer to a group of variables	group_ref="mooring"	field_group
id	allow to identify a tag	id="nemo"	accepted by all tags except simulation
level	output priority of a field: 0 (high) to 10 (low)	level="1"	field family
long_name	define the long_name attribute in the NetCDF file	long_name="Vertical T levels"	field
min_digits	specify the minimum of digits used in the core number in the name of the NetCDF file	min_digits="4"	file family
name	name of a variable or a file. If the name of a file is undefined, its id is used as a name	name="tos"	field or file families
name_suffix	suffix to be inserted after the name and before the cpu number and the ".nc" termination of a file	name_suffix="_myzoom"	file family
attribute name	description	example	accepted by
operation	type of temporal operation: average, accumulate, instantaneous, min, max and once	operation="average"	field family
output_freq	operation frequency. units can be ts (timestep), y, mo, d, h, mi, s.	output_freq="1d12h"	field family

attribute name	description	example	accepted by
output_level	output priority of variables in a file: 0 (high) to 10 (low). All variables listed in the file with a level smaller or equal to output_level will be output. Other variables won't be output even if they are listed in the file.	output_level="10"	file family
positive	convention used for the orientation of vertical axis (positive downward in <i>NEMO</i> ).	positive="down"	axis family
prec	output precision: real 4 or real 8	prec="4"	field family
split_freq	frequency at which to temporally split output files. Units can be ts (timestep), y, mo, d, h, mi, s. Useful for long runs to prevent over-sized output files.	split_freq="1mo"	file family
split_freq_format	date format used in the name of temporally split output files. Can be specified using the following syntaxes: %y, %mo, %d, %h %mi and %s	split_freq_format="y%mo%d"	file family
src	allow to include a file	src="/field_def.xml"	accepted by all tags except simulation
standard_name	define the standard_name attribute in the NetCDF file	standard_name="Eastward_Sea_Ice_Transport"	field
sync_freq	NetCDF file synchronization frequency (update of the time_counter). units can be ts (timestep), y, mo, d, h, mi, s.	sync_freq="10d"	file family
attribute name	description	example	accepted by



attribute name	description	example	accepted by
time_origin	specify the origin of the time counter	time_origin="1900-01-01 00:00:00"	context
type (1)	specify if the output files are to be split spatially (multiple_file) or not (one_file)	type="multiple_file"	file family
type (2)	define the type of a variable tag	type="boolean"	variable
unit	unit of a variable or the vertical axis	unit="m"	field and axis families
zoom_ibegin	starting point along x direction of the zoom. Automatically defined for TAO/RAMA/PIRATA moorings	zoom_ibegin="1"	domain family
zoom_jbegin	starting point along y direction of the zoom. Automatically defined for TAO/RAMA/PIRATA moorings	zoom_jbegin="1"	domain family
zoom_ni	zoom extent along x direction	zoom_ni="1"	domain family
zoom_nj	zoom extent along y direction	zoom_nj="1"	domain family

### 11.2.6 CF metadata standard compliance

Output from the XIOS-1.0 IO server is compliant with [version 1.5](#) of the CF metadata standard. Therefore while a user may wish to add their own metadata to the output files (as demonstrated in example 4 of section [11.2.5](#)) the metadata should, for the most part, comply with the CF-1.5 standard.

Some metadata that may significantly increase the file size (horizontal cell areas and vertices) are controlled by the namelist parameter *ln\_cfmata* in the *namrun* namelist. This must be set to true if these metadata are to be included in the output files.

## 11.3 NetCDF4 Support (key\_netcdf4)

Since version 3.3, support for NetCDF4 chunking and (loss-less) compression has been included. These options build on the standard NetCDF output and allow the user control over the size of the chunks via namelist settings. Chunking and compression can lead to significant reductions in file sizes for a small runtime

overhead. For a fuller discussion on chunking and other performance issues the reader is referred to the NetCDF4 documentation found [here](#).

The new features are only available when the code has been linked with a NetCDF4 library (version 4.1 onwards, recommended) which has been built with HDF5 support (version 1.8.4 onwards, recommended). Datasets created with chunking and compression are not backwards compatible with NetCDF3 "classic" format but most analysis codes can be relinked simply with the new libraries and will then read both NetCDF3 and NetCDF4 files. NEMO executables linked with NetCDF4 libraries can be made to produce NetCDF3 files by setting the *ln\_nc4zip* logical to false in the *namnc4* namelist:

```
!-----
&namnc4      ! netcdf4 chunking and compression settings      ("key_netcdf4")
!-----
  nn_nchunks_i= 4      ! number of chunks in i-dimension
  nn_nchunks_j= 4      ! number of chunks in j-dimension
  nn_nchunks_k= 31     ! number of chunks in k-dimension
  !               ! setting nn_nchunks_k = jpk will give a chunk size of 1 in the vertical which
  !               ! is optimal for postprocessing which works exclusively with horizontal slabs
  ln_nc4zip = .true.   ! (T) use netcdf4 chunking and compression
  !               ! (F) ignore chunking information and produce netcdf3-compatible files
/
```

If **key\_netcdf4** has not been defined, these namelist parameters are not read. In this case, *ln\_nc4zip* is set false and dummy routines for a few NetCDF4-specific functions are defined. These functions will not be used but need to be included so that compilation is possible with NetCDF3 libraries.

When using NetCDF4 libraries, **key\_netcdf4** should be defined even if the intention is to create only NetCDF3-compatible files. This is necessary to avoid duplication between the dummy routines and the actual routines present in the library. Most compilers will fail at compile time when faced with such duplication. Thus when linking with NetCDF4 libraries the user must define **key\_netcdf4** and control the type of NetCDF file produced via the namelist parameter.

Chunking and compression is applied only to 4D fields and there is no advantage in chunking across more than one time dimension since previously written chunks would have to be read back and decompressed before being added to. Therefore, user control over chunk sizes is provided only for the three space dimensions. The user sets an approximate number of chunks along each spatial axis. The actual size of the chunks will depend on global domain size for mono-processors or, more likely, the local processor domain size for distributed processing. The derived values are subject to practical minimum values (to avoid wastefully small chunk sizes) and cannot be greater than the domain size in any dimension. The algorithm used is:

```
ichunksz(1) = MIN( idomain_size, MAX( (idomain_size-1)/nn_nchunks_i + 1, 16 ) )
ichunksz(2) = MIN( jdomain_size, MAX( (jdomain_size-1)/nn_nchunks_j + 1, 16 ) )
ichunksz(3) = MIN( kdomain_size, MAX( (kdomain_size-1)/nn_nchunks_k + 1, 1 ) )
ichunksz(4) = 1
```

As an example, setting:

```
nn_nchunks_i=4, nn_nchunks_j=4 and nn_nchunks_k=31
```

**Table 11.3:** Filesize comparison between NetCDF3 and NetCDF4 with chunking and compression

Filename	NetCDF3 filesize (KB)	NetCDF4 filesize (KB)	Reduction %
ORCA2_restart_0000.nc	16420	8860	47%
ORCA2_restart_0001.nc	16064	11456	29%
ORCA2_restart_0002.nc	16064	9744	40%
ORCA2_restart_0003.nc	16420	9404	43%
ORCA2_restart_0004.nc	16200	5844	64%
ORCA2_restart_0005.nc	15848	8172	49%
ORCA2_restart_0006.nc	15848	8012	50%
ORCA2_restart_0007.nc	16200	5148	69%
ORCA2_2d_grid_T_0000.nc	2200	1504	32%
ORCA2_2d_grid_T_0001.nc	2200	1748	21%
ORCA2_2d_grid_T_0002.nc	2200	1592	28%
ORCA2_2d_grid_T_0003.nc	2200	1540	30%
ORCA2_2d_grid_T_0004.nc	2200	1204	46%
ORCA2_2d_grid_T_0005.nc	2200	1444	35%
ORCA2_2d_grid_T_0006.nc	2200	1428	36%
ORCA2_2d_grid_T_0007.nc	2200	1148	48%
...	...	...	..
ORCA2_2d_grid_W_0000.nc	4416	2240	50%
ORCA2_2d_grid_W_0001.nc	4416	2924	34%
ORCA2_2d_grid_W_0002.nc	4416	2512	44%
ORCA2_2d_grid_W_0003.nc	4416	2368	47%
ORCA2_2d_grid_W_0004.nc	4416	1432	68%
ORCA2_2d_grid_W_0005.nc	4416	1972	56%
ORCA2_2d_grid_W_0006.nc	4416	2028	55%
ORCA2_2d_grid_W_0007.nc	4416	1368	70%

for a standard ORCA2.LIM configuration gives chunksizes of  $46 \times 38 \times 1$  respectively in the mono-processor case (i.e. global domain of  $182 \times 149 \times 31$ ). An illustration of the potential space savings that NetCDF4 chunking and compression provides is given in table 11.3 which compares the results of two short runs of the ORCA2.LIM reference configuration with a  $4 \times 2$  mpi partitioning. Note the variation in the compression ratio achieved which reflects chiefly the dry to wet volume ratio of each processing region.

When **key\_omput** is activated with **key\_netcdf4** chunking and compression parameters for fields produced via *iom\_put* calls are set via an equivalent and identically named namelist to *namnc4* in *xmlio\_server.def*. Typically this namelist serves the mean files whilst the *namnc4* in the main namelist file continues to serve the restart files. This duplication is unfortunate but appropriate since, if us-

ing `io_servers`, the domain sizes of the individual files produced by the `io_server` processes may be different to those produced by the individual processing regions and different chunking choices may be desired.

## 11.4 Tracer/Dynamics Trends (*namtrd*)

```

!-----
&namtrd      !   trend diagnostics                               (default F)
!-----
ln_glo_trd = .false.  ! (T) global domain averaged diag for T, T^2, KE, and PE
ln_dyn_trd = .false.  ! (T) 3D momentum trend output
ln_dyn_mxl = .false.  ! (T) 2D momentum trends averaged over the mixed layer (not coded yet)
ln_vor_trd = .false.  ! (T) 2D barotropic vorticity trends (not coded yet)
ln_KE_trd  = .false.  ! (T) 3D Kinetic Energy trends
ln_PE_trd  = .false.  ! (T) 3D Potential Energy trends
ln_tra_trd = .false.  ! (T) 3D tracer trend output
ln_tra_mxl = .false.  ! (T) 2D tracer trends averaged over the mixed layer (not coded yet)
nn_trd     = 365      ! print frequency (ln_glo_trd=T) (unit=time step)
/

```

Each trend of the dynamics and/or temperature and salinity time evolution equations can be sent to *trddyn.F90* and/or *trdra.F90* modules (see TRD directory) just after their computation (*i.e.* at the end of each *dyn...F90* and/or *tra...F90* routines). This capability is controlled by options offered in *namtrd* namelist. Note that the output are done with xIOS, and therefore the **key IOM** is required.

What is done depends on the *namtrd* logical set to *true*:

***ln\_glo\_trd*** : at each *nn\_trd* time-step a check of the basin averaged properties of the momentum and tracer equations is performed. This also includes a check of  $T^2$ ,  $S^2$ ,  $\frac{1}{2}(u^2 + v^2)$ , and potential energy time evolution equations properties ;

***ln\_dyn\_trd*** : each 3D trend of the evolution of the two momentum components is output ;

***ln\_dyn\_mxl*** : each 3D trend of the evolution of the two momentum components averaged over the mixed layer is output ;

***ln\_vor\_trd*** : a vertical summation of the moment tendencies is performed, then the curl is computed to obtain the barotropic vorticity tendencies which are output ;

***ln\_KE\_trd*** : each 3D trend of the Kinetic Energy equation is output ;

***ln\_tra\_trd*** : each 3D trend of the evolution of temperature and salinity is output ;

***ln\_tra\_mxl*** : each 2D trend of the evolution of temperature and salinity averaged over the mixed layer is output ;

Note that the mixed layer tendency diagnostic can also be used on biogeochemical models via the **key\_trdtrc** and **key\_trdmld\_trc** CPP keys.

**Note that** in the current version (v3.6), many changes has been introduced but not fully tested. In particular, options associated with *ln\_dyn\_mxl*, *ln\_vor\_trd*, and

*ln\_tra\_mxl* are not working, and none of the option have been tested with variable volume (*i.e.* **key\_vvl** defined).

## 11.5 On-line Floats trajectories (FLO) (key\_floats)

```

!-----
&namflo      !   float parameters                                ("key_float")
!-----
!-----
jpnfl       = 1          ! total number of floats during the run
jpnnewflo   = 0          ! number of floats for the restart
ln_rstflo   = .false.   ! float restart (T) or not (F)
nn_writefl  = 75        ! frequency of writing in float output file
nn_stockfl  = 5475      ! frequency of creation of the float restart file
ln_argo     = .false.   ! Argo type floats (stay at the surface each 10 days)
ln_flork4   = .false.   ! trajectories computed with a 4th order Runge-Kutta (T)
!           ! or computed with Blanke' scheme (F)
ln_ariane   = .true.    ! Input with Ariane tool convention(T)
ln_flo_ascii= .true.    ! Output with Ariane tool netcdf convention(F) or ascii file (T)
/

```

The on-line computation of floats advected either by the three dimensional velocity field or constraint to remain at a given depth ( $w = 0$  in the computation) have been introduced in the system during the CLIPPER project. Options are defined by *namflo* namelis variables. The algorithm used is based either on the work of [Blanke and Raynaud \[1997\]](#) (default option), or on a 4<sup>th</sup> Runge-Hutta algorithm (*ln\_flork4=true*). Note that the [Blanke and Raynaud \[1997\]](#) algorithm have the advantage of providing trajectories which are consistent with the numeric of the code, so that the trajectories never intercept the bathymetry.

### Input data: initial coordinates

Initial coordinates can be given with Ariane Tools convention ( IJK coordinates ,(*ln\_ariane=true*) ) or with longitude and latitude.

In case of Ariane convention, input filename is *init\_float\_ariane*. Its format is:

```
I J K nisobfl itrash itrash
```

with:

- I,J,K : indexes of initial position
- nisobfl: 0 for an isobar float, 1 for a float following the w velocity
- itrash : set to zero; it is a dummy variable to respect Ariane Tools convention
- itrash :set to zero; it is a dummy variable to respect Ariane Tools convention

Example:

```

100.00000 90.00000 -1.50000 1.00000 0.00000
102.00000 90.00000 -1.50000 1.00000 0.00000
104.00000 90.00000 -1.50000 1.00000 0.00000
106.00000 90.00000 -1.50000 1.00000 0.00000
108.00000 90.00000 -1.50000 1.00000 0.00000

```

In the other case ( longitude and latitude ), input filename is *init\_float*. Its format is:

```
Long Lat depth nisobfl ngrpfl itrash
```

with:

- Long, Lat, depth : Longitude, latitude, depth
- nisobfl: 0 for an isobar float, 1 for a float following the w velocity
- ngrpfl : number to identify searcher group
- itrash :set to 1; it is a dummy variable.

Example:

```
20.0 0.0 0.0 0 1 1
-21.0 0.0 0.0 0 1 1
-22.0 0.0 0.0 0 1 1
-23.0 0.0 0.0 0 1 1
-24.0 0.0 0.0 0 1 1
```

*jpnfl* is the total number of floats during the run. When initial positions are read in a restart file ( *ln\_rstflo*= .TRUE. ), *jpnflnewflo* can be added in the initialization file.

### Output data

*mn\_writefl* is the frequency of writing in float output file and *nn\_stockfl* is the frequency of creation of the float restart file.

Output data can be written in ascii files (*ln\_flo\_ascii* = .TRUE. ). In that case, output filename is *trajec\_float*.

Another possibility of writing format is Netcdf (*ln\_flo\_ascii* = .FALSE. ). There are 2 possibilities:

- if (**key\_iomput**) is used, outputs are selected in *iodef.xml*. Here it is an example of specification to put in files description section:

```
<group id="ld_grid_T" name="auto" description="ocean T grid variables" > }
  <file id="floats" description="floats variables"> }\\
    <field ref="traj_lon" name="floats_longitude" freq_op="86400" />
    <field ref="traj_lat" name="floats_latitude" freq_op="86400" />
    <field ref="traj_dep" name="floats_depth" freq_op="86400" />
    <field ref="traj_temp" name="floats_temperature" freq_op="86400" />
    <field ref="traj_salt" name="floats_salinity" freq_op="86400" />
    <field ref="traj_dens" name="floats_density" freq_op="86400" />
    <field ref="traj_group" name="floats_group" freq_op="86400" />
  </file>
</group>
```

- if (**key\_iomput**) is not used, a file called *trajec\_float.nc* will be created by IOIPSL library.

See also [here](#) the web site describing the off-line use of this marvellous diagnostic tool.

## 11.6 Harmonic analysis of tidal constituents (key\_diaharm)

A module is available to compute the amplitude and phase of tidal waves. This on-line Harmonic analysis is activated with **key\_diaharm**. Some parameters are available in namelist *namdia\_harm* :

- *nit000\_han* is the first time step used for harmonic analysis
- *nitend\_han* is the last time step used for harmonic analysis
- *nstep\_han* is the time step frequency for harmonic analysis
- *nb\_ana* is the number of harmonics to analyse
- *tname* is an array with names of tidal constituents to analyse

*nit000\_han* and *nitend\_han* must be between *nit000* and *nitend* of the simulation. The restart capability is not implemented.

The Harmonic analysis solve the following equation:

$$h_i - A_0 + \sum_{j=1}^{nb\_ana} [A_j \cos(\nu_j t_j - \phi_j)] = e_i \quad (11.1)$$

With  $A_j, \nu_j, \phi_j$ , the amplitude, frequency and phase for each wave and  $e_i$  the error.  $h_i$  is the sea level for the time  $t_i$  and  $A_0$  is the mean sea level.

We can rewrite this equation:

$$h_i - A_0 + \sum_{j=1}^{nb\_ana} [C_j \cos(\nu_j t_j) + S_j \sin(\nu_j t_j)] = e_i \quad (11.2)$$

with  $A_j = \sqrt{C_j^2 + S_j^2}$  et  $\phi_j = \arctan(S_j/C_j)$ .

We obtain in output  $C_j$  and  $S_j$  for each tidal wave.

## 11.7 Transports across sections (key\_diadct)

```
!-----
&namdct      ! transports through some sections                                ("key_diadct")
!-----
  nn_dct      = 15      ! time step frequency for transports computing
  nn_dctwri   = 15      ! time step frequency for transports writing
  nn_secdebug= 112     !      0 : no section to debug
  !           !      -1 : debug all section
  !           !      0 < n : debug section number n
/
```

A module is available to compute the transport of volume, heat and salt through sections. This diagnostic is activated with **key\_diadct**.

Each section is defined by the coordinates of its 2 extremities. The pathways between them are constructed using tools which can be found in NEMOGCM/TOOLS/SECTIONS\_DIADCT and are written in a binary file *section\_ijglobal.diadct\_ORCA2\_LIM* which is later read in by NEMO to compute on-line transports.

The on-line transports module creates three output ascii files:

- *volume\_transport* for volume transports ( unit:  $10^6 m^3 s^{-1}$  )
- *heat\_transport* for heat transports ( unit:  $10^{15} W$  )
- *salt\_transport* for salt transports ( unit:  $10^9 Kgs^{-1}$  )

Namelist variables in *namdct* control how frequently the flows are summed and the time scales over which they are averaged, as well as the level of output for debugging:

*nn\_dct*: frequency of instantaneous transports computing  
*nn\_dctwri*: frequency of writing ( mean of instantaneous transports )  
*nn\_debug*: debugging of the section

### Creating a binary file containing the pathway of each section

In NEMOGCM/TOOLS/SECTIONS\_DIADCT/run, the file *list\_sections.ascii\_global* contains a list of all the sections that are to be computed (this list of sections is based on MERSEA project metrics).

Another file is available for the GYRE configuration ( *list\_sections.ascii\_GYRE*).

Each section is defined by:

```
long1 lat1 long2 lat2 nclass (ok/no)strpond (no)ice section_name
with:
```

- long1 lat1 , coordinates of the first extremity of the section;
- long2 lat2 , coordinates of the second extremity of the section;
- nclass the number of bounds of your classes (e.g. 3 bounds for 2 classes);
- okstrpond to compute heat and salt transport, nostrpond if no;
- ice to compute surface and volume ice transports, noice if no.

The results of the computing of transports, and the directions of positive and negative flow do not depend on the order of the 2 extremities in this file.

If nclass  $\neq$  0, the next lines contain the class type and the nclass bounds:

```
long1 lat1 long2 lat2 nclass (ok/no)strpond (no)ice section_name
classtype
zbound1
zbound2
.
.
nclass-1
nclass
```

where classtype can be:

- zsal for salinity classes
- ztem for temperature classes
- zlay for depth classes
- zsigi for insitu density classes
- zsigp for potential density classes

The script *job.ksh* computes the pathway for each section and creates a binary file *section\_ijglobal.diadct\_ORCA2\_LIM* which is read by NEMO.



It is possible to use this tools for new configurations: `job.ksh` has to be updated with the coordinates file name and path.

Examples of two sections, the ACC\_Drake\_Passage with no classes, and the ATL\_Cuba\_Florida with 4 temperature classes (5 class bounds), are shown:

```
-68.  -54.5 -60.  -64.7 00 okstrpond noice ACC_Drake_Passage
-80.5 22.5 -80.5 25.5 05 nostrpond noice ATL_Cuba_Florida
ztem
-2.0
 4.5
 7.0
12.0
40.0
```

### To read the output files

The output format is :

```
date, time-step number, section number, section name, section
slope coefficient, class number, class name, class bound 1 ,
classe bound2, transport_direction1 , transport_direction2, transport_total
```

For sections with classes, the first `nclass-1` lines correspond to the transport for each class and the last line corresponds to the total transport summed over all classes. For sections with no classes, class number 1 corresponds to total class and this class is called N, meaning none.

```
transport_direction1 is the positive part of the transport ( > = 0 ).
transport_direction2 is the negative part of the transport ( < = 0 ).
```

The section slope coefficient gives information about the significance of transports signs and direction:

section slope coefficient	section type	direction 1	direction 2	total transport
0.	horizontal	northward	southward	postive: northward
1000.	vertical	eastward	westward	postive: eastward
$\neq 0, \neq 1000.$	diagonal	eastward	westward	postive: eastward

## 11.8 Diagnosing the Steric effect in sea surface height

Changes in steric sea level are caused when changes in the density of the water column imply an expansion or contraction of the column. It is essentially produced through surface heating/cooling and to a lesser extent through non-linear effects of the equation of state (cabbeling, thermobaricity...). Non-Boussinesq models contain all ocean effects within the ocean acting on the sea level. In particular, they

include the steric effect. In contrast, Boussinesq models, such as *NEMO*, conserve volume, rather than mass, and so do not properly represent expansion or contraction. The steric effect is therefore not explicitly represented. This approximation does not represent a serious error with respect to the flow field calculated by the model [Greatbatch 1994], but extra attention is required when investigating sea level, as steric changes are an important contribution to local changes in sea level on seasonal and climatic time scales. This is especially true for investigation into sea level rise due to global warming.

Fortunately, the steric contribution to the sea level consists of a spatially uniform component that can be diagnosed by considering the mass budget of the world ocean [Greatbatch 1994]. In order to better understand how global mean sea level evolves and thus how the steric sea level can be diagnosed, we compare, in the following, the non-Boussinesq and Boussinesq cases.

Let denote  $\mathcal{M}$  the total mass of liquid seawater ( $\mathcal{M} = \int_D \rho dv$ ),  $\mathcal{V}$  the total volume of seawater ( $\mathcal{V} = \int_D dv$ ),  $\mathcal{A}$  the total surface of the ocean ( $\mathcal{A} = \int_S ds$ ),  $\bar{\rho}$  the global mean seawater (*in situ*) density ( $\bar{\rho} = 1/\mathcal{V} \int_D \rho dv$ ), and  $\bar{\eta}$  the global mean sea level ( $\bar{\eta} = 1/\mathcal{A} \int_S \eta ds$ ).

A non-Boussinesq fluid conserves mass. It satisfies the following relations:

$$\begin{aligned}\mathcal{M} &= \mathcal{V} \bar{\rho} \\ \mathcal{V} &= \mathcal{A} \bar{\eta}\end{aligned}\tag{11.3}$$

Temporal changes in total mass is obtained from the density conservation equation :

$$\frac{1}{e_3} \partial_t (e_3 \rho) + \nabla(\rho \mathbf{U}) = \frac{emp}{e_3} \Big|_{surface}\tag{11.4}$$

where  $\rho$  is the *in situ* density, and *emp* the surface mass exchanges with the other media of the Earth system (atmosphere, sea-ice, land). Its global averaged leads to the total mass change

$$\partial_t \mathcal{M} = \mathcal{A} \overline{emp}\tag{11.5}$$

where  $\overline{emp} = \int_S emp ds$  is the net mass flux through the ocean surface. Bringing (11.5) and the time derivative of (11.3) together leads to the evolution equation of the mean sea level

$$\partial_t \bar{\eta} = \frac{\overline{emp}}{\bar{\rho}} - \frac{\mathcal{V}}{\mathcal{A}} \frac{\partial_t \bar{\rho}}{\bar{\rho}}\tag{11.6}$$

The first term in equation (11.6) alters sea level by adding or subtracting mass from the ocean. The second term arises from temporal changes in the global mean density; *i.e.* from steric effects.

In a Boussinesq fluid,  $\rho$  is replaced by  $\rho_o$  in all the equation except when  $\rho$  appears multiplied by the gravity (*i.e.* in the hydrostatic balance of the primitive Equations). In particular, the mass conservation equation, (11.4), degenerates into the incompressibility equation:

$$\frac{1}{e_3} \partial_t (e_3) + \nabla(\mathbf{U}) = \frac{emp}{\rho_o e_3} \Big|_{surface}\tag{11.7}$$

and the global average of this equation now gives the temporal change of the total volume,

$$\partial_t \mathcal{V} = \mathcal{A} \frac{\overline{emp}}{\rho_o} \quad (11.8)$$

Only the volume is conserved, not mass, or, more precisely, the mass which is conserved is the Boussinesq mass,  $\mathcal{M}_o = \rho_o \mathcal{V}$ . The total volume (or equivalently the global mean sea level) is altered only by net volume fluxes across the ocean surface, not by changes in mean mass of the ocean: the steric effect is missing in a Boussinesq fluid.

Nevertheless, following [Greatbatch 1994], the steric effect on the volume can be diagnosed by considering the mass budget of the ocean. The apparent changes in  $\mathcal{M}$ , mass of the ocean, which are not induced by surface mass flux must be compensated by a spatially uniform change in the mean sea level due to expansion/contraction of the ocean [Greatbatch 1994]. In others words, the Boussinesq mass,  $\mathcal{M}_o$ , can be related to  $\mathcal{M}$ , the total mass of the ocean seen by the Boussinesq model, via the steric contribution to the sea level,  $\eta_s$ , a spatially uniform variable, as follows:

$$\mathcal{M}_o = \mathcal{M} + \rho_o \eta_s \mathcal{A} \quad (11.9)$$

Any change in  $\mathcal{M}$  which cannot be explained by the net mass flux through the ocean surface is converted into a mean change in sea level. Introducing the total density anomaly,  $\mathcal{D} = \int_D d_a dv$ , where  $d_a = (\rho - \rho_o)/\rho_o$  is the density anomaly used in *NEMO* (cf. §5.8.1) in (11.9) leads to a very simple form for the steric height:

$$\eta_s = -\frac{1}{\mathcal{A}} \mathcal{D} \quad (11.10)$$

The above formulation of the steric height of a Boussinesq ocean requires four remarks. First, one can be tempted to define  $\rho_o$  as the initial value of  $\mathcal{M}/\mathcal{V}$ , *i.e.* set  $\mathcal{D}_{t=0} = 0$ , so that the initial steric height is zero. We do not recommend that. Indeed, in this case  $\rho_o$  depends on the initial state of the ocean. Since  $\rho_o$  has a direct effect on the dynamics of the ocean (it appears in the pressure gradient term of the momentum equation) it is definitively not a good idea when inter-comparing experiments. We better recommend to fixe once for all  $\rho_o$  to  $1035 \text{ Kg m}^{-3}$ . This value is a sensible choice for the reference density used in a Boussinesq ocean climate model since, with the exception of only a small percentage of the ocean, density in the World Ocean varies by no more than 2% from this value (Gill [1982], page 47).

Second, we have assumed here that the total ocean surface,  $\mathcal{A}$ , does not change when the sea level is changing as it is the case in all global ocean GCMs (wetting and drying of grid point is not allowed).

Third, the discretisation of (11.10) depends on the type of free surface which is considered. In the non linear free surface case, *i.e.* **key\_vvl** defined, it is given by

$$\eta_s = -\frac{\sum_{i,j,k} d_a e_{1t} e_{2t} e_{3t}}{\sum_{i,j,k} e_{1t} e_{2t} e_{3t}} \quad (11.11)$$

whereas in the linear free surface, the volume above the  $z=0$  surface must be explicitly taken into account to better approximate the total ocean mass and thus the steric sea level:

$$\eta_s = -\frac{\sum_{i,j,k} d_a e_{1t} e_{2t} e_{3t} + \sum_{i,j} d_a e_{1t} e_{2t} \eta}{\sum_{i,j,k} e_{1t} e_{2t} e_{3t} + \sum_{i,j} e_{1t} e_{2t} \eta} \quad (11.12)$$

The fourth and last remark concerns the effective sea level and the presence of sea-ice. In the real ocean, sea ice (and snow above it) depresses the liquid seawater through its mass loading. This depression is a result of the mass of sea ice/snow system acting on the liquid ocean. There is, however, no dynamical effect associated with these depressions in the liquid ocean sea level, so that there are no associated ocean currents. Hence, the dynamically relevant sea level is the effective sea level, *i.e.* the sea level as if sea ice (and snow) were converted to liquid seawater [Campin et al. 2008]. However, in the current version of *NEMO* the sea-ice is levitating above the ocean without mass exchanges between ice and ocean. Therefore the model effective sea level is always given by  $\eta + \eta_s$ , whether or not there is sea ice present.

In AR5 outputs, the thermosteric sea level is demanded. It is steric sea level due to changes in ocean density arising just from changes in temperature. It is given by:

$$\eta_s = -\frac{1}{\mathcal{A}} \int_D d_a(T, S_o, p_o) dv \quad (11.13)$$

where  $S_o$  and  $p_o$  are the initial salinity and pressure, respectively.

Both steric and thermosteric sea level are computed in *diaar5.F90* which needs the **key\_diaar5** defined to be called.

## 11.9 Other Diagnostics (**key\_diahth**, **key\_diaar5**)

Aside from the standard model variables, other diagnostics can be computed on-line. The available ready-to-add diagnostics modules can be found in directory DIA.

### 11.9.1 Depth of various quantities (*diahth.F90*)

Among the available diagnostics the following ones are obtained when defining the **key\_diahth** CPP key:

- the mixed layer depth (based on a density criterion [de Boyer Montégut et al. 2004]) (*diahth.F90*)
- the turbocline depth (based on a turbulent mixing coefficient criterion) (*diahth.F90*)
- the depth of the 20°C isotherm (*diahth.F90*)
- the depth of the thermocline (maximum of the vertical temperature gradient) (*diahth.F90*)

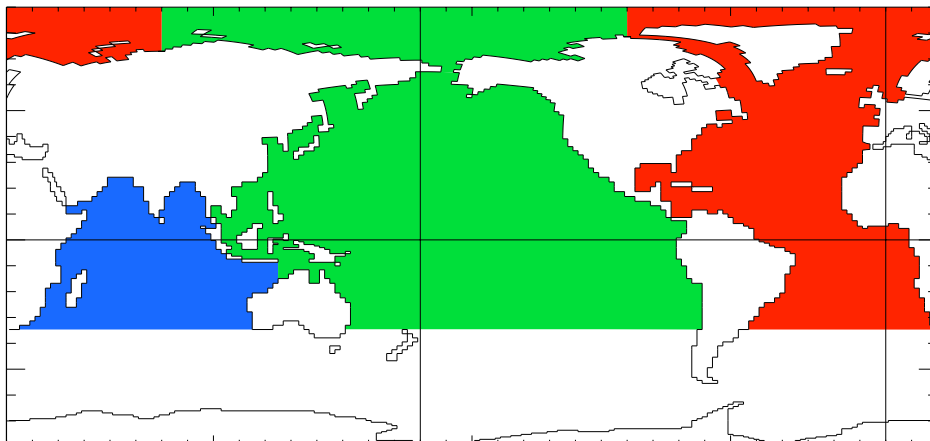


**Figure 11.1:** Decomposition of the World Ocean (here ORCA2) into sub-basin used in to compute the heat and salt transports as well as the meridional stream-function: Atlantic basin (red), Pacific basin (green), Indian basin (bleue), Indo-Pacific basin (bleue+green). Note that semi-enclosed seas (Red, Med and Baltic seas) as well as Hudson Bay are removed from the sub-basins. Note also that the Arctic Ocean has been split into Atlantic and Pacific basins along the North fold line.

### 11.9.2 Poleward heat and salt transports (*diaptr.F90*)

```
!-----
&namptr      ! Poleward Transport Diagnostic (default F)
!-----
  ln_diaptr   = .false.  ! Poleward heat and salt transport (T) or not (F)
  ln_subbas   = .false.  ! Atlantic/Pacific/Indian basins computation (T) or not
/
```

The poleward heat and salt transports, their advective and diffusive component, and the meridional stream function can be computed on-line in *diaptr.F90* *ln\_diaptr* to true (see the *namptr* namelist below). When *ln\_subbas* = true, transports and stream function are computed for the Atlantic, Indian, Pacific and Indo-Pacific Oceans (defined north of 30°S) as well as for the World Ocean. The sub-basin decomposition requires an input file (*subbasins.nc*) which contains three 2D mask arrays, the Indo-Pacific mask been deduced from the sum of the Indian and Pacific mask (Fig 11.1).

### 11.9.3 CMIP specific diagnostics (*diaar5.F90*)

A series of diagnostics has been added in the *diaar5.F90*. They corresponds to outputs that are required for AR5 simulations (CMIP5) (see also Section 11.8 for one of them). Activating those outputs requires to define the **key\_diaar5** CPP key.

### 11.9.4 25 hour mean output for tidal models

```
!-----
```

```

&nam_dia25h ! 25h Mean Output (default F)
!-----
ln_dia25h = .false. ! Choose 25h mean output or not
/

```

A module is available to compute a crudely detided M2 signal by obtaining a 25 hour mean. The 25 hour mean is available for daily runs by summing up the 25 hourly instantaneous hourly values from midnight at the start of the day to midnight at the day end. This diagnostic is activated with the logical *ln\_dia25h*

### 11.9.5 Top Middle and Bed hourly output

```

!-----
&nam_diatmb ! Top Middle Bottom Output (default F)
!-----
ln_diatmb = .false. ! Choose Top Middle and Bottom output or not
/

```

A module is available to output the surface (top), mid water and bed diagnostics of a set of standard variables. This can be a useful diagnostic when hourly or sub-hourly output is required in high resolution tidal outputs. The tidal signal is retained but the overall data usage is cut to just three vertical levels. Also the bottom level is calculated for each cell. This diagnostic is activated with the logical *ln\_diatmb*

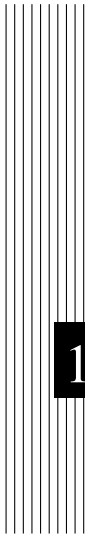
### 11.9.6 Courant numbers

Courant numbers provide a theoretical indication of the model's numerical stability. The advective Courant numbers can be calculated according to

$$C_u = |u| \frac{\Delta t}{e_{1u}}, \quad C_v = |v| \frac{\Delta t}{e_{2v}}, \quad C_w = |w| \frac{\Delta t}{e_{3w}} \quad (11.14)$$

in the zonal, meridional and vertical directions respectively. The vertical component is included although it is not strictly valid as the vertical velocity is calculated from the continuity equation rather than as a prognostic variable. Physically this represents the rate at which information is propagated across a grid cell. Values greater than 1 indicate that information is propagated across more than one grid cell in a single time step.

The variables can be activated by setting the *nn\_diacfl* namelist parameter to 1 in the *namctl* namelist. The diagnostics will be written out to an ascii file named *cfl\_diagnostics.ascii*. In this file the maximum value of  $C_u$ ,  $C_v$ , and  $C_w$  are printed at each timestep along with the coordinates of where the maximum value occurs. At the end of the model run the maximum value of  $C_u$ ,  $C_v$ , and  $C_w$  for the whole model run is printed along with the coordinates of each. The maximum values from the run are also copied to the *ocean.output* file.



# 12 Observation and model comparison (OBS)

Authors: D. Lea, M. Martin, K. Mogensen, A. Vidard, A. Weaver, A. Ryan, ...

## Contents

---

<b>12.1</b>	<b>Running the observation operator code example</b>	<b>246</b>
<b>12.2</b>	<b>Technical details</b>	<b>247</b>
12.2.1	Profile feedback type observation file header	248
12.2.2	Sea level anomaly feedback type observation file header	250
12.2.3	Sea surface temperature feedback type observation file header	252
<b>12.3</b>	<b>Theoretical details</b>	<b>253</b>
12.3.1	Horizontal interpolation methods	253
12.3.2	Grid search	255
12.3.3	Parallel aspects of horizontal interpolation	255
12.3.4	Vertical interpolation operator	258
<b>12.4</b>	<b>Offline observation operator</b>	<b>259</b>
12.4.1	Concept	259
12.4.2	Using the offline observation operator	259
12.4.3	Configuring the offline observation operator	260
12.4.4	Advanced usage	264
<b>12.5</b>	<b>Observation Utilities</b>	<b>265</b>
12.5.1	Obstools	265
12.5.2	building the obstools	268
12.5.3	Dataplot	268

---

The observation and model comparison code (OBS) reads in observation files (profile temperature and salinity, sea surface temperature, sea level anomaly, sea ice concentration, and velocity) and calculates an interpolated model equivalent value at the observation location and nearest model timestep. The resulting data are saved in a “feedback” file (or files). The code was originally developed for use with the NEMOVAR data assimilation code, but can be used for validation or verification of the model or with any other data assimilation system.

The OBS code is called from *nemogcm.F90* for model initialisation and to calculate the model equivalent values for observations on the 0th timestep. The code is then called again after each timestep from *step.F90*. The code is only activated if the namelist logical *ln\_diaobs* is set to true.

For all data types a 2D horizontal interpolator is needed to interpolate the model fields to the observation location. For *in situ* profiles, a 1D vertical interpolator is needed in addition to provide model fields at the observation depths. Currently this only works in z-level model configurations, but is being developed to work with a generalised vertical coordinate system.

Some profile observation types (e.g. tropical moored buoys) are made available as daily averaged quantities. The observation operator code can be set-up to calculate the equivalent daily average model temperature fields using the *nn\_profdavtypes* namelist array. Some SST observations are equivalent to a night-time average value and the observation operator code can calculate equivalent night-time average model SST fields by setting the namelist value *ln\_sstnight* to true. Otherwise the model value from the nearest timestep to the observation time is used.

The code is controlled by the namelist *nam\_obs*. See the following sections for more details on setting up the namelist.

Section 12.1 introduces a test example of the observation operator code including where to obtain data and how to setup the namelist. Section 12.2 introduces some more technical details of the different observation types used and also shows a more complete namelist. Section 12.3 introduces some of the theoretical aspects of the observation operator including interpolation methods and running on multiple processors. Section 12.4 describes the offline observation operator code. Section 12.5 introduces some utilities to help working with the files produced by the OBS code.

## 12.1 Running the observation operator code example

This section describes an example of running the observation operator code using profile data which can be freely downloaded. It shows how to adapt an existing run and build of NEMO to run the observation operator.

1. Compile NEMO.



2. Download some EN4 data from <http://www.metoffice.gov.uk/hadobs>. Choose observations which are valid for the period of your test run because the observation operator compares the model and observations for a matching date and time.
3. Compile the OBSTOOLS code using:

```
./maketools -n OBSTOOLS -m [ARCH].
```

4. Convert the EN4 data into feedback format:

```
enact2fb.exe profiles_01.nc EN.4.1.1.f.profiles.g10.YYYYMM.nc
```

5. Include the following in the NEMO namelist to run the observation operator on this data:

Options are defined through the *namobs* namelist variables. The options *ln\_t3d* and *ln\_s3d* switch on the temperature and salinity profile observation operator code. The filename or array of filenames are specified using the *cn\_prof\_files* variable. The model grid points for a particular observation latitude and longitude are found using the grid searching part of the code. This can be expensive, particularly for large numbers of observations, setting *ln\_grid\_search\_lookup* allows the use of a lookup table which is saved into an “xypos” file (or files). This will need to be generated the first time if it does not exist in the run directory. However, once produced it will significantly speed up future grid searches. Setting *ln\_grid\_global* means that the code distributes the observations evenly between processors. Alternatively each processor will work with observations located within the model subdomain (see section 12.3.3).

A number of utilities are now provided to plot the feedback files, convert and recombine the files. These are explained in more detail in section 12.5. Utilities to convert other input data formats into the feedback format are also described in section 12.5.

## 12.2 Technical details

Here we show a more complete example namelist *namobs* and also show the NetCDF headers of the observation files that may be used with the observation operator

```
!-----
&namobs      ! observation usage switch
!-----
ln_diaobs   = .false.      ! Logical switch for the observation operator
ln_t3d     = .false.      ! Logical switch for T profile observations
ln_s3d     = .false.      ! Logical switch for S profile observations
ln_sla     = .false.      ! Logical switch for SLA observations
ln_sst     = .false.      ! Logical switch for SST observations
ln_sic     = .false.      ! Logical switch for Sea Ice observations
ln_vel3d   = .false.      ! Logical switch for velocity observations
```

```

ln_altbias = .false.           ! Logical switch for altimeter bias correction
ln_nea     = .false.           ! Logical switch for rejection of observations near land
ln_grid_global = .true.        ! Logical switch for global distribution of observations
ln_grid_search_lookup = .false. ! Logical switch for obs grid search w/lookup table
ln_ignmis  = .true.           ! Logical switch for ignoring missing files
ln_s_at_t  = .false.          ! Logical switch for computing model S at T obs if not there
ln_sstnight = .false.         ! Logical switch for calculating night-time average for SST obs
! All of the *files* variables below are arrays. Use namelist_cfg to add more files
cn_profbf_files = 'profiles_01.nc' ! Profile feedback input observation file names
cn_slafbf_files = 'sla_01.nc'      ! SLA feedback input observation file names
cn_sstfb_files = 'sst_01.nc'      ! SST feedback input observation file names
cn_sicfb_files = 'sic_01.nc'      ! SIC feedback input observation file names
cn_velfb_files = 'vel_01.nc'      ! Velocity feedback input observation file names
cn_altbiasfile = 'altbias.nc'     ! Altimeter bias input file name
cn_gridsearchfile='gridsearch.nc' ! Grid search file name
rn_gridsearchres = 0.5            ! Grid search resolution
rn_dobsini       = 00010101.000000 ! Initial date in window YYYYMMDD.HHMMSS
rn_dobsend       = 00010102.000000 ! Final date in window YYYYMMDD.HHMMSS
nn_ldint         = 0               ! Type of vertical interpolation method
nn_2dint         = 0               ! Type of horizontal interpolation method
nn_msshc         = 0               ! MSSH correction scheme
rn_mdtdcorr      = 1.61            ! MDT correction
rn_mdtdcutoff    = 65.0            ! MDT cutoff for computed correction
nn_profdavtypes = -1              ! Profile daily average types - array
ln_sstbias       = .false.         !
cn_sstbias_files = 'sstbias.nc'   !
/

```

The observation operator code uses the "feedback" observation file format for all data types. All the observation files must be in NetCDF format. Some example headers (produced using *ncdump -h*) for profile data, sea level anomaly and sea surface temperature are in the following subsections.

### 12.2.1 Profile feedback type observation file header

```

netcdf profiles_01 {
dimensions:
    N_OBS = 603 ;
    N_LEVELS = 150 ;
    N_VARS = 2 ;
    N_QCF = 2 ;
    N_ENTRIES = 1 ;
    N_EXTRA = 1 ;
    STRINGNAM = 8 ;
    STRINGGRID = 1 ;
    STRINGWMO = 8 ;
    STRINGTYP = 4 ;
    STRINGJULD = 14 ;
variables:
    char VARIABLES(N_VARS, STRINGNAM) ;
        VARIABLES:long_name = "List of variables in feedback files" ;
    char ENTRIES(N_ENTRIES, STRINGNAM) ;
        ENTRIES:long_name = "List of additional entries for each variable in feedback files" ;
    char EXTRA(N_EXTRA, STRINGNAM) ;
        EXTRA:long_name = "List of extra variables" ;
    char STATION_IDENTIFIER(N_OBS, STRINGWMO) ;
        STATION_IDENTIFIER:long_name = "Station identifier" ;
    char STATION_TYPE(N_OBS, STRINGTYP) ;
        STATION_TYPE:long_name = "Code instrument type" ;
    double LONGITUDE(N_OBS) ;
        LONGITUDE:long_name = "Longitude" ;
        LONGITUDE:units = "degrees_east" ;
        LONGITUDE:_Fillvalue = 99999.f ;
    double LATITUDE(N_OBS) ;
        LATITUDE:long_name = "Latitude" ;
        LATITUDE:units = "degrees_north" ;
        LATITUDE:_Fillvalue = 99999.f ;
    double DEPTH(N_OBS, N_LEVELS) ;
        DEPTH:long_name = "Depth" ;
        DEPTH:units = "metre" ;
        DEPTH:_Fillvalue = 99999.f ;
    int DEPTH_QC(N_OBS, N_LEVELS) ;
        DEPTH_QC:long_name = "Quality on depth" ;
        DEPTH_QC:Conventions = "q where q=[0,9]" ;
        DEPTH_QC:_Fillvalue = 0 ;
    int DEPTH_QC_FLAGS(N_OBS, N_LEVELS, N_QCF) ;

```

```

DEPTH_QC_FLAGS:long_name = "Quality flags on depth" ;
DEPTH_QC_FLAGS:Conventions = "NEMOVAR flag conventions" ;
double JULD(N_OBS) ;
JULD:long_name = "Julian day" ;
JULD:units = "days since JULD_REFERENCE" ;
JULD:Conventions = "relative julian days with decimal part (as parts of day)" ;
JULD:Fillvalue = 99999.f ;
char JULD_REFERENCE(StringJULD) ;
JULD_REFERENCE:long_name = "Date of reference for julian days" ;
JULD_REFERENCE:Conventions = "YYYYMMDDHHMMSS" ;
int OBSERVATION_QC(N_OBS) ;
OBSERVATION_QC:long_name = "Quality on observation" ;
OBSERVATION_QC:Conventions = "q where q =[0,9]" ;
OBSERVATION_QC:Fillvalue = 0 ;
int OBSERVATION_QC_FLAGS(N_OBS, N_QCF) ;
OBSERVATION_QC_FLAGS:long_name = "Quality flags on observation" ;
OBSERVATION_QC_FLAGS:Conventions = "NEMOVAR flag conventions" ;
OBSERVATION_QC_FLAGS:Fillvalue = 0 ;
int POSITION_QC(N_OBS) ;
POSITION_QC:long_name = "Quality on position (latitude and longitude)" ;
POSITION_QC:Conventions = "q where q =[0,9]" ;
POSITION_QC:Fillvalue = 0 ;
int POSITION_QC_FLAGS(N_OBS, N_QCF) ;
POSITION_QC_FLAGS:long_name = "Quality flags on position" ;
POSITION_QC_FLAGS:Conventions = "NEMOVAR flag conventions" ;
POSITION_QC_FLAGS:Fillvalue = 0 ;
int JULD_QC(N_OBS) ;
JULD_QC:long_name = "Quality on date and time" ;
JULD_QC:Conventions = "q where q =[0,9]" ;
JULD_QC:Fillvalue = 0 ;
int JULD_QC_FLAGS(N_OBS, N_QCF) ;
JULD_QC_FLAGS:long_name = "Quality flags on date and time" ;
JULD_QC_FLAGS:Conventions = "NEMOVAR flag conventions" ;
JULD_QC_FLAGS:Fillvalue = 0 ;
int ORIGINAL_FILE_INDEX(N_OBS) ;
ORIGINAL_FILE_INDEX:long_name = "Index in original data file" ;
ORIGINAL_FILE_INDEX:Fillvalue = -99999 ;
float POTM_OBS(N_OBS, N_LEVELS) ;
POTM_OBS:long_name = "Potential temperature" ;
POTM_OBS:units = "Degrees Celsius" ;
POTM_OBS:Fillvalue = 99999.f ;
float POTM_Hx(N_OBS, N_LEVELS) ;
POTM_Hx:long_name = "Model interpolated potential temperature" ;
POTM_Hx:units = "Degrees Celsius" ;
POTM_Hx:Fillvalue = 99999.f ;
int POTM_QC(N_OBS) ;
POTM_QC:long_name = "Quality on potential temperature" ;
POTM_QC:Conventions = "q where q =[0,9]" ;
POTM_QC:Fillvalue = 0 ;
int POTM_QC_FLAGS(N_OBS, N_QCF) ;
POTM_QC_FLAGS:long_name = "Quality flags on potential temperature" ;
POTM_QC_FLAGS:Conventions = "NEMOVAR flag conventions" ;
POTM_QC_FLAGS:Fillvalue = 0 ;
int POTM_LEVEL_QC(N_OBS, N_LEVELS) ;
POTM_LEVEL_QC:long_name = "Quality for each level on potential temperature" ;
POTM_LEVEL_QC:Conventions = "q where q =[0,9]" ;
POTM_LEVEL_QC:Fillvalue = 0 ;
int POTM_LEVEL_QC_FLAGS(N_OBS, N_LEVELS, N_QCF) ;
POTM_LEVEL_QC_FLAGS:long_name = "Quality flags for each level on potential temperature" ;
POTM_LEVEL_QC_FLAGS:Conventions = "NEMOVAR flag conventions" ;
POTM_LEVEL_QC_FLAGS:Fillvalue = 0 ;
int POTM_IOBSI(N_OBS) ;
POTM_IOBSI:long_name = "ORCA grid search I coordinate" ;
int POTM_IOBSJ(N_OBS) ;
POTM_IOBSJ:long_name = "ORCA grid search J coordinate" ;
int POTM_IOBSK(N_OBS, N_LEVELS) ;
POTM_IOBSK:long_name = "ORCA grid search K coordinate" ;
char POTM_GRID(StringGRID) ;
POTM_GRID:long_name = "ORCA grid search grid (I,U,V)" ;
float PSAL_OBS(N_OBS, N_LEVELS) ;
PSAL_OBS:long_name = "Practical salinity" ;
PSAL_OBS:units = "PSU" ;
PSAL_OBS:Fillvalue = 99999.f ;
float PSAL_Hx(N_OBS, N_LEVELS) ;
PSAL_Hx:long_name = "Model interpolated practical salinity" ;
PSAL_Hx:units = "PSU" ;
PSAL_Hx:Fillvalue = 99999.f ;
int PSAL_QC(N_OBS) ;
PSAL_QC:long_name = "Quality on practical salinity" ;
PSAL_QC:Conventions = "q where q =[0,9]" ;
PSAL_QC:Fillvalue = 0 ;
int PSAL_QC_FLAGS(N_OBS, N_QCF) ;
PSAL_QC_FLAGS:long_name = "Quality flags on practical salinity" ;
PSAL_QC_FLAGS:Conventions = "NEMOVAR flag conventions" ;

```

```

        PSAL_QC_FLAGS:_Fillvalue = 0 ;
    int PSAL_LEVEL_QC(N_OBS, N_LEVELS) ;
        PSAL_LEVEL_QC:long_name = "Quality for each level on practical salinity" ;
        PSAL_LEVEL_QC:Conventions = "q where q =[0,9]" ;
        PSAL_LEVEL_QC:_Fillvalue = 0 ;
    int PSAL_LEVEL_QC_FLAGS(N_OBS, N_LEVELS, N_QCF) ;
        PSAL_LEVEL_QC_FLAGS:long_name = "Quality flags for each level on practical salinity" ;
        PSAL_LEVEL_QC_FLAGS:Conventions = "NEMOVAR flag conventions" ;
        PSAL_LEVEL_QC_FLAGS:_Fillvalue = 0 ;
    int PSAL_IOBSI(N_OBS) ;
        PSAL_IOBSI:long_name = "ORCA grid search I coordinate" ;
    int PSAL_IOBSJ(N_OBS) ;
        PSAL_IOBSJ:long_name = "ORCA grid search J coordinate" ;
    int PSAL_IOBSK(N_OBS, N_LEVELS) ;
        PSAL_IOBSK:long_name = "ORCA grid search K coordinate" ;
    char PSAL_GRID(StringGrid) ;
        PSAL_GRID:long_name = "ORCA grid search grid (T,U,V)" ;
    float TEMP(N_OBS, N_LEVELS) ;
        TEMP:long_name = "Insitu temperature" ;
        TEMP:units = "Degrees Celsius" ;
        TEMP:_Fillvalue = 99999.f ;

// global attributes:
    :title = "NEMO observation operator output" ;
    :Convention = "NEMO unified observation operator output" ;
}

```

## 12.2.2 Sea level anomaly feedback type observation file header

```

netcdf sla_01 {
dimensions:
    N_OBS = 41301 ;
    N_LEVELS = 1 ;
    N_VARS = 1 ;
    N_QCF = 2 ;
    N_ENTRIES = 1 ;
    N_EXTRA = 1 ;
    STRINGNAM = 8 ;
    STRINGGRID = 1 ;
    STRINGWMO = 8 ;
    STRINGTYP = 4 ;
    STRINGJULD = 14 ;
variables:
    char VARIABLES(N_VARS, STRINGNAM) ;
        VARIABLES:long_name = "List of variables in feedback files" ;
    char ENTRIES(N_ENTRIES, STRINGNAM) ;
        ENTRIES:long_name = "List of additional entries for each variable in feedback files" ;
    char EXTRA(N_EXTRA, STRINGNAM) ;
        EXTRA:long_name = "List of extra variables" ;
    char STATION_IDENTIFIER(N_OBS, STRINGWMO) ;
        STATION_IDENTIFIER:long_name = "Station identifier" ;
    char STATION_TYPE(N_OBS, STRINGTYP) ;
        STATION_TYPE:long_name = "Code instrument type" ;
    double LONGITUDE(N_OBS) ;
        LONGITUDE:long_name = "Longitude" ;
        LONGITUDE:units = "degrees_east" ;
        LONGITUDE:_Fillvalue = 99999.f ;
    double LATITUDE(N_OBS) ;
        LATITUDE:long_name = "Latitude" ;
        LATITUDE:units = "degrees_north" ;
        LATITUDE:_Fillvalue = 99999.f ;
    double DEPTH(N_OBS, N_LEVELS) ;
        DEPTH:long_name = "Depth" ;
        DEPTH:units = "metre" ;
        DEPTH:_Fillvalue = 99999.f ;
    int DEPTH_QC(N_OBS, N_LEVELS) ;
        DEPTH_QC:long_name = "Quality on depth" ;
        DEPTH_QC:Conventions = "q where q =[0,9]" ;
        DEPTH_QC:_Fillvalue = 0 ;
    int DEPTH_QC_FLAGS(N_OBS, N_LEVELS, N_QCF) ;
        DEPTH_QC_FLAGS:long_name = "Quality flags on depth" ;
        DEPTH_QC_FLAGS:Conventions = "NEMOVAR flag conventions" ;
    double JULD(N_OBS) ;
        JULD:long_name = "Julian day" ;
        JULD:units = "days since JULD_REFERENCE" ;
        JULD:Conventions = "relative julian days with decimal part (as parts of day)" ;
        JULD:_Fillvalue = 99999.f ;
    char JULD_REFERENCE(StringJULD) ;
        JULD_REFERENCE:long_name = "Date of reference for julian days" ;
}

```

```

    JULD_REFERENCE:Conventions = "YYYYMMDDHHMMSS" ;
int OBSERVATION_QC(N_OBS) ;
    OBSERVATION_QC:long_name = "Quality on observation" ;
    OBSERVATION_QC:Conventions = "q where q =[0,9]" ;
    OBSERVATION_QC:Fillvalue = 0 ;
int OBSERVATION_QC_FLAGS(N_OBS, N_QCF) ;
    OBSERVATION_QC_FLAGS:long_name = "Quality flags on observation" ;
    OBSERVATION_QC_FLAGS:Conventions = "NEMOVAR flag conventions" ;
    OBSERVATION_QC_FLAGS:Fillvalue = 0 ;
int POSITION_QC(N_OBS) ;
    POSITION_QC:long_name = "Quality on position (latitude and longitude)" ;
    POSITION_QC:Conventions = "q where q =[0,9]" ;
    POSITION_QC:Fillvalue = 0 ;
int POSITION_QC_FLAGS(N_OBS, N_QCF) ;
    POSITION_QC_FLAGS:long_name = "Quality flags on position" ;
    POSITION_QC_FLAGS:Conventions = "NEMOVAR flag conventions" ;
    POSITION_QC_FLAGS:Fillvalue = 0 ;
int JULD_QC(N_OBS) ;
    JULD_QC:long_name = "Quality on date and time" ;
    JULD_QC:Conventions = "q where q =[0,9]" ;
    JULD_QC:Fillvalue = 0 ;
int JULD_QC_FLAGS(N_OBS, N_QCF) ;
    JULD_QC_FLAGS:long_name = "Quality flags on date and time" ;
    JULD_QC_FLAGS:Conventions = "NEMOVAR flag conventions" ;
    JULD_QC_FLAGS:Fillvalue = 0 ;
int ORIGINAL_FILE_INDEX(N_OBS) ;
    ORIGINAL_FILE_INDEX:long_name = "Index in original data file" ;
    ORIGINAL_FILE_INDEX:Fillvalue = -99999 ;
float SLA_OBS(N_OBS, N_LEVELS) ;
    SLA_OBS:long_name = "Sea level anomaly" ;
    SLA_OBS:units = "metre" ;
    SLA_OBS:Fillvalue = 99999.f ;
float SLA_Hx(N_OBS, N_LEVELS) ;
    SLA_Hx:long_name = "Model interpolated sea level anomaly" ;
    SLA_Hx:units = "metre" ;
    SLA_Hx:Fillvalue = 99999.f ;
int SLA_QC(N_OBS) ;
    SLA_QC:long_name = "Quality on sea level anomaly" ;
    SLA_QC:Conventions = "q where q =[0,9]" ;
    SLA_QC:Fillvalue = 0 ;
int SLA_QC_FLAGS(N_OBS, N_QCF) ;
    SLA_QC_FLAGS:long_name = "Quality flags on sea level anomaly" ;
    SLA_QC_FLAGS:Conventions = "NEMOVAR flag conventions" ;
    SLA_QC_FLAGS:Fillvalue = 0 ;
int SLA_LEVEL_QC(N_OBS, N_LEVELS) ;
    SLA_LEVEL_QC:long_name = "Quality for each level on sea level anomaly" ;
    SLA_LEVEL_QC:Conventions = "q where q =[0,9]" ;
    SLA_LEVEL_QC:Fillvalue = 0 ;
int SLA_LEVEL_QC_FLAGS(N_OBS, N_LEVELS, N_QCF) ;
    SLA_LEVEL_QC_FLAGS:long_name = "Quality flags for each level on sea level anomaly" ;
    SLA_LEVEL_QC_FLAGS:Conventions = "NEMOVAR flag conventions" ;
    SLA_LEVEL_QC_FLAGS:Fillvalue = 0 ;
int SLA_IOBSI(N_OBS) ;
    SLA_IOBSI:long_name = "ORCA grid search I coordinate" ;
int SLA_IOBSJ(N_OBS) ;
    SLA_IOBSJ:long_name = "ORCA grid search J coordinate" ;
int SLA_IOBSK(N_OBS, N_LEVELS) ;
    SLA_IOBSK:long_name = "ORCA grid search K coordinate" ;
char SLA_GRID(StringGRID) ;
    SLA_GRID:long_name = "ORCA grid search grid (T,U,V)" ;
float MDT(N_OBS, N_LEVELS) ;
    MDT:long_name = "Mean Dynamic Topography" ;
    MDT:units = "metre" ;
    MDT:Fillvalue = 99999.f ;

// global attributes
: title = "NEMO observation operator output" ;
: Convention = "NEMO unified observation operator output" ;
}

```

The mean dynamic topography (MDT) must be provided in a separate file defined on the model grid called *slaReferenceLevel.nc*. The MDT is required in order to produce the model equivalent sea level anomaly from the model sea surface height. Below is an example header for this file (on the ORCA025 grid).

```

dimensions:
    x = 1442 ;

```

```

        y = 1021 ;
variables:
  float nav_lon(y, x) ;
      nav_lon:units = "degrees_east" ;
  float nav_lat(y, x) ;
      nav_lat:units = "degrees_north" ;
  float sossheig(y, x) ;
      sossheig:FillValue = -1.e+30f ;
      sossheig:coordinates = "nav_lon nav_lat" ;
      sossheig:long_name = "Mean Dynamic Topography" ;
      sossheig:units = "metres" ;
      sossheig:grid = "orca025T" ;

```

### 12.2.3 Sea surface temperature feedback type observation file header

```

netcdf sst_01 {
dimensions:
  N_OBS = 33099 ;
  N_LEVELS = 1 ;
  N_VARS = 1 ;
  N_QCF = 2 ;
  N_ENTRIES = 1 ;
  STRINGNAM = 8 ;
  STRINGGRID = 1 ;
  STRINGWMO = 8 ;
  STRINGTYP = 4 ;
  STRINGJULD = 14 ;
variables:
  char VARIABLES(N_VARS, STRINGNAM) ;
      VARIABLES:long_name = "List of variables in feedback files" ;
  char ENTRIES(N_ENTRIES, STRINGNAM) ;
      ENTRIES:long_name = "List of additional entries for each variable in feedback files" ;
  char STATION_IDENTIFIER(N_OBS, STRINGWMO) ;
      STATION_IDENTIFIER:long_name = "Station identifier" ;
  char STATION_TYPE(N_OBS, STRINGTYP) ;
      STATION_TYPE:long_name = "Code instrument type" ;
  double LONGITUDE(N_OBS) ;
      LONGITUDE:long_name = "Longitude" ;
      LONGITUDE:units = "degrees_east" ;
      LONGITUDE:Fillvalue = 99999.f ;
  double LATITUDE(N_OBS) ;
      LATITUDE:long_name = "Latitude" ;
      LATITUDE:units = "degrees_north" ;
      LATITUDE:Fillvalue = 99999.f ;
  double DEPTH(N_OBS, N_LEVELS) ;
      DEPTH:long_name = "Depth" ;
      DEPTH:units = "metre" ;
      DEPTH:Fillvalue = 99999.f ;
  int DEPTH_QC(N_OBS, N_LEVELS) ;
      DEPTH_QC:long_name = "Quality on depth" ;
      DEPTH_QC:Conventions = "q where q =[0,9]" ;
      DEPTH_QC:Fillvalue = 0 ;
  int DEPTH_QC_FLAGS(N_OBS, N_LEVELS, N_QCF) ;
      DEPTH_QC_FLAGS:long_name = "Quality flags on depth" ;
      DEPTH_QC_FLAGS:Conventions = "NEMOVAR flag conventions" ;
  double JULD(N_OBS) ;
      JULD:long_name = "Julian day" ;
      JULD:units = "days since JULD_REFERENCE" ;
      JULD:Conventions = "relative julian days with decimal part (as parts of day)" ;
      JULD:Fillvalue = 99999.f ;
  char JULD_REFERENCE(STRINGJULD) ;
      JULD_REFERENCE:long_name = "Date of reference for julian days" ;
      JULD_REFERENCE:Conventions = "YYYYMMDDHHMMSS" ;
  int OBSERVATION_QC(N_OBS) ;
      OBSERVATION_QC:long_name = "Quality on observation" ;
      OBSERVATION_QC:Conventions = "q where q =[0,9]" ;
      OBSERVATION_QC:Fillvalue = 0 ;
  int OBSERVATION_QC_FLAGS(N_OBS, N_QCF) ;
      OBSERVATION_QC_FLAGS:long_name = "Quality flags on observation" ;
      OBSERVATION_QC_FLAGS:Conventions = "NEMOVAR flag conventions" ;
      OBSERVATION_QC_FLAGS:Fillvalue = 0 ;
  int POSITION_QC(N_OBS) ;
      POSITION_QC:long_name = "Quality on position (latitude and longitude)" ;
      POSITION_QC:Conventions = "q where q =[0,9]" ;
      POSITION_QC:Fillvalue = 0 ;
  int POSITION_QC_FLAGS(N_OBS, N_QCF) ;
      POSITION_QC_FLAGS:long_name = "Quality flags on position" ;
      POSITION_QC_FLAGS:Conventions = "NEMOVAR flag conventions" ;
      POSITION_QC_FLAGS:Fillvalue = 0 ;

```

```

int JULD_QC(N_OBS) ;
    JULD_QC:long_name = "Quality on date and time" ;
    JULD_QC:Conventions = "q where q =[0,9]" ;
    JULD_QC:Fillvalue = 0 ;
int JULD_QC_FLAGS(N_OBS, N_QCF) ;
    JULD_QC_FLAGS:long_name = "Quality flags on date and time" ;
    JULD_QC_FLAGS:Conventions = "NEMOVAR flag conventions" ;
    JULD_QC_FLAGS:Fillvalue = 0 ;
int ORIGINAL_FILE_INDEX(N_OBS) ;
    ORIGINAL_FILE_INDEX:long_name = "Index in original data file" ;
    ORIGINAL_FILE_INDEX:Fillvalue = -99999 ;
float SST_OBS(N_OBS, N_LEVELS) ;
    SST_OBS:long_name = "Sea surface temperature" ;
    SST_OBS:units = "Degree centigrade" ;
    SST_OBS:Fillvalue = 99999.f ;
float SST_Hx(N_OBS, N_LEVELS) ;
    SST_Hx:long_name = "Model interpolated sea surface temperature" ;
    SST_Hx:units = "Degree centigrade" ;
    SST_Hx:Fillvalue = 99999.f ;
int SST_QC(N_OBS) ;
    SST_QC:long_name = "Quality on sea surface temperature" ;
    SST_QC:Conventions = "q where q =[0,9]" ;
    SST_QC:Fillvalue = 0 ;
int SST_QC_FLAGS(N_OBS, N_QCF) ;
    SST_QC_FLAGS:long_name = "Quality flags on sea surface temperature" ;
    SST_QC_FLAGS:Conventions = "NEMOVAR flag conventions" ;
    SST_QC_FLAGS:Fillvalue = 0 ;
int SST_LEVEL_QC(N_OBS, N_LEVELS) ;
    SST_LEVEL_QC:long_name = "Quality for each level on sea surface temperature" ;
    SST_LEVEL_QC:Conventions = "q where q =[0,9]" ;
    SST_LEVEL_QC:Fillvalue = 0 ;
int SST_LEVEL_QC_FLAGS(N_OBS, N_LEVELS, N_QCF) ;
    SST_LEVEL_QC_FLAGS:long_name = "Quality flags for each level on sea surface temperature" ;
    SST_LEVEL_QC_FLAGS:Conventions = "NEMOVAR flag conventions" ;
    SST_LEVEL_QC_FLAGS:Fillvalue = 0 ;
int SST_IOBSI(N_OBS) ;
    SST_IOBSI:long_name = "ORCA grid search I coordinate" ;
int SST_IOBSJ(N_OBS) ;
    SST_IOBSJ:long_name = "ORCA grid search J coordinate" ;
int SST_IOBSK(N_OBS, N_LEVELS) ;
    SST_IOBSK:long_name = "ORCA grid search K coordinate" ;
char SST_GRID(STRINGGRID) ;
    SST_GRID:long_name = "ORCA grid search grid (T,U,V)" ;

// global attributes:
: title = "NEMO observation operator output" ;
: Convention = "NEMO unified observation operator output" ;
}

```

## 12.3 Theoretical details

### 12.3.1 Horizontal interpolation methods

Consider an observation point  $P$  with with longitude and latitude  $(\lambda_P, \phi_P)$  and the four nearest neighbouring model grid points  $A, B, C$  and  $D$  with longitude and latitude  $(\lambda_A, \phi_A), (\lambda_B, \phi_B)$  etc. All horizontal interpolation methods implemented in NEMO estimate the value of a model variable  $x$  at point  $P$  as a weighted linear combination of the values of the model variables at the grid points  $A, B$  etc.:

$$x_P = \frac{1}{w} (w_A x_A + w_B x_B + w_C x_C + w_D x_D) \quad (12.1)$$

where  $w_A, w_B$  etc. are the respective weights for the model field at points  $A, B$  etc., and  $w = w_A + w_B + w_C + w_D$ .

Four different possibilities are available for computing the weights.

1. **Great-Circle distance-weighted interpolation.** The weights are computed as a function of the great-circle distance  $s(P, \cdot)$  between  $P$  and the model

grid points  $A, B$  etc. For example, the weight given to the field  $x_A$  is specified as the product of the distances from  $P$  to the other points:

$$w_A = s(P, B) s(P, C) s(P, D)$$

where

$$s(P, M) = \cos^{-1} \{ \sin \phi_P \sin \phi_M + \cos \phi_P \cos \phi_M \cos(\lambda_M - \lambda_P) \} \quad (12.2)$$

and  $M$  corresponds to  $B, C$  or  $D$ . A more stable form of the great-circle distance formula for small distances ( $x$  near 1) involves the arcsine function (*e.g.* see p. 101 of [Daley and Barker \[2001\]](#)):

$$s(P, M) = \sin^{-1} \left\{ \sqrt{1 - x^2} \right\}$$

where

$$x = a_M a_P + b_M b_P + c_M c_P$$

and

$$\begin{aligned} a_M &= \sin \phi_M, \\ a_P &= \sin \phi_P, \\ b_M &= \cos \phi_M \cos \lambda_M, \\ b_P &= \cos \phi_P \cos \lambda_P, \\ c_M &= \cos \phi_M \sin \lambda_M, \\ c_P &= \cos \phi_P \sin \lambda_P. \end{aligned}$$

2. **Great-Circle distance-weighted interpolation with small angle approximation.** Similar to the previous interpolation but with the distance  $s$  computed as

$$s(P, M) = \sqrt{(\phi_M - \phi_P)^2 + (\lambda_M - \lambda_P)^2 \cos^2 \phi_M} \quad (12.3)$$

where  $M$  corresponds to  $A, B, C$  or  $D$ .

3. **Bilinear interpolation for a regular spaced grid.** The interpolation is split into two 1D interpolations in the longitude and latitude directions, respectively.
4. **Bilinear remapping interpolation for a general grid.** An iterative scheme that involves first mapping a quadrilateral cell into a cell with coordinates  $(0,0)$ ,  $(1,0)$ ,  $(0,1)$  and  $(1,1)$ . This method is based on the SCRIP interpolation package [[Jones 1998](#)].



### 12.3.2 Grid search

For many grids used by the NEMO model, such as the ORCA family, the horizontal grid coordinates  $i$  and  $j$  are not simple functions of latitude and longitude. Therefore, it is not always straightforward to determine the grid points surrounding any given observational position. Before the interpolation can be performed, a search algorithm is then required to determine the corner points of the quadrilateral cell in which the observation is located. This is the most difficult and time consuming part of the 2D interpolation procedure. A robust test for determining if an observation falls within a given quadrilateral cell is as follows. Let  $P(\lambda_P, \phi_P)$  denote the observation point, and let  $A(\lambda_A, \phi_A)$ ,  $B(\lambda_B, \phi_B)$ ,  $C(\lambda_C, \phi_C)$  and  $D(\lambda_D, \phi_D)$  denote the bottom left, bottom right, top left and top right corner points of the cell, respectively. To determine if  $P$  is inside the cell, we verify that the cross-products

$$\begin{aligned} \mathbf{r}_{PA} \times \mathbf{r}_{PC} &= [(\lambda_A - \lambda_P)(\phi_C - \phi_P) - (\lambda_C - \lambda_P)(\phi_A - \phi_P)] \hat{\mathbf{k}} \\ \mathbf{r}_{PB} \times \mathbf{r}_{PA} &= [(\lambda_B - \lambda_P)(\phi_A - \phi_P) - (\lambda_A - \lambda_P)(\phi_B - \phi_P)] \hat{\mathbf{k}} \\ \mathbf{r}_{PC} \times \mathbf{r}_{PD} &= [(\lambda_C - \lambda_P)(\phi_D - \phi_P) - (\lambda_D - \lambda_P)(\phi_C - \phi_P)] \hat{\mathbf{k}} \\ \mathbf{r}_{PD} \times \mathbf{r}_{PB} &= [(\lambda_D - \lambda_P)(\phi_B - \phi_P) - (\lambda_B - \lambda_P)(\phi_D - \phi_P)] \hat{\mathbf{k}} \end{aligned} \quad (12.4)$$

point in the opposite direction to the unit normal  $\hat{\mathbf{k}}$  (i.e., that the coefficients of  $\hat{\mathbf{k}}$  are negative), where  $\mathbf{r}_{PA}$ ,  $\mathbf{r}_{PB}$ , etc. correspond to the vectors between points  $P$  and  $A$ ,  $P$  and  $B$ , etc.. The method used is similar to the method used in the SCRIP interpolation package [Jones 1998].

In order to speed up the grid search, there is the possibility to construct a lookup table for a user specified resolution. This lookup table contains the lower and upper bounds on the  $i$  and  $j$  indices to be searched for on a regular grid. For each observation position, the closest point on the regular grid of this position is computed and the  $i$  and  $j$  ranges of this point searched to determine the precise four points surrounding the observation.

### 12.3.3 Parallel aspects of horizontal interpolation

For horizontal interpolation, there is the basic problem that the observations are unevenly distributed on the globe. In numerical models, it is common to divide the model grid into subgrids (or domains) where each subgrid is executed on a single processing element with explicit message passing for exchange of information along the domain boundaries when running on a massively parallel processor (MPP) system. This approach is used by *NEMO*.

For observations there is no natural distribution since the observations are not equally distributed on the globe. Two options have been made available: 1) geographical distribution; and 2) round-robin.

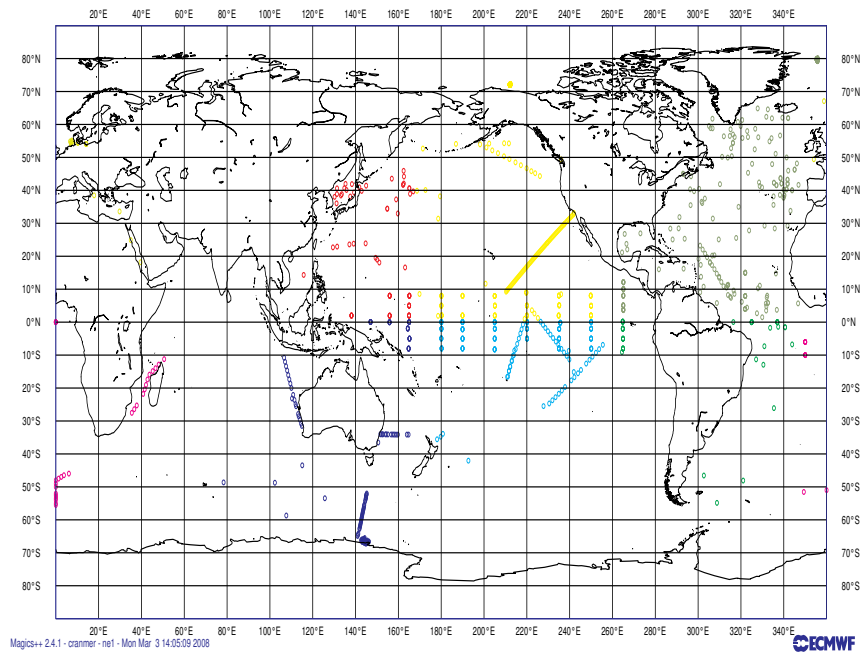


**Figure 12.1:** Example of the distribution of observations with the geographical distribution of observational data.

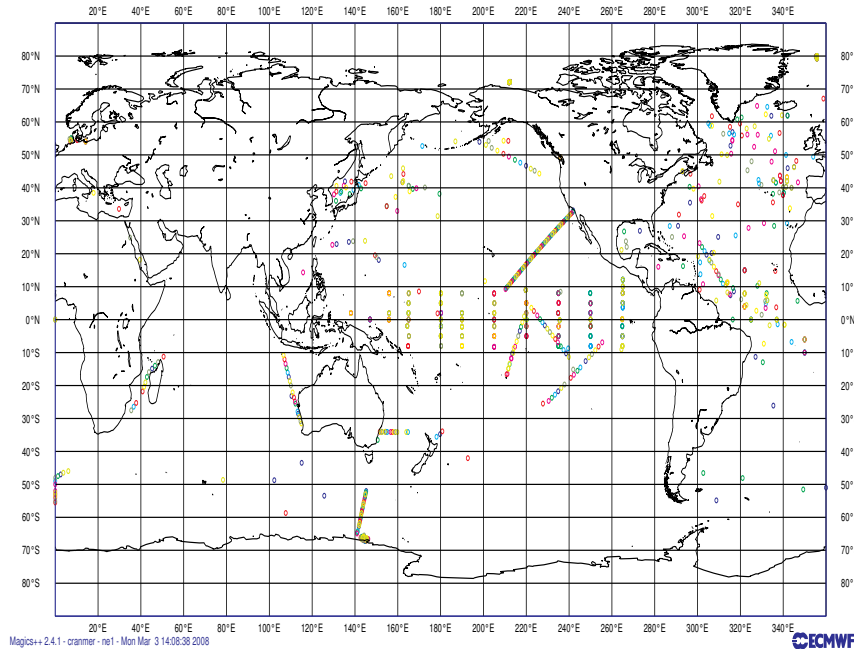


**Figure 12.2:** Example of the distribution of observations with the round-robin distribution of observational data.

### Geographical distribution of observations among processors

This is the simplest option in which the observations are distributed according to the domain of the grid-point parallelization. Figure 12.1 shows an example of the distribution of the *in situ* data on processors with a different colour for each observation on a given processor for a  $4 \times 2$  decomposition with ORCA2. The grid-point domain decomposition is clearly visible on the plot.

The advantage of this approach is that all information needed for horizontal interpolation is available without any MPP communication. Of course, this is under the assumption that we are only using a  $2 \times 2$  grid-point stencil for the interpolation (e.g., bilinear interpolation). For higher order interpolation schemes this is no longer valid. A disadvantage with the above scheme is that the number of observations on each processor can be very different. If the cost of the actual interpolation is expensive relative to the communication of data needed for interpolation, this could lead to load imbalance.

### Round-robin distribution of observations among processors

An alternative approach is to distribute the observations equally among processors and use message passing in order to retrieve the stencil for interpolation. The simplest distribution of the observations is to distribute them using a round-robin scheme. Figure 12.2 shows the distribution of the *in situ* data on processors for the round-robin distribution of observations with a different colour for each observation on a given processor for a  $4 \times 2$  decomposition with ORCA2 for the same input data as in Fig. 12.1. The observations are now clearly randomly distributed on the globe. In order to be able to perform horizontal interpolation in this case, a subroutine has been developed that retrieves any grid points in the global space.

#### 12.3.4 Vertical interpolation operator

Vertical interpolation is achieved using either a cubic spline or linear interpolation. For the cubic spline, the top and bottom boundary conditions for the second derivative of the interpolating polynomial in the spline are set to zero. At the bottom boundary, this is done using the land-ocean mask.

## 12.4 Offline observation operator

### 12.4.1 Concept

The obs oper maps model variables to observation space. It is possible to apply this mapping without running the model. The software which performs this functionality is known as the **offline obs oper**. The obs oper is divided into three stages. An initialisation phase, an interpolation phase and an output phase. The implementation of which is outlined in the previous sections. During the interpolation phase the offline obs oper populates the model arrays by reading saved model fields from disk.

There are two ways of exploiting this offline capacity. The first is to mimic the behaviour of the online system by supplying model fields at regular intervals between the start and the end of the run. This approach results in a single model counterpart per observation. This kind of usage produces feedback files the same file format as the online obs oper. The second is to take advantage of the offline setting in which multiple model counterparts can be calculated per observation. In this case it is possible to consider all forecasts verifying at the same time. By forecast, I mean any method which produces an estimate of physical reality which is not an observed value. In the case of class 4 files this means forecasts, analyses, persisted analyses and climatological values verifying at the same time. Although the class 4 file format doesn't account for multiple ensemble members or multiple experiments per observation, it is possible to include these components in the same or multiple files.

### 12.4.2 Using the offline observation operator

#### Building

In addition to *OPA\_SRC* the offline obs oper requires the inclusion of the *OOO\_SRC* directory. *OOO\_SRC* contains a replacement **nemo.f90** and **nemogcm.F90** which overwrites the resultant **nemo.exe**. This is the approach taken by *SAS\_SRC* and *OFF\_SRC*.

#### Running

The simplest way to use the executable is to edit and append the **ooo.nml** namelist to a full NEMO namelist and then to run the executable as if it were nemo.exe.

#### Quick script

A useful Python utility to control the namelist options can be found in **OBSTOOLS/OOO**. The functions which locate model fields and observation files can be manually specified. The package can be installed by appropriate use of the included setup.py script.

Documentation can be auto-generated by Sphinx by running *make html* in the **doc** directory.

### 12.4.3 Configuring the offline observation operator

The observation files and settings understood by **namobs** have been outlined in the online obs oper section. In addition there are two further namelists which control the operation of the offline obs oper. **namooo** which controls the input model fields and **namcl4** which controls the production of class 4 files.

#### Single field

In offline mode model arrays are populated at appropriate time steps via input files. At present, **tsn** and **sshn** are populated by the default read routines. These routines will be expanded upon in future versions to allow the specification of any model variable. As such, input files must be global versions of the model domain with **votemper**, **vosaline** and optionally **sshn** present.

For each field read there must be an entry in the **namooo** namelist specifying the name of the file to read and the index along the *time\_counter*. For example, to read the second time counter from a single file the namelist would be.

```
!-----
!           namooo Offline obs_oper namelist
!-----
!   ooo_files   specifies the files containing the model counterpart
!   nn_ooo_idx  specifies the time_counter index within the model file
&namooo
   ooo_files = "foo.nc"
   nn_ooo_idx = 2
/
```

#### Multiple fields per run

Model field iteration is controlled via **nn\_ooo\_freq** which specifies the number of model steps at which the next field gets read. For example, if 12 hourly fields are to be interpolated in a setup where 288 steps equals 24 hours.

```
!-----
!           namooo Offline obs_oper namelist
!-----
!   ooo_files   specifies the files containing the model counterpart
!   nn_ooo_idx  specifies the time_counter index within the model file
!   nn_ooo_freq specifies number of time steps between read operations
&namooo
   ooo_files = "foo.nc" "foo.nc"
   nn_ooo_idx = 1 2
   nn_ooo_freq = 144
/
```

The above namelist will result in feedback files whose first 12 hours contain the first field of foo.nc and the second 12 hours contain the second field.

**Note** Missing files can be denoted as "nofile".

It is easy to see how a collection of fields taken from a number of files at different indices can be combined at a particular frequency in time to generate a pseudo model evolution. As long as all that is needed is a single model counterpart at a regular interval then `namooo` is all that needs to be edited. However, a far more interesting approach can be taken in which multiple forecasts, analyses, persisted analyses and climatologies are considered against the same set of observations. For this a slightly more complicated approach is needed. It is referred to as *Class 4* since it is the fourth metric defined by the GODAE intercomparison project.

#### Multiple model counterparts per observation a.k.a Class 4

A generalisation of feedback files to allow multiple model components per observation. For a single observation, as well as previous forecasts verifying at the same time there are also analyses, persisted analyses and climatologies.

The above namelist performs two basic functions. It organises the fields given in `namooo` into groups so that observations can be matched up multiple times. It also controls the metadata and the output variable of the class 4 file when a write routine is called.

**Note:** `ln_cl4` must be set to `.TRUE.` in `namobs` to use class 4 outputs.

#### Class 4 naming convention

The standard class 4 file naming convention is as follows.

`${prefix}_${yyyymmdd}_${sys}_${cfg}_${vn}_${kind}_${nproc}.nc`

Much of the namelist is devoted to specifying this convention. The following namelist settings control the elements of the output file names. Each should be specified as a single string of character data.

**cl4\_prefix** Prefix for class 4 files e.g. class4

**cl4\_date** YYYYMMDD validity date

**cl4\_sys** The name of the class 4 model system e.g. FOAM

**cl4\_cfg** The name of the class 4 model configuration e.g. orca025

**cl4\_vn** The name of the class 4 model version e.g. 12.0

The kind is specified by the observation type internally to the obs oper. The processor number is specified internally in NEMO.

### Class 4 file global attributes

Global attributes necessary to fulfill the class 4 file definition. These are also useful pieces of information when collaborating with external partners.

**cl4\_contact** Contact email for class 4 files.

**cl4\_inst** The name of the producers institution.

**cl4\_cfg** The name of the class 4 model configuration e.g. orca025

**cl4\_vn** The name of the class 4 model version e.g. 12.0

The `obs_type`, creation date and validity time are specified internally to the `obs oper`.

### Class 4 model counterpart configuration

As seen previously it is possible to perform a single sweep of the `obs oper` and specify a collection of model fields equally spaced along that sweep. In the class 4 case the single sweep is replaced with multiple sweeps and a certain amount of book keeping is needed to ensure each model counterpart makes its way to the correct piece of memory in the output files.

In terms of book keeping, the offline `obs oper` needs to know how many full sweeps need to be performed. This is specified via the **cl4\_match\_len** variable and is the total number of model counterparts per observation. For example, a 3 forecasts plus 3 persistence fields plus an analysis field would be 7 counterparts per observation.

```
cl4_match_len = 7
```

Then to correctly allocate a class 4 file the forecast axis must be defined. This is controlled via **cl4\_fcst\_len**, which in our above example would be 3.

```
cl4_fcst_len = 3
```

Then for each model field it is necessary to designate what class 4 variable and index along the forecast dimension the model counterpart should be stored in the output file. As well as a value for that lead time in hours, this will be useful when interpreting the data afterwards.

```
cl4_vars = "forecast" "forecast" "forecast" "persistence" "persistence"
           "persistence" "best_estimate"
cl4_fcst_idx = 1 2 3 1 2 3 1
cl4_leadtime = 12 36 60
```



In terms of files and indices of fields inside each file the class 4 approach makes use of the **namooo** namelist. If our fields are in separate files with a single field per file our example inputs will be specified.

```
ooo_files = "F.1.nc" "F.2.nc" "F.3.nc" "P.1.nc" "P.2.nc" "P.3.nc" "A.1.nc"
nn_ooo_idx = 1 1 1 1 1 1 1
```

When we combine all of the naming conventions, global attributes and i/o instructions the class 4 namelist becomes.

```
!-----
!          namooo Offline obs_oper namelist
!-----
!  ooo_files    specifies the files containing the model counterpart
!  nn_ooo_idx   specifies the time_counter index within the model file
!  nn_ooo_freq  specifies number of time steps between read operations
&namooo
  ooo_files = "F.1.nc" "F.2.nc" "F.3.nc" "P.1.nc" "P.2.nc" "P.3.nc" "A.1.nc"
  nn_ooo_idx = 1 1 1 1 1 1 1
/
!-----
!          namcl4 Offline obs_oper class 4 namelist
!-----
!
!  Naming convention
!  -----
!  cl4_prefix   specifies the output file prefix
!  cl4_date     specifies the output file validity date
!  cl4_sys      specifies the model counterpart system
!  cl4_cfg      specifies the model counterpart configuration
!  cl4_vn       specifies the model counterpart version
!  cl4_inst     specifies the model counterpart institute
!  cl4_contact  specifies the file producers contact details
!
!  I/O specification
!  -----
!  cl4_vars     specifies the names of the output file netcdf variable
!  cl4_fcst_idx specifies output file forecast index
!  cl4_fcst_len specifies forecast axis length
!  cl4_match_len specifies number of unique matches per observation
!  cl4_leadtime specifies the forecast axis lead time
!
&namcl4
  cl4_match_len = 7
  cl4_fcst_len = 3
  cl4_fcst_idx = 1 2 3 1 2 3 1
  cl4_vars = "forecast" "forecast" "forecast" "persistence" "persistence"
             "persistence" "best_estimate"
  cl4_leadtime = 12 36 60
  cl4_prefix = "class4"
  cl4_date = "20130101"
  cl4_vn = "12.0"
  cl4_sys = "FOAM"
  cl4_cfg = "AMM7"
  cl4_contact = "example@example.com"
  cl4_inst = "UK Met Office"
/
```

### Climatology interpolation

The climatological counterpart is generated at the start of the run by restarting the model from climatology through appropriate use of **namtsd**. To override the offline observation operator read routine and to take advantage of the restart settings, specify the first entry in **cl4\_vars** as "climatology". This will then pipe the restart from climatology into the output class 4 file. As in every other class 4 matchup the input file, input index and output index must be specified. These can be replaced

with dummy data since they are not used but they must be present to cycle through the matchups correctly.

#### 12.4.4 Advanced usage

In certain cases it may be desirable to include both multiple model fields per observation window with multiple match ups per observation. This can be achieved by specifying `nn_ooo_freq` as well as the class 4 settings. Care must be taken in generating the `ooo_files` list such that the files are arranged into consecutive blocks of single match ups. For example, 2 forecast fields of 12 hourly data would result in 4 separate read operations but only 2 write operations, 1 per forecast.

```
ooo_files = "F1.nc" "F1.nc" "F2.nc" "F2.nc"  
...  
cl4_fcst_idx = 1 2
```

The above notation reveals the internal split between match up iterators and file iterators. This technique has not been used before so experimentation is needed before results can be trusted.

## 12.5 Observation Utilities

Some tools for viewing and processing of observation and feedback files are provided in the NEMO repository for convenience. These include OBSTOOLS which are a collection of Fortran programs which are helpful to deal with feedback files. They do such tasks as observation file conversion, printing of file contents, some basic statistical analysis of feedback files. The other tool is an IDL program called dataplot which uses a graphical interface to visualise observations and feedback files. OBSTOOLS and dataplot are described in more detail below.

### 12.5.1 Obstoools

A series of Fortran utilities is provided with NEMO called OBSTOOLS. This are helpful in handling observation files and the feedback file output from the NEMO observation operator. The utilities are as follows

#### **c4comb**

The program c4comb combines multiple class 4 files produced by individual processors in an MPI run of NEMO offline obs\_oper into a single class 4 file. The program is called in the following way:

```
c4comb.exe outputfile inputfile1 inputfile2 ...
```

#### **corio2fb**

The program corio2fb converts profile observation files from the Coriolis format to the standard feedback format. The program is called in the following way:

```
corio2fb.exe outputfile inputfile1 inputfile2 ...
```

#### **enact2fb**

The program enact2fb converts profile observation files from the ENACT format to the standard feedback format. The program is called in the following way:

```
enact2fb.exe outputfile inputfile1 inputfile2 ...
```

### **fbcomb**

The program `fbcomb` combines multiple feedback files produced by individual processors in an MPI run of NEMO into a single feedback file. The program is called in the following way:

```
fbcomb.exe outputfile inputfile1 inputfile2 ...
```

### **fbmatchup**

The program `fbmatchup` will match observations from two feedback files. The program is called in the following way:

```
fbmatchup.exe outputfile inputfile1 varname1 inputfile2 varname2 ...
```

### **fbprint**

The program `fbprint` will print the contents of a feedback file or files to standard output. Selected information can be output using optional arguments. The program is called in the following way:

```
fbprint.exe [options] inputfile
```

options:

<code>-b</code>	shorter output
<code>-q</code>	Select observations based on QC flags
<code>-Q</code>	Select observations based on QC flags
<code>-B</code>	Select observations based on QC flags
<code>-u</code>	unsorted
<code>-s ID</code>	select station ID
<code>-t TYPE</code>	select observation type
<code>-v NUM1-NUM2</code>	select variable range to print by number (default all)
<code>-a NUM1-NUM2</code>	select additional variable range to print by number (default all)
<code>-e NUM1-NUM2</code>	select extra variable range to print by number (default all)
<code>-d</code>	output date range
<code>-D</code>	print depths
<code>-z</code>	use zipped files

**fbssel**

The program fbssel will select or subsample observations. The program is called in the following way:

```
fbssel.exe <input filename> <output filename>
```

**fbstat**

The program fbstat will output summary statistics in different global areas into a number of files. The program is called in the following way:

```
fbstat.exe [-nmlev] <filenames>
```

**fbthin**

The program fbthin will thin the data to 1 degree resolution. The code could easily be modified to thin to a different resolution. The program is called in the following way:

```
fbthin.exe inputfile outputfile
```

**sla2fb**

The program sla2fb will convert an AVISO SLA format file to feedback format. The program is called in the following way:

```
sla2fb.exe [-s type] outputfile inputfile1 inputfile2 ...
```

Option:

```
-s          Select altimeter data_source
```

**vel2fb**

The program vel2fb will convert TAO/PIRATA/RAMA currents files to feedback format. The program is called in the following way:

```
vel2fb.exe outputfile inputfile1 inputfile2 ...
```

### 12.5.2 building the obstools

To build the obstools use in the tools directory use `./maketools -n OBSTOOLS -m [ARCH]`.

### 12.5.3 Dataplot

An IDL program called `dataplot` is included which uses a graphical interface to visualise observations and feedback files. It is possible to zoom in, plot individual profiles and calculate some basic statistics. To plot some data run IDL and then:

```
IDL> dataplot, "filename"
```

To read multiple files into `dataplot`, for example multiple feedback files from different processors or from different days, the easiest method is to use the `spawn` command to generate a list of files which can then be passed to `dataplot`.

```
IDL> spawn, 'ls profb*.nc', files
IDL> dataplot, files
```

Fig 12.3 shows the main window which is launched when `dataplot` starts. This is split into three parts. At the top there is a menu bar which contains a variety of drop down menus. `Areas` - zooms into prespecified regions; `plot` - plots the data as a timeseries or a T-S diagram if appropriate; `Find` - allows data to be searched; `Config` - sets various configuration options.

The middle part is a plot of the geographical location of the observations. This will plot the observation value, the model background value or observation minus background value depending on the option selected in the radio button at the bottom of the window. The plotting colour range can be changed by clicking on the colour bar. The title of the plot gives some basic information about the date range and depth range shown, the extreme values, and the mean and rms values. It is possible to zoom in using a drag-box. You may also zoom in or out using the mouse wheel.

The bottom part of the window controls what is visible in the plot above. There are two bars which select the level range plotted (for profile data). The other bars below select the date range shown. The bottom of the figure allows the option to plot the mean, root mean square, standard deviation or mean square values. As mentioned above you can choose to plot the observation value, the model background value or observation minus background value. The next group of radio buttons selects the map projection. This can either be regular latitude longitude grid, or north or south polar stereographic. The next group of radio buttons will plot bad observations, switch to salinity and plot density for profile observations. The rightmost group of buttons will print the plot window as a postscript, save it as png, or exit from `dataplot`.

If a profile point is clicked with the mouse button a plot of the observation and background values as a function of depth (Fig 12.4).

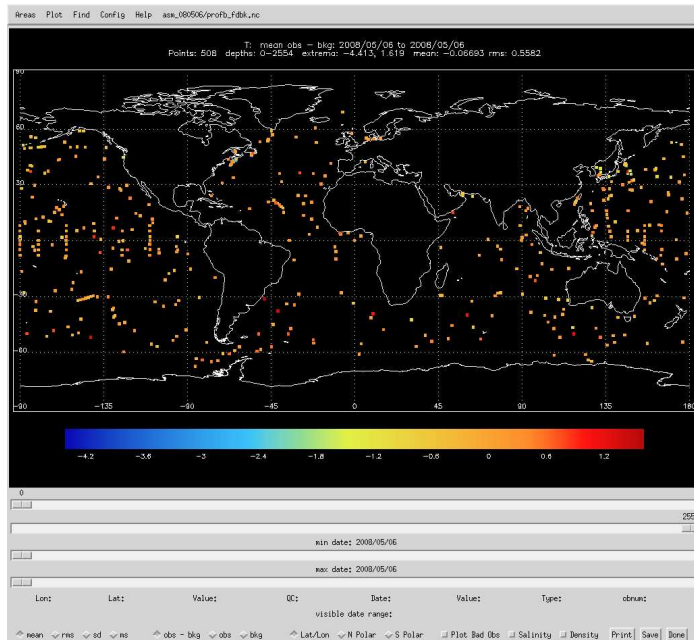


Figure 12.3: Main window of dataplot.

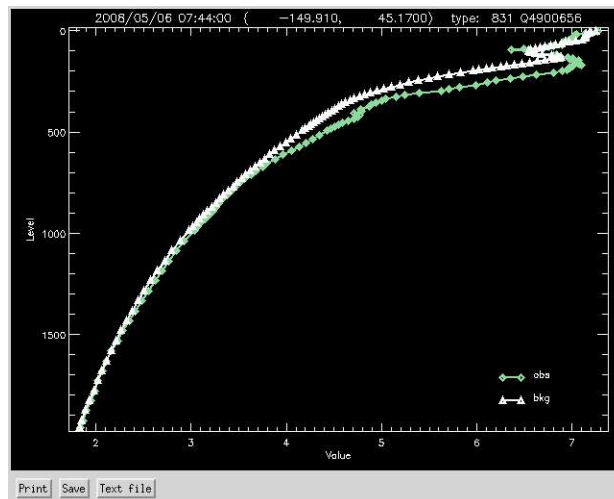
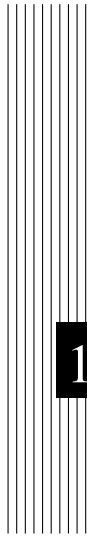


Figure 12.4: Profile plot from dataplot produced by right clicking on a point in the main window.







# 13 Apply assimilation increments (ASM)

Authors: D. Lea, M. Martin, K. Mogensen, A. Weaver, ...

## Contents

---

<b>13.1 Direct initialization</b>	<b>272</b>
<b>13.2 Incremental Analysis Updates</b>	<b>272</b>
<b>13.3 Divergence damping initialisation</b>	<b>273</b>
<b>13.4 Implementation details</b>	<b>273</b>

---

The ASM code adds the functionality to apply increments to the model variables: temperature, salinity, sea surface height, velocity and sea ice concentration. These are read into the model from a NetCDF file which may be produced by separate data assimilation code. The code can also output model background fields which are used as an input to data assimilation code. This is all controlled by the namelist *nam\_asminc*. There is a brief description of all the namelist options provided. To build the ASM code key **asminc** must be set.

### 13.1 Direct initialization

Direct initialization (DI) refers to the instantaneous correction of the model background state using the analysis increment. DI is used when *ln\_asmdin* is set to true.

### 13.2 Incremental Analysis Updates

Rather than updating the model state directly with the analysis increment, it may be preferable to introduce the increment gradually into the ocean model in order to minimize spurious adjustment processes. This technique is referred to as Incremental Analysis Updates (IAU) [Bloom et al. 1996]. IAU is a common technique used with 3D assimilation methods such as 3D-Var or OI. IAU is used when *ln\_asmiau* is set to true.

With IAU, the model state trajectory  $\mathbf{x}$  in the assimilation window ( $t_0 \leq t_i \leq t_N$ ) is corrected by adding the analysis increments for temperature, salinity, horizontal velocity and SSH as additional tendency terms to the prognostic equations:

$$\mathbf{x}^a(t_i) = M(t_i, t_0)[\mathbf{x}^b(t_0)] + F_i \delta \tilde{\mathbf{x}}^a \quad (13.1)$$

where  $F_i$  is a weighting function for applying the increments  $\delta \tilde{\mathbf{x}}^a$  defined such that  $\sum_{i=1}^N F_i = 1$ .  $\mathbf{x}^b$  denotes the model initial state and  $\mathbf{x}^a$  is the model state after the increments are applied. To control the adjustment time of the model to the increment, the increment can be applied over an arbitrary sub-window,  $t_m \leq t_i \leq t_n$ , of the main assimilation window, where  $t_0 \leq t_m \leq t_i$  and  $t_i \leq t_n \leq t_N$ . Typically the increments are spread evenly over the full window. In addition, two different weighting functions have been implemented. The first function employs constant weights,

$$F_i^{(1)} = \begin{cases} 0 & \text{if } t_i < t_m \\ 1/M & \text{if } t_m < t_i \leq t_n \\ 0 & \text{if } t_i > t_n \end{cases} \quad (13.2)$$

where  $M = m - n$ . The second function employs peaked hat-like weights in order to give maximum weight in the centre of the sub-window, with the weighting

reduced linearly to a small value at the window end-points:

$$F_i^{(2)} = \begin{cases} 0 & \text{if } t_i < t_m \\ \alpha i & \text{if } t_m \leq t_i \leq t_{M/2} \\ \alpha (M - i + 1) & \text{if } t_{M/2} < t_i \leq t_n \\ 0 & \text{if } t_i > t_n \end{cases} \quad (13.3)$$

where  $\alpha^{-1} = \sum_{i=1}^{M/2} 2i$  and  $M$  is assumed to be even. The weights described by (13.3) provide a smoother transition of the analysis trajectory from one assimilation cycle to the next than that described by (13.2).

### 13.3 Divergence damping initialisation

The velocity increments may be initialized by the iterative application of a divergence damping operator. In iteration step  $n$  new estimates of velocity increments  $u_I^n$  and  $v_I^n$  are updated by:

$$\begin{cases} u_I^n = u_I^{n-1} + \frac{1}{e_{1u}} \delta_{i+1/2} (A_D \chi_I^{n-1}) \\ v_I^n = v_I^{n-1} + \frac{1}{e_{2v}} \delta_{j+1/2} (A_D \chi_I^{n-1}) \end{cases}, \quad (13.4)$$

where

$$\chi_I^{n-1} = \frac{1}{e_{1t} e_{2t} e_{3t}} (\delta_i [e_{2u} e_{3u} u_I^{n-1}] + \delta_j [e_{1v} e_{3v} v_I^{n-1}]). \quad (13.5)$$

By the application of (13.4) and (13.4) the divergence is filtered in each iteration, and the vorticity is left unchanged. In the presence of coastal boundaries with zero velocity increments perpendicular to the coast the divergence is strongly damped. This type of the initialisation reduces the vertical velocity magnitude and alleviates the problem of the excessive unphysical vertical mixing in the first steps of the model integration [Talagrand 1972, Dobricic et al. 2007]. Diffusion coefficients are defined as  $A_D = \alpha e_{1t} e_{2t}$ , where  $\alpha = 0.2$ . The divergence damping is activated by assigning to *nn\_divdmp* in the *nam\_asminc* namelist a value greater than zero. By choosing this value to be of the order of 100 the increments in the vertical velocity will be significantly reduced.

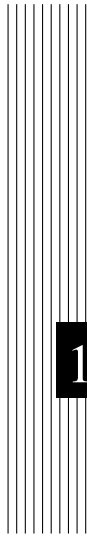
### 13.4 Implementation details

Here we show an example *namasm* namelist and the header of an example assimilation increments file on the ORCA2 grid.

The header of an assimilation increments file produced using the NetCDF tool *ncdump -h* is shown below

```
netcdf assim_background_increments {
dimensions:
    x = 182 ;
    y = 149 ;
    z = 31 ;
    t = UNLIMITED ; // (1 currently)
variables:
    float nav_lon(y, x) ;
    float nav_lat(y, x) ;
    float nav_lev(z) ;
    double time_counter(t) ;
    double time ;
    double z_inc_dateb ;
    double z_inc_datef ;
    double bckint(t, z, y, x) ;
    double bckins(t, z, y, x) ;
    double bckinu(t, z, y, x) ;
    double bckinv(t, z, y, x) ;
    double bckineta(t, y, x) ;

// global attributes:
        :DOMAIN_number_total = 1 ;
        :DOMAIN_number = 0 ;
        :DOMAIN_dimensions_ids = 1, 2 ;
        :DOMAIN_size_global = 182, 149 ;
        :DOMAIN_size_local = 182, 149 ;
        :DOMAIN_position_first = 1, 1 ;
        :DOMAIN_position_last = 182, 149 ;
        :DOMAIN_halo_size_start = 0, 0 ;
        :DOMAIN_halo_size_end = 0, 0 ;
        :DOMAIN_type = "BOX" ;
}
```



# 14 Stochastic parametrization of EOS (STO)

Authors: P.-A. Bouttier

## Contents

---

<b>14.1 Stochastic processes</b> . . . . .	<b>276</b>
<b>14.2 Implementation details</b> . . . . .	<b>277</b>

---

The stochastic parametrization module aims to explicitly simulate uncertainties in the model. More particularly, Brankart [2013] has shown that, because of the nonlinearity of the seawater equation of state, unresolved scales represent a major source of uncertainties in the computation of the large scale horizontal density gradient (from T/S large scale fields), and that the impact of these uncertainties can be simulated by random processes representing unresolved T/S fluctuations.

The stochastic formulation of the equation of state can be written as:

$$\rho = \frac{1}{2} \sum_{i=1}^m \{ \rho[T + \Delta T_i, S + \Delta S_i, p_o(z)] + \rho[T - \Delta T_i, S - \Delta S_i, p_o(z)] \} \quad (14.1)$$

where  $p_o(z)$  is the reference pressure depending on the depth and,  $\Delta T_i$  and  $\Delta S_i$  are a set of T/S perturbations defined as the scalar product of the respective local T/S gradients with random walks  $\xi$ :

$$\Delta T_i = \xi_i \cdot \nabla T \quad \text{and} \quad \Delta S_i = \xi_i \cdot \nabla S \quad (14.2)$$

$\xi_i$  are produced by a first-order autoregressive processes (AR-1) with a parametrized decorrelation time scale, and horizontal and vertical standard deviations  $\sigma_s$ .  $\xi$  are uncorrelated over the horizontal and fully correlated along the vertical.

## 14.1 Stochastic processes

The starting point of our implementation of stochastic parameterizations in NEMO is to observe that many existing parameterizations are based on autoregressive processes, which are used as a basic source of randomness to transform a deterministic model into a probabilistic model. A generic approach is thus to add one single new module in NEMO, generating processes with appropriate statistics to simulate each kind of uncertainty in the model (see Brankart et al. [2015] for more details).

In practice, at every model grid point, independent Gaussian autoregressive processes  $\xi^{(i)}$ ,  $i = 1, \dots, m$  are first generated using the same basic equation:

$$\xi_{k+1}^{(i)} = a^{(i)} \xi_k^{(i)} + b^{(i)} w^{(i)} + c^{(i)} \quad (14.3)$$

where  $k$  is the index of the model timestep; and  $a^{(i)}$ ,  $b^{(i)}$ ,  $c^{(i)}$  are parameters defining the mean ( $\mu^{(i)}$ ) standard deviation ( $\sigma^{(i)}$ ) and correlation timescale ( $\tau^{(i)}$ ) of each process:

- for order 1 processes,  $w^{(i)}$  is a Gaussian white noise, with zero mean and standard deviation equal to 1, and the parameters  $a^{(i)}$ ,  $b^{(i)}$ ,  $c^{(i)}$  are given by:

$$\begin{cases} a^{(i)} = \varphi \\ b^{(i)} = \sigma^{(i)} \sqrt{1 - \varphi^2} \\ c^{(i)} = \mu^{(i)} (1 - \varphi) \end{cases} \quad \text{with} \quad \varphi = \exp(-1/\tau^{(i)}) \quad (14.4)$$

- for order  $n > 1$  processes,  $w^{(i)}$  is an order  $n - 1$  autoregressive process, with zero mean, standard deviation equal to  $\sigma^{(i)}$ ; correlation timescale equal to  $\tau^{(i)}$ ; and the parameters  $a^{(i)}$ ,  $b^{(i)}$ ,  $c^{(i)}$  are given by:

$$\begin{cases} a^{(i)} = \varphi \\ b^{(i)} = \frac{n-1}{2(4n-3)} \sqrt{1-\varphi^2} \\ c^{(i)} = \mu^{(i)} (1-\varphi) \end{cases} \quad \text{with} \quad \varphi = \exp(-1/\tau^{(i)}) \quad (14.5)$$

In this way, higher order processes can be easily generated recursively using the same piece of code implementing Eq. (14.3), and using successively processes from order 0 to  $n - 1$  as  $w^{(i)}$ . The parameters in Eq. (14.5) are computed so that this recursive application of Eq. (14.3) leads to processes with the required standard deviation and correlation timescale, with the additional condition that the  $n - 1$  first derivatives of the autocorrelation function are equal to zero at  $t = 0$ , so that the resulting processes become smoother and smoother as  $n$  is increased.

Overall, this method provides quite a simple and generic way of generating a wide class of stochastic processes. However, this also means that new model parameters are needed to specify each of these stochastic processes. As in any parameterization of lacking physics, a very important issues then to tune these new parameters using either first principles, model simulations, or real-world observations.

## 14.2 Implementation details

```
!-----
&namsto      ! Stochastic parametrization of EOS                (default: NO)
!-----
ln_sto_eos = .false.    ! stochastic equation of state
nn_sto_eos = 1         ! number of independent random walks
rn_eos_stdxy= 1.4      ! random walk horz. standard deviation (in grid points)
rn_eos_stdz = 0.7      ! random walk vert. standard deviation (in grid points)
rn_eos_tcor = 1440.    ! random walk time correlation (in timesteps)
nn_eos_ord = 1         ! order of autoregressive processes
nn_eosflt = 0          ! passes of Laplacian filter
rn_eos_lim = 2.0       ! limitation factor (default = 3.0)
ln_rststo = .false.    ! start from mean parameter (F) or from restart file (T)
ln_rstseed = .true.    ! read seed of RNG from restart file
cn_storst_in = "restart_sto" ! suffix of stochastic parameter restart file (input)
cn_storst_out = "restart_sto" ! suffix of stochastic parameter restart file (output)
/
```

The computer code implementing stochastic parametrisations can be found in the STO directory. It involves three modules :

**stopar.F90** : define the Stochastic parameters and their time evolution.

**stornr.F90** : a random number generator based on (and includes) the 64-bit KISS (Keep It Simple Stupid) random number generator distributed by George Marsaglia (see [here](#))

*stopts.F90* : stochastic parametrisation associated with the non-linearity of the equation of seawater, implementing Eq 14.2 and specific piece of code in the equation of state implementing Eq 14.1.

The *stopar.F90* module has 3 public routines to be called by the model (in our case, NEMO):

The first routine (*sto\_par*) is a direct implementation of Eq. (14.3), applied at each model grid point (in 2D or 3D), and called at each model time step ( $k$ ) to update every autoregressive process ( $i = 1, \dots, m$ ). This routine also includes a filtering operator, applied to  $w^{(i)}$ , to introduce a spatial correlation between the stochastic processes.

The second routine (*sto\_par\_init*) is an initialization routine mainly dedicated to the computation of parameters  $a^{(i)}$ ,  $b^{(i)}$ ,  $c^{(i)}$  for each autoregressive process, as a function of the statistical properties required by the model user (mean, standard deviation, time correlation, order of the process, ...).

Parameters for the processes can be specified through the following *namsto* namelist parameters:

*nn\_sto\_eos* : number of independent random walks

*rn\_eos\_stdxy* : random walk horz. standard deviation (in grid points)

*rn\_eos\_stdz* : random walk vert. standard deviation (in grid points)

*rn\_eos\_tcor* : random walk time correlation (in timesteps)

*nn\_eos\_ord* : order of autoregressive processes

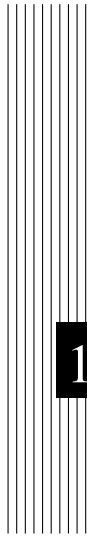
*nn\_eos\_ftt* : passes of Laplacian filter

*rn\_eos\_lim* : limitation factor (default = 3.0)

This routine also includes the initialization (seeding) of the random number generator.

The third routine (*sto\_rst\_write*) writes a restart file (which suffix name is given by *cn\_storst\_out* namelist parameter) containing the current value of all autoregressive processes to allow restarting a simulation from where it has been interrupted. This file also contains the current state of the random number generator. When *ln\_rststo* is set to *true*, the restart file (which suffix name is given by *cn\_storst\_in* namelist parameter) is read by the initialization routine (*sto\_par\_init*). The simulation will continue exactly as if it was not interrupted only when *ln\_rstseed* is set to *true*, *i.e.* when the state of the random number generator is read in the restart file.





# 15 Miscellaneous Topics

## Contents

---

<b>15.1 Representation of Unresolved Straits</b> . . . . .	<b>280</b>
15.1.1 Hand made geometry changes . . . . .	280
<b>15.2 Closed seas (<i>closea.F90</i>)</b> . . . . .	<b>282</b>
<b>15.3 Sub-Domain Functionality</b> . . . . .	<b>282</b>
15.3.1 Simple subsetting of input files via netCDF attributes .	282
<b>15.4 Accuracy and Reproducibility (<i>lib_fortran.F90</i>)</b> . . . . .	<b>283</b>
15.4.1 Issues with intrinsic SIGN function ( <b>key_nosignedzero</b> )	283
15.4.2 MPP reproducibility . . . . .	284
15.4.3 MPP scalability . . . . .	284
<b>15.5 Model Optimisation, Control Print and Benchmark</b> . . . . .	<b>285</b>

---

## 15.1 Representation of Unresolved Straits

In climate modeling, it often occurs that a crucial connections between water masses is broken as the grid mesh is too coarse to resolve narrow straits. For example, coarse grid spacing typically closes off the Mediterranean from the Atlantic at the Strait of Gibraltar. In this case, it is important for climate models to include the effects of salty water entering the Atlantic from the Mediterranean. Likewise, it is important for the Mediterranean to replenish its supply of water from the Atlantic to balance the net evaporation occurring over the Mediterranean region. This problem occurs even in eddy permitting simulations. For example, in ORCA 1/4° several straits of the Indonesian archipelago (Ombai, Lombok...) are much narrow than even a single ocean grid-point.

We describe briefly here the three methods that can be used in *NEMO* to handle such improperly resolved straits. The first two consist of opening the strait by hand while ensuring that the mass exchanges through the strait are not too large by either artificially reducing the surface of the strait grid-cells or, locally increasing the lateral friction. In the third one, the strait is closed but exchanges of mass, heat and salt across the land are allowed. Note that such modifications are so specific to a given configuration that no attempt has been made to set them in a generic way. However, examples of how they can be set up is given in the ORCA 2° and 0.5° configurations. For example, for details of implementation in ORCA2, search:

```
IF( cp_cfg == "orca" .AND. jp_cfg == 2 )
```

### 15.1.1 Hand made geometry changes

- reduced scale factor in the cross-strait direction to a value in better agreement with the true mean width of the strait. (Fig. 15.1). This technique is sometime called "partially open face" or "partially closed cells". The key issue here is only to reduce the faces of *T*-cell (*i.e.* change the value of the horizontal scale factors at *u*- or *v*-point) but not the volume of the *T*-cell. Indeed, reducing the volume of strait *T*-cell can easily produce a numerical instability at that grid point that would require a reduction of the model time step. The changes associated with strait management are done in *domhgr.F90*, just after the definition or reading of the horizontal scale factors.

- increase of the viscous boundary layer thickness by local increase of the *fmask* value at the coast (Fig. 15.1). This is done in *dommsk.F90* together with the setting of the coastal value of *fmask* (see Section 8.1)

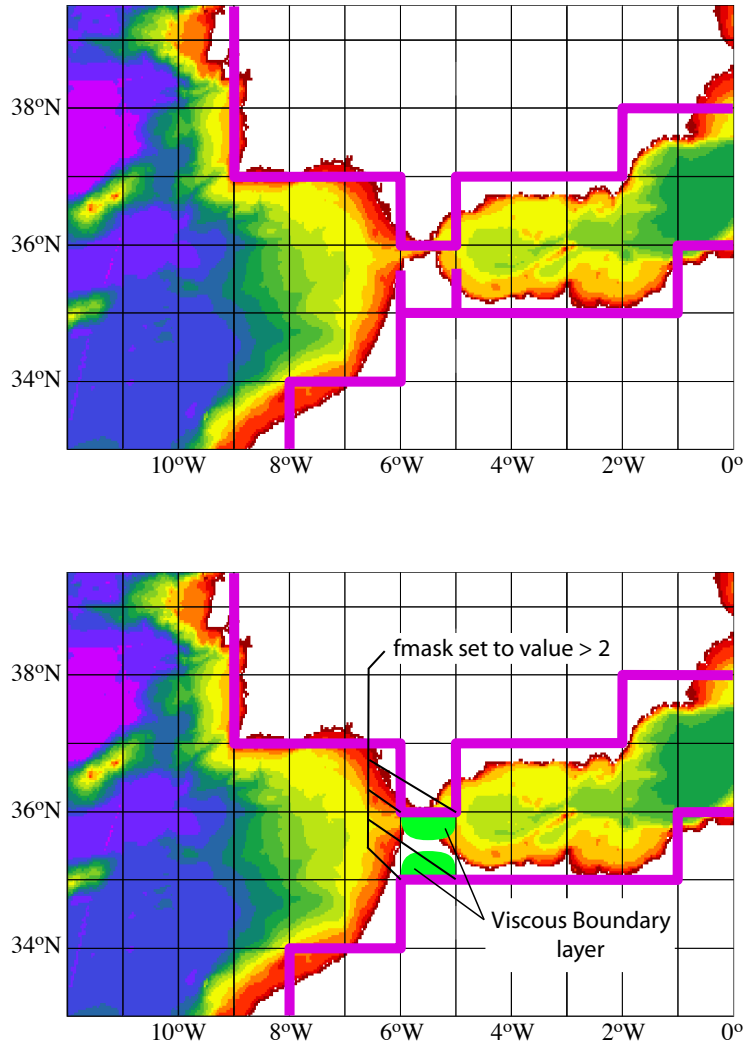


**Figure 15.1:** Example of the Gibraltar strait defined in a  $1^\circ \times 1^\circ$  mesh. *Top:* using partially open cells. The meridional scale factor at  $v$ -point is reduced on both sides of the strait to account for the real width of the strait (about 20 km). Note that the scale factors of the strait  $T$ -point remains unchanged. *Bottom:* using viscous boundary layers. The four  $f_{\text{mask}}$  parameters along the strait coastlines are set to a value larger than 4, *i.e.* "strong" no-slip case (see Fig.8.2) creating a large viscous boundary layer that allows a reduced transport through the strait.

## 15.2 Closed seas (*closea.F90*)

Add here a short description of the way closed seas are managed

## 15.3 Sub-Domain Functionality

### 15.3.1 Simple subsetting of input files via netCDF attributes

The extended grids for use with the under-shelf ice cavities will result in redundant rows around Antarctica if the ice cavities are not active. A simple mechanism for subsetting input files associated with the extended domains has been implemented to avoid the need to maintain different sets of input fields for use with or without active ice cavities. The existing 'zoom' options are overly complex for this task and marked for deletion anyway. This alternative subsetting operates for the j-direction only and works by optionally looking for and using a global file attribute (named: *open\_ocean\_jstart*) to determine the starting j-row for input. The use of this option is best explained with an example: Consider an ORCA1 configuration using the extended grid bathymetry and coordinate files:

```
eORCA1_bathymetry_v2.nc
eORCA1_coordinates.nc
```

These files define a horizontal domain of 362x332. Assuming the first row with open ocean wet points in the non-*isf* bathymetry for this set is row 42 (Fortran indexing) then the formally correct setting for *open\_ocean\_jstart* is 41. Using this value as the first row to be read will result in a 362x292 domain which is the same size as the original ORCA1 domain. Thus the extended coordinates and bathymetry files can be used with all the original input files for ORCA1 if the ice cavities are not active (*ln\_isfcav = .false.*). Full instructions for achieving this are:

Add the new attribute to any input files requiring a j-row offset, i.e:

```
ncatted -a open_ocean_jstart,global,a,d,41 eORCA1_coordinates.nc
ncatted -a open_ocean_jstart,global,a,d,41 eORCA1_bathymetry_v2.nc
```

Add the logical switch to *namcfg* in the configuration namelist and set true:

```
!-----
&namcfg      ! parameters of the configuration      ! (default: user defined GYRE)
!-----
  ln_read_cfg = .false.  ! (=T) read the domain configuration file
  !              ! (=F) user defined configuration ==>>> see usrdef(...) modules
  cn_domcfg = "domain_cfg"      ! domain configuration filename
  !
  ln_write_cfg = .false.  ! (=T) create the domain configuration file
  cn_domcfg_out = "domain_cfg_out" ! newly created domain configuration filename
  !
  ln_use_jattr = .false.  ! use (T) the file attribute: open_ocean_jstart, if present
  !              ! in netcdf input files, as the start j-row for reading
/
```

Note the j-size of the global domain is the (extended j-size minus *open\_ocean\_jstart* + 1) and this must match the size of all datasets other than bathymetry and coordinates currently. However the option can be extended to any global, 2D and 3D, netcdf, input field by adding the:

```
lrowattr=ln_use_jattr
```

optional argument to the appropriate *iom\_get* call and the *open\_ocean\_jstart* attribute to the corresponding input files. It remains the users responsibility to set *jpjdt* and *jpglo* values in the *namelist\_cfg* file according to their needs.

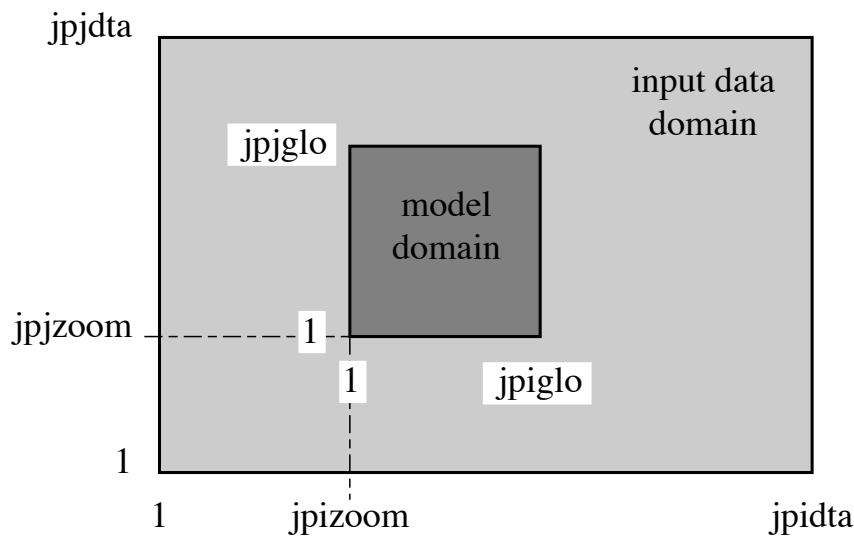


**Figure 15.2:** Position of a model domain compared to the data input domain when the zoom functionality is used.

## 15.4 Accuracy and Reproducibility (*lib\_fortran.F90*)

### 15.4.1 Issues with intrinsic SIGN function (*key\_nosignedzero*)

The  $\text{SIGN}(A, B)$  is the FORTRAN intrinsic function delivers the magnitude of  $A$  with the sign of  $B$ . For example,  $\text{SIGN}(-3.0, 2.0)$  has the value  $3.0$ . The problematic case is when the second argument is zero, because, on platforms that support IEEE arithmetic, zero is actually a signed number. There is a positive zero and a negative zero.

In FORTRAN 90, the processor was required always to deliver a positive result for  $\text{SIGN}(A, B)$  if  $B$  was zero. Nevertheless, in FORTRAN 95, the processor is allowed to do the correct thing and deliver  $\text{ABS}(A)$  when  $B$  is a positive zero and  $-\text{ABS}(A)$  when  $B$  is a negative zero. This change in the specification becomes apparent only when  $B$  is of type real, and is zero, and the processor is capable of distinguishing between positive and negative zero, and  $B$  is negative real zero. Then  $\text{SIGN}$  delivers a negative result where, under FORTRAN 90 rules, it used to

return a positive result. This change may be especially sensitive for the ice model, so we overwrite the intrinsic function with our own function simply performing :

```

      IF ( B >= 0.e0 ) THEN      ;    SIGN (A, B) = ABS (A)
      ELSE                      ;    SIGN (A, B) = -ABS (A)
      ENDIF

```

This feature can be found in *lib\_fortran.F90* module and is effective when **key\_nosignedzero** is defined. We use a CPP key as the overwriting of a intrinsic function can present performance issues with some computers/compilers.

### 15.4.2 MPP reproducibility

The numerical reproducibility of simulations on distributed memory parallel computers is a critical issue. In particular, within NEMO global summation of distributed arrays is most susceptible to rounding errors, and their propagation and accumulation cause uncertainty in final simulation reproducibility on different numbers of processors. To avoid so, based on [He and Ding \[2001\]](#) review of different technics, we use a so called self-compensated summation method. The idea is to estimate the roundoff error, store it in a buffer, and then add it back in the next addition.

Suppose we need to calculate  $b = a_1 + a_2 + a_3$ . The following algorithm will allow to split the sum in two ( $sum_1 = a_1 + a_2$  and  $b = sum_2 = sum_1 + a_3$ ) with exactly the same rounding errors as the sum performed all at once.

$$\begin{aligned}
 sum_1 &= a_1 + a_2 \\
 error_1 &= a_2 + (a_1 - sum_1) \\
 sum_2 &= sum_1 + a_3 + error_1 \\
 error_2 &= a_3 + error_1 + (sum_1 - sum_2) \\
 b &= sum_2
 \end{aligned}$$

An example of this feature can be found in *lib\_fortran.F90* module. It is systematicallt used in *glob\_sum* function (summation over the entire basin excluding duplicated rows and columns due to cyclic or north fold boundary condition as well as overlap MPP areas). The self-compensated summation method should be used in all summation in i- and/or j-direction. See *closea.F90* module for an example. Note also that this implementation may be sensitive to the optimization level.

### 15.4.3 MPP scalability

The default method of communicating values across the north-fold in distributed memory applications (**key\_mpp\_mpi**) uses a `MPI_ALLGATHER` function to exchange values from each processing region in the northern row with every other processing region in the northern row. This enables a global width array containing the top 4 rows to be collated on every northern row processor and then folded

with a simple algorithm. Although conceptually simple, this "All to All" communication will hamper performance scalability for large numbers of northern row processors. From version 3.4 onwards an alternative method is available which only performs direct "Peer to Peer" communications between each processor and its immediate "neighbours" across the fold line. This is achieved by using the default MPI\_ALLGATHER method during initialisation to help identify the "active" neighbours. Stored lists of these neighbours are then used in all subsequent north-fold exchanges to restrict exchanges to those between associated regions. The collated global width array for each region is thus only partially filled but is guaranteed to be set at all the locations actually required by each individual for the fold operation. This alternative method should give identical results to the default ALLGATHER method and is recommended for large values of *jpni*. The new method is activated by setting *ln\_nogather* to be true (**nammpp**). The reproducibility of results using the two methods should be confirmed for each new, non-reference configuration.

## 15.5 Model Optimisation, Control Print and Benchmark

```

!-----
&namctl      ! Control prints
!-----
ln_ctl       = .false. ! trends control print (expensive!)
nn_print     = 0       ! level of print (0 no extra print)
nn_ictls     = 0       ! start i indice of control sum (use to compare mono versus
nn_ictle     = 0       ! end i indice of control sum      multi processor runs
nn_jctls     = 0       ! start j indice of control          over a subdomain)
nn_jctle     = 0       ! end j indice of control
nn_isplt     = 1       ! number of processors in i-direction
nn_jsplt     = 1       ! number of processors in j-direction
ln_timing    = .false. ! timing by routine write out in timing.output file
ln_diacfl    = .false. ! CFL diagnostics write out in cfl_diagnostics.ascii
/

```

Options are defined through the *namctl* namelist variables.

- Vector optimisation:

**key\_vectopt\_loop** enables the internal loops to collapse. This is very a very efficient way to increase the length of vector calculations and thus to speed up the model on vector computers.

- Control print

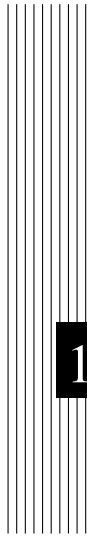
1- *ln\_ctl* : compute and print the trends averaged over the interior domain in all TRA, DYN, LDF and ZDF modules. This option is very helpful when diagnosing the origin of an undesired change in model results.

2- also *ln\_ctl* but using the *nictl* and *njctl* namelist parameters to check the source of differences between mono and multi processor runs.

3- last digit comparison (*nn\_bit\_cmp*). In an MPP simulation, the computation of a sum over the whole domain is performed as the summation over all processors of each of their sums over their interior domains. This double sum never gives exactly the same result as a single sum over the whole domain, due to truncation differences. The "bit comparison" option has been introduced in order to be able to check that mono-processor and multi-processor runs give exactly the same results.

- Benchmark (*nn\_bench*). This option defines a benchmark run based on a GYRE configuration (see §16.4) in which the resolution remains the same whatever the domain size. This allows a very large model domain to be used, just by changing the domain size (*jpiglo*, *jpglo*) and without adjusting either the time-step or the physical parameterisations.





# 16 Configurations

## Contents

---

<b>16.1 Introduction</b>	<b>288</b>
<b>16.2 Water column model: 1D model (C1D) (key_c1d)</b>	<b>288</b>
<b>16.3 ORCA family: global ocean with tripolar grid</b>	<b>289</b>
16.3.1 ORCA tripolar grid	289
16.3.2 ORCA pre-defined resolution	292
<b>16.4 GYRE family: double gyre basin</b>	<b>293</b>
<b>16.5 AMM: atlantic margin configuration</b>	<b>294</b>

---

## 16.1 Introduction

The purpose of this part of the manual is to introduce the *NEMO* reference configurations. These configurations are offered as means to explore various numerical and physical options, thus allowing the user to verify that the code is performing in a manner consistent with that we are running. This form of verification is critical as one adopts the code for his or her particular research purposes. The reference configurations also provide a sense for some of the options available in the code, though by no means are all options exercised in the reference configurations.

Configuration is defined mainly through the *namcfg* namelist variables:

```

!-----
&namcfg      ! parameters of the configuration                               ! (default: user defined GYRE)
!-----
  ln_read_cfg = .false.  ! (=T) read the domain configuration file
                        ! (=F) user defined configuration ==>>> see usrdef(...) modules
  cn_domcfg = "domain_cfg" ! domain configuration filename
                        !
  ln_write_cfg = .false. ! (=T) create the domain configuration file
                        ! cn_domcfg_out = "domain_cfg_out" ! newly created domain configuration filename
                        !
  ln_use_jattr = .false. ! use (T) the file attribute: open_ocean_jstart, if present
                        ! in netcdf input files, as the start j-row for reading
/

```

## 16.2 Water column model: 1D model (C1D) (key\_c1d)

BE careful: to be re-written according to suppression of jpzoom and jppzoom !!!!

The 1D model option simulates a stand alone water column within the 3D *NEMO* system. It can be applied to the ocean alone or to the ocean-ice system and can include passive tracers or a biogeochemical model. It is set up by defining the position of the 1D water column in the grid (see *CONFIG/SHARED/namelist\_ref*). The 1D model is a very useful tool (*a*) to learn about the physics and numerical treatment of vertical mixing processes ; (*b*) to investigate suitable parameterisations of unresolved turbulence (surface wave breaking, Langmuir circulation, ...) ; (*c*) to compare the behaviour of different vertical mixing schemes ; (*d*) to perform sensitivity studies on the vertical diffusion at a particular point of an ocean domain ; (*d*) to produce extra diagnostics, without the large memory requirement of the full 3D model.

The methodology is based on the use of the zoom functionality over the smallest possible domain : a 3x3 domain centered on the grid point of interest, with some extra routines. There is no need to define a new mesh, bathymetry, initial state or forcing, since the 1D model will use those of the configuration it is a zoom

of. The chosen grid point is set in *namcfg* namelist by setting the *jpizoom* and *npjzoom* parameters to the indices of the location of the chosen grid point.

The 1D model has some specifics. First, all the horizontal derivatives are assumed to be zero, and second, the two components of the velocity are moved on a *T*-point. Therefore, defining **key\_c1d** changes five main things in the code behaviour:

- (1) the lateral boundary condition routine (*lbc\_lnk*) set the value of the central column of the 3x3 domain is imposed over the whole domain ;
- (3) a call to *lbc\_lnk* is systematically done when reading input data (*i.e.* in *iom.F90*) ;
- (3) a simplified *stp* routine is used (*stp\_c1d*, see *step\_c1d.F90* module) in which both lateral tendency terms and lateral physics are not called ;
- (4) the vertical velocity is zero (so far, no attempt at introducing a Ekman pumping velocity has been made) ;
- (5) a simplified treatment of the Coriolis term is performed as *U*- and *V*-points are the same (see *dyncor\_c1d.F90*).

All the relevant *\_c1d* modules can be found in the NEMOGCM/NEMO/OPA\_SRC/C1D directory of the *NEMO* distribution.

## 16.3 ORCA family: global ocean with tripolar grid

The ORCA family is a series of global ocean configurations that are run together with the LIM sea-ice model (ORCA-LIM) and possibly with PISCES biogeochemical model (ORCA-LIM-PISCES), using various resolutions. The appropriate namelist is available in *CONFIG/ORCA2\_LIM3\_PISCES/EXP00/namelist\_cfg* for ORCA2 and in *CONFIG/SHARED/README\_configs\_namcfg\_namdom* for other resolutions

### 16.3.1 ORCA tripolar grid

The ORCA grid is a tripolar is based on the semi-analytical method of [Madec and Imbard \[1996\]](#). It allows to construct a global orthogonal curvilinear ocean mesh which has no singularity point inside the computational domain since two north mesh poles are introduced and placed on lands. The method involves defining an analytical set of mesh parallels in the stereographic polar plan, computing the associated set of mesh meridians, and projecting the resulting mesh onto the sphere. The set of mesh parallels used is a series of embedded ellipses which foci are the two mesh north poles (Fig. 16.1). The resulting mesh presents no loss of continuity in either the mesh lines or the scale factors, or even the scale factor derivatives over the whole ocean domain, as the mesh is not a composite mesh.

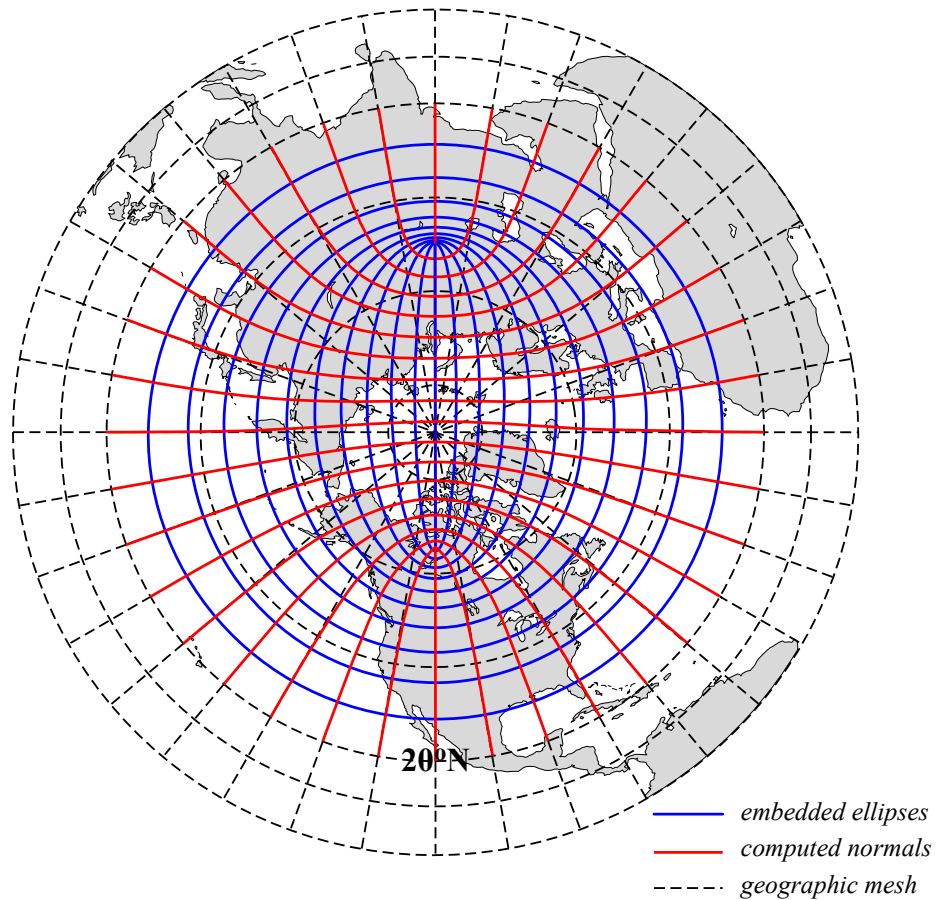


**Figure 16.1:** ORCA mesh conception. The departure from an isotropic Mercator grid start poleward of  $20^{\circ}N$ . The two "north pole" are the foci of a series of embedded ellipses (blue curves) which are determined analytically and form the i-lines of the ORCA mesh (pseudo latitudes). Then, following Madec and Imbard [1996], the normal to the series of ellipses (red curves) is computed which provide the j-lines of the mesh (pseudo longitudes).

The method is applied to Mercator grid (*i.e.* same zonal and meridional grid spacing) poleward of  $20^{\circ}N$ , so that the Equator is a mesh line, which provides a better numerical solution for equatorial dynamics. The choice of the series of embedded ellipses (position of the foci and variation of the ellipses) is a compromise between maintaining the ratio of mesh anisotropy ( $e_1/e_2$ ) close to one in the ocean (especially in area of strong eddy activities such as the Gulf Stream) and keeping the smallest scale factor in the northern hemisphere larger than the smallest one in the southern hemisphere. The resulting mesh is shown in Fig. 16.1 and 16.2 for a half a degree grid (ORCA\_R05). The smallest ocean scale factor is found in along Antarctica, while the ratio of anisotropy remains close to one except near the

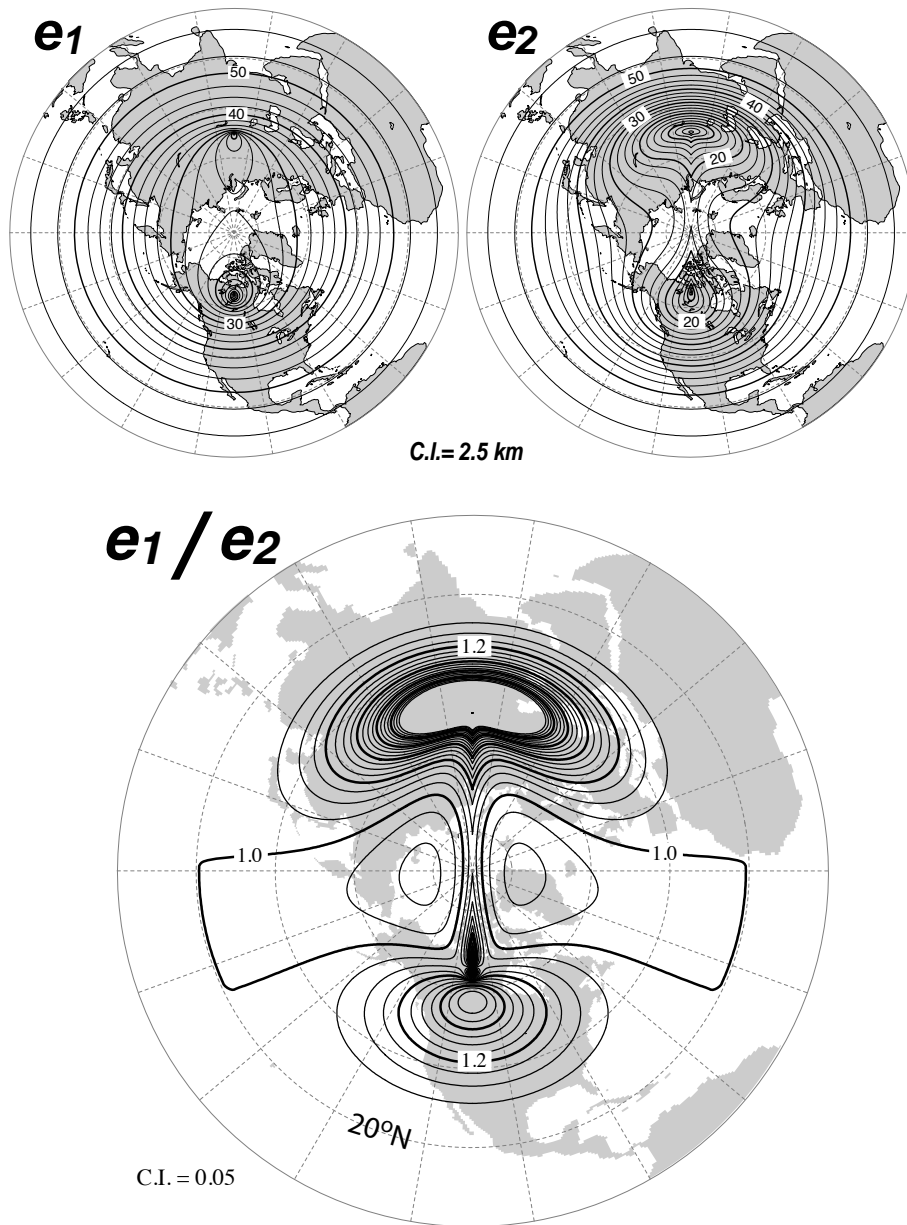


**Figure 16.2:** *Top:* Horizontal scale factors ( $e_1$ ,  $e_2$ ) and *Bottom:* ratio of anisotropy ( $e_1/e_2$ ) for ORCA  $0.5^\circ$  mesh. South of  $20^\circ N$  a Mercator grid is used ( $e_1 = e_2$ ) so that the anisotropy ratio is 1. Poleward of  $20^\circ N$ , the two "north pole" introduce a weak anisotropy over the ocean areas ( $< 1.2$ ) except in vicinity of Victoria Island (Canadian Arctic Archipelago).

**Table 16.1:** Set of predefined parameters for ORCA family configurations. In all cases, the flag for configurations of ORCA family is set to 1 in *domain\_cfg*

Horizontal Grid	<i>ORCA_index</i>	<i>jpglo</i>	<i>jpglo</i>
$\tilde{4}^\circ$	4	92	76
$\tilde{2}^\circ$	2	182	149
$\tilde{1}^\circ$	1	362	292
$\tilde{0.5}^\circ$	05	722	511
$\tilde{0.25}^\circ$	025	1442	1021

Victoria Island in the Canadian Archipelago.

### 16.3.2 ORCA pre-defined resolution

The NEMO system is provided with five built-in ORCA configurations which differ in the horizontal resolution. The value of the resolution is given by the resolution at the Equator expressed in degrees. Each of configuration is set through the *domain\_cfg* file, which sets the grid size and configuration name parameters (Tab. 16.1).

The ORCA\_R2 configuration has the following specificity : starting from a  $2^\circ$  ORCA mesh, local mesh refinements were applied to the Mediterranean, Red, Black and Caspian Seas, so that the resolution is  $1^\circ$  there. A local transformation were also applied with in the Tropics in order to refine the meridional resolution up to  $0.5^\circ$  at the Equator.

The ORCA\_R1 configuration has only a local tropical transformation to refine the meridional resolution up to  $1/3^\circ$  at the Equator. Note that the tropical mesh refinements in ORCA\_R2 and R1 strongly increases the mesh anisotropy there.

The ORCA\_R05 and higher global configurations do not incorporate any regional refinements.

For ORCA\_R1 and R025, setting the configuration key to 75 allows to use 75 vertical levels, otherwise 46 are used. In the other ORCA configurations, 31 levels are used (see Tab. 4.2 and Fig. 4.6).

Only the ORCA\_R2 is provided with all its input files in the *NEMO* distribution. It is very similar to that used as part of the climate model developed at IPSL for the 4th IPCC assessment of climate change (Marti et al., 2009). It is also the basis for the *NEMO* contribution to the Coordinate Ocean-ice Reference Experiments (COREs) documented in Griffies et al. [2009].

This version of ORCA\_R2 has 31 levels in the vertical, with the highest resolution (10m) in the upper 150m (see Tab. 4.2 and Fig. 4.6). The bottom topography and the coastlines are derived from the global atlas of Smith and Sandwell (1997). The default forcing uses the boundary forcing from Large and Yeager [2004] (see §7.5.1), which was developed for the purpose of running global coupled ocean-ice simulations without an interactive atmosphere. This Large and Yeager [2004]

dataset is available through the [GFDL web site](#). The "normal year" of [Large and Yeager \[2004\]](#) has been chosen of the *NEMO* distribution since release v3.3.

ORCA\_R2 pre-defined configuration can also be run with an AGRIF zoom over the Agulhas current area ( **key\_agrif** defined) and, by setting the appropriate variables, see *CONFIG/SHARED/namelist\_ref* a regional Arctic or peri-Antarctic configuration is extracted from an ORCA\_R2 or R05 configurations using sponge layers at open boundaries.

## 16.4 GYRE family: double gyre basin

The GYRE configuration [[Lévy et al. 2010](#)] has been built to simulate the seasonal cycle of a double-gyre box model. It consists in an idealized domain similar to that used in the studies of [Drijfhout \[1994\]](#) and [Hazeleger and Drijfhout \[1998; 1999; 2000b;a\]](#), over which an analytical seasonal forcing is applied. This allows to investigate the spontaneous generation of a large number of interacting, transient mesoscale eddies and their contribution to the large scale circulation.

The domain geometry is a closed rectangular basin on the  $\beta$ -plane centred at  $\sim 30^\circ N$  and rotated by  $45^\circ$ , 3180 km long, 2120 km wide and 4 km deep (Fig. 15.1). The domain is bounded by vertical walls and by a flat bottom. The configuration is meant to represent an idealized North Atlantic or North Pacific basin. The circulation is forced by analytical profiles of wind and buoyancy fluxes. The applied forcings vary seasonally in a sinusoidal manner between winter and summer extrema [[Lévy et al. 2010](#)]. The wind stress is zonal and its curl changes sign at  $22^\circ N$  and  $36^\circ N$ . It forces a subpolar gyre in the north, a subtropical gyre in the wider part of the domain and a small recirculation gyre in the southern corner. The net heat flux takes the form of a restoring toward a zonal apparent air temperature profile. A portion of the net heat flux which comes from the solar radiation is allowed to penetrate within the water column. The fresh water flux is also prescribed and varies zonally. It is determined such as, at each time step, the basin-integrated flux is zero. The basin is initialised at rest with vertical profiles of temperature and salinity uniformly applied to the whole domain.

The GYRE configuration is set like an analytical configuration, through *ln\_read\_cfg=true* in *namcfg* namelist defined in the reference configuration *CONFIG/GYRE/EXP00/namelist\_cfg*. Its horizontal resolution (and thus the size of the domain) is determined by setting *nn\_GYRE* in *namusr\_def*:

$$jpiglo = 30 \times nn\_GYRE + 2$$

$$jjpglo = 20 \times nn\_GYRE + 2$$

Obviously, the namelist parameters have to be adjusted to the chosen resolution, see the Configurations pages on the NEMO web site (Using NEMOConfigurations) . In the vertical, GYRE uses the default 30 ocean levels (*jpk=31*) (Fig. 4.6).

The GYRE configuration is also used in benchmark test as it is very simple to increase its resolution and as it does not requires any input file. For example, keeping a same model size on each processor while increasing the number of pro-

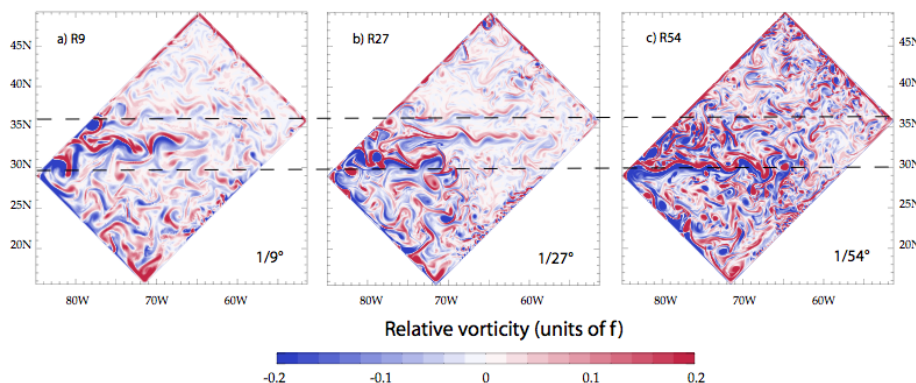


**Figure 16.3:** Snapshot of relative vorticity at the surface of the model domain in GYRE R9, R27 and R54. From Lévy et al. [2010].

cessor used is very easy, even though the physical integrity of the solution can be compromised. Benchmark is activate via `ln_bench=true` in `namusr_def` in namelist `CONFIG/GYRE/EXP00/namelist_cfg`.

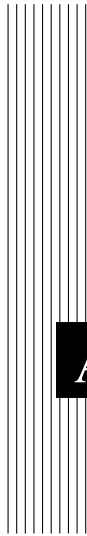
## 16.5 AMM: atlantic margin configuration

The AMM, Atlantic Margins Model, is a regional model covering the Northwest European Shelf domain on a regular lat-lon grid at approximately 12km horizontal resolution. The appropriate `&namcfg` namelist is available in `CONFIG/AMM12/EXP00/namelist_cfg`. It is used to build the correct dimensions of the AMM domain.

This configuration tests several features of NEMO functionality specific to the shelf seas. In particular, the AMM uses  $S$ -coordinates in the vertical rather than  $z$ -coordinates and is forced with tidal lateral boundary conditions using a flather boundary condition from the BDY module. The AMM configuration uses the GLS (`key_zdfgls`) turbulence scheme, the VVL non-linear free surface (`key_vvl`) and time-splitting (`key_dynspg_ts`).

In addition to the tidal boundary condition the model may also take open boundary conditions from a North Atlantic model. Boundaries may be completely omitted by setting `ln_bdy` to false. Sample surface fluxes, river forcing and a sample initial restart file are included to test a realistic model run. The Baltic boundary is included within the river input file and is specified as a river source. Unlike ordinary river points the Baltic inputs also include salinity and temperature data.





# **A** Curvilinear $s$ –Coordinate Equations

## **Contents**

---

<b>A.1</b>	<b>The chain rule for <math>s</math>–coordinates . . . . .</b>	<b>296</b>
<b>A.2</b>	<b>Continuity Equation in <math>s</math>–coordinates . . . . .</b>	<b>296</b>
<b>A.3</b>	<b>Momentum Equation in <math>s</math>–coordinate . . . . .</b>	<b>298</b>
<b>A.4</b>	<b>Tracer Equation . . . . .</b>	<b>302</b>

---

## A.1 The chain rule for $s$ –coordinates

In order to establish the set of Primitive Equation in curvilinear  $s$ -coordinates (*i.e.* an orthogonal curvilinear coordinate in the horizontal and an Arbitrary Lagrangian Eulerian (ALE) coordinate in the vertical), we start from the set of equations established in §2.3.2 for the special case  $k = z$  and thus  $e_3 = 1$ , and we introduce an arbitrary vertical coordinate  $a = a(i, j, z, t)$ . Let us define a new vertical scale factor by  $e_3 = \partial z / \partial s$  (which now depends on  $(i, j, z, t)$ ) and the horizontal slope of  $s$ –surfaces by :

$$\sigma_1 = \frac{1}{e_1} \left. \frac{\partial z}{\partial i} \right|_s \quad \text{and} \quad \sigma_2 = \frac{1}{e_2} \left. \frac{\partial z}{\partial j} \right|_s \quad (\text{A.1})$$

The chain rule to establish the model equations in the curvilinear  $s$ –coordinate system is:

$$\begin{aligned} \left. \frac{\partial \bullet}{\partial t} \right|_z &= \left. \frac{\partial \bullet}{\partial t} \right|_s - \frac{\partial \bullet}{\partial s} \frac{\partial s}{\partial t} \\ \left. \frac{\partial \bullet}{\partial i} \right|_z &= \left. \frac{\partial \bullet}{\partial i} \right|_s - \frac{\partial \bullet}{\partial s} \frac{\partial s}{\partial i} = \left. \frac{\partial \bullet}{\partial i} \right|_s - \frac{e_1}{e_3} \sigma_1 \frac{\partial \bullet}{\partial s} \\ \left. \frac{\partial \bullet}{\partial j} \right|_z &= \left. \frac{\partial \bullet}{\partial j} \right|_s - \frac{\partial \bullet}{\partial s} \frac{\partial s}{\partial j} = \left. \frac{\partial \bullet}{\partial j} \right|_s - \frac{e_2}{e_3} \sigma_2 \frac{\partial \bullet}{\partial s} \\ \frac{\partial \bullet}{\partial z} &= \frac{1}{e_3} \frac{\partial \bullet}{\partial s} \end{aligned} \quad (\text{A.2})$$

In particular applying the time derivative chain rule to  $z$  provides the expression for  $w_s$ , the vertical velocity of the  $s$ –surfaces referenced to a fix  $z$ -coordinate:

$$w_s = \left. \frac{\partial z}{\partial t} \right|_s = \frac{\partial z}{\partial s} \frac{\partial s}{\partial t} = e_3 \frac{\partial s}{\partial t} \quad (\text{A.3})$$

## A.2 Continuity Equation in $s$ –coordinates

Using (A.2) and the fact that the horizontal scale factors  $e_1$  and  $e_2$  do not depend on the vertical coordinate, the divergence of the velocity relative to the  $(i, j, z)$  coordinate system is transformed as follows in order to obtain its expression in the

curvilinear  $s$ -coordinate system:

$$\begin{aligned}
\nabla \cdot \mathbf{U} &= \frac{1}{e_1 e_2} \left[ \frac{\partial(e_2 u)}{\partial i} \Big|_z + \frac{\partial(e_1 v)}{\partial j} \Big|_z \right] + \frac{\partial w}{\partial z} \\
&= \frac{1}{e_1 e_2} \left[ \frac{\partial(e_2 u)}{\partial i} \Big|_s - \frac{e_1}{e_3} \sigma_1 \frac{\partial(e_2 u)}{\partial s} + \frac{\partial(e_1 v)}{\partial j} \Big|_s - \frac{e_2}{e_3} \sigma_2 \frac{\partial(e_1 v)}{\partial s} \right] + \frac{\partial w}{\partial s} \frac{\partial s}{\partial z} \\
&= \frac{1}{e_1 e_2} \left[ \frac{\partial(e_2 u)}{\partial i} \Big|_s + \frac{\partial(e_1 v)}{\partial j} \Big|_s \right] + \frac{1}{e_3} \left[ \frac{\partial w}{\partial s} - \sigma_1 \frac{\partial u}{\partial s} - \sigma_2 \frac{\partial v}{\partial s} \right] \\
&= \frac{1}{e_1 e_2 e_3} \left[ \frac{\partial(e_2 e_3 u)}{\partial i} \Big|_s - e_2 u \frac{\partial e_3}{\partial i} \Big|_s + \frac{\partial(e_1 e_3 v)}{\partial j} \Big|_s - e_1 v \frac{\partial e_3}{\partial j} \Big|_s \right] \\
&\quad + \frac{1}{e_3} \left[ \frac{\partial w}{\partial s} - \sigma_1 \frac{\partial u}{\partial s} - \sigma_2 \frac{\partial v}{\partial s} \right]
\end{aligned}$$

Noting that  $\frac{1}{e_1} \frac{\partial e_3}{\partial i} \Big|_s = \frac{1}{e_1} \frac{\partial^2 z}{\partial i \partial s} \Big|_s = \frac{\partial}{\partial s} \left( \frac{1}{e_1} \frac{\partial z}{\partial i} \Big|_s \right) = \frac{\partial \sigma_1}{\partial s}$  and  $\frac{1}{e_2} \frac{\partial e_3}{\partial j} \Big|_s = \frac{\partial \sigma_2}{\partial s}$ , it becomes:

$$\begin{aligned}
\nabla \cdot \mathbf{U} &= \frac{1}{e_1 e_2 e_3} \left[ \frac{\partial(e_2 e_3 u)}{\partial i} \Big|_s + \frac{\partial(e_1 e_3 v)}{\partial j} \Big|_s \right] \\
&\quad + \frac{1}{e_3} \left[ \frac{\partial w}{\partial s} - u \frac{\partial \sigma_1}{\partial s} - v \frac{\partial \sigma_2}{\partial s} - \sigma_1 \frac{\partial u}{\partial s} - \sigma_2 \frac{\partial v}{\partial s} \right] \\
&= \frac{1}{e_1 e_2 e_3} \left[ \frac{\partial(e_2 e_3 u)}{\partial i} \Big|_s + \frac{\partial(e_1 e_3 v)}{\partial j} \Big|_s \right] + \frac{1}{e_3} \frac{\partial}{\partial s} [w - u \sigma_1 - v \sigma_2]
\end{aligned}$$

Here,  $w$  is the vertical velocity relative to the  $z$ -coordinate system. Introducing the dia-surface velocity component,  $\omega$ , defined as the volume flux across the moving  $s$ -surfaces per unit horizontal area:

$$\omega = w - w_s - \sigma_1 u - \sigma_2 v \quad (\text{A.5})$$

with  $w_s$  given by (A.3), we obtain the expression for the divergence of the velocity in the curvilinear  $s$ -coordinate system:

$$\begin{aligned}
\nabla \cdot \mathbf{U} &= \frac{1}{e_1 e_2 e_3} \left[ \frac{\partial(e_2 e_3 u)}{\partial i} \Big|_s + \frac{\partial(e_1 e_3 v)}{\partial j} \Big|_s \right] + \frac{1}{e_3} \frac{\partial \omega}{\partial s} + \frac{1}{e_3} \frac{\partial w_s}{\partial s} \\
&= \frac{1}{e_1 e_2 e_3} \left[ \frac{\partial(e_2 e_3 u)}{\partial i} \Big|_s + \frac{\partial(e_1 e_3 v)}{\partial j} \Big|_s \right] + \frac{1}{e_3} \frac{\partial \omega}{\partial s} + \frac{1}{e_3} \frac{\partial}{\partial s} (e_3 \frac{\partial s}{\partial t}) \\
&= \frac{1}{e_1 e_2 e_3} \left[ \frac{\partial(e_2 e_3 u)}{\partial i} \Big|_s + \frac{\partial(e_1 e_3 v)}{\partial j} \Big|_s \right] + \frac{1}{e_3} \frac{\partial \omega}{\partial s} + \frac{\partial}{\partial s} \frac{\partial s}{\partial t} + \frac{1}{e_3} \frac{\partial s}{\partial t} \frac{\partial e_3}{\partial s} \\
&= \frac{1}{e_1 e_2 e_3} \left[ \frac{\partial(e_2 e_3 u)}{\partial i} \Big|_s + \frac{\partial(e_1 e_3 v)}{\partial j} \Big|_s \right] + \frac{1}{e_3} \frac{\partial \omega}{\partial s} + \frac{1}{e_3} \frac{\partial e_3}{\partial t}
\end{aligned}$$

As a result, the continuity equation (2.1c) in the  $s$ -coordinates is:

$$\frac{1}{e_3} \frac{\partial e_3}{\partial t} + \frac{1}{e_1 e_2 e_3} \left[ \frac{\partial(e_2 e_3 u)}{\partial i} \Big|_s + \frac{\partial(e_1 e_3 v)}{\partial j} \Big|_s \right] + \frac{1}{e_3} \frac{\partial \omega}{\partial s} = 0 \quad (\text{A.7})$$

A additional term has appeared that take into account the contribution of the time variation of the vertical coordinate to the volume budget.

### A.3 Momentum Equation in $s$ -coordinate

Here we only consider the first component of the momentum equation, the generalization to the second one being straightforward.

• **Total derivative in vector invariant form**

Let us consider (2.13), the first component of the momentum equation in the vector invariant form. Its total  $z$ -coordinate time derivative,  $\frac{Du}{Dt}\Big|_z$  can be transformed as follows in order to obtain its expression in the curvilinear  $s$ -coordinate system:

$$\begin{aligned}\frac{Du}{Dt}\Big|_z &= \frac{\partial u}{\partial t}\Big|_z - \zeta\Big|_z v + \frac{1}{2e_1} \frac{\partial(u^2+v^2)}{\partial i}\Big|_z + w \frac{\partial u}{\partial z} \\ &= \frac{\partial u}{\partial t}\Big|_z - \zeta\Big|_z v + \frac{1}{e_1 e_2} \left[ \frac{\partial(e_2 v)}{\partial i}\Big|_z - \frac{\partial(e_1 u)}{\partial j}\Big|_z \right] v + \frac{1}{2e_1} \frac{\partial(u^2+v^2)}{\partial i}\Big|_z + w \frac{\partial u}{\partial z}\end{aligned}$$

introducing the chain rule (A.2)

$$\begin{aligned}&= \frac{\partial u}{\partial t}\Big|_z - \frac{1}{e_1 e_2} \left[ \frac{\partial(e_2 v)}{\partial i}\Big|_s - \frac{\partial(e_1 u)}{\partial j}\Big|_s - \frac{e_1}{e_3} \sigma_1 \frac{\partial(e_2 v)}{\partial s} + \frac{e_2}{e_3} \sigma_2 \frac{\partial(e_1 u)}{\partial s} \right] v \\ &\quad + \frac{1}{2e_1} \left( \frac{\partial(u^2+v^2)}{\partial i}\Big|_s - \frac{e_1}{e_3} \sigma_1 \frac{\partial(u^2+v^2)}{\partial s} \right) + \frac{w}{e_3} \frac{\partial u}{\partial s} \\ &= \frac{\partial u}{\partial t}\Big|_z + \zeta\Big|_s v + \frac{1}{2e_1} \frac{\partial(u^2+v^2)}{\partial i}\Big|_s \\ &\quad + \frac{w}{e_3} \frac{\partial u}{\partial s} - \left[ \frac{\sigma_1}{e_3} \frac{\partial v}{\partial s} - \frac{\sigma_2}{e_3} \frac{\partial u}{\partial s} \right] v - \frac{\sigma_1}{2e_3} \frac{\partial(u^2+v^2)}{\partial s} \\ &= \frac{\partial u}{\partial t}\Big|_z + \zeta\Big|_s v + \frac{1}{2e_1} \frac{\partial(u^2+v^2)}{\partial i}\Big|_s \\ &\quad + \frac{1}{e_3} \left[ w \frac{\partial u}{\partial s} + \sigma_1 v \frac{\partial v}{\partial s} - \sigma_2 v \frac{\partial u}{\partial s} - \sigma_1 u \frac{\partial u}{\partial s} - \sigma_1 v \frac{\partial v}{\partial s} \right] \\ &= \frac{\partial u}{\partial t}\Big|_z + \zeta\Big|_s v + \frac{1}{2e_1} \frac{\partial(u^2+v^2)}{\partial i}\Big|_s + \frac{1}{e_3} [w - \sigma_2 v - \sigma_1 u] \frac{\partial u}{\partial s}\end{aligned}$$

Introducing  $\omega$ , the dia-a-surface velocity given by (A.5)

$$= \frac{\partial u}{\partial t}\Big|_z + \zeta\Big|_s v + \frac{1}{2e_1} \frac{\partial(u^2+v^2)}{\partial i}\Big|_s + \frac{1}{e_3} (\omega - w_s) \frac{\partial u}{\partial s}$$

Applying the time derivative chain rule (first equation of (A.2)) to  $u$  and using (A.3) provides the expression of the last term of the right hand side,

$$w_s \frac{\partial u}{\partial s} = \frac{\partial s}{\partial t} \frac{\partial u}{\partial s} = \frac{\partial u}{\partial t}\Big|_s - \frac{\partial u}{\partial t}\Big|_z \quad ,$$

leads to the  $s$ -coordinate formulation of the total  $z$ -coordinate time derivative, *i.e.* the total  $s$ -coordinate time derivative :

$$\frac{Du}{Dt}\Big|_s = \frac{\partial u}{\partial t}\Big|_s + \zeta\Big|_s v + \frac{1}{2e_1} \frac{\partial(u^2+v^2)}{\partial i}\Big|_s + \frac{1}{e_3} \omega \frac{\partial u}{\partial s} \quad (\text{A.9})$$

Therefore, the vector invariant form of the total time derivative has exactly the same mathematical form in  $z$ - and  $s$ -coordinates. This is not the case for the flux form as shown in next paragraph.

• **Total derivative in flux form**

Let us start from the total time derivative in the curvilinear  $s$ -coordinate system we have just establish. Following the procedure used to establish (2.11), it can be transformed into :

$$\begin{aligned} \frac{Du}{Dt} \Big|_s &= \frac{\partial u}{\partial t} \Big|_s - \zeta v + \frac{1}{2e_1} \frac{\partial(u^2+v^2)}{\partial i} + \frac{1}{e_3} \omega \frac{\partial u}{\partial s} \\ &= \frac{\partial u}{\partial t} \Big|_s + \frac{1}{e_1 e_2} \left( \frac{\partial(e_2 u u)}{\partial i} + \frac{\partial(e_1 u v)}{\partial j} \right) + \frac{1}{e_3} \frac{\partial(\omega u)}{\partial s} \\ &\quad - u \left[ \frac{1}{e_1 e_2} \left( \frac{\partial(e_2 u)}{\partial i} + \frac{\partial(e_1 v)}{\partial j} \right) + \frac{1}{e_3} \frac{\partial \omega}{\partial s} \right] \\ &\quad - \frac{v}{e_1 e_2} \left( v \frac{\partial e_2}{\partial i} - u \frac{\partial e_1}{\partial j} \right) \end{aligned}$$

Introducing the vertical scale factor inside the horizontal derivative of the first two terms (*i.e.* the horizontal divergence), it becomes :

$$\begin{aligned} \frac{Du}{Dt} \Big|_s &= \frac{\partial u}{\partial t} \Big|_s + \frac{1}{e_1 e_2 e_3} \left( \frac{\partial(e_2 e_3 u^2)}{\partial i} + \frac{\partial(e_1 e_3 u v)}{\partial j} - e_2 u u \frac{\partial e_3}{\partial i} - e_1 u v \frac{\partial e_3}{\partial j} \right) + \frac{1}{e_3} \frac{\partial(\omega u)}{\partial s} \\ &\quad - u \left[ \frac{1}{e_1 e_2 e_3} \left( \frac{\partial(e_2 e_3 u)}{\partial i} + \frac{\partial(e_1 e_3 v)}{\partial j} - e_2 u \frac{\partial e_3}{\partial i} - e_1 v \frac{\partial e_3}{\partial j} \right) - \frac{1}{e_3} \frac{\partial \omega}{\partial s} \right] \\ &\quad - \frac{v}{e_1 e_2} \left( v \frac{\partial e_2}{\partial i} - u \frac{\partial e_1}{\partial j} \right) \\ &= \frac{\partial u}{\partial t} \Big|_s + \frac{1}{e_1 e_2 e_3} \left( \frac{\partial(e_2 e_3 u u)}{\partial i} + \frac{\partial(e_1 e_3 u v)}{\partial j} \right) + \frac{1}{e_3} \frac{\partial(\omega u)}{\partial s} \\ &\quad - u \left[ \frac{1}{e_1 e_2 e_3} \left( \frac{\partial(e_2 e_3 u)}{\partial i} + \frac{\partial(e_1 e_3 v)}{\partial j} \right) - \frac{1}{e_3} \frac{\partial \omega}{\partial s} \right] - \frac{v}{e_1 e_2} \left( v \frac{\partial e_2}{\partial i} - u \frac{\partial e_1}{\partial j} \right) \end{aligned}$$

Introducing a more compact form for the divergence of the momentum fluxes, and using (A.7), the  $s$ -coordinate continuity equation, it becomes :

$$= \frac{\partial u}{\partial t} \Big|_s + \nabla \cdot (\mathbf{U} u) \Big|_s + u \frac{1}{e_3} \frac{\partial e_3}{\partial t} - \frac{v}{e_1 e_2} \left( v \frac{\partial e_2}{\partial i} - u \frac{\partial e_1}{\partial j} \right)$$

which leads to the  $s$ -coordinate flux formulation of the total  $s$ -coordinate time derivative, *i.e.* the total  $s$ -coordinate time derivative in flux form :

$$\frac{Du}{Dt} \Big|_s = \frac{1}{e_3} \frac{\partial(e_3 u)}{\partial t} \Big|_s + \nabla \cdot (\mathbf{U} u) \Big|_s - \frac{v}{e_1 e_2} \left( v \frac{\partial e_2}{\partial i} - u \frac{\partial e_1}{\partial j} \right) \quad (\text{A.11})$$

which is the total time derivative expressed in the curvilinear  $s$ -coordinate system. It has the same form as in the  $z$ -coordinate but for the vertical scale factor that has appeared inside the time derivative which comes from the modification of (A.7), the continuity equation.

• **horizontal pressure gradient**

The horizontal pressure gradient term can be transformed as follows:

$$\begin{aligned} -\frac{1}{\rho_o e_1} \frac{\partial p}{\partial i} \Big|_z &= -\frac{1}{\rho_o e_1} \left[ \frac{\partial p}{\partial i} \Big|_s - \frac{e_1}{e_3} \sigma_1 \frac{\partial p}{\partial s} \right] \\ &= -\frac{1}{\rho_o e_1} \frac{\partial p}{\partial i} \Big|_s + \frac{\sigma_1}{\rho_o e_3} (-g \rho e_3) \\ &= -\frac{1}{\rho_o e_1} \frac{\partial p}{\partial i} \Big|_s - \frac{g \rho}{\rho_o} \sigma_1 \end{aligned}$$

Applying similar manipulation to the second component and replacing  $\sigma_1$  and  $\sigma_2$  by their expression (A.1), it comes:

$$\begin{aligned} -\frac{1}{\rho_o e_1} \frac{\partial p}{\partial i} \Big|_z &= -\frac{1}{\rho_o e_1} \left( \frac{\partial p}{\partial i} \Big|_s + g \rho \frac{\partial z}{\partial i} \Big|_s \right) \\ -\frac{1}{\rho_o e_2} \frac{\partial p}{\partial j} \Big|_z &= -\frac{1}{\rho_o e_2} \left( \frac{\partial p}{\partial j} \Big|_s + g \rho \frac{\partial z}{\partial j} \Big|_s \right) \end{aligned} \quad (\text{A.12})$$

An additional term appears in (A.14) which accounts for the tilt of  $s$ -surfaces with respect to geopotential  $z$ -surfaces.

As in  $z$ -coordinate, the horizontal pressure gradient can be split in two parts following Marsaleix et al. [2008]. Let defined a density anomaly,  $d$ , by  $d = (\rho - \rho_o)/\rho_o$ , and a hydrostatic pressure anomaly,  $p'_h$ , by  $p'_h = g \int_z^\eta d e_3 dk$ . The pressure is then given by:

$$\begin{aligned} p &= g \int_z^\eta \rho e_3 dk = g \int_z^\eta (\rho_o d + 1) e_3 dk \\ &= g \rho_o \int_z^\eta d e_3 dk + g \int_z^\eta e_3 dk \end{aligned}$$

Therefore,  $p$  and  $p'_h$  are linked through:

$$p = \rho_o p'_h + g(z + \eta) \quad (\text{A.13})$$

and the hydrostatic pressure balance expressed in terms of  $p'_h$  and  $d$  is:

$$\frac{\partial p'_h}{\partial k} = -d g e_3$$

Substituting (A.13) in (A.14) and using the definition of the density anomaly it comes the expression in two parts:

$$\begin{aligned} -\frac{1}{\rho_o e_1} \frac{\partial p}{\partial i} \Big|_z &= -\frac{1}{e_1} \left( \frac{\partial p'_h}{\partial i} \Big|_s + g d \frac{\partial z}{\partial i} \Big|_s \right) - \frac{g}{e_1} \frac{\partial \eta}{\partial i} \\ -\frac{1}{\rho_o e_2} \frac{\partial p}{\partial j} \Big|_z &= -\frac{1}{e_2} \left( \frac{\partial p'_h}{\partial j} \Big|_s + g d \frac{\partial z}{\partial j} \Big|_s \right) - \frac{g}{e_2} \frac{\partial \eta}{\partial j} \end{aligned} \quad (\text{A.14})$$

This formulation of the pressure gradient is characterised by the appearance of a term depending on the the sea surface height only (last term on the right hand side of expression (A.14)). This term will be loosely termed *surface pressure gradient* whereas the first term will be termed the *hydrostatic pressure gradient* by analogy to the  $z$ -coordinate formulation. In fact, the the true surface pressure gradient is  $1/\rho_o \nabla(\rho\eta)$ , and  $\eta$  is implicitly included in the computation of  $p'_h$  through the upper bound of the vertical integration.

#### • The other terms of the momentum equation

The coriolis and forcing terms as well as the the vertical physics remain unchanged as they involve neither time nor space derivatives. The form of the lateral physics is discussed in appendix B.

#### • Full momentum equation

To sum up, in a curvilinear  $s$ -coordinate system, the vector invariant momentum equation solved by the model has the same mathematical expression as the one in a curvilinear  $z$ -coordinate, except for the pressure gradient term :

$$\begin{aligned} \frac{\partial u}{\partial t} &= +(\zeta + f) v - \frac{1}{2e_1} \frac{\partial}{\partial i} (u^2 + v^2) - \frac{1}{e_3} \omega \frac{\partial u}{\partial k} \\ &\quad - \frac{1}{e_1} \left( \frac{\partial p'_h}{\partial i} + g d \frac{\partial z}{\partial i} \right) - \frac{g}{e_1} \frac{\partial \eta}{\partial i} + D_u^{\mathbf{U}} + F_u^{\mathbf{U}} \end{aligned} \quad (\text{A.15a})$$

$$\begin{aligned} \frac{\partial v}{\partial t} &= -(\zeta + f) u - \frac{1}{2e_2} \frac{\partial}{\partial j} (u^2 + v^2) - \frac{1}{e_3} \omega \frac{\partial v}{\partial k} \\ &\quad - \frac{1}{e_2} \left( \frac{\partial p'_h}{\partial j} + g d \frac{\partial z}{\partial j} \right) - \frac{g}{e_2} \frac{\partial \eta}{\partial j} + D_v^{\mathbf{U}} + F_v^{\mathbf{U}} \end{aligned} \quad (\text{A.15b})$$

whereas the flux form momentum equation differ from it by the formulation of both the time derivative and the pressure gradient term :

$$\begin{aligned} \frac{1}{e_3} \frac{\partial (e_3 u)}{\partial t} &= \nabla \cdot (\mathbf{U} u) + \left\{ f + \frac{1}{e_1 e_2} \left( v \frac{\partial e_2}{\partial i} - u \frac{\partial e_1}{\partial j} \right) \right\} v \\ &\quad - \frac{1}{e_1} \left( \frac{\partial p'_h}{\partial i} + g d \frac{\partial z}{\partial i} \right) - \frac{g}{e_1} \frac{\partial \eta}{\partial i} + D_u^{\mathbf{U}} + F_u^{\mathbf{U}} \end{aligned} \quad (\text{A.16a})$$

$$\begin{aligned} \frac{1}{e_3} \frac{\partial (e_3 v)}{\partial t} = & -\nabla \cdot (\mathbf{U} v) + \left\{ f + \frac{1}{e_1 e_2} \left( v \frac{\partial e_2}{\partial i} - u \frac{\partial e_1}{\partial j} \right) \right\} u \\ & - \frac{1}{e_2} \left( \frac{\partial p'_h}{\partial j} + g d \frac{\partial z}{\partial j} \right) - \frac{g}{e_2} \frac{\partial \eta}{\partial j} + D_v^{\mathbf{U}} + F_v^{\mathbf{U}} \quad (\text{A.16b}) \end{aligned}$$

Both formulations share the same hydrostatic pressure balance expressed in terms of hydrostatic pressure and density anomalies,  $p'_h$  and  $d = (\frac{\rho}{\rho_o} - 1)$ :

$$\frac{\partial p'_h}{\partial k} = -d g e_3 \quad (\text{A.17})$$

It is important to realize that the change in coordinate system has only concerned the position on the vertical. It has not affected  $(\mathbf{i}, \mathbf{j}, \mathbf{k})$ , the orthogonal curvilinear set of unit vectors.  $(u, v)$  are always horizontal velocities so that their evolution is driven by *horizontal* forces, in particular the pressure gradient. By contrast,  $\omega$  is not  $w$ , the third component of the velocity, but the dia-surface velocity component, *i.e.* the volume flux across the moving  $s$ -surfaces per unit horizontal area.

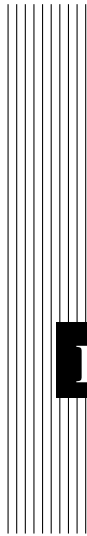
#### A.4 Tracer Equation

The tracer equation is obtained using the same calculation as for the continuity equation and then regrouping the time derivative terms in the left hand side :

$$\begin{aligned} \frac{1}{e_3} \frac{\partial (e_3 T)}{\partial t} = & -\frac{1}{e_1 e_2 e_3} \left[ \frac{\partial}{\partial i} (e_2 e_3 T u) + \frac{\partial}{\partial j} (e_1 e_3 T v) \right] \\ & + \frac{1}{e_3} \frac{\partial}{\partial k} (T w) + D^T + F^T \quad (\text{A.18}) \end{aligned}$$

The expression for the advection term is a straight consequence of (A.4), the expression of the 3D divergence in the  $s$ -coordinates established above.





## **B** Appendix B : Diffusive Operators

### **Contents**

---

<b>B.1</b>	<b>Horizontal/Vertical 2nd Order Tracer Diffusive Operators</b>	<b>304</b>
<b>B.2</b>	<b>Iso/diapycnal 2nd Order Tracer Diffusive Operators . . . . .</b>	<b>306</b>
<b>B.3</b>	<b>Lateral/Vertical Momentum Diffusive Operators . . . . .</b>	<b>308</b>

---

## B.1 Horizontal/Vertical 2nd Order Tracer Diffusive Operators

### In $z$ -coordinates

In  $z$ -coordinates, the horizontal/vertical second order tracer diffusion operator is given by:

$$D^T = \frac{1}{e_1 e_2} \left[ \frac{\partial}{\partial i} \left( \frac{e_2}{e_1} A^{lT} \frac{\partial T}{\partial i} \Big|_z \right) \Big|_z + \frac{\partial}{\partial j} \left( \frac{e_1}{e_2} A^{lT} \frac{\partial T}{\partial j} \Big|_z \right) \Big|_z \right] + \frac{\partial}{\partial z} \left( A^{vT} \frac{\partial T}{\partial z} \right) \quad (\text{B.1})$$

### In generalized vertical coordinates

In  $s$ -coordinates, we defined the slopes of  $s$ -surfaces,  $\sigma_1$  and  $\sigma_2$  by (A.1) and the vertical/horizontal ratio of diffusion coefficient by  $\epsilon = A^{vT}/A^{lT}$ . The diffusion operator is given by:

$$D^T = \nabla|_s \cdot \left[ A^{lT} \mathfrak{R} \cdot \nabla|_s T \right] \quad \text{where } \mathfrak{R} = \begin{pmatrix} 1 & 0 & -\sigma_1 \\ 0 & 1 & -\sigma_2 \\ -\sigma_1 & -\sigma_2 & \epsilon + \sigma_1^2 + \sigma_2^2 \end{pmatrix} \quad (\text{B.2})$$

or in expanded form:

$$D^T = \frac{1}{e_1 e_2 e_3} \left[ \begin{aligned} & e_2 e_3 A^{lT} \frac{\partial}{\partial i} \left( \frac{1}{e_1} \frac{\partial T}{\partial i} \Big|_s - \frac{\sigma_1}{e_3} \frac{\partial T}{\partial s} \right) \Big|_s \\ & + e_1 e_3 A^{lT} \frac{\partial}{\partial j} \left( \frac{1}{e_2} \frac{\partial T}{\partial j} \Big|_s - \frac{\sigma_2}{e_3} \frac{\partial T}{\partial s} \right) \Big|_s \\ & + e_1 e_2 A^{lT} \frac{\partial}{\partial s} \left( -\frac{\sigma_1}{e_1} \frac{\partial T}{\partial i} \Big|_s - \frac{\sigma_2}{e_2} \frac{\partial T}{\partial j} \Big|_s + (\epsilon + \sigma_1^2 + \sigma_2^2) \frac{1}{e_3} \frac{\partial T}{\partial s} \right) \Big] \end{aligned}$$

Equation (B.2) is obtained from (B.1) without any additional assumption. Indeed, for the special case  $k = z$  and thus  $e_3 = 1$ , we introduce an arbitrary vertical coordinate  $s = s(i, j, z)$  as in Appendix A and use (A.1) and (A.2). Since no cross horizontal derivative  $\partial_i \partial_j$  appears in (B.1), the  $(i, z)$  and  $(j, z)$  planes are independent. The derivation can then be demonstrated for the  $(i, z) \rightarrow (j, s)$  transformation

without any loss of generality:

$$\begin{aligned}
D^T &= \frac{1}{e_1 e_2} \frac{\partial}{\partial i} \left( \frac{e_2}{e_1} A^{lT} \frac{\partial T}{\partial i} \Big|_z \right) \Big|_z + \frac{\partial}{\partial z} \left( A^{vT} \frac{\partial T}{\partial z} \right) \\
&= \frac{1}{e_1 e_2} \left[ \frac{\partial}{\partial i} \left( \frac{e_2}{e_1} A^{lT} \left( \frac{\partial T}{\partial i} \Big|_s - \frac{e_1 \sigma_1}{e_3} \frac{\partial T}{\partial s} \right) \right) \Big|_s \right. \\
&\quad \left. - \frac{e_1 \sigma_1}{e_3} \frac{\partial}{\partial s} \left( \frac{e_2}{e_1} A^{lT} \left( \frac{\partial T}{\partial i} \Big|_s - \frac{e_1 \sigma_1}{e_3} \frac{\partial T}{\partial s} \right) \Big|_s \right) \right] + \frac{1}{e_3} \frac{\partial}{\partial s} \left[ \frac{A^{vT}}{e_3} \frac{\partial T}{\partial s} \right] \\
&= \frac{1}{e_1 e_2 e_3} \left[ \frac{\partial}{\partial i} \left( \frac{e_2 e_3}{e_1} A^{lT} \frac{\partial T}{\partial i} \Big|_s \right) \Big|_s - \frac{e_2}{e_1} A^{lT} \frac{\partial e_3}{\partial i} \Big|_s \frac{\partial T}{\partial i} \Big|_s \right. \\
&\quad - e_3 \frac{\partial}{\partial i} \left( \frac{e_2 \sigma_1}{e_3} A^{lT} \frac{\partial T}{\partial s} \right) \Big|_s - e_1 \sigma_1 \frac{\partial}{\partial s} \left( \frac{e_2}{e_1} A^{lT} \frac{\partial T}{\partial i} \Big|_s \right) \\
&\quad \left. - e_1 \sigma_1 \frac{\partial}{\partial s} \left( - \frac{e_2 \sigma_1}{e_3} A^{lT} \frac{\partial T}{\partial s} \right) + \frac{\partial}{\partial s} \left( \frac{e_1 e_2}{e_3} A^{vT} \frac{\partial T}{\partial s} \right) \right]
\end{aligned}$$

Noting that  $\frac{1}{e_1} \frac{\partial e_3}{\partial i} \Big|_s = \frac{\partial \sigma_1}{\partial s}$ , it becomes:

$$\begin{aligned}
&= \frac{1}{e_1 e_2 e_3} \left[ \frac{\partial}{\partial i} \left( \frac{e_2 e_3}{e_1} A^{lT} \frac{\partial T}{\partial i} \Big|_s \right) \Big|_s - e_3 \frac{\partial}{\partial i} \left( \frac{e_2 \sigma_1}{e_3} A^{lT} \frac{\partial T}{\partial s} \right) \Big|_s \right. \\
&\quad - e_2 A^{lT} \frac{\partial \sigma_1}{\partial s} \frac{\partial T}{\partial i} \Big|_s - e_1 \sigma_1 \frac{\partial}{\partial s} \left( \frac{e_2}{e_1} A^{lT} \frac{\partial T}{\partial i} \Big|_s \right) \\
&\quad \left. + e_1 \sigma_1 \frac{\partial}{\partial s} \left( \frac{e_2 \sigma_1}{e_3} A^{lT} \frac{\partial T}{\partial s} \right) + \frac{\partial}{\partial s} \left( \frac{e_1 e_2}{e_3} A^{vT} \frac{\partial T}{\partial s} \right) \right] \\
&= \frac{1}{e_1 e_2 e_3} \left[ \frac{\partial}{\partial i} \left( \frac{e_2 e_3}{e_1} A^{lT} \frac{\partial T}{\partial i} \Big|_s \right) \Big|_s - \frac{\partial}{\partial i} \left( e_2 \sigma_1 A^{lT} \frac{\partial T}{\partial s} \right) \Big|_s \right. \\
&\quad + \frac{e_2 \sigma_1}{e_3} A^{lT} \frac{\partial T}{\partial s} \frac{\partial e_3}{\partial i} \Big|_s - e_2 A^{lT} \frac{\partial \sigma_1}{\partial s} \frac{\partial T}{\partial i} \Big|_s \\
&\quad - e_2 \sigma_1 \frac{\partial}{\partial s} \left( A^{lT} \frac{\partial T}{\partial i} \Big|_s \right) + \frac{\partial}{\partial s} \left( \frac{e_1 e_2 \sigma_1^2}{e_3} A^{lT} \frac{\partial T}{\partial s} \right) \\
&\quad \left. - \frac{\partial (e_1 e_2 \sigma_1)}{\partial s} \left( \frac{\sigma_1}{e_3} A^{lT} \frac{\partial T}{\partial s} \right) + \frac{\partial}{\partial s} \left( \frac{e_1 e_2}{e_3} A^{vT} \frac{\partial T}{\partial s} \right) \right]
\end{aligned}$$

using the same remark as just above, it becomes:

$$\begin{aligned}
&= \frac{1}{e_1 e_2 e_3} \left[ \frac{\partial}{\partial i} \left( \frac{e_2 e_3}{e_1} A^{lT} \frac{\partial T}{\partial i} \Big|_s - e_2 \sigma_1 A^{lT} \frac{\partial T}{\partial s} \right) \Big|_s \right. \\
&\quad + \frac{e_1 e_2 \sigma_1}{e_3} A^{lT} \frac{\partial T}{\partial s} \frac{\partial \sigma_1}{\partial s} - \frac{\sigma_1}{e_3} A^{lT} \frac{\partial (e_1 e_2 \sigma_1)}{\partial s} \frac{\partial T}{\partial s} \\
&\quad - e_2 \left( A^{lT} \frac{\partial \sigma_1}{\partial s} \frac{\partial T}{\partial i} \Big|_s + \frac{\partial}{\partial s} \left( \sigma_1 A^{lT} \frac{\partial T}{\partial i} \Big|_s \right) - \frac{\partial \sigma_1}{\partial s} A^{lT} \frac{\partial T}{\partial i} \Big|_s \right) \\
&\quad \left. + \frac{\partial}{\partial s} \left( \frac{e_1 e_2 \sigma_1^2}{e_3} A^{lT} \frac{\partial T}{\partial s} + \frac{e_1 e_2}{e_3} A^{vT} \frac{\partial T}{\partial s} \right) \right]
\end{aligned}$$

Since the horizontal scale factors do not depend on the vertical coordinate, the last term of the first line and the first term of the last line cancel, while the second line reduces to a single vertical derivative, so it becomes:

$$= \frac{1}{e_1 e_2 e_3} \left[ \frac{\partial}{\partial i} \left( \frac{e_2 e_3}{e_1} A^{lT} \frac{\partial T}{\partial i} \Big|_s - e_2 \sigma_1 A^{lT} \frac{\partial T}{\partial s} \right) \Big|_s + \frac{\partial}{\partial s} \left( -e_2 \sigma_1 A^{lT} \frac{\partial T}{\partial i} \Big|_s + A^{lT} \frac{e_1 e_2}{e_3} (\varepsilon + \sigma_1^2) \frac{\partial T}{\partial s} \right) \right]$$

in other words, the horizontal/vertical Laplacian operator in the  $(i,s)$  plane takes the following form:

$$\frac{1}{e_1 e_2 e_3} \left( \frac{\partial(e_2 e_3 \bullet)}{\partial i} \Big|_s \right) \cdot \left[ A^{lT} \begin{pmatrix} 1 & -\sigma_1 \\ -\sigma_1 & \varepsilon + \sigma_1^2 \end{pmatrix} \cdot \left( \frac{1}{e_1} \frac{\partial \bullet}{\partial i} \Big|_s \right) \left( \frac{1}{e_3} \frac{\partial \bullet}{\partial s} \right) (T) \right]$$

## B.2 Iso/diapycnal 2nd Order Tracer Diffusive Operators

### In $z$ -coordinates

The iso/diapycnal diffusive tensor  $\mathbf{A}_I$  expressed in the  $(i,j,k)$  curvilinear coordinate system in which the equations of the ocean circulation model are formulated, takes the following form [Redi 1982]:

$$\mathbf{A}_I = \frac{A^{lT}}{(1 + a_1^2 + a_2^2)} \begin{bmatrix} 1 + a_1^2 & -a_1 a_2 & -a_1 \\ -a_1 a_2 & 1 + a_2^2 & -a_2 \\ -a_1 & -a_2 & \varepsilon + a_1^2 + a_2^2 \end{bmatrix} \quad (\text{B.3})$$

where  $(a_1, a_2)$  are the isopycnal slopes in  $(\mathbf{i}, \mathbf{j})$  directions, relative to geopotentials:

$$a_1 = \frac{e_3}{e_1} \left( \frac{\partial \rho}{\partial i} \right) \left( \frac{\partial \rho}{\partial k} \right)^{-1}, \quad a_2 = \frac{e_3}{e_2} \left( \frac{\partial \rho}{\partial j} \right) \left( \frac{\partial \rho}{\partial k} \right)^{-1}$$

In practice, isopycnal slopes are generally less than  $10^{-2}$  in the ocean, so  $\mathbf{A}_I$  can be simplified appreciably [Cox 1987]:

$$\mathbf{A}_I \approx A^{lT} \mathfrak{R} \text{ where } \mathfrak{R} = \begin{bmatrix} 1 & 0 & -a_1 \\ 0 & 1 & -a_2 \\ -a_1 & -a_2 & \varepsilon + a_1^2 + a_2^2 \end{bmatrix}, \quad (\text{B.4a})$$

and the iso/dianeutral diffusive operator in  $z$ -coordinates is then

$$D^T = \nabla|_z \cdot \left[ A^{lT} \mathfrak{R} \cdot \nabla|_z T \right]. \quad (\text{B.4b})$$

Physically, the full tensor (B.3) represents strong isoneutral diffusion on a plane parallel to the isoneutral surface and weak dianeutral diffusion perpendicular to

this plane. However, the approximate ‘weak-slope’ tensor (B.4a) represents strong diffusion along the isoneutral surface, with weak *vertical* diffusion – the principal axes of the tensor are no longer orthogonal. This simplification also decouples the  $(i,z)$  and  $(j,z)$  planes of the tensor. The weak-slope operator therefore takes the same form, (B.4), as (B.2), the diffusion operator for geopotential diffusion written in non-orthogonal  $i, j, s$ -coordinates. Written out explicitly,

$$D^T = \frac{1}{e_1 e_2} \left\{ \frac{\partial}{\partial i} \left[ A_h \left( \frac{e_2}{e_1} \frac{\partial T}{\partial i} - a_1 \frac{e_2}{e_3} \frac{\partial T}{\partial k} \right) \right] + \frac{\partial}{\partial j} \left[ A_h \left( \frac{e_1}{e_2} \frac{\partial T}{\partial j} - a_2 \frac{e_1}{e_3} \frac{\partial T}{\partial k} \right) \right] \right\} + \frac{1}{e_3} \frac{\partial}{\partial k} \left[ A_h \left( -\frac{a_1}{e_1} \frac{\partial T}{\partial i} - \frac{a_2}{e_2} \frac{\partial T}{\partial j} + \frac{(a_1^2 + a_2^2 + \varepsilon)}{e_3} \frac{\partial T}{\partial k} \right) \right] \quad (\text{B.5})$$

The isopycnal diffusion operator (B.4), (B.5) conserves tracer quantity and dissipates its square. The demonstration of the first property is trivial as (B.4) is the divergence of fluxes. Let us demonstrate the second one:

$$\iiint_D T \nabla \cdot (\mathbf{A}_I \nabla T) \, dv = - \iiint_D \nabla T \cdot (\mathbf{A}_I \nabla T) \, dv,$$

and since

$$\begin{aligned} \nabla T \cdot (\mathbf{A}_I \nabla T) &= A^{IT} \left[ \left( \frac{\partial T}{\partial i} \right)^2 - 2a_1 \frac{\partial T}{\partial i} \frac{\partial T}{\partial k} + \left( \frac{\partial T}{\partial j} \right)^2 \right. \\ &\quad \left. - 2a_2 \frac{\partial T}{\partial j} \frac{\partial T}{\partial k} + (a_1^2 + a_2^2 + \varepsilon) \left( \frac{\partial T}{\partial k} \right)^2 \right] \\ &= A_h \left[ \left( \frac{\partial T}{\partial i} - a_1 \frac{\partial T}{\partial k} \right)^2 + \left( \frac{\partial T}{\partial j} - a_2 \frac{\partial T}{\partial k} \right)^2 + \varepsilon \left( \frac{\partial T}{\partial k} \right)^2 \right] \\ &\geq 0 \end{aligned}$$

the property becomes obvious.

### In generalized vertical coordinates

Because the weak-slope operator (B.4), (B.5) is decoupled in the  $(i,z)$  and  $(j,z)$  planes, it may be transformed into generalized  $s$ -coordinates in the same way as (B.1) was transformed into (B.2). The resulting operator then takes the simple form

$$D^T = \nabla|_s \cdot \left[ A^{IT} \mathfrak{R} \cdot \nabla|_s T \right] \quad \text{where } \mathfrak{R} = \begin{pmatrix} 1 & 0 & -r_1 \\ 0 & 1 & -r_2 \\ -r_1 & -r_2 & \varepsilon + r_1^2 + r_2^2 \end{pmatrix}, \quad (\text{B.6})$$

where  $(r_1, r_2)$  are the isopycnal slopes in  $(\mathbf{i}, \mathbf{j})$  directions, relative to  $s$ -coordinate surfaces:

$$r_1 = \frac{e_3}{e_1} \left( \frac{\partial \rho}{\partial i} \right) \left( \frac{\partial \rho}{\partial s} \right)^{-1}, \quad r_2 = \frac{e_3}{e_2} \left( \frac{\partial \rho}{\partial j} \right) \left( \frac{\partial \rho}{\partial s} \right)^{-1}.$$

To prove (B.7) by direct re-expression of (B.5) is straightforward, but laborious. An easier way is first to note (by reversing the derivation of (B.2) from (B.1)) that the weak-slope operator may be *exactly* reexpressed in non-orthogonal  $i, j, \rho$ -coordinates as

$$D^T = \nabla|_{\rho} \cdot \left[ A'^T \mathfrak{R} \cdot \nabla|_{\rho} T \right] \quad \text{where } \mathfrak{R} = \begin{pmatrix} 1 & 0 & 0 \\ 0 & 1 & 0 \\ 0 & 0 & \varepsilon \end{pmatrix}. \quad (\text{B.7})$$

Then direct transformation from  $i, j, \rho$ -coordinates to  $i, j, s$ -coordinates gives (B.6) immediately.

Note that the weak-slope approximation is only made in transforming from the (rotated, orthogonal) isoneutral axes to the non-orthogonal  $i, j, \rho$ -coordinates. The further transformation into  $i, j, s$ -coordinates is exact, whatever the steepness of the  $s$ -surfaces, in the same way as the transformation of horizontal/vertical Laplacian diffusion in  $z$ -coordinates, (B.1) onto  $s$ -coordinates is exact, however steep the  $s$ -surfaces.

### B.3 Lateral/Vertical Momentum Diffusive Operators

The second order momentum diffusion operator (Laplacian) in the  $z$ -coordinate is found by applying (2.7e), the expression for the Laplacian of a vector, to the horizontal velocity vector :

$$\begin{aligned} \Delta \mathbf{U}_h &= \nabla (\nabla \cdot \mathbf{U}_h) - \nabla \times (\nabla \times \mathbf{U}_h) \\ &= \begin{pmatrix} \frac{1}{e_1} \frac{\partial \chi}{\partial i} \\ \frac{1}{e_2} \frac{\partial \chi}{\partial j} \\ \frac{1}{e_3} \frac{\partial \chi}{\partial k} \end{pmatrix} - \begin{pmatrix} \frac{1}{e_2} \frac{\partial \zeta}{\partial j} - \frac{1}{e_3} \frac{\partial}{\partial k} \left( \frac{1}{e_3} \frac{\partial u}{\partial k} \right) \\ \frac{1}{e_3} \frac{\partial}{\partial k} \left( -\frac{1}{e_3} \frac{\partial v}{\partial k} \right) - \frac{1}{e_1} \frac{\partial \zeta}{\partial i} \\ \frac{1}{e_1 e_2} \left[ \frac{\partial}{\partial i} \left( \frac{e_2}{e_3} \frac{\partial u}{\partial k} \right) - \frac{\partial}{\partial j} \left( -\frac{e_1}{e_3} \frac{\partial v}{\partial k} \right) \right] \end{pmatrix} \\ &= \begin{pmatrix} \frac{1}{e_1} \frac{\partial \chi}{\partial i} - \frac{1}{e_2} \frac{\partial \zeta}{\partial j} \\ \frac{1}{e_2} \frac{\partial \chi}{\partial j} + \frac{1}{e_1} \frac{\partial \zeta}{\partial i} \\ 0 \end{pmatrix} + \frac{1}{e_3} \begin{pmatrix} \frac{\partial}{\partial k} \left( \frac{1}{e_3} \frac{\partial u}{\partial k} \right) \\ \frac{\partial}{\partial k} \left( \frac{1}{e_3} \frac{\partial v}{\partial k} \right) \\ \frac{\partial \chi}{\partial k} - \frac{1}{e_1 e_2} \left( \frac{\partial^2 (e_2 u)}{\partial i \partial k} + \frac{\partial^2 (e_1 v)}{\partial j \partial k} \right) \end{pmatrix} \end{aligned}$$

Using (2.7b), the definition of the horizontal divergence, the third component of the second vector is obviously zero and thus :

$$\Delta \mathbf{U}_h = \nabla_h (\chi) - \nabla_h \times (\zeta) + \frac{1}{e_3} \frac{\partial}{\partial k} \left( \frac{1}{e_3} \frac{\partial \mathbf{U}_h}{\partial k} \right)$$

Note that this operator ensures a full separation between the vorticity and horizontal divergence fields (see Appendix C). It is only equal to a Laplacian applied to each component in Cartesian coordinates, not on the sphere.

The horizontal/vertical second order (Laplacian type) operator used to diffuse horizontal momentum in the  $z$ -coordinate therefore takes the following form :

$$\mathbf{D}^U = \nabla_h \left( A^{lm} \chi \right) - \nabla_h \times \left( A^{lm} \zeta \mathbf{k} \right) + \frac{1}{e_3} \frac{\partial}{\partial k} \left( \frac{A^{vm}}{e_3} \frac{\partial \mathbf{U}_h}{\partial k} \right) \quad (\text{B.8})$$

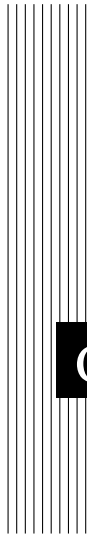
that is, in expanded form:

$$\begin{aligned} D_u^U &= \frac{1}{e_1} \frac{\partial (A^{lm} \chi)}{\partial i} - \frac{1}{e_2} \frac{\partial (A^{lm} \zeta)}{\partial j} + \frac{1}{e_3} \frac{\partial u}{\partial k} \\ D_v^U &= \frac{1}{e_2} \frac{\partial (A^{lm} \chi)}{\partial j} + \frac{1}{e_1} \frac{\partial (A^{lm} \zeta)}{\partial i} + \frac{1}{e_3} \frac{\partial v}{\partial k} \end{aligned}$$

Note Bene: introducing a rotation in (B.8) does not lead to a useful expression for the iso/diapycnal Laplacian operator in the  $z$ -coordinate. Similarly, we did not found an expression of practical use for the geopotential horizontal/vertical Laplacian operator in the  $s$ -coordinate. Generally, (B.8) is used in both  $z$ - and  $s$ -coordinate systems, that is a Laplacian diffusion is applied on momentum along the coordinate directions.







# C Discrete Invariants of the Equations

## Contents

---

<b>C.1 Introduction / Notations</b> . . . . .	<b>312</b>
<b>C.2 Continuous conservation</b> . . . . .	<b>313</b>
<b>C.3 Discrete total energy conservation : vector invariant form</b> .	<b>316</b>
C.3.1 Total energy conservation . . . . .	316
C.3.2 Vorticity term (coriolis + vorticity part of the advection)	316
C.3.3 Pressure Gradient Term . . . . .	320
<b>C.4 Discrete total energy conservation : flux form</b> . . . . .	<b>322</b>
C.4.1 Total energy conservation . . . . .	322
C.4.2 Coriolis and advection terms: flux form . . . . .	323
<b>C.5 Discrete enstrophy conservation</b> . . . . .	<b>324</b>
<b>C.6 Conservation Properties on Tracers</b> . . . . .	<b>326</b>
C.6.1 Advection Term . . . . .	326
<b>C.7 Conservation Properties on Lateral Momentum Physics</b> . .	<b>327</b>
C.7.1 Conservation of Potential Vorticity . . . . .	327
C.7.2 Dissipation of Horizontal Kinetic Energy . . . . .	328
C.7.3 Dissipation of Enstrophy . . . . .	329
C.7.4 Conservation of Horizontal Divergence . . . . .	329
C.7.5 Dissipation of Horizontal Divergence Variance . . . . .	329
<b>C.8 Conservation Properties on Vertical Momentum Physics</b> . .	<b>330</b>
<b>C.9 Conservation Properties on Tracer Physics</b> . . . . .	<b>333</b>
C.9.1 Conservation of Tracers . . . . .	333
C.9.2 Dissipation of Tracer Variance . . . . .	334

---

## C.1 Introduction / Notations

Notation used in this appendix in the demonstrations :

fluxes at the faces of a  $T$ -box:

$$U = e_{2u} e_{3u} u \quad V = e_{1v} e_{3v} v \quad W = e_{1w} e_{2w} w$$

volume of cells at  $u$ -,  $v$ -, and  $T$ -points:

$$b_u = e_{1u} e_{2u} e_{3u} \quad b_v = e_{1v} e_{2v} e_{3v} \quad b_t = e_{1t} e_{2t} e_{3t}$$

partial derivative notation:  $\partial_{\bullet} = \frac{\partial}{\partial \bullet}$

$dv = e_1 e_2 e_3 di dj dk$  is the volume element, with only  $e_3$  that depends on time.  $D$  and  $S$  are the ocean domain volume and surface, respectively. No wetting/drying is allow (*i.e.*  $\frac{\partial S}{\partial t} = 0$ ) Let  $k_s$  and  $k_b$  be the ocean surface and bottom, resp. (*i.e.*  $s(k_s) = \eta$  and  $s(k_b) = -H$ , where  $H$  is the bottom depth).

$$z(k) = \eta - \int_{\tilde{k}=k}^{\tilde{k}=k_s} e_3(\tilde{k}) d\tilde{k} = \eta - \int_k^{k_s} e_3 d\tilde{k}$$

Continuity equation with the above notation:

$$\frac{1}{e_{3t}} \partial_t (e_{3t}) + \frac{1}{b_t} \left\{ \delta_i [U] + \delta_j [V] + \delta_k [W] \right\} = 0$$

A quantity,  $Q$  is conserved when its domain averaged time change is zero, that is when:

$$\partial_t \left( \int_D Q dv \right) = 0$$

Noting that the coordinate system used .... blah blah

$$\partial_t \left( \int_D Q dv \right) = \int_D \partial_t (e_3 Q) e_1 e_2 di dj dk = \int_D \frac{1}{e_3} \partial_t (e_3 Q) dv = 0$$

equation of evolution of  $Q$  written as the time evolution of the vertical content of  $Q$  like for tracers, or momentum in flux form, the quadratic quantity  $\frac{1}{2} Q^2$  is conserved when :

$$\begin{aligned} \partial_t \left( \int_D \frac{1}{2} Q^2 dv \right) &= \int_D \frac{1}{2} \partial_t \left( \frac{1}{e_3} (e_3 Q)^2 \right) e_1 e_2 di dj dk \\ &= \int_D Q \partial_t (e_3 Q) e_1 e_2 di dj dk - \int_D \frac{1}{2} Q^2 \partial_t (e_3) e_1 e_2 di dj dk \end{aligned}$$

that is in a more compact form :

$$\partial_t \left( \int_D \frac{1}{2} Q^2 dv \right) = \int_D \frac{Q}{e_3} \partial_t (e_3 Q) dv - \frac{1}{2} \int_D \frac{Q^2}{e_3} \partial_t (e_3) dv \quad (\text{C.1})$$

equation of evolution of  $Q$  written as the time evolution of  $Q$  like for momentum in vector invariant form, the quadratic quantity  $\frac{1}{2}Q^2$  is conserved when :

$$\begin{aligned} \partial_t \left( \int_D \frac{1}{2} Q^2 dv \right) &= \int_D \frac{1}{2} \partial_t (e_3 Q^2) e_1 e_2 di dj dk \\ &= \int_D Q \partial_t Q e_1 e_2 e_3 di dj dk + \int_D \frac{1}{2} Q^2 \partial_t e_3 e_1 e_2 di dj dk \end{aligned}$$

that is in a more compact form :

$$\partial_t \left( \int_D \frac{1}{2} Q^2 dv \right) = \int_D Q \partial_t Q dv + \frac{1}{2} \int_D \frac{1}{e_3} Q^2 \partial_t e_3 dv \quad (\text{C.2})$$

## C.2 Continuous conservation

The discretization of primitive equation in  $s$ -coordinate (*i.e.* time and space varying vertical coordinate) must be chosen so that the discrete equation of the model satisfy integral constraints on energy and enstrophy.

Let us first establish those constraint in the continuous world. The total energy (*i.e.* kinetic plus potential energies) is conserved :

$$\partial_t \left( \int_D \left( \frac{1}{2} \mathbf{U}_h^2 + \rho g z \right) dv \right) = 0 \quad (\text{C.3})$$

under the following assumptions: no dissipation, no forcing (wind, buoyancy flux, atmospheric pressure variations), mass conservation, and closed domain.

This equation can be transformed to obtain several sub-equalities. The transformation for the advection term depends on whether the vector invariant form or the flux form is used for the momentum equation. Using (C.2) and introducing (A.15) in (C.3) for the former form and Using (C.1) and introducing (A.16) in (C.3) for the latter form leads to:

advection term (vector invariant form):

$$\int_D \zeta (\mathbf{k} \times \mathbf{U}_h) \cdot \mathbf{U}_h dv = 0 \quad (\text{C.4a})$$

$$\int_D \mathbf{U}_h \cdot \nabla_h \left( \frac{\mathbf{U}_h^2}{2} \right) dv + \int_D \mathbf{U}_h \cdot \nabla_z \mathbf{U}_h dv - \int_D \frac{\mathbf{U}_h^2}{2} \frac{1}{e_3} \partial_t e_3 dv = 0 \quad (\text{C.4b})$$

advection term (flux form):

$$\int_D \frac{1}{e_1 e_2} (v \partial_i e_2 - u \partial_j e_1) (\mathbf{k} \times \mathbf{U}_h) \cdot \mathbf{U}_h dv = 0 \quad (\text{C.4c})$$

$$\int_D \mathbf{U}_h \cdot \left( \begin{array}{c} \nabla \cdot (\mathbf{U} u) \\ \nabla \cdot (\mathbf{U} v) \end{array} \right) dv + \frac{1}{2} \int_D \mathbf{U}_h^2 \frac{1}{e_3} \partial_t e_3 dv = 0 \quad (\text{C.4d})$$

coriolis term

$$\int_D f (\mathbf{k} \times \mathbf{U}_h) \cdot \mathbf{U}_h dv = 0 \quad (\text{C.4e})$$

pressure gradient:

$$- \int_D \nabla p|_z \cdot \mathbf{U}_h dv = - \int_D \nabla \cdot (\rho \mathbf{U}) g z dv + \int_D g \rho \partial_t z dv \quad (\text{C.4f})$$

where  $\nabla_h = \nabla|_k$  is the gradient along the  $s$ -surfaces.

blah blah...

The prognostic ocean dynamics equation can be summarized as follows:

$$\text{NXT} = \left( \begin{array}{c} \text{VOR} + \text{KEG} + \text{ZAD} \\ \text{COR} + \text{ADV} \end{array} \right) + \text{HPG} + \text{SPG} + \text{LDF} + \text{ZDF}$$

Vector invariant form:

$$\int_D \mathbf{U}_h \cdot \text{VOR} dv = 0 \quad (\text{C.5a})$$

$$\int_D \mathbf{U}_h \cdot \text{KEG} dv + \int_D \mathbf{U}_h \cdot \text{ZAD} dv - \int_D \frac{\mathbf{U}_h^2}{2} \frac{1}{e_3} \partial_t e_3 dv = 0 \quad (\text{C.5b})$$

$$- \int_D \mathbf{U}_h \cdot (\text{HPG} + \text{SPG}) dv = - \int_D \nabla \cdot (\rho \mathbf{U}) g z dv + \int_D g \rho \partial_t z dv \quad (\text{C.5c})$$

Flux form:

$$\int_D \mathbf{U}_h \cdot \text{COR} dv = 0 \quad (\text{C.6a})$$

$$\int_D \mathbf{U}_h \cdot \text{ADV} dv + \frac{1}{2} \int_D \mathbf{U}_h^2 \frac{1}{e_3} \partial_t e_3 dv = 0 \quad (\text{C.6b})$$

$$-\int_D \mathbf{U}_h \cdot (\text{HPG} + \text{SPG}) \, dv = -\int_D \nabla \cdot (\rho \mathbf{U}) \, g z \, dv + \int_D g \rho \, \partial_t z \, dv \quad (\text{C.6c})$$

(C.6c) is the balance between the conversion KE to PE and PE to KE. Indeed the left hand side of (C.6c) can be transformed as follows:

$$\begin{aligned} \partial_t \left( \int_D \rho g z \, dv \right) &= + \int_D \frac{1}{e_3} \partial_t(e_3 \rho) \, g z \, dv + \int_D g \rho \, \partial_t z \, dv \\ &= - \int_D \nabla \cdot (\rho \mathbf{U}) \, g z \, dv + \int_D g \rho \, \partial_t z \, dv \\ &= + \int_D \rho g \left( \mathbf{U}_h \cdot \nabla_h z + \omega \frac{1}{e_3} \partial_k z \right) \, dv + \int_D g \rho \, \partial_t z \, dv \\ &= + \int_D \rho g (\omega + \partial_t z + \mathbf{U}_h \cdot \nabla_h z) \, dv \\ &= + \int_D g \rho \, w \, dv \end{aligned}$$

where the last equality is obtained by noting that the brackets is exactly the expression of  $w$ , the vertical velocity referenced to the fixe  $z$ -coordinate system (see (A.5)).

The left hand side of (C.6c) can be transformed as follows:

$$\begin{aligned} - \int_D \nabla p|_z \cdot \mathbf{U}_h \, dv &= - \int_D (\nabla_h p + \rho g \nabla_h z) \cdot \mathbf{U}_h \, dv \\ &= - \int_D \nabla_h p \cdot \mathbf{U}_h \, dv - \int_D \rho g \nabla_h z \cdot \mathbf{U}_h \, dv \\ &= + \int_D p \nabla_h \cdot \mathbf{U}_h \, dv + \int_D \rho g (\omega - w + \partial_t z) \, dv \\ &= - \int_D p \left( \frac{1}{e_3} \partial_t e_3 + \frac{1}{e_3} \partial_k \omega \right) \, dv + \int_D \rho g (\omega - w + \partial_t z) \, dv \\ &= - \int_D \frac{p}{e_3} \partial_t e_3 \, dv + \int_D \frac{1}{e_3} \partial_k p \, \omega \, dv + \int_D \rho g (\omega - w + \partial_t z) \, dv \\ &= - \int_D \frac{p}{e_3} \partial_t e_3 \, dv - \int_D \rho g \omega \, dv + \int_D \rho g (\omega - w + \partial_t z) \, dv \end{aligned}$$

$$= - \int_D \frac{p}{e_3} \partial_t e_3 \, dv - \int_D \rho g w \, dv + \int_D \rho g \partial_t z \, dv$$

introducing the hydrostatic balance  $\partial_k p = -\rho g e_3$  in the last term, it becomes:

$$\begin{aligned} &= - \int_D \frac{p}{e_3} \partial_t e_3 \, dv - \int_D \rho g w \, dv - \int_D \frac{1}{e_3} \partial_k p \partial_t z \, dv \\ &= - \int_D \frac{p}{e_3} \partial_t e_3 \, dv - \int_D \rho g w \, dv + \int_D \frac{p}{e_3} \partial_t (\partial_k z) \, dv \\ &= - \int_D \rho g w \, dv \end{aligned}$$

### C.3 Discrete total energy conservation : vector invariant form

#### C.3.1 Total energy conservation

The discrete form of the total energy conservation, (C.3), is given by:

$$\partial_t \left( \sum_{i,j,k} \left\{ \frac{u^2}{2} b_u + \frac{v^2}{2} b_v + \rho g z_t b_t \right\} \right) = 0$$

which in vector invariant forms, it leads to:

$$\begin{aligned} &\sum_{i,j,k} \left\{ u \partial_t u b_u + v \partial_t v b_v \right\} + \frac{1}{2} \sum_{i,j,k} \left\{ \frac{u^2}{e_{3u}} \partial_t e_{3u} b_u + \frac{v^2}{e_{3v}} \partial_t e_{3v} b_v \right\} \\ &= - \sum_{i,j,k} \left\{ \frac{1}{e_{3t}} \partial_t (e_{3t} \rho) g z_t b_t \right\} - \sum_{i,j,k} \left\{ \rho g \partial_t (z_t) b_t \right\} \end{aligned} \quad (\text{C.7})$$

Substituting the discrete expression of the time derivative of the velocity either in vector invariant, leads to the discrete equivalent of the four equations (C.6).

#### C.3.2 Vorticity term (coriolis + vorticity part of the advection)

Let  $q$ , located at  $f$ -points, be either the relative ( $q = \zeta/e_{3f}$ ), or the planetary ( $q = f/e_{3f}$ ), or the total potential vorticity ( $q = (\zeta + f)/e_{3f}$ ). Two discretisation of the vorticity term (ENE and EEN) allows the conservation of the kinetic energy.

**Vorticity Term with ENE scheme (*ln\_dynvor\_ene=.true.*)**

For the ENE scheme, the two components of the vorticity term are given by :

$$-e_3 q \mathbf{k} \times \mathbf{U}_h \equiv \begin{pmatrix} +\frac{1}{e_{1u}} q \overline{(e_{1v} e_{3v} v)}^{i+1/2^j} \\ -\frac{1}{e_{2v}} q \overline{(e_{2u} e_{3u} u)}^{j+1/2^i} \end{pmatrix}$$

This formulation does not conserve the enstrophy but it does conserve the total kinetic energy. Indeed, the kinetic energy tendency associated to the vorticity term and averaged over the ocean domain can be transformed as follows:

$$\begin{aligned} \int_D - (e_3 q \mathbf{k} \times \mathbf{U}_h) \cdot \mathbf{U}_h dv & \\ \equiv \sum_{i,j,k} \left\{ \frac{1}{e_{1u}} q \overline{V}^{i+1/2^j} u b_u - \frac{1}{e_{2v}} q \overline{U}^{j+1/2^i} v b_v \right\} & \\ \equiv \sum_{i,j,k} \left\{ q \overline{V}^{i+1/2^j} U - q \overline{U}^{j+1/2^i} V \right\} & \\ \equiv \sum_{i,j,k} q \left\{ \overline{V}^{i+1/2} \overline{U}^{j+1/2} - \overline{U}^{j+1/2} \overline{V}^{i+1/2} \right\} & \equiv 0 \end{aligned}$$

In other words, the domain averaged kinetic energy does not change due to the vorticity term.

**Vorticity Term with EEN scheme (*ln\_dynvor\_een=.true.*)**

With the EEN scheme, the vorticity terms are represented as:

$$\begin{cases} +q e_3 v \equiv +\frac{1}{e_{1u}} \sum_{i_p, k_p}^{i+1/2-i_p} Q_{j_p}^{i_p} (e_{1v} e_{3v} v)_{j+j_p}^{i+i_p-1/2} \\ -q e_3 u \equiv -\frac{1}{e_{2v}} \sum_{i_p, k_p}^i Q_{j_p}^{i_p} (e_{2u} e_{3u} u)_{j+j_p-1/2}^{i+i_p} \end{cases} \quad (\text{C.8})$$

where the indices  $i_p$  and  $j_p$  take the following value:  $i_p = -1/2$  or  $1/2$  and  $j_p = -1/2$  or  $1/2$ , and the vorticity triads,  ${}^i_j Q_{j_p}^{i_p}$ , defined at  $T$ -point, are given by:

$${}^j_i Q_{j_p}^{i_p} = \frac{1}{12} \left( q_{j+j_p}^{i-i_p} + q_{j+i_p}^{i+j_p} + q_{j-j_p}^{i+i_p} \right) \quad (\text{C.9})$$

This formulation does conserve the total kinetic energy. Indeed,

$$\begin{aligned}
& \int_D -\mathbf{U}_h \cdot (\zeta \mathbf{k} \times \mathbf{U}_h) \, dv \\
& \equiv \sum_{i,j,k} \left\{ \left[ \sum_{i_p, k_p}^{i+1/2-i_p} \mathbb{Q}_{j_p}^{i_p} V_{j+j_p}^{i+1/2-i_p} \right] U_j^{i+1/2} - \left[ \sum_{i_p, k_p}^i \mathbb{Q}_{j_p}^{i_p} U_{j+1/2-j_p}^{i+i_p} \right] V_{j+1/2}^i \right\} \\
& \equiv \sum_{i,j,k} \sum_{i_p, k_p} \left\{ \begin{aligned} & \mathbb{Q}_{j_p}^{i+1/2-i_p} V_{j+j_p}^{i+1/2-i_p} U_j^{i+1/2} - \mathbb{Q}_{j_p}^i U_{j+1/2-j_p}^{i+i_p} V_{j+1/2}^i \end{aligned} \right\}
\end{aligned}$$

Expanding the summation on  $i_p$  and  $k_p$ , it becomes:

$$\begin{aligned}
& \equiv \sum_{i,j,k} \left\{ \begin{aligned} & \mathbb{Q}_{+1/2}^{i+1} V_{j+1/2}^{i+1} U_j^{i+1/2} - \mathbb{Q}_{+1/2}^{-i} U_j^{i-1/2} V_{j+1/2}^i \\ & + \mathbb{Q}_{-1/2}^{i+1} V_{j-1/2}^{i+1} U_j^{i+1/2} - \mathbb{Q}_{-1/2}^{-i} U_{j+1}^{i-1/2} V_{j+1/2}^i \\ & + \mathbb{Q}_{+1/2}^{+i} V_{j+1/2}^i U_j^{i+1/2} - \mathbb{Q}_{+1/2}^{+i} U_j^{i+1/2} V_{j+1/2}^i \\ & + \mathbb{Q}_{-1/2}^{+i} V_{j-1/2}^i U_j^{i+1/2} - \mathbb{Q}_{-1/2}^{+i} U_{j+1}^{i+1/2} V_{j+1/2}^i \end{aligned} \right\}
\end{aligned}$$

The summation is done over all  $i$  and  $j$  indices, it is therefore possible to introduce a shift of  $-1$  either in  $i$  or  $j$  direction in some of the term of the summation (first term of the first and second lines, second term of the second and fourth lines). By doing so, we can regroup all the terms of the summation by triad at a  $(i,j)$  point. In other words, we regroup all the terms in the neighbourhood that contain a triad at the same  $(i,j)$  indices. It becomes:

$$\begin{aligned}
& \equiv \sum_{i,j,k} \left\{ \begin{aligned} & \mathbb{Q}_{+1/2}^{i-1} \left[ V_{j+1/2}^i U_j^{i-1/2} - U_j^{i-1/2} V_{j+1/2}^i \right] \\ & + \mathbb{Q}_{-1/2}^{i-1} \left[ V_{j-1/2}^i U_j^{i-1/2} - U_j^{i-1/2} V_{j-1/2}^i \right] \\ & + \mathbb{Q}_{+1/2}^{+i} \left[ V_{j+1/2}^i U_j^{i+1/2} - U_j^{i+1/2} V_{j+1/2}^i \right] \\ & + \mathbb{Q}_{-1/2}^{+i} \left[ V_{j-1/2}^i U_j^{i+1/2} - U_{j-1}^{i+1/2} V_{j-1/2}^i \right] \end{aligned} \right\} \equiv 0
\end{aligned}$$



### Gradient of Kinetic Energy / Vertical Advection

The change of Kinetic Energy (KE) due to the vertical advection is exactly balanced by the change of KE due to the horizontal gradient of KE :

$$\int_D \mathbf{U}_h \cdot \frac{1}{e_3} \omega \partial_k \mathbf{U}_h \, dv = - \int_D \mathbf{U}_h \cdot \nabla_h \left( \frac{1}{2} \mathbf{U}_h^2 \right) \, dv + \frac{1}{2} \int_D \frac{\mathbf{U}_h^2}{e_3} \partial_t (e_3) \, dv$$

Indeed, using successively (4.11) (*i.e.* the skew symmetry property of the  $\delta$  operator) and the continuity equation, then (4.11) again, then the commutativity of operators  $\bar{\cdot}$  and  $\delta$ , and finally (4.12) (*i.e.* the symmetry property of the  $\bar{\cdot}$  operator) applied in the horizontal and vertical directions, it becomes:

$$\begin{aligned} & - \int_D \mathbf{U}_h \cdot \text{KEG} \, dv = - \int_D \mathbf{U}_h \cdot \nabla_h \left( \frac{1}{2} \mathbf{U}_h^2 \right) \, dv \\ \equiv & - \sum_{i,j,k} \frac{1}{2} \left\{ \frac{1}{e_{1u}} \delta_{i+1/2} [\bar{u}^{2^i} + \bar{v}^{2^j}] u b_u + \frac{1}{e_{2v}} \delta_{j+1/2} [\bar{u}^{2^i} + \bar{v}^{2^j}] v b_v \right\} \\ \equiv & + \sum_{i,j,k} \frac{1}{2} (\bar{u}^{2^i} + \bar{v}^{2^j}) \left\{ \delta_i [U] + \delta_j [V] \right\} \\ \equiv & - \sum_{i,j,k} \frac{1}{2} (\bar{u}^{2^i} + \bar{v}^{2^j}) \left\{ \frac{b_t}{e_{3t}} \partial_t (e_{3t}) + \delta_k [W] \right\} \\ \equiv & + \sum_{i,j,k} \frac{1}{2} \delta_{k+1/2} [\bar{u}^{2^i} + \bar{v}^{2^j}] W - \sum_{i,j,k} \frac{1}{2} (\bar{u}^{2^i} + \bar{v}^{2^j}) \partial_t b_t \\ \equiv & + \sum_{i,j,k} \frac{1}{2} \left( \overline{\delta_{k+1/2} [u^2]}^i + \overline{\delta_{k+1/2} [v^2]}^j \right) W - \sum_{i,j,k} \left( \frac{u^2}{2} \partial_t \bar{b}_t^{i+1/2} + \frac{v^2}{2} \partial_t \bar{b}_t^{j+1/2} \right) \end{aligned}$$

Assuming that  $b_u = \bar{b}_t^{i+1/2}$  and  $b_v = \bar{b}_t^{j+1/2}$ , or at least that the time derivative of these two equations is satisfied, it becomes:

$$\begin{aligned} \equiv & \sum_{i,j,k} \frac{1}{2} \left\{ \overline{W}^{i+1/2} \delta_{k+1/2} [u^2] + \overline{W}^{j+1/2} \delta_{k+1/2} [v^2] \right\} - \sum_{i,j,k} \left( \frac{u^2}{2} \partial_t b_u + \frac{v^2}{2} \partial_t b_v \right) \\ \equiv & \sum_{i,j,k} \left\{ \overline{W}^{i+1/2} \bar{u}^{k+1/2} \delta_{k+1/2} [u] + \overline{W}^{j+1/2} \bar{v}^{k+1/2} \delta_{k+1/2} [v] \right\} - \sum_{i,j,k} \left( \frac{u^2}{2} \partial_t b_u + \frac{v^2}{2} \partial_t b_v \right) \\ \equiv & \sum_{i,j,k} \left\{ \frac{1}{b_u} \overline{\overline{W}^{i+1/2} \delta_{k+1/2} [u]}^k u b_u + \frac{1}{b_v} \overline{\overline{W}^{j+1/2} \delta_{k+1/2} [v]}^k v b_v \right\} - \sum_{i,j,k} \left( \frac{u^2}{2} \partial_t b_u + \frac{v^2}{2} \partial_t b_v \right) \end{aligned}$$

The first term provides the discrete expression for the vertical advection of momentum (ZAD), while the second term corresponds exactly to (C.7), therefore:

$$\begin{aligned} &\equiv \int_D \mathbf{U}_h \cdot \text{ZAD} \, dv + \frac{1}{2} \int_D \mathbf{U}_h^2 \frac{1}{e_3} \partial_t(e_3) \, dv \\ &\equiv \int_D \mathbf{U}_h \cdot w \partial_k \mathbf{U}_h \, dv + \frac{1}{2} \int_D \mathbf{U}_h^2 \frac{1}{e_3} \partial_t(e_3) \, dv \end{aligned}$$

There is two main points here. First, the satisfaction of this property links the choice of the discrete formulation of the vertical advection and of the horizontal gradient of KE. Choosing one imposes the other. For example KE can also be discretized as  $1/2 (\bar{u}^2 + \bar{v}^2)$ . This leads to the following expression for the vertical advection:

$$\frac{1}{e_3} \omega \partial_k \mathbf{U}_h \equiv \left( \begin{array}{c} \frac{1}{e_{1u} e_{2u} e_{3u}} \overline{\overline{e_{1t} e_{2t} \omega \delta_{k+1/2} [\bar{u}^{i+1/2}]}}^{i+1/2,k} \\ \frac{1}{e_{1v} e_{2v} e_{3v}} \overline{\overline{e_{1t} e_{2t} \omega \delta_{k+1/2} [\bar{v}^{j+1/2}]}}^{j+1/2,k} \end{array} \right)$$

a formulation that requires an additional horizontal mean in contrast with the one used in NEMO. Nine velocity points have to be used instead of 3. This is the reason why it has not been chosen.

Second, as soon as the chosen  $s$ -coordinate depends on time, an extra constraint arises on the time derivative of the volume at  $u$ - and  $v$ -points:

$$\begin{aligned} e_{1u} e_{2u} \partial_t(e_{3u}) &= \overline{\overline{e_{1t} e_{2t} \partial_t(e_{3t})}}^{i+1/2} \\ e_{1v} e_{2v} \partial_t(e_{3v}) &= \overline{\overline{e_{1t} e_{2t} \partial_t(e_{3t})}}^{j+1/2} \end{aligned}$$

which is (over-)satisfied by defining the vertical scale factor as follows:

$$e_{3u} = \frac{1}{e_{1u} e_{2u}} \overline{\overline{e_{1t} e_{2t} e_{3t}}}^{i+1/2} \quad (\text{C.10})$$

$$e_{3v} = \frac{1}{e_{1v} e_{2v}} \overline{\overline{e_{1t} e_{2t} e_{3t}}}^{j+1/2} \quad (\text{C.11})$$

Blah blah required on the the step representation of bottom topography.....

### C.3.3 Pressure Gradient Term

When the equation of state is linear (*i.e.* when an advection-diffusion equation for density can be derived from those of temperature and salinity) the change of KE due to the work of pressure forces is balanced by the change of potential energy due to buoyancy forces:

$$- \int_D \nabla p|_z \cdot \mathbf{U}_h \, dv = - \int_D \nabla \cdot (\rho \mathbf{U}) \, g z \, dv + \int_D g \rho \partial_t(z) \, dv$$

This property can be satisfied in a discrete sense for both  $z$ - and  $s$ -coordinates. Indeed, defining the depth of a  $T$ -point,  $z_t$ , as the sum of the vertical scale factors at  $w$ -points starting from the surface, the work of pressure forces can be written as:

$$-\int_D \nabla p|_z \cdot \mathbf{U}_h \, dv \equiv \sum_{i,j,k} \left\{ -\frac{1}{e_{1u}} \left( \delta_{i+1/2}[p_t] - g \bar{\rho}^{i+1/2} \delta_{i+1/2}[z_t] \right) u \, b_u - \frac{1}{e_{2v}} \left( \delta_{j+1/2}[p_t] - g \bar{\rho}^{j+1/2} \delta_{j+1/2}[z_t] \right) v \, b_v \right\}$$

Using successively (4.11), *i.e.* the skew symmetry property of the  $\delta$  operator, (6.4), the continuity equation, (6.20), the hydrostatic equation in the  $s$ -coordinate, and  $\delta_{k+1/2}[z_t] \equiv e_{3w}$ , which comes from the definition of  $z_t$ , it becomes:

$$\begin{aligned} &\equiv + \sum_{i,j,k} g \left\{ \bar{\rho}^{i+1/2} U \delta_{i+1/2}[z_t] + \bar{\rho}^{j+1/2} V \delta_{j+1/2}[z_t] + \left( \delta_i[U] + \delta_j[V] \right) \frac{p_t}{g} \right\} \\ &\equiv + \sum_{i,j,k} g \left\{ \bar{\rho}^{i+1/2} U \delta_{i+1/2}[z_t] + \bar{\rho}^{j+1/2} V \delta_{j+1/2}[z_t] - \left( \frac{b_t}{e_{3t}} \partial_t(e_{3t}) + \delta_k[W] \right) \frac{p_t}{g} \right\} \\ &\equiv + \sum_{i,j,k} g \left\{ \bar{\rho}^{i+1/2} U \delta_{i+1/2}[z_t] + \bar{\rho}^{j+1/2} V \delta_{j+1/2}[z_t] + \frac{W}{g} \delta_{k+1/2}[p_t] - \frac{p_t}{g} \partial_t b_t \right\} \\ &\equiv + \sum_{i,j,k} g \left\{ \bar{\rho}^{i+1/2} U \delta_{i+1/2}[z_t] + \bar{\rho}^{j+1/2} V \delta_{j+1/2}[z_t] - W e_{3w} \bar{\rho}^{k+1/2} - \frac{p_t}{g} \partial_t b_t \right\} \\ &\equiv + \sum_{i,j,k} g \left\{ \bar{\rho}^{i+1/2} U \delta_{i+1/2}[z_t] + \bar{\rho}^{j+1/2} V \delta_{j+1/2}[z_t] + W \bar{\rho}^{k+1/2} \delta_{k+1/2}[z_t] - \frac{p_t}{g} \partial_t b_t \right\} \\ &\equiv - \sum_{i,j,k} g \, z_t \left\{ \delta_i \left[ U \bar{\rho}^{i+1/2} \right] + \delta_j \left[ V \bar{\rho}^{j+1/2} \right] + \delta_k \left[ W \bar{\rho}^{k+1/2} \right] \right\} - \sum_{i,j,k} \left\{ p_t \, \partial_t b_t \right\} \\ &\equiv + \sum_{i,j,k} g \, z_t \left\{ \partial_t(e_{3t} \rho) \right\} b_t - \sum_{i,j,k} \left\{ p_t \, \partial_t b_t \right\} \end{aligned}$$

The first term is exactly the first term of the right-hand-side of (C.7). It remains to demonstrate that the last term, which is obviously a discrete analogue of  $\int_D \frac{p}{e_3} \partial_t(e_3) \, dv$  is equal to the last term of (C.7). In other words, the following property must be satisfied:

$$\sum_{i,j,k} \left\{ p_t \, \partial_t b_t \right\} \equiv \sum_{i,j,k} \left\{ \rho \, g \, \partial_t(z_t) \, b_t \right\}$$

Let introduce  $p_w$  the pressure at  $w$ -point such that  $\delta_k[p_w] = -\rho \, g \, e_{3t}$ . The right-hand-side of the above equation can be transformed as follows:

$$\begin{aligned}
\sum_{i,j,k} \left\{ \rho g \partial_t(z_t) b_t \right\} &\equiv - \sum_{i,j,k} \left\{ \delta_k[p_w] \partial_t(z_t) e_{1t} e_{2t} \right\} \\
&\equiv + \sum_{i,j,k} \left\{ p_w \delta_{k+1/2}[\partial_t(z_t)] e_{1t} e_{2t} \right\} \equiv + \sum_{i,j,k} \left\{ p_w \partial_t(e_{3w}) e_{1t} e_{2t} \right\} \\
&\equiv + \sum_{i,j,k} \left\{ p_w \partial_t(b_w) \right\}
\end{aligned}$$

therefore, the balance to be satisfied is:

$$\sum_{i,j,k} \left\{ p_t \partial_t(b_t) \right\} \equiv \sum_{i,j,k} \left\{ p_w \partial_t(b_w) \right\}$$

which is a purely vertical balance:

$$\sum_k \left\{ p_t \partial_t(e_{3t}) \right\} \equiv \sum_k \left\{ p_w \partial_t(e_{3w}) \right\}$$

Defining  $p_w = \bar{p}_t^{k+1/2}$

Note that this property strongly constrains the discrete expression of both the depth of  $T$ -points and of the term added to the pressure gradient in the  $s$ -coordinate. Nevertheless, it is almost never satisfied since a linear equation of state is rarely used.

## C.4 Discrete total energy conservation : flux form

### C.4.1 Total energy conservation

The discrete form of the total energy conservation, (C.3), is given by:

$$\partial_t \left( \sum_{i,j,k} \left\{ \frac{u^2}{2} b_u + \frac{v^2}{2} b_v + \rho g z_t b_t \right\} \right) = 0$$

which in flux form, it leads to:

$$\begin{aligned}
\sum_{i,j,k} \left\{ \frac{u}{e_{3u}} \frac{\partial(e_{3u}u)}{\partial t} b_u + \frac{v}{e_{3v}} \frac{\partial(e_{3v}v)}{\partial t} b_v \right\} - \frac{1}{2} \sum_{i,j,k} \left\{ \frac{u^2}{e_{3u}} \frac{\partial e_{3u}}{\partial t} b_u + \frac{v^2}{e_{3v}} \frac{\partial e_{3v}}{\partial t} b_v \right\} \\
= - \sum_{i,j,k} \left\{ \frac{1}{e_{3t}} \frac{\partial e_{3t} \rho}{\partial t} g z_t b_t \right\} - \sum_{i,j,k} \left\{ \rho g \frac{\partial z_t}{\partial t} b_t \right\}
\end{aligned}$$

Substituting the discrete expression of the time derivative of the velocity either in vector invariant or in flux form, leads to the discrete equivalent of the

### C.4.2 Coriolis and advection terms: flux form

#### Coriolis plus “metric” Term

In flux from the vorticity term reduces to a Coriolis term in which the Coriolis parameter has been modified to account for the “metric” term. This altered Coriolis parameter is discretised at an f-point. It is given by:

$$f + \frac{1}{e_1 e_2} \left( v \frac{\partial e_2}{\partial i} - u \frac{\partial e_1}{\partial j} \right) \equiv f + \frac{1}{e_{1f} e_{2f}} \left( \bar{v}^{i+1/2} \delta_{i+1/2} [e_{2u}] - \bar{u}^{j+1/2} \delta_{j+1/2} [e_{1u}] \right)$$

Either the ENE or EEN scheme is then applied to obtain the vorticity term in flux form. It therefore conserves the total KE. The derivation is the same as for the vorticity term in the vector invariant form (§C.3.2).

#### Flux form advection

The flux form operator of the momentum advection is evaluated using a centered second order finite difference scheme. Because of the flux form, the discrete operator does not contribute to the global budget of linear momentum. Because of the centered second order scheme, it conserves the horizontal kinetic energy, that is :

$$- \int_D \mathbf{U}_h \cdot \begin{pmatrix} \nabla \cdot (\mathbf{U} u) \\ \nabla \cdot (\mathbf{U} v) \end{pmatrix} dv - \frac{1}{2} \int_D \mathbf{U}_h^2 \frac{1}{e_3} \frac{\partial e_3}{\partial t} dv = 0 \quad (\text{C.12})$$

Let us first consider the first term of the scalar product (*i.e.* just the the terms associated with the i-component of the advection) :

$$\begin{aligned} & - \int_D u \cdot \nabla \cdot (\mathbf{U} u) dv \\ \equiv & - \sum_{i,j,k} \left\{ \frac{1}{b_u} \left( \delta_{i+1/2} [\bar{U}^i \bar{u}^i] + \delta_j [\bar{V}^{i+1/2} \bar{u}^{j+1/2}] + \delta_k [\bar{W}^{i+1/2} \bar{u}^{k+1/2}] \right) \right\} b_u u \\ \equiv & - \sum_{i,j,k} \left\{ \delta_{i+1/2} [\bar{U}^i \bar{u}^i] + \delta_j [\bar{V}^{i+1/2} \bar{u}^{j+1/2}] + \delta_k [\bar{W}^{i+1/2} \bar{u}^{k+1/2}] \right\} u \\ \equiv & + \sum_{i,j,k} \left\{ \bar{U}^i \bar{u}^i \delta_i [u] + \bar{V}^{i+1/2} \bar{u}^{j+1/2} \delta_{j+1/2} [u] + \bar{W}^{i+1/2} \bar{u}^{k+1/2} \delta_{k+1/2} [u] \right\} \\ \equiv & + \frac{1}{2} \sum_{i,j,k} \left\{ \bar{U}^i \delta_i [u^2] + \bar{V}^{i+1/2} \delta_{j+1/2} [u^2] + \bar{W}^{i+1/2} \delta_{k+1/2} [u^2] \right\} \\ \equiv & - \sum_{i,j,k} \frac{1}{2} \left\{ U \delta_{i+1/2} [\bar{u}^2]^i + V \delta_{j+1/2} [\bar{u}^2]^i + W \delta_{k+1/2} [\bar{u}^2]^i \right\} \\ \equiv & - \sum_{i,j,k} \frac{1}{2} \bar{u}^2{}^i \left\{ \delta_{i+1/2} [U] + \delta_{j+1/2} [V] + \delta_{k+1/2} [W] \right\} \end{aligned}$$

$$\equiv + \sum_{i,j,k} \frac{1}{2} \overline{u^2}^i \left\{ \left( \frac{1}{e_{3t}} \frac{\partial e_{3t}}{\partial t} \right) b_t \right\}$$

Applying similar manipulation applied to the second term of the scalar product leads to :

$$- \int_D \mathbf{U}_h \cdot \begin{pmatrix} \nabla \cdot (\mathbf{U} u) \\ \nabla \cdot (\mathbf{U} v) \end{pmatrix} dv \equiv + \sum_{i,j,k} \frac{1}{2} (\overline{u^2}^i + \overline{v^2}^j) \left\{ \left( \frac{1}{e_{3t}} \frac{\partial e_{3t}}{\partial t} \right) b_t \right\}$$

which is the discrete form of  $\frac{1}{2} \int_D u \cdot \nabla \cdot (\mathbf{U} u) dv$ . (C.12) is thus satisfied.

When the UBS scheme is used to evaluate the flux form momentum advection, the discrete operator does not contribute to the global budget of linear momentum (flux form). The horizontal kinetic energy is not conserved, but forced to decay (*i.e.* the scheme is diffusive).

## C.5 Discrete enstrophy conservation

### Vorticity Term with ENS scheme (*ln\_dynvor\_ens=true.*)

In the ENS scheme, the vorticity term is discretized as follows:

$$\begin{cases} + \frac{1}{e_{1u}} \overline{q}^i & \overline{\overline{(e_{1v} e_{3v} v)}}^{i,j+1/2} \\ - \frac{1}{e_{2v}} \overline{q}^j & \overline{\overline{(e_{2u} e_{3u} u)}}^{i+1/2,j} \end{cases} \quad (\text{C.13})$$

The scheme does not allow but the conservation of the total kinetic energy but the conservation of  $q^2$ , the potential enstrophy for a horizontally non-divergent flow (*i.e.* when  $\chi=0$ ). Indeed, using the symmetry or skew symmetry properties of the operators (Eqs (4.12) and (4.11)), it can be shown that:

$$\int_D q \mathbf{k} \cdot \frac{1}{e_3} \nabla \times (e_3 q \mathbf{k} \times \mathbf{U}_h) dv \equiv 0 \quad (\text{C.14})$$

where  $dv = e_1 e_2 e_3 di dj dk$  is the volume element. Indeed, using (C.13), the discrete form of the right hand side of (C.14) can be transformed as follow:

$$\begin{aligned} & \int_D q \mathbf{k} \cdot \frac{1}{e_3} \nabla \times (e_3 q \mathbf{k} \times \mathbf{U}_h) dv \\ & \equiv \sum_{i,j,k} q \left\{ \delta_{i+1/2} \left[ -\overline{q}^i \overline{\overline{U}}^{i,j+1/2} \right] - \delta_{j+1/2} \left[ \overline{q}^j \overline{\overline{V}}^{i+1/2,j} \right] \right\} \\ & \equiv \sum_{i,j,k} \left\{ \delta_i [q] \overline{q}^i \overline{\overline{U}}^{i,j+1/2} + \delta_j [q] \overline{q}^j \overline{\overline{V}}^{i+1/2,j} \right\} \\ & \equiv \frac{1}{2} \sum_{i,j,k} \left\{ \delta_i [q^2] \overline{\overline{U}}^{i,j+1/2} + \delta_j [q^2] \overline{\overline{V}}^{i+1/2,j} \right\} \\ & \equiv -\frac{1}{2} \sum_{i,j,k} q^2 \left\{ \delta_{i+1/2} \left[ \overline{\overline{U}}^{i,j+1/2} \right] + \delta_{j+1/2} \left[ \overline{\overline{V}}^{i+1/2,j} \right] \right\} \end{aligned}$$

Since  $\overline{\cdot}$  and  $\delta$  operators commute:  $\delta_{i+1/2} [\overline{a^i}] = \overline{\delta_i [a]}^{i+1/2}$ , and introducing the horizontal divergence  $\chi$ , it becomes:

$$\equiv \sum_{i,j,k} -\frac{1}{2} q^2 \overline{e_{1t} e_{2t} e_{3t} \chi}^{i+1/2, j+1/2} \equiv 0$$

The later equality is obtain only when the flow is horizontally non-divergent, *i.e.*  $\chi=0$ .

#### Vorticity Term with EEN scheme (*ln\_dynvor\_een=.true.*)

With the EEN scheme, the vorticity terms are represented as:

$$\begin{cases} +q e_3 v \equiv +\frac{1}{e_{1u}} \sum_{i_p, k_p}^{i+1/2-i_p} \mathbb{Q}_{j_p}^{i_p} (e_{1v} e_{3v} v)_{j+j_p}^{i+i_p-1/2} \\ -q e_3 u \equiv -\frac{1}{e_{2v}} \sum_{i_p, k_p}^i \mathbb{Q}_{j_p}^{i_p} (e_{2u} e_{3u} u)_{j+j_p-1/2}^{i+i_p} \end{cases} \quad (\text{C.15})$$

where the indices  $i_p$  and  $k_p$  take the following value:  $i_p = -1/2$  or  $1/2$  and  $j_p = -1/2$  or  $1/2$ , and the vorticity triads,  ${}^i_j \mathbb{Q}_{j_p}^{i_p}$ , defined at  $T$ -point, are given by:

$${}^j_i \mathbb{Q}_{j_p}^{i_p} = \frac{1}{12} \left( q_{j+j_p}^{i-i_p} + q_{j+i_p}^{i+j_p} + q_{j-j_p}^{i+i_p} \right) \quad (\text{C.16})$$

This formulation does conserve the potential enstrophy for a horizontally non-divergent flow (*i.e.*  $\chi = 0$ ).

Let consider one of the vorticity triad, for example  ${}^i_j \mathbb{Q}_{+1/2}^{+1/2}$ , similar manipulation can be done for the 3 others. The discrete form of the right hand side of (C.14) applied to this triad only can be transformed as follow:

$$\begin{aligned} & \int_D q \mathbf{k} \cdot \frac{1}{e_3} \nabla \times (e_3 q \mathbf{k} \times \mathbf{U}_h) dv \\ & \equiv \sum_{i,j,k} q \left\{ \delta_{i+1/2} \left[ -{}^i_j \mathbb{Q}_{+1/2}^{+1/2} U_j^{i+1/2} \right] - \delta_{j+1/2} \left[ {}^i_j \mathbb{Q}_{+1/2}^{+1/2} V_{j+1/2}^i \right] \right\} \\ & \equiv \sum_{i,j,k} \left\{ \delta_i [q] {}^i_j \mathbb{Q}_{+1/2}^{+1/2} U_j^{i+1/2} + \delta_j [q] {}^i_j \mathbb{Q}_{+1/2}^{+1/2} V_{j+1/2}^i \right\} \\ & \dots \\ & \text{Demonstration to be done...} \\ & \dots \\ & \equiv \frac{1}{2} \sum_{i,j,k} \left\{ \delta_i \left[ \left( {}^i_j \mathbb{Q}_{+1/2}^{+1/2} \right)^2 \right] \overline{U}^{i, j+1/2} + \delta_j \left[ \left( {}^i_j \mathbb{Q}_{+1/2}^{+1/2} \right)^2 \right] \overline{V}^{i+1/2, j} \right\} \end{aligned}$$

$$\begin{aligned}
&\equiv -\frac{1}{2} \sum_{i,j,k} \left( {}^i_j \mathbb{Q}_{+1/2}^{+1/2} \right)^2 \left\{ \delta_{i+1/2} \left[ \overline{\overline{U}}^{i,j+1/2} \right] + \delta_{j+1/2} \left[ \overline{\overline{V}}^{i+1/2,j} \right] \right\} \\
&\equiv \sum_{i,j,k} -\frac{1}{2} \left( {}^i_j \mathbb{Q}_{+1/2}^{+1/2} \right)^2 \overline{\overline{b}}_t^{i+1/2,j+1/2} \chi \\
&\equiv 0
\end{aligned}$$

## C.6 Conservation Properties on Tracers

All the numerical schemes used in NEMO are written such that the tracer content is conserved by the internal dynamics and physics (equations in flux form). For advection, only the CEN2 scheme (*i.e.*  $2^{nd}$  order finite different scheme) conserves the global variance of tracer. Nevertheless the other schemes ensure that the global variance decreases (*i.e.* they are at least slightly diffusive). For diffusion, all the schemes ensure the decrease of the total tracer variance, except the iso-neutral operator. There is generally no strict conservation of mass, as the equation of state is non linear with respect to  $T$  and  $S$ . In practice, the mass is conserved to a very high accuracy.

### C.6.1 Advection Term

conservation of a tracer,  $T$ :

$$\frac{\partial}{\partial t} \left( \int_D T \, dv \right) = \int_D \frac{1}{e_3} \frac{\partial (e_3 T)}{\partial t} \, dv = 0$$

conservation of its variance:

$$\frac{\partial}{\partial t} \left( \int_D \frac{1}{2} T^2 \, dv \right) = \int_D \frac{1}{e_3} Q \frac{\partial (e_3 T)}{\partial t} \, dv - \frac{1}{2} \int_D T^2 \frac{1}{e_3} \frac{\partial e_3}{\partial t} \, dv$$

Whatever the advection scheme considered it conserves of the tracer content as all the scheme are written in flux form. Indeed, let  $T$  be the tracer and  $\tau_u$ ,  $\tau_v$ , and  $\tau_w$  its interpolated values at velocity point (whatever the interpolation is), the conservation of the tracer content due to the advection tendency is obtained as follows:

$$\begin{aligned}
&\int_D \frac{1}{e_3} \frac{\partial (e_3 T)}{\partial t} \, dv = - \int_D \nabla \cdot (T \mathbf{U}) \, dv \\
&\equiv - \sum_{i,j,k} \left\{ \frac{1}{b_t} (\delta_i [U \tau_u] + \delta_j [V \tau_v]) + \frac{1}{e_{3t}} \delta_k [w \tau_w] \right\} b_t \\
&\equiv - \sum_{i,j,k} \{ \delta_i [U \tau_u] + \delta_j [V \tau_v] + \delta_k [W \tau_w] \} \\
&\equiv 0
\end{aligned}$$



The conservation of the variance of tracer due to the advection tendency can be achieved only with the CEN2 scheme, *i.e.* when  $\tau_u = \bar{T}^{i+1/2}$ ,  $\tau_v = \bar{T}^{j+1/2}$ , and  $\tau_w = \bar{T}^{k+1/2}$ . It can be demonstrated as follows:

$$\begin{aligned}
& \int_D \frac{1}{e_3} Q \frac{\partial (e_3 T)}{\partial t} dv = - \int_D \tau \nabla \cdot (T \mathbf{U}) dv \\
& \equiv - \sum_{i,j,k} T \left\{ \delta_i [U \bar{T}^{i+1/2}] + \delta_j [V \bar{T}^{j+1/2}] + \delta_k [W \bar{T}^{k+1/2}] \right\} \\
& \equiv + \sum_{i,j,k} \left\{ U \bar{T}^{i+1/2} \delta_{i+1/2} [T] + V \bar{T}^{j+1/2} \delta_{j+1/2} [T] + W \bar{T}^{k+1/2} \delta_{k+1/2} [T] \right\} \\
& \equiv + \frac{1}{2} \sum_{i,j,k} \left\{ U \delta_{i+1/2} [T^2] + V \delta_{j+1/2} [T^2] + W \delta_{k+1/2} [T^2] \right\} \\
& \equiv - \frac{1}{2} \sum_{i,j,k} T^2 \left\{ \delta_i [U] + \delta_j [V] + \delta_k [W] \right\} \\
& \equiv + \frac{1}{2} \sum_{i,j,k} T^2 \left\{ \frac{1}{e_{3t}} \frac{\partial e_{3t} T}{\partial t} \right\}
\end{aligned}$$

which is the discrete form of  $\frac{1}{2} \int_D T^2 \frac{1}{e_3} \frac{\partial e_3}{\partial t} dv$ .

## C.7 Conservation Properties on Lateral Momentum Physics

The discrete formulation of the horizontal diffusion of momentum ensures the conservation of potential vorticity and the horizontal divergence, and the dissipation of the square of these quantities (*i.e.* enstrophy and the variance of the horizontal divergence) as well as the dissipation of the horizontal kinetic energy. In particular, when the eddy coefficients are horizontally uniform, it ensures a complete separation of vorticity and horizontal divergence fields, so that diffusion (dissipation) of vorticity (enstrophy) does not generate horizontal divergence (variance of the horizontal divergence) and *vice versa*.

These properties of the horizontal diffusion operator are a direct consequence of properties (4.9) and (4.10). When the vertical curl of the horizontal diffusion of momentum (discrete sense) is taken, the term associated with the horizontal gradient of the divergence is locally zero.

### C.7.1 Conservation of Potential Vorticity

The lateral momentum diffusion term conserves the potential vorticity :

$$\int_D \frac{1}{e_3} \mathbf{k} \cdot \nabla \times \left[ \nabla_h (A^{lm} \chi) - \nabla_h \times (A^{lm} \zeta \mathbf{k}) \right] dv$$

$$\begin{aligned}
&= \int_D -\frac{1}{e_3} \mathbf{k} \cdot \nabla \times \left[ \nabla_h \times \left( A^{lm} \zeta \mathbf{k} \right) \right] dv \\
&\equiv \sum_{i,j} \left\{ \delta_{i+1/2} \left[ \frac{e_{2v}}{e_{1v} e_{3v}} \delta_i \left[ A_f^{lm} e_{3f} \zeta \right] \right] + \delta_{j+1/2} \left[ \frac{e_{1u}}{e_{2u} e_{3u}} \delta_j \left[ A_f^{lm} e_{3f} \zeta \right] \right] \right\}
\end{aligned}$$

Using (4.11), it follows:

$$\equiv \sum_{i,j,k} - \left\{ \frac{e_{2v}}{e_{1v} e_{3v}} \delta_i \left[ A_f^{lm} e_{3f} \zeta \right] \delta_i [1] + \frac{e_{1u}}{e_{2u} e_{3u}} \delta_j \left[ A_f^{lm} e_{3f} \zeta \right] \delta_j [1] \right\} \equiv 0$$

### C.7.2 Dissipation of Horizontal Kinetic Energy

The lateral momentum diffusion term dissipates the horizontal kinetic energy:

$$\begin{aligned}
&\int_D \mathbf{U}_h \cdot \left[ \nabla_h \left( A^{lm} \chi \right) - \nabla_h \times \left( A^{lm} \zeta \mathbf{k} \right) \right] dv \\
&\equiv \sum_{i,j,k} \left\{ \frac{1}{e_{1u}} \delta_{i+1/2} \left[ A_T^{lm} \chi \right] - \frac{1}{e_{2u} e_{3u}} \delta_j \left[ A_f^{lm} e_{3f} \zeta \right] \right\} e_{1u} e_{2u} e_{3u} u \\
&\quad + \left\{ \frac{1}{e_{2u}} \delta_{j+1/2} \left[ A_T^{lm} \chi \right] + \frac{1}{e_{1v} e_{3v}} \delta_i \left[ A_f^{lm} e_{3f} \zeta \right] \right\} e_{1v} e_{2u} e_{3v} v \\
&\equiv \sum_{i,j,k} \left\{ e_{2u} e_{3u} u \delta_{i+1/2} \left[ A_T^{lm} \chi \right] - e_{1u} u \delta_j \left[ A_f^{lm} e_{3f} \zeta \right] \right\} \\
&\quad + \left\{ e_{1v} e_{3v} v \delta_{j+1/2} \left[ A_T^{lm} \chi \right] + e_{2v} v \delta_i \left[ A_f^{lm} e_{3f} \zeta \right] \right\} \\
&\equiv \sum_{i,j,k} - \left( \delta_i \left[ e_{2u} e_{3u} u \right] + \delta_j \left[ e_{1v} e_{3v} v \right] \right) A_T^{lm} \chi \\
&\quad - \left( \delta_{i+1/2} \left[ e_{2v} v \right] - \delta_{j+1/2} \left[ e_{1u} u \right] \right) A_f^{lm} e_{3f} \zeta \\
&\equiv \sum_{i,j,k} - A_T^{lm} \chi^2 e_{1t} e_{2t} e_{3t} - A_f^{lm} \zeta^2 e_{1f} e_{2f} e_{3f} \leq 0
\end{aligned}$$

### C.7.3 Dissipation of Enstrophy

The lateral momentum diffusion term dissipates the enstrophy when the eddy coefficients are horizontally uniform:

$$\begin{aligned}
& \int_D \zeta \mathbf{k} \cdot \nabla \times \left[ \nabla_h \left( A^{lm} \chi \right) - \nabla_h \times \left( A^{lm} \zeta \mathbf{k} \right) \right] dv \\
&= A^{lm} \int_D \zeta \mathbf{k} \cdot \nabla \times \left[ \nabla_h \times \left( \zeta \mathbf{k} \right) \right] dv \\
&\equiv A^{lm} \sum_{i,j,k} \zeta e_{3f} \left\{ \delta_{i+1/2} \left[ \frac{e_{2v}}{e_{1v} e_{3v}} \delta_i [e_{3f} \zeta] \right] + \delta_{j+1/2} \left[ \frac{e_{1u}}{e_{2u} e_{3u}} \delta_j [e_{3f} \zeta] \right] \right\}
\end{aligned}$$

Using (4.11), it follows:

$$\equiv -A^{lm} \sum_{i,j,k} \left\{ \left( \frac{1}{e_{1v} e_{3v}} \delta_i [e_{3f} \zeta] \right)^2 b_v + \left( \frac{1}{e_{2u} e_{3u}} \delta_j [e_{3f} \zeta] \right)^2 b_u \right\} \leq 0$$

### C.7.4 Conservation of Horizontal Divergence

When the horizontal divergence of the horizontal diffusion of momentum (discrete sense) is taken, the term associated with the vertical curl of the vorticity is zero locally, due to (4.10). The resulting term conserves the  $\chi$  and dissipates  $\chi^2$  when the eddy coefficients are horizontally uniform.

$$\begin{aligned}
& \int_D \nabla_h \cdot \left[ \nabla_h \left( A^{lm} \chi \right) - \nabla_h \times \left( A^{lm} \zeta \mathbf{k} \right) \right] dv = \int_D \nabla_h \cdot \nabla_h \left( A^{lm} \chi \right) dv \\
&\equiv \sum_{i,j,k} \left\{ \delta_i \left[ A_u^{lm} \frac{e_{2u} e_{3u}}{e_{1u}} \delta_{i+1/2} [\chi] \right] + \delta_j \left[ A_v^{lm} \frac{e_{1v} e_{3v}}{e_{2v}} \delta_{j+1/2} [\chi] \right] \right\}
\end{aligned}$$

Using (4.11), it follows:

$$\equiv \sum_{i,j,k} - \left\{ \frac{e_{2u} e_{3u}}{e_{1u}} A_u^{lm} \delta_{i+1/2} [\chi] \delta_{i+1/2} [1] + \frac{e_{1v} e_{3v}}{e_{2v}} A_v^{lm} \delta_{j+1/2} [\chi] \delta_{j+1/2} [1] \right\} \equiv 0$$

### C.7.5 Dissipation of Horizontal Divergence Variance

$$\begin{aligned}
& \int_D \chi \nabla_h \cdot \left[ \nabla_h \left( A^{lm} \chi \right) - \nabla_h \times \left( A^{lm} \zeta \mathbf{k} \right) \right] dv = A^{lm} \int_D \chi \nabla_h \cdot \nabla_h (\chi) dv \\
&\equiv A^{lm} \sum_{i,j,k} \frac{1}{e_{1t} e_{2t} e_{3t}} \chi \left\{ \delta_i \left[ \frac{e_{2u} e_{3u}}{e_{1u}} \delta_{i+1/2} [\chi] \right] + \delta_j \left[ \frac{e_{1v} e_{3v}}{e_{2v}} \delta_{j+1/2} [\chi] \right] \right\} e_{1t} e_{2t} e_{3t}
\end{aligned}$$

Using (4.11), it turns out to be:

$$\equiv -A^{lm} \sum_{i,j,k} \left\{ \left( \frac{1}{e_{1u}} \delta_{i+1/2} [\chi] \right)^2 b_u + \left( \frac{1}{e_{2v}} \delta_{j+1/2} [\chi] \right)^2 b_v \right\} \leq 0$$

## C.8 Conservation Properties on Vertical Momentum Physics

As for the lateral momentum physics, the continuous form of the vertical diffusion of momentum satisfies several integral constraints. The first two are associated with the conservation of momentum and the dissipation of horizontal kinetic energy:

$$\int_D \frac{1}{e_3} \frac{\partial}{\partial k} \left( \frac{A^{vm}}{e_3} \frac{\partial \mathbf{U}_h}{\partial k} \right) dv = \vec{\mathbf{0}}$$

and

$$\int_D \mathbf{U}_h \cdot \frac{1}{e_3} \frac{\partial}{\partial k} \left( \frac{A^{vm}}{e_3} \frac{\partial \mathbf{U}_h}{\partial k} \right) dv \leq 0$$

The first property is obvious. The second results from:

$$\begin{aligned} & \int_D \mathbf{U}_h \cdot \frac{1}{e_3} \frac{\partial}{\partial k} \left( \frac{A^{vm}}{e_3} \frac{\partial \mathbf{U}_h}{\partial k} \right) dv \\ & \equiv \sum_{i,j,k} \left( u \delta_k \left[ \frac{A_u^{vm}}{e_{3uw}} \delta_{k+1/2} [u] \right] e_{1u} e_{2u} + v \delta_k \left[ \frac{A_v^{vm}}{e_{3vw}} \delta_{k+1/2} [v] \right] e_{1v} e_{2v} \right) \end{aligned}$$

since the horizontal scale factor does not depend on  $k$ , it follows:

$$\equiv - \sum_{i,j,k} \left( \frac{A_u^{vm}}{e_{3uw}} (\delta_{k+1/2} [u])^2 e_{1u} e_{2u} + \frac{A_v^{vm}}{e_{3vw}} (\delta_{k+1/2} [v])^2 e_{1v} e_{2v} \right) \leq 0$$

The vorticity is also conserved. Indeed:

$$\int_D \frac{1}{e_3} \mathbf{k} \cdot \nabla \times \left( \frac{1}{e_3} \frac{\partial}{\partial k} \left( \frac{A^{vm}}{e_3} \frac{\partial \mathbf{U}_h}{\partial k} \right) \right) dv$$

$$\equiv \sum_{i,j,k} \frac{1}{e_{3f}} \frac{1}{e_{1f} e_{2f}} \left\{ \begin{aligned} & \delta_{i+1/2} \left( \frac{e_{2v}}{e_{3v}} \delta_k \left[ \frac{1}{e_{3vw}} \delta_{k+1/2} [v] \right] \right) \\ & - \delta_{j+1/2} \left( \frac{e_{1u}}{e_{3u}} \delta_k \left[ \frac{1}{e_{3uw}} \delta_{k+1/2} [u] \right] \right) \end{aligned} \right\} e_{1f} e_{2f} e_{3f} \equiv 0$$

If the vertical diffusion coefficient is uniform over the whole domain, the enstrophy is dissipated, *i.e.*

$$\int_D \zeta \mathbf{k} \cdot \nabla \times \left( \frac{1}{e_3} \frac{\partial}{\partial k} \left( \frac{A^{vm}}{e_3} \frac{\partial \mathbf{U}_h}{\partial k} \right) \right) dv = 0$$

This property is only satisfied in  $z$ -coordinates:

$$\begin{aligned} & \int_D \zeta \mathbf{k} \cdot \nabla \times \left( \frac{1}{e_3} \frac{\partial}{\partial k} \left( \frac{A^{vm}}{e_3} \frac{\partial \mathbf{U}_h}{\partial k} \right) \right) dv \\ & \equiv \sum_{i,j,k} \zeta e_{3f} \left\{ \begin{aligned} & \delta_{i+1/2} \left( \frac{e_{2v}}{e_{3v}} \delta_k \left[ \frac{A_v^{vm}}{e_{3vw}} \delta_{k+1/2} [v] \right] \right) \\ & - \delta_{j+1/2} \left( \frac{e_{1u}}{e_{3u}} \delta_k \left[ \frac{A_u^{vm}}{e_{3uw}} \delta_{k+1/2} [u] \right] \right) \end{aligned} \right\} \\ & \equiv \sum_{i,j,k} \zeta e_{3f} \left\{ \begin{aligned} & \frac{1}{e_{3v}} \delta_k \left[ \frac{A_v^{vm}}{e_{3vw}} \delta_{k+1/2} [\delta_{i+1/2} [e_{2v} v]] \right] \\ & - \frac{1}{e_{3u}} \delta_k \left[ \frac{A_u^{vm}}{e_{3uw}} \delta_{k+1/2} [\delta_{j+1/2} [e_{1u} u]] \right] \end{aligned} \right\} \end{aligned}$$

Using the fact that the vertical diffusion coefficients are uniform, and that in  $z$ -coordinate, the vertical scale factors do not depend on  $i$  and  $j$  so that:  $e_{3f} = e_{3u} = e_{3v} = e_{3t}$  and  $e_{3w} = e_{3uw} = e_{3vw}$ , it follows:

$$\equiv A^{vm} \sum_{i,j,k} \zeta \delta_k \left[ \frac{1}{e_{3w}} \delta_{k+1/2} [\delta_{i+1/2} [e_{2v} v] - \delta_{j+1/2} [e_{1u} u]] \right]$$

$$\equiv -A^{vm} \sum_{i,j,k} \frac{1}{e_{3w}} (\delta_{k+1/2} [\zeta])^2 e_{1f} e_{2f} \leq 0$$

Similarly, the horizontal divergence is obviously conserved:

$$\int_D \nabla \cdot \left( \frac{1}{e_3} \frac{\partial}{\partial k} \left( \frac{A^{vm}}{e_3} \frac{\partial \mathbf{U}_h}{\partial k} \right) \right) dv = 0$$

and the square of the horizontal divergence decreases (*i.e.* the horizontal divergence is dissipated) if the vertical diffusion coefficient is uniform over the whole domain:

$$\int_D \chi \nabla \cdot \left( \frac{1}{e_3} \frac{\partial}{\partial k} \left( \frac{A^{vm}}{e_3} \frac{\partial \mathbf{U}_h}{\partial k} \right) \right) dv = 0$$

This property is only satisfied in the  $z$ -coordinate:

$$\int_D \chi \nabla \cdot \left( \frac{1}{e_3} \frac{\partial}{\partial k} \left( \frac{A^{vm}}{e_3} \frac{\partial \mathbf{U}_h}{\partial k} \right) \right) dv$$

$$\equiv \sum_{i,j,k} \frac{\chi}{e_{1t} e_{2t}} \left\{ \delta_{i+1/2} \left( \frac{e_{2u}}{e_{3u}} \delta_k \left[ \frac{A_u^{vm}}{e_{3uw}} \delta_{k+1/2} [u] \right] \right) + \delta_{j+1/2} \left( \frac{e_{1v}}{e_{3v}} \delta_k \left[ \frac{A_v^{vm}}{e_{3vw}} \delta_{k+1/2} [v] \right] \right) \right\} e_{1t} e_{2t} e_{3t}$$

$$\equiv A^{vm} \sum_{i,j,k} \chi \left\{ \delta_{i+1/2} \left( \delta_k \left[ \frac{1}{e_{3uw}} \delta_{k+1/2} [e_{2u} u] \right] \right) + \delta_{j+1/2} \left( \delta_k \left[ \frac{1}{e_{3vw}} \delta_{k+1/2} [e_{1v} v] \right] \right) \right\}$$

$$\begin{aligned}
&\equiv -A^{vm} \sum_{i,j,k} \frac{\delta_{k+1/2} [\chi]}{e_{3w}} \left\{ \delta_{k+1/2} \left[ \delta_{i+1/2} [e_{2u} u] + \delta_{j+1/2} [e_{1v} v] \right] \right\} \\
&\equiv -A^{vm} \sum_{i,j,k} \frac{1}{e_{3w}} \delta_{k+1/2} [\chi] \delta_{k+1/2} [e_{1t} e_{2t} \chi] \\
&\equiv -A^{vm} \sum_{i,j,k} \frac{e_{1t} e_{2t}}{e_{3w}} (\delta_{k+1/2} [\chi])^2 \equiv 0
\end{aligned}$$

## C.9 Conservation Properties on Tracer Physics

The numerical schemes used for tracer subgridscale physics are written such that the heat and salt contents are conserved (equations in flux form). Since a flux form is used to compute the temperature and salinity, the quadratic form of these quantities (*i.e.* their variance) globally tends to diminish. As for the advection term, there is conservation of mass only if the Equation Of Seawater is linear.

### C.9.1 Conservation of Tracers

constraint of conservation of tracers:

$$\begin{aligned}
&\int_D \nabla \cdot (A \nabla T) \, dv \\
&\equiv \sum_{i,j,k} \left\{ \delta_i \left[ A_u^{lT} \frac{e_{2u} e_{3u}}{e_{1u}} \delta_{i+1/2} [T] \right] + \delta_j \left[ A_v^{lT} \frac{e_{1v} e_{3v}}{e_{2v}} \delta_{j+1/2} [T] \right] \right. \\
&\quad \left. + \delta_k \left[ A_w^{vT} \frac{e_{1t} e_{2t}}{e_{3t}} \delta_{k+1/2} [T] \right] \right\} \equiv 0
\end{aligned}$$

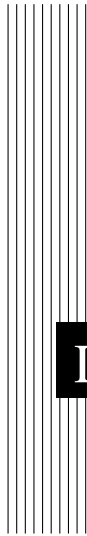
In fact, this property simply results from the flux form of the operator.

### C.9.2 Dissipation of Tracer Variance

constraint on the dissipation of tracer variance:

$$\begin{aligned}
 & \int_D T \nabla \cdot (A \nabla T) \, dv \\
 & \equiv \sum_{i,j,k} T \left\{ \delta_i \left[ A_u^{lT} \frac{e_{2u} e_{3u}}{e_{1u}} \delta_{i+1/2} [T] \right] + \delta_j \left[ A_v^{lT} \frac{e_{1v} e_{3v}}{e_{2v}} \delta_{j+1/2} [T] \right] \right. \\
 & \qquad \qquad \qquad \left. + \delta_k \left[ A_w^{vT} \frac{e_{1t} e_{2t}}{e_{3t}} \delta_{k+1/2} [T] \right] \right\} \\
 & \equiv - \sum_{i,j,k} \left\{ A_u^{lT} \left( \frac{1}{e_{1u}} \delta_{i+1/2} [T] \right)^2 e_{1u} e_{2u} e_{3u} \right. \\
 & \qquad \qquad \qquad + A_v^{lT} \left( \frac{1}{e_{2v}} \delta_{j+1/2} [T] \right)^2 e_{1v} e_{2v} e_{3v} \\
 & \qquad \qquad \qquad \left. + A_w^{vT} \left( \frac{1}{e_{3w}} \delta_{k+1/2} [T] \right)^2 e_{1w} e_{2w} e_{3w} \right\} \leq 0
 \end{aligned}$$





# D Iso-neutral diffusion and eddy advection using triads

## Contents

---

<b>D.1</b>	<b>Choice of <i>namtra_ldf</i> namelist parameters . . . . .</b>	<b>336</b>
<b>D.2</b>	<b>Triad formulation of iso-neutral diffusion . . . . .</b>	<b>337</b>
D.2.1	The iso-neutral diffusion operator . . . . .	337
D.2.2	The standard discretization . . . . .	338
D.2.3	Expression of the skew-flux in terms of triad slopes . . .	339
D.2.4	The full triad fluxes . . . . .	341
D.2.5	Ensuring the scheme does not increase tracer variance	342
D.2.6	Triad volumes in Griffes's scheme and in <i>NEMO</i> . . .	343
D.2.7	Summary of the scheme . . . . .	344
D.2.8	Treatment of the triads at the boundaries . . . . .	345
D.2.9	Limiting of the slopes within the interior . . . . .	347
D.2.10	Tapering within the surface mixed layer . . . . .	347
<b>D.3</b>	<b>Eddy induced advection formulated as a skew flux . . . . .</b>	<b>350</b>
D.3.1	The continuous skew flux formulation . . . . .	350
D.3.2	The discrete skew flux formulation . . . . .	352
D.3.3	Treatment of the triads at the boundaries . . . . .	353
D.3.4	Limiting of the slopes within the interior . . . . .	354
D.3.5	Tapering within the surface mixed layer . . . . .	354
D.3.6	Streamfunction diagnostics . . . . .	354

---

## D.1 Choice of *namtra\_ldf* namelist parameters

```

!-----
&namtra_ldf ! lateral diffusion scheme for tracers (default: NO selection)
!-----
!
! Operator type:
ln_traldf_NONE = .false. ! No explicit diffusion
ln_traldf_lap = .false. ! laplacian operator
ln_traldf_blp = .false. ! bilaplacian operator
!
! Direction of action:
ln_traldf_lev = .false. ! iso-level
ln_traldf_hor = .false. ! horizontal (geopotential)
ln_traldf_iso = .false. ! iso-neutral (standard operator)
ln_traldf_triad = .false. ! iso-neutral (triad operator)
!
! iso-neutral options:
ln_traldf_msc = .false. ! Method of Stabilizing Correction (both operators)
rn_slpmax = 0.01 ! slope limit (both operators)
ln_triad_iso = .false. ! pure horizontal mixing in ML (triad only)
rn_sw_triad = 1 ! =1 switching triad ; =0 all 4 triads used (triad only)
ln_botmix_triad = .false. ! lateral mixing on bottom (triad only)
!
! Coefficients:
nn_aht_ijk_t = 0 ! space/time variation of eddy coef
! ! =-20 (= -30) read in eddy_diffusivity_2D.nc (..._3D.nc) file
! ! = 0 constant
! ! = 10 F(k) =ldf_c1d
! ! = 20 F(i,j) =ldf_c2d
! ! = 21 F(i,j,t) =Treguier et al. JPO 1997 formulation
! ! = 30 F(i,j,k) =ldf_c2d * ldf_c1d
! ! = 31 F(i,j,k,t)=F(local velocity and grid-spacing)
rn_aht_0 = 2000. ! lateral eddy diffusivity (lap. operator) [m2/s]
rn_bht_0 = 1.e+12 ! lateral eddy diffusivity (bilap. operator) [m4/s]
/

```

Two schemes are available to perform the iso-neutral diffusion. If the namelist logical *ln\_traldf\_triad* is set true, *NEMO* updates both active and passive tracers using the Griffies triad representation of iso-neutral diffusion and the eddy-induced advective skew (GM) fluxes. If the namelist logical *ln\_traldf\_iso* is set true, the filtered version of Cox's original scheme (the Standard scheme) is employed (§9.1). In the present implementation of the Griffies scheme, the advective skew fluxes are implemented even if *ln\_traldf\_eiv* is false.

Values of iso-neutral diffusivity and GM coefficient are set as described in §9.3. Note that when GM fluxes are used, the eddy-advective (GM) velocities are output for diagnostic purposes using *xIOS*, even though the eddy advection is accomplished by means of the skew fluxes.

The options specific to the Griffies scheme include:

*ln\_triad\_iso* See §D.2.10. If this is set false (the default), then 'iso-neutral' mixing is accomplished within the surface mixed-layer along slopes linearly decreasing with depth from the value immediately below the mixed-layer to zero (flat) at the surface (§D.2.10). This is the same treatment as used in the default implementation §9.1.2; Fig. 9.2. Where *ln\_triad\_iso* is set true, the vertical skew flux is further reduced to ensure no vertical buoyancy flux, giving an almost pure horizontal diffusive tracer flux within the mixed layer. This is similar to the tapering suggested by Gerdes et al. [1991]. See §D.2.10

*ln\_botmix\_triad* See §D.2.8. If this is set false (the default) then the lateral diffusive fluxes associated with triads partly masked by topography are neglected. If it is set true, however, then these lateral diffusive fluxes are applied, giving smoother bottom tracer fields at the cost of introducing diapycnal mixing.

*rn\_sw\_triad* blah blah to be added....

The options shared with the Standard scheme include:

*ln\_traldf\_msc* blah blah to be added

*rn\_slpmax* blah blah to be added

## D.2 Triad formulation of iso-neutral diffusion

We have implemented into *NEMO* a scheme inspired by Griffies et al. [1998], but formulated within the *NEMO* framework, using scale factors rather than grid-sizes.

### D.2.1 The iso-neutral diffusion operator

The iso-neutral second order tracer diffusive operator for small angles between iso-neutral surfaces and geopotentials is given by (2.35):

$$D^{lT} = -\nabla \cdot \mathbf{f}^{lT} \equiv -\frac{1}{e_1 e_2 e_3} \left[ \frac{\partial}{\partial i} (f_1^{lT} e_2 e_3) + \frac{\partial}{\partial j} (f_2^{lT} e_2 e_3) + \frac{\partial}{\partial k} (f_3^{lT} e_1 e_2) \right], \quad (\text{D.1a})$$

where the diffusive flux per unit area of physical space

$$\mathbf{f}^{lT} = -A^{lT} \mathfrak{R} \cdot \nabla T, \quad (\text{D.1b})$$

$$\text{with } \mathfrak{R} = \begin{pmatrix} 1 & 0 & -r_1 \\ 0 & 1 & -r_2 \\ -r_1 & -r_2 & r_1^2 + r_2^2 \end{pmatrix} \quad \text{and} \quad \nabla T = \begin{pmatrix} \frac{1}{e_1} \frac{\partial T}{\partial i} \\ \frac{1}{e_2} \frac{\partial T}{\partial j} \\ \frac{1}{e_3} \frac{\partial T}{\partial k} \end{pmatrix}. \quad (\text{D.1c})$$

Here (2.36)

$$\begin{aligned} r_1 &= -\frac{e_3}{e_1} \left( \frac{\partial \rho}{\partial i} \right) \left( \frac{\partial \rho}{\partial k} \right)^{-1} \\ &= -\frac{e_3}{e_1} \left( -\alpha \frac{\partial T}{\partial i} + \beta \frac{\partial S}{\partial i} \right) \left( -\alpha \frac{\partial T}{\partial k} + \beta \frac{\partial S}{\partial k} \right)^{-1} \end{aligned}$$

is the  $i$ -component of the slope of the iso-neutral surface relative to the computational surface, and  $r_2$  is the  $j$ -component.

We will find it useful to consider the fluxes per unit area in  $i, j, k$  space; we write

$$\mathbf{F}_{\text{iso}} = \left( f_1^{lT} e_2 e_3, f_2^{lT} e_1 e_3, f_3^{lT} e_1 e_2 \right). \quad (\text{D.2})$$

Additionally, we will sometimes write the contributions towards the fluxes  $\mathbf{f}$  and  $\mathbf{F}_{\text{iso}}$  from the component  $R_{ij}$  of  $\mathfrak{R}$  as  $f_{ij}$ ,  $F_{\text{iso } ij}$ , with  $f_{ij} = R_{ij} e_i^{-1} \partial T / \partial x_i$  (no summation) etc.

The off-diagonal terms of the small angle diffusion tensor (2.35), (D.1c) produce skew-fluxes along the  $i$ - and  $j$ -directions resulting from the vertical tracer gradient:

$$f_{13} = + A^{lT} r_1 \frac{1}{e_3} \frac{\partial T}{\partial k}, \quad f_{23} = + A^{lT} r_2 \frac{1}{e_3} \frac{\partial T}{\partial k} \quad (\text{D.3})$$

and in the  $k$ -direction resulting from the lateral tracer gradients

$$f_{31} + f_{32} = A^{lT} r_1 \frac{1}{e_1} \frac{\partial T}{\partial i} + A^{lT} r_2 \frac{1}{e_1} \frac{\partial T}{\partial i} \quad (\text{D.4})$$

The vertical diffusive flux associated with the  $33$  component of the small angle diffusion tensor is

$$f_{33} = -A^{lT} (r_1^2 + r_2^2) \frac{1}{e_3} \frac{\partial T}{\partial k}. \quad (\text{D.5})$$

Since there are no cross terms involving  $r_1$  and  $r_2$  in the above, we can consider the iso-neutral diffusive fluxes separately in the  $i$ - $k$  and  $j$ - $k$  planes, just adding together the vertical components from each plane. The following description will describe the fluxes on the  $i$ - $k$  plane.

There is no natural discretization for the  $i$ -component of the skew-flux, (D.3), as although it must be evaluated at  $u$ -points, it involves vertical gradients (both for the tracer and the slope  $r_1$ ), defined at  $w$ -points. Similarly, the vertical skew flux, (D.4), is evaluated at  $w$ -points but involves horizontal gradients defined at  $u$ -points.

## D.2.2 The standard discretization

The straightforward approach to discretize the lateral skew flux (D.3) from tracer cell  $i, k$  to  $i + 1, k$ , introduced in 1995 into OPA, (5.10), is to calculate a mean vertical gradient at the  $u$ -point from the average of the four surrounding vertical tracer gradients, and multiply this by a mean slope at the  $u$ -point, calculated from the averaged surrounding vertical density gradients. The total area-integrated skew-flux (flux per unit area in  $ijk$  space) from tracer cell  $i, k$  to  $i + 1, k$ , noting that the  $e_{3i+1/2}^k$  in the area  $e_{3i+1/2}^k e_{2i+1/2} i^k$  at the  $u$ -point cancels out with the  $1/e_{3i+1/2}^k$  associated with the vertical tracer gradient, is then (5.10)

$$(F_u^{13})_{i+\frac{1}{2}}^k = A_{i+\frac{1}{2}}^k e_{2i+1/2}^k \overline{\overline{r_1}}^{i,k} \overline{\overline{\delta_k T}}^{i,k},$$

where

$$\overline{\overline{r_1}}^{i,k} = - \frac{e_{3u_{i+1/2}}^k}{e_{1u_{i+1/2}}^k} \frac{\delta_{i+1/2}[\rho]}{\overline{\overline{\delta_k \rho}}^{i,k}},$$

and here and in the following we drop the  $lT$  superscript from  $A^{lT}$  for simplicity. Unfortunately the resulting combination  $\overline{\overline{\delta_k \bullet}}^{i,k}$  of a  $k$  average and a  $k$  difference

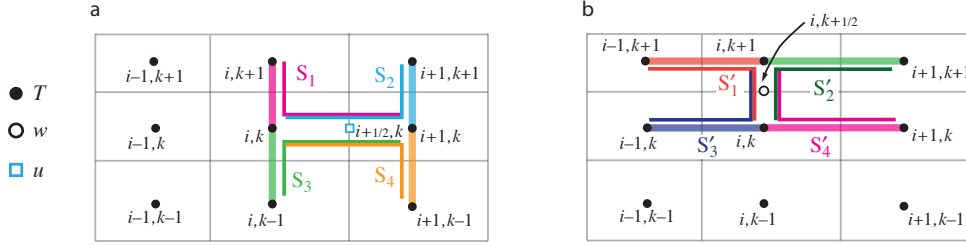


**Figure D.1:** (a) Arrangement of triads  $S_i$  and tracer gradients to give lateral tracer flux from box  $i, k$  to  $i + 1, k$  (b) Triads  $S'_i$  and tracer gradients to give vertical tracer flux from box  $i, k$  to  $i, k + 1$ .

reduces to  $\bullet_{k+1} - \bullet_{k-1}$ , so two-grid-point oscillations are invisible to this discretization of the iso-neutral operator. These *computational modes* will not be damped by this operator, and may even possibly be amplified by it. Consequently, applying this operator to a tracer does not guarantee the decrease of its global-average variance. To correct this, we introduced a smoothing of the slopes of the iso-neutral surfaces (see §9). This technique works for  $T$  and  $S$  in so far as they are active tracers (*i.e.* they enter the computation of density), but it does not work for a passive tracer.

### D.2.3 Expression of the skew-flux in terms of triad slopes

[Griffies et al. 1998] introduce a different discretization of the off-diagonal terms that nicely solves the problem. They get the skew flux from the products of the vertical gradients at each  $w$ -point surrounding the  $u$ -point with the corresponding ‘triad’ slope calculated from the lateral density gradient across the  $u$ -point divided by the vertical density gradient at the same  $w$ -point as the tracer gradient. See Fig. D.1a, where the thick lines denote the tracer gradients, and the thin lines the corresponding triads, with slopes  $s_1, \dots, s_4$ . The total area-integrated skew-flux from tracer cell  $i, k$  to  $i + 1, k$

$$\begin{aligned} (F_u^{13})_{i+\frac{1}{2}}^k &= A_{i+1}^k a_1 s_1 \delta_{k+\frac{1}{2}} [T^{i+1}] / e_{3w_{i+1}}^{k+\frac{1}{2}} + A_i^k a_2 s_2 \delta_{k+\frac{1}{2}} [T^i] / e_{3w_{i+1}}^{k+\frac{1}{2}} \\ &+ A_{i+1}^k a_3 s_3 \delta_{k-\frac{1}{2}} [T^{i+1}] / e_{3w_{i+1}}^{k+\frac{1}{2}} + A_i^k a_4 s_4 \delta_{k-\frac{1}{2}} [T^i] / e_{3w_{i+1}}^{k+\frac{1}{2}}, \quad (\text{D.6}) \end{aligned}$$

where the contributions of the triad fluxes are weighted by areas  $a_1, \dots, a_4$ , and  $A$  is now defined at the tracer points rather than the  $u$ -points. This discretization gives a much closer stencil, and disallows the two-point computational modes.

The vertical skew flux (D.4) from tracer cell  $i, k$  to  $i, k + 1$  at the  $w$ -point  $i, k + \frac{1}{2}$  is constructed similarly (Fig. D.1b) by multiplying lateral tracer gradients

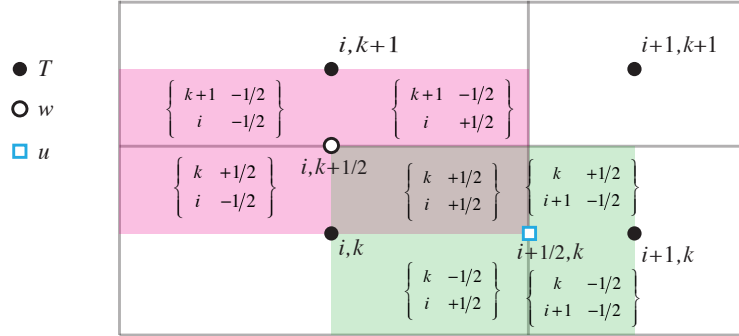


**Figure D.2:** Triad notation for quarter cells.  $T$ -cells are inside boxes, while the  $i + \frac{1}{2}, k$   $u$ -cell is shaded in green and the  $i, k + \frac{1}{2}$   $w$ -cell is shaded in pink.

from each of the four surrounding  $u$ -points by the appropriate triad slope:

$$\begin{aligned} (F_w^{31})_i^{k+\frac{1}{2}} &= A_i^{k+1} a'_1 s'_1 \delta_{i-\frac{1}{2}} [T^{k+1}] / e_{3u_{i-\frac{1}{2}}^{k+1}} + A_i^{k+1} a'_2 s'_2 \delta_{i+\frac{1}{2}} [T^{k+1}] / e_{3u_{i+\frac{1}{2}}^{k+1}} \\ &+ A_i^k a'_3 s'_3 \delta_{i-\frac{1}{2}} [T^k] / e_{3u_{i-\frac{1}{2}}^k} + A_i^k a'_4 s'_4 \delta_{i+\frac{1}{2}} [T^k] / e_{3u_{i+\frac{1}{2}}^k}. \end{aligned} \quad (\text{D.7})$$

We notate the triad slopes  $s_i$  and  $s'_i$  in terms of the ‘anchor point’  $i, k$  (appearing in both the vertical and lateral gradient), and the  $u$ - and  $w$ -points  $(i + i_p, k)$ ,  $(i, k + k_p)$  at the centres of the ‘arms’ of the triad as follows (see also Fig. D.1):

$${}^k \mathbb{R}_{i_p}^{k_p} = - \frac{e_{3w_i}^{k+k_p}}{e_{1u_{i+i_p}}^k} \frac{\alpha_i^k \delta_{i+i_p} [T^k] - \beta_i^k \delta_{i+i_p} [S^k]}{\alpha_i^k \delta_{k+k_p} [T^i] - \beta_i^k \delta_{k+k_p} [S^i]}. \quad (\text{D.8})$$

In calculating the slopes of the local neutral surfaces, the expansion coefficients  $\alpha$  and  $\beta$  are evaluated at the anchor points of the triad, while the metrics are calculated at the  $u$ - and  $w$ -points on the arms.

Each triad  $\{i, i_p\}^k$  is associated (Fig. D.2) with the quarter cell that is the intersection of the  $i, k$   $T$ -cell, the  $i + i_p, k$   $u$ -cell and the  $i, k + k_p$   $w$ -cell. Expressing the slopes  $s_i$  and  $s'_i$  in (D.6) and (D.7) in this notation, we have e.g.  $s_1 = s'_1 = {}^k \mathbb{R}_{1/2}^{1/2}$ . Each triad slope  ${}^k \mathbb{R}_{i_p}^{k_p}$  is used once (as an  $s$ ) to calculate the lateral flux along its  $u$ -arm, at  $(i + i_p, k)$ , and then again as an  $s'$  to calculate the vertical flux along its  $w$ -arm at  $(i, k + k_p)$ . Each vertical area  $a_i$  used to calculate the lateral flux and horizontal area  $a'_i$  used to calculate the vertical flux can also be identified as the area across the  $u$ - and  $w$ -arms of a unique triad, and we notate these areas, similarly to the triad slopes, as  ${}^k \mathbb{A}_{u_{i_p}}^{k_p}$ ,  ${}^k \mathbb{A}_{w_{i_p}}^{k_p}$ , where e.g. in (D.6)  $a_1 = {}^k \mathbb{A}_{u_{1/2}}^{1/2}$ , and in (D.7)  $a'_1 = {}^k \mathbb{A}_{w_{1/2}}^{1/2}$ .

### D.2.4 The full triad fluxes

A key property of iso-neutral diffusion is that it should not affect the (locally referenced) density. In particular there should be no lateral or vertical density flux. The lateral density flux disappears so long as the area-integrated lateral diffusive flux from tracer cell  $i, k$  to  $i + 1, k$  coming from the  $_{11}$  term of the diffusion tensor takes the form

$$(F_u^{11})_{i+\frac{1}{2}}^k = - \left( A_i^{k+1} a_1 + A_i^{k+1} a_2 + A_i^k a_3 + A_i^k a_4 \right) \frac{\delta_{i+1/2} [T^k]}{e_{1u}^k}_{i+1/2}, \quad (\text{D.9})$$

where the areas  $a_i$  are as in (D.6). In this case, separating the total lateral flux, the sum of (D.6) and (D.9), into triad components, a lateral tracer flux

$${}^k \mathbb{F}_{u i_p}^{k_p}(T) = -A_i^k {}^k \mathbb{A}_{u i_p}^{k_p} \left( \frac{\delta_{i+i_p} [T^k]}{e_{1u}^k}_{i+i_p} - {}^k \mathbb{R}_{i_p}^{k_p} \frac{\delta_{k+k_p} [T^i]}{e_{3w}^k}_{k+k_p} \right) \quad (\text{D.10})$$

can be identified with each triad. Then, because the same metric factors  $e_{3w}^k$  and  $e_{1u}^k$  are employed for both the density gradients in  ${}^k \mathbb{R}_{i_p}^{k_p}$  and the tracer gradients, the lateral density flux associated with each triad separately disappears.

$$\mathbb{F}_{u i_p}^{k_p}(\rho) = -\alpha_i^k {}^k \mathbb{F}_{u i_p}^{k_p}(T) + \beta_i^k {}^k \mathbb{F}_{u i_p}^{k_p}(S) = 0 \quad (\text{D.11})$$

Thus the total flux  $(F_u^{31})_{i,k+\frac{1}{2}}^i + (F_u^{11})_{i,k+\frac{1}{2}}^i$  from tracer cell  $i, k$  to  $i + 1, k$  must also vanish since it is a sum of four such triad fluxes.

The squared slope  $r_1^2$  in the expression (D.5) for the  $_{33}$  component is also expressed in terms of area-weighted squared triad slopes, so the area-integrated vertical flux from tracer cell  $i, k$  to  $i, k + 1$  resulting from the  $r_1^2$  term is

$$(F_w^{33})_i^{k+\frac{1}{2}} = - \left( A_i^{k+1} a'_1 s_1'^2 + A_i^{k+1} a'_2 s_2'^2 + A_i^k a'_3 s_3'^2 + A_i^k a'_4 s_4'^2 \right) \delta_{k+\frac{1}{2}} [T^{i+1}], \quad (\text{D.12})$$

where the areas  $a'$  and slopes  $s'$  are the same as in (D.7). Then, separating the total vertical flux, the sum of (D.7) and (D.12), into triad components, a vertical flux

$${}^k \mathbb{F}_{w i_p}^{k_p}(T) = A_i^k {}^k \mathbb{A}_{w i_p}^{k_p} \left( {}^k \mathbb{R}_{i_p}^{k_p} \frac{\delta_{i+i_p} [T^k]}{e_{1u}^k}_{i+i_p} - \left( {}^k \mathbb{R}_{i_p}^{k_p} \right)^2 \frac{\delta_{k+k_p} [T^i]}{e_{3w}^k}_{k+k_p} \right) \quad (\text{D.13})$$

$$= - \left( {}^k \mathbb{A}_{w i_p}^{k_p} / {}^k \mathbb{A}_{u i_p}^{k_p} \right) {}^k \mathbb{R}_{i_p}^{k_p} {}^k \mathbb{F}_{u i_p}^{k_p}(T) \quad (\text{D.14})$$

may be associated with each triad. Each vertical density flux  ${}^k \mathbb{F}_{w i_p}^{k_p}(\rho)$  associated with a triad then separately disappears (because the lateral flux  ${}^k \mathbb{F}_{u i_p}^{k_p}(\rho)$  disappears). Consequently the total vertical density flux  $(F_w^{31})_i^{k+\frac{1}{2}} + (F_w^{33})_i^{k+\frac{1}{2}}$  from tracer cell  $i, k$  to  $i, k + 1$  must also vanish since it is a sum of four such triad fluxes.

We can explicitly identify (Fig. D.2) the triads associated with the  $s_i$ ,  $a_i$ , and  $s'_i$ ,  $a'_i$  used in the definition of the  $u$ -fluxes and  $w$ -fluxes in (D.7), (D.6), (D.9) (D.12) and Fig. D.1 to write out the iso-neutral fluxes at  $u$ - and  $w$ -points as sums of the triad fluxes that cross the  $u$ - and  $w$ -faces:

$$\mathbf{F}_{\text{iso}}(T) \equiv \sum_{i_p, k_p} \begin{pmatrix} {}^k_{i+1/2-i_p} \mathbb{F}_{u_{i_p}}^{k_p}(T) \\ {}^{k+1/2-k_p} \mathbb{F}_{w_{i_p}}^{k_p}(T) \end{pmatrix}. \quad (\text{D.15})$$

### D.2.5 Ensuring the scheme does not increase tracer variance

We now require that this operator should not increase the globally-integrated tracer variance. Each triad slope  ${}^k \mathbb{R}_{i_p}^{k_p}$  drives a lateral flux  ${}^k \mathbb{F}_{u_{i_p}}^{k_p}(T)$  across the  $u$ -point  $i + i_p, k$  and a vertical flux  ${}^k \mathbb{F}_{w_{i_p}}^{k_p}(T)$  across the  $w$ -point  $i, k + k_p$ . The lateral flux drives a net rate of change of variance, summed over the two  $T$ -points  $i + i_p - \frac{1}{2}, k$  and  $i + i_p + \frac{1}{2}, k$ , of

$$\begin{aligned} & b_{T_{i+i_p-1/2}}^k \left( \frac{\partial T}{\partial t} T \right)_{i+i_p-1/2}^k + b_{T_{i+i_p+1/2}}^k \left( \frac{\partial T}{\partial t} T \right)_{i+i_p+1/2}^k \\ &= -T_{i+i_p-1/2}^k {}^k \mathbb{F}_{u_{i_p}}^{k_p}(T) + T_{i+i_p+1/2}^k {}^k \mathbb{F}_{u_{i_p}}^{k_p}(T) \\ &= {}^k \mathbb{F}_{u_{i_p}}^{k_p}(T) \delta_{i+i_p}[T^k], \end{aligned} \quad (\text{D.16})$$

while the vertical flux similarly drives a net rate of change of variance summed over the  $T$ -points  $i, k + k_p - \frac{1}{2}$  (above) and  $i, k + k_p + \frac{1}{2}$  (below) of

$${}^k \mathbb{F}_{w_{i_p}}^{k_p}(T) \delta_{k+k_p}[T^i]. \quad (\text{D.17})$$

The total variance tendency driven by the triad is the sum of these two. Expanding  ${}^k \mathbb{F}_{u_{i_p}}^{k_p}(T)$  and  ${}^k \mathbb{F}_{w_{i_p}}^{k_p}(T)$  with (D.10) and (D.13), it is

$$\begin{aligned} & -A_i^k \left\{ {}^k \mathbb{A}_{u_{i_p}}^{k_p} \left( \frac{\delta_{i+i_p}[T^k]}{e_{1u_{i+i_p}}^k} - {}^k \mathbb{R}_{i_p}^{k_p} \frac{\delta_{k+k_p}[T^i]}{e_{3w_i}^{k+k_p}} \right) \delta_{i+i_p}[T^k] \right. \\ & \quad \left. - {}^k \mathbb{A}_{w_{i_p}}^{k_p} \left( \frac{\delta_{i+i_p}[T^k]}{e_{1u_{i+i_p}}^k} - {}^k \mathbb{R}_{i_p}^{k_p} \frac{\delta_{k+k_p}[T^i]}{e_{3w_i}^{k+k_p}} \right) {}^k \mathbb{R}_{i_p}^{k_p} \delta_{k+k_p}[T^i] \right\}. \end{aligned}$$

The key point is then that if we require  ${}^k \mathbb{A}_{u_{i_p}}^{k_p}$  and  ${}^k \mathbb{A}_{w_{i_p}}^{k_p}$  to be related to a triad volume  ${}^k \mathbb{V}_{i_p}^{k_p}$  by

$${}^k \mathbb{V}_{i_p}^{k_p} = {}^k \mathbb{A}_{u_{i_p}}^{k_p} e_{1u_{i+i_p}}^k = {}^k \mathbb{A}_{w_{i_p}}^{k_p} e_{3w_i}^{k+k_p}, \quad (\text{D.18})$$



the variance tendency reduces to the perfect square

$$-A_i^k \mathbb{V}_i^{k_p} \left( \frac{\delta_{i+i_p}[T^k]}{e_{1u}^k} - \mathbb{R}_i^{k_p} \frac{\delta_{k+k_p}[T^i]}{e_{3w}^{k+k_p}} \right)^2 \leq 0. \quad (\text{D.19})$$

Thus, the constraint (D.18) ensures that the fluxes (D.10, D.13) associated with a given slope triad  $\mathbb{R}_i^{k_p}$  do not increase the net variance. Since the total fluxes are sums of such fluxes from the various triads, this constraint, applied to all triads, is sufficient to ensure that the globally integrated variance does not increase.

The expression (D.18) can be interpreted as a discretization of the global integral

$$\frac{\partial}{\partial t} \int \frac{1}{2} T^2 dV = \int \mathbf{F} \cdot \nabla T dV, \quad (\text{D.20})$$

where, within each triad volume  $\mathbb{V}_i^{k_p}$ , the lateral and vertical fluxes/unit area

$$\mathbf{F} = \left( \mathbb{F}_{u_i^p}^{k_p}(T) / \mathbb{A}_{u_i^p}^{k_p}, \mathbb{F}_{w_i^p}^{k_p}(T) / \mathbb{A}_{w_i^p}^{k_p} \right)$$

and the gradient

$$\nabla T = \left( \delta_{i+i_p}[T^k] / e_{1u}^k, \delta_{k+k_p}[T^i] / e_{3w}^{k+k_p} \right)$$

### D.2.6 Triad volumes in Griffes's scheme and in NEMO

To complete the discretization we now need only specify the triad volumes  $\mathbb{V}_i^{k_p}$ . Griffes et al. [1998] identify these  $\mathbb{V}_i^{k_p}$  as the volumes of the quarter cells, defined in terms of the distances between  $T$ ,  $u$ ,  $f$  and  $w$ -points. This is the natural discretization of (D.20). The NEMO model, however, operates with scale factors instead of grid sizes, and scale factors for the quarter cells are not defined. Instead, therefore we simply choose

$$\mathbb{V}_i^{k_p} = \frac{1}{4} b_{u_{i+i_p}}^k, \quad (\text{D.21})$$

as a quarter of the volume of the  $u$ -cell inside which the triad quarter-cell lies. This has the nice property that when the slopes  $\mathbb{R}$  vanish, the lateral flux from tracer cell  $i, k$  to  $i+1, k$  reduces to the classical form

$$-\bar{A}_{i+1/2}^k \frac{b_{u_{i+1/2}}^k}{e_{1u}^k} \frac{\delta_{i+1/2}[T^k]}{e_{1u}^k} = -\bar{A}_{i+1/2}^k \frac{e_{1w}^k e_{1v}^k}{e_{1u}^k} \frac{\delta_{i+1/2}[T^k]}{e_{1u}^k}. \quad (\text{D.22})$$

In fact if the diffusive coefficient is defined at  $u$ -points, so that we employ  $A_{i+i_p}^k$  instead of  $A_i^k$  in the definitions of the triad fluxes (D.10) and (D.13), we can replace  $\bar{A}_{i+1/2}^k$  by  $A_{i+1/2}^k$  in the above.

### D.2.7 Summary of the scheme

The iso-neutral fluxes at  $u$ - and  $w$ -points are the sums of the triad fluxes that cross the  $u$ - and  $w$ -faces (D.15):

$$\mathbf{F}_{\text{iso}}(T) \equiv \sum_{i_p, k_p} \begin{pmatrix} {}^k_{i+1/2-i_p} \mathbb{F}_{u_{i_p}}^{k_p}(T) \\ {}^{k+1/2-k_p} \mathbb{F}_{w_{i_p}}^{k_p}(T) \end{pmatrix}, \quad (\text{D.23a})$$

where (D.10):

$${}^k \mathbb{F}_{u_{i_p}}^{k_p}(T) = -A_i^k \frac{{}^k \mathbb{V}_{i_p}^{k_p}}{e_{1u}^k e_{i+i_p}^k} \left( \frac{\delta_{i+i_p}[T^k]}{e_{1u}^k e_{i+i_p}^k} - {}^k \mathbb{R}_{i_p}^{k_p} \frac{\delta_{k+k_p}[T^i]}{e_{3w}^k e_{i+i_p}^k} \right), \quad (\text{D.23b})$$

and

$${}^k \mathbb{F}_{w_{i_p}}^{k_p}(T) = A_i^k \frac{{}^k \mathbb{V}_{i_p}^{k_p}}{e_{3w}^k e_{i+i_p}^k} \left( {}^k \mathbb{R}_{i_p}^{k_p} \frac{\delta_{i+i_p}[T^k]}{e_{1u}^k e_{i+i_p}^k} - \left( {}^k \mathbb{R}_{i_p}^{k_p} \right)^2 \frac{\delta_{k+k_p}[T^i]}{e_{3w}^k e_{i+i_p}^k} \right), \quad (\text{D.23c})$$

with (D.21)

$${}^k \mathbb{V}_{i_p}^{k_p} = \frac{1}{4} b_{u_{i+i_p}}^k. \quad (\text{D.23d})$$

The divergence of the expression (D.15) for the fluxes gives the iso-neutral diffusion tendency at each tracer point:

$$D_l^T = \frac{1}{b_T} \sum_{i_p, k_p} \left\{ \delta_i \left[ {}^k_{i+1/2-i_p} \mathbb{F}_{u_{i_p}}^{k_p} \right] + \delta_k \left[ {}^{k+1/2-k_p} \mathbb{F}_{w_{i_p}}^{k_p} \right] \right\} \quad (\text{D.24})$$

where  $b_T = e_{1T} e_{2T} e_{3T}$  is the volume of  $T$ -cells. The diffusion scheme satisfies the following six properties:

- **horizontal diffusion** The discretization of the diffusion operator recovers (D.22) the traditional five-point Laplacian in the limit of flat iso-neutral direction :

$$D_l^T = \frac{1}{b_T} \delta_i \left[ \frac{e_{2u} e_{3u}}{e_{1u}} \bar{A}^i \delta_{i+1/2}[T] \right] \quad \text{when} \quad {}^k \mathbb{R}_{i_p}^{k_p} = 0 \quad (\text{D.25})$$

- **implicit treatment in the vertical** Only tracer values associated with a single water column appear in the expression (D.12) for the  $33$  fluxes, vertical fluxes driven by vertical gradients. This is of paramount importance since it means that a time-implicit algorithm can be used to solve the vertical diffusion equation. This is necessary since the vertical eddy diffusivity associated with this term,

$$\frac{1}{b_w} \sum_{i_p, k_p} \left\{ {}^k \mathbb{V}_{i_p}^{k_p} A_i^k \left( {}^k \mathbb{R}_{i_p}^{k_p} \right)^2 \right\} = \frac{1}{4b_w} \sum_{i_p, k_p} \left\{ b_{u_{i+i_p}}^k A_i^k \left( {}^k \mathbb{R}_{i_p}^{k_p} \right)^2 \right\}, \quad (\text{D.26})$$

(where  $b_w = e_{1w} e_{2w} e_{3w}$  is the volume of  $w$ -cells) can be quite large.

- **pure iso-neutral operator** The iso-neutral flux of locally referenced potential density is zero. See (D.11) and (D.14).
- **conservation of tracer** The iso-neutral diffusion conserves tracer content, *i.e.*

$$\sum_{i,j,k} \{D_l^T b_T\} = 0 \quad (\text{D.27})$$

This property is trivially satisfied since the iso-neutral diffusive operator is written in flux form.

- **no increase of tracer variance** The iso-neutral diffusion does not increase the tracer variance, *i.e.*

$$\sum_{i,j,k} \{T D_l^T b_T\} \leq 0 \quad (\text{D.28})$$

The property is demonstrated in §D.2.5 above. It is a key property for a diffusion term. It means that it is also a dissipation term, *i.e.* it dissipates the square of the quantity on which it is applied. It therefore ensures that, when the diffusivity coefficient is large enough, the field on which it is applied becomes free of grid-point noise.

- **self-adjoint operator** The iso-neutral diffusion operator is self-adjoint, *i.e.*

$$\sum_{i,j,k} \{S D_l^T b_T\} = \sum_{i,j,k} \{D_l^S T b_T\} \quad (\text{D.29})$$

In other word, there is no need to develop a specific routine from the adjoint of this operator. We just have to apply the same routine. This property can be demonstrated similarly to the proof of the ‘no increase of tracer variance’ property. The contribution by a single triad towards the left hand side of (D.29), can be found by replacing  $\delta[T]$  by  $\delta[S]$  in (D.16) and (D.17). This results in a term similar to (D.19),

$$-A_i^k \frac{k}{i} \nabla_{i_p}^{k_p} \left( \frac{\delta_{i+i_p}[T^k]}{e_{1u}^k} - \frac{k}{i} \mathbb{R}_{i_p}^{k_p} \frac{\delta_{k+k_p}[T^i]}{e_{3w}^k} \right) \left( \frac{\delta_{i+i_p}[S^k]}{e_{1u}^k} - \frac{k}{i} \mathbb{R}_{i_p}^{k_p} \frac{\delta_{k+k_p}[S^i]}{e_{3w}^k} \right). \quad (\text{D.30})$$

This is symmetrical in  $T$  and  $S$ , so exactly the same term arises from the discretization of this triad’s contribution towards the RHS of (D.29).

## D.2.8 Treatment of the triads at the boundaries

The triad slope can only be defined where both the grid boxes centred at the end of the arms exist. Triads that would poke up through the upper ocean surface into the atmosphere, or down into the ocean floor, must be masked out. See Fig. D.3. Surface layer triads  $\frac{1}{i} \mathbb{R}_{1/2}^{-1/2}$  (magenta) and  $\frac{1}{i+1} \mathbb{R}_{-1/2}^{-1/2}$  (blue) that require density to be specified above the ocean surface are masked (Fig. D.3a):

this ensures that lateral tracer gradients produce no flux through the ocean surface. However, to prevent surface noise, it is customary to retain the  ${}_{11}$  contributions towards the lateral triad fluxes  ${}^1\mathbb{F}_{u_{1/2}}^{-1/2}$  and  ${}^1\mathbb{F}_{u_{-1/2}}^{-1/2}$ ; this drives diapycnal tracer fluxes. Similar comments apply to triads that would intersect the ocean floor (Fig. D.3b). Note that both near bottom triad slopes  ${}^k\mathbb{R}_{1/2}^{1/2}$  and  ${}^k\mathbb{R}_{-1/2}^{1/2}$  are masked when either of the  $i, k + 1$  or  $i + 1, k + 1$  tracer points is masked, i.e. the  $i, k + 1$   $u$ -point is masked. The associated lateral fluxes (grey-black dashed line) are masked if `ln_botmix_triad=false`, but left unmasked, giving bottom mixing, if `ln_botmix_triad=true`.

The default option `ln_botmix_triad=false` is suitable when the bbl mixing option is enabled (**key\_trabbl**, with `nn_bbl_ldf=1`), or for simple idealized problems. For setups with topography without bbl mixing, `ln_botmix_triad=true` may be necessary.

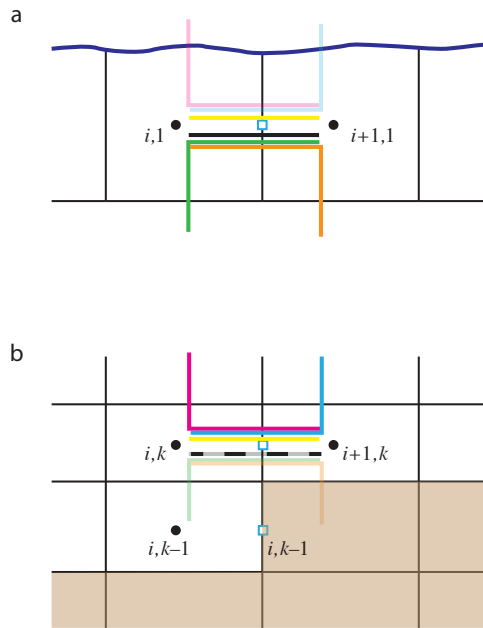


**Figure D.3:** (a) Uppermost model layer  $k = 1$  with  $i, 1$  and  $i + 1, 1$  tracer points (black dots), and  $i + 1/2, 1$   $u$ -point (blue square). Triad slopes  ${}^1\mathbb{R}_{1/2}^{-1/2}$  (magenta) and  ${}^1\mathbb{R}_{-1/2}^{-1/2}$  (blue) poking through the ocean surface are masked (faded in figure). However, the lateral  ${}_{11}$  contributions towards  ${}^1\mathbb{F}_{u_{1/2}}^{-1/2}$  and  ${}^1\mathbb{F}_{u_{-1/2}}^{-1/2}$  (yellow line) are still applied, giving diapycnal diffusive fluxes. (b) Both near bottom triad slopes  ${}^k\mathbb{R}_{1/2}^{1/2}$  and  ${}^k\mathbb{R}_{-1/2}^{1/2}$  are masked when either of the  $i, k + 1$  or  $i + 1, k + 1$  tracer points is masked, i.e. the  $i, k + 1$   $u$ -point is masked. The associated lateral fluxes (grey-black dashed line) are masked if `botmix_triad=false`, but left unmasked, giving bottom mixing, if `botmix_triad=true`.

### D.2.9 Limiting of the slopes within the interior

As discussed in §9.1.2, iso-neutral slopes relative to geopotentials must be bounded everywhere, both for consistency with the small-slope approximation and for numerical stability [Cox 1987, Griffies 2004]. The bound chosen in *NEMO* is applied to each component of the slope separately and has a value of 1/100 in the ocean interior. It is of course relevant to the iso-neutral slopes  $\tilde{r}_i = r_i + \sigma_i$  relative to geopotentials (here the  $\sigma_i$  are the slopes of the coordinate surfaces relative to geopotentials) (2.39) rather than the slope  $r_i$  relative to coordinate surfaces, so we require

$$|\tilde{r}_i| \leq \tilde{r}_{\max} = 0.01.$$

and then recalculate the slopes  $r_i$  relative to coordinates. Each individual triad slope

$${}^k\mathbb{R}_{i_p}^{k_p} = {}^k\mathbb{R}_{i_p}^{k_p} + \frac{\delta_{i+i_p}[z_T^k]}{e_{1u}^k{}_{i+i_p}} \quad (\text{D.31})$$

is limited like this and then the corresponding  ${}^k\mathbb{R}_{i_p}^{k_p}$  are recalculated and combined to form the fluxes. Note that where the slopes have been limited, there is now a non-zero iso-neutral density flux that drives dianeutral mixing. In particular this iso-neutral density flux is always downwards, and so acts to reduce gravitational potential energy.

### D.2.10 Tapering within the surface mixed layer

Additional tapering of the iso-neutral fluxes is necessary within the surface mixed layer. When the Griffies triads are used, we offer two options for this.

#### Linear slope tapering within the surface mixed layer

This is the option activated by the default choice *ln\_triad\_iso=false*. Slopes  $\tilde{r}_i$  relative to geopotentials are tapered linearly from their value immediately below the mixed layer to zero at the surface, as described in option (c) of Fig. 9.2, to values

$$\tilde{r}_{\text{ML}i} = -\frac{z}{h} \tilde{r}_i|_{z=-h} \quad \text{for } z > -h, \quad (\text{D.32a})$$

and then the  $r_i$  relative to vertical coordinate surfaces are appropriately adjusted to

$$r_{\text{ML}i} = \tilde{r}_{\text{ML}i} - \sigma_i \quad \text{for } z > -h. \quad (\text{D.32b})$$

Thus the diffusion operator within the mixed layer is given by:

$$D^{lT} = \nabla \cdot \left( A^{lT} \mathfrak{R} \nabla T \right) \quad \text{with} \quad \mathfrak{R} = \begin{pmatrix} 1 & 0 & -r_{\text{ML}1} \\ 0 & 1 & -r_{\text{ML}2} \\ -r_{\text{ML}1} & -r_{\text{ML}2} & r_{\text{ML}1}^2 + r_{\text{ML}2}^2 \end{pmatrix} \quad (\text{D.33})$$

This slope tapering gives a natural connection between tracer in the mixed-layer and in isopycnal layers immediately below, in the thermocline. It is consistent with the way the  $\tilde{r}_i$  are tapered within the mixed layer (see §D.3.5 below) so as to ensure a uniform GM eddy-induced velocity throughout the mixed layer. However, it gives a downwards density flux and so acts so as to reduce potential energy in the same way as does the slope limiting discussed above in §D.2.9.

As in §D.2.9 above, the tapering (D.32a) is applied separately to each triad  ${}^k_i\tilde{\mathbb{R}}_{i_p}^{k_p}$ , and the  ${}^k_i\mathbb{R}_{i_p}^{k_p}$  adjusted. For clarity, we assume  $z$ -coordinates in the following; the conversion from  $\mathbb{R}$  to  $\tilde{\mathbb{R}}$  and back to  $\mathbb{R}$  follows exactly as described above by (D.31).

1. Mixed-layer depth is defined so as to avoid including regions of weak vertical stratification in the slope definition. At each  $i, j$  (simplified to  $i$  in Fig. D.4), we define the mixed-layer by setting the vertical index of the tracer point immediately below the mixed layer,  $k_{\text{ML}}$ , as the maximum  $k$  (shallowest tracer point) such that the potential density  $\rho_{0i,k} > \rho_{0i,k_{10}} + \Delta\rho_c$ , where  $i, k_{10}$  is the tracer gridbox within which the depth reaches 10 m. See the left side of Fig. D.4. We use the  $k_{10}$ -gridbox instead of the surface gridbox to avoid problems e.g. with thin daytime mixed-layers. Currently we use the same  $\Delta\rho_c = 0.01 \text{ kg m}^{-3}$  for ML triad tapering as is used to output the diagnosed mixed-layer depth  $h_{\text{ML}} = |z_W|_{k_{\text{ML}}+1/2}$ , the depth of the  $w$ -point above the  $i, k_{\text{ML}}$  tracer point.
2. We define ‘basal’ triad slopes  ${}^k_i\mathbb{R}_{i_p}^{\text{base } k_p}$  as the slopes of those triads whose vertical ‘arms’ go down from the  $i, k_{\text{ML}}$  tracer point to the  $i, k_{\text{ML}} - 1$  tracer point below. This is to ensure that the vertical density gradients associated with these basal triad slopes  ${}^k_i\mathbb{R}_{i_p}^{\text{base } k_p}$  are representative of the thermocline. The four basal triads defined in the bottom part of Fig. D.4 are then

$${}^k_i\mathbb{R}_{i_p}^{\text{base } k_p} = {}^{k_{\text{ML}}-k_p-1/2}_i\mathbb{R}_{i_p}^{\text{base } k_p}, \quad (\text{D.34})$$

with e.g. the green triad

$${}^{k_{\text{ML}}-1/2}_i\mathbb{R}_{i_p}^{\text{base } k_p} = {}^{k_{\text{ML}}-1/2}_i\mathbb{R}_{i_p}^{\text{base } k_p}.$$

The vertical flux associated with each of these triads passes through the  $w$ -point  $i, k_{\text{ML}} - 1/2$  lying *below* the  $i, k_{\text{ML}}$  tracer point, so it is this depth

$$z_{\text{base } i} = z_{w, k_{\text{ML}}-1/2} \quad (\text{D.35})$$

(one gridbox deeper than the diagnosed ML depth  $z_{\text{ML}}$ ) that sets the  $h$  used to taper the slopes in (D.32a).

3. Finally, we calculate the adjusted triads  ${}^k_i\mathbb{R}_{i_p}^{\text{ML } k_p}$  within the mixed layer, by multiplying the appropriate  ${}^k_i\mathbb{R}_{i_p}^{\text{base } k_p}$  by the ratio of the depth of the  $w$ -point

$z_{wk+k_p}$  to  $z_{\text{base } i}$ . For instance the green triad centred on  $i, k$

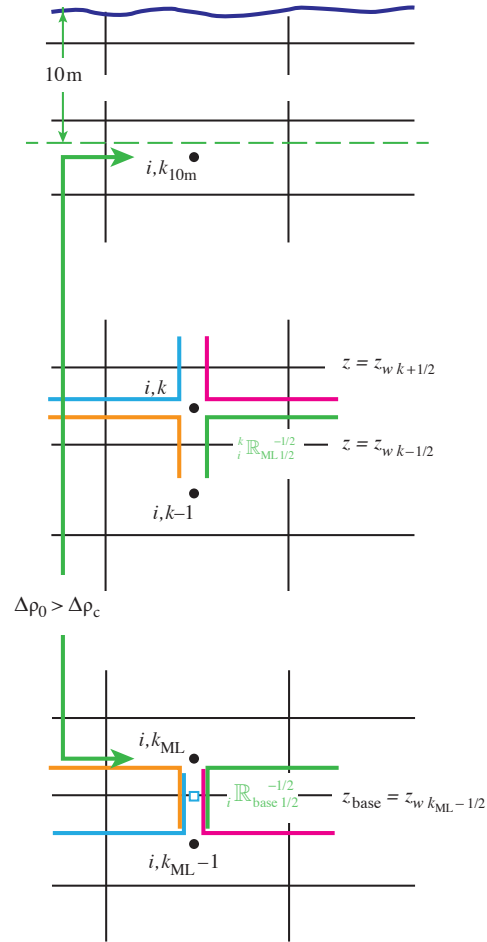
$${}_i^k \mathbb{R}_{\text{ML}}^{-1/2} = \frac{z_{wk-1/2}}{z_{\text{base } i}} {}_i \mathbb{R}_{\text{base}}^{-1/2}$$

and more generally

$${}_i^k \mathbb{R}_{\text{ML}}^{k_p} = \frac{z_{wk+k_p}}{z_{\text{base } i}} {}_i \mathbb{R}_{\text{base}}^{k_p}. \quad (\text{D.36})$$

**Figure D.4:** Definition of mixed-layer depth and calculation of linearly tapered triads. The figure shows a water column at a given  $i, j$  (simplified to  $i$ ), with the ocean surface at the top. Tracer points are denoted by bullets, and black lines the edges of the tracer cells;  $k$  increases upwards.

We define the mixed-layer by setting the vertical index of the tracer point immediately below the mixed layer,  $k_{\text{ML}}$ , as the maximum  $k$  (shallowest tracer point) such that  $\rho_{0i,k} > \rho_{0i,k_{10}} + \Delta\rho_c$ , where  $i, k_{10}$  is the tracer gridbox within which the depth reaches 10 m. We calculate the triad slopes within the mixed layer by linearly tapering them from zero (at the surface) to the ‘basal’ slopes, the slopes of the four triads passing through the  $w$ -point  $i, k_{\text{ML}} - 1/2$  (blue square),  ${}_i \mathbb{R}_{\text{base}}^{k_p}$ . Triads with different  $i_p, k_p$ , denoted by different colours, (e.g. the green triad  $i_p = 1/2, k_p = -1/2$ ) are tapered to the appropriate basal triad.



### Additional truncation of skew iso-neutral flux components

The alternative option is activated by setting `ln_triad_iso = true`. This retains the same tapered slope  $r_{\text{ML } i}$  described above for the calculation of the  $33$  term of

the iso-neutral diffusion tensor (the vertical tracer flux driven by vertical tracer gradients), but replaces the  $r_{\text{ML}i}$  in the skew term by

$$r_{\text{ML}i}^* = \tilde{r}_{\text{ML}i}^2 / \tilde{r}_i - \sigma_i, \quad (\text{D.37})$$

giving a ML diffusive operator

$$D^{lT} = \nabla \cdot \left( A^{lT} \mathfrak{R} \nabla T \right) \quad \text{with} \quad \mathfrak{R} = \begin{pmatrix} 1 & 0 & -r_{\text{ML}1}^* \\ 0 & 1 & -r_{\text{ML}2}^* \\ -r_{\text{ML}1}^* & -r_{\text{ML}2}^* & r_{\text{ML}1}^2 + r_{\text{ML}2}^2 \end{pmatrix}. \quad (\text{D.38})$$

This operator<sup>1</sup> then has the property it gives no vertical density flux, and so does not change the potential energy. This approach is similar to multiplying the iso-neutral diffusion coefficient by  $\tilde{r}_{\text{max}}^{-2} \tilde{r}_i^{-2}$  for steep slopes, as suggested by Gerdes et al. [1991] (see also Griffies [2004]). Again it is applied separately to each triad  ${}^k \mathbb{R}_{i_p}^{k_p}$

In practice, this approach gives weak vertical tracer fluxes through the mixed-layer, as well as vanishing density fluxes. While it is theoretically advantageous that it does not change the potential energy, it may give a discontinuity between the fluxes within the mixed-layer (purely horizontal) and just below (along iso-neutral surfaces).

## D.3 Eddy induced advection formulated as a skew flux

### D.3.1 The continuous skew flux formulation

When Gent and McWilliams's [1990] diffusion is used, an additional advection term is added. The associated velocity is the so called eddy induced velocity, the formulation of which depends on the slopes of iso-neutral surfaces. Contrary to the case of iso-neutral mixing, the slopes used here are referenced to the geopotential surfaces, *i.e.* (9.1) is used in  $z$ -coordinate, and the sum (9.1) + (9.2) in  $z^*$  or  $s$ -coordinates.

The eddy induced velocity is given by:

$$\begin{aligned} u^* &= -\frac{1}{e_3} \partial_i \psi_1, \\ v^* &= -\frac{1}{e_3} \partial_j \psi_2, \\ w^* &= \frac{1}{e_1 e_2} \{ \partial_i (e_2 \psi_1) + \partial_j (e_1 \psi_2) \}, \end{aligned} \quad (\text{D.39a})$$

where the streamfunctions  $\psi_i$  are given by

$$\begin{aligned} \psi_1 &= A_e \tilde{r}_1, \\ \psi_2 &= A_e \tilde{r}_2, \end{aligned} \quad (\text{D.39b})$$

<sup>1</sup>To ensure good behaviour where horizontal density gradients are weak, we in fact follow Gerdes et al. [1991] and set  $r_{\text{ML}i}^* = \text{sgn}(\tilde{r}_i) \min(|\tilde{r}_{\text{ML}i}^2 / \tilde{r}_i|, |\tilde{r}_i|) - \sigma_i$ .



with  $A_e$  the eddy induced velocity coefficient, and  $\tilde{r}_1$  and  $\tilde{r}_2$  the slopes between the iso-neutral and the geopotential surfaces.

The traditional way to implement this additional advection is to add it to the Eulerian velocity prior to computing the tracer advection. This is implemented if `key_traldf_eiv` is set in the default implementation, where `ln_traldf_triad` is set false. This allows us to take advantage of all the advection schemes offered for the tracers (see §5.1) and not just a 2<sup>nd</sup> order advection scheme. This is particularly useful for passive tracers where *positivity* of the advection scheme is of paramount importance.

However, when `ln_traldf_triad` is set true, *NEMO* instead implements eddy induced advection according to the so-called skew form [Griffies 1998]. It is based on a transformation of the advective fluxes using the non-divergent nature of the eddy induced velocity. For example in the  $(\mathbf{i}, \mathbf{k})$  plane, the tracer advective fluxes per unit area in  $ijk$  space can be transformed as follows:

$$\begin{aligned} \mathbf{F}_{\text{eiv}}^T &= \begin{pmatrix} e_2 e_3 u^* \\ e_1 e_2 w^* \end{pmatrix} T = \begin{pmatrix} -\partial_k (e_2 \psi_1) T \\ +\partial_i (e_2 \psi_1) T \end{pmatrix} \\ &= \begin{pmatrix} -\partial_k (e_2 \psi_1 T) \\ +\partial_i (e_2 \psi_1 T) \end{pmatrix} + \begin{pmatrix} +e_2 \psi_1 \partial_k T \\ -e_2 \psi_1 \partial_i T \end{pmatrix} \end{aligned}$$

and since the eddy induced velocity field is non-divergent, we end up with the skew form of the eddy induced advective fluxes per unit area in  $ijk$  space:

$$\mathbf{F}_{\text{eiv}}^T = \begin{pmatrix} +e_2 \psi_1 \partial_k T \\ -e_2 \psi_1 \partial_i T \end{pmatrix} \quad (\text{D.40})$$

The total fluxes per unit physical area are then

$$\begin{aligned} f_1^* &= \frac{1}{e_3} \psi_1 \partial_k T \\ f_2^* &= \frac{1}{e_3} \psi_2 \partial_k T \\ f_3^* &= -\frac{1}{e_1 e_2} \{e_2 \psi_1 \partial_i T + e_1 \psi_2 \partial_j T\}. \end{aligned} \quad (\text{D.41})$$

Note that Eq. (D.41) takes the same form whatever the vertical coordinate, though of course the slopes  $\tilde{r}_i$  which define the  $\psi_i$  in (D.39b) are relative to geopotentials. The tendency associated with eddy induced velocity is then simply the convergence of the fluxes (D.40, D.41), so

$$\frac{\partial T}{\partial t} = -\frac{1}{e_1 e_2 e_3} \left[ \frac{\partial}{\partial i} (e_2 \psi_1 \partial_k T) + \frac{\partial}{\partial j} (e_1 \psi_2 \partial_k T) - \frac{\partial}{\partial k} (e_2 \psi_1 \partial_i T + e_1 \psi_2 \partial_j T) \right] \quad (\text{D.42})$$

It naturally conserves the tracer content, as it is expressed in flux form. Since it has the same divergence as the advective form it also preserves the tracer variance.

### D.3.2 The discrete skew flux formulation

The skew fluxes in (D.41, D.40), like the off-diagonal terms (D.3, D.4) of the small angle diffusion tensor, are best expressed in terms of the triad slopes, as in Fig. D.1 and Eqs (D.6, D.7); but now in terms of the triad slopes  $\tilde{\mathbb{R}}$  relative to geopotentials instead of the  $\mathbb{R}$  relative to coordinate surfaces. The discrete form of (D.40) using the slopes (D.8) and defining  $A_e$  at  $T$ -points is then given by:

$$\mathbf{F}_{\text{eiv}}(T) \equiv \sum_{i_p, k_p} \begin{pmatrix} {}^k_{i+1/2-i_p} \mathbb{S}_{u_{i_p}}^{k_p}(T) \\ {}^{k+1/2-k_p}_i \mathbb{S}_{w_{i_p}}^{k_p}(T) \end{pmatrix}, \quad (\text{D.43a})$$

where the skew flux in the  $i$ -direction associated with a given triad is (D.10, D.23b):

$${}^k_i \mathbb{S}_{u_{i_p}}^{k_p}(T) = +\frac{1}{4} A_e {}^k_i \frac{b_{u_{i+i_p}}^k}{e_{1u}^k} \frac{{}^k_i \tilde{\mathbb{R}}_{i_p}^{k_p}}{e_{3w}^k} \frac{\delta_{k+k_p}[T^i]}{e_{3w}^k}, \quad (\text{D.43b})$$

and (D.23c) in the  $k$ -direction, changing the sign to be consistent with (D.40):

$${}^k_i \mathbb{S}_{w_{i_p}}^{k_p}(T) = -\frac{1}{4} A_e {}^k_i \frac{b_{u_{i+i_p}}^k}{e_{3w}^k} \frac{{}^k_i \tilde{\mathbb{R}}_{i_p}^{k_p}}{e_{1u}^k} \frac{\delta_{i+i_p}[T^k]}{e_{1u}^k}. \quad (\text{D.43c})$$

Such a discretisation is consistent with the iso-neutral operator as it uses the same definition for the slopes. It also ensures the following two key properties.

#### No change in tracer variance

The discretization conserves tracer variance, *i.e.* it does not include a diffusive component but is a ‘pure’ advection term. This can be seen by considering the fluxes associated with a given triad slope  ${}^k_i \mathbb{R}_{i_p}^{k_p}(T)$ . For, following §D.2.5 and (D.16), the associated horizontal skew-flux  ${}^k_i \mathbb{S}_{u_{i_p}}^{k_p}(T)$  drives a net rate of change of variance, summed over the two  $T$ -points  $i + i_p - \frac{1}{2}, k$  and  $i + i_p + \frac{1}{2}, k$ , of

$${}^k_i \mathbb{S}_{u_{i_p}}^{k_p}(T) \delta_{i+i_p}[T^k], \quad (\text{D.44})$$

while the associated vertical skew-flux gives a variance change summed over the  $T$ -points  $i, k + k_p - \frac{1}{2}$  (above) and  $i, k + k_p + \frac{1}{2}$  (below) of

$${}^k_i \mathbb{S}_{w_{i_p}}^{k_p}(T) \delta_{k+k_p}[T^i]. \quad (\text{D.45})$$

Inspection of the definitions (D.43b, D.43c) shows that these two variance changes (D.44, D.45) sum to zero. Hence the two fluxes associated with each triad make no net contribution to the variance budget.

### Reduction in gravitational PE

The vertical density flux associated with the vertical skew-flux always has the same sign as the vertical density gradient; thus, so long as the fluid is stable (the vertical density gradient is negative) the vertical density flux is negative (downward) and hence reduces the gravitational PE.

For the change in gravitational PE driven by the  $k$ -flux is

$$ge_{3w_i}^{k+k_p} \mathbb{S}_{w_{i_p}}^{k_p}(\rho) = ge_{3w_i}^{k+k_p} \left[ -\alpha_i^k \mathbb{S}_{w_{i_p}}^{k_p}(T) + \beta_i^k \mathbb{S}_{w_{i_p}}^{k_p}(S) \right].$$

Substituting  $\mathbb{S}_{w_{i_p}}^{k_p}$  from (D.43c), gives

$$\begin{aligned} &= -\frac{1}{4} g A e_i^k b_{u_{i+i_p}}^k \mathbb{R}_{i_p}^{k_p} \frac{-\alpha_i^k \delta_{i+i_p}[T^k] + \beta_i^k \delta_{i+i_p}[S^k]}{e_{1u_{i+i_p}}^k} \\ &= +\frac{1}{4} g A e_i^k b_{u_{i+i_p}}^k \left( \mathbb{R}_{i_p}^{k_p} + \frac{\delta_{i+i_p}[z_T^k]}{e_{1u_{i+i_p}}^k} \right) \mathbb{R}_{i_p}^{k_p} \frac{-\alpha_i^k \delta_{k+k_p}[T^i] + \beta_i^k \delta_{k+k_p}[S^i]}{e_{3w_i}^{k+k_p}}, \end{aligned} \quad (\text{D.46})$$

using the definition of the triad slope  $\mathbb{R}_{i_p}^{k_p}$ , (D.8) to express  $-\alpha_i^k \delta_{i+i_p}[T^k] + \beta_i^k \delta_{i+i_p}[S^k]$  in terms of  $-\alpha_i^k \delta_{k+k_p}[T^i] + \beta_i^k \delta_{k+k_p}[S^i]$ .

Where the coordinates slope, the  $i$ -flux gives a PE change

$$\begin{aligned} &g \delta_{i+i_p}[z_T^k] \left[ -\alpha_i^k \mathbb{S}_{u_{i_p}}^{k_p}(T) + \beta_i^k \mathbb{S}_{u_{i_p}}^{k_p}(S) \right] \\ &= +\frac{1}{4} g A e_i^k b_{u_{i+i_p}}^k \frac{\delta_{i+i_p}[z_T^k]}{e_{1u_{i+i_p}}^k} \left( \mathbb{R}_{i_p}^{k_p} + \frac{\delta_{i+i_p}[z_T^k]}{e_{1u_{i+i_p}}^k} \right) \frac{-\alpha_i^k \delta_{k+k_p}[T^i] + \beta_i^k \delta_{k+k_p}[S^i]}{e_{3w_i}^{k+k_p}}, \end{aligned} \quad (\text{D.47})$$

(using (D.43b)) and so the total PE change (D.46) + (D.47) associated with the triad fluxes is

$$\begin{aligned} &ge_{3w_i}^{k+k_p} \mathbb{S}_{w_{i_p}}^{k_p}(\rho) + g \delta_{i+i_p}[z_T^k] \mathbb{S}_{u_{i_p}}^{k_p}(\rho) \\ &= +\frac{1}{4} g A e_i^k b_{u_{i+i_p}}^k \left( \mathbb{R}_{i_p}^{k_p} + \frac{\delta_{i+i_p}[z_T^k]}{e_{1u_{i+i_p}}^k} \right)^2 \frac{-\alpha_i^k \delta_{k+k_p}[T^i] + \beta_i^k \delta_{k+k_p}[S^i]}{e_{3w_i}^{k+k_p}}. \end{aligned} \quad (\text{D.48})$$

Where the fluid is stable, with  $-\alpha_i^k \delta_{k+k_p}[T^i] + \beta_i^k \delta_{k+k_p}[S^i] < 0$ , this PE change is negative.

### D.3.3 Treatment of the triads at the boundaries

Triad slopes  $\mathbb{R}_{i_p}^{k_p}$  used for the calculation of the eddy-induced skew-fluxes are masked at the boundaries in exactly the same way as are the triad slopes  $\mathbb{R}_{i_p}^{k_p}$  used for the iso-neutral diffusive fluxes, as described in §D.2.8 and Fig. D.3. Thus surface layer triads  $\mathbb{R}_{1/2}^{-1/2}$  and  $\mathbb{R}_{i+1}^{-1/2}$  are masked, and both near bottom triad

slopes  ${}^k\tilde{\mathbb{R}}_{1/2}^{1/2}$  and  ${}^{k+1}\tilde{\mathbb{R}}_{-1/2}^{1/2}$  are masked when either of the  $i, k+1$  or  $i+1, k+1$  tracer points is masked, i.e. the  $i, k+1$   $u$ -point is masked. The namelist parameter *ln\_botmix\_triad* has no effect on the eddy-induced skew-fluxes.

### D.3.4 Limiting of the slopes within the interior

Presently, the iso-neutral slopes  $\tilde{r}_i$  relative to geopotentials are limited to be less than  $1/100$ , exactly as in calculating the iso-neutral diffusion, §D.2.9. Each individual triad  ${}^k\tilde{\mathbb{R}}_{i_p}^{k_p}$  is so limited.

### D.3.5 Tapering within the surface mixed layer

The slopes  $\tilde{r}_i$  relative to geopotentials (and thus the individual triads  ${}^k\tilde{\mathbb{R}}_{i_p}^{k_p}$ ) are always tapered linearly from their value immediately below the mixed layer to zero at the surface (D.32a), as described in §D.2.10. This is option (c) of Fig. 9.2. This linear tapering for the slopes used to calculate the eddy-induced fluxes is unaffected by the value of *ln\_triad\_iso*.

The justification for this linear slope tapering is that, for  $A_e$  that is constant or varies only in the horizontal (the most commonly used options in *NEMO*: see §9.3), it is equivalent to a horizontal eiv (eddy-induced velocity) that is uniform within the mixed layer (D.39a). This ensures that the eiv velocities do not re-stratify the mixed layer [Tréguier et al. 1997, Danabasoglu et al. 2008]. Equivalently, in terms of the skew-flux formulation we use here, the linear slope tapering within the mixed-layer gives a linearly varying vertical flux, and so a tracer convergence uniform in depth (the horizontal flux convergence is relatively insignificant within the mixed-layer).

### D.3.6 Streamfunction diagnostics

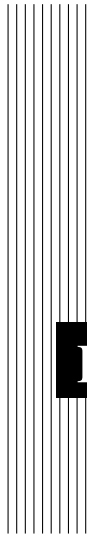
Where the namelist parameter *ln\_traldf\_gdia=true*, diagnosed mean eddy-induced velocities are output. Each time step, streamfunctions are calculated in the  $i$ - $k$  and  $j$ - $k$  planes at  $uw$  (integer  $+1/2$   $i$ , integer  $j$ , integer  $+1/2$   $k$ ) and  $vw$  (integer  $i$ , integer  $+1/2$   $j$ , integer  $+1/2$   $k$ ) points (see Table 4.1) respectively. We follow [Griffies 2004] and calculate the streamfunction at a given  $uw$ -point from the surrounding four triads according to:

$$\psi_{i+1/2}^{k+1/2} = \frac{1}{4} \sum_{i_p, k_p} A_{e_{i+1/2-i_p}^{k+1/2-k_p}} \mathbb{R}_{i+1/2-i_p}^{k_p}. \quad (\text{D.49})$$

The streamfunction  $\psi_1$  is calculated similarly at  $vw$  points. The eddy-induced velocities are then calculated from the straightforward discretisation of (D.39a):

$$\begin{aligned}
 u_{i+1/2}^{*k} &= -\frac{1}{e_{3u_i}^k} \left( \psi_{1i+1/2}^{k+1/2} - \psi_{1i+1/2}^{k+1/2} \right), \\
 v_{j+1/2}^{*k} &= -\frac{1}{e_{3v_j}^k} \left( \psi_{2j+1/2}^{k+1/2} - \psi_{2j+1/2}^{k+1/2} \right), \\
 w_{i,j}^{*k+1/2} &= \frac{1}{e_{1t}e_{2t}} \left\{ e_{2u_{i+1/2}}^{k+1/2} \psi_{1i+1/2}^{k+1/2} - e_{2u_{i-1/2}}^{k+1/2} \psi_{1i-1/2}^{k+1/2} + \right. \\
 &\quad \left. e_{2v_{j+1/2}}^{k+1/2} \psi_{2j+1/2}^{k+1/2} - e_{2v_{j-1/2}}^{k+1/2} \psi_{2j-1/2}^{k+1/2} \right\},
 \end{aligned} \tag{D.50}$$





# **E** Coding Rules

## **Contents**

---

<b>E.1</b>	<b>The program structure</b>	<b>358</b>
<b>E.2</b>	<b>Coding conventions</b>	<b>358</b>
<b>E.3</b>	<b>Naming Conventions</b>	<b>360</b>
<b>E.4</b>	<b>The program structure</b>	<b>361</b>

---

A "model life" is more than ten years. Its software, composed of a few hundred modules, is used by many people who are scientists or students and do not necessarily know every aspect of computing very well. Moreover, a well thought-out program is easier to read and understand, less difficult to modify, produces fewer bugs and is easier to maintain. Therefore, it is essential that the model development follows some rules :

- well planned and designed
- well written
- well documented (both on- and off-line)
- maintainable
- easily portable
- flexible.

To satisfy part of these aims, *NEMO* is written with a coding standard which is close to the ECMWF rules, named DOCTOR [Gibson 1986]. These rules present some advantages like :

- to provide a well presented program
- to use rules for variable names which allow recognition of their type (integer, real, parameter, local or shared variables, etc. ).

This facilitates both the understanding and the debugging of an algorithm.

## E.1 The program structure

Each program begins with a set of headline comments containing :

- the program title
- the purpose of the routine
- the method and algorithms used
- the detail of input and output interfaces
- the external routines and functions used (if they exist)
- references (if they exist)
- the author name(s), the date of creation and any updates.
- Each program is split into several well separated sections and sub-sections with an underlined title and specific labelled statements.
- A program has not more than 200 to 300 lines.

A template of a module style can be found on the NEMO depository in the following file : NEMO/OPA\_SRC/module\_example.

## E.2 Coding conventions

- Use of the universal language FORTRAN 90, and try to avoid obsolescent features like statement functions, do not use GO TO and EQUIVALENCE statements.



- A continuation line begins with the character & indented by three spaces compared to the previous line, while the previous line ended with the character &.
- All the variables must be declared. The code is usually compiled with implicit none.
- Never use continuation lines in the declaration of a variable. When searching a variable in the code through a *grep* command, the declaration line will be found.
- In the declaration of a PUBLIC variable, the comment part at the end of the line should start with the two characters ”! :”. the following UNIX command,  

```
grep var_name *90 \ grep \!:
```

will display the module name and the line where the var\_name declaration is.
- Always use a three spaces indentation in DO loop, CASE, or IF-ELSEIF-ELSE-ENDIF statements.
- use a space after a comma, except when it appears to separate the indices of an array.
- use call to `ctl_stop` routine instead of just a STOP.

### E.3 Naming Conventions

The purpose of the naming conventions is to use prefix letters to classify model variables. These conventions allow the variable type to be easily known and rapidly identified. The naming conventions are summarised in the Table below:

Type / Status	integer	real	logical	character	structure	double precision	complex
public or module variable	<b>m n</b> <i>but not</i> <b>nn_ np_</b>	<b>a b e f g h</b> <b>o q r</b> <b>t to x</b> <i>but not</i> <b>fs rn_</b>	<b>l</b> <i>but not</i> <b>lp ld</b> <b>ll ln_</b>	<b>c</b> <i>but not</i> <b>cp cd</b> <b>cl cn_</b>	<b>s</b> <i>but not</i> <b>sd sd</b> <b>sl sn_</b>	<b>d</b> <i>but not</i> <b>dp dd</b> <b>dl dn_</b>	<b>y</b> <i>but not</i> <b>yp yd</b> <b>yl yn</b>
dummy argument	<b>k</b> <i>but not</i> <b>kf</b>	<b>p</b> <i>but not</i> <b>pp pf</b>	<b>ld</b>	<b>cd</b>	<b>sd</b>	<b>dd</b>	<b>yd</b>
local variable	<b>i</b>	<b>z</b>	<b>ll</b>	<b>cl</b>	<b>sl</b>	<b>dl</b>	<b>yl</b>
loop control	<b>j</b> <i>but not</i> <b>jp</b>						
parameter	<b>jp np_</b>	<b>pp</b>	<b>lp</b>	<b>cp</b>	<b>sp</b>	<b>dp</b>	<b>yp</b>
namelist	<b>nn_</b>	<b>rn_</b>	<b>ln_</b>	<b>cn_</b>	<b>sn_</b>	<b>dn_</b>	<b>yn_</b>
CPP macro	<b>kf</b>	<b>fs</b>					

N.B. Parameter here, in not only parameter in the FORTRAN acceptance, it is also used for code variables that are read in namelist and should never be modified during a simulation. It is the case, for example, for the size of a domain (jpi,jpj,jpk).

## **E.4 The program structure**

To be done....



# Index

## CPP keys, 7

- key\_agrif, 291
- key\_asminc, 270
- key\_c1d, 286, 287
- key\_cice, 151
- key\_coupled, 138
- key\_cpl\_carbon\_cycle, 139
- key\_diaar5, 240, 241
- key\_diadct, 235
- key\_diaharm, 234, 235
- key\_diahth, 240
- key\_diainstant, 212
- key\_dynldf\_c1d, 178
- key\_dynldf\_c2d, 178, 179
- key\_dynldf\_c3d, 178, 179
- key\_dynspg\_exp, 113, 206
- key\_dynspg\_ft, 116, 206
- key\_dynspg\_ts, 113, 206
- key\_floats, 233
- key\_IOM, 232
- key\_iomput, 212, 231, 234
- key\_lim3, 139, 151
- key\_mpp\_mpi, 54, 147, 160, 213, 282
- key\_nemocice\_decomp, 151
- key\_netcdf4, 229–231
- key\_nosignedzero, 281, 282
- key\_oasis3, 138
- key\_pisces, 138
- key\_top, 138
- key\_trabbl, 87, 88, 184, 344
- key\_traldf\_c1d, 178
- key\_traldf\_c2d, 178, 179
- key\_traldf\_c3d, 178, 179
- key\_traldf\_eiv, 179, 180, 349
- key\_trddyn, 100
- key\_trdmld\_trc, 232
- key\_trdtrc, 232
- key\_trdvor, 100
- key\_vectopt\_loop, 283
- key\_vvl, 102, 110, 112, 113, 116, 120, 142, 193, 233, 239
- key\_zdfcst, 184, 185
- key\_zdfddm, 82, 199, 200
- key\_zdfgls, 194, 195, 199
- key\_zdftric, 185

- key\_zdftke, 186, 191, 199
- key\_zdftmx, 207
- key\_zdftmx\_new, 209
- h90 file
  - ldfdyn\_substitute, 178
  - ldftra\_substitute, 178
  - traldf\_c1d, 178
- Input NetCDF files
  - bathy\_level.nc, 59
  - bathy\_meter.nc, 59
  - bfr\_coef.nc, 203
  - coordinates.nc, 55
  - geothermal\_heating.nc, 87
  - isf\_draft\_meter.nc, 59
  - isfdraft\_meter.nc, 60
  - mask\_itf.nc, 208
  - subbasins.nc, 241
- Model parameters
  - jpi, 160
  - jpiglo, 284
  - jpgj, 160
  - jpglo, 284
  - jpk, 57, 60–62, 160, 291
  - jpni, 160, 161
  - jpni\_j, 160, 161
  - jpni\_j, 160, 161
  - jprecj, 160
  - lk\_vvl, 92
- Modules
  - closea, 280
  - daymod, 134
  - diar5, 240, 241
  - diahth, 240
  - diaptr, 241
  - diawri, 134, 212
  - divcur, 101, 142, 144
  - domhgr, 54, 55, 278
  - dommsk, 278
  - domzgr, 54, 57, 60, 67
  - dtatsd, 68
  - dynadv, 107
  - dynadv\_ubs, 108, 109
  - dynbfr, 202, 203, 205, 206
  - dyncor\_c1d, 287
  - dynhpg, 96, 109
  - dynkeg, 106
  - dynldf, 100, 116
  - dynnxt, 40, 113, 120, 121
  - dynsp\_ft, 121
  - dynspg, 112, 139
  - dynspg\_exp, 113
  - dynspg\_ft, 113
  - dynspg\_ts, 205
  - dynvor, 102, 103, 107
  - dynzad, 106
  - dynzdf, 100, 118, 127, 184
  - dynzdf\_imp, 205
  - eosbn2, 70, 93, 95, 96, 200
  - fldread, 10, 90, 128
  - geo2ocean, 149
  - iom, 134, 287
  - istate, 68
  - lbclnk, 157–159
  - lbcnfd, 158
  - ldfdyn, 178
  - ldfdyn\_c2d, 179
  - ldfeiv, 180
  - ldfslp, 77, 173
  - ldftra, 178
  - lib\_fortran, 281, 282
  - lib\_mpp, 158, 160
  - nemogcm, 134, 244
  - par\_oce, 160
  - phycst, 55, 70, 93
  - sbc\_ana\_gyre, 135
  - sbcana, 134, 135
  - sbcapr, 139
  - sbcblk\_clio, 135, 136
  - sbcblk\_core, 135
  - sbcblk\_mfs, 135, 137
  - sbcctl, 138
  - sbcscy, 147
  - sbcflx, 135
  - sbcfwb, 152
  - sbcice\_cice, 151
  - sbcice\_if, 151

- sbcisf, 142
- sbcmod, 82, 127, 134
- sbcnrf, 141
- sbcetas, 134
- sbcssr, 139, 150
- sbctide, 140
- sbcwave, 152
- sshwzv, 101
- step, 134, 244
- step\_cld, 287
- stopar, 275, 276
- stopts, 276
- stornq, 275
- stpctl, 134
- traadv, 71
- traadv\_cen, 73
- traadv\_eiv, 180
- traadv\_fct, 74
- traadv\_mus, 75
- traadv\_qck, 77
- traadv\_ubs, 76
- trabbc, 85
- trabbl, 87
- tradmp, 90
- traldf, 8, 77, 96, 178
- traldf\_iso, 78, 80
- traldf\_lap, 79
- traldf\_lap\_blp, 78
- traldf\_triad, 78, 80
- tranpc, 70
- tranxt, 40, 92, 93
- traqsr, 83, 85, 127
- trasbc, 82, 127
- trazdf, 80, 81, 93, 184
- trc\_oce, 85
- trddyn, 232
- trdra, 232
- userdef\_hgr, 54
- userdef\_zgr, 54
- zdfbfr, 201–203, 205, 206
- zdfddm, 200
- zdfgls, 184
- zdfini, 184
- zdfkpp, 199
- zdfric, 184
- zdfcke, 184
- zpsdhe, 110
- zpsdhe, 79, 96, 98
- Namelist, 7
- Namelist Group Name
  - namnc4, 231
  - nam\_asminc, 270
  - nam\_dynldf, 172
  - nam\_tide, 140
  - nam\_traldf, 172
  - namasm, 271
  - nambbl, 87
  - nambdy, 163
  - nambdy\_dta, 163
  - nambdy\_dta2, 163
  - nambdy\_index, 163
  - nambdy\_tide, 169
  - namberg, 146
  - nambfr, 201
  - namcfg, 52, 54, 55, 57, 60, 62, 157, 280, 286
  - namctl, 242, 283
  - namdct, 236
  - namdia\_harm, 235
  - namdom, 57, 59, 62, 92, 120
  - namdyn\_adv, 102, 107
  - namdyn\_hpg, 109
  - namdyn\_ldf, 116
  - namdyn\_spg, 112
  - namdyn\_vor, 103
  - namelist\_cfg, 73
  - namelist\_ref, 73
  - nameos, 94
  - namflo, 233
  - namlbc, 154
  - nammpp, 160, 161
  - namobs, 245
  - namptr, 241
  - namrun, 46, 229
  - namsrc, 125, 139, 143, 147, 150, 152
  - namsrc\_clio, 137

- namsbc\_core, 136
- namsbc\_mfs, 137
- namsbc\_rnf, 141
- namsbc\_sas, 134
- namsbc\_ssr, 150
- namsbc\_wave, 152
- namsbc\_ana, 135
- namsbc\_cpl, 139
- namsbc\_flux, 135
- namsto, 276
- namtra\_adv, 73
- namtra\_bbc, 87
- namtra\_dmp, 90
- namtra\_ldf, 77, 334
- namtra\_qsr, 84
- namtrd, 232
- namtsd, 68
- namusr\_def, 291
- namzdf, 81, 119, 185, 197, 199
- namzdf\_ddm, 200
- namzdf\_gls, 195
- namzdf\_ric, 185
- namzdf\_tmx, 207
- namzdf\_tmx\_new, 210
- namzdfy\_tke, 187
- namzgr, 57, 58
- namzgr\_sco, 64
- Namelist variables
  - botmix\_triad, 344
  - clname, 140
  - cn\_dir, 128, 136
  - cn\_domcfg, 54
  - cn\_mask\_file, 166
  - cn\_profbbfiles, 245
  - cn\_resto, 90
  - cn\_storst\_in, 276
  - cn\_storst\_out, 276
  - cp\_cfg, 91
  - cp\_cpz, 91
  - init\_float\_ariane, 233
  - iom\_get, 281
  - iom\_put, 231
  - jp\_cfg, 91
  - jperio, 57, 59, 91, 157
  - jphgr\_mesh, 55–57
  - jpglo, 52, 160, 290, 291
  - jpindt, 166
  - jpinfo, 166
  - jpizoom, 286
  - jpgdta, 281
  - jpglo, 52, 160, 281, 290, 291
  - jpgnob, 166
  - jpgzoom, 286
  - jpglo, 52
  - jpgnfl, 234
  - jpgnflnewflo, 234
  - jpgni, 283
  - ln\_ana, 125
  - ln\_apr\_dyn, 120, 126, 139
  - ln\_apr\_obc, 140
  - ln\_ariane, 233
  - ln\_asmdin, 270
  - ln\_asmiau, 270
  - ln\_bdy, 163, 292
  - ln\_bench=true, 291
  - ln\_bfr2d, 203
  - ln\_bfrimp, 205–207
  - ln\_blk\_clio, 125
  - ln\_blk\_core, 125, 147
  - ln\_blk\_mfs, 125
  - ln\_botmix\_triad, 81, 334, 344, 352
  - ln\_bt\_av, 114, 115
  - ln\_bt\_fw, 114, 115
  - ln\_bt\_nn\_auto, 113
  - ln\_cdgw, 126, 152
  - ln\_cfmeta, 229
  - ln\_clio, 135, 136, 148
  - ln\_coast, 92
  - ln\_coords\_file, 163
  - ln\_core, 135, 148
  - ln\_cpl, 126, 138
  - ln\_crban, 195
  - ln\_ctl, 147, 283
  - ln\_custom, 92
  - ln\_diaobs, 244
  - ln\_diaptr, 241
  - ln\_dm2dc, 126, 147
  - ln\_dyn\_mx1, 232

- [ln\\_dyn\\_trd](#), 232
- [ln\\_dynadv\\_cen2](#), 107, 108
- [ln\\_dynadv\\_ubs](#), 107, 108, 180
- [ln\\_dynhpg\\_djc](#), 110
- [ln\\_dynhpg\\_imp](#), 111, 112
- [ln\\_dynhpg\\_isf](#), 110, 111
- [ln\\_dynhpg\\_prj](#), 110
- [ln\\_dynhpg\\_sco](#), 110
- [ln\\_dynhpg\\_vec](#), 120
- [ln\\_dynhpg\\_zco](#), 109
- [ln\\_dynhpg\\_zps](#), 110
- [ln\\_dynldf\\_bilap](#), 108, 118, 180
- [ln\\_dynldf\\_hor](#), 117, 173
- [ln\\_dynldf\\_iso](#), 117
- [ln\\_dynldf\\_lap](#), 108, 117, 180
- [ln\\_dynvor\\_eeen](#), 104, 315, 323
- [ln\\_dynvor\\_ene](#), 103, 315
- [ln\\_dynvor\\_ens](#), 103, 322
- [ln\\_dynvor\\_mix](#), 103
- [ln\\_dynzad\\_zts](#), 106
- [ln\\_flo\\_ascii](#), 234
- [ln\\_flork4](#), 233
- [ln\\_fix](#), 125, 135, 147, 148, 150
- [ln\\_fixqsr](#), 84
- [ln\\_full\\_field](#), 91, 92
- [ln\\_glo\\_trd](#), 232
- [ln\\_grid\\_global](#), 245
- [ln\\_grid\\_search\\_lookup](#), 245
- [ln\\_hsb = true](#), 145
- [ln\\_icebergs](#), 146
- [ln\\_iscpl = true](#), 145
- [ln\\_isf](#), 126
- [ln\\_isfcav](#), 58–60, 96, 110, 111, 143, 144, 204
- [ln\\_isfcav = .false.](#), 280
- [ln\\_KE\\_trd](#), 232
- [ln\\_lc](#), 190
- [ln\\_length\\_lim](#), 196
- [ln\\_linssh](#), 58, 59, 66, 71, 72, 83
- [ln\\_loglayer](#), 204
- [ln\\_med\\_red\\_seas](#), 91
- [ln\\_mevar](#), 210
- [ln\\_mfs](#), 135, 137
- [ln\\_mixcpl](#), 126, 133
- [ln\\_mldw](#), 186
- [ln\\_mus\\_ups](#), 75
- [ln\\_mx10](#), 189
- [ln\\_nc4zip](#), 230
- [ln\\_nnogather](#), 283
- [ln\\_old\\_31\\_lev\\_code](#), 91
- [ln\\_qsr\\_2bd](#), 84
- [ln\\_qsr\\_bio](#), 85
- [ln\\_qsr\\_rgb](#), 85
- [ln\\_read\\_cfg=true](#), 291
- [ln\\_ref\\_apr](#), 139
- [ln\\_rnf](#), 126
- [ln\\_rnf\\_depth](#), 141
- [ln\\_rnf\\_sal](#), 141
- [ln\\_rnf\\_temp](#), 141
- [ln\\_rstflo](#), 234
- [ln\\_rstseed](#), 276
- [ln\\_rststo](#), 276
- [ln\\_s3d](#), 245
- [ln\\_s\\_SF12](#), 64, 65
- [ln\\_s\\_SH94](#), 64
- [ln\\_sco](#), 58, 64, 79, 173
- [ln\\_sigcrit](#), 66
- [ln\\_ssr](#), 126
- [ln\\_sstnight](#), 244
- [ln\\_subbas](#), 241
- [ln\\_t3d](#), 245
- [ln\\_taudif](#), 136
- [ln\\_tide](#), 120, 140
- [ln\\_tide\\_pot](#), 120, 140
- [ln\\_tmx\\_itf](#), 208
- [ln\\_tra\\_mxl](#), 71, 232, 233
- [ln\\_tra\\_trd](#), 71, 232
- [ln\\_traadv\\_cen](#), 73
- [ln\\_traadv\\_fct](#), 74
- [ln\\_traadv\\_mus](#), 75
- [ln\\_traadv\\_NONE](#), 71
- [ln\\_traadv\\_qck](#), 77
- [ln\\_traadv\\_tvd\\_zts](#), 106
- [ln\\_traadv\\_ubs](#), 75
- [ln\\_trabbc](#), 87
- [ln\\_tradmp](#), 90, 91
- [ln\\_traldf\\_blp](#), 78, 79
- [ln\\_traldf\\_eiv](#), 334



- ln\_traldf\_gdia, 352
- ln\_traldf\_grif, 80
- ln\_traldf\_hor, 78–80, 173
- ln\_traldf\_iso, 78–80, 334
- ln\_traldf\_lap, 78–80
- ln\_traldf\_lev, 78, 79
- ln\_traldf\_msc, 78, 81, 335
- ln\_traldf\_NONE, 78
- ln\_traldf\_triad, 78, 80, 334, 349
- ln\_tranpc, 196
- ln\_traqsr, 127
- ln\_triad\_iso, 81, 334, 345, 347, 352
- ln\_tsd\_ini, 68
- ln\_tsd\_init, 90
- ln\_tsd\_tradmp, 90
- ln\_tsdiff, 210
- ln\_useCT, 94
- ln\_vor\_trd, 232
- ln\_zco, 58, 60, 78–80
- ln\_zdfevd, 198, 199
- ln\_zdfexp, 42, 82, 119, 184, 199, 205
- ln\_zdfnpc, 197, 199
- ln\_zdfmx\_itf, 208
- ln\_zero\_top\_layer, 92
- ln\_zps, 58, 62, 79, 80, 96, 97
- lzoom\_e, 91
- lzoom\_n, 91
- lzoom\_s, 91
- lzoom\_w, 91
- namelist\_cfg, 281
- nb\_ana, 235
- nb\_bdy, 163
- nb\_harmo, 140
- nbdysegn, 166
- nit000, 235
- nit000\_han, 235
- nitend, 235
- nitend\_han, 235
- nn\_atfp, 121
- nn\_baro, 113, 114, 206
- nn\_bathy, 59
- nn\_bbl\_adv, 88
- nn\_bbl\_ldf, 88, 344
- nn\_bench, 284
- nn\_bit\_cmp, 283
- nn\_botfr, 202–204
- nn\_cen\_h, 73
- nn\_cen\_v, 73, 74, 76
- nn\_chdta, 85
- nn\_clo, 195
- nn\_clos, 195
- nn\_dct, 236
- nn\_dctwri, 236
- nn\_debug, 236
- nn\_diacfl, 242
- nn\_divdmp, 271
- nn\_drown, 145
- nn\_dttc, 222
- nn\_dynhpg\_rst, 46, 112
- nn\_ediff, 187
- nn\_ediss, 187
- nn\_eeen\_e3f, 104
- nn\_eos, 93–95, 174
- nn\_eos\_ft, 276
- nn\_eos\_ord, 276
- nn\_etau, 191
- nn\_evdm, 199
- nn\_fct\_h, 74
- nn\_fct\_v, 74, 75
- nn\_fct\_zts, 75
- nn\_fsbc, 126, 127, 130, 148, 151, 222
- nn\_fwb, 126, 152
- nn\_gammablck = 0, 143
- nn\_gammablck = 1, 143
- nn\_gammablck = 2, 143
- nn\_geoflx, 87
- nn\_geoflx\_cst, 87
- nn\_GYRE, 291
- nn\_hdmp, 92
- nn\_ice, 126, 150
- nn\_ice\_embd, 120
- nn\_isf, 143, 144
- nn\_isfblk, 143
- nn\_msh, 57, 91, 161
- nn\_mx1, 187, 188
- nn\_nit000, 146

- nn\_npc, 197
- nn\_pdl, 187
- nn\_profdavtypes, 244
- nn\_ric, 185
- nn\_rimwidth, 165
- nn\_sample\_rate, 147
- nn\_stab\_func, 195
- nn\_sto\_eos, 276
- nn\_stockfl, 234
- nn\_tau000, 135
- nn\_test\_box, 146
- nn\_test\_icebergs, 146
- nn\_tkebc\_bot, 195
- nn\_tkebc\_surf, 195
- nn\_tra, 164
- nn\_tra\_dta, 164
- nn\_trd, 232
- nn\_verbose\_level, 147
- nn\_verbose\_write, 147
- nn\_volctl, 167
- nn\_writefl, 234
- nn\_zdfexp, 42, 82, 119
- nn\_zdmp, 91
- nn\_zpyc, 210
- nstep\_han, 235
- nz\_rnf, 141
- open\_ocean\_jstart, 280, 281
- ORCA\_index, 290
- ppa0, 62
- ppa1, 62
- ppacr, 62
- ppacr=0, 60
- ppdzmin, 62
- ppe1\_deg, 55, 56
- ppe1\_m, 56
- ppe2\_deg, 55
- ppe2\_m, 56
- ppglam0, 57
- ppglamt0, 56
- ppgphi0, 56, 57
- pphmax, 60, 62
- ppkth, 62
- ppsur, 62
- rn\_a0, 95
- rn\_abs, 84
- rn\_aeiv, 180
- rn\_ahm0, 178, 179
- rn\_ahmb0, 180
- rn\_aht0, 178, 179
- rn\_ahtb0, 180
- rn\_ahtbbl, 88
- rn\_alp, 185
- rn\_alpha, 65
- rn\_atfp, 41, 92
- rn\_avevd, 199
- rn\_avm0, 185, 187
- rn\_avmri, 185
- rn\_avt0, 185, 187
- rn\_b0, 95
- rn\_bb, 65
- rn\_bfeb2, 203
- rn\_bfri1, 202, 203
- rn\_bfri2, 203, 204
- rn\_bfri2\_max, 204
- rn\_bfrien, 203
- rn\_bfrz0, 204
- rn\_bits\_erosion\_fraction, 147
- rn\_bot, 92
- rn\_bt\_cmax, 113
- rn\_chnrn, 195
- rn\_clim\_galp, 196
- rn\_crban, 195
- rn\_dep, 92
- rn\_e3zps\_min, 62
- rn\_e3zps\_rat, 64
- rn\_ebb, 187, 189
- rn\_efac, 136
- rn\_efr, 191
- rn\_emin, 187
- rn\_emin0, 190
- rn\_emp0, 135
- rn\_eos\_lim, 276
- rn\_eos\_stdxy, 276
- rn\_eos\_stdz, 276
- rn\_eos\_tcor, 276
- rn\_fiscpl, 145
- rn\_gambbl, 89
- rn\_gammas0, 143

- rn\_gammat0, 143
  - rn\_hc, 65
  - rn\_hisf\_tbl, 143, 144
  - rn\_htmx, 207
  - rn\_initial\_mass, 146
  - rn\_initial\_thickness, 146
  - rn\_isfhmin, 67
  - rn\_lambda1, 95
  - rn\_lambda2, 95
  - rn\_lc, 190
  - rn\_mass\_scaling, 146
  - rn\_me, 207
  - rn\_mldmax, 186
  - rn\_mldmin, 186
  - rn\_mu1, 95
  - rn\_mu2, 95
  - rn\_mx10, 188
  - rn\_n2min, 208
  - rn\_nu, 95
  - rn\_pfac, 136
  - rn\_qns0, 135
  - rn\_qsr0, 135
  - rn\_rdt, 206, 222
  - rn\_rmax, 64
  - rn\_sbot\_max, 64
  - rn\_sbot\_min, 64
  - rn\_shlat, 154, 155, 157
  - rn\_si0, 84
  - rn\_slpmax, 81, 335
  - rn\_surf, 92
  - rn\_sw\_triad, 81, 335
  - rn\_tfe, 207
  - rn\_tfe\_itf, 208
  - rn\_tfri2, 204
  - rn\_tfri2\_max, 204
  - rn\_tfrz0, 204
  - rn\_theta, 65
  - rn\_utau0, 135
  - rn\_vfac, 136
  - rn\_vtau0, 135
  - rn\_wtmix, 186
  - rn\_wvmix, 186
  - rn\_zb\_a, 65
  - rn\_zb\_b, 65
  - rn\_zqt, 136
  - rn\_zs, 65
  - rn\_zu, 136
  - sbc\_wave, 152
  - sn\_apr, 139
  - sn\_clc, 137
  - sn\_depmax\_isf, 144
  - sn\_depmin\_isf, 144
  - sn\_fwfisf, 144
  - sn\_humi, 136
  - sn\_icb, 146
  - sn\_Leff\_isf, 144
  - sn\_msl, 138
  - sn\_prec, 136, 138
  - sn\_qlw, 136
  - sn\_qsr, 136, 148
  - sn\_rhm, 138
  - sn\_rnfisf, 144
  - sn\_sal, 68, 90
  - sn\_snow, 136
  - sn\_tair, 136, 138
  - sn\_tdif, 136
  - sn\_tem, 68, 90
  - sn\_windi, 137
  - sn\_windj, 137
  - sn\_wndi, 136
  - sn\_wndj, 136
  - tname, 235
  - traldf\_grif, 172, 174
  - traldf\_grif\_iso, 175
  - xmlio\_server.def, 231
- Routines
- dyn\_spg\_ts, 206
  - fld\_read, 128, 132
  - hgr\_read, 55
  - inimpp2, 161
  - istate\_t\_s, 68
  - lbc\_lnk, 159, 287
  - ldf\_dyn\_c2d\_orca, 179
  - ldfslp\_init, 173
  - sbc\_blk\_init, 128
  - sbc\_isf\_div, 144
  - sbc\_rnf\_div, 142

sto\_par, [276](#)  
sto\_par\_init, [276](#)  
sto\_rst\_write, [276](#)  
stp, [287](#)  
stp\_c1d, [287](#)  
stp\_ctl, [134](#)  
tra\_dmp\_init, [90](#)  
traldf\_blp, [79](#)  
traldf\_lap, [79](#)  
trc\_oce\_rgb, [85](#)  
zdf\_bfr, [207](#)



## Bibliography

- Adcroft, A. and J.-M. Campin, 2004: Re-scaled height coordinates for accurate representation of free-surface flows in ocean circulation models. *Ocean Modelling*, **7**, 269–284, doi:10.1016/j.ocemod.2003.09.003, URL <http://dx.doi.org/10.1016/j.ocemod.2003.09.003>.
- Arakawa, A. and Y.-J. G. Hsu, 1990: Energy conserving and potential-enstrophy dissipating schemes for the shallow water equations. *Mon. Wea. Rev.*, **118** (10), 1960–1969.
- Arakawa, A. and V. R. Lamb, 1981: A potential enstrophy and energy conserving scheme for the shallow water equations. *Mon. Wea. Rev.*, **109** (1), 18–36.
- Asselin, R., 1972: Frequency filter for time integrations. *Mon. Wea. Rev.*, **100** (6), 487–490.
- Axell, L. B., 2002: Wind-driven internal waves and langmuir circulations in a numerical ocean model of the southern baltic sea. *J. Geophys. Res.*, **107**, doi:10.1029/2001JC000922, URL <http://dx.doi.org/10.1029/2001JC000922>.
- Barnier, B., G. Madec, T. Penduff, J.-M. Molines, A.-M. Treguier, J. L. Sommer, A. Beckmann, A. Biastoch, C. Boning, J. Dengg, C. Derval, E. Durand, S. Gulev, E. Remy, C. Talandier, S. Theetten, M. Maltrud, J. McClean, and B. D. Cuevas, 2006: Impact of partial steps and momentum advection schemes in a global ocean circulation model at eddy-permitting resolution. *Ocean Dyn.*, **56**, 543–567, doi:10.1007/s10236-006-0082-1, URL <http://dx.doi.org/10.1007/s10236-006-0082-1>.

- Beckmann, A. and R. Döscher, 1997: A method for improved representation of dense water spreading over topography in geopotential-coordinate models. *J. Phys. Oceanogr.*, **27**, 581–591.
- Beckmann, A. and H. Goosse, 2003: A parameterization of ice shelf-ocean interaction for climate models. *Ocean Modelling*, **5**, 157–170.
- Beckmann, A. and D. B. Haidvogel, 1993: Numerical simulation of flow around a tall isolated seamount. part i - problem formulation and model accuracy. *J. Phys. Oceanogr.*, **23** (8), 1736–1753.
- Bernie, D., E. Guilyardi, G. Madec, J. M. Slingo, and S. J. Woolnough, 2007: Impact of resolving the diurnal cycle in an ocean–atmosphere gcm. part 1: a diurnally forced ogcm. *Clim. Dyn.*, **29** (6), 575–590.
- Bernie, D. J., S. J. Woolnough, J. M. Slingo, and E. Guilyardi, 2005: Modelling diurnal and intraseasonal variability of the ocean mixed layer. *J. Climate*, **18** (8), 1190–1200.
- Bignami, F., S. Marullo, R. Santoleri, and M. E. Schiano, 1995: Longwave radiation budget in the mediterranean sea. *J. Geophys. Res.*, **100** (C2), 2501–2514, doi:10.1029/94JC02496.
- Blanke, B. and P. Delecluse, 1993: Low frequency variability of the tropical atlantic ocean simulated by a general circulation model with mixed layer physics. *J. Phys. Oceanogr.*, **23**, 1363–1388.
- Blanke, B. and S. Raynaud, 1997: Kinematics of the pacific equatorial undercurrent: An eulerian and lagrangian approach from gcm results. *J. Phys. Oceanogr.*, **27** (6), 1038–1053.
- Bloom, S. C., L. L. Takacs, A. M. D. Silva, and D. Ledvina, 1996: Data assimilation using incremental analysis updates. *Mon. Wea. Rev.*, **124**, 1256–1271.
- Bouffard, D. and L. Boegman, 2013: A diapycnal diffusivity model for stratified environmental flows. *Dyn. Atmos. Ocean*, **61–62**, 14–34, doi:10.1016/j.dynatmoce.2013.02.002, URL <http://dx.doi.org/10.1016/j.dynatmoce.2013.02.002>.
- Bougeault, P. and P. Lacarrere, 1989: Parameterization of orography-induced turbulence in a mesobeta–scale model. *Mon. Wea. Rev.*, **117** (8), 1872–1890.
- Bouillon, S., M. M. Maqueda, V. Legat, and T. Fichefet, 2009: An elastic-viscous-plastic sea ice model formulated on arakawa b and c grids. *Ocean Modelling*, **27**, 174–184, doi:10.1016/j.ocemod.2009.01.004, URL <http://dx.doi.org/10.1016/j.ocemod.2009.01.004>.

- Brankart, J.-M., 2013: Impact of uncertainties in the horizontal density gradient upon low resolution global ocean modelling. *Ocean Modelling*, **66**, 64–76, doi:<http://dx.doi.org/10.1016/j.ocemod.2013.02.004>, URL <http://www.sciencedirect.com/science/article/pii/S1463500313000309>.
- Brankart, J.-M., G. Candille, F. Garnier, C. Calone, A. Melet, P.-A. Bouttier, P. Brasseur, and J. Verron, 2015: A generic approach to explicit simulation of uncertainty in the nemo ocean model. *Geoscientific Model Development*, **8** (5), 1285–1297, doi:10.5194/gmd-8-1285-2015, URL <http://www.geosci-model-dev.net/8/1285/2015/>.
- Brodeau, L., B. Barnier, A.-M. Tréguier, T. Penduff, and S. Gulev, 2009: An era40-based atmospheric forcing for global ocean circulation models. *Ocean Modelling*, **31** (3-4), 88–104.
- Brown, J. A. and K. A. Campana, 1978: An economical time-differencing system for numerical weather prediction. *Mon. Wea. Rev.*, **106** (8), 1125–1136.
- Burchard, H., 2002: Energy-conserving discretisation of turbulent shear and buoyancy production. *Ocean Modelling*, **4** (3-4), 347–361, doi:10.1016/S1463-5003(02)00009-4, URL [http://dx.doi.org/10.1016/S1463-5003\(02\)00009-4](http://dx.doi.org/10.1016/S1463-5003(02)00009-4).
- Campin, J.-M., A. Adcroft, C. Hill, and J. Marshall, 2004: Conservation of properties in a free-surface model. *Ocean Modelling*, **6** (3-4), 221–244.
- Campin, J.-M. and H. Goosse, 1999: Parameterization of density-driven downsloping flow for a coarse-resolution ocean model in z-coordinate. *Tellus*, **51**, 412–430.
- Campin, J.-M., J. Marshall, and D. Ferreira, 2008: Sea ice-ocean coupling using a rescaled vertical coordinate  $z^*$ . *Ocean Modelling*, **24** (1-2), 1–14, doi:10.1016/j.ocemod.2008.05.005, URL <http://dx.doi.org/10.1016/j.ocemod.2008.05.005>.
- Canuto, V. M., A. Howard, Y. Cheng, and M. S. Dubovikov, 2001: Ocean turbulence. parti: One-point closure model-momentum and heat vertical diffusivities. *J. Phys. Oceanogr.*, **24** (12), 2546–2559.
- Carrère, L. and F. Lyard, 2003: Modelling the barotropic response of the global ocean to atmospheric wind and pressure forcing - comparisons with observations. *Geophys. Res. Lett.*, **30** (6), doi:10.1029/2002GL016473, URL <http://dx.doi.org/10.1029/2002GL016473>.
- Castellari, S., N. Pinardi, and K. Leaman, 1998: A model study of air-sea interactions in the mediterranean sea. *J. Mar. Sys.*, **18**, 89–114.

- Chanut, J., 2005: Nesting code for nemo. Tech. rep., European Union: Marine Environment and Security for the European Area (MERSEA) Integrated Project, mERSEA-WP09-MERCA-TASK-9.1.1.
- Chassignet, E. P., L. T. Smith, and G. R. Halliwell, 2003: North atlantic simulations with the hybrid coordinate ocean model (hycom): Impact of the vertical coordinate choice, reference pressure, and thermobaricity. *J. Phys. Oceanogr.*, **33**, 2504–2526.
- Cox, M., 1987: Isopycnal diffusion in a z-coordinate ocean model. *Ocean Modelling*, **74**, 1–9.
- Craig, P. D. and M. L. Banner, 1994: Modeling wave-enhanced turbulence in the ocean surface layer. *J. Phys. Oceanogr.*, **24** (12), 2546–2559.
- Craik, A. D. D. and S. Leibovich, 1976: A rational model for langmuir circulations. *J. Fluid Mech.*, **73**, 401–426.
- D’Alessio, S. J. D., K. Abdella, and N. A. McFarlane, 1998: A new second-order turbulence closure scheme for modeling the oceanic mixed layer. *J. Phys. Oceanogr.*, **28**, 1624–1641.
- Daley, R. and E. Barker, 2001: *NAVDAS Source Book 2001*. NRL/PU/7530-01-441, Available from the Naval Research Laboratory, Monterey, CA., 93943-5502, 163pp pp.
- Danabasoglu, G., R. Ferrari, and J. C. McWilliams, 2008: Sensitivity of an ocean general circulation model to a parameterization of near-surface eddy fluxes. *J. Climate*, **21**, 1192–1208, doi:10.1175/2007JCLI1508.1, URL <http://dx.doi.org/10.1175/2007JCLI1508.1>.
- Davies, H., 1976: A lateral boundary formulation for multi-level prediction models. *Quart. J. Roy. Meteor. Soc.*, **102**, 405–418.
- de Boyer Montégut, C., G. Madec, A. Fischer, A. Lazar, and D. Iudicone, 2004: Mixed layer depth over the global ocean: An examination of profile data and a profile-based climatology. *J. Geophys. Res.*, **109**, C12 003, doi:10.1029/2004JC002378, URL <http://dx.doi.org/10.1029/2004JC002378>.
- de Lavergne, C., G. Madec, J. L. Sommer, A. J. G. Nurser, and A. C. N. Garabato, 2016: The impact of a variable mixing efficiency on the abyssal overturning. *Journal of Physical Oceanography*, **46**, 663–681, doi:10.1175/JPO-D-14-0259.1, URL <http://dx.doi.org/10.1175/JPO-D-14-0259.1>.
- Debreu, L., C. Vouland, and E. Blayo, 2008: Agrif: Adaptive grid refinement in fortran. *Computers and Geosciences*, **34**, 8–13.



- Delecluse, P. and G. Madec, 2000: Ocean modelling and the role of the ocean in the climate system. In *Modeling the Earth's Climate and its Variability, Les Houches, Session, LXVII 1997*, Eds. W. R. Holland, S. Joussaume and F. David, Elsevier Science, 237–313.
- Demange, J., 2014: Schémas numériques d'advection et de propagation ondes de gravité dans les modèles de circulation océanique. Ph.D. thesis, Doctorat es Applied Mathematiques, Grenoble University, France.
- Dobricic, S., N. Pinardi, M. Adani, M. Tonani, C. Fratianni, A. Bonazzi, and V. Fernandez, 2007: Daily oceanographic analysis by the mediterranean basin scale assimilation system. *Ocean Sc.*, **3**, 149–157.
- Drijfhout, S. S., 1994: Heat transport by mesoscale eddies in an ocean circulation model. *J. Phys. Oceanogr.*, **24**, 353–369.
- Dukowicz, J. K. and R. D. Smith, 1994: Implicit free-surface method for the bryan-cox-semtner ocean model. *J. Geophys. Res.*, **99**, 7991–8014.
- Egbert, G. and R. Ray, 2000: Significant dissipation of tidal energy in the deep ocean inferred from satellite altimeter data. *Nature*, **405**, 775–778.
- , 2001: Estimates of m<sup>2</sup> tidal energy dissipation from topex/poseidon altimeter data. *J. Geophys. Res.*, **106**, 22 475–22 502.
- Eiseman, P. R. and A. P. Stone, 1980: Conservation laws of fluid dynamics – a survey. *SIAM Review*, **22**, 12–27.
- Emile-Geay, J. and G. Madec, 2009: Geothermal heating, diapycnal mixing and the abyssal circulation. *Ocean Sc.*, **5**, 281–325.
- Engerdahl, H., 1995: Use of the flow relaxation scheme in a three-dimensional baroclinic ocean model with realistic topography. *Tellus*, **47A**, 365–382.
- Farge, M., 1987: Dynamique non lineaire des ondes et des tourbillons dans les equations de saint venant. Ph.D. thesis, Doctorat es Mathematiques, Paris VI University, France.
- Farrow, D. E. and D. P. Stevens, 1995: A new tracer advection scheme for bryan-cox type ocean general circulation models. *J. Phys. Oceanogr.*, **25**, 1731–1741.
- Flather, R., 1994: A storm surge prediction model for the northern bay of bengal with application to the cyclone disaster in april 1991. *J. Phys. Oceanogr.*, **24**, 172–190.
- Fujio, S. and N. Imasato, 1991: Diagnostic calculation for circulation and water mass movement in the deep pacific. *J. Geophys. Res.*, **96**, 759–774.

- Galperin, B., L. H. Kantha, S. Hassid, and A. Rosati, 1988: A quasi-equilibrium turbulent energy model for geophysical flows. *J. Atmos. Sc.*, **45**, 55–62.
- Gargett, A. E., 1984: Vertical eddy diffusivity in the ocean interior. *J. Mar. Res.*, **42**.
- Gaspar, P., Y. Grégoris, and J.-M. Lefevre, 1990: A simple eddy kinetic energy model for simulations of the oceanic vertical mixing Tests at station papa and long-term upper ocean study site. *J. Geophys. Res.*, **95** (C9).
- Gent, P. R. and J. C. McWilliams, 1990: Isopycnal mixing in ocean circulation models. *J. Phys. Oceanogr.*, **20** (1), 150–155.
- Gerdes, R., 1993a: A primitive equation ocean circulation model using a general vertical coordinate transformation 1. description and testing of the model. *J. Geophys. Res.*, **98**.
- , 1993b: A primitive equation ocean circulation model using a general vertical coordinate transformation 2. application to an overflow problem. *J. Geophys. Res.*, **98**, 14 703–14 726.
- Gerdes, R., C. Köberle, and J. Willebrand, 1991: The influence of numerical advection schemes on the results of ocean general circulation models. *Clim. Dynamics*, **5** (4), 211–226, doi:10.1007/BF00210006, URL <http://dx.doi.org/10.1007/BF00210006>.
- Gibson, J. K., 1986: Standard software development and maintenance. Tech. rep., Operational Dep., ECMWF, Reading, UK.
- Gill, A. E., 1982: *Atmosphere-Ocean Dynamics*. International Geophysics Series, Academic Press, New-York.
- Goff, J. A., 2010: Global prediction of abyssal hill root-mean-square heights from small-scale altimetric gravity variability. *Journal of Geophysical Research: Solid Earth*, **115** (B12), B12 104, doi:10.1029/2010JB007867, URL <http://dx.doi.org/10.1029/2010JB007867>.
- Goosse, H., E. Deleersnijder, T. Fichefet, and M. England, 1999: Sensitivity of a global coupled ocean-sea ice model to the parameterization of vertical mixing. *J. Geophys. Res.*, **104**, 13,681–13,695.
- Graham, F. and T. McDougall, 2013: Quantifying the nonconservative production of conservative temperature, potential temperature, and entropy. *J. Phys. Oceanogr.*, **43**, 838–862, URL <http://dx.doi.org/10.1175/JPO-D-11-0188.1>.
- Greatbatch, R. J., 1994: A note on the representation of steric sea level in models that conserve volume rather than mass. *J. Geophys. Res.*, **99** (C6), 12,767–12,771.

- Griffies, S., 1998: The gent-mcwilliams skew-flux. *J. Phys. Oceanogr.*, **28**, 831–841.
- , 2004: *Fundamentals of ocean climate models*. Princeton University Press, 434pp.
- Griffies, S., A. Biastoch, C. Boning, F. Bryan, G. Danabasoglu, E. P. Chassignet, M. H. England, R. Gerdes, H. Haak, R. W. Hallberg, W. Hazeleger, J. Jungclaus, W. G. Large, G. Madec, A. Pirani, B. L. Samuels, M. Scheinert, A. S. Gupta, C. A. Severijns, H. L. Simmons, A.-M. Treguier, M. Winton, S. Yeager, and J. Yin, 2009: Coordinated ocean-ice reference experiments (cores). *Ocean Modelling*, **26** (1-2), 1–46, doi:10.1016/j.ocemod.2008.08.007, URL <http://dx.doi.org/10.1016/j.ocemod.2008.08.007>.
- Griffies, S., A. Gnanadesikan, R. Pacanowski, V. Larichev, J. Dukowicz, and R. Smith, 1998: Isonutral diffusion in a z-coordinate ocean model. *J. Phys. Oceanogr.*, **28** (5), 805–830.
- Griffies, S., R. Pacanowski, M. Schmidt, and V. Balaji, 2001: Tracer conservation with an explicit free surface method for z-coordinate ocean models. *Mon. Wea. Rev.*, **129** (5), 1081–1098.
- Guilyardi, E., G. Madec, and L. Terray, 2001: The role of lateral ocean physics in the upper ocean thermal balance of a coupled ocean-atmosphere gcm. *Clim. Dyn.*, **17** (8), 589–599.
- Haney, R. L., 1991: On the pressure gradient force over steep topography in sigma coordinate ocean models. *J. Phys. Oceanogr.*, **21** (4), 610–619.
- Hazeleger, W. and S. S. Drijfhout, 1998: Mode water variability in a model of the subtropical gyre: response to anomalous forcing. *J. Phys. Oceanogr.*, **28**, 266–288.
- , 1999: Stochastically forced mode water variability. *J. Phys. Oceanogr.*, **29**, 1772–1786.
- , 2000a: Eddy subduction in a model of the subtropical gyre. *J. Phys. Oceanogr.*, **30**, 677–695.
- , 2000b: A model study on internally generated variability in subtropical mode water formation. *J. Geophys. Res.*, **105**, 13,965–13,979.
- He, Y. and C. H. Q. Ding, 2001: Using accurate arithmetics to improve numerical reproducibility and stability in parallel applications. *J. Supercomputing.*, **18**, 259–277.
- Hellerman, S. and M. Rosenstein, 1983: Normal monthly wind stress over the world ocean with error estimates. *J. Phys. Oceanogr.*, **13**, 1093–1104.

- Hirt, C. W., A. A. Amsden, and J. L. Cook, 1974: An arbitrary lagrangian–eulerian computing method for all flow speeds. *J. Comput. Phys.*, **14**, 227–253.
- Hofmeister, R., H. Burchard, and J.-M. Beckers, 2009: Non-uniform adaptive vertical grids for 3d numerical ocean models. *Ocean Modelling*, **33**, 70–86, doi:10.1016/j.ocemod.2009.12.003, URL <http://dx.doi.org/10.1016/j.ocemod.2009.12.003>.
- Holland, D. and A. Jenkins, 1999: Modeling thermodynamic ice-ocean interactions at the base of an ice shelf. *J. Phys. Oceanogr.*, **29**, 1787–1800.
- Hunke, E. and W. Lipscomb, 2008: Cice: the los alamos sea ice model documentation and software user’s manual, version 4.0. Tech. rep., Los Alamos National Laboratory, N.M.
- Hunter, J. R., 2006: Specification for test models of ice shelf cavities. Tech. rep., Antarctic Climate & Ecosystems Cooperative Research Centre Private Bag 80, Hobart, Tasmania 7001.
- IOC, SCOR, and IAPSO, 2010: The international thermodynamic equation of seawater - 2010: Calculation and use of thermodynamic properties. Tech. rep., Intergovernmental Oceanographic Commission, URL [http://www.teos-10.org/pubs/TEOS-10\\_Manual.pdf](http://www.teos-10.org/pubs/TEOS-10_Manual.pdf).
- Jackson, P. R. and C. R. Rehmann, 2014: Experiments on differential scalar mixing in turbulence in a sheared, stratified flow. *J. Phys. Oceanogr.*, **44** (10), 2661–2680, doi:10.1175/JPO-D-14-0027.1, URL <http://dx.doi.org/10.1175/JPO-D-14-0027.1>.
- Jenkins, A., 1991: A one-dimensional model of ice shelf-ocean interaction. *J. Geophys. Res.*, **96** (C11), 2298–2312.
- , 2010: observation and parameterization of ablation at the base of ronne ice shelf, antarctica. *J. Phys. Oceanogr.*, **40** (10), 2298–2312.
- Jones, P. W., 1998: A user’s guide for scrip: A spherical coordinate remapping and interpolation package. version 1.4. Tech. rep., Los Alamos National Laboratory, URL <http://climate.lanl.gov/Software/SCRIP/SCRIPusers.pdf>.
- Kantha, L. and S. Carniel, 2005: Comment on ”generic length-scale equation for geophysical turbulence models” by l. umlauf and h. burchard. *J. Mar. Sys.*, **61**, 693–702.
- Kantha, L. H. and C. A. Clayson, 1994: An improved mixed layer model for geophysical applications. *J. Geophys. Res.*, **99**, 25,235–25,266.
- Kasahara, A., 1974: Various vertical coordinate systems used for numerical weather prediction. *Mon. Wea. Rev.*, **102**, 509–522.

- Killworth, P., D. Stainforth, D. Webb, and S. Paterson, 1991: The development of a free-surface bryan-cox-semtner ocean model. *J. Phys. Oceanogr.*, **21** (9), 1333–1348.
- Killworth, P. D., 1989: On the parameterization of deep convection in ocean models. *Parameterization of small-scale processes*, winter workshop, H., Ed., University of Hawaii at Manoa.
- , 1992: An equivalent-barotropic mode in the fine resolution antarctic model. *J. Phys. Oceanogr.*, **22**, 1379–1387.
- Koch-Larrouy, A., M. Lengaigne, P. Terray, G. Madec, and S. Masson, 2010: Tidal mixing in the indonesian seas and its effect on the tropical climate system. *Clim. Dyn.*, **34** (6), 891–904, doi:10.1007/s00382-009-0642-4, URL <http://dx.doi.org/10.1007/s00382-009-0642-4>.
- Koch-Larrouy, A., G. Madec, B. Blanke, and R. Molcard, 2008a: Water mass transformation along the indonesian throughflow in an ogcm. *Ocean Dyn.*, **58** (3-4), 289–309, doi:10.1007/s10236-008-0155-4, URL <http://dx.doi.org/10.1007/s10236-008-0155-4>.
- Koch-Larrouy, A., G. Madec, P. Bouruet-Aubertot, T. Gerkema, L. Bessieres, and R. Molcard, 2007: Tidal mixing in the indonesian seas and its effect on the tropical climate system. *Geophys. Res. Lett.*, **34**, L04 604, doi:10.1029/2006GL028405, URL <http://dx.doi.org/10.1029/2006GL028405>.
- Koch-Larrouy, A., G. Madec, D. Iudicone, A. Atmadipoera, and R. Molcard, 2008b: Physical processes contributing to the water mass transformation of the indonesian throughflow. *Ocean Dyn.*, **58** (3-4), 275–288, doi:10.1007/s10236-008-0154-5, URL <http://dx.doi.org/10.1007/s10236-008-0154-5>.
- Kolmogorov, A. N., 1942: The equation of turbulent motion in an incompressible fluid. *Izv. Akad. Nauk SSSR, Ser. Fiz.*, **6**, 56–58.
- Kondo, J., 1975: Air-sea bulk transfer coefficients in diabatic conditions. *Boundary-Layer Meteorol.*, **9**, 91–112.
- Large, W. G. and S. Yeager, 2004: *Diurnal to decadal global forcing for ocean and sea-ice models: the data sets and flux climatologies*. NCAR Technical Note, NCAR/TN-460+STR, CGD Division of the National Center for Atmospheric Research.
- Lazar, A., 1997: La branche froide de la circulation thermohaline - sensibilité à la diffusion turbulente dans un modèle de circulation générale idéalisée. Ph.D. thesis, Université Pierre et Marie Curie, Paris, France, 200pp.

- Lazar, A., G. Madec, and P. Delecluse, 1999: The deep interior downwelling, the veronis effect, and mesoscale tracer transport parameterizations in an ogcm. *J. Phys. Oceanogr.*, **29** (11), 2945–2961.
- Le Sommer, J., T. Penduff, S. Theetten, G. Madec, and B. Barnier, 2009: How momentum advection schemes influence current-topography interactions at eddy permitting resolution. *Ocean Modelling*, **29** (1), 1–14, doi:10.1016/j.ocemod.2008.11.007, URL <http://dx.doi.org/10.1016/j.ocemod.2008.11.007>.
- Leclair, M., 2010: introduction d'une coordonnée verticale arbitrairement lagrangienne eulérienne dans le code nemo, 180pp. Ph.D. thesis, Université Pierre and Marie Curie.
- Leclair, M. and G. Madec, 2009: A conservative leap-frog time stepping method. *Ocean Modelling*, **30** (2-3), 88–94, doi:10.1016/j.ocemod.2009.06.006, URL <http://dx.doi.org/10.1016/j.ocemod.2009.06.006>.
- , 2011:  $\tilde{z}$ -coordinate, an arbitrary lagrangian-eulerian coordinate separating high and low frequency. *Ocean Modelling*, **37**, 139–152, doi:10.1016/j.ocemod.2011.02.001, URL <http://dx.doi.org/10.1016/j.ocemod.2011.02.001>.
- Lele, S., 1992: Compact finite difference schemes with spectral-like resolution. *J. Comput. Phys.*, **103**, 16–42.
- Lemarié, F., L. Debreu, J. Demange, G. Madec, J. Molines, and M. Honnorat, 2015: Stability constraints for oceanic numerical models: Implications for the formulation of time and space discretizations. *Ocean Modelling*, **92**, 124–148, doi:10.1016/j.ocemod.2015.06.006, URL <http://dx.doi.org/10.1016/j.ocemod.2015.06.006>.
- Lemarié, F., L. Debreu, A. Shchepetkin, and J. McWilliams, 2012: On the stability and accuracy of the harmonic and biharmonic isoneutral mixing operators in ocean models. *Ocean Modelling*, **5253**, 9–35, doi:http://dx.doi.org/10.1016/j.ocemod.2012.04.007, URL <http://www.sciencedirect.com/science/article/pii/S1463500312000674>.
- Lengaigne, M., G. Madec, G. Alory, and C. Menkes, 2003: Sensitivity of the tropical pacific ocean to isopycnal diffusion on tracer and dynamics. *J. Geophys. Res.*, **108** (C11), 3345, doi:10.1029/2002JC001704, URL <http://dx.doi.org/10.1029/2002JC001704>.
- Lengaigne, M., C. Menkes, O. Aumont, T. Gorgues, L. Bopp, and J.-M. A. G. Madec, 2007: Bio-physical feedbacks on the tropical pacific climate in a coupled general circulation model. *Clim. Dyn.*, **28**, 503–516.

- Leonard, B. P., 1979: A stable and accurate convective modelling procedure based on quadratic upstream interpolation. *Computer Methods in Applied Mechanics and Engineering*, **19**, 59–98.
- , 1991: The ultimate conservative difference scheme applied to unsteady one-dimensional advection. *Computer Methods in Applied Mechanics and Engineering*, 17–74.
- Lermusiaux, P. F. J., 2001: Evolving the subspace of three-dimensional multiscale ocean variability: Massachusetts bay. *J. Mar. Sys.*, **29**, 385–422.
- Levier, B., A.-M. Tréguier, G. Madec, and V. Garnier, 2007: Free surface and variable volume in the nemo code. Tech. rep., MERSEA MERSEA IP report WP09-CNRS-STR-03-1A, 47pp, available on the NEMO web site.
- Lévy, M., A. Estubier, and G. Madec, 2001: Choice of an advection scheme for biogeochemical models. *Geophys. Res. Lett.*, **28**.
- Lévy, M., P. Klein, A.-M. Tréguier, D. Iovino, G. Madec, S. Masson, and T. Takahashi, 2010: Impacts of sub-mesoscale physics on idealized gyres. *Ocean Modelling*, **34** (1-2), doi:10.1016/j.ocemod.2010.04.001, URL <http://dx.doi.org/10.1016/j.ocemod.2010.04.001>.
- Li, M. and C. Garrett, 1993: Cell merging and the jet/downwelling ratio in langmuir circulation. *J. Mar. Res.*, **51**, 737–769.
- Losch, M., 2008: Modeling ice shelf cavities in a z coordinate ocean general circulation model. *J. Geophys. Res.*, **113** (C13).
- Lott, F., G. Madec, and J. Verron, 1990: Topographic experiments in an ocean general circulation model. *Ocean Modelling*, **88**, 1–4.
- Madec, G., M. Chartier, and M. Crépon, 1991a: Effect of thermohaline forcing variability on deep water formation in the northwestern mediterranean sea - a high resolution three-dimensional study. *Dyn. Atmos. Ocean*, **15**, 301–332.
- Madec, G., M. Chartier, P. Delecluse, and M. Crépon, 1991b: A three-dimensional numerical study of deep water formation in the northwestern mediterranean sea. *J. Phys. Oceanogr.*, **21**, 1349–1371.
- Madec, G. and M. Crépon, 1991: *Deep convection and deep water formation in the oceans*, chap. Thermohaline-driven deep water formation in the Northwestern Mediterranean Sea, 241–265. Elsevier Oceanographic Series, P.C. Chu and J.C. Gascard (Eds.).
- Madec, G. and P. Delecluse, 1997: The opa/arpege and opa/lmd global ocean-atmosphere coupled model. *Int. WOCE Newsletter*, **26**, 12–15.

- Madec, G., P. Delecluse, M. Imbard, and C. Levy, 1998: Opa 8 ocean general circulation model - reference manual. Tech. rep., LODYC/IPSL Note 11.
- Madec, G. and M. Imbard, 1996: A global ocean mesh to overcome the north pole singularity. *Clim. Dyn.*, **12**, 381–388.
- Madec, G., F. Lott, P. Delecluse, and M. Crépon, 1996: Large-scale preconditioning of deep-water formation in the northwestern mediterranean sea. *J. Phys. Oceanogr.*, **26** (8), 1393–1408.
- Maggiore, A., M. Zavatarelli, M. G. Angelucci, and N. Pinardi, 1998: Surface heat and water fluxes in the adriatic sea: seasonal and interannual variability. *Phys Chem Earth*, **23**, 561–567.
- Maltrud, M. E., R. D. Smith, A. J. Semtner, and R. C. Malone, 1998: Global eddy-resolving ocean simulations driven by 1985-1995 atmospheric winds. *J. Geophys. Res.*, **103** (C13), 30,825–30,854.
- Marsaleix, P., F. Auclair, J. W. Floor, M. J. Herrmann, C. Estournel, I. Pairaud, and C. Ulses, 2008: Energy conservation issues in sigma-coordinate free-surface ocean models. *Ocean Modelling*, **20** (1), 61–89, doi:10.1016/j.ocemod.2007.07.005, URL <http://dx.doi.org/10.1016/j.ocemod.2007.07.005>.
- Marsh, R., V. O. Ivchenko, N. Skliris, S. Alderson, G. R. Bigg, G. Madec, A. T. Blaker, Y. Aksenov, B. Sinha, A. C. Coward, J. L. Sommer, N. Merino, and V. B. Zalesny, 2015: Nemo-icb (v1.0): interactive icebergs in the nemo ocean model globally configured at eddy-permitting resolution. *Geoscientific Model Development*, **8** (5), 1547–1562, doi:10.5194/gmd-8-1547-2015, URL [HTTP://www.geosci-model-dev.net/8/1547/2015/](http://www.geosci-model-dev.net/8/1547/2015/).
- Marti, O., 1992: Etude de l’océan mondial : modélisation de la circulation et du transport de traceurs anthropogéniques. Ph.D. thesis, Université Pierre et Marie Curie, Paris, France, 201pp.
- Marti, O., G. Madec, and P. Delecluse, 1992: Comment on ”net diffusivity in ocean general circulation models with nonuniform grids” by f. l. yin and i. y. fung. *J. Geophys. Res.*, **97**, 12,763–12,766.
- Martin, T. and A. Adcroft, 2010: Parameterizing the fresh-water flux from land ice to ocean with interactive icebergs in a coupled climate model. *Ocean Modelling*, **34** (3–4), 111–124, doi:10.1016/j.ocemod.2010.05.001, URL <http://dx.doi.org/10.1016/j.ocemod.2010.05.001>.
- McDougall, T. J., 1987: Neutral surfaces. *J. Phys. Oceanogr.*, **17** (11), 1950–1964.
- McDougall, T. J. and J. R. Taylor, 1984: Flux measurements across a finger interface at low values of the stability ratio. *J. Mar. Res.*, **42**, 1–14.



- Mellor, G. and A. Blumberg, 2004: Wave breaking and ocean surface layer thermal response. *J. Phys. Oceanogr.*, **34** (3), 693–698, doi:10.1175/2517.1, URL <http://journals.ametsoc.org/doi/abs/10.1175/2517.1>.
- Mellor, G. L. and T. Yamada, 1982: Development of a turbulence closure model for geophysical fluid problems. *Rev. Geophys. Space Phys.*, **20**, 851–875.
- Merryfield, W. J., G. Holloway, and A. E. Gargett, 1999: A global ocean model with double-diffusive mixing. *J. Phys. Oceanogr.*, **29** (6), 1124–1142.
- Mesinger, F. and A. Arakawa, 1976: *Numerical methods used in Atmospheric models*. GARP Publication Series No 17.
- Morel, A., 1988: Optical modeling of the upper ocean in relation to its biogenous matter content (case i waters). *J. Geophys. Res.*, **93**, 10,749–10,768.
- Morel, A. and J.-F. Berthon, 1989: Surface pigments, algal biomass profiles, and potential production of the euphotic layer: Relationships reinvestigated in view of remote-sensing applications. *Limnol. Oceanogr.*, **34**(8), 1545–1562.
- Morel, A. and S. Maritorena, 2001: Bio-optical properties of oceanic waters: a reappraisal. *J. Geophys. Res.*, **106** (C4), 7163–7180.
- Murray, R. J., 1996: Explicit generation of orthogonal grids for ocean models. *J. Comput. Phys.*, **126** (2), 251–273.
- Oddo, P., M. Adani, N. Pinardi, C. Fratianni, M. Tonani, and D. Pettenuzzo, 2009: A nested atlantic-mediterranean sea general circulation model for operational forecasting. *Ocean Sc.*, **5**, 1–13.
- Osborn, T., 1980: Estimates of the local rate of vertical diffusion from dissipation measurements. *J. Phys. Oceanogr.*, **10**, 83–89.
- Pacanowski, R. and S. Philander, 1981: Parameterization of vertical mixing in numerical models of tropical oceans. *J. Phys. Oceanogr.*, **11** (11), 1443–1451.
- Pacanowski, R. C. and A. Gnanadesikan, 1998: Transient response in a z-level ocean model that resolves topography with partial-cells. *Mon. Wea. Rev.*, **126**, 3248–3270.
- Paulson, C. A. and J. J. Simpson, 1977: Irradiance measurements in the upper ocean. *J. Phys. Oceanogr.*, **7** (6), 952–956.
- Payne, R. E., 1972: Albedo of the sea surface. *J. Atmos. Sc.*, **29**, 959–970.
- Penduff, T., J. L. Sommer, B. Barnier, A. Treguier, J. Molines, and G. Madec, 2007: Influence of numerical schemes on current-topography interactions in 1/4° global ocean simulations. *Ocean Sc.*, **3**, 509–524.

- Redi, M. H., 1982: Oceanic isopycnal mixing by coordinate rotation. *J. Phys. Oceanogr.*, **13**, 1154–1158.
- Reed, R. K., 1977: On estimating insolation over the ocean. *J. Phys. Oceanogr.*, **1**, 874–971.
- Reverdin, G., P. Delecluse, C. Lévy, P. Andrich, A. Morlière, and J. M. Verstraete, 1991: The near surface tropical atlantic in 1982-1984 : results from a numerical simulation and a data analysis. *Prog. Oceanogr.*, **27**, 273–340.
- Richtmyer, R. D. and K. W. Morton, 1967: *Difference methods for initial-value problems*. Interscience Publisher, Second Edition, 405pp pp.
- Robert, A. J., 1966: The integration of a low order spectral form of the primitive meteorological equations. *J. Met. Soc. Japan*, **44** (2).
- Rodgers, K. B., O. Aumont, S. E. Mikaloff Fletcher, Y. Plancherel, L. Bopp, C. de Boyer Montégut, D. Iudicone, R. F. Keeling, G. Madec, and R. Wanninkhof, 2014: Strong sensitivity of southern ocean carbon uptake and nutrient cycling to wind stirring. *Biogeosciences*, **11** (15), 4077–4098, doi:10.5194/bg-11-4077-2014, URL [HTTP://www.biogeosciences.net/11/4077/2014/](http://www.biogeosciences.net/11/4077/2014/).
- Rodi, W., 1987: Examples of calculation methods for flow and mixing in stratified fluids. *J. Geophys. Res.*, **92** (C5), 5305–5328.
- Roquet, F., G. Madec, L. Brodeau, and J. Nycander, 2015a: Defining a simplified yet realistic equation of state for seawater. *J. Phys. Oceanogr.*, **45**, 2564–2579, doi:10.1175/JPO-D-15-0080.1, URL <http://dx.doi.org/10.1175/JPO-D-15-0080.1>.
- Roquet, F., G. Madec, T. McDougall, and P. Barker, 2015b: Accurate polynomial expressions for the density and specific volume of seawater using the teos-10 standard. *Ocean Modelling*, **90**, 29–43, doi:10.1016/j.ocemod.2015.04.002, URL <http://dx.doi.org/10.1016/j.ocemod.2015.04.002>.
- Roullet, G. and G. Madec, 2000: salt conservation, free surface, and varying levels: a new formulation for ocean general circulation models. *J. Geophys. Res.*, **105**, 23,927–23,942.
- Sarmiento, J. L. and K. Bryan, 1982: Ocean transport model for the north atlantic. *J. Geophys. Res.*, **87**, 394–409.
- Shchepetkin, A. F. and J. C. McWilliams, 2005: The regional oceanic modeling system (roms) - a split-explicit, free-surface, topography-following-coordinate oceanic model. *Ocean Modelling*, **9** (4), 347–404.

- , 2008: *Handbook of Numerical Analysis, Vol. XIV: Computational Methods for the Ocean and the Atmosphere*, pp 121-183. P. G. Ciarlet, editor, R. Temam and J. Tribbia, guest eds., Elsevier Science, 784 pp.
- Siddorn, J. and R. Furner, 2012: An analytical stretching function that combines the best attributes of geopotential and terrain-following vertical coordinates. *Ocean Modelling*, submitted.
- Simmons, H. L., S. R. Jayne, L. C. St. Laurent, and A. J. Weaver, 2004: Tidally driven mixing in a numerical model of the ocean general circulation. *Ocean Modelling*, 245–263.
- Song, Y. and D. Haidvogel, 1994: A semi-implicit ocean circulation model using a generalized topography-following coordinate system. *J. Comput. Phys.*, **115** (1), 228–244.
- Song, Y. T., 1998: A general pressure gradient formulation for ocean models. part i: Scheme design and diagnostic analysis. *Mon. Wea. Rev.*, **126** (12), 3213–3230.
- St. Laurent, L. and J. D. Nash, 2004: An examination of the radiative and dissipative properties of deep ocean internal tides. *Deep-Sea Res.*, **II** (51), 3029–3042, doi:10.1016/j.dsr2.2004.09.008, URL <http://dx.doi.org/10.1016/j.dsr2.2004.09.008>.
- St. Laurent, L., H. Simmons, and S. Jayne, 2002: Estimating tidally driven mixing in the deep ocean. *Geophys. Res. Lett.*, **29**, 2106, doi:10.1029/2002GL015633, URL <http://dx.doi.org/10.1029/2002GL015633>.
- Stacey, M. W., 1999: Simulations of the wind-forced near-surface circulation in knight inlet: A parameterization of the roughness length. *J. Phys. Oceanogr.*, **29**, 1363–1367.
- Steele, M., R. Morley, and W. Ermold, 2001: Phc- a global ocean hydrography with a high-quality arctic ocean. *J. Climate*, **14** (9), 2079–2087.
- Stein, C. A. and S. Stein, 1992: A model for the global variation in oceanic depth and heat flow with lithospheric age. *Nature*, **359**, 123–129.
- Talagrand, O., 1972: On the damping of high-frequency motions in four-dimensional assimilation of meteorological data. *J. Atmos. Sc.*, **29**, 1571–1574.
- Tonani, M., N. Pinardi, S. Dobricic, I. Pujol, and C. Fratianni, 2008: A high-resolution free-surface model of the mediterranean sea. *Ocean Sc.*, **4**, 1–14.
- Tréguier, A., 1992: Kinetic energy analysis of an eddy resolving, primitive equation north atlantic model. *J. Geophys. Res.*, **97**, 687–701.
- Tréguier, A.-M., J. Dukowicz, and K. Bryan, 1996: Properties of nonuniform grids used in ocean general circulation models. *J. Geophys. Res.*, **101**, 20,877–20,881.

- Tréguier, A. M., I. M. Held, and V. D. Larichev, 1997: Parameterization of quasi-geostrophic eddies in primitive equation ocean models. *J. Phys. Oceanogr.*, **27** (4), 567–580.
- Umlauf, L. and H. Burchard, 2003: A generic length-scale equation for geophysical turbulence models. *J. Mar. Sys.*, **61** (2), 235–265.
- , 2005: Second-order turbulence closure models for geophysical boundary layers. a review of recent work. *J. Mar. Sys.*, **25**, 795–827.
- UNESCO, 1983: *Algorithms for computation of fundamental property of sea water*. Techn. Paper in Mar. Sci, 44, UNESCO.
- Valcke, S., 2006: Oasis3 user guide (prism.2-5). Tech. rep., PRISM Support Initiative Report No 3, CERFACS, Toulouse, France.
- Vallis, G. K., 2006: *Atmospheric and Oceanic Fluid Dynamics*. Cambridge University Press, Cambridge, U.K., 745 pp.
- Vancoppenolle, M., T. Fichefet, and H. Goosse, 2009a: Simulating the mass balance and salinity of arctic and antarctic sea ice. 2. importance of sea ice salinity variations. *Ocean Modelling*, **27**, 54–69.
- Vancoppenolle, M., T. Fichefet, H. Goosse, S. Bouillon, G. Madec, and M. A. M. Maqueda, 2009b: Simulating the mass balance and salinity of arctic and antarctic sea ice. 1. model description and validation. *Ocean Modelling*, **27**, 33–53, doi:10.1016/j.ocemod.2008.10.005, URL <http://dx.doi.org/10.1016/j.ocemod.2008.10.005>.
- Warner, J. C., C. R. Sherwood, H. G. Arango, and R. P. Signell, 2005: Performance of four turbulence closure models implemented using a generic length scale method. *Ocean Modelling*, **8**, 81–113, doi:10.1016/j.ocemod.2003.12.003, URL <http://dx.doi.org/j.ocemod.2003.12.003>.
- Weatherly, G. L., 1984: An estimate of bottom frictional dissipation by gulf stream fluctuations. *J. Mar. Res.*, **42** (2), 289–301.
- Weaver, A. J. and M. Eby, 1997: On the numerical implementation of advection schemes for use in conjunction with various mixing parameterizations in the gfdl ocean model. *J. Phys. Oceanogr.*, **27**.
- Webb, D. J., B. A. de Cuevas, and C. S. Richmond, 1998: Improved advection schemes for ocean models. *J. Atmos. Ocean Tech.*, **15** (5), 1171–1187.
- White, L., A. Adcroft, and R. Hallberg, 2009: High-order regridding-remapping schemes for continuous isopycnal and generalized coordinates in ocean models. *J. Climate*, **228**, 8665–8692.

- Wilcox, D. C., 1988: Reassessment of the scale-determining equation for advanced turbulence models. *AIAA journal*, **26** (11), 1299–1310.
- Willebrand, J., B. Barnier, C. Boning, C. Dieterich, P. D. Killworth, C. L. Provost, Y. Jia, J.-M. Molines, and A. L. New, 2001: Circulation characteristics in three eddy-permitting models of the north atlantic. *Prog. Oceanogr.*, **48** (2), 123–161.
- Zalesak, S. T., 1979: Fully multidimensional flux corrected transport algorithms for fluids. *J. Comput. Phys.*, **31**.
- Zhang, R.-H. and M. Endoh, 1992: A free surface general circulation model for the tropical pacific ocean. *J. Geophys. Res.*, **97**, 11,237–11,255.